The Crystal Engineering of Two Anti-bacterial Pharmaceutical Ingredients: Cocrystals and Molecular Salts of a Series of Sulfa-Drugs and the Polymorphism and Cocrystals of an Isoniazid Derivative.

By

Matthew Clarke Scheepers

Submitted in accordance with the requirements for the degree of

Doctor of Philosophy

In the subject

Chemistry

At the

UNIVERSITY OF THE WITWATERSRAND

Supervisor: Prof. A. Lemmerer
January 2023

DECLARATION

I declare that **"The Crystal Engineering of Two Anti-bacterial Pharmaceutical Ingredients: Cocrystals and Molecular Salts of a Series of Sulfa-Drugs and the Polymorphism and Cocrystals of an Isoniazid Derivative."** is my own unaided work and that all sources I have used or quoted have been indicated and acknowledged by means of complete references. It has not been submitted before for any degree or examination at any other University.



Matthew Clarke Scheepers

31 January 2023

Date

Abstract

Crystal engineering is the design and synthesis of new solid forms by using the knowledge of intermolecular interactions and crystal packing. The goal of crystal engineering is to improve the properties of materials without altering the chemical identity of the materials. This work can be divided into three major parts. The first part deals with a series of sulfa drugs and its cocrystals. The second part deals with exploring the cocrystals of 3,5-dinitrobenzoic acid, in particular using Hirshfeld surfaces. The last part deals with the polymorphism of an isoniazid derivative and the cocrystals formed with it. In all cases these new solids were characterized by single crystal X-ray diffraction (SC-XRD), powder X-ray diffraction (PXRD), differential scanning calorimetry (DSC), thermal gravimetric analysis (TGA), and Fourier-transform infrared spectroscopy (FTIR).

When designing new solid forms (cocrystals and molecular salts) it would be ideal to use a knowledge based system on the use of synthons. Sometimes this knowledge is limited and can hinder future work. Sulfa drugs such as sulfamethazine (**sz**), sulfapyridine (**sp**), sulfathiazole (**st**) and sulfamethoxazole (**sm**) have been shown to exhibit unique solid-state behaviour such as cocrystal-salt polymorphism and tautomerism. The number of known cocrystals and molecular salts consisting of the mentioned drugs are limited, which hinders research into exploring this interesting solid-state behaviour. Therefore, the structural landscape of these sulfa drugs was expanded in hopes of observing new cases where this solid-state behaviour is observed. Cocrystals and molecular salts of these sulfa drugs were synthesized using various techniques, such as solvent evaporation and mechanochemical grinding (both dry and liquid-assisted grinding). Twenty-five different coformers were chosen to use for these cocrystallization experiments, most of which are either benzoic acid/benzoic acid derivatives or a pyridine derivative. **sz** formed eight successful cocrystals and one molecular salt with benzoic acid and its derivatives. SC-XRD showed that eight of the coformers that interacted

with **sz** formed the sulfonamide-carboxyl synthon; the only exception to this was **sz** + 4-hydroxybenzoic acid, which the sulfonimide-carboxyl synthon formed instead. Five cocrystals and one molecular salt containing **st**, three cocrystals and one molecular salt of **sm**, and four cocrystals and one molecular salt containing **sp** were also synthesized. Most of these included using 2-aminopyridine or one of its derivatives.

The second part deals with the cocrystals and molecular salts of 3,5-dinitrobenzoic acid (**dnba**). **dnba** is often used as a popular coformer for crystal engineering purpose. However, very little work centered on **dnba** with coformers has been reported. In this work we report new multi-component crystals containing **dnba**, which include one hydrate, one solvate, one molecular salt, and four cocrystals. The coformers include: 2-acetylpyridine, 3-cyanopyridine, flufenamic acid, 4-dimethylaminobenzophenone, pyridoxine, theophylline, and thiourea. In addition to the strong hydrogen bonding expected, several weaker intermolecular interactions were identified using Hirshfeld surfaces, which included C−H···π bonding, π-hole, and π···π interactions. The Hirshfeld surfaces indicated that these weaker interactions had a significant effect on the packing of these multi-component crystals. These multi-component crystals were compared with the crystal structures reported in the Cambridge structural database (CSD), which has given some significant insights in the structural landscape of **dnba**.

Isoniazid (**inh**) is a simple, useful active pharmaceutical ingredient (API) used to treat *Myobacterium tuberculosis*. It is composed of a hydrazine and pyridine ring. The hydrazine group can be modified in a multitude of ways, including using a Schiff-base condensation reaction. This is achieved by using an appropriate ketone or aldehyde. In this work isoniazid was derivitised using diacetone alcohol (4-hydroxy-4-methyl-2-pentanone), generating *N*'-[(2*E*)-4-hydroxy-4-methylpentan-2-ylidene]pyridine-4-carbohydrazide (**iz4h4m2p**). This derivative was found to be polymorphic, existing in two forms, form **I** and form **II**. The

difference between these two forms is distinguished by the major hydrogen bond pattern, which is either a chain hydrogen bond motif formed between the hydroxyl group and amide groups (the pyridine ring is not involved) or a ring based hydrogen bond motif that forms dimers with the hydroxyl group forming a hydrogen bond to the pyridine ring. Form **I** was found to be metastable with respect to form **II**, with form **I** converting to form **II** upon heating before melting. Form **II** does not convert to form **I**. In addition to exploring the polymorphism of **iz4h4m2p**, several cocrystals of **iz4h4m2p** were synthesized. The coformers chosen were benzoic acid derivatives. Most of these cocrystals formed a hydrogen bond between the carboxylic acid and pyridine ring. This left the hydroxyl group of **iz4h4m2p** to form a hydrogen bond to the amide group, forming a chain hydrogen bond motif similar to the one observed in form **I**. The only deviation from this was observed in cocrystals where the benzoic acid included a hydroxyl group of its own, such as 2,5-dihydroxybenzoic acid.

Acknowledgements

First, I would like to thank my supervisor, Prof. Andreas Lemmerer, for his unwavering support, dedication, patience and kindness. Under your supervision, not only have I have grown my knowledge and skills but I have also grown as a person. I also thank you for allowing me to attend a few conferences and the crystallographic school that gave me insight into the nature of research in crystallography.

I would also like to thank Prof. Manuel Fernandes and Prof. Demetrius Levendis for their time, advice and kindness. I would also like to thank the rest of the structural chemistry group over the past 6 years for their support, including Cara, Prathapa, Delbert, Attiyah and Tracy.

Lastly I would like to thank my family for their endless support and unconditional love, making it possible for me to achieve my hopes and dreams.

Poster

Poster presented: Synthesis and characterization of a series of multicomponent crystals with sulfanilamide derivatives, presented at the 11th Bologna's convention on crystal forms held online 10-11 September 2021

The structure and outputs of the Thesis

There are several styles present in this work. The introductory, experimental and concluding chapters have been written in a uniform style. The central chapters (Chapters 3-5) have been published in different journals, each with its own respective style required for that journal. The published work has been presented as the essential research chapters since the significant findings from a large amount of work have been presented in a concise way. In chapters 3-5 a brief description of the papers is present preceding the papers.

Contributions from the authors

There were five papers published for this thesis. The conceptual ideas, as well as most of the experimental work and analysis was developed and carried out by myself. I wrote the papers largely by myself. Prof. Andreas Lemmerer provided supervision and academic insight. Prof. Manuel Fernandes carried out the *PIXEL* calculations presented in chapter 5, which was requested by the reviewers of the paper, which he helped write the related parts in that paper. This was his only contribution.

Contents

Chapter 1: The Crystal Engineering of Active Pharmaceutical Ingredients as an attempt to improve solid-state properties 6

1.1 Crystals 6

1.1.1 Introduction 6

1.1.2 Crystal Growth 8

1.2. Crystal Engineering and Supramolecular Chemistry 10

1.2.1 Introduction 10

1.2.2 Intermolecular interactions 10

1.2.3 Hydrogen Bonding 11

1.2.4 $\pi\cdots\pi$ stacking 12

1.2.5 Polymorphism 13

1.2.6 Cocrystals and Molecular Salts 19

1.2.7 Tautomerism 24

1.3 Hirshfeld Surfaces 25

1.4 Sulfa Drugs 30

1.4.1 Sulfapyridine 32

1.4.2. Sulfathiazole 33

1.4.3. Sulfamethoxazole 34

1.4.4. Sulfamethazine 35

1.5 Isoniazid 35

1.5.1 Introduction to isoniazid 35

1.5.2 Blocking the hydrazine group 36

1.5.3 Polymorphism of isoniazid and its derivatives/cocrystals 37

1.6 Aims and Objectives 37

Chapter 2 Experimental Procedures and Aims and Objectives 39

2.1 Cocrystal/molecular salt synthetic methods 39

2.2 Synthesis of iz4h4m2p 40

2.3 Single Crystal X-Ray Diffraction 40

2.4 Powder X-Ray Diffraction 41

2.5 Infrared Spectroscopy 41

2.6 Differential Scanning Calorimetry 41

2.7 Hirshfeld Surface Analysis 42

2.8 Hot Stage Microscopy 42

2.**9 Thermalgravimetric Analysis** 42

Chapter 3 Synthesis and Characterization of a series of Sulfamethazine multi-component crystals with Various Benzoic Acids. 43

3.1 introduction 43

Chapter 4 In Pursuit of Multicomponent Crystals of the Sulfa Drugs Sulfapyridine, Sulftahiazole and Sulfamethoxazole 55

4.1 Introduction 55

Chapter 5 Exploring the Crystal Structure Landscape of 3,5-Dinitrobenzoic Acid through Various Multicomponent Molecular Complexes 81

5.1 Introduction 81

Chapter 6 Chains or rings? Polymorphism of an isoniazid derivative derivatized with diacetone alcohol 95

6.1 Introduction 95

Chapter 7 Design of a series of cocrystals featuring isoniazid modified with diacetone alcohol 103

7.1 Introduction 103

Chapter 8 Conclusions 115

References 118

Appendix 125

List of Figures

Figure 1.1.1 The 14 Bravais lattices.

Figure 1.1.2 Schematic illustration of the size dependence of the energetics of nucleation.

Figure 1.2.4.1. The three different types of π···π stacking: (a) cofacial parallel packing, (b) parallel displaced packing and (c) Edge-to-face T-shaped packing.
Figure 1.2.4.2 Graphical representation explaining why a cofacial parallel stack is unfavourable to parallel displaced, and a case where cofacial parallel stack might be feasible.

Figure 1.2.5.1 Enantiotropic vs. monotropic energy-temperature diagrams

Fig. 1.2.5.2 Schematic of the reaction coordinates for the crystallization of a dimorphic system.

Scheme 1.2.7. The tautomerism of adenine: (A – major tautomer of adenine) hydrogen bonded to thymine (T) on the left versus adenine's minor tautomer (A') hydrogen bonded to cytosine (C) on the right.

Figure 1.3.1 A plain surface showing the definition of d_i and d_e of 4-hydroxybenzoic acid (Refcode JOZZHI01).

Figure 1.3.2 The Hirshfeld surface of 4hba (Refcode JOZZHI01) showing (a) d_i, (b) d_e, (c) d_{norm}, (d) the shape index and (e) the curvedness.

Figure 1.3.3 A fingerprint plot of 4hba (Refcode JOZZHI01).

Scheme 1.4. The basic structure of sulfonanilamide.

Scheme 1.4.1 Basic structure of sulfapyridine showing its tautomerism.

Scheme 1.4.2 The structure of st showing the sulfonamide tautomer.

Scheme 1.4.3 Structure of **sm**.

Scheme 1.4.4. Structure of **sz** showing the sulfonamide tautomer (right) and sulfonimide tautomer (left).

Scheme. 1.5.3. General scheme of the Schiff-base condensation reaction of isoniazid with a ketone or aldehyde (R_1 = H).

Scheme 2.2 Reaction scheme for the synthesis of **iz4h4m2p**.

List of Tables

Table 2.1 List of coformers used in this work.

List of Abbreviations

2ap: 2-aminopyridine

3ap: 3-aminopyridine

4ap: 4-aminopyridine

2a3np: 2-amino-3-nitropyridine

2a5np: 2-amino-5-nitropyridine

2a5clp: 2-amino-5-chloropyridine

bipy: 4,4'-bipyridine

BCS: Biopharmaceutics Classification System

2hba: 2-hydroxybenzoic acid (salicylic acid)

3hba: 3-hydroxybenzoic acid

4hba: 4-hydroxybenzoic acid

2hp: 2-hydroxypyridine

3hp: 3-hydroxypyridine

4hp: 4-hydroxypyridine

2c4n: 2-chloro-4-nitrobenzoic acid

2c5n: 2-chloro-5-nitrobenzoic acid

3cnp: 3-cyanopyridine

4cnp: 4-cyanopyridine

ca: cinnamic acid

CSD: Cambridge structural database

dnba: 3,5-dinitrobenzoic acid

dcba: 3,4-dichlorobenzoic acid

DSC: Differential Scanning Calorimetry

FTIR: Fourier-transforminfrared spectroscopy

4hba: 4-hydroxybenzoic acid

inh : isoniazid

iz4h4m2p: *N*'-[(2E)-4-hydroxy-4-methylpentan-2-ylidene]pyridine-4-carbohydrazide

LAG: Liquid-assisted grinding

PXRD: Powder X-Ray Diffraction

PABA: 4-aminobenzoic acid

sa: succinic acid

sac: saccharine

SC-XRD: Single Crystal X-Ray Diffraction

sm : sulfamethoxazole

sp : sulfapyridine

st : sulfathiazole

sz : sulfamethazine

ta: Toluic acid

Chapter 1: The Crystal Engineering of Active Pharmaceutical Ingredients as an attempt to improve solid-state properties

1.1 Crystals

1.1.1 Introduction

A crystal is a solid made up of a periodic and ordered arrangement of atoms, ions and/or molecules in three-dimensional space known as a lattice. The crystal structure is best represented by using a unit cell, which can replicate the entire crystal structure by using only translation. Depending on the lattice, several possible unit cells may be defined, however, only one unit cell is considered. The one chosen is one that best represents the different symmetries that are present in the crystal structure while minimizing the size required to recreate the entire crystal structure.

All crystals exist in one of seven possible crystal systems. These crystal systems are: triclinic, monoclinic, orthorhombic, tetragonal, trigonal, hexagonal and cubic. These seven crystal systems are then classified further as being part of one of fourteen Bravais lattices (**Fig. 1.1.1**). These are further classified by space groups, which presents all the symmetry present in the crystal structure. Symmetry operations include inversion, rotations, mirror planes, screw axes and glide planes, in addition to the identity operation *E*. There are 230 space groups in total, with each space group named after the major symmetry operation(s) present in each crystal structures.

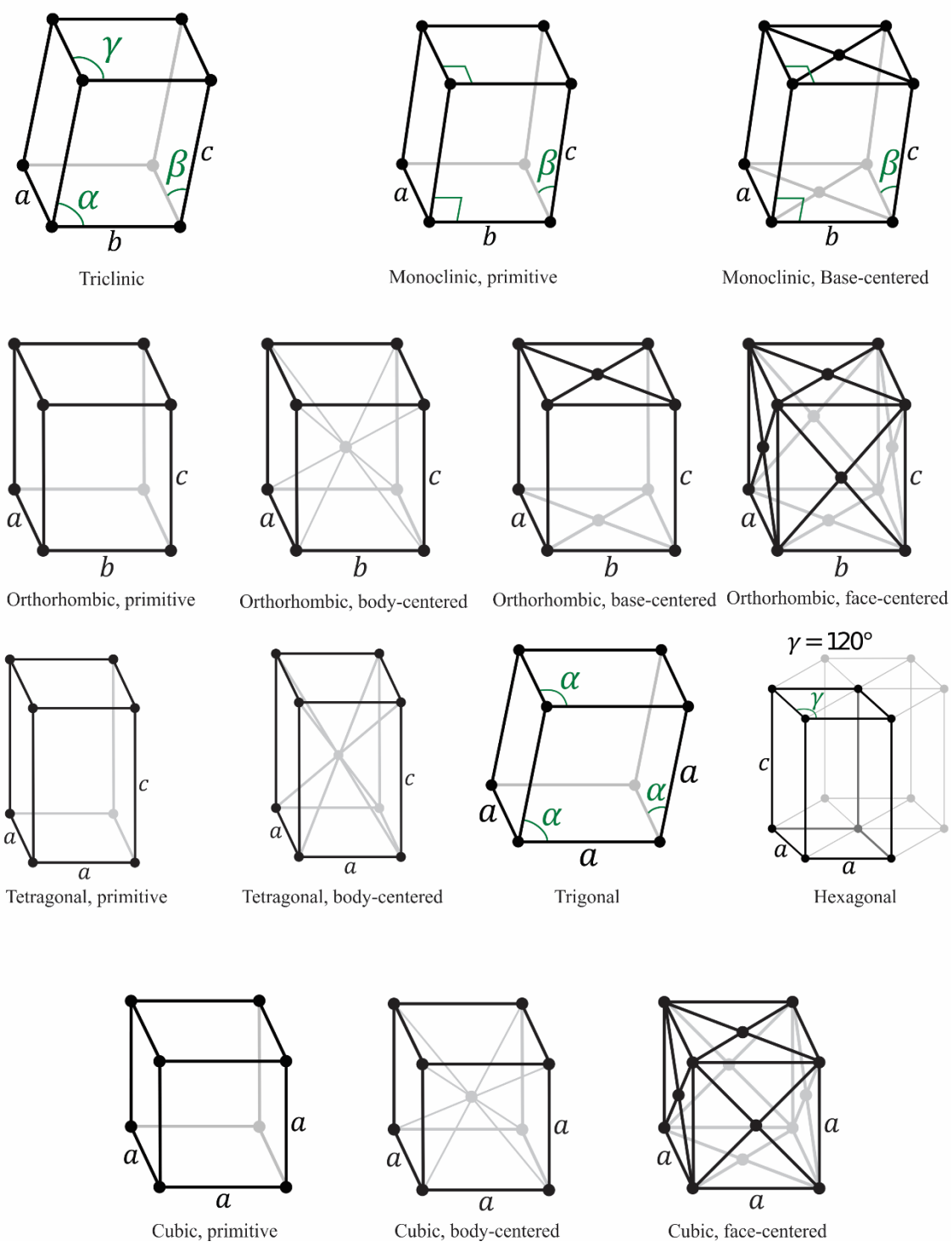


Figure 1.1.1 The 14 Bravais lattices (images adapted from Wikipedia page[1]).

For molecular crystals consisting of organic compounds, approximately 75% of reported organic crystals appears in just five space groups, which are: $P2_1/c$, $P\bar{1}$, $P2_1$, $P2_12_12_1$ and $C2/c$.[2]

Many solids of interest form in a crystal, and the study of crystals forms the basis of many areas of research. The properties of solids arise from the arrangement of atoms of molecules in the solid state, as well as the interactions between atoms and/or molecules present in the solid state. Therefore, in order to understand how a material behaves, the solid state structure needs to be first determined, and understood from an atomistic or molecular viewpoint.

1.1.2 Crystal Growth

A standard method for purifying organic compounds typically involves using recrystallization. Here, the impure compound is dissolved in a suitable solvent. This solution is then filtered (leaving behind insoluble impurities) and then evaporated (either through heating or slow evaporation). The process then ultimately leaves behind crystals of the (hopefully) pure compound. A series of questions remains: "How did these crystals form?" "How did the individual molecules come together to form these crystals?"

Crystallization is the process where atoms, molecules or ions aggregate together to form crystals. Crystallization is governed by two steps: nucleation and growth. Nucleation is the first step where a first order phase transition occurs, that is the change from being part of an aqueous solution, liquid or gas phase transforms into the solid phase. Two different types of nucleation exists: heterogeneous nucleation and homogenous nucleation. Homogenous nucleation occurs in the absence of the influence of foreign materials, for example, nucleation that occurs in the bulk or "centre" of a solution (not necessarily aqueous). Heterogeneous nucleation occurs at the surface of another material, for example the walls of glassware. Heterogeneous nucleation is the most dominant form of nucleation, which serves as the rationale for scratching the surface of glass walls to promote crystal growth. In order for nucleation to occur, the Gibbs free energy for the pre-existing phase (solution, liquid, gas) must become greater than the Gibbs free energy of the emerging phase.[3,4] The Gibbs energy of the emerging nucleus is dependent on two

factors. The first is the Gibbs free energy per unit volume, i.e. the bulk. This energy is always negative. The second is related to the surface energy of the emerging nucleus, which is always positive. **Fig. 1.1.2** represents these two energies. Small nuclei will consist of being more of a surface than consisting of bulk. These molecules will be loosely bound to the rest of the nucleus, which will result in the destabilisation of the nucleus and thus its dissolution. As more molecules aggregate to the developing nucleus, its bulk increases. At the critical radius r_{crit}, the Gibbs free energy between the interfacial and bulk energy reaches a maximum. Additional molecules at this point decreases this Gibbs free energy, which results in the growth of the nucleus. Heterogeneous nucleation is more prevalent than homogenous nucleation because the surface of the growing nucleus is substantially smaller than that of a free-growing nucleus, which ultimately causes crystal growth to occur using smaller nuclei.

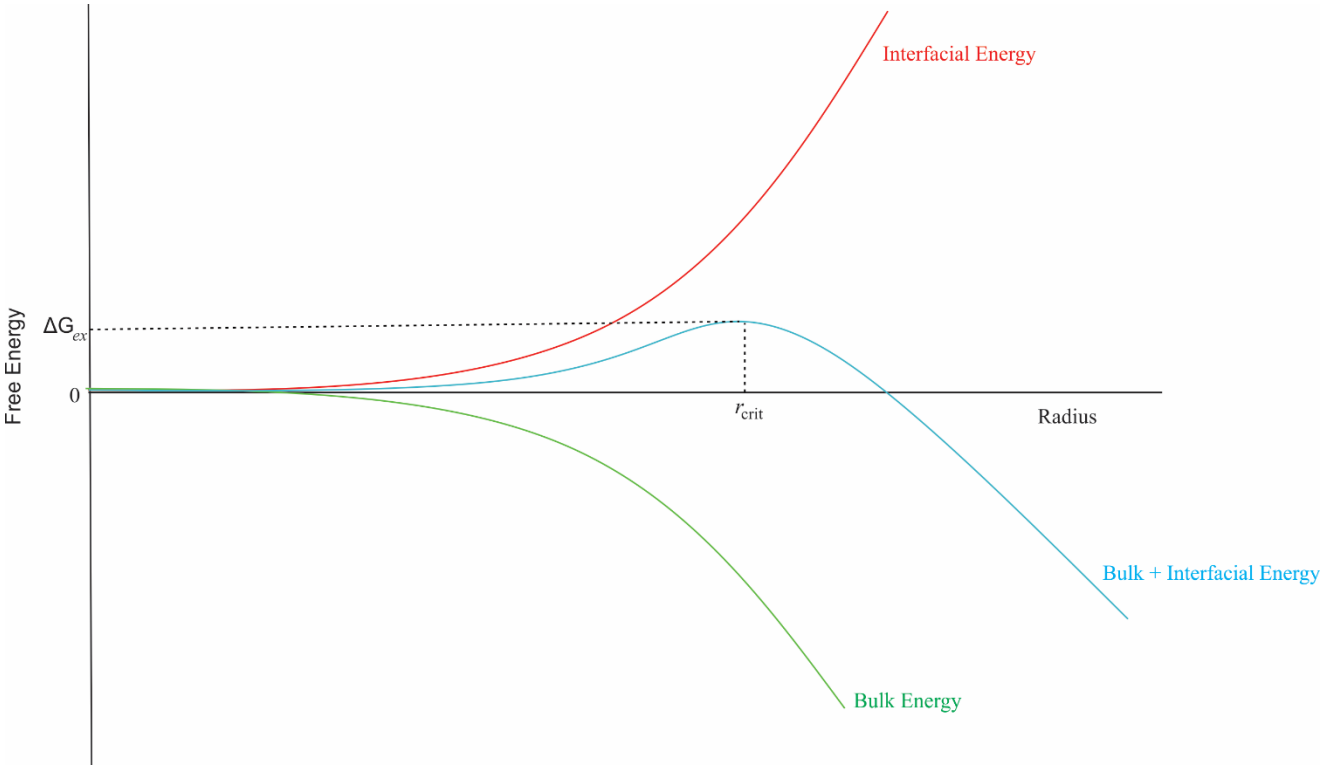


Figure 1.1.2 Schematic illustration of the size dependence of the energetics of nucleation.

1.2. Crystal Engineering and Supramolecular Chemistry

1.2.1 Introduction

Organic chemists often use the process of recrystallization to purify organic samples. This involves the assembly of a random collection of molecules in solution to form an organized assembly that results in a crystal. If chemistry is about the control of chemical processes, is it possible to control the crystallization of molecules? Is it possible to change the assembly of molecules? Is there any benefit in doing so?

The answer to these questions is yes, it is possible to manipulate the crystallization process (to an extent, at least), which forms part of the field of crystal engineering. Crystal engineering can be defined as the "understanding of intermolecular interactions in the context of crystal packing and in the utilization of such understanding in the design of new solids with desired physical and chemical properties."[5] This is achieved through the understanding of the intermolecular interactions between atoms, molecules and ions, which ultimately affects how they will pack in the solid state.

1.2.2 Intermolecular interactions

The arrangement of molecules in crystal structures is driven by molecular recognition. Molecular recognition is the aspect where certain intermolecular interactions are favoured and co-ordination of molecules occurs due to these interactions. Non-covalent interactions such as hydrogen bonding, π···π, metal co-ordination (chelation), van der Waals and electrostatic interactions often dictate the overall geometry and direction molecules form in the network. For e.g., DNA consists of two nucleobase strands held together by hydrogen bonds.[6] It was the recognition that the nucleobases can only bond with its counterpart (eg. adenine with thymine, guanine with cytosine) that eventually led to elucidation of the overall structure determination

of DNA and hence its function.[6] The understanding of the possible interactions can allow one to gain insight into how molecules form their respective crystal structures and hence predict/explain the resulting physical properties.

1.2.3 Hydrogen Bonding

The hydrogen bond is one of the most important intermolecular interactions to consider in the design of molecular crystals. The IUPAC definition for the hydrogen bond is as follows:

> The hydrogen bond is an attractive interaction between a hydrogen atom from a molecule or a molecular fragment X–H in which X is more electronegative than H, and an atom or a group of atoms in the same or a different molecule, in which there is evidence of bond formation. [7]

If the hydrogen bond is represented as X—H···A, X—H is defined as the hydrogen bond donor and A as the hydrogen bond acceptor. It is possible for a hydrogen bond donor or hydrogen bond acceptor to form more than one hydrogen bond simultaneously. If an atom forms two hydrogen bonds (either as a hydrogen bond donor or a hydrogen bond acceptor), the arrangement is referred to as a bifurcated hydrogen bond. Cases where an atom shares three hydrogen bonds is referred to as a trifurcated hydrogen bond, although such cases are rare.[8] The bond energies of hydrogen bonds are typically in the range of 10-65 kJ mol^{-1}, which are significantly higher in energy than that of the van der Waals forces (<8 kJ mol^{-1}).[9] The length of the hydrogen bond (X···A) can vary between 2.45 – 3.35 Å, while hydrogen bond angles (∠ X—H···A) can range between 90° - 180°. [8,10]

The hydrogen bond is a directional force in molecular crystals, which is significant enough that a formal notation based on Graph Sets can be used to describe the arrangement of the molecule based on the hydrogen bonds present. These patterns are defined according to the number of hydrogen bond donors, acceptors and the number of atoms involved in making up the motif.

The patterns in which hydrogen bonding forms between neighbouring molecules may be described as one of four pattern types: chains (*C*), Rings (*R*), Discrete (*D*) or Self (*S*).[11] Graph sets are presented in the following form $\boldsymbol{G_d^a(n)}$, where $\boldsymbol{G}$ represents the pattern, $\boldsymbol{a}$ represents the total number of hydrogen bond acceptors, $\boldsymbol{d}$ the total number of hydrogen bond donors and $\boldsymbol{n}$ represents the total number of atoms involved. The reasoning for using such definitions is that hydrogen bonding can be reduced from a complex pattern to that of a simple descriptive one, such that the resulting properties from such bonding can be explained with ease, and to attempt to predict such complex patterns.

1.2.4 π···π stacking

Many organic molecules feature aromatic systems. These rings consists of a series of overlapping π-orbitals, which cause the electrons to be delocalized. It has been observed that there is an electrostatic interaction that exists between two or more rings, although the exact nature of this interaction is still not fully understood.[12] π···π stacking forms part of several different areas of research, including biology and physics.[12,13] Three main types of π···π stacking exists: edge-to-face T-shaped, parallel displaced, and cofacial parallel stacked (**Fig. 1.2.4.1**). π···π stacking is the result of a combination of both dispersion and electrostatic effects. Hunter and Sanders proposed a simple model for π···π stacking where a positively charged σ-framework is sandwiched between two negatively charged π-systems.[13] Edge-to-face T shaped and parallel displaced π···π stacking systems are the most common, since most aromatic systems contain a partially positive hydrogen covalently bonded to the aromatic carbon ring. These partially positive hydrogens can form an attractive interaction with the partially negative π-systems. Cofacial parallel stacked remains the rarest of the three since the negatively charged π-systems will most likely repel each other. The only case where a cofacial parallel π···π stacking system could exist is where one of the coformers has strong electron withdrawing

functional groups present, such as the case of the cocrystal containing hexafluorobenzene and benzene (**Fig. 1.2.4.2)**.[14]

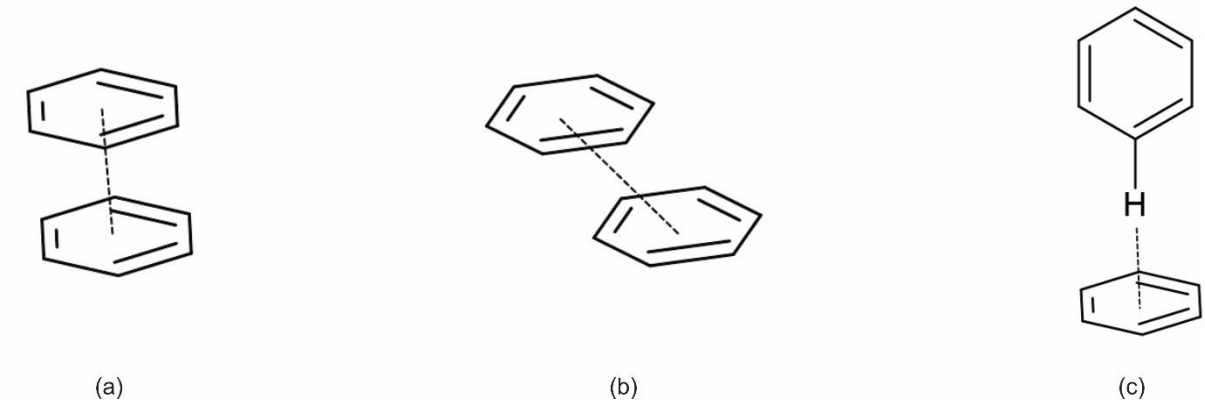


Figure 1.2.4.1. The three different types of π···π stacking: (a) cofacial parallel packing, (b) parallel displaced packing and (c) Edge-to-face T-shaped packing.

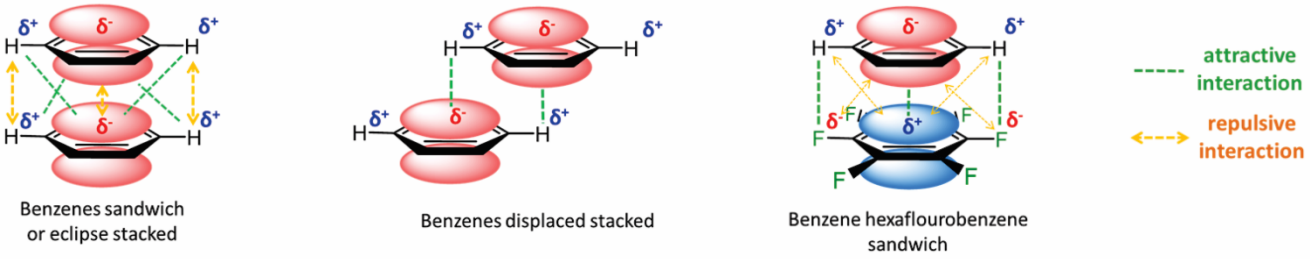


Figure 1.2.4.2 Graphical representation explaining why a cofacial parallel stack is unfavourable to parallel displaced, and a case where cofacial parallel stack might be feasible. (Graphics adapted from Chemistry Libre texts)[15]

1.2.5 Polymorphism

1.2.5.1. Introduction

Polymorphism refers to the phenomenon where molecules or ions can exist in more than one crystal form, either through different conformations of the molecules (conformational polymorphism) or packing arrangements (packing polymorphism).[16] Allotropy is where elements can have different solid state forms (such as diamond and graphite for carbon). Several thousand cases of polymorphism have been reported in the literature, with crystal

structures of organic and organometallic systems stored in the Cambridge Structural Database (CSD).[17] Cocrystals can also exhibit polymorphism.[18] The result of polymorphism is that different properties can arise. This can range from appearance (colour, shape etc.) to different electronic and thermal properties.[19] In the pharmaceutical industry, polymorphism plays a major role in the research and development of API's. Properties such as the dissolution rate and the solubility affect the bioavailability and therefore the effectiveness of the API.[20] Since each polymorph will have properties that differ between each other, it becomes critical to determine and characterize all possible forms. Polymorphs also offer the advantage of becoming new intellectual property.

McCrone once claimed that all compounds are polymorphic, and that the number of polymorphs discovered is proportional to the time and effort placed in finding them.[21] Over the course of the last few decades it became apparent that polymorphism is the norm instead of being the exception. However, the number of polymorphs reported for different compounds can differ drastically. Some compounds such as salicylic acid and sucrose have only one form reported at ambient conditions, while other compounds such as 5-methyl-2-[(2-nitrophenyl)-amino]thiophene-3-carbonitrile, also known as ROY (Red, Orange, Yellow, named after the colours its polymorphic forms can exhbit), can have more than nine forms reported.[22] Some compounds can be identified as monomorphic for several years before its first polymorphic form can be discovered, such as isoniazid[23] or aspirin.[24,25] It is even possible for different polymorphs to arise from the same crystallization event, a phenomenon known as concomitant polymorphism.[21,26,27] There are cases where a polymorphic form that has been reported previously cannot be obtained from using the same conditions as before, a phenomenon known as "disappearing polymorphs." The impact of polymorphism has only become more relevant over the past few decades.[21,27] For example, the protease inhibitor Ritonavir, a drug used to treat HIV was initially marketed by Abbott (now AbbVie) in a capsule form that was sold as

Norvir oral liquid and Norvir semi-solid capsules.[28] This first form (Form **I**) could easily dissolve in the desired water/ethanol mix. However, in 1998 a new, more thermodynamically stable form (Form **II**) appeared, which was identified from batches that failed the dissolution tests. As a result the new batches threatened the supply of this drug on the market as the new form could not be processed into the desired product, which resulted in massive recalls and became a major loss for the company.

1.2.5.2 Kinetics and Thermodynamics of polymorphism

How does a crystal crystallise in a particular form? What are the conditions for one form to be favoured over the other? The formation of a particular form over the other will depend on both thermodynamic and kinetic factors. These factors play a role in both the initial crystallization process (from nucleation) and in solid-to-solid phase transformations. When comparing polymorphic forms, it is typical that one form is more thermodynamically stable than the others at some given temperature. The most thermodynamically stable polymorphic form is called the thermodynamic form while polymorphic forms that are more unstable than the thermodynamic form are referred to as metastable forms. It is expected that any metastable form will convert to the more thermodynamic form. The rate at which the metastable form transforms to the thermodynamically stable form is determined by kinetic factors. The rate at which this occurs can be fast (to the point as if the metastable form never existed) to slow (to the point where it seems as if nothing is happening). For example, diamond and coal are two allotropes of carbon, with diamond being the metastable phase and graphite the thermodynamically favoured form. It is expected that diamond should transform to graphite but the rate at which it does is so slow that practically the transformation does not occur.

It is possible that under heating one polymorphic form will convert to another at some temperature. Consider a compound that consists of exactly two polymorphic forms: Form **I** and

Form **II**. The different polymorphic forms of molecular crystals are named using either a numeric approach (1,2,3… or I, II, III…) or using the Greek alphabet (α, β, γ…).[29] Typically forms are named in order of discovery, but otherwise they are ordered in terms of melting points starting with the form with the lowest melting point. Let's say that for our hypothetical compound we initially obtained Form **I**, which converts to Form **II** at some transition temperature T_p, i.e. a typical dimorphic system. If the transition of Form **I** to Form **II** is reversible at T_p, the process is enantiotropic. If the process is irreversible, it is monotropic. It should be noted that some phase transitions can be enantiotropic despite being irreversible due to kinetic reasons. Therefore, in order to decide conclusively if the phase transition is enantiotropic or monotropic, several rules need to be considered.

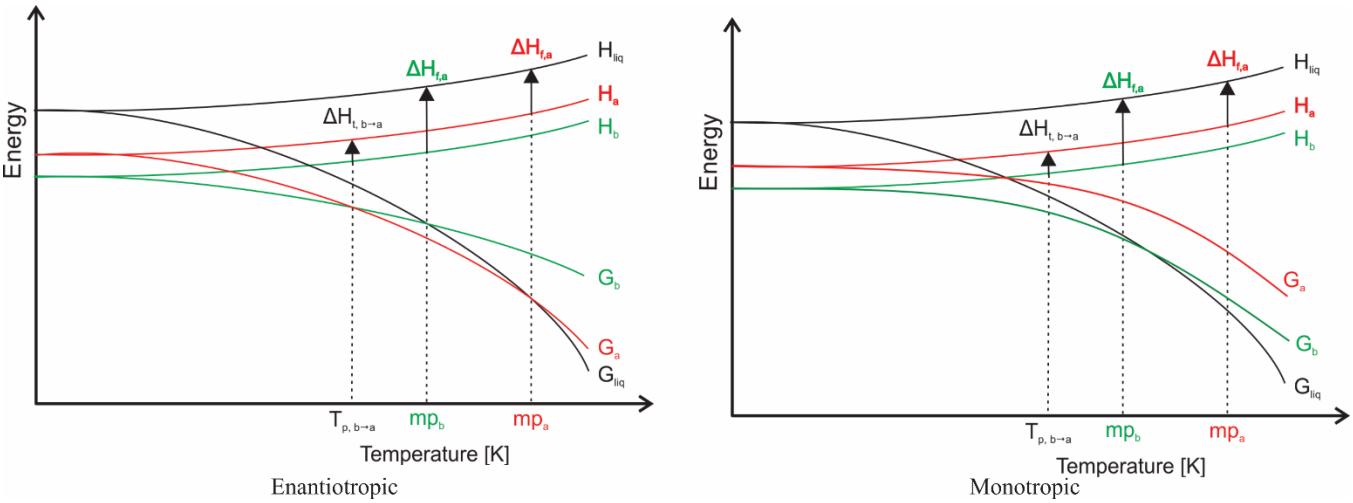


Figure 1.2.5.1 Enantiotropic vs. monotropic energy-temperature diagrams

The first rule to consider is the Heat-of-transition rule. It is stated as follows:

"*If an endothermal transition is observed at some temperature it may be assumed that there is a transition point below it, i.e. the two forms are related enantiotropically*."

"*If an exothermal transition is observed at some temperature it may be assumed that there is no transition point below it, i.e. the two forms are either related monotropically or the transition temperature is higher*."[30]

This rule was derived based on the observation that ΔH and ΔS are usually positive, and that H curves do not intersect while the G curves intersects only once (**Fig. 1.2.5.1**). This rule has been obeyed by 99% of all polymorphic cases.[30]

In the case that the transition point cannot be measured easily, the Heat-of-fusion rule can be used. It states:

"*If the higher melting form has the lower heat of fusion the two forms are usually enantiotropic, otherwise they are monotropic.*"[30]

This rule is obeyed if H curves follow the behaviour observed in **Fig. 1.2.5.1**. Deviation from this rule exists when the H curves diverge significantly or the difference between the melting points of both forms is more than 30 K.[31] The success of this rule is essentially equivalent to the Heat-of-transition rule.

In the case the Heat-of-fusion rule is unable to be used, the Entropy-of-fusion rule can be applied. The entropy of fusion is given by:

$$\Delta S = \frac{\Delta H_f}{T}$$

Then the rule states that if the form with the higher melting point has the lower entropy of fusion then the two forms are enantiotropically related, otherwise they are monotropically related.

Kinetics plays a role in selecting the polymorphic form that crystallises first. Consider our dimorphic system in which either form can crystallise. There are two possible reaction pathways: one pathway has a low activation energy barrier but the overall free energy is higher while the other pathway has a higher activation energy barrier but the free energy is much lower (**Fig. 1.2.5.2**). Most often the metastable phase forms over the thermodynamic phase simply because the activation energy is lower. During nucleation, the phase boundary (between the surface of the nucleus and the surrounding environment) is associated with an increase in free energy. The system in turn, must overall decrease in free energy, which is achieved by increasing the size of the nucleus. The observation in which the metastable phase forms first due to having a lower activation barrier was first made by Ostwald, which he stated in his "Rule of Stages." Although it is apparently true for many cases, exceptions arise such as in the case of concomitant polymorphism. It also becomes problematic when describing systems which are "apparently monomorphic."

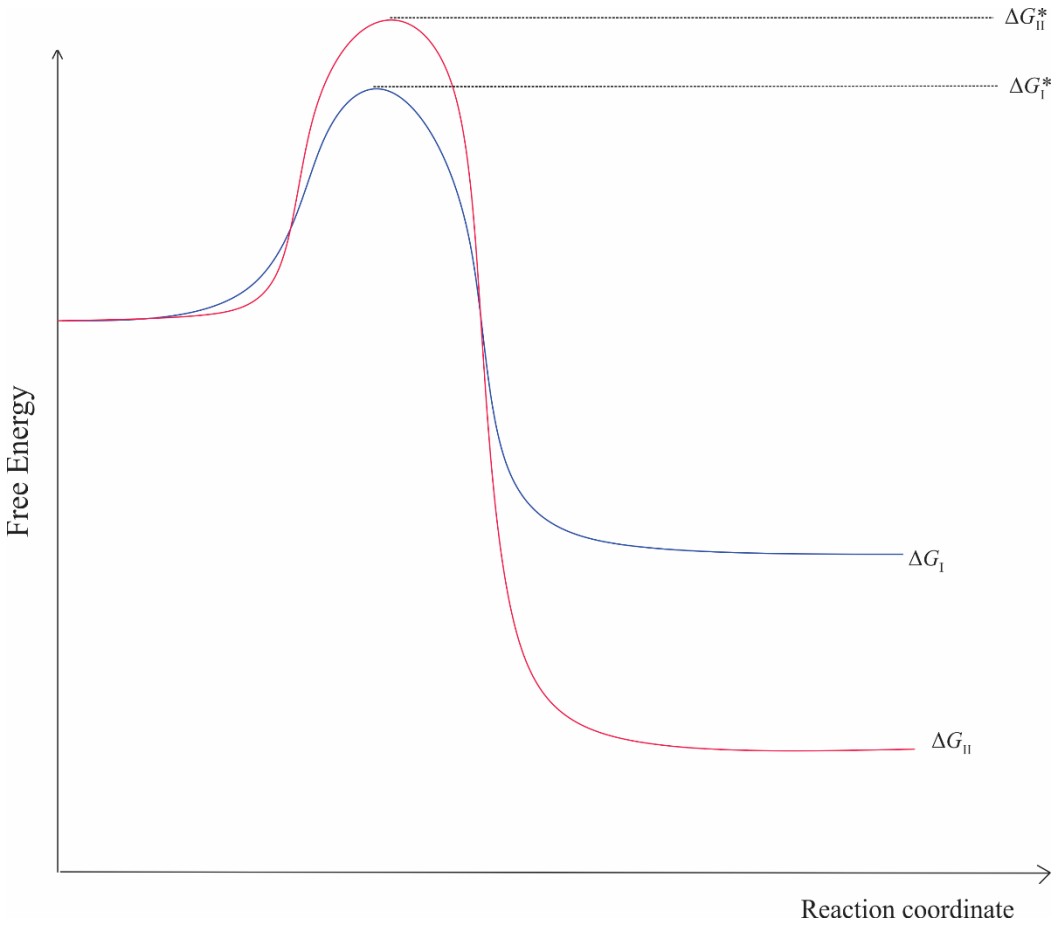


Fig. 1.2.5.2 Schematic of the reaction coordinates for the crystallization of a dimorphic system.

1.2.6 Cocrystals and Molecular Salts

Multi-component complexes such as co-crystals and molecular salts are systems designed to contain more than one component in the solid state, and are a rapidly growing area of interest in modern chemistry. Cocrystals are the combination of two or more neutral molecules that interact with each other in a way that makes up the supramolecular complex.[32] This distinguishes them from molecular salts where a proton transfer has occurred, leading to the formation of an ionic bond. In addition, cocrystals are further distinguished from hydrates and solvates in the sense that all the co-formers involved must be solid at ambient conditions. It should also be noted the spelling “cocrystal” and “co-crystal” are used by different authors and

journals and refer to the same thing, although agreement on which term to use has not been made.

1.2.5.1 pK_a and the ΔpK_a Rule

As stated previously, molecular salts are solids where proton transfer as occurred. This results in the formation of a set of ions (cation and anion), with both species held together by an electrostatic attraction. It becomes important to consider the acidic and basic nature of many compounds in the crystal engineering of organic molecules. Many organic compounds are acids and bases, although most are weak in nature. In solution, both ionized and non-ionized species exist in equilibrium. For some generic acid HA, this equilibrium is expressed as:

$$HA \rightleftharpoons H^+ + A^-$$

For which the acid dissociation constant K_a can be represented as:

$$K_a = \frac{[H^+][A^-]}{[HA]}$$

One useful means of comparing the extent to which an acid may be deprotonated (or a base protonated) is through the use of the pK_a which is defined as follows:

$$pK_a = -\log K_a$$

The pK_a can also be used for bases by using the conjugate acid. Strong acids will have small or negative pK_a's while strong bases will have large positive pK_a's. Amphoterism is the case where a compound can act both as an acid or a base, and as such these compounds can have multiple pK_a's. An acid or base in solution will change the *p*H of the solution. This change is given by the Henderson-Hasselbalch equation below:

$$pH = pK_a + \log\frac{[A^-]}{[HA]}$$

The Henderson-Hasselbalch equation indicates that in solution a mixture of an acid and its conjugate base (or a base and its conjugate acid) will exist, and the pH will affect the amount of acid (or conjugate acid) relative to its conjugative base (or base).

The pK_a is often used to compare the strength of an acid or a base with other acids and bases. The pK_a of a compound is usually listed in tables or databases alongside many others. Although useful, there are several limitations to this. The first is that the pK_a of many compounds are reported only for using water as the solvent. This presents a problem since different solvents have different effects on the solute. For example, according to a paper by Rossini *et al.*,[33] which examines both experimental and theoretical pK_a's of various compounds in different solvents, the pK_a of benzoic acid in water, acetonitrile, dimethyl sulfoxide and methanol is respectively 4.22, 20.10, 11.10 and 9.40. This makes sense, as solvents like water and methanol are protic solvents which will facilitate the proton transfer easier than an aprotic solvent like acetonitrile. This becomes problematic when the pK_a for a compound in a particular solvent has not been determined experimentally (or even theoretically). Another issue is temperature. The pK_a of many compounds has been reported at standard temperature (25 °C). Although the pK_a does not change drastically within a few degrees, it becomes more significant at much higher temperatures. For example, solutions are often heated to allow complete dissolution of the solute, in which case the pK_a will change. This change is determined according to the van't Hoff equation below:

$$\frac{d}{dT}\ln K = \frac{\Delta H^o}{RT^2}$$

Where K is the equilibrium constant, R is the universal gas constant and ΔH^o is the standard enthalpy. Accordingly, heating the solution will increase the K_a, which decreases the pK_a. These factors need to be considered for solution-based cocrystallization strategies.

How does one predict whether a salt or a co-crystal will form (and if they form)? In order for a salt to form, in the case of most organic systems, a proton needs to be transferred. So molecules with no ionisable sites cannot exist as a salt. For molecules where ionisable sites exist, a rule of thumb related to their pK_a exists.[34] Accordingly, one looks at the value of ΔpK_a = pK_a (conjugate acid of base) – pK_a (acid). If ΔpK_a is less than 0 a co-crystal should be synthesized, whereas a value greater than 2-3 should lead to a salt. Values between 0-3 can predict either case and are dependent on the nature of the components in question.

An example of where the pK_a rule has been used is the work by Lemmerer *et al*.[35] In this work a series of co-crystals and molecular salts consisting of 2-chloro-4-nitrobenzoic acid with pyridines with varying pK_a's were synthesized, with the aim being to determine if calculated pK_a's were applicable to predicting the formation of a cocrystal or molecular salt. The ΔpK_a of each crystal system along with other co-crystals and salts containing 2-chloro-4-nitrobenzoic acid and similar compounds reported in the CSD was calculated. The results showed that most of the salts formed when the ΔpK_a was greater than three and most of the cocrystals formed when the ΔpK_a was less than zero. Results between zero and three varied. The conclusion of the study shows that the ΔpK_a rule seems to work rather well.

1.2.5.2. Pharmaceutical Cocrystals

The development of an API from concept to market can take several years and can cost millions of dollars. API's in development undergo several tests and evaluations to prove their safety and effectiveness, with most failing before being able to reach the market. Therefore, it can be more economically feasible to improve currently existing drugs than to develop new drugs from scratch or modify them. Most API's exist in the solid form, either in tablet or capsule form. As such it can exist in different solid-state forms. Amorphous API's have no long-range or

periodic order, and typically have higher dissolution rates and higher bioavailability than their more crystalline form.[36] However, amorphous forms are undesired because most are unstable, and will convert to a crystalline form anyway. Polymorphs offer the potential of having different physicochemical properties, which can be used to select one form with the best properties. The disadvantage of this is that typically the metastable forms are usually the most desirable since they typically have the best properties among all other known forms. This can prove problematic when the metastable form is unable to be obtained consistently ("disappearing polymorphs") or converts to a more stable form. Salt formation remains one of the most popular means of improving API's, with more than half of the API's available on the market in a salt form.[37] The problem with salt formation is that the API must have an ionisable site, which may not be present. Considering all this, without modifying the API, cocrystals can overcome the limitations mentioned above.

Cocrystals are becoming increasingly more important due to the different physical properties that can arise. For example, flufenamic acid is a drug reported to have poor water solubility. A co-crystal of flufenamic acid with 2-chloro-4-nitrobenzoic acid was determined to have a solubility of 5 times that of the pure flufenamic acid.[38] In some cases, multi-component crystals can include two or more API's into one solid form. For example, sulfamethoxazole is often used with trimethoprim to treat bacterial infections.[39] By involving these two API's into one solid form, it offers the advantage of combining drugs with different modes of action into one oral dose. The improvement of the physical properties of the API or the inclusion of several APIs into one form can not only allow pharmaceutical companies to offer a superior product but can also save time and money by avoiding repeating clinical trials.

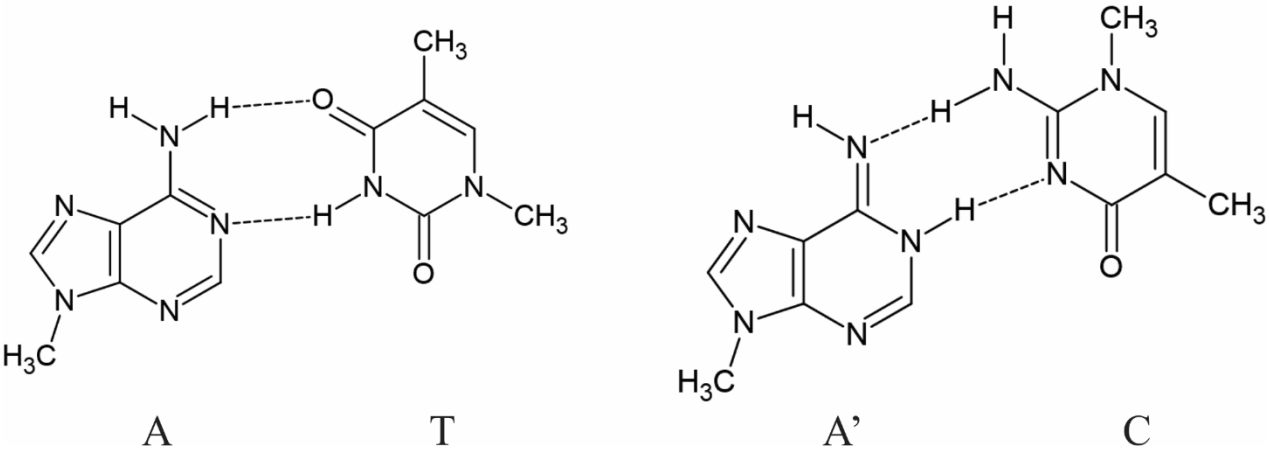
It is not possible to predict whether the formation of a cocrystal is guaranteed.[40] Several approaches to designing cocrystals exist. One of the most common approaches to cocrystal design is to focus on the use of synthons. Synthons are "structural units within supermolecules

which can be formed and/or assembled by known or conceivable synthetic operations involving intermolecular interactions."[41] Many organic compounds with the same functional groups tend to share similar synthons. For example, most primary amides and carboxylic acids tend to form dimers with the $R_2^2(8)$ hydrogen bond motif in the solid state. Synthons made up of identical functional groups are termed as homosynthons, while synthons made up of different functional groups as heterosynthons. One of the best heterosynthons to use for designing cocrystals is that of the pyridine···carboxylic acid pair. An analysis of the CSD showed that this synthon was present in 98% of crystal structures containing said functional groups.[42]

1.2.7 Tautomerism

Tautomerism refers to the ability to convert between two isomers in which only the electrons and/or protons have shifted position. Tautomers are considered to be distinct chemical species, with each form having unique spectra identifying each one. For example ketones can generally undergo tautomerism to form the enol form, although the keto form will be more dominant in general. Different tautomers can be observed in crystal structures, for example, Form **VI** of sulfapyridine exhibits both the sulfonamide and sulfonimide forms in the same crystal structure.[43] Sulfasalazine's two polymorphs each exhibit different tautomers from each other. Sulfamethazine has been observed to form both the sulfonamide and sulfonimide forms in the same cocrystal with theophylline.[44] The tautomer that is favoured may be dependent on the phase the material is in. For example sulfapyridine in the gas phase favours the sulfonamide form,[45] while in the solid state the more stable polymorphic forms (**I**-**V**) all favoured the sulfonimide form.[43,46–48] Tautomerism has gained significant attention over the past years, over the implications of molecular recognition. For example, adenine in its most stable tautomer, pairs with thymine in DNA. However, under irradiation of UV light, adenine undergoes tautomerism. This new tautomer is then mistaken as guanine, which then pairs with cytosine,

resulting in a miscoded pair (**Fig. 1.2.7**).[49] For the solid state not only does protic tautomerism offer possible variable synthons for crystal engineering possibilities, it also offers possible applications for photochromism, thermochromism, photochemical hole-burning and hydrogen-bonded dielectrics.[49] Therefore, it would be of interest to determine the conditions required to obtain the different tautomers, and exploit them for these various applications.



Scheme 1.2.7. The tautomerism of adenine: (A – major tautomer of adenine) hydrogen bonded to thymine (T) on the left versus adenine's minor tautomer (A') hydrogen bonded to cytosine (C) on the right.

1.3 Hirshfeld Surfaces

The Hirshfeld surface is a method used to visualise the space molecules occupy in the crystal structure. It provides information on various intermolecular interactions occurring in the crystal structure, including weak intermolecular interactions such as weak C-H hydrogen bonding, C-H···π interactions, π-π stacking etc. This method was named in honour of F.L. Hirshfeld after his "stockholder partitioning scheme" but the method itself was developed by McKinnon, Spackman, Mitchell *et al*. [50]

The Hirshfeld method is based on partitioning the molecular crystal's electron density into regions where the electron density is a sum of the spherical atoms of the molecule (the promolecule) that dominates over the sum of the molecule. A weighing function $w(\mathbf{r})$ defined as:

$$w(\boldsymbol{r}) = \sum_{a \in molecule} \rho_a(\boldsymbol{r}) \Big/ \sum_{a \in crystal} \rho_a(\boldsymbol{r})$$

$$= \rho_{promolecule}(\boldsymbol{r}) / \rho_{procrystal}(\boldsymbol{r})$$

$$\simeq \rho_{molecule}(\boldsymbol{r}) / \rho_{crystal}(\boldsymbol{r})$$

Where $\rho(\mathbf{r})$ is the spherically averaged Hartree-Fock atomic electron density function. The weighing function is a continuous function in the $0 \leq w(\mathbf{r}) \leq 1$ region. The Hirshfeld surface is defined as where $w(\mathbf{r}) = 0.5$, also called the isosurface. Using this, changes to the molecule will yield changes to the surface. This means that intermolecular interactions such as hydrogen bonding will have an effect on this surface.

Different types of surfaces can be defined from the Hirshfeld surface, which can describe different interactions between the molecule(s) and surfaces. Surfaces are colour-coded in different colour ranges depending on the property of interest. The first set is the distance between a molecule inside the surface to the surface d_i and the distance between the surface to a molecule outside the surface d_e (**Fig. 1.3.1**). These two variables are combined together to form d_{norm}, which is defined as follows:

$$d_{norm} = \frac{d_i - {r_i}^{vdW}}{{r_i}^{vdW}} + \frac{d_e - {r_e}^{vdW}}{{r_e}^{vdW}}$$

Where r^{vdW} represents the van der Waals radius of the respective atom of the internal or external molecule. On a colour-code scheme for d_{norm}, the colours range from red through white to blue. Red spots indicate close contacts while blue spots indicate distant contacts. Observe in **Fig.**

1.3.2 the red spots in both d_i and d_e for **4hba**. The bright red spot in d_i is located at the O-H portion of the carboxylate of **4hba** while the red spot in the d_e represent the C=O portion of the carboxylate. The O-H portion represents the hydrogen bond donor and C=O represents the hydrogen bond acceptor. These spots are red indicating short contacts, which is expected since these groups are involved in hydrogen bonding. The d_{norm} shows both groups to be red since it represents the combination of the d_i and d_e.

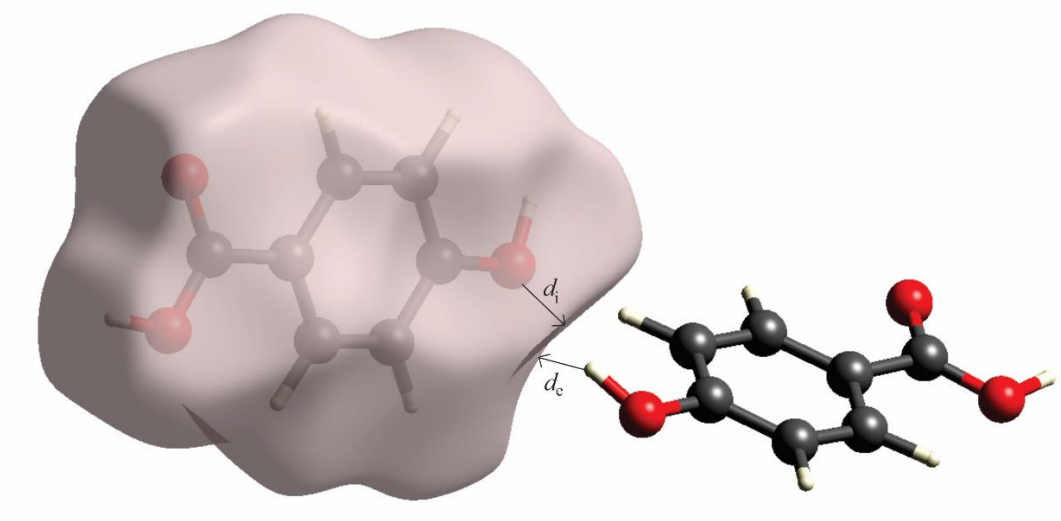


Figure 1.3.1 A plain surface showing the definition of d_i and d_e of 4-hydroxybenzoic acid (Refcode JOZZHI01).

The d_i, d_e and d_{norm} are not the only important surfaces to consider. The shape index and curvedness are two surface that are also important to consider. Before the shape index and curvedness can be defined, two variables called the principal curvature, κ_1 and κ_2 must first be defined. These are defined as follows:

$$\kappa_1 = -\frac{1}{|\boldsymbol{n}|}\frac{\partial^2 w}{\partial u^2}$$

$$\kappa_2 = -\frac{1}{|\boldsymbol{n}|}\frac{\partial^2 w}{\partial v^2}$$

Where **n** is the gradient and *u* and *v* are the respective principal directions. From these two equations, the shape index *S* and curvedness *C* are defined below:

$$S = \frac{2}{\pi} arctan\left(\frac{\kappa_1 + \kappa_2}{\kappa_1 - \kappa_2}\right)$$

$$C = \frac{2}{\pi} \ln \sqrt{\frac{{\kappa_1}^2 + {\kappa_2}^2}{2}}$$

The shape index are colour coded from red through to orange, yellow, green to blue. It is a qualitative measure of the "bump" (blue) and "hollows" (red) in a surface. The curvedness indicates regions where the surface is flat. The curvedness and shape index is useful for identifying weaker interactions. π···π stacking for example, can be identified by looking for flat regions in the curvedness surface, while blue and red triangles pointing at each other in the shape index indicates the presence of π···π stacking.

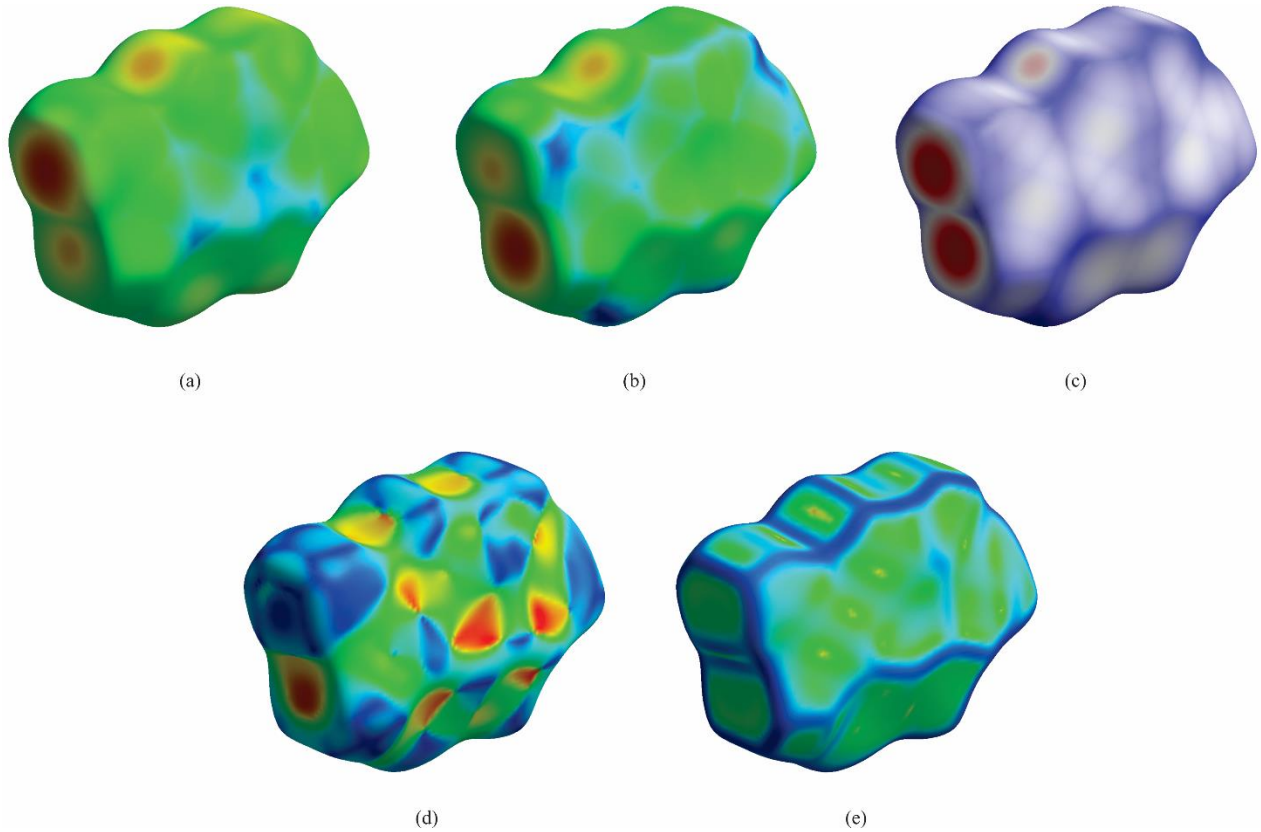


Figure 1.3.2 The Hirshfeld surface of **4hba** (Refcode JOZZHI01) showing (a) d_i, (b) d_e, (c) d_{norm}, (d) the shape index and (e) the curvedness.

Another useful feature of Hirshfeld surfaces are the fingerprint plot. The fingerprint plots are a 2D representation of the different contacts between different atoms to the surface.[50] These are made by plotting the d_i (*x*-axis) against the d_e (*y*-axis), using distance ranges from 0.6 Å to 2.4 Å (**Fig. 1.3.3)**. Visually these plots represent dots, spikes and wings, for example, **Fig. 1.3.3.** represents the fingerprint plot of **4hba**. The spikes with tips at the 1.0 Å mark represent the O···H set of contacts. This is expected since the major intermolecular interaction present in **4hba** was hydrogen bonding, which would be composed of short contacts. Longer contacts that form in the > 2.0 Å regions are composed of C···H contacts, which correspond to the weaker C-H hydrogen bonds.

Overall, Hirshfeld surfaces prove useful in the analysis of crystal structures, especially for polymorphs and multicomponent crystals. Molecules in different polymorphic forms will adopt either different conformations or exhibit different intermolecular interactions. These can be easily examined by comparing either the Hirshfeld surfaces themselves or the fingerprint plots.

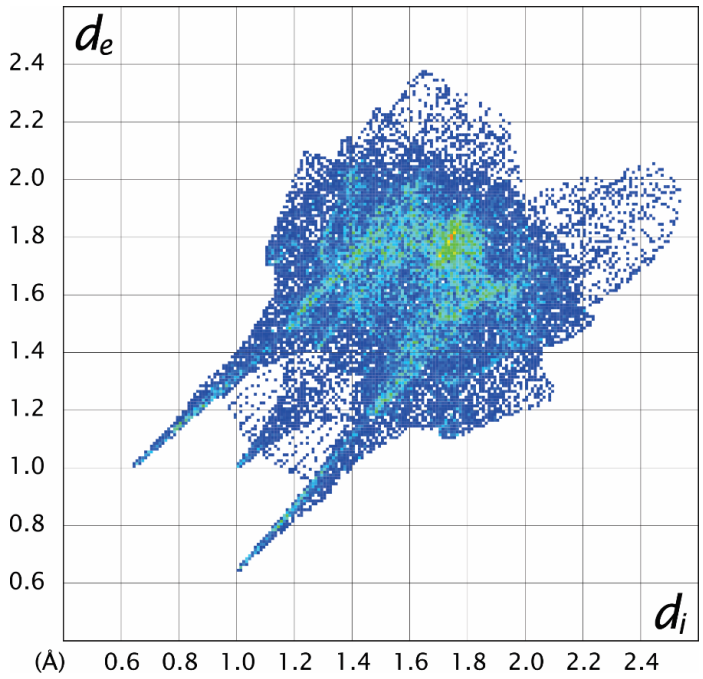


Figure 1.3.3 A fingerprint plot of 4hba (Refcode JOZZHI01).

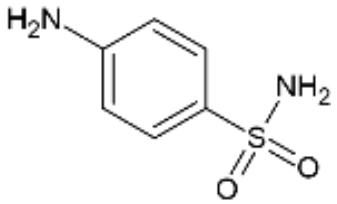
1.4 Sulfa Drugs

"*And thus, we had the powder of life, born from stone, the sulfa drug.*"

Dr. Stone, Riichiro Inagaki, Chapter 40

In the early 1920s and 1930s the number of bacterial infections reported across the world was high, and the number of possible treatments were limited. These infections would prove fatal and a demand for a synthetic treatment was born. Sulfanilamide (**Scheme 1.4**) was first synthesized as early as the 1910s, but its significance was not recognized until much later. In the 1920s, Bayer (a subsidiary of I.G. Farben back then) investigated the use of dyes as a potential source to use as an antibacterial.[51] It was assumed that the inclusion of a sulfonamide group within the dye would yield a molecule with anti-bacterial properties. Under Gerhard Domagk, these compounds were tested *in vivo* of mice. The first successful result of this series of investigations was prontosil, a prodrug which is metabolised *in vivo* to form sulfanilamide and 5-aminosalicylic acid. Prontosil would later go on to save several thousands of lives and earn Domagk the Nobel Prize for medicine in 1939. It was initially believed that prontosil acted as a bactericidal agent (an agent which directly killed the bacteria) as opposed to being a

bacteriostatic agent (an agent which prevented the growth and spread of new bacteria), and the dye portion of the molecule was integral in its anti-bacterial properties. Only much later was it proven that the opposite was true. The demand for sulfa drugs declined after penicillin entered the market as a superior anti-bacterial drug. Nevertheless sulfa drugs are still being used for both human and veterinarian purposes.



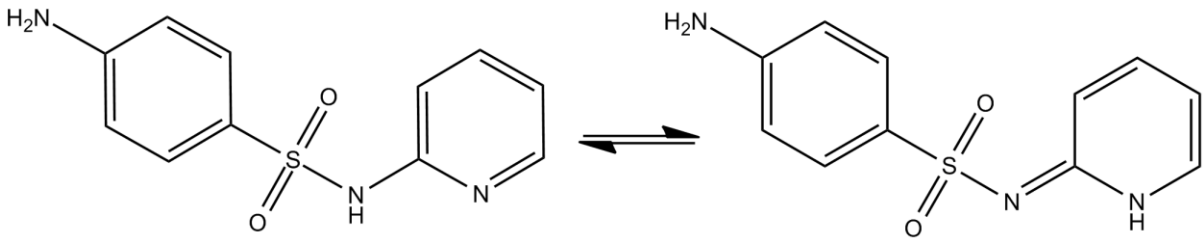
Scheme 1.4. The basic structure of sulfonanilamide.

As the name implies, sulfonamides consist of a sulfonyl group bonded directly to an amine group. For the purpose of this work, only derivatives based closely on sulfonanilamide will be considered. In particular, for this work, the sulfa drugs sulfapyridine (**sp**), sulfamethazine (**sz**), sulfamethoxazole (**sm**) and sulfathiazole (**st**) were investigated.

The mechanism of action of sulfanilamides involves the inhibition of folic acid synthesis, which is a necessary component for the growth of new bacteria. Sulfanilamides are structural analogues of 4-aminobenzoic acid (PABA), an important precursor necessary for folic acid synthesis. Sulfanilamides compete for the dihydropteroate synthetase enzyme with PABA,[52] which outcompetes PABA and thus prevents the conversion of PABA to folic acid.

1.4.1 Sulfapyridine

sp (**Scheme 1.4.1**) was first reported as an improved treatment for pneumococcal infections over prontosil in 1938 by Lionel Whitby.[53] It would later be used in the Second World War to save many lives, including Winston Churchill who fell ill with pneumonia.[54] **sp** consists of the sulfanilamide molecule with one hydrogen from the sulfonamide group replaced with a pyridine group at the 2' position of the pyridine. **sp** is polymorphic, consisting of at least six reported forms,[43,46,48,55,56] although identifying the forms between works has been inconsistent.[48] In all forms sulfapyridine exists in the imidine form, with the exception being form **VI** where both tautomers exist in the same structure.[43] According to Adsmond and Grant, sulfapyridine existing in the sulfonimide form as opposed to the sulfonamide form in the solid state is an exception to the norm.[57]



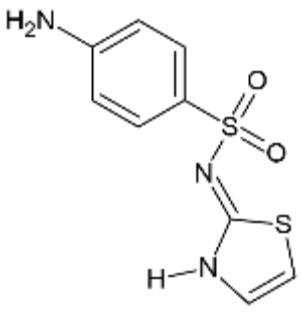
Scheme 1.4.1 Basic structure of sulfapyridine showing its tautomerism.

Multicomponent crystals containing **sp** are rare. A few crystal structures of **sp** solvates containing **sp** exists.[47,58,59] Prior to this work the only cocrystals and molecular salts reported were done by Shunje.[60] Shunje reported that **sp** formed cocrystals with 3-nitrobenzoic acid, **dmap** and 5-bromosalicylic acid and molecular salts with **4nba**, 3,5-dinitrosalicylic acid and 3,5-dibromosalicylic acid. **sp** showed diversity in the major hydrogen bonds observed.

1.4.2. Sulfathiazole

st is a sulfanilamide derivative with a 1,3-thiazole ring attached to the sulfonamide group at the 2' position. It first entered the market in 1940, being developed by several different companies at the time.[61] Sulfathiazole is polymorphic, with five forms reported so far. Accordingly, the thermal stability of these polymorphs is in the order of **III** ≈ **IV** > **II** > **I**, with **I** being the metastable form.[62] Form **I** also forms a unique dimer different to the other polymorphic forms of sulfathiazole. This is a $R_2^2(8)$ ring hydrogen bond motif, called the α-dimer. While the other forms share a common second level dimer, referred to as the β-dimer. Form **I** shows no other phase transitions on heating before melting at 201 °C. Forms II-V convert to Form **I** on heating, before melting at 201 °C. In all cases sulfathiazole exists in the sulfonimide form.

One point to note about sulfathiazole is its ability to form solvates. It has been claimed that over one hundred solvates have been reported in the literature,[63] but only a fraction of crystal structures of the solvates have been reported.[62,64,65] Some notable cocrystals featuring **st** include forming cocrystals with: theophylline,[66] sulfanilamide,[66] **4nba**,[67] 4-aminobenzamide,[68] and glutaric acid.[69] In all entries of the CSD containing the neutral form of **st**, the sulfonimide tautomer of **st** was reported with no entries reporting the sulfonamide form. This suggests that the sulfonimide form is the most dominant form in the solid state, although no extensive study on the tautomerism of **st** (either in the solid state or solution) has been done.

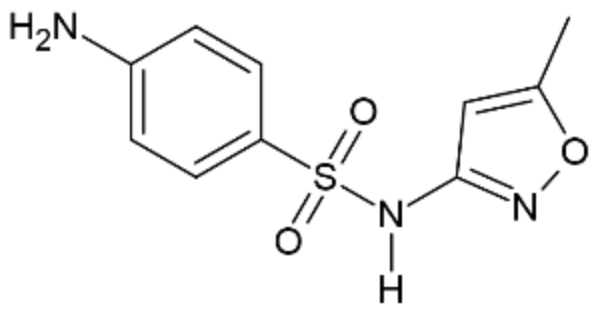


Scheme 1.4.2 The structure of **st** showing the sulfonimide tautomer.

1.4.3. Sulfamethoxazole

sm (**Scheme 1.4.3**) is a sulfanilamide derivative with a 5-methyl-1,2-oxazole present at the 3' position. **sm** is still used today, packaged together with trimethoprim to form co-trimoxazole, and sold under the brand names Bactrim® or Spetrin®. According to the Biopharmaceutics Classification System (BCS), sulfamethoxazole is classified as a class IV drug, which means that it has both low solubility and low permeability. Sulfamethoxazole, like most of the other sulfa drugs, is polymorphic consisting of at least five reported forms.[70–73] The first two forms are both monoclinic crystal system *C*2/*c* first reported in the 1980s.[71,73] The third and fourth forms were obtained using polymer heteronuclei seeding and crystallized in the monoclinic crystal system with space groups $P2_1/c$ and $P2_1/n$, respectively. A fifth polymorph was reported in the 1980s, but crystallographic information regarding it is scarce.[70]

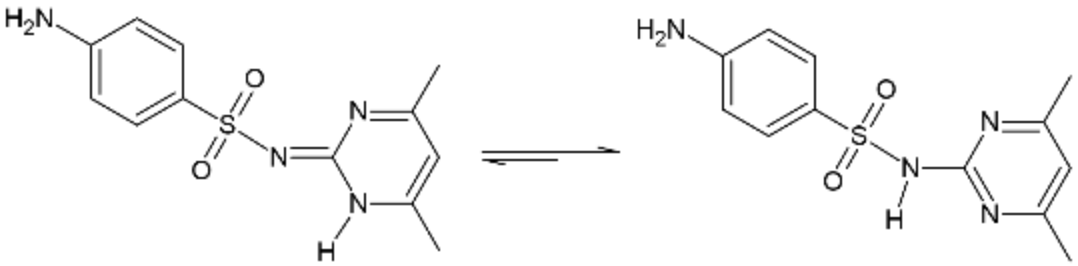
The most notable multi-component crystal with sulfamethoxazole is the molecular salt consisting of sulfamethoxazole and trimethoprim. First reported as a cocrystal by Giuseppetti and Tandini in 1980,[74] it was later rectified as a molecular salt by Nakai *et al.*[75] by use of IR analysis in 1984. This salt consists of an ionic hydrogen bond ring between the pyrimidine ring of trimethoprim and the oxazole/sulfamide group of sulfamthoxazole. Otherwise very few crystal structures of multi-component crystals consisting of sulfamethoxazole have been reported, with other notable examples including coformers with pyridine rings.[76]



Scheme 1.4.3 Structure of **sm**.

1.4.4. Sulfamethazine

sz (**Scheme 1.4.4.**), also referred to as sulfadimidine, consists of the sulfanilamide with a 4,6-dimethylpyrimidine ring attached. Sulfamethazine was first synthesized in 1941 and used during the 1950s until it was discovered to be carcinogenic.[77,78] However, it is still used for veterinarian purposes.[78] Unlike most of the other sulfa drugs presented here, only one crystal form of **sz** has been reported, although it can exist in multiple crystal habits.[79] **sz** has been featured in several crystal engineering studies exhibiting often rare structural features not often observed in other crystal systems. For example, a study done by Perumalla *et al.* on a system consisting of sulfamethazine and saccharine showed a case of salt-cocrystal polymorphism: a case where one polymorphic form is a cocrystal while the other is a molecular salt.[80] Another unusual case is a 2:1 cocrystal containing **sz** and **thp** in which both tautomers were present.[44] Overall, it seems **sz** readily forms cocrystals with carboxylic acids.[77,81–84] In most of these cases **sz** adopts the sulfonamide tautomer with the only notable exception being the case of the cocrystal with **4hba**, where it adopts the sulfonimide form.[82]



Scheme 1.4.4. Structure of **sz** showing the sulfonamide tautomer (right) and sulfonimide tautomer (left).

1.5 Isoniazid

1.5.1 Introduction to isoniazid

Isoniazid (**inh**), an anti-bacterial prodrug that was initially combined with *p*-aminosalicylic acid (PABA) and streptomycin as a treatment for tuberculosis (TB) in the 1940s.[85] **inh** was

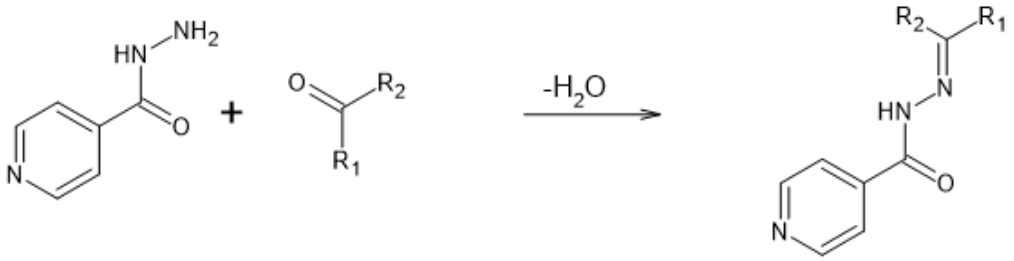
later combined with rifampicin, pyrazinamide and ethambutol in a fixed dose concentration tablet that proved to be a more effective treatment towards the late 20th century.[85,86] **inh** is a simple molecule, consisting of a pyridine and a hydrazine group. The mechanism of action involves the conversion of **inh** to the active form isonicotinic acyl radical by the catalase-peroxidase enzyme KatG present in *Mycobacterium tuberculosis* bacterium.[87] This isonicotinic acyl radical couples with NADH which forms a nicotinoyl-NAD adduct. This complex binds enoyl-acyl carrier protein reductase InhA, which blocks the natural enoyl-AcpM substrate and the action of fatty acid synthase. This ultimately prevents the synthesis of mycolic acid which is a key component of the cell walls of *Mycobacterium tuberculosis*. **Inh** has attracted much attention from the crystal engineering community for its simple structure and its effective ability to form cocrystals and molecular salts readily.

For a long extent of its history **inh** was considered to be monomorphic,[88–91] with new polymorphic forms only discovered recently.[23] Three forms have been reported so far, with single crystal structure data available for two of them. Form **I** (Z' = 1) consists of a series of infinitely hydrogen bond chain motifs, formed by the interactions of hydrazide groups. Form **II** (Z' = 4) consists of dimers formed between the hydrogen bonded interactions between the oxygen of the amide with one of the hydrogens from the hydrazide group. From this, it can be observed that the hydrazine group dominates most of the hydrogen bond interactions.

1.5.2 Blocking the hydrazine group

From a crystal engineering perspective, it may prove to be difficult to work with several hydrogen bond donors/acceptors. Sometimes it may be necessary to remove some of these hydrogen bond donors/acceptors in order to simplify the major hydrogen bonding schemes or the dimensionality of the structure. Previous work by Lemmerer experimented with using

"covalent-assisted supramolecular chemistry" which involved using a ketone and reacting it with isoniazid in a Schiff-base reaction. [90,92–94] Here the hydrazine is replaced with an imine, effectively removing two hydrogen bond donors (Scheme 1.5.3).



Scheme. 1.5.3. General scheme of the Schiff-base condensation reaction of isoniazid with a ketone or aldehyde (R_1 = H).

1.5.3 Polymorphism of isoniazid and its derivatives/cocrystals

Some derivatives of **inh** were also found to be polymorphic, a few of which are described below. One of the most remarkable polymorphic systems of an **inh** derivative is that of **inh** reacted with acetophenone, to form (*E*)-(1-phenylethylidene)hydrazide (**IPH**), reported by Hean *et al*.[95] Hean and co-workers reported six polymorphic forms for this compound, all of which were obtained using standard methods and materials. These forms were ordered in terms of increasing melting points. All forms, with the exception of form **II**, form catamers between the amide groups of neighbouring **IPH** molecules, while form **II** and the one pair of molecules in the asymmetric unit of form **I** form a ring hydrogen bond motif. It should be noted that the pyridine ring only forms a strong hydrogen bond in form **I**. Cocrystals of **inh** can also exhibit polymorphism, with coformers such as **ca** (and its derivatives),[96–98] PABA,[86] **4hba** hydrate,[99] and various simple dicarboxylic acids such as **sa**, fumaric acid and adipic acid.[100]

1.6 Aims and Objectives

As noted from Chapter 1.4 many of the sulfa drugs discussed exhibit interesting properties such as tautomerism and polymorphism. With the exception of **sz**, each sulfa drug discussed has at

least five polymorphs. Usually polymorphic compounds make good coformers due to the greater structural flexibility.[101] Structures of **sz**, **st** and **sp** show the possibility of solid-state tautomerism. Tautomerism in the solid state is still poorly understood, and its understanding depends on finding cases where it exists. Therefore it becomes critical to find these cases. For the sulfa drugs, the number of reported cocrystals and molecular salts is relatively small. The design and synthesis of new crystal forms often requires knowledge of the types of intermolecular interactions that occur. The lack of this knowledge can hamper the design of new solids. Therefore it becomes crucial to explore unknown structural landscapes of these sulfa drugs.

3,5-dinitrobenzoic acid (**dnba**) is a popular co-former used in crystal engineering studies. At the start of this work, at least 362 entries containg **dnba** (or its benzoate form) were reported. Despite this, very few studies centred on **dnba** exists. To my knowledge, there are no other significant applications for this compound, other than being an excellent co-crystalizing agent. Due to the ring of **dnba** being π-electron poor due to the strong electron withdrawing groups, it makes a potential charge transfer acceptor molecule. Therefore, it would be of interest to explore the multi-component structural landscape of **dnba** by using a diverse range of coformers.

To summarize, the main objectives of this work are to explore and expand the crystal structural landscape of the previously described sulfa drugs, isoniazid derivatives and **dnba**. In particular:

- Design and synthesize new cocrystals and molecular salts of the sulfa drugs **sz**, **st**, **sm** and **sp**.
- Design and synthesize new cocrystals and molecular salts of **dnba**, and explore the weaker intermolecular interactions using Hirshfeld surfaces.

- Synthesize and characterize the polymorphs of the diacetone alcohol derivative of isoniazid (**iz4h4m2p**), as well as its cocrystals.

Chapter 2 Experimental Procedures and Aims and Objectives

2.1 Cocrystal/molecular salt synthetic methods

Various methods, both solvent-based and mechanochemical-based, have been used to synthesize the multi-component crystals presented in this work. 4,4'-bipyridine was purchased from Alfa-Aeser. All other materials were purchased from Sigma-Aldrich. All solvents were of analytical grade. **Table 2.1** lists all the coformers used as part of the cocrystallization attempts in this work.

Table 2.1 List of coformers used in this work.

Compound name		
3-cyanopyridine	4-hydroxypyridine	2-hydroxybenzoic acid (Salicylic acid)
4-cyanopyridine	2-amino-3-nitropyridine	3-hydroxybenoic acid
4-dimethylaminopyridine	2-amino-5-nitropyridine	4-hydroxybenzoic acid
2-aminopyridine	4,4'-bipyridine	3,4-dichlorobenzoic acid
3-aminopyridine	2-amino-5-chloropyridine	toluic Acid
4-aminopyridine	3,5-dinitrobenzoic acid	saccharine
2-hydroxypyridine	4-nitrobenzoic acid	succinic acid
3-hydroxypyridine	2-chloro-4-nitrobenzoic acid	
cinnamic Acid (*trans*)	2-chloro-5-nitrobenzoic acid	

Solution Based Methods

Varying stoichiometric amounts of co-former:API (or **dnba** for chapter 5) were completely dissolved in an appropriate solvent system. In most cases some heating was used to achieve complete dissolution. This solution was then left partially open to allow solvent evaporation for several days, with the aim of leaving crystals suitable for X-ray diffraction behind.

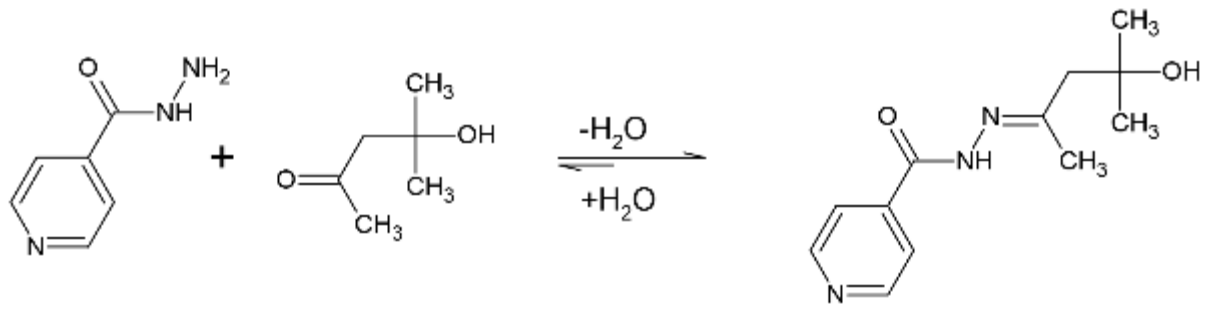
Mechanochemical Methods

Stoichiometric amounts of the co-formers were placed in a Teflon-coated milling jar (18 mm diameter, 65 mm length) with two steel balls (5 mm diameter). In some cases a few drops of an appropriate solvent was added to the mixture. The jars were then placed on a Retsch MM200 vibratory mill and were milled at 20 Hz for some time (typically between 20-60 minutes).

To obtain single crystals suitable for single crystal X-ray diffraction (SC-XRD) from these powders, the same solution based methods described previously were used, where some of the powder obtained from milling was used as seed crystals.

2.2 Synthesis of iz4h4m2p

A general method of obtaining **iz4h4m2p** is given as follows: 0.250 g of isoniazid (1.82 mmol) was dissolved in 10 mL of ethanol (absolute). A few drops (0.5 mL) of 4h4m2p was added to this mixture. This solution was refluxed for 18 h, after which it was transferred to a vial, which was kept loosely open. Crystals were grown from this mixture after several days.



Scheme 2.2 Reaction scheme for the synthesis of **iz4h4m2p**.

2.3 Single Crystal X-Ray Diffraction

The Bruker D8 VENTURE PHOTON CMOS area detector diffractometer, equipped with a graphite monochromated Mo-Kα_1 sealed tube (50 kV, 30 mA), was used to collect all the intensity data. The program *SAINT+*, vers. 6.02[102] was used to integrate the data and the program *SADABS*[23] was used to make empirical absorption corrections. Space group assignments were made using *XPREP*[102] on all compounds. In all cases, the structures were

solved in the *WinGX* Suite of programs[103] by direct methods using *SHELXS-97*[104] and refined using full-matrix least-squares/difference Fourier techniques on F^2 using *SHELXL-97*.[105] All non-hydrogen atoms were refined anisotropically. Thereafter, all hydrogen atoms attached to N or O atoms, except where otherwise stated, were located in the difference Fourier map and their coordinates and isotropic thermal displacement parameters were refined freely. Diagrams and publication material were generated using *ORTEP-3*[106] and *MERCURY*.[107]

2.4 Powder X-Ray Diffraction

Powder X-ray diffraction is done to determine the phase purity of the bulk material. PXRD data for all compounds were measured at 293 K on a Bruker D2 Phaser diffractometer which employs a sealed-tube Co X-ray source (λ = 1.78896 Å), operating at 30 kV and 10 mA, and LynxEye PSD detector in Bragg-Brentano geometry. Powder patterns for each sample are presented in the supporting information, where the experimentally obtained data were compared with the calculated patterns obtained from the SC-XRD data.

2.5 Infrared Spectroscopy

FTIR spectra were collected using Bruker Tensor 27 and a Bruker Alpha II model equipped with the Eco-ATR sampling module. Background noise was subtracted and a small amount of the sample of interest was placed onto the ATR crystal. Spectra were measured from 600 to 4000 cm^{-1} range, resolution 4 cm^{-1} with 24 scans per sample. The FTIR spectrophotometers were in a room with conditioning at 22 °C. After spectral acquisition the ATR crystal was cleaned using isopropanol.

2.6 Differential Scanning Calorimetry

Differential scanning calorimetry data were collected using a Mettler Toledo 822^e and a Mettler Toledo DSC 3 with aluminium pans under nitrogen gas (flow rate = 10 mL/min). Exothermic events were shown as peaks. Samples were heated and cooled to determine melting points as

well as any additional phase transitions. The temperature and energy calibrations were performed using pure indium (purity 99.99%, m.p. 156.6 °C, heat of fusion: 28.45 J g^{-1}) and pure zinc (purity 99.99%, m.p. 479.5 °C, heat of fusion: 107.5 J g^{-1}). Samples were heated and cooled to different temperatures at different rates.

2.7 Hirshfeld Surface Analysis

The Hirshfeld surfaces and fingerprint plots presented were generated using the program *Crystal Explorer* (vers. 17.5).[108] All surfaces were generated using a High (standard) resolution.

2.8 Hot Stage Microscopy

Hot stage microscopy was done on an Olympus SZ61 equipped with a Kofler hot bench. Images were captured using an Olympus EP50 camera. Various heating and cooling techniques were applied to capture the phase transitions.

2.9 Thermogravimetric Analysis

Thermogravimetric analysis (TGA) was done using a PerkinElmer TGA 6000 thermogravimetric analyzer using high-purity nitrogen at a heating rate of 10 °C/min and gas flow rate of 10 mL/min.

Chapter 3 Synthesis and Characterization of a series of Sulfamethazine multi-component crystals with Various Benzoic Acids.

3.1 introduction

Nine cocrystals containing **sz** and a carboxylic acid were synthesized and characterized. These cocrystals were synthesized using both solution and mechanochemical methods. It should be noted that for **sz** both carboxylic acids and pyridines were used for cocrystallization attempts in the same way as for **sp**, **st** and **sm**. No new crystal structures containing **sz** and a pyridine derivative was successfully synthesized, which resulted in the theme of the paper being centred on the success of the multi-component crystals containing **sz** with benzoic acid and its derivatives.

Authors: Scheepers, M.C., Lemmerer A.
Journal: *Crystal Growth & Design*
Date Published: 3 December 2019
Volume Number: 20
Pages: 813-823
Number of citations as of 10 November 2022: 7

CRYSTAL GROWTH & DESIGN

Article

Cite This: Cryst. Growth Des. 2020, 20, 813−823

pubs.acs.org/crystal

Synthesis and Characterization of a Series of Sulfamethazine Multicomponent Crystals with Various Benzoic Acids

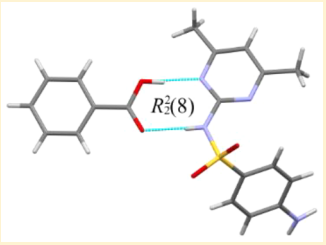
Published as part of a Crystal Growth and Design virtual special issue Remembering the Contributions and Life of Prof. Joel Bernstein

Matthew C. Scheepers and Andreas Lemmerer*

Molecular Sciences Institute, School of Chemistry, University of the Witwatersrand, 2050, Johannesburg, South Africa

Supporting Information

ABSTRACT: Nine multicomponent crystals consisting of sulfamethazine (**sz**) with benzoic acid and its derivatives were synthesized and characterized. Eight of the nine multicomponent crystals are cocrystals, while one is a molecular salt. The coformers used to form multicomponent crystals with **sz** include 2-chloro-4-nitrobenzoic acid (**2c4n**), 2-chloro-5-nitrobenzoic acid (**2c5n**), salicylic acid (**2hba**), 3-hydroxybenzoic acid (**3hba**), 4-hydroxybenzoic acid (**4hba**), 4-bromobenzoic acid (**4Brba**), benzoic acid (**ba**), cinnamic acid (**ca**), and toluic acid (**ta**). These multicomponent crystals were characterized by single-crystal X-ray diffraction (SC-XRD), powder X-ray diffraction (PXRD), and differential scanning calorimetry (DSC). SC-XRD showed that eight of the coformers that interacted with **sz** formed the amidine-carboxyl synthon; the only exception to this was **sz** + **4hba**, which formed the imidine-carboxyl synthon formed instead. PXRD confirmed that the single crystals were representative of the bulk material. DSC showed most of the multicomponent crystals to have only a melting phase transition, which differed from the melting points of the coformers. The only exceptions were **sz** + **4brba** and **sz** + **ca**, where an additional endothermic peak was observed, which corresponds to an amorphous phase transition before melting.



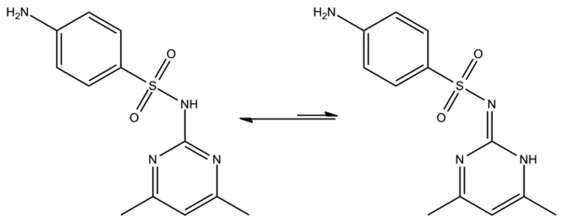
INTRODUCTION

The need for designing new crystal forms of potentially useful active pharmaceutical ingredients (APIs) has been rising in the past few decades. Promising drug candidates often have poor physiochemical properties, especially poor water solubility and dissolution rates.[1,2] One common approach to altering the poor physiochemical properties of an API is to incorporate them into multicomponent crystals.[3] Multicomponent crystals often have different properties, if not superior properties, with respect to its coformers.[4] Therefore, there is a great interest in exploring new multicomponent crystals of various APIs.

Sulfamethazine (**sz**), also referred to as sulfadimidine, is an antibacterial drug used to treat urinary tract infection, chlamydia, malaria, rheumatoid fever, and toxoplasmosis in humans as well as for veterinary purposes.[5] **Sz** is also known to be tautomeric,[5,6] consisting of an amidine form and an imidine form (Scheme 1). Both forms have been reported to appear in the solid state.[5−7] However, the amidine form tends to be the more dominant form, appearing more frequently than the imidine form. In its pure form, **sz** is able to crystallize into several different crystal habits, but has only one crystal structure.[8] In addition to the amidine/imidine group, an amino group is present to act as an additional hydrogen bond donor, and the sulfoxide and second nitrogen of the pyrimidine ring can act as an additional hydrogen bond acceptor. This allows a wide variety of possible hydrogen bond interactions to occur.

Several different cocrystals and solvates of sulfamethazine have already been reported in the literature. The major synthon

Scheme 1. Sulfamethazine Showing the Amidine Form (Left) and Imidine Form (Right)



that forms between **sz** and the corresponding coformers involves the amidine/imidine functional group. Several multicomponent crystals of **sz** containing a coformer with a carboxylic acid usually interact with the amidine/imidine group as seen in synthon (i) and (ii) (Scheme 2). In such a case, this should leave the amino and sulfoxide groups free to interact with each other (Synthon (iii), Scheme 2).

In this work,we present the synthesis of nine multicomponent crystals of sulfamethazine, with eight cocrystals and one molecular salt. Six of these multicomponent crystals are novel, while three have been previously reported but produced under slightly different conditions. The benzoic acids chosen for this work were either structural isomers of each other (**2hba**, **3hba**, **4hba**, etc.) or did not contain any additional hydrogen bonding groups

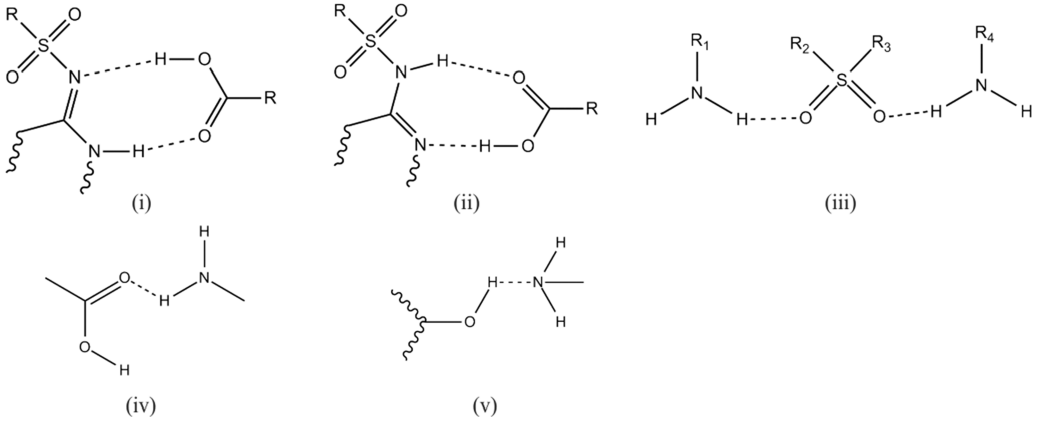
Received: September 12, 2019
Revised: December 3, 2019
Published: December 18, 2019

Downloaded via UNIV OF THE WITWATERSRAND on June 13, 2022 at 09:14:07 (UTC).
See https://pubs.acs.org/sharingguidelines for options on how to legitimately share published articles.

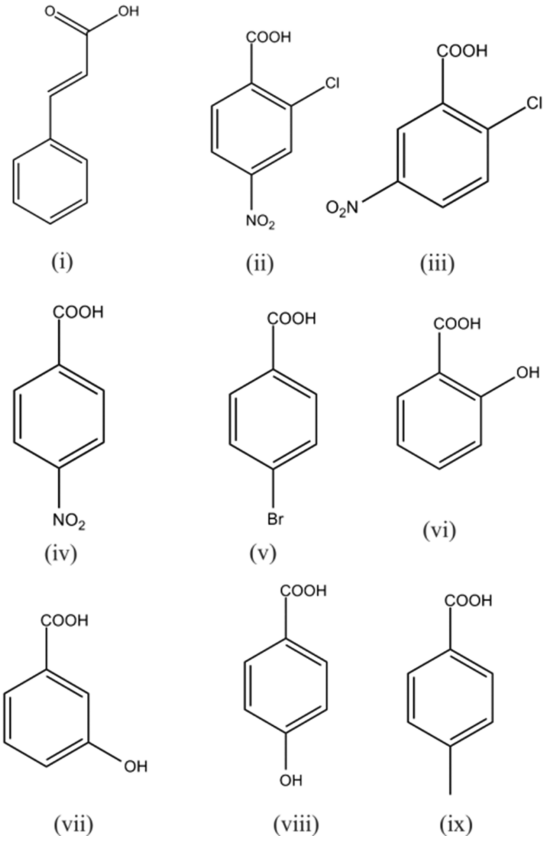
© 2019 American Chemical Society

DOI: 10.1021/acs.cgd.9b01209
Cryst. Growth Des. 2020, 20, 813−823

Scheme 2. Some of the Synthons Expected for This Work: (i) Amidine-Carboxyl Synthon, (ii) Imidine-Carboxyl Synthon, (iii) Sulfoxide-Amino Chains, (iv) Amino-Carboxyl Synthon, (v) Hydroxyl-Amino Synthon



Scheme 3. Coformers Used for This Work: (i) Cinnamic Acid (ca), (ii) 2-Chloro-4-nitrobenzoic Acid (2c4n), (iii) 2-Chloro-5-nitrobenzoic acid (2c5n), (iv) 4-Nitrobenzoic Acid (4nba), (v) 4-Bromobenzoic Acid (4brba), (vi) 2-Hydroxybenzoic Acid/Salicylic Acid (2hba), (vii) 3-Hydroxybenzoic Acid (3hba), (viii) 4-Hydroxybenzoic Acid (4hba), (ix) Toluic Acid (ta)



(e.g., **ca**, **ba**, **ta**). These multicomponent crystals were characterized by single crystal X-ray diffraction (SC-XRD), powder X-ray diffraction (PXRD), and differential scanning calorimetry (DSC).

EXPERIMENTAL SECTION

Crystal Preparation. All reagents used were purchased from Sigma-Aldrich and were used without further purification.

Table 1. Grouping of the Multicomponent Crystals As Well As the Motivation for Such Groupings

group	motivation for grouping together
sz + 4Brba	**sz +4Brba** is in its own group since it does not fit in with the other three group list below.
sz + ca, **sz + ba**, **sz + ta**	The coformers consist of a carboxylic acid group which acts as the sole source for hydrogen bonding.
sz +2hba, **sz +3hba**, **sz +4hba**	The coformers are structural isomers of each other.
sz +2c4n, **sz +2c5n**	The coformers are structural isomers of each other; in particular, it is the shift of the nitro group from the 4′ position to the 5′ position.

Most of the cocrystals presented here have been prepared almost exclusively by solvent evaporation methods. Equimolar amounts of **sz** and the respective coformer were dissolved together in a 1:1 v/v ratio of ethanol/acetonitrile, which was allowed to stir for an additional 10 min with some heating. Afterward, samples were left slightly open at room temperature to allow solvent evaporation. Crystals were grown from this solution after several days.

For the case of **sz + 2c5n** and **sz + ca**, ball milling followed by solvent evaporation methods was deployed. Equimolar amounts of **sz** and the respective coformer were placed in Teflon-coated milling jar (18 mm diameter, 65 mm length) with two steel balls (5 mm diameter). A few drops of acetonitrile were added to this mixture. The jars were then placed on a Retsch MM200 vibratory mill and were milled at 20 Hz for 20 min. Afterward, the solvent evaporation methods described previously were used, with some of the powder from the ball milling used as seeds.

Powder X-ray Diffraction (PXRD). Powder X-ray diffraction is done to determine the phase purity of the bulk material. PXRD data for all compounds were measured at 293 K on a Bruker D2 Phaser diffractometer, which employs a sealed tube Co X-ray source (λ = 1.78896 Å), operating at 30 kV and 10 mA, and LynxEye PSD detector in Bragg–Brentano geometry. Powder patterns for each sample are presented in the Supporting Information, where the experimentally obtained data are compared to the calculated patterns obtained from the SC-XRD data.

Single Crystal X-ray Diffraction (SC-XRD). The Bruker D8 VENTURE PHOTON CMOS area detector diffractometer, equipped with a graphite monochromated Mo Kα_1 sealed tube (50 kV, 30 mA), was used to collect all the intensity data. The program *SAINT+*, vers. 6.02[9] was used to integrate the data, and the program *SADABS*[10] was used to make empirical absorption corrections. Space group assignments were made using *XPREP*[10] on all compounds. In all cases, the structures were solved in the *WinGX* Suite of programs[11] by direct methods using *SHELXS-97*[10] and refined using full-matrix least-squares/difference Fourier techniques on F^2 using *SHELXL-97*.[10] All non-hydrogen atoms

DOI: 10.1021/acs.cgd.9b01209
Cryst. Growth Des. 2020, 20, 813–823

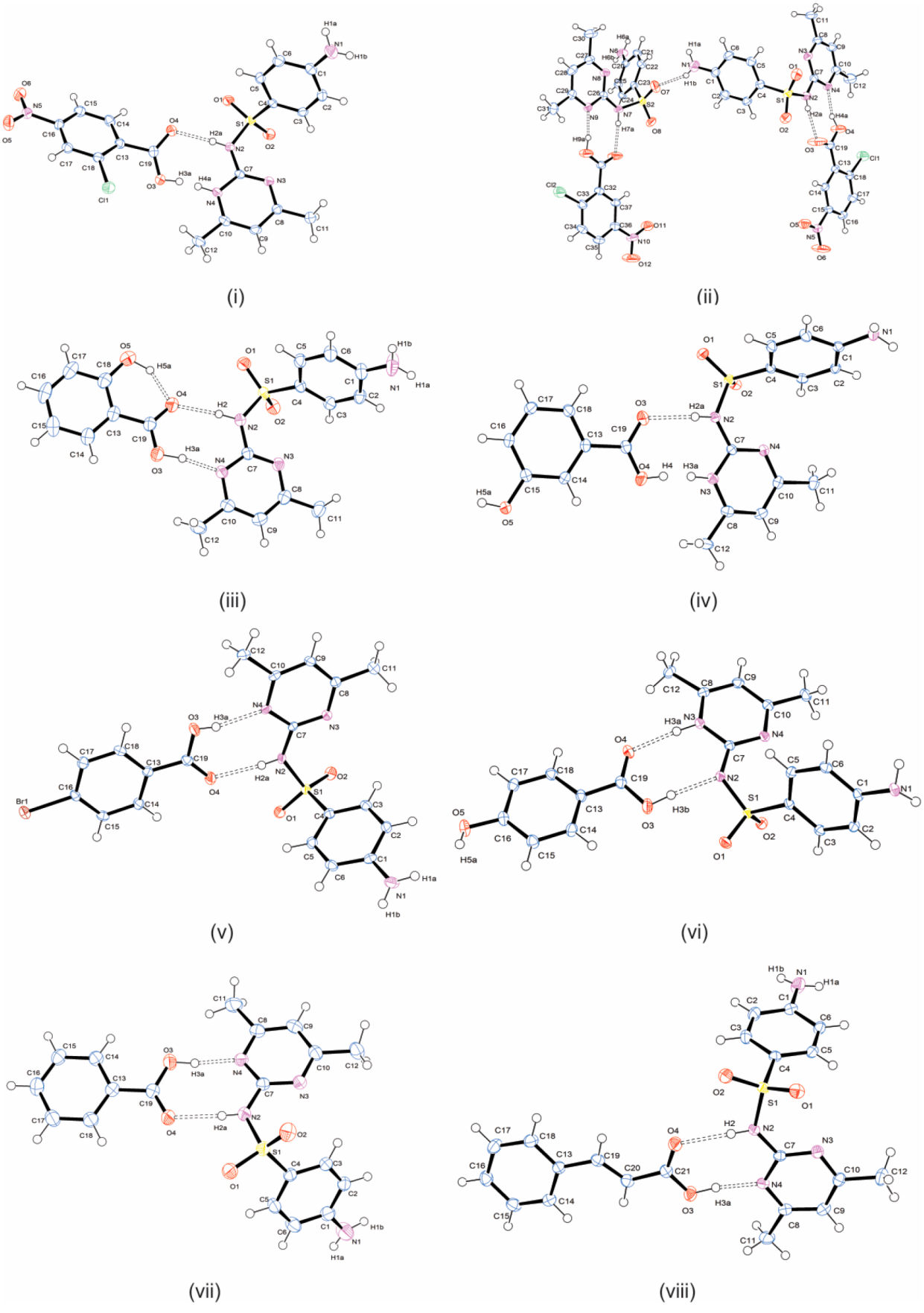


Figure 1. Ortep diagram for (i) **sz + 2c4n**, (ii) **sz + 2c5n**, (iii) **sz + 2hba**, (iv) **sz + 3hba**, (v) **sz + 4brba**, (vi) **sz + 4hba**, (vii) **sz + ba**, and (viii) **sz + ca**.

DOI: 10.1021/acs.cgd.9b01209
Cryst. Growth Des. 2020, 20, 813−823

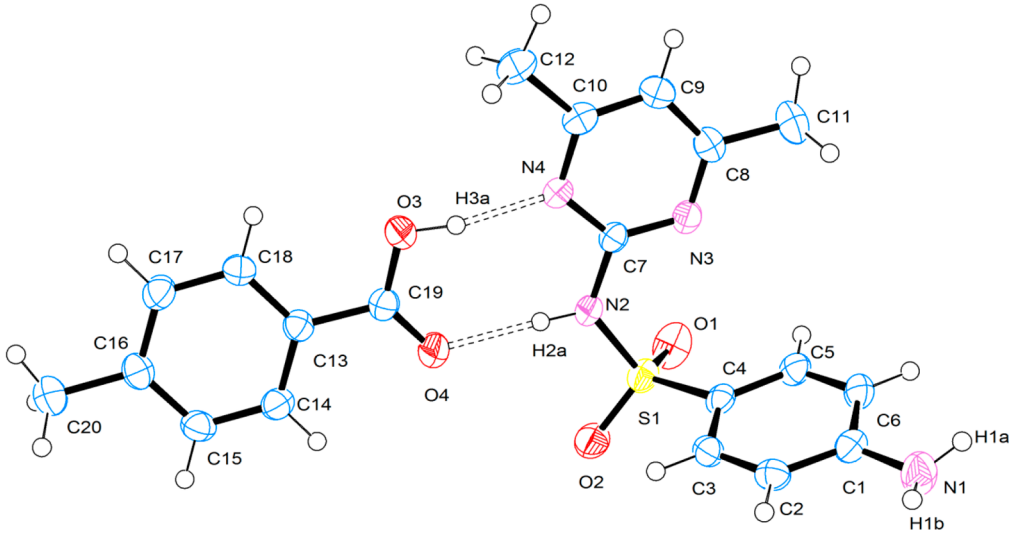


Figure 2. Ortep diagram for **sz** + **ta**.

were refined anisotropically. Thereafter, all hydrogen atoms attached to N or O atoms, except where otherwise stated, were located in the difference Fourier map, and their coordinates and isotropic thermal displacement parameters were refined freely. All C−H hydrogen atoms were placed at idealized positions and refined as riding atoms with isotropic parameters 1.2 or 1.5 times those of the "heavy" atoms to which they are attached. Diagrams and publication material were generated using *ORTEP-3*[11] and *Mercury*.[12]

Differential Scanning Calorimetry (DSC). Differential scanning calorimetry data were collected using a Mettler Toledo 822^e with aluminum pans under nitrogen gas (flow rate = 10 L/min). Exothermic events were shown as peaks. Cocrystals were heated and cooled to determine melting points as well as any additional phase transitions. The temperature and energy calibrations were performed using pure indium (purity 99.99%, mp 156.6 °C, heat of fusion: 28.45 J g^{-1}).

Infrared Spectroscopy. Infrared spectra were collected on a Bruker Tensor 27. Samples were used as is without further processing. Spectra were collected in the range of 4000−600 cm^{-1}, and band intensities were expressed as transmittance %.

RESULTS AND DISCUSSION

Nine multicomponent crystal forms containing sulfamethazine are reported. Six of these crystal forms are new. These crystal forms were characterized by SC-XRD. PXRD was used to confirm that the bulk material matched the calculated pattern in order to ensure purity. DSC was used to determine the melting points as well as any other potential phase transitions.

SC-XRD Results. **Sz** formed nine multicomponent crystals which were characterized by SC-XRD. For most of these crystal systems, the intermolecular interactions are similar and possess some structural and packing similarities. For the purpose of this work, several multicomponent crystals are grouped and discussed together below. Table 1 gives a list of which multicomponent crystals are grouped together and reasons for such grouping. In addition, Table 4 contains a list of the bond lengths of the carboxyl group obtained from each of the multicomponent crystals as well as if a salt or cocrystal was formed. The ratios of the C−O bond lengths indicate that most of the crystals systems are cocrystals, with the exception of **sz** + **2c4n** and **sz** + **3hba**, which show incomplete proton transfer.

Crystal Structures of sz + 4brba. The cocrystal of **sz** + **4brba** crystallizes in the $P2_1/n$ space group with the asymmetric unit consisting of one molecule of each **sz** and **4brBA**. Sz forms in the amidine tautomer, forming the expected amidine-carboxyl synthon. **Sz** adopts a v-conformation, which forms wavelike columns along the *c*-axis (Figure 3(i)), with **4brba** sitting in between adjacent columns. However, the pyrimidine rings of **sz** and **4brba** forms a layered structure, with layers separated from each other via the aniline ring of **sz**.

Crystal Structures of sz + ba, sz + ca, and sz + ta. The crystal structure of **sz** + **ba** has been previously reported,[22] while **sz** + **ca** and **sz** + **ta** are novel to this work. Cocrystals of **sz** + **ba**, **sz** + **ca**, and **sz** + **ta** are described and compared together since the coformers only consist of one hydrogen bond donor/acceptor—the carboxyl group. From this, it should be reasoned that differences in the crystal structures should arise due to the unique aspects of the respective coformer. Cocrystals of **sz** + **ba**, **sz** + **ca**, and **sz** + **ta** crystallize in the *Pbca*, $P2_1/n$, and $P2_1$ space groups, respectively. In each case, the asymmetric unit is made up of one molecule of **sz** and one molecule of the respective coformer. The coformers **ta**, **ba**, and **ca** contain only one functional group that can form hydrogen bonds—the carboxyl group. In each case, the amidine-carboxyl synthon (Synthon (ii), see Scheme 2) formed. **Sz** + **ca** and **sz** + **ta** formed the sulfoxide-amino chain synthon (Synthon (iii), see Scheme 2), while **sz** + **ba** did not. Instead, in **sz** + **ba** the amino group forms a hydrogen bond to one of the oxygen atoms of the sulfoxide group, while the other hydrogen bonds to the carboxyl group of **ba** (Synthon (iv) see Scheme 2).

In the packing of the cocrystal of **sz** + **ba** (Figure 4(ii)), the pyrimidine ring of sz and rings of ba form rows of the aniline ring of **sz** in the *b*-axis direction separating clusters of **sz** + **ba** apart. Adjacent dimers of **sz** + **ba** running in the *a*-axis appear T-shaped, with rows interlocking together. In the packing of **sz** + **ca**, molecules of **sz** lie in rows down the *b*-axis, alternating between the aniline and pyrimidine rings. This results in the **sz** molecules forming parallel zigzag formations, with molecules of ca. filling in the gaps between the **sz**-rows.

Crystal Structures of sz + Hydroxybenzoic Acids. The cocrystals of **sz** + **2hba** and **sz** + **3hba** both crystallize in the *Pbca* space group, while the cocrystal of **sz** + **4hba** crystallizes in the $P\bar{1}$ space group. In each case, the asymmetric unit is composed of one molecule of **sz** and each respective conformer. The crystal structures of **sz** + **4hba** and **sz** + **2hba** have been previously reported in the literature.[5,23] Despite using slightly different crystallizing conditions (**sz** + **2hba** used acetone as the solvent, while **sz** + **4hba** used pure acetonitrile), the same crystal structures were

DOI: 10.1021/acs.cgd.9b01209
Cryst. Growth Des. 2020, 20, 813−823

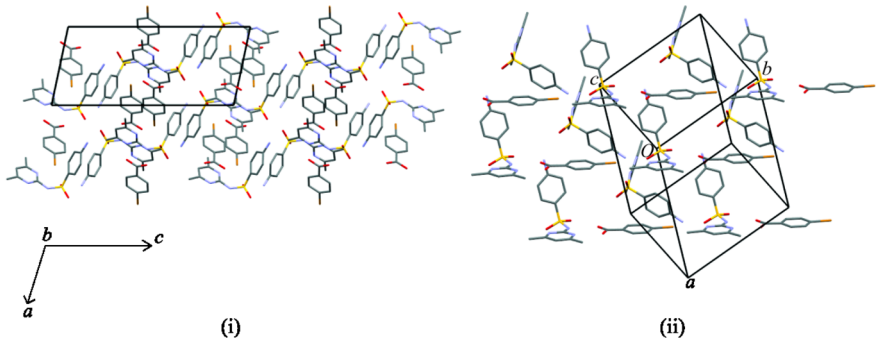


Figure 3. Crystal structure of **sz** + **4brba** showing (i) the packing viewed down the *b*-axis, (ii) the layers of the pyrimidine of **sz** and **4brba** separated by the aniline rings.

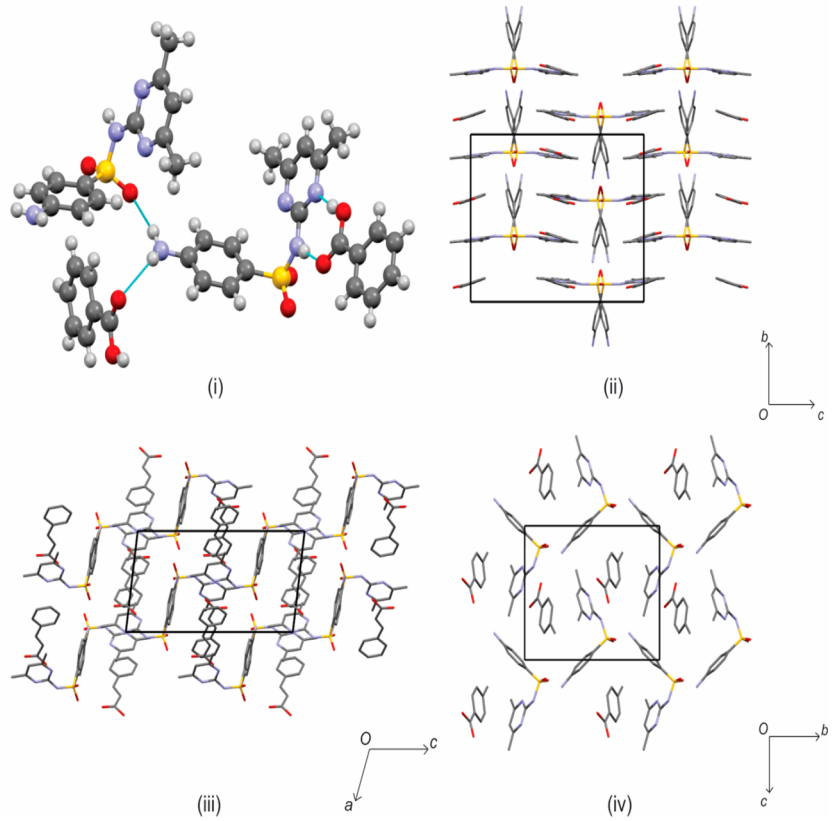


Figure 4. Crystal structure of **sz** + **ba** showing the hydrogen bonding patterns (i) and its packing (ii). The packing diagrams for **sz** + **ca** (iii) and **sz** + **ta** (iv).

obtained. The cocrystal of **sz** + **3hba** is novel; hence, the synthesis of the former proved useful in comparing the changes that may occur due to the shift of the hydroxyl group. In the cocrystal of **sz** + **3hba**, it was observed that the carboxylic acid proton had only partially transferred to the **sz**. In the difference Fourier map, there were two clear areas of electron density near O3 and N4. Subsequently, we decided to place a hydroxyl (H3A) and aromatic (H4) hydrogen atom geometrically and give each one a site occupancy of a half. This behavior is reflected in the ratio of the C−O bonds given in Table 3. For a typical carboxylic acid, the ratio should be greater than 1.5. For a carboxylate, the value should be close to 1.0. In this case, the ratio was found to be 1.027. Hence, we will refer to **sz** + **3hba** as a mixed salt/cocrystal. **sz** + **2hba** and **sz** + **3hba** form the amidine-carboxyl synthon, while **sz** + **4hba** formed the imidine-carboxyl synthon instead. **sz** + **2hba** and **sz** + **3hba** form the sulfoxide-amino chains, while **Sz** + **4hba** do not. Instead, only one of the oxygen atoms of the sulfoxide group forms a hydrogen bond with the amino group (N1−H1A···O2). The hydroxyl group for **sz** + **2hba** forms an intramolecular hydrogen bond as expected. For both **sz** + **3hba** and **sz** + **4hba**, the hydroxyl group forms a hydrogen bond interaction with the amino group of **sz** (Synthon (v), see Scheme 2).

The packing of the crystal structures of **sz** + **2hba** and **sz** + **3hba** are isomorphous, as seen in Figure 5(i) and (ii). Like many of the other crystal structures reported in this work, **sz** adopts a v-shaped conformation. Both **sz** + **2hba** and **sz** + **3hba** form long chains of **sz** connected by the sulfoxide-amino hydrogen bond, which essentially forms long columns with the hydroxybenzoic acid attached. These columns overall appear in a wavelike structure.

The packing of **sz** + **4hba** deviates from the previous two. Two molecules of each **sz** and **4hba** form tetramers, which stack together to form a ladder. This ladder is made up of the pyrimidine rings of **sz** and **4hba** making up the steps, while the aniline

DOI: 10.1021/acs.cgd.9b01209
Cryst. Growth Des. 2020, 20, 813−823

Table 2. Crystallographic Data and Structure Refinement Data for sz Multicomponent Crystals

	sz + 2c4n	sz + 2c5n	sz + 2hba	sz + 3hba	sz + 4hba
empirical formula	$C_{19}H_{18}ClN_5O_6S$	$C_{19}H_{18}ClN_5O_6S$	$C_{19}H_{20}N_4O_5S$	$C_{19}H_{20}N_4O_5S$	$C_{19}H_{20}N_4O_5S$
formula weight/g·mol^{-1}	479.89	479.89	416.45	416.45	416.45
temperature/K	173(2)	173(2)	173(2)	173(2)	173(2)
wavelength/Å	0.71073	0.71073	0.71073	0.71073	0.71073
crystal system	orthorhombic	monoclinic	orthorhombic	orthorhombic	triclinic
space group	$Pbc2_1$	$P2_1$	$Pbca$	$Pbca$	$P\bar{1}$
a/Å	19.2999(6)	6.96450(10)	10.1289(3)	9.9985(3)	7.9638(9)
b/Å	7.7198(2)	19.3894(3)	15.7422(4)	15.7375(4)	9.3601(10)
c/Å	13.9038(4)	15.7238(2)	25.0535(7)	24.6844(7)	13.2882(14)
α/°	90	90	90	90	74.123(4)
β/°	90	90.7000(10)	90	90	75.616(4)
γ/°	90	90	90	90	85.727(4)
V/Å^3	2071.55(10)	2123.14(5)	3994.81(19)	3884.12(19)	922.85(18)
Z	4	4	8	8	2
density (calculated)/ Mg m^{-3}	1.539	1.501	1.385	1.424	1.499
μ/mm^{-1}	0.335	0.326	0.201	0.207	0.218
F(000)	992	992	1744	1744	436
crystal size/mm^3	0.214 × 0.248 × 0.317	0.349 × 0.189 × 0.130	0.441 × 0.284 × 0.238	0.315 × 0.257 × 0.129	0.163 × 0.146 × 0.052
theta range for data/° collection	2.110 to 28.238	1.295 to 28.215	3.057 to 28.334	2.924 to 28.360	3.126 to 28.334
reflections collected	24549	58621	58505	47634	36343
independent reflections	5046 [R(int) = 0.0545]	10439 [R(int) = 0.0482]	4953 [R(int) = 0.0405]	4831 [R(int) = 0.0748]	4592 [R(int) = 0.0511]
goodness-of-fit on F^2	1.030	1.059	1.021	1.072	1.046
final R indices [$I > 2\sigma(I)$]	R_1 = 0.0366	R_1 = 0.0392	R_1 = 0.0373	R_1 = 0.0452	R_1 = 0.0416
	wR_2 = 0.0707	wR_2 = 0.0854	wR_2 = 0.0926	wR_2 = 0.1134	wR_2 = 0.0977
R indices (all data)	R_1 = 0.0560	R_1 = 0.0595	$R1$ = 0.0484	R_1 = 0.0693	R_1 = 0.0555
	wR_2 = 0.0785	wR_2 = 0.0935	wR_2 = 0.0999	wR_2 = 0.1250	wR_2 = 0.1039
CCDC no.	1952592	1952593	1952594	1952595	1952596

	sz + 4brba	sz + ba	sz + ca	sz + ta
empirical formula	$C_{19}H_{19}BrN_4O_4S$	$C_{19}H_{20}N_4O_4S$	$C_{21}H_{22}N_4O_4S$	$C_{20}H_{22}N_4O_4S$
formula weight/g·mol^{-1}	479.35	400.45	426.48	414.47
temperature/K	173(2)	173(2)	173(2)	173(2)
wavelength/Å	0.71073	0.71073	0.71073	0.71073
crystal system	monoclinic	orthorhombic	monoclinic	monoclinic
space group	$P2_1/n$	$Pbca$	$P2_1/n$	$P2_1$
a/Å	8.5979(7)	15.1817(3)	8.3614(2)	7.3454(6)
b/Å	11.8215(10)	14.0288(3)	14.6091(4)	13.3001(11)
c/Å	19.5587(16)	17.9844(4)	16.9318(5)	11.2172(10)
α/°	90	90	90	90
β/°	102.009(3)	90	98.2910(10)	107.585(3)
γ/°	90	90	90	90
V/Å^3	1944.4(3)	3830.34(14)	2046.65(10)	1044.65(15)
Z	4	8	4	2
density (calculated)/Mg m^{-3}	1.637	1.389	1.384	1.318
μ/mm^{-1}	2.257	0.203	0.195	0.188
F(000)	976	1680	896	436
crystal size/mm^3	0.365 × 0.086 × 0.066	0.347 × 0.248 × 0.160	0.514 × 0.317 × 0.254	0.325 × 0.258 × 0.136
theta range for data collection	2.983 to 28.356°	2.265 to 30.749°	2.899 to 28.315°	2.909 to 28.356°
reflections collected	26446	46609	40194	19104
independent reflections	4840 [R(int) = 0.0864]	5970 [R(int) = 0.0892]	5084 [R(int) = 0.0413]	5182 [R(int) = 0.0224]
goodness-of-fit on F^2	1.050	1.011	1.081	1.064
final R indices [$I > 2\sigma(I)$]	R_1 = 0.0485	R_1 = 0.0465	R_1 = 0.0372	R_1 = 0.0336
	wR_2 = 0.0748	wR_2 = 0.1101	wR_2 = 0.0955	wR_2 = 0.0932
R indices (all data)	R_1 = 0.0889	R_1 = 0.0917	R_1 = 0.0478	R_1 = 0.0375
	wR_2 = 0.0840	wR_2 = 0.1314	wR_2 = 0.1011	wR_2 = 0.1025
CCDC no.	1952597	1952598	1952599	1952600

ring makes up the rail. This description matches the one previously reported.[5]

Crystal Structures of sz + 2c4n and sz + 2c5n. The multicomponent crystals of **sz + 2c4n** and **sz + 2c5n** form a molecular salt and a cocrystal, respectively. **Sz + 2c4n** and **sz + 2c5n** crystallize in the $Pca2_1$ and $P2_1$ space groups, respectively. The asymmetric unit for **sz + 2c4n** consists of one molecule of each **sz** and **2c4n**, while the one for **sz + 2c5n** consists of two molecules of **sz** and **2c5n**. As was the case for **sz + 3hba**, **sz + 2c4n** was observed to have a positional disorder of the carboxylic H atom.

DOI: 10.1021/acs.cgd.9b01209
Cryst. Growth Des. 2020, 20, 813−823

Table 3. Hydrogen Bond Table for the Multicomponent Crystals Represented in This Work[a]

D−H···A	d(D−H)	d(H···A)	d(D···A)	∠(DHA)
sz + 2c4n				
N1−H1A···O4[a]	0.89(5)	2.40(5)	3.083(4)	134(4)
N1−H1B···O5[b]	0.78(5)	2.30(5)	3.032(5)	156(5)
N2−H2A···O4	0.83(5)	1.91(5)	2.731(4)	176(5)
N4−H4A···O3	0.88	1.68	2.560(4)	173
sz + 2c5n				
N1−H1A···O8[c]	0.90(4)	2.20(4)	3.067(5)	159(4)
N1−H1B···O7	0.80(5)	2.15(5)	2.899(4)	156(4)
N2−H2A···O3	0.73(4)	2.06(4)	2.793(4)	172(4)
O4−H4A···N4	0.88(5)	1.80(5)	2.647(4)	159(5)
N6−H6A···O2[d]	0.84(5)	2.36(5)	3.021(4)	136(4)
N6−H6B···O1[e]	0.87(4)	2.14(4)	2.976(4)	162(3)
N7−H7A···O10	0.85(5)	1.92(5)	2.762(4)	173(4)
O9−H9A···N9	0.90(6)	1.74(6)	2.631(4)	172(6)
sz + 3hba				
N2−H2A···O3	0.88	1.93	2.751(2)	155
N1−H1A···O1[f]	0.88(2)	2.24(2)	3.124(2)	177(2)
N1−H1A···S1[f]	0.88(2)	2.95(2)	3.7743(18)	155(18)
N1−H1B···O2[g]	0.88(2)	2.26(2)	3.039(2)	148(2)
O4−H4···N3	0.84	1.89	2.722(2)	171
O5−H5A···N1[h]	0.89(3)	2.01(3)	2.878(2)	165(3)
N3−H3A···O4	0.88	1.86	2.722(2)	166
sz + 4brba				
N1−H1A···O1[c]	0.85(4)	2.27(4)	3.103(4)	169(3)
N1−H1B···O2[i]	0.82(3)	2.36(3)	3.166(4)	168(3)
N2−H2A···O3	0.80(3)	3.12(3)	3.706(4)	132(3)
O3−H3A···N4	0.78(4)	1.93(4)	2.693(3)	168(4)
sz + 4hba				
N1−H1A···O2[c]	0.85(2)	2.23(3)	3.0697(19)	168(2)
N1−H1A···S1[c]	0.85(2)	2.95(3)	3.7585(16)	158(19)

D−H···A	d(D−H)	d(H···A)	d(D···A)	∠(DHA)
sz + 4hba				
N1−H1B···N4[j]	0.88(2)	2.56(2)	3.430(2)	168(19)
N1−H1B···O2[j]	0.88(2)	2.63(2)	3.1212(18)	116(17)
N3−H3A···O3	0.91(2)	3.06(2)	3.7433(19)	133(17)
O3−H3B···N2	0.93(3)	1.86(3)	2.7765(19)	173(3)
O3−H3B···S1	0.93(3)	2.76(3)	3.5270(14)	141(2)
O5−H5A···N1[k]	0.85(3)	1.97(3)	2.800(2)	165(2)
sz + ba				
N1−H1A···O3[g]	0.83(3)	2.40(3)	3.084(3)	140(2)
N1−H1B···O2[l]	0.92(3)	2.04(3)	2.955(3)	172(2)
N2−H2A···O3	0.80(3)	2.00(3)	2.792(2)	174(3)
O4−H4···N4	0.94(3)	1.70(3)	2.640(2)	174(2)
sz + ca				
N2−H2···O3	0.84(2)	3.04(2)	3.6632(15)	134(16)
O3−H3A···N4	0.97(2)	1.71(2)	2.6757(15)	171(2)
N1−H1A···O2[c]	0.85(2)	2.27(2)	3.0828(18)	159(18)
N1−H1B···O1[i]	0.83(2)	2.27(2)	3.0859(18)	168(2)
sz + 2hba				
N2−H2···O4	0.88(2)	1.90(2)	2.7789(16)	175(18)
N1−H1A···O2[a]	0.85(2)	2.14(2)	2.9478(19)	160(2)
N1−H1B···S1[b]	0.91(2)	2.99(2)	3.8674(18)	164(17)
N1−H1B···O1[b]	0.91(2)	2.16(2)	3.057(2)	168(19)
O3−H3A···N4	0.99(3)	1.64(3)	2.6283(15)	171(3)
O5−H5A···O3	0.99(3)	3.56(3)	4.1468(17)	120(19)
sz + ta				
N1−H1A···O1[o]	0.87(3)	2.08(3)	2.896(3)	155(3)
N1−H1B···O2[n]	0.83(3)	2.19(3)	2.961(3)	154(3)
N2−H2A···O4	0.86(3)	1.90(3)	2.759(2)	177(3)
O3−H3A···N4	0.94(4)	1.81(4)	2.732(2)	168(4)

[a]Symmetry transformations used to generate equivalent atoms. (a) $-x+1, -y+2, z-1/2$. (b) $x-1/2, -y+2, z-1$. (c) $x+1, y, z$. (d) $x, y, z+1$. (e) $x-1, y, z+1$. (f) $-x+1/2, y+1/2, z$. (g) $-x+1, y+1/2, -z+1/2$. (h) $-x+1/2, -y+1, z+1/2$. (i) $-x+3/2, y-1/2, -z+1/2$. (j) $-x+2, -y+1, -z$. (k) $-x+1, -y, -z+1$. (l) $-x+3/2, y+1/2, z$. (m) $-x+1, y-1/2, -z+3/2$. (n) $-x+1, y-1/2, -z+2$. (o) $-x, y-1/2, -z+2$.

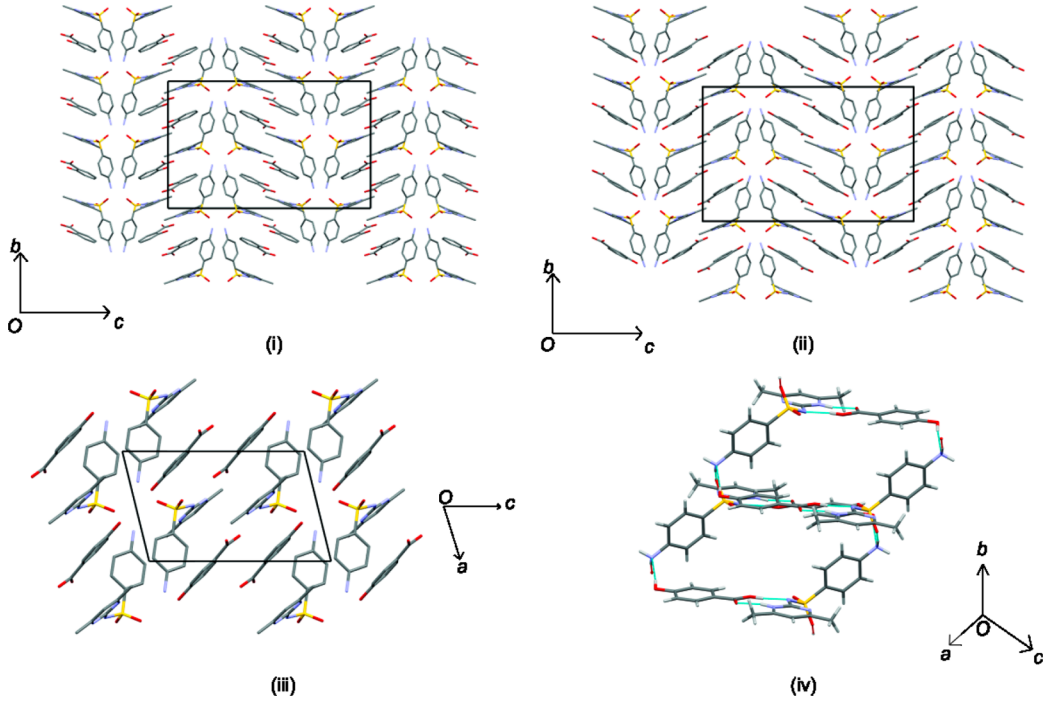


Figure 5. Packing diagram for (i) **sz + 2hba** as viewed down the *a*-axis, (ii) **sz + 3hba** as viewed down the *a*-axis, (iii) **sz + 4hba** as viewed down the *b*-axis, and (iv) two tetramers of **sz + 4hba** stacked to show the ladder.

DOI: 10.1021/acs.cgd.9b01209
Cryst. Growth Des. 2020, 20, 813−823

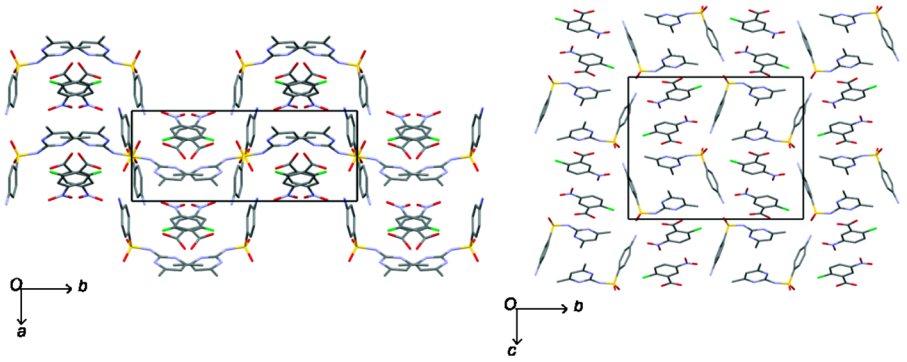


Figure 6. Packing diagrams of the multicomponent crystals of **sz** + **2c4n** as viewed down the *c*-axis (left) and **sz** + **2c5n** with the *a*-axis coming out of the plane (right).

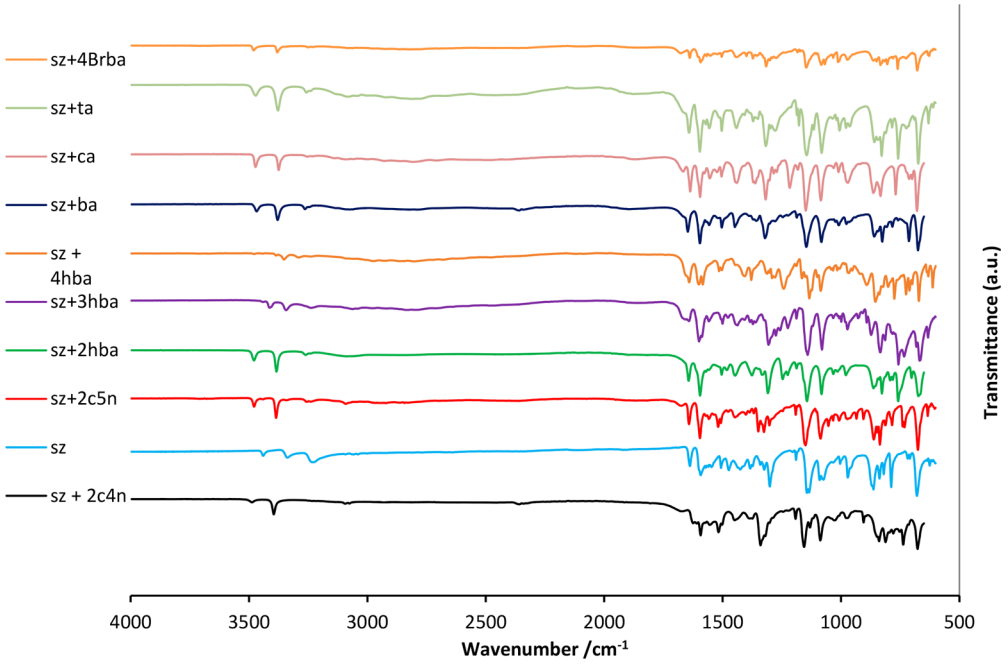


Figure 7. FTIR spectra obtained for the **sz** and the multicomponent crystals of **sz**.

Table 4. Comparison of the Bond Lengths of the Carboxyl Group of the Coformer

compound	C19−O3/Å	C19−O4/Å	ratio (long over short)	long C−O bond of respective coformer in native crystal structure/Å	short C−O bond of respective coformer in native crystal structure/Å
sz + **2c4n(salt/cc)**	1.266(4)	1.237(4)	1.023	1.247 (**Form I**) 1.288/1309/1.301/1.313 (**Form II**) 13[c]	1.233 (**Form I**) 1.221/1.216/1.214/1.222 (**Form II**)[13]
sz + **2c5n**[a] (cc)	1.202(4)/ 1.197(4)	1.285(4)/ 1.279(4)	1.069/1.068	1.295[14]	1.220[14]
sz + **3hba(salt/cc)**	1.250(2)	1.284(2)	1.027	1.317[15]	1.208[15]
sz + **4brba** (cc)	1.311(4)	1.227(4)	1.069	1.309[16]	1.223[16]
sz + **4hba** (cc)	1.318(2)	1.227(2)	1.074	1.278[17]	1.267[17]
sz + **ba** (cc)	1.306(2)	1.228(2)	1.064	1.275[18]	1.264[18]
sz + **ca**[b] (cc)	1.3127(17)	1.2299(16)	1.067	1.292[19]	1.254[19]
sz + **2hba** (cc)	1.2921(19)	1.2476(18)	1.036	1.311[20]	1.245[20]
sz + **ta** (cc)	1.311(3)	1.224(3)	1.053	1.302[21]	1.248[21]

[a]For the case of **sz** + **2c5n**, the second molecule of 2c5n is also included, as C38−O10 and C38−O9 respectively, separated by a slash. [b]For the case of **sz** + **ca**, it is the C21−O3 and C21−O4 bond respectively instead. [c]2c4n is polymorphic, with **Form I** having one 2c4n molecule in the asymmetric unit, while **Form II** has four 2c4n molecules.

In the difference Fourier map, there were two clear areas of electron density near O3 and N4. Subsequently, we decided to place a hydroxyl (H4) and aromatic (H3a) hydrogen atom geometrically and give each one a site occupancy of a half. The bond lengths of C19−O3 and C19−O4 for **sz** + **2c4n** are 1.266(4) and 1.237(4) respectively, giving a ratio of 1.023 and indicating again a mixed salt/cocrystal. Despite being close isomers of each other, **2c4n** and **2c5n** will exhibit different acid strengths. One approach to determine if a cocrystal or a molecular salt will form is to use the pK_a of the coformers. If the ΔpK_a (ΔpK_a = pK_a

DOI: 10.1021/acs.cgd.9b01209
Cryst. Growth Des. 2020, 20, 813−823

(conjugate acid of base) − pK_a (acid)) is greater than 2−3, a molecular salt will form.[24] Anything less than 1 will almost always indicate the formation of a cocrystal. Values between 0 and 3 are an intermediate case where either a molecular salt or cocrystal could form. For water the pK_a's for **sz**, **2c4n**, and **2c5n** respectively are 2.07,[25] 1.96, and 2.17, and give ΔpK_a's for **sz** + **2c4n** and **sz** + **2c5n** as 0.11 and −0.10 respectively. Although this ΔpK_a could only be truly valid if these crystals were grown from water solution, it still correlates well for the case of **sz** + **2c5n**.

In addition to being different in being a salt and a cocrystal, some hydrogen bonding patterns are different. The cocrystal of **sz** + **2c5n** is comparable to many of the other cocrystals presented in this work: the formation of the amidine-carboxyl and the amino-sulfoxide synthons. The nitro group of **2c5n** is involved in some weak hydrogen bonding with a neighboring **2c5n** molecule (C16−H16···O12−N10 and C35−H35···O6−N6). In contrast, the sulfoxide group of **sz** in the salt of **sz** + **2c4n** does not form the sulfoxide-amino chains that are observed in the other crystal structures. Instead, the amino group of **sz** forms hydrogen bonds with the carboxylate group and nitro group of **2c4n** (N1−H1B···O5 and N1−H1A···O4 respectively). The sulfoxide group forms only weak hydrogen bonds (C11−H11···O1, C14−H14···O2, and C6−H6···O2).

The packing of the crystal structures of **sz** + **2c4n** and **sz** + **2c5n** is similar. In both cases, **sz** adopts a v-shaped conformation that has been observed in the other crystal structures. The packing of **sz** molecules forms channels formed by four sz molecules, which the molecules of **2c4n** and **2c5n** occupy.

Infrared Spectroscopy. Infrared spectroscopy can be used to determine the formation of molecular salts or cocrystals by comparing the spectrum of the multicomponent crystal with the spectra of the parent coformers. A shift of a peak between the spectrum of the parent coformer and the spectrum of the multicomponent crystal is typically expected. For this work, FT-IR spectra were obtained and are presented in Figure 7.The stretching frequencies of the primary amino group of **sz** (−NH_2) and the sulfonamide group (−NH) are then compared to that of the parent coformer. Table 5 contains the wavenumbers associated with the *sym* and *asym* stretching frequencies of the primary amino group and the stretching frequency of the sulfonamide group. It is clear that for most of the multicomponent crystals, there is a shift in the expected stretching frequencies.

In particular, it should be noted that for the spectrum of **sz** + **2c4n**, a broad band is observed over the 1500−1650 cm^{-1} region, which is not observed for the other multicomponent crystals presented in this work. This broad band is typically associated with a carboxylate, which infers that the multicomponent crystal of **sz** + **2c4n** is indeed a molecular salt, in contrast to the refinement model we used in the crystal structure.

Differential Scanning Calorimetry Results. The multicomponent crystals were analyzed by DSC. Samples were heated at a rate of 10 °C/min from 25 to 250 °C, which were then cooled back to 25 °C at a rate of 10 °C/min. In each case, upon cooling, no further thermal events were observed. With the exception of **sz** + **4brba** and **sz** + **ca**, the DSC curve for each sample showed only one single endothermic peak, which corresponds to melting. These curves are plotted in Figure 8, with thermodynamic data in Table 2. The DSC curves for **sz** + **4brba** and **sz** + **ca** were plotted separately and are in Figure 9. **sz** + **4brba** show two endothermic peaks: one broad peak occurring at 125 °C and one peak at 204 °C. **sz** + **ca** show two peaks occurring at 188 and 209 °C respectively.

In order to determine what the additional peaks observed in the crystals of **sz** + **4Brba** and **sz** + **ca** are, crystals were mounted

Table 5. Peak Shift Assignments for the IR Spectra of sz and the Multicomponent Crystals of sz[a]

peak assignment	wavenumber/cm^{-1}
sz	
amine $\nu(NH_2)$ *sym*	3346
amine $\nu(NH_2)$ *asym*	3445
sulfonamide (NH)	3238
sz + 2c4n	
amine $\nu(NH_2)$ *sym*	3396 (+50)
amine $\nu(NH_2)$ *asym*	3488 (+43)
sulfonamide (NH)	3094 (−144)
sz + 2c5n	
amine $\nu(NH_2)$ *sym*	3388 (+42)
amine $\nu(NH_2)$ *asym*	3483 (+38)
sulfonamide (NH)	3247 (+9)
sz + 2hba	
amine $\nu(NH_2)$ *sym*	3380 (+34)
amine $\nu(NH_2)$ *asym*	3485 (+40)
sulfonamide (NH)	3251 (+13)
sz + 3hba	
amine $\nu(NH_2)$ *sym*	3352 (+6)
amine $\nu(NH_2)$ *asym*	3419 (−26)
sulfonamide (NH)	3230 (−8)
sz + 4hba	
amine $\nu(NH_2)$ *sym*	3359 (+13)
amine $\nu(NH_2)$ *asym*	3376 (−69)
sulfonamide (NH)	3283 (+45)
sz+4Brba	
amine $\nu(NH_2)$ *sym*	3384 (+38)
amine $\nu(NH_2)$ *asym*	3486 (+41)
sulfonamide (NH)	3241 (+3)
sz + ba	
amine $\nu(NH_2)$ *sym*	3373 (+27)
amine $\nu(NH_2)$ *asym*	3460 (+15)
sulfonamide (NH)	3271 (+33)
sz + ca	
amine $\nu(NH_2)$ *sym*	3371 (+25)
amine $\nu(NH_2)$ *asym*	3477 (+32)
sulfonamide (NH)	3265 (+29)
sz+ta	
amine $\nu(NH_2)$ *sym*	3381 (+35)
amine $\nu(NH_2)$ *asym*	3480 (+32)
sulfonamide (NH)	3247 (+9)

[a]Note: values in brackets indicate the shift of the peak compared to pure **sz**.

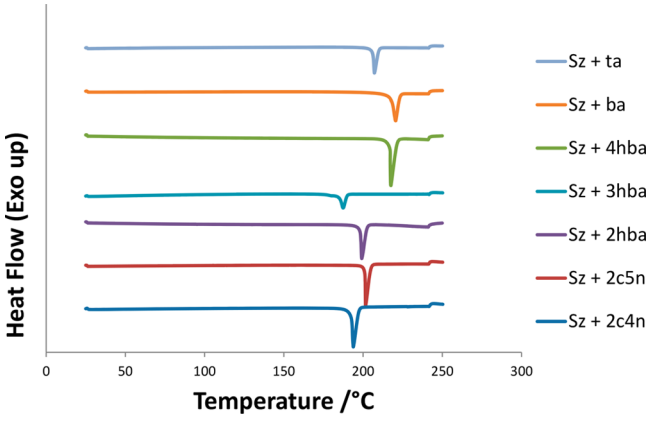


Figure 8. DSC curves for cocrystals which only show melting.

DOI: 10.1021/acs.cgd.9b01209
Cryst. Growth Des. 2020, 20, 813−823

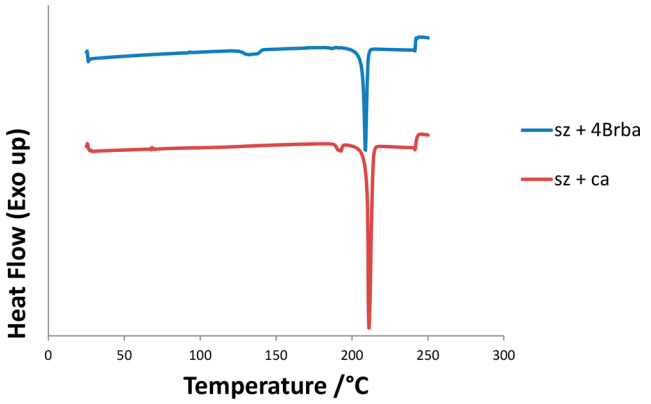


Figure 9. DSC curves for **sz + 4brba** and **sz + ca** showing the additional endothermic peaks.

Table 6. Thermodynamic Data for the Endothermic Peaks of the Multicomponent Crystals

cocrystal/salt	onset/°C	peak/°C	enthalpy/ kJ mol^{-1}
sz + 2c4n	192.1	193.8	72.5
sz + 2c5n	200.8	201.6	72.6
sz + 2hba	198.0	199.2	64.1
sz + 3hba	184.8	187.4	75.3
sz + 4hba	214.2	217.6	57.5
sz + 4Brba (crystalline → amorphous phase transition)	126.1	132.8	10.5
sz + 4Brba (melting phase transition)	206.6	208.8	58.3
sz + ca (crystalline → amorphous phase transition)	188.7	192.7	2.3
sz + ca (melting phase transition)	209.8	211.2	51.2
sz + ba	217.4	220.5	66.4
sz + ta	203.9	208.0	54.0

on a glass fiber and heated in situ in the diffractometer. These crystals were heated from 25 °C up to the temperature at which the first thermal event was observed. The unit cell parameters were collected at every 10 °C interval to monitor if any significant change occurs. In both cases, as soon as the crystal reached the temperature at which the first thermal event occurs, no diffraction spots were observed in the diffraction image. These crystals were observed to have changed from being transparent to being opaque. This implies that the phase change associated with the first thermal event of the DSC curves for both cases is a phase change from being crystalline to being amorphous.

CONCLUSIONS

Nine multicomponent crystals were synthesized and characterized. Among **sz + ba**, **sz + ca**, and **sz + ta**, structural feature varied widely despite having the same set of hydrogen bond synthons. **sz + 2hba** and **sz + 3hba** were found to be isomorphous and favored the amidine-carboxyl synthon, while **sz + 4hba** differed from the previous two both in terms of packing as well as the imidine-carboxyl synthon. **sz + 2c4n** and **sz + 2c5n** formed a salt and cocrystal respectively and showed vast differences between the two in terms of packing and synthons despite being isomers of each other. Finally, the DSC showed that the multicomponent crystals have different melting points from each other and the coformers that make it up. Thus, coformers containing the carboxyl group have great potential for forming a multicomponent crystal with **sz**. Therefore, **sz** could prove useful as a potential coformer itself for compounds or even other APIs that feature carboxylic acid functional groups.

ASSOCIATED CONTENT

Supporting Information

The Supporting Information is available free of charge at https://pubs.acs.org/doi/10.1021/acs.cgd.9b01209.

Powder X-ray patterns (PXRD) (PDF)

Accession Codes

CCDC 1952592−1952600 contain the supplementary crystallographic data for this paper. These data can be obtained free of charge via www.ccdc.cam.ac.uk/data_request/cif, or by emailing data_request@ccdc.cam.ac.uk, or by contacting The Cambridge Crystallographic Data Centre, 12 Union Road, Cambridge CB2 1EZ, UK; fax: +44 1223 336033.

AUTHOR INFORMATION

Corresponding Author

*Molecular Sciences Institute, School of Chemistry, University of the Witwatersrand, Private Bag 3, 2050, Johannesburg, South Africa. E-mail: andreas.lemmerer@wits.ac.za. Fax: +27-11-717-6749. Tel: +27-11-717-6711.

ORCID

Andreas Lemmerer: 0000-0003-1569-2831

Notes

The authors declare no competing financial interest.

REFERENCES

(1) Blagden, N.; de Matas, M.; Gavan, P. T.; York, P. Crystal engineering of active pharmaceutical ingredients to improve solubility and dissolution rates. *Adv. Drug Delivery Rev.* **2007**, *59*, 617−630.

(2) Pouton, C. W. Formulation of poorly water-soluble drugs for oral administration: Physicochemical and physiological issues and the lipid formulation classification system. *Eur. J. Pharm. Sci.* **2006**, *29*, 278−287.

(3) Schultheiss, N.; Newman, A. Pharmaceutical Cocrystals and Their Physicochemical Properties. *Cryst. Growth Des.* **2009**, *9*, 2950−2967.

(4) Vishweshwar, P.; McMahon, J. A.; Bis, J. A.; Zaworotko, M. J. Pharmaceutical co-crystals. *J. Pharm. Sci.* **2006**, *95*, 499−516.

(5) Ghosh, S.; Bag, P. P.; Reddy, C. M. Co-Crystals of Sulfamethazine with Some Carboxylic Acids and Amides: Co-Former Assisted Tautomerism in an Active Pharmaceutical Ingredient and Hydrogen Bond Competition Study. *Cryst. Growth Des.* **2011**, *11*, 3489−3503.

(6) Lu, J.; Cruz-Cabeza, A. J.; Rohani, S.; Jennings, M. C. A 2:1 sulfamethazine−theophylline cocrystal exhibiting two tautomers of sulfamethazine. *Acta Crystallogr., Sect. C: Cryst. Struct. Commun.* **2011**, *C67*, o306−o309.

(7) Kumar, V.; Thaimattam, R.; Dutta, S.; Munshi, P.; Ramanan, A. Structural landscape of multicomponent solids based on sulfa drugs. *CrystEngComm* **2017**, *19*, 2914−2924.

(8) Maury, L.; Rambaud, J.; Pauvert, B.; Lasserre, Y.; Berge, G. Physicochemical and structural study of sulfamethazine. *J. Pharm. Sci.* **1985**, *74*, 1344.

(9) *SAINT+, version 6.02 (including XPREP)*; Bruker AXS Inc.: Madison, WI, USA, 1999. *CrystEngComm*, **2012**, *14*, 6362−6365.

(10) Sheldrick, G. M. *SHELX, release 97−2 (includes SHELXS and SHELXL)*; University of Göttingen, 1997.

(11) Farrugia, L. ORTEP-3 for Windows - a version of ORTEP-III with a Graphical User Interface (GUI). *J. Appl. Crystallogr.* **1997**, *30*, 565.

(12) Macrae, C. F.; Edgington, P. R.; McCabe, P.; Pidcock, E.; Shields, G. P.; Taylor, R.; Towler, M.; van de Streek, J. Mercury: visualization and analysis of crystal structures. *J. Appl. Crystallogr.* **2006**, *39*, 453−457.

(13) Barsky, I.; Bernstein, J.; Stephens, P. W.; Stone, K. H. The study of the polymorphic system of 2-chloro-4-nitrobenzoic acid. *New J. Chem.* **2008**, *32*, 1747.

DOI: 10.1021/acs.cgd.9b01209
Cryst. Growth Des. 2020, 20, 813−823

(14) Ferguson, G.; Sim, G. A. 336. X-ray studies of molecular overcrowding. Part IV. The cystal and molecular structure of 2-chloro-5-nitrobenzonic acid. *J. Chem. Soc.* **1962**, *336*, 1767.
(15) Clevers, S.; Simon, F.; Sanselme, M.; Dupray, V.; Coquerel, G. Monotropic Transition Mechanism of m-Hydroxybenzoic Acid Investigated by Temperature-Resolved Second Harmonic Generation. *Cryst. Growth Des.* **2013**, *13*, 3697−3704.
(16) Ohkura, K.; Kashino, S.; Haisa. The Crystal and Molecular Structure of p-Bromobenzoic Acid. *Bull. Chem. Soc. Jpn.* **1972**, *45*, 2651−2652.
(17) Du, J. J.; Stanton, S. A.; Williams, P. A.; Ong, J. A.; Groundwater, P. W.; Overgaard, J.; Platts, J. A.; Hibbs, D. E. *Using Electron Density to Predict Synthon Formation in a 4-Hydroxybenzoic Acid: 4,4′-Bipyridine Cocrystal. Cryst. Growth Des.* **2018**, *18*, 1786−1798.
(18) Bruno, G.; Randaccio, L. A refinement of the benzoic acid structure at room temperature. *Acta Crystallogr., Sect. B: Struct. Crystallogr. Cryst. Chem.* **1980**, *B36*, 1711−1712.
(19) Wierda, D. A.; Feng, T. L.; Barron, A. R. Structure of α-trans-cinnamic acid. *Acta Crystallogr., Sect. C: Cryst. Struct. Commun.* **1989**, *C45*, 338−339.
(20) Munshi, P.; Guru Row, T. N. Intra- and intermolecular interactions in small bioactive molecules: cooperative features from experimental and theoretical charge-density analysis. *Acta Crystallogr., Sect. B: Struct. Sci.* **2006**, *B62*, 612−626.
(21) Hathwar, V. R.; Thakur, T. S.; Row, T. N. G.; Desiraju, G. R. Transferability of Multipole Charge Density Parameters for Supramolecular Synthons: A New Tool for Quantitative Crystal Engineering. *Cryst. Growth Des.* **2011**, *11*, 616−623.
(22) Arman, H. D.; Kaulgud, T.; Tiekink, E. R. T. *4-Amino-N-(4,6-dimethylpyrimidin-2-yl)-benzenesulfonamide−benzoic acid (1/1). Acta Crystallogr., Sect. E: Struct. Rep. Online* **2010**, *E66*, o2430.
(23) Patel, U.; Haridas, M.; Singh, T. P. Structure of the 1:1 complex between 4-amino-N-(4,6-dimethyl-2-pyrimidinyl)benzenesulfonamide (sulfadimidine) and 2-hydroxybenzoic acid (salicylic acid). *Acta Crystallogr., Sect. C: Cryst. Struct. Commun.* **1988**, *C44*, 1264−1267.
(24) Cruz-Cabeza, A. J. *Acid−base crystalline complexes and the pK_a rule. CrystEngComm* **2012**, *14*, 6362−6365.
(25) Qiang, Z.; Adams, C. Potentiometric determination of acid dissociation constants (pKa) for human and veterinary antibiotics. *Water Res.* **2004**, *38*, 2874−2890.

DOI: 10.1021/acs.cgd.9b01209
Cryst. Growth Des. 2020, 20, 813−823

Chapter 4 In Pursuit of Multicomponent Crystals of the Sulfa Drugs Sulfapyridine, Sulfathiazole and Sulfamethoxazole

4.1 Introduction

In this paper several cocrystals and molecular salts containing either **sp**, **sm** or **st** were synthesized and characterized. These cocrystals and molecular salts were synthesized using both mechanochemical and solution-based methods. Fifteen new cocrystals and molecular salts were synthesized: 5 containing **sp**, four containing **sm** and six containing **st**.

Authors: Scheepers, M.C., Lemmerer A.

Journal: *Crystal Growth & Design*

Date Published: 14 December 2021

Volume Number: 22

Pages: 98-122

Number of citations as of 10 November 2022: 2

CRYSTAL GROWTH & DESIGN

pubs.acs.org/crystal

Article

In Pursuit of Multicomponent Crystals of the Sulfa Drugs Sulfapyridine, Sulfathiazole, and Sulfamethoxazole

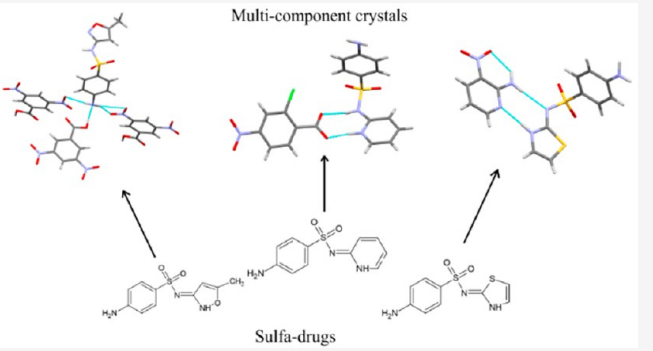
Matthew C. Scheepers and Andreas Lemmerer*

Cite This: *Cryst. Growth Des.* 2022, 22, 98−122

Read Online

ACCESS | Metrics & More | Article Recommendations | Supporting Information

ABSTRACT: An attempt to synthesize and characterize a series of multicomponent crystals (molecular salts or cocrystals) containing sulfamethoxazole, sulfapyridine, and sulfathiazole was made. Twenty-five different coformers were selected to synthesize cocrystals or molecular salts, and of those, 15 multicomponent crystals were isolated: five cocrystals and one molecular salt containing sulfathiazole, three cocrystals and one molecular salt of sulfamethoxazole, and four cocrystals and one molecular salt containing sulfapyridine. Synthesis was attempted using solution crystallization, as well as dry and liquid-assisted grinding, experiments. These crystals were characterized by single crystal X-ray diffraction, differential scanning calorimetry, thermal gravimetric analysis, and infrared spectroscopy. Many of the successful crystallizations yielded multicomponent crystals with a diverse range of hydrogen bonding networks. The predominant set of coformers responsible for the most successful synthesis attempts were 2-aminopyridine and its derivatives. These coformers formed a ring-based hydrogen bond motif with the corresponding sulfa drug, in addition to several different hydrogen bonds, which contribute to a larger hydrogen bonded network. The multicomponent crystals containing the sulfa drug and a benzoic acid derivative formed a hydrogen bond either between the carboxylic acid and the sulfonamide group or between the carboxylic acid group and the aniline group, in which a proton transfer occurred depending on the specific case.

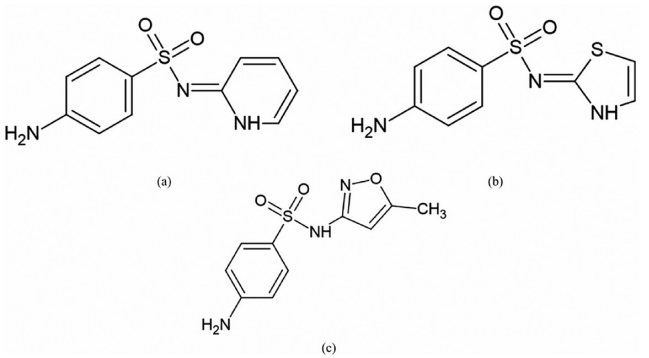


Downloaded via UNIV OF THE WITWATERSRAND on June 13, 2022 at 09:13:20 (UTC).
See https://pubs.acs.org/sharingguidelines for options on how to legitimately share published articles.

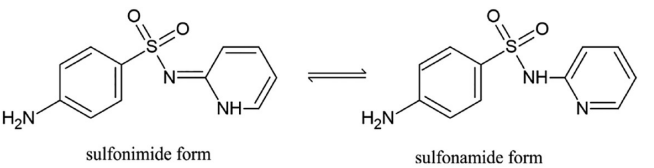
INTRODUCTION

There is a constant need for the design and development of new drugs. These new drugs are usually designed with the goal of targeting a specific drug target while minimizing side effects or drug resistance. New promising drugs are often impeded by poor physicochemical properties such as solubility, dissolution rates, tabletability, etc.[1−3] Crystal engineering is a means that can be used to solve these types of problems rather than attempting to design new drug molecules from scratch.[2,4] Crystal engineering more specifically is the design, synthesis, and characterization of new solid state forms, which can include either new polymorphs or multicomponent crystals (molecular salts or cocrystals). The design of new solid forms of active pharmaceutical ingredients (APIs) usually involves understanding the crystal packing and the different intermolecular interactions that the API could form

Scheme 1. Structure of the Predominant Tautomer in the Solid State of (a) Sulfapyridine (Imidine Form), (b) Sulfathiazole (Imidine Form), and (c) Sulfamethoxazole (Amidine Form)



Scheme 2. Tatutomerism of Sulfapyridine



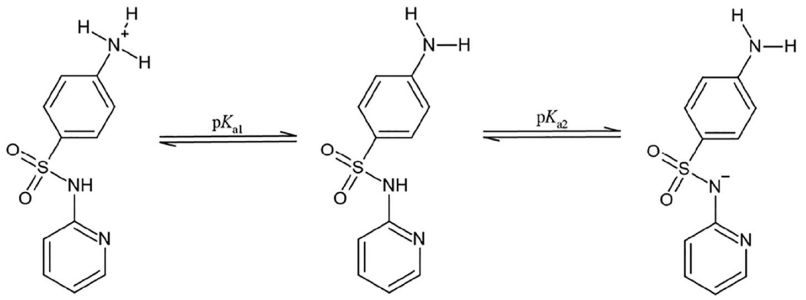
Received: April 16, 2021
Revised: November 30, 2021
Published: December 14, 2021



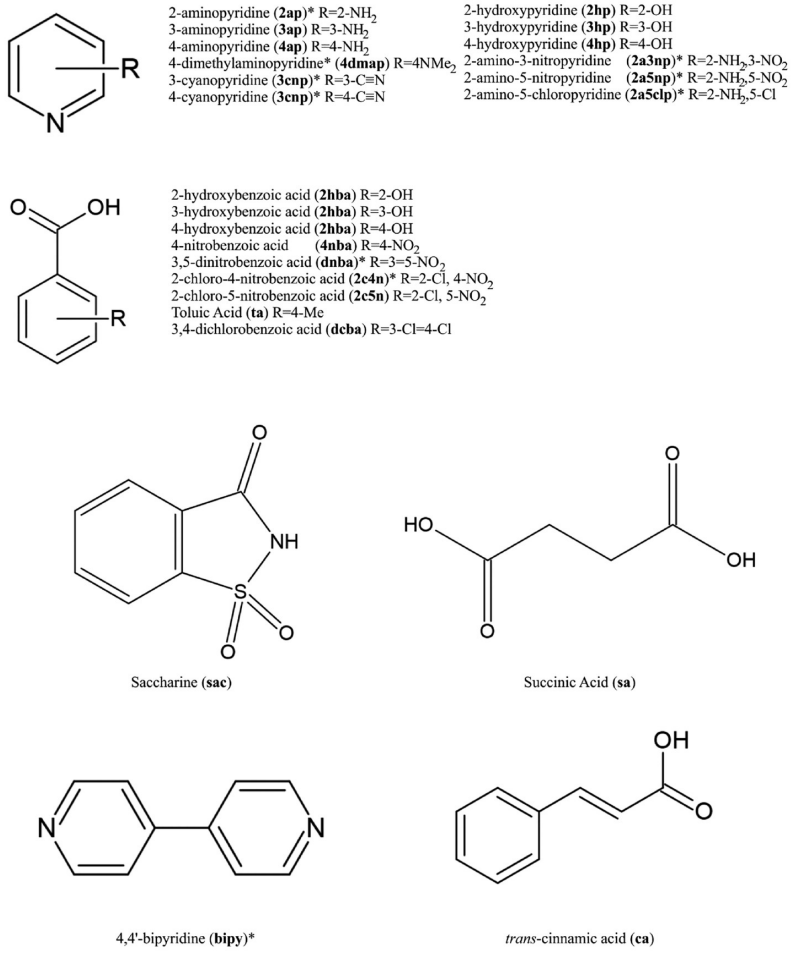
ACS Publications

© 2021 American Chemical Society

Scheme 3. Relationship between the Different pK_a Values



Scheme 4. List of Coformers Used for This Work[a]



[a]Coformers marked with an asterisk (*) were successful in forming a cocrystal or a molecular salt with one of the sulfa drugs.

and then using these to design new solid forms with, hopefully, new physical and chemical properties.[5,6] Typically, strong hydrogen bonds are the most significant of the intermolecular forces that are exploited, but weaker interactions such as halogen bonding and $\pi\cdots\pi$ and C−H···O interactions can also be of significance, depending on the nature of the crystal engineering target.

Cocrystals can be defined as crystalline solids that contain two or more neutral components (coformers), coexisting in the same crystal structure, with the components being solids at ambient conditions.[7,8] Molecular salts on the other hand contain ionized components and are treated as being on one end of the multicomponent crystal spectrum (with cocrystals containing only neutral components being on the other end). For the case of pharmaceutical cocrystals, the target API is combined with a coformer(s) that is ideally either another API or a generally regarded as safe (GRAS) compound.[4] This is done either to combine APIs with synergistic effects[9] or to minimize the potential toxic effects from the coformer by using a GRAS compound. In practice, the successful synthesis of a multicomponent crystal can prove to be challenging. For example, the number of APIs or GRAS compounds that can be used as a suitable coformer is extremely limited. The formation of successful cocrystals and molecular salts is never guaranteed,

https://doi.org/10.1021/acs.cgd.1c00448
Cryst. Growth Des. 2022, 22, 98−122

Table 1. Summary of Crystallographic Data for Cocrystals and Molecular Salt Containing st

	cocrystal or salt		
	st + 2a3np	**st + 2a5clp**	**st + 2a5np**
empirical formula	$(C_9H_9N_3O_2S_2)\cdot(C_5H_5N_3O_2)$	$(C_9H_9N_3O_2S_2)\cdot(C_5H_5ClN_2)$	$(C_9H_9N_3O_2S_2)_2\cdot(C_5H_5N_3O_2)$
formula weight	394.43	383.87	649.76
temp (K)	173(2)	173(2)	173(2)
cryst syst	triclinic	monoclinic	triclinic
space group	$P\bar{1}$	$P2_1/n$	$P\bar{1}$
a (Å)	8.3346(6)	8.39680(10)	8.2866(4) Å
b (Å)	9.7463(7)	19.1690(3)	11.5419(6)
c (Å)	10.5348(8)	10.7913(2)	15.4143(8)
α (deg)	101.762(3)	90	79.817(2)
β (deg)	93.929(3)	105.6050(10)	88.639(2)
γ (deg)	93.843(3)	90	76.525(2)
V (Å^3)	832.94(11)	1672.92(5)	1410.87(12)
Z	2	4	4
density (g/cm^3)	1.573	1.524	1.529
μ (mm^{-1})	0.356	0.496	0.394
F(000)	408	792	672
cryst size (mm^3)	0.124 × 0.034 × 0.026	0.257 × 0.252 × 0.165	0.459 × 0.036 × 0.025
2Θ range for data collection (deg)	3.025−28.309	2.125−28.338	2.464−28.303
reflns collected	29440	69074	53460
independent reflns	4124 [R(int) = 0.0433]	4169 [R(int) = 0.0307]	6994 [R(int) = 0.0275]
GOF on F^2	1.053	1.029	1.145
final R indexes [$I \geq 2\sigma(I)$]	R_1 = 0.0390, wR_2 = 0.0873	R_1 = 0.0274, wR_2 = 0.0722	R_1 = 0.0327, wR_2 = 0.0890
final R indexes [all data]	R_1 = 0.0529, wR_2 = 0.0927	R_1 = 0.0324, wR_2 = 0.0758	R_1 = 0.0408, wR_2 = 0.1024
CCDC	2078044	2078045	2078046
	cocrystal or salt		
	st + 2ap	**st + bipy**	**stH$^+$ + dnba$^-$**
empirical formula	$(C_9H_9N_3O_2S_2)\cdot(C_5H_6N_2)$	$(C_9H_9N_3O_2S_2)_2\cdot(C_{10}H_8N_2)$	$(C_7H_4N_3O_6)^-\cdot(C_9H_9N_2O_2S_2)^+$
formula weight	349.43	666.81	435.37
temp (K)	173(2)	173(2)	173(2)
cryst syst	monoclinic	monoclinic	orthorhombic
space group	$P2_1/n$	$P2_1/n$	$P2_12_12_1$
a (Å)	8.4667(10)	8.4105(2)	6.0301(2)
b (Å)	18.657(2)	31.6737(7)	8.0388(2)
c (Å)	10.4390(13)	11.6376(2)	38.8995(10)
α (deg)	90	90	90
β (deg)	104.445(4)	95.1050(10)	90
γ (deg)	90°.	90	90
V (Å^3)	1596.9(3)	3087.86(11)	1885.64(9)
Z	4	4	4
density (g/cm^3)	1.453	1.434	1.534
μ (mm^{-1})	0.350	0.357	0.230
F(000)	728	1384	896
cryst size (mm^3)	0.217 × 0.298 × 0.421	0.220 × 0.179 × 0.086	0.360 × 0.228 × 0.108
2Θ range for data collection (deg)	2.971−28.309	1.871−28.367	1.047−28.389
reflns collected	27689	97333	34784
independent reflns	3944 [R(int) = 0.0602]	7707 [R(int) = 0.1220]	4662 [R(int) = 0.0646]
GOF on F^2	1.089	1.021	1.030
final R indexes [$I \geq 2\sigma(I)$]	R_1 = 0.0405, wR_2 = 0.1089	R_1 = 0.0519, wR_2 = 0.1109	R_1 = 0.0427, wR_2 = 0.0852
final R indexes [all data]	R_1 = 0.0558, wR_2 = 0.1187	R_1 = 0.1156, wR_2 = 0.1335	R_1 = 0.0596, wR_2 = 0.0978
CCDC	2078047	2078048	2078049

even with the aid of powerful computational aids and thorough cocrystal screening methods. Sometimes, a successful method for producing a specific multicomponent crystal may not be obvious.[10] Despite these challenges, the potential advantages of cocrystals and salts over their single component forms are numerous. Apart from potentially new (and hopefully improved) properties, cocrystals and molecular salts can also provide control over APIs with "problematic" polymorphism (such as the case of the infamous ritonavir), as well as provide legal advantages (intellectual property, patents, etc.).

Sulfonamides are a class of compounds used as antihypertensive, antibacterial, antiprotozoal, antifungal, and anti-inflammatory agents, nonpeptidic vasopressin receptor antagonists, and translation initiation inhibitors.[11,12] Historically, derivatives of sulfanilamide were developed as the first antibiotics, with Prontosil being the first to be marketed by

https://doi.org/10.1021/acs.cgd.1c00448
Cryst. Growth Des. 2022, 22, 98−122

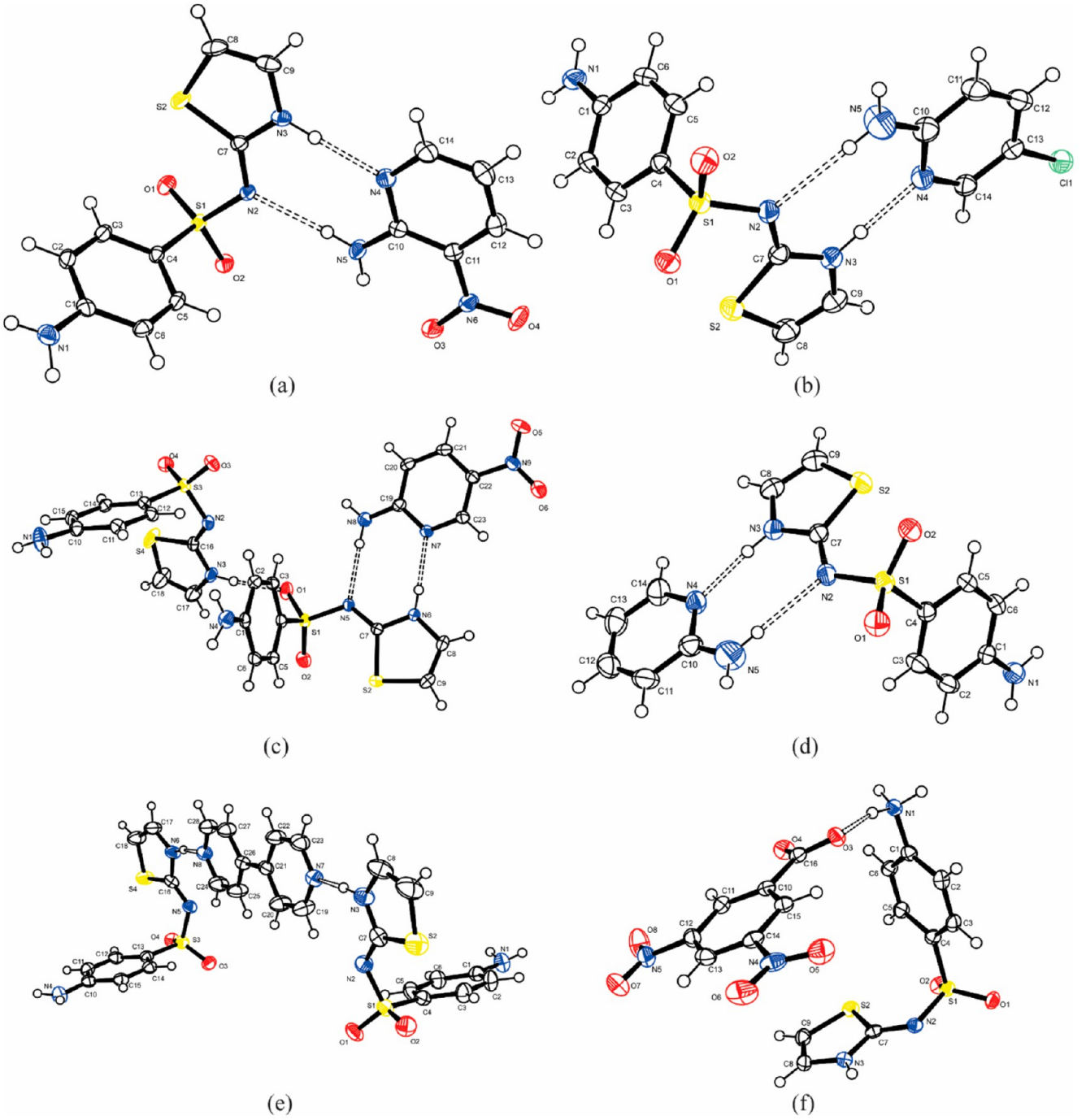


Figure 1. Ortep diagrams showing the asymmetric units of (a) **st** + **2a3np**, (b) **st** + **2a5clp** (c) **st** + **2a5np**, (d) **st** + **2ap**, (e) **st** + **bipy**, and (f) **stH**$^{+}$ + **dnba**$^{-}$.

Bayer. These compounds proved to be successful, with further development leading to new generations of sulfa drugs being marketed and sold worldwide. For this work, the second-generation drugs sulfapyridine (**sp**), sulfathiazole (**st**), and sulfamethoxazole (**sm**) were investigated (Scheme 1). Although **sp** and **st** are no longer used to treat humans, they are still used for veterinarian purposes. **sm** is commonly used in combination with trimethoprim, known as co-trimoxazole, to treat various bacterial infections, and is marketed under several different brand names such as Septrin and Bactrim. These sulfanilamide compounds consist of at least three hydrogen bond donors (the amine and sulfonamide groups) and four hydrogen bond acceptors (sulfonyl group (sulfonamide), amine and pyridyl nitrogen from heterocyclic ring). **sp**, **st**, and **sm** are highly polymorphic, with six different polymorphic forms reported for **sp**,[13−15] five polymorphs reported for **st**,[16−18] and four reported for **sm**.[19,20] Compounds that exhibit polymorphism in the solid state tend to have a higher chance of forming a cocrystal due to having structural flexibility.[21] The structural flexibility for these sulfa drugs lies in the multiple combinations of different hydrogen bond pairs that could form, as observed between the different structural features of each polymorphic form.

Prototropic tautomerism of molecules exists within the solid state, although this phenomenon has not been extensively explored as compared to studies of tautomers in solution.[22,23] From a theoretical perspective, each of the mentioned sulfa

https://doi.org/10.1021/acs.cgd.1c00448
Cryst. Growth Des. 2022, 22, 98−122

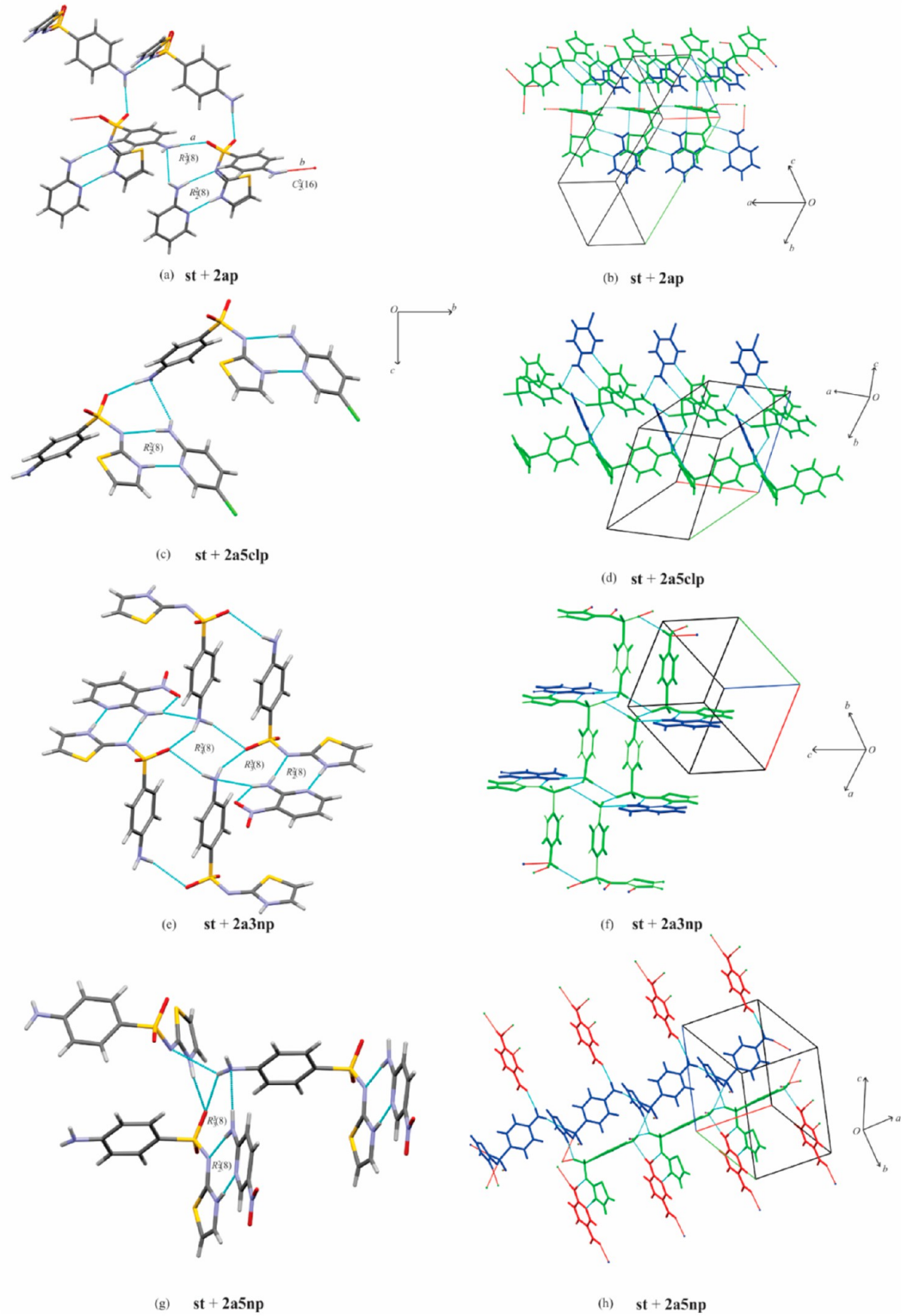


Figure 2. Crystal structures of **st + 2ap**, **st + 2a5clp**, **st + 2a3np**, and **st + 2a5np** showing (a) some of the hydrogen bond interactions present within **st + 2ap**, (b) the packing of **st + 2ap**, (c) some of the hydrogen bond interactions present within **st + 2a5clp**, (d) the packing of **st + 2a5clp**, (e) some of the hydrogen bond interactions present within **st + 2a3np**, (f) the packing of **st + 2a3np**, (g) some of the hydrogen bond interactions present within **st + 2a5np**, and (h) the packing of **st + 2a5np**.

https://doi.org/10.1021/acs.cgd.1c00448
Cryst. Growth Des. 2022, 22, 98−122

Table 2. Hydrogen Bond Table for Cocrystals and Molecular Salt Containing st

D−H···A[a]	d(D−H)	d(H···A)	d(D···A)	∠(DHA)
		st + 2a3np		
N1−H1B···O2 (i)	0.85(3)	2.24(3)	3.050(2)	158(2)
N5−H5B···N2	0.86(3)	2.16(3)	3.019(2)	177(2)
N1−H1A···O2 (ii)	0.89(2)	2.43(2)	3.116(2)	134(2)
N5−H5A···O3	0.84(3)	2.07(3)	2.662(2)	127(2)
N5−H5A···N1 (iii)	0.84(3)	2.38(3)	3.066(2)	139(2)
N3−H3A···N4	0.92(3)	1.93(3)	2.847(2)	178(2)
		st + 2a5clp		
N1−H1A···O1 (iv)	0.836(19)	2.199(19)	3.0077(16)	163(2)
N1−H1B···O2 (i)	0.865(19)	2.183(19)	3.0293(17)	166(2)
N3−H3A···N4	0.90(2)	1.87(2)	2.7721(17)	177(2)
N5−H5A···N2	0.86(2)	2.28(2)	3.134(2)	176(2)
N5−H5B···N1 (iii)	0.82(2)	2.61(2)	3.149(2)	125(2)
		st + 2a5np		
N1−H1A···O4 (iii)	0.86(3)	2.16(3)	2.994(2)	164(3)
N1−H1B···O6 (v)	0.85(3)	2.27(3)	3.102(2)	165(2)
N3−H3A···O1	0.89(2)	1.90(2)	2.7899(19)	173(2)
N4−H4A···N2 (iii)	0.92(3)	2.67(2)	3.311(2)	128(2)
N4−H4A···O1 (iii)	0.92(3)	2.62(2)	3.413(2)	145(2)
N4−H4B···O3 (vi)	0.79(2)	2.26(2)	3.029(2)	167(2)
N6−H6A···N7	0.84(2)	2.00(2)	2.8350(19)	176(2)
N8−H8A···N5	0.82(3)	2.19(3)	3.003(2)	176(2)
N8−H8B···N4 (i)	0.89(2)	2.27(2)	3.051(2)	146(2)
		st + 2ap		
N3−H3A···N4	0.88	1.85	2.730(2)	173
N5−H5B···N1 (i)	0.84(3)	2.66(3)	3.239(3)	127(3)
N5−H5A···N2	0.85(4)	2.27(4)	3.111(3)	170(4)
N1−H1A···O1 (iii)	0.88(3)	2.12(3)	2.990(3)	171(2)
N1−H1B···O2 (viii)	0.87(3)	2.12(3)	2.975(2)	169(2)
		st + bipy		
N1−H1A···O1 (xi)	0.82(4)	2.21(4)	3.017(3)	170(3)
N1−H1B···O2 (xii)	0.98(4)	1.95(4)	2.915(3)	167(3)
N3−H3A···N7	1.03(3)	1.71(3)	2.733(3)	172(3)
N4−H4A···O4 (iii)	0.84(3)	2.14(3)	2.955(3)	165(3)
N4−H4B···O1 (xiii)	0.92(3)	2.03(3)	2.935(3)	169(3)
N6−H6A···N8	0.93(3)	1.87(3)	2.784(3)	170(3)
		stH$^+$ + dnba$^-$		
N1−H1C···O1 (xiv)	0.93(4)	2.56(4)	3.167(4)	123(3)
N1−H1C···N2 (xiv)	0.93(4)	2.01(4)	2.929(4)	170(4)
N3−H3A···O4 (xv)	0.92(5)	1.83(5)	2.701(4)	157(4)
N1−H1B···O1(xvi)	0.88(4)	2.08(4)	2.939(4)	166(4)
N1−H1A···O3	1.09(4)	1.53(4)	2.603(4)	165(4)

[a]Symmetry transformations used to generate equivalent atoms: (i) $x-1, y, z$; (ii) $-x+1, -y+2, -z+2$; (iii) $x+1, y, z$; (iv) $x-1/2, -y+1/2, z+1/2$; (v) $x+1, y-1, z+1$; (vi) $-x+1, -y+1, -z+1$; (vii) $x-1/2, -y+1/2, z-1/2$; (viii) $x+1/2, -y+1/2, z-1/2$; (ix) $-x+1, -y+1, -z$; (x) $x, y, z+1$; (xi) $x-1/2, -y+3/2, z+1/2$; (xii) $x-1, y, z$; (xiii) $-x+2, -y+1, -z$; (xiv) $x, y+1, z$; (xv) $x, y-1, z$; (xvi) $x+1/2, -y+3/2, -z+1$.

drugs could exist in two different tautomeric forms: the sulfonamide and sulfonimide forms (Scheme 2). This involves a proton shift from the sulfonamide to the N-containing heterocycle. In the solid state, based on the polymorphs of **st**, **sp**, and **sm**,[13−20] **sp** and **st** favor the imidine form, while **sm** favors the amidine form. However, NMR studies of **sp** and **sm** in solution indicate that the amidine form is favored then.[24,25] Furthermore, computational studies done by Velraj and co-workers on **sp** show that in solution the amidine form is the energetically stable form, with an energy difference between the two tautomers in the range 15−25 kJ mol^{-1}, with this energy gap being dependent on the solvent polarity, with values increasing with an increase in solvent polarity.[24] **sp** has only appeared in its amidine form, polymorph VI, together with the imidine form,[14] although this metastable form converts quickly to form III over a period of time. These observations imply several things: (i) typically only one tautomer is favored in the solid state, which can differ from how the molecule would behave in solution, and (ii) during crystallization from solution a tautomeric shift occurs for **sp** (and possibly for **st** as well), shifting from the amidine to the imidine forms. It has been observed for certain sulfamethazine cocrystals the imidine tautomeric form (the higher energy form) can appear, as opposed to the more typical (lower energy) amidine form.[26−30] Such behavior has yet to be observed in a crystal structure of other structurally similar sulfa drugs in the CSD.

https://doi.org/10.1021/acs.cgd.1c00448
Cryst. Growth Des. 2022, 22, 98−122

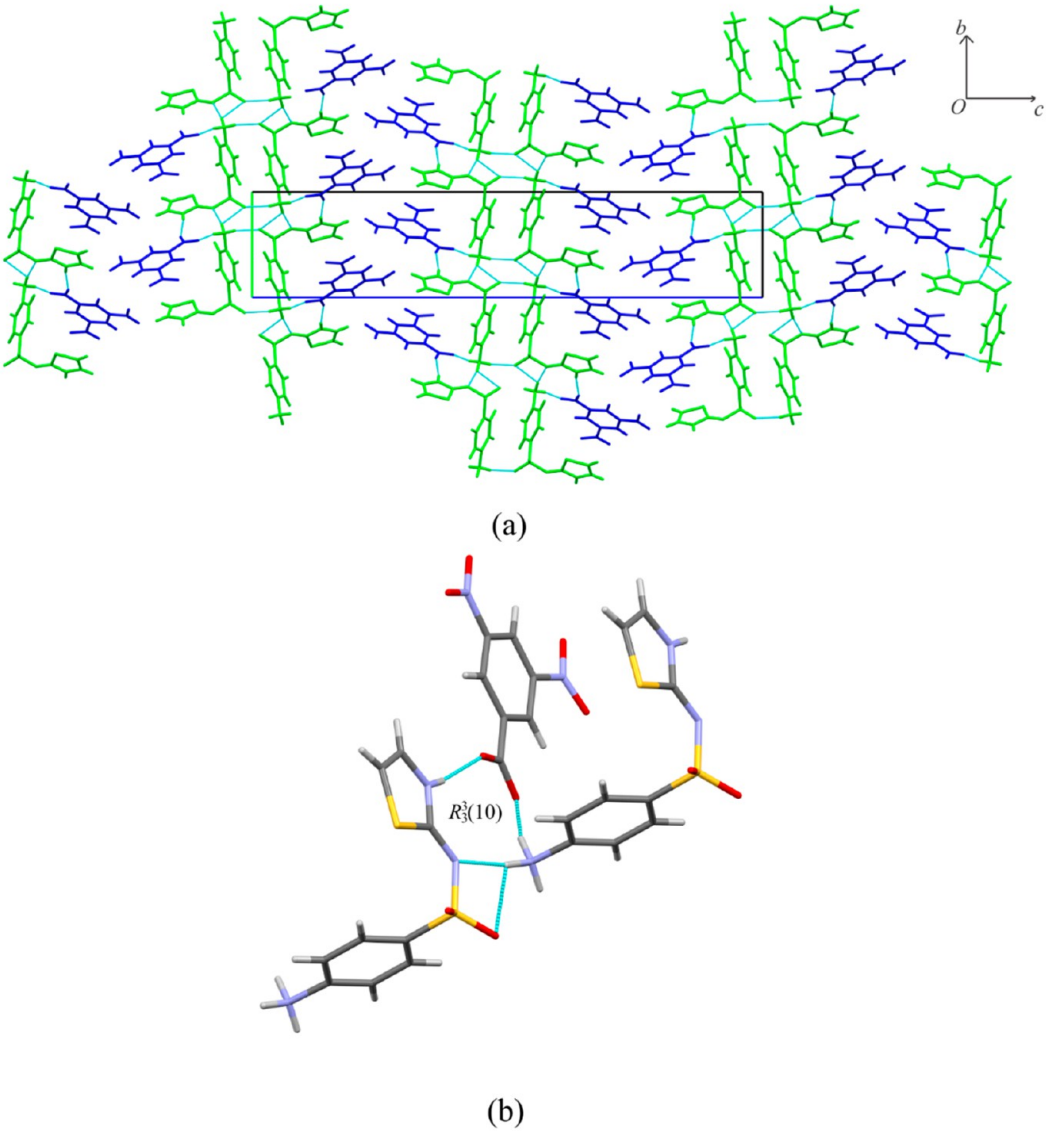


Figure 3. Crystal structure of **stH**$^+$ + **dnba**$^-$ showing (a) the packing and (b) the trimer formed.

From a crystal engineering perspective, tautomerism could provide greater flexibility to the possible hydrogen bonds that could form.[31] For example, the sulfonimide form could form an intramolecular hydrogen bond between the hydrogen attached to the nitrogen of the heterocyclic ring and the sulfone ring.[32] In multicomponent crystals, usually the coformer disrupts the formation of this intramolecular hydrogen bond, but the sulfonimide form is stabilized by other hydrogen bonds present, which depends on a case-by-case basis.

As noted before, the sulfa drugs could be ionized and form a molecular salt if a proton transfer is involved. A rule of thumb exists to predict whether a cocrystal or a molecular salt would form based on the pK_a values of a compound.[33,34] According to this rule, if the ΔpK_a (ΔpK_a = pK_a(conjugate acid of base) − pK_a(acid)) is greater than two or three, the result will be a molecular salt. If the value is less than zero, a cocrystal would form (if it forms). Results between zero and three vary, and will be dependent on the crystal system in question. For derivatives of sulfonamides, two major sites where proton transfer could occur exist: the amino group of the aniline ring and the sulfonamide group (see Scheme 3), based on the crystal structures reported in previous works.[35−38] For these sulfa drugs there does not seem to be any particular trend or pattern that could be used to verify which hydrogen bond site would undergo hydrogen bonding or proton transfer between the sulfa drug and conformer, and from the literature,[33−36] it seems the site preferred depends on the crystal system in question.

The purpose of this work is to explore the scope of the multicomponent landscape of **st**, **sp**, and **sm** and expand the library of known multicomponent crystals of said compounds. In particular, we wanted to expand the number of cocrystals or molecular salts of **sp**, as previously reported instances of multicomponent crystals consisting of **sp** are limited in most cases to solvates.[39,40] This work also includes an attempt to obtain multicomponent crystals containing different tautomers of **st**, **sp**, and **sm**, that if successful could yield some insight in solid-state tautomerism of sulfa drugs. Twenty-five coformers were chosen based on successes with other sulfonanilamide derivatives, having structural similarity with each other (isomers), having robust and well-defined hydrogen bond motifs, or being API/GRAS compounds.[26,29,35,41−43] The coformers chosen are listed and represented in Scheme 4.

https://doi.org/10.1021/acs.cgd.1c00448
Cryst. Growth Des. 2022, 22, 98−122

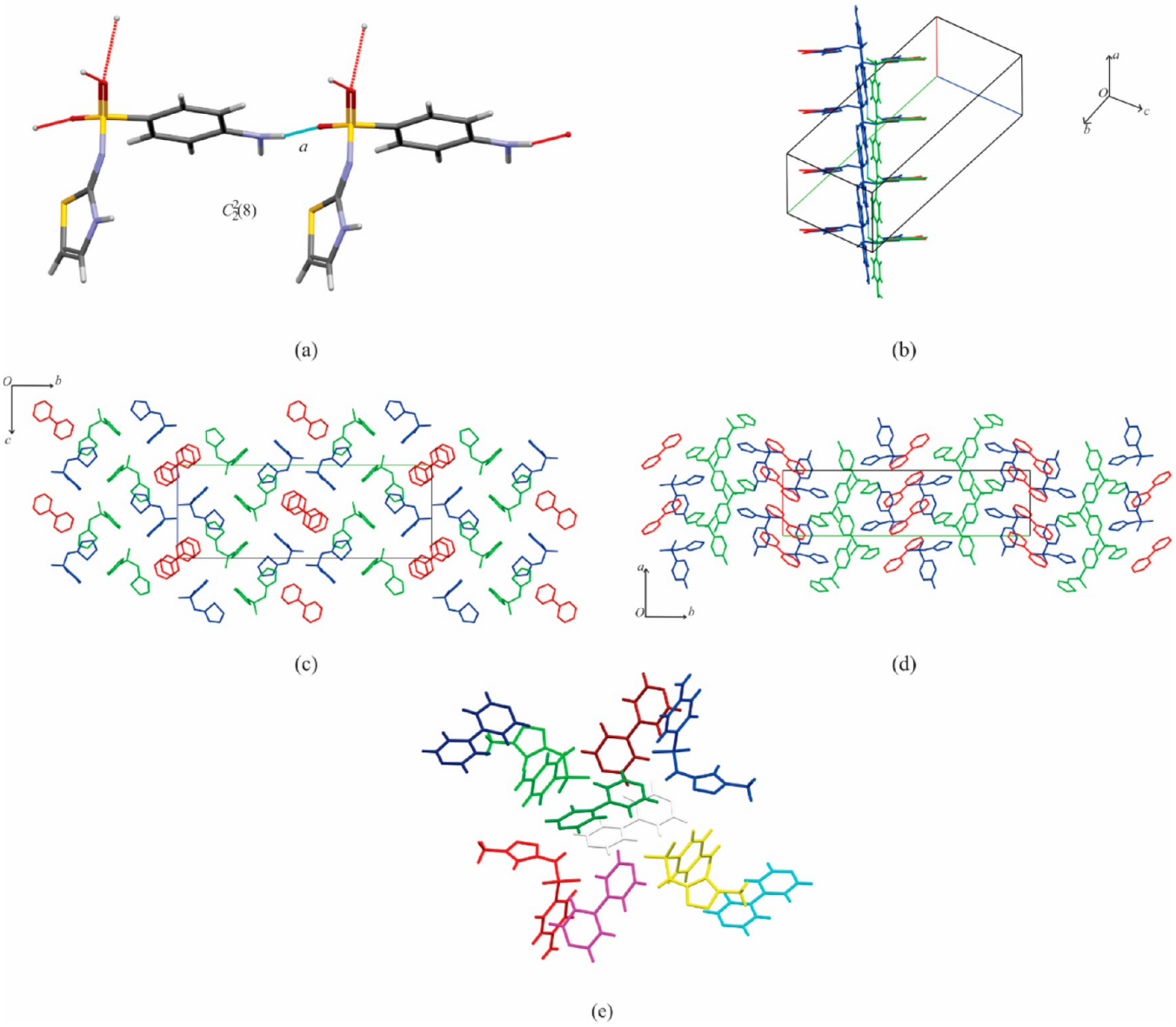


Figure 4. Crystal structure of **st + bipy** showing the (a) the chain hydrogen bond motif, (b) a portion of the planar stacks of **st + bipy** (with **bipy** in red and **st** in blue and green), the packing viewed down the (c) *a*-axis and (d) *c*-axis, and (e) the asymmetric unit of **sm + bipy**.

EXPERIMENTAL SECTION

4,4′-Bipyridine was purchased from Alfa-Aesar. All other compounds used were purchased from Sigma-Aldrich. All materials and solvents were used as is without further purification. In order to obtain a multicomponent crystal consisting of the sulfa drug and corresponding coformer, both mechanochemical and solution based methods were used to see which method would be the most effective. Mechanochemical methods have the advantage of not relying on compatible solubilities of the components, as well as being "solvent-free".

For solution based synthesis, the typical procedure includes dissolving both the sulfa drug and the respective coformer in the respective solvent system (for the mass scale used in this work, 5 mL of the solvent system was used) and heating until no solid remained. This solution would then be kept slightly opened in a dark room for several days until crystals formed. Several different solvents, solvent combinations, and molar ratios were used. The solvent system used to grow successful multicomponent crystals is listed in Table S2 of the Supporting Information. Heating was required in most cases, as the sulfa drugs did not readily dissolve in the chosen solvent at room temperature. Various molar ratios of sulfa drug to coformer were used, including 1:1, 2:1, and 1:2, but a 1:1 molar ratio of sulfa drug/coformer was found to be the most prominent ratio in crystal structures of various sulfa drug multicomponent crystals.

For dry mechanochemical methods, the same amounts of the sulfa drug and the respective coformer used for the solution-based synthesis was used (see again Table 2 of the Supporting Information) and were placed in a Teflon-coated milling jar (18 mm diameter, 65 mm length) with two steel balls (5 mm diameter). The jars were then placed on a Retsch MM200 vibratory mill and were milled at 20 Hz for 60 min, with a 5 min break after 30 min. This break was to prevent overheating of the mill. As part of this investigation, a few drops (~0.05 mL) of the 1:1 vol/vol acetonitrile/ethanol mixture was added to some batches to determine if this would increase the chance of obtaining a multi-component crystal.

Single Crystal X-ray Diffraction (SC-XRD). The Bruker D8 VENTURE PHOTON CMOS area detector diffractometer, equipped with a graphite monochromated Mo Kα_1 sealed tube (50 kV, 30 mA), was used to collect all the intensity data. The program SAINT+, v. 6.02[44] was used to integrate the data, and the program SADABS[23] was used to make empirical absorption corrections. Space group assignments were made using XPREP[44] on all compounds. In all cases,

https://doi.org/10.1021/acs.cgd.1c00448
Cryst. Growth Des. 2022, 22, 98−122

Table 3. Summary of Crystallographic Data for Cocrystals and Molecular Salt Containing sm

	cocrystal or salt			
	sm + 4cnp	sm + 3cnp	$sm^- + 4dmapH^+$	sm + dnba
empirical formula	$(C_{10}H_{11}N_3O_3S)\cdot(C_6H_4N_2)$	$(C_{10}H_{11}N_3O_3S)\cdot(C_6H_4N_2)$	$(C_7H_{11}N_2)^+\cdot(C_{10}H_{10}N_3O_3S)^-$	$(C_{10}H_{10}N_3O_3S)\cdot(C_7H_4N_2O_6)$
formula weight	357.39	357.39	375.45	310.27
temp (K)	173(2)	173(2)	173(2)	173(2)
cryst syst	monoclinic	monoclinic	monoclinic	monoclinic
space group	$P2_1/n$	$P2_1/n$	$P2_1/n$	$P2_1/c$
a (Å)	7.1902(8)	9.3371(9)	7.99300(10)	10.9019(4)
b (Å)	20.031(2)	16.2431(16)	17.9943(3)	14.8066(6)
c (Å)	12.2966(14)	11.6029(11)	12.7173(2)	12.4850(5)
α (deg)	90	90	90	90
β (deg)	105.870(4)	110.264(3)	101.2510(10)	91.6280(10)
γ (deg)	90	90	90	90
V (Å^3)	1703.5(3)	1650.8(3)	1793.96(5)	2014.52(14)
Z	4	4	4	4
density (g/cm^3)	1.393	1.438	1.390	1.534
μ (mm^{-1})	0.216	0.223	0.209	0.224
$F(000)$	744	744	792	960
cryst size (mm^3)	0.249 × 0.235 × 0.125	0.562 × 0.539 × 0.447	0.384 × 0.331 × 0.272	0.842 × 0.389 × 0.346
2Θ range for data collection (deg)	3.116−25.799	2.252−28.424	1.987−28.304	2.807−28.339
reflns collected	21143	29688	63765	87447
independent reflns	3250 [R(int) = 0.1049]	4150 [R(int) = 0.0402]	4464 [R(int) = 0.0368]	5009 [R(int) = 0.0234]
GOF on F^2	1.142	1.059	1.025	1.038
final R indexes [$I \geq 2\sigma(I)$]	R_1 = 0.0808, wR_2 = 0.1861	R_1 = 0.0339, wR_2 = 0.0887	R_1 = 0.0346, wR_2 = 0.0903	R_1 = 0.0328, wR_2 = 0.0859
final R indexes [all data]	R_1 = 0.1032, wR_2 = 0.1974	R_1 = 0.0370, wR_2 = 0.0914	R_1 = 0.0446, wR_2 = 0.0971	R_1 = 0.0357, wR_2 = 0.0882
CCDC	2078040	2078043	2078041	2078042

the structures were solved in the WinGX Suite of programs[45] by direct methods using SHELXS-97[46] and refined using full-matrix least-squares/difference Fourier techniques on F^2 using SHELXL-97.[46] All non-hydrogen atoms were refined anisotropically. Thereafter, all hydrogen atoms attached to N or O atoms, except where otherwise stated, were located in the difference Fourier map, and their coordinates and isotropic thermal displacement parameters were refined freely. Diagrams and publication material were generated using ORTEP-3[47] and Mercury.[48]

Powder X-ray Diffraction (PXRD). Powder X-ray diffraction data for all compounds were measured at 293 K on a Bruker D2 Phaser diffractometer, which employs a sealed tube Co X-ray source (λ = 1.78896 Å) operating at 30 kV and 10 mA and LynxEye PSD detector in Bragg−Brentano geometry. Powder patterns for each sample are present in the Supporting Information, where the experimentally obtained data is compared to the calculated patterns obtained from the SC-XRD data.

Thermal Analysis (DSC and TGA). Differential scanning calorimetry data were collected using a Mettler Toledo DSC 3 with aluminum pans under nitrogen gas (flow rate = 10 mL/min). Exothermic events were shown as peaks. Samples were heated and cooled to determine melting points as well as any additional phase transitions. The temperature and energy calibrations were performed using pure indium (purity 99.99%, mp 156.6 °C, heat of fusion 28.45 J g^{-1}) and pure zinc (purity 99.99%, mp 479.5 °C, heat of fusion 107.5 J g^{-1}). Samples were heated to 250 °C from 25 °C before being cooled back down at 25 °C at a heating or cooling rate of 10 °C/min.

Thermogravimetric analysis (TGA) was done using a PerkinElmer TGA 6000 thermogravimetric analyzer using high-purity nitrogen at a heating rate of 10 °C/min and gas flow rate of 10 mL/min.

FTIR Analysis. FTIR spectra were collected using the Bruker Alpha II model equipped with the Eco-ATR sampling module. A small amount of the sample of interest was placed onto the ATR crystal. Spectra were measured from 600 to 4000 cm^{-1} range, resolution 4 cm^{-1}, with 24 scans per sample. Background noise was subtracted. The ATR-FTIR was in a room with conditioning at 22 °C. After spectral acquisition, the ATR crystal was cleaned using isopropanol.

Cambridge Structural Database Analysis. The Cambridge Structural Database (CSD)[49] was used to analyze and determine any previous records of crystal structures that include **sp**, **st**, or **sm**. The only restriction was that entries must be classified as being organic. Mercury[48] was used to inspect the crystal structures.

RESULTS AND DISCUSSION

Twenty-three coformers were chosen and used in an attempt to synthesize cocrystals and molecular salts containing **st**, **sm**, and **st**. Fifteen cocrystals and molecular salts are presented, of which only 13 were new. Five cocrystals and one molecular salt containing **st**, three cocrystals and one molecular salt containing **sm**, and four cocrystals and one molecular salt containing **sp** were synthesized and characterized. These multicomponent crystals are presented together according to the sulfa drug present (ordered **st**, **sm**, and the **sp**) and similarity of the coformer (for example, multicomponent crystals containing **2a3np**, **2a5np**, and **2a5clp** were described and grouped together with **2ap** since they are derivatives of **2ap**). It should be noted that the following combinations were obtained but are not presented in detail in this work since they have been reported and described in the literature previously: **st** + **4nba**,[43] **sm** + **4ap**,[35] **sm** + **bipy**,[41] **sm** + **2hp**,[41] and **sp** + **4nba**.[50] However, the crystal structures of **st** + **2ap** and **st** + **2a5clp** were presented in another work recently;[51] in this case, we present an alternative method for obtaining the same crystal form and additional characterization such as FTIR, TGA, and DSC data, which was not included in the previous work.

Where relevant, we will denote the abbreviations for a molecular salt of the sulfa drug as XH^+ in order to differentiate and emphasize the formation of the ionic form over the neutral form. In which case, the ion coformer will contain a negative charge at the end of its usual abbreviation.

https://doi.org/10.1021/acs.cgd.1c00448
Cryst. Growth Des. 2022, 22, 98−122

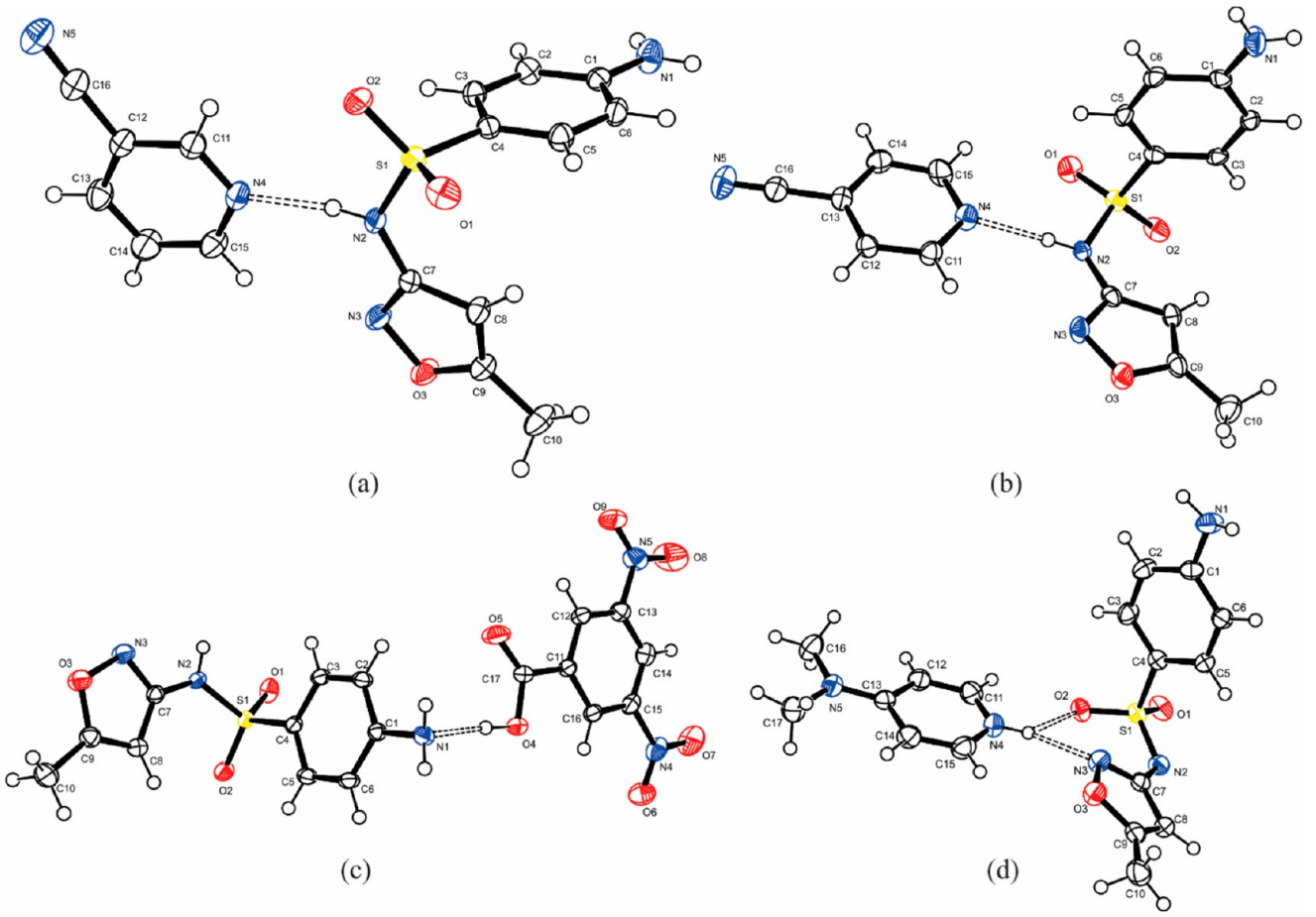


Figure 5. Ortep diagram showing the asymmetric units of (a) **sm** + **3cnp**, (b) **sm** + **4cnp**, (c) **sm** + **dnba**, and (d) $\mathbf{sm}^{-}$ + $\mathbf{4dmapH}^{+}$.

Results of Mechanochemical Syntheses. For this work, both dry milling and liquid assisted grinding (LAG) was used. In all of the dry milling attempts, no noticeable change was observed in the PXRD patterns of the mixtures, indicating that only a physical mixture of the components was obtained and no new crystalline phases of multicomponent complexes. For the LAG experiments, we obtained the same multicomponent crystals of **st** and **sp** as the ones obtained from traditional solvent evaporation methods, as the PXRD peaks matched for the respective mixtures. For **sm**, the addition of solvent made no difference and, again, only physical mixtures were obtained. We conclude that dry mechanochemical synthesis is not feasible but some solvent is necessary for obtaining the multicomponent crystals in mechanochemical methods for the sulfa drugs **st** and **sp**, which are presented below.

Crystal Structures of Cocrystals st + 2ap, st + 2a3np, st + 2a5np, and st + 2a5clp. **st** formed four separate cocrystals with **2ap**, **2a3np**, **2a5np**, and **2a5clp**, forming yellow needles, orange needles, yellow needles, and colorless needles, respectively (Table 1). As noted by Wojnarska et al. the crystal structures of **st** + **2ap** and **st** + **2a5clp** are isostructural.[51] **st** + **2a3np** and **st** + **2a5np** crystallize in the same space group, $P\bar{1}$. The asymmetric unit for each of these is one molecule each of **st** and the respective pyridine, with the exception of the crystal structure of **st** + **2a5np**, where two molecules of **st** are present instead, giving a 2:1 molar ratio of **st** to **2a5np** (Figure 1a–d). The hydrogen H3A in the crystal structure of **st** + **2ap** was placed geometrically with respect to N3, since it could not be located precisely in the Fourier map. In each case, the respective pyridine forms a hydrogen bond ring motif, $R_2^2(8)$, with the sulfonamide group of **st** (N5–H5B···N2 and N3–H3A···N4 for **st** + **2a3np**, N5–H5A···N2 and N3–H3A···N4 for **st** + **2a5clp** and **st** + **2ap**, N8–H5A···N2 and N6–H6A···N7 for **st** + **2a5np**), as seen in Figure 2a,c,e,g (see Table 2 for bond distances and angles). Other hydrogen bonds formed in these structures begin to deviate between the different crystal structures. For example, with the exception of **st** + **2ap** and **st** + **2a5clp**, the remaining hydrogen on the amino group (H8B for **st** + **2a5np** and H5A for **st** + **2a3np**) forms a hydrogen bond to a neighboring **st** molecule. For **st** + **2ap** and **st** + **2a5clp**, the aniline group of **st** forms a chain hydrogen bond motif with the sulfone group, with hydrogen bond pairs N1–H1A···O1 and N1–H1B···O2 in both structures. This is contrasted with the structures of **st** + **2a3np** and **st** + **2a5np**, where the sulfone group forms part of a series of hydrogen bond ring motifs in the former (see Figure 2e) or in the latter a nitro group and thiazole ring form a hydrogen bond to the sulfone group (N1–H1B···O6 and N3–H3A···O1 respectively). The packing of **st** + **2ap**, **st** + **2a5np**, and **st** + **2a5clp** is made up of a series of 1D tapes of **st** molecules, with the **2ap** derivatives separating the tapes (Figure 2b,d,h). The packing of **st** + **2a3np** is made up of a layers of **2a3np** and the thiazole portion of **st** with the aniline portion separating said layers, as observed in Figure 2f. Overall the structures of **st** + **2ap** and the derivatives of **2ap** share a common set of hydrogen bonds but can diverge when in the presence of other groups that could hydrogen bond (the nitro

https://doi.org/10.1021/acs.cgd.1c00448
Cryst. Growth Des. 2022, 22, 98–122

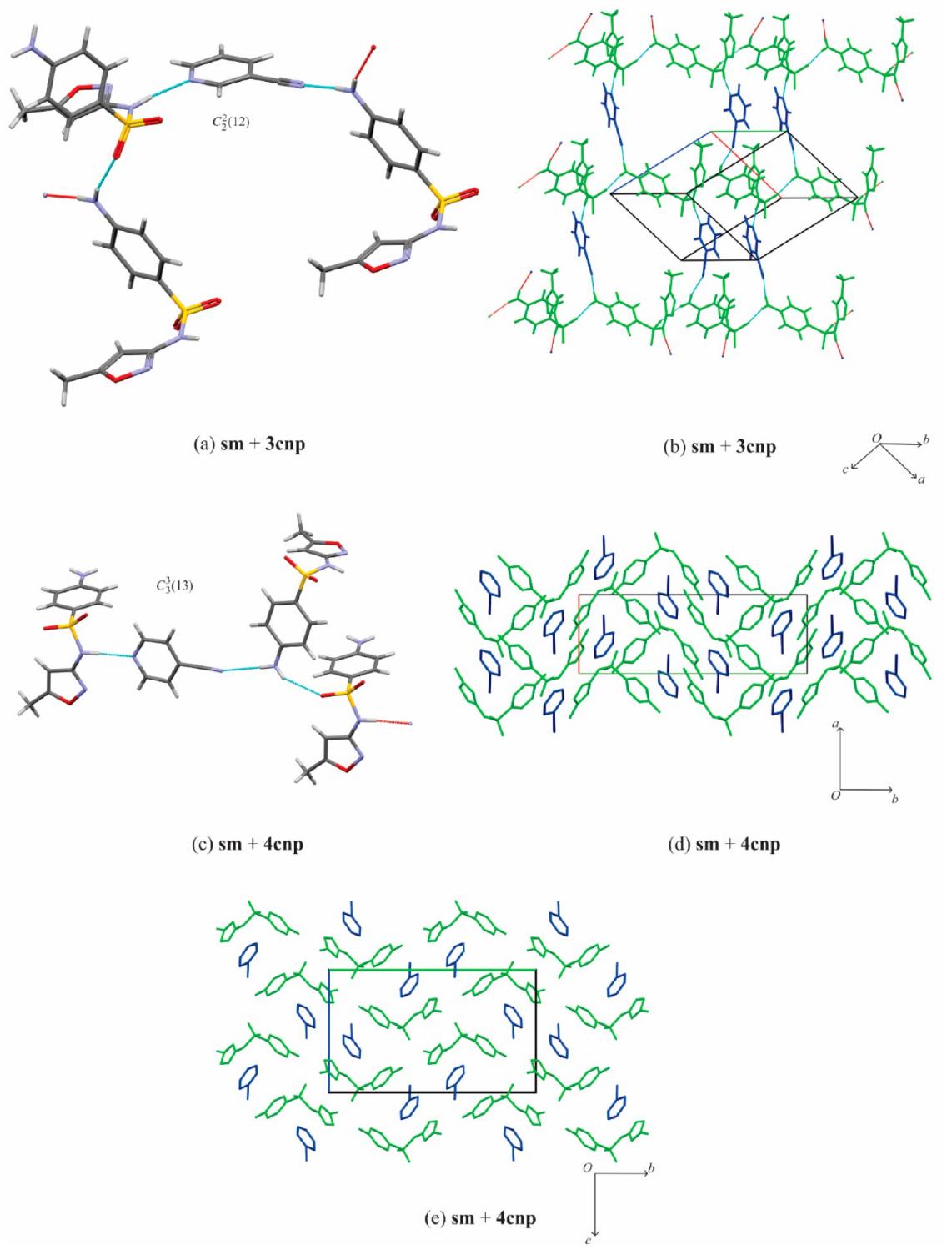


Figure 6. Crystal structure diagrams showing (a) the chain hydrogen bond motif present in **sm + 3cnp**, (b) the packing of **sm + 3cnp**, (c) the chain hydrogen bond motif present in **sm + 4cnp**, (d) the packing of **sm + 4cnp** viewed down the *c*-axis (with hydrogens omitted for clarity), and (e) the packing of **sm + 4cnp** viewed down the *a*-axis (with hydrogens omitted for clarity).

group), which in this case expectedly also results in different crystal structure packing.

Crystal Structure of Molecular Salt stH$^+$ + dnba$^-$. In all our attempts to obtain cocrystals or molecular salts containing **st** and benzoic acid (or one of its derivatives), we were only able to obtain a single molecular salt successfully with 3,5-dintrobenzoic acid (**dnba**). This molecular salt crystallized as yellow prisms. The asymmetric unit consists of one ion of each **stH$^+$** and **dnba**, and it crystallizes into the $P2_12_12_1$ space group. A proton transfer occurs between the carboxylic acid of **dnba** and the aniline group of **st**. A trimer consisting of two ions of **st** and one ion of **dnba**, with a $R_3^3(10)$ ring motif, is formed (Figure 3b). This motif is formed from both aniline rings forming two hydrogen bonds: one to the sulfonamide group of **st** (N1−H1C···N2) and one to

https://doi.org/10.1021/acs.cgd.1c00448
Cryst. Growth Des. 2022, 22, 98−122

Table 4. Hydrogen Bond Geometries for Cocrystals and Molecular Salt Containing sm

D−H···A[a]	d(D−H)	d(H···A)	d(D···A)	∠(DHA)
		sm + 3cnp		
N1−H1A···O1 (i)	0.848(19)	2.242(19)	3.0682(16)	165(2)
N1−H1B···N5 (ii)	0.854(18)	2.315(18)	3.1451(19)	164(2)
N2−H2A···N4	0.895(19)	1.930(19)	2.8168(15)	170(2)
		sm + 4cnp		
N1−H1A···N5 (iii)	0.82(5)	2.29(5)	3.111(6)	178(5)
N1−H1B···O2 (iv)	0.79(5)	2.38(5)	3.050(5)	144(4)
N2−H2···N4	0.86(5)	1.98(5)	2.839(5)	178(4)
		sm$^-$ + 4dmapH$^+$		
N1−H1A···O2 (v)	0.88(2)	2.29(2)	3.0820(17)	150(2)
N1−H1B···N2 (vi)	0.91(2)	2.07(2)	2.9711(18)	171(2)
N4−H4A···N3	0.88(2)	2.05(2)	2.8603(18)	152(2)
N4−H4A···O2	0.88(2)	2.33(2)	2.9173(17)	124(2)
		sm + dnba		
N1−H1A···O6 (viii)	0.895(18)	2.296(18)	3.1365(14)	156(2)
N1−H1B···O8 (vii)	0.875(19)	2.182(19)	3.0261(16)	161(2)
O4−H4A···N1	0.95(2)	1.74(2)	2.6839(14)	175(2)
N2−H2A···N3 (ix)	0.841(18)	2.078(18)	2.9131(15)	172(2)
N1−H1A···O6 (viii)	0.895(18)	2.296(18)	3.1365(14)	156(2)

[a]Symmetry transformations used to generate equivalent atoms: (i) $x - 1/2, -y + 3/2, z + 1/2$; (ii) $x - 3/2, -y + 3/2, z - 1/2$; (iii) $x + 3/2, -y + 3/2, z - 1/2$; (iv) $x + 1/2, -y + 3/2, z + 1/2$; (v) $x - 1, y, z$; (vi) $x - 1/2, -y + 1/2, z + 1/2$; (vii) $-x + 1, y - 1/2, -z + 3/2$; (viii) $-x + 2, y - 1/2, -z + 3/2$; (ix) $-x + 1, -y + 1, -z$.

the carboxylate group of **dnba** (N1−H1A···O3). This ring is then completed with the thiazole ring of **st** forming a hydrogen bond to the carboxylate of **dnba** (N3−H3A···O4). **st** molecules are also connected with neighboring **st** molecules with a hydrogen bond formed between the sulfone group and aniline group (N1−H1B···O2). The packing of **st** + **dnba** forms a 1D tape structure along the *b*-axis with **st** ions located in the inner portion of the tape (shown in green in Figure 3a) and the **dnba** molecules located along the edge (shown in blue in Figure 3a).

Crystal Structure of st + bipy. **st** forms a cocrystal with **bipy**, crystallizing as yellow needles. The asymmetric unit consists of two molecules of **st** and one molecule of **bipy**, and it crystallizes into the $P2_1/n$ space group. The two rings of **bipy** are relatively planar with respect to each other, with a torsional angle of 7.3(4)° (C20−C21−C25−C26). **bipy** molecules exhibit $\pi\cdots\pi$ stacking with other nearby **bipy** molecules. The two molecules of **st** form a hydrogen bond to **bipy** from the thiazole ring of both **st** molecules to each pyridyl nitrogen of **bipy** (N3−H3A···N7 and N6−H6A···N8). The aniline group of **st** forms a hydrogen bond to the oxygen of the sulfone group of a neighboring **st** molecule (N4−H4B···O1, N1−H1B···O2), which effectively forms a chain hydrogen bond motif (Figure 4a). The packing of **st** + **bipy** consists of a planar layers of the aniline rings of **st**, with the **bipy** molecules and the thiazole portion of **st** sitting perpendicular to this layer (Figure 4b). These planar layers form rows of **bipy** molecules separated by the **st** molecules (Figure 4c,d).

One structure to compare **st** + **bipy** to in particular is that of **sm** + **bipy**, reported by Alsubaie et al.[41] **sm** + **bipy** (refcode **QIBCIQ**) was reported to crystallize in the *P*1 space group, although the authors noted that it could have been the $P\bar{1}$ if an extensive disorder model was used. The resulting structure had four molecules of **sm** and six molecules of **bipy** (Figure 4e) in the asymmetric unit. The torsional angles for the rings of the **bipy** molecules in **sm** + **bipy** range from 10° to 40° with at least four **bipy** molecules in the 20° to 30° range. Accordingly, the energy related to this torsional rotation tends to be at the lowest in the 30° to 50° range and increases when out of this range. The small torsional angle of **bipy** in **st** + **bipy** can most likely be a result of the formation of $\pi\cdots\pi$ stacking being more favorable, which can offset the high energy associated with this low torsional angle. Despite **sm** and **st** being similar molecules, a significant difference in the crystal structures of **sm** + **bipy** and **st** + **bipy** was observed.

Crystal Structures of the Cocrystals of sm + 3cnp and sm + 4cnp. **sm** forms two separate cocrystals with **3cnp** and **4cnp**, crystallizing as colorless plates and colorless needles, respectively (Table 3). The asymmetric unit in each cocrystal consists of one molecule of **sm** and one molecule of **3cnp** or **4cnp** (Figure 5), and both cocrystals crystallize in the $P2_1/n$ space group. In each structure, the cyanopyridine molecule acts as a bridge between two **sm** molecules by forming a hydrogen bond between the pyridyl nitrogen and sulfonamide group's hydrogen (N2−H2···N4 for both structures) and the nitrile group to the aniline group (N1−H1B···N5 for **sm** + **3cnp** and N1−H1A···N5 for **sm** + **4cnp**), as seen in Figure 6a,c (see Table 4 for bond distances and angles). These interactions along with the hydrogen bond between the aniline group and an oxygen atom from the sulfonamide group forms a chain hydrogen bond motif (Figure 6a,c). However, a difference arises between **sm** + **3cnp** and **sm** + **4cnp**: there is an additional **sm** molecule in the chain hydrogen bond motif of **sm** + **4cnp** (Figure 6a). The packing between the two structures are distinctively different. The structure of **sm** + **3cnp** forms a ladder-like structure, with the rungs being made from **3cnp** molecules and the oxazole ring of **sm** and the aniline rings form the sides (Figure 6b), while **sm** molecules in **sm** + **4cnp** form wave-like rows with rows of **4cnp** molecules between them (Figure 6d,e).

Crystal Structure of sm + dnba. **sm** forms a cocrystal with **dnba**, crystallizing as yellow needles. The asymmetric unit consists of one molecule of each **sm** and **dnba**, and it crystallizes into the $P2_1/c$ space group. **sm** molecules form homodimers via the ring hydrogen bond motif $R_2^2(8)$, which has

https://doi.org/10.1021/acs.cgd.1c00448
Cryst. Growth Des. 2022, 22, 98−122

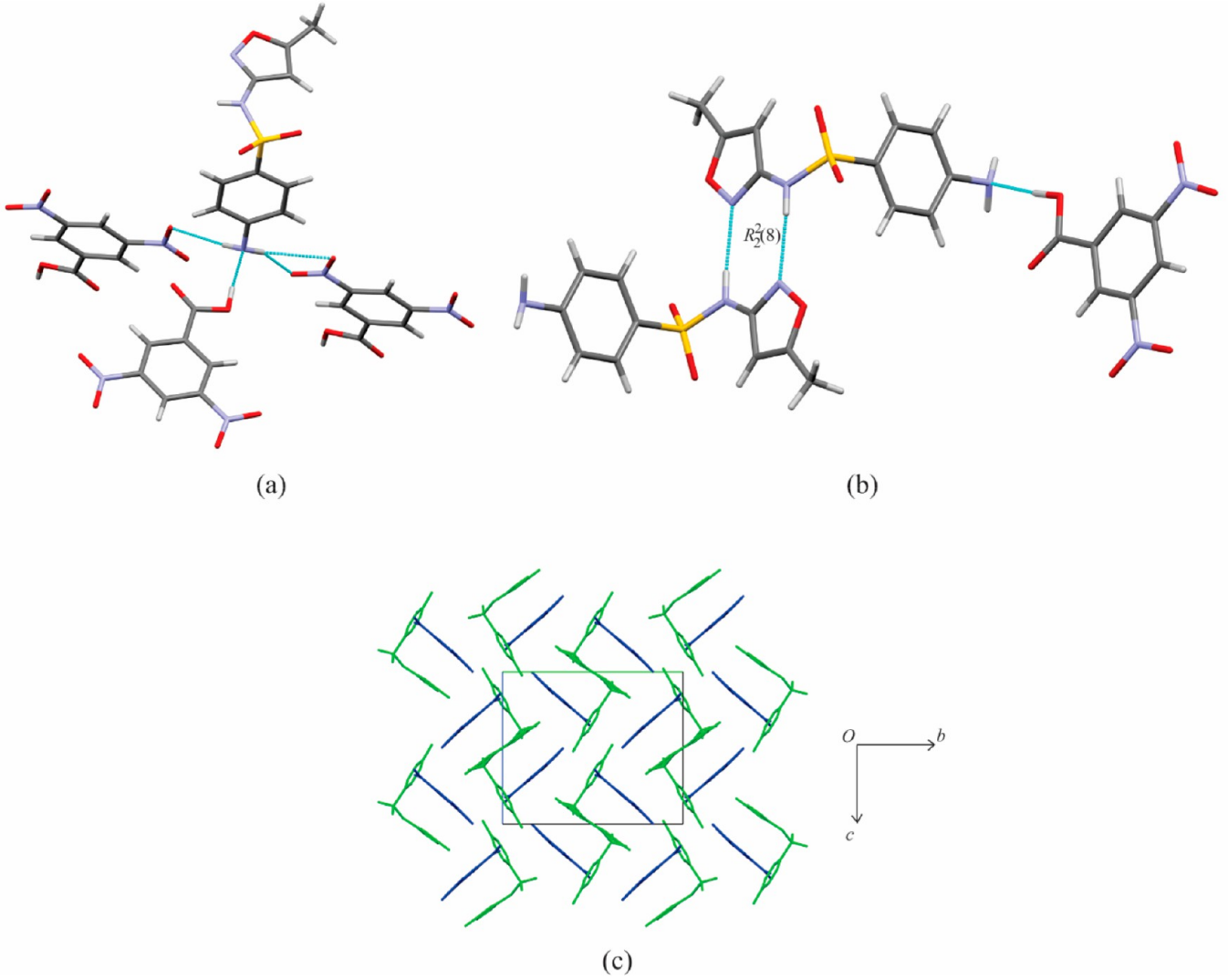


Figure 7. Crystal structure of **sm** + **dnba** showing (a) hydrogen bond interactions surrounding the amino group of the aniline ring, (b) the **sm** dimer, and (c) the packing as viewed down the *a*-axis.

been observed in polymorph II of **sm**[52] (Figure 7b). This differs significantly from the trimer formed in **st** + **dnba**. **dnba** forms a hydrogen bond with the aniline group of **sm** (synthon iii). The bond angle H1A−N1−H1B is 109.3°, which makes the amino group adopt a more pyramidal geometry over the more planar geometry observed in the other structures reported here. However, based on the bond lengths of the carboxylic acid of **dnba** (C17−O4 = 1.3169(14) Å and C17−O5 = 1.2041(15) Å), we conclude that the proton has not been transferred. Comparing **sm** + **dnba** with **st** + **dnba**, the hydrogen bonding site is the same, although a proton transfer has occurred in **stH**$^+$ + **dnba**$^-$. According to Table 5 below, the aniline group in **st** is more basic than that of **sm**, with a pK_a difference between the two being 0.3. In essence this makes it less likely for the proton to transfer from **dnba** to **sm** according to the pK_a rule.[33,34] The aniline group forms part of a chain hydrogen bond motif ($C_2^2(10)$) involving N1−H1B···O8 and O4−H4···N1. This result is an example of a saturated hydrogen bonding site, that is, all possible hydrogen bonding pairs are present surrounding the amino group of the aniline ring (Figure 7a). It is interesting to note that there are no hydrogen bonds between the sulfone group and the aniline

Table 5. List of the pK_a Values of Compounds Used for This Work[a]

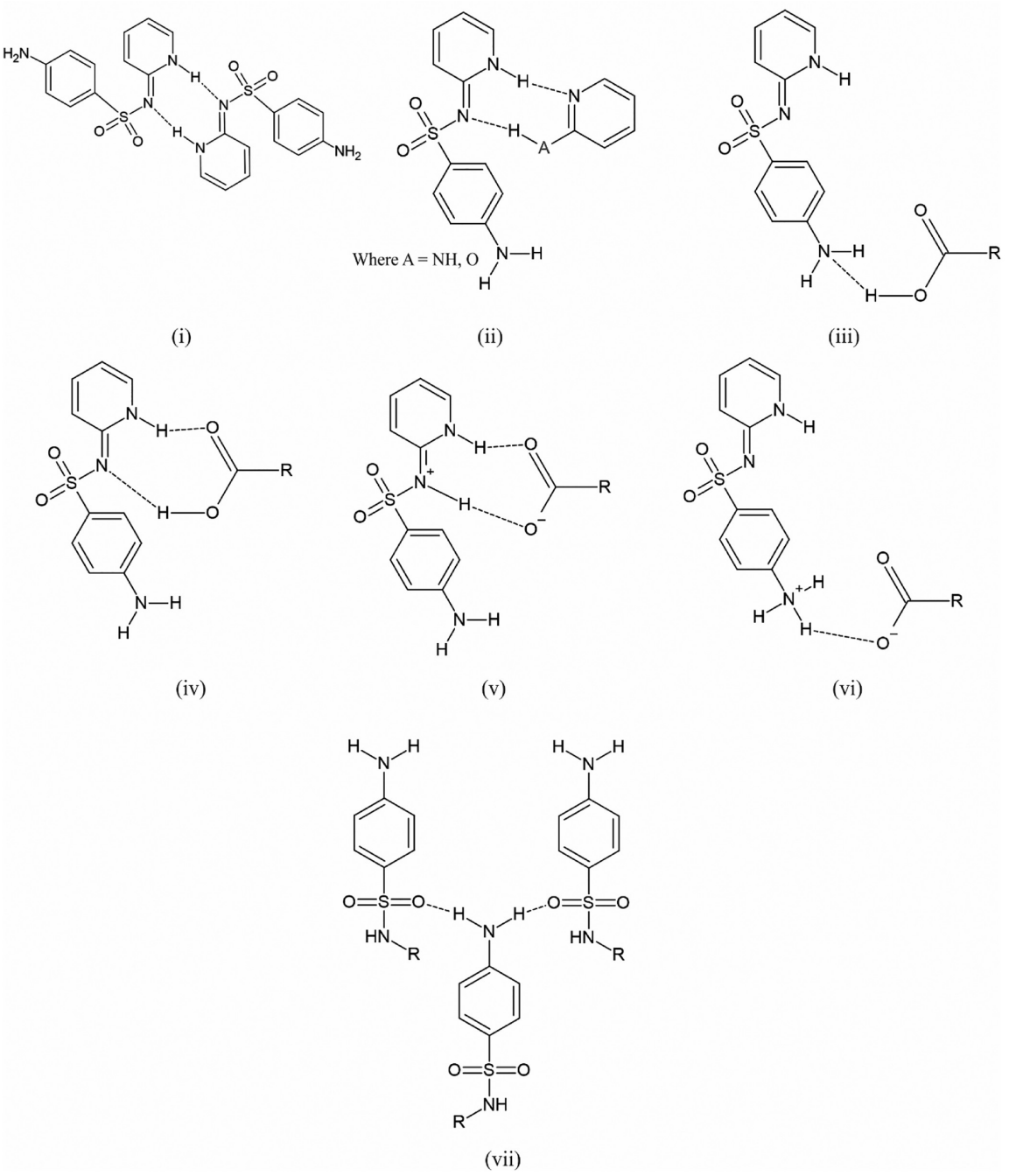
compd	pK_{a1}	pK_{a2}
st	2.19	7.24
sp	2.13	8.43
sm	1.83	5.60
2ap	6.67	
2a5clp	4.67	
2a3np	2.40	
2a5np	2.82	
bipy	3.27	
3cnp	1.78	
4cnp	1.92	
dnba	2.77	
2c4n	2.04	
dmap	9.52	

[a]pK_a values were obtained from *Scifinder*.[55]

(Scheme 5, synthon vii), which makes this structure rather unusual with respect to the other structures reported here as well as those reported in the literature. The packing consists of

https://doi.org/10.1021/acs.cgd.1c00448
Cryst. Growth Des. 2022, 22, 98−122

Scheme 5. List of Synthons Expected to Form for This Work



1D wave-like tape structures of **sm** with **dnba** interlocked between sections of **sm** (Figure 7c).

Crystal Structure of Molecular Salt sm$^-$ + 4dampH$^+$. **sm**$^-$ forms a molecular salt with **4dampH**$^+$, crystallizing as colorless prisms. The asymmetric unit consists of one ion of each **sm**$^-$ and **4dampH**$^+$, crystallizing in the $P2_1/n$ space group. A bifurcated hydrogen bond forms between H1B and O1 and O2 of **sm**$^-$ (Figure 8a), which results in the formation of a ribbon motif consisting of **sm**$^-$ ions connected to each other via these chain hydrogen bond motifs. The remaining aniline hydrogen H1A forms a hydrogen bond to the oxazole ring of **sm**$^-$, which connects parallel chains to each other. A proton is transferred from the sulfonamide/oxazole ring of **sm**$^-$ to the pyridine ring of **4dampH**$^+$, which contrasts to the other molecular salts presented in this work. The transferred proton forms part of a set of bifurcated hydrogen bonds to the sulfone group (N4−H4A···O2) and to the nitrogen of the oxazole ring (N4−H4A···N3) (Figure 8a). This bifurcated hydrogen bond connects **4dampH**$^+$. The packing of **sm**$^-$ + **4dmap**$^+$ resembles channels with its walls made up of **sm**$^-$ with **4dampH**$^+$ sitting within them (Figure 8b).

Crystal Structures of Cocrystals sp + 2ap, sp + 2a3np, sp + 2a5np, and sp + 2a5clp. **sp** formed four separate cocrystals with **2ap**, **2a3np**, **2a5np**, and **2a5clp**, forming colorless, yellow, colorless, and colorless block-like crystals, respectively (Table 6, Figure 9). With the exception of **sp** + **2a3np**,

https://doi.org/10.1021/acs.cgd.1c00448
Cryst. Growth Des. 2022, 22, 98−122

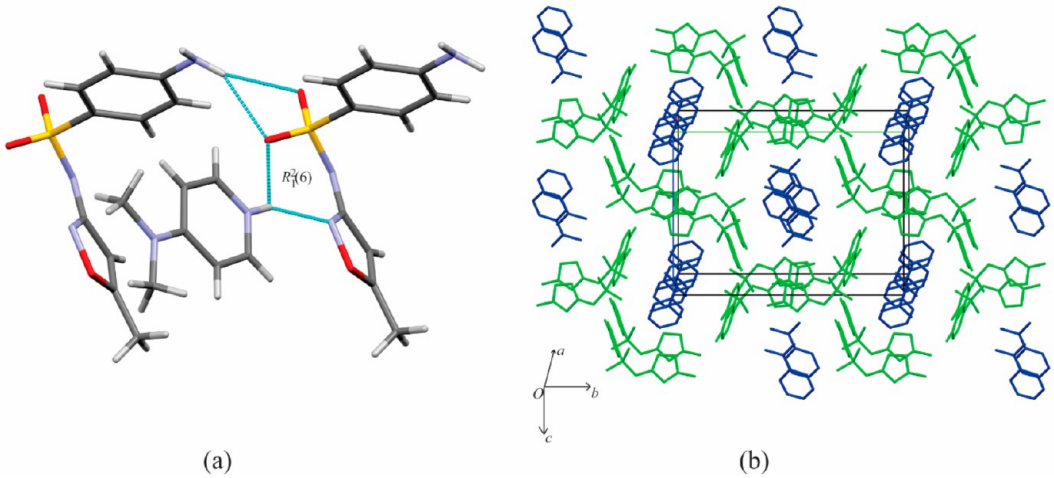


Figure 8. Crystal of **sm**$^-$ + **4dampH**$^+$ showing (a) the two sets of bifurcated hydrogen bonds and (b) the packing (with hydrogens omitted).

Table 6. Summary of Crystallographic Data for Cocrystals and Molecular Salt Containing sp

	cocrystal or salt				
	sp + 2a3np	**sp + 2ap**	**sp + 2a5np**	**sp + 2a5clp**	**spH$^+$ + 2c4n$^-$**
empirical formula	$(C_5N_3O_2H_5)\cdot(C_{11}H_{11}N_3O_2S)$	$(C_5N_2H_6)\cdot(C_{11}H_{11}N_3O_2S)$	$(C_5N_3O_2H_5)\cdot(C_{11}H_{11}N_3O_2S)$	$(C_{11}H_{11}N_3O_2S)\cdot(C_5H_5N_2Cl)$	$(C_7H_3O_4NCl)\cdot(C_{11}H_{12}O_2N_3S)^+$
formula weight	388.41	343.40	388.41	377.85	450.85
temp (K)	173(2)	173(2)	173(2)	173(2)	173(2)
cryst syst	triclinic	monoclinic	monoclinic	monoclinic	orthorhombic
space group	$P\bar{1}$	$P2_1/n$	$P2_1/n$	$P2_1/n$	$Pca2_1$
a (Å)	8.22100(10)	8.3965(3)	8.3305(2)	8.2918(2)	18.732(3)
b (Å)	10.1618(2)	19.1556(7)	18.8604(4)	18.9211(4)	8.4760(13)
c (Å)	10.2403(2)	10.3031(4)	11.0032(3)	11.0643(2)	12.187(2)
α (deg)	101.8080(10)	90	90	90	90
β (deg)	90.0390(10)	102.9410(10)	100.1800(10)	105.4610(10)	90
γ (deg)	93.7200(10)	90	90	90	90
V (Å^3)	835.52(3)	1615.06(10)	1701.57(7)	1673.06(6)	1934.9(5)
Z	2	4	4	4	4
density (g/cm^3)	1.544	1.412	1.516	1.500	1.548
μ (mm^{-1})	0.233	0.220	0.229	0.375	0.351
$F(000)$	404	720	808	784	928
cryst size (mm^3)	0.365 × 0.217 × 0.106	0.245 × 0.154 × 0.116	0.371 × 0.240 × 0.172	0.277 × 0.222 × 0.174	0.243 × 0.215 × 0.116
2Θ range for data collection (deg)	2.032−28.328	2.939−28.292	2.160−28.366	2.153−28.373	3.123−28.268
reflns collected	27738	68258	50479	55915	30691
independent reflns	4158 [R(int) = 0.0357	4006 [R(int) = 0.0541	4254 [R(int) = 0.0278, $R(\sigma)$ = 0.0139]	4178 [R(int) = 0.0706, $R(\sigma)$ = 0.0434]	4783 [R(int) = 0.0569, $R(\sigma)$ = 0.0410]
GOF on F^2	1.038	1.098	1.052	1.075	1.059
final R indexes [$I \geq 2\sigma(I)$]	R_1 = 0.0345, wR_2 = 0.0938	R_1 = 0.0473, wR_2 = 0.1084	R_1 = 0.0327, wR_2 = 0.0884	R_1 = 0.0437, wR_2 = 0.1045	R_1 = 0.0394, wR_2 = 0.0838
final R indexes [all data]	R_1 = 0.0402, wR_2 = 0.0981	R_1 = 0.0613, wR_2 = 0.1146	R_1 = = 0.0375, wR_2 = 0.0922	R_1 = 0.0759, wR_2 = 0.1182	R_1 = 0.0500, wR_2 = 0.0876
CCDC	2078050	2078053	2078052	2078045	2078054

each of the cocrystals crystallizes in the $P2_1/n$ space group. **sp + 2a3np** crystallizes in the $P\bar{1}$ space group. In addition, **sp + 2a5clp** and **sp + 2a5np** are isostructural (having similar unit cell parameters), as seen in Figure 10g. The structure of **sp + 2ap** shares similar structural features with those of **sp + 2a5clp** and **sp + 2a5np** but is not isostructural, as seen comparing Figure 10d,f. With the exception of **st + 2a5np**, the space group and unit cell parameters for **sp** and **st** corresponding cocrystal pairs are very similar, however those for **st** are not isostructural, as the molecules in each asymmetric unit do not overlap. Like the corresponding cocrystals containing **st** and **2ap** and its derivatives, a ring hydrogen bond motif $R_2^2(8)$ is formed between the **2ap** ring and the sulfonamide and pyridine ring of **sp**, with the remaining hydrogen of the amino group from **2ap** or its derivatives forming a hydrogen bond to the aniline group of a nearby **sp** molecule, as seen in Figure 10a,c,e. Like the case with the **st + 2ap** and **2ap** derivatives, the remaining hydrogen bonds in the **sp + 2ap** and it derivatives differ in each structure. In **sp + 2a3np**, the hydrogen bonding is identical to that observed in **st + 2a3np**, which features a series of ring based

https://doi.org/10.1021/acs.cgd.1c00448
Cryst. Growth Des. 2022, 22, 98−122

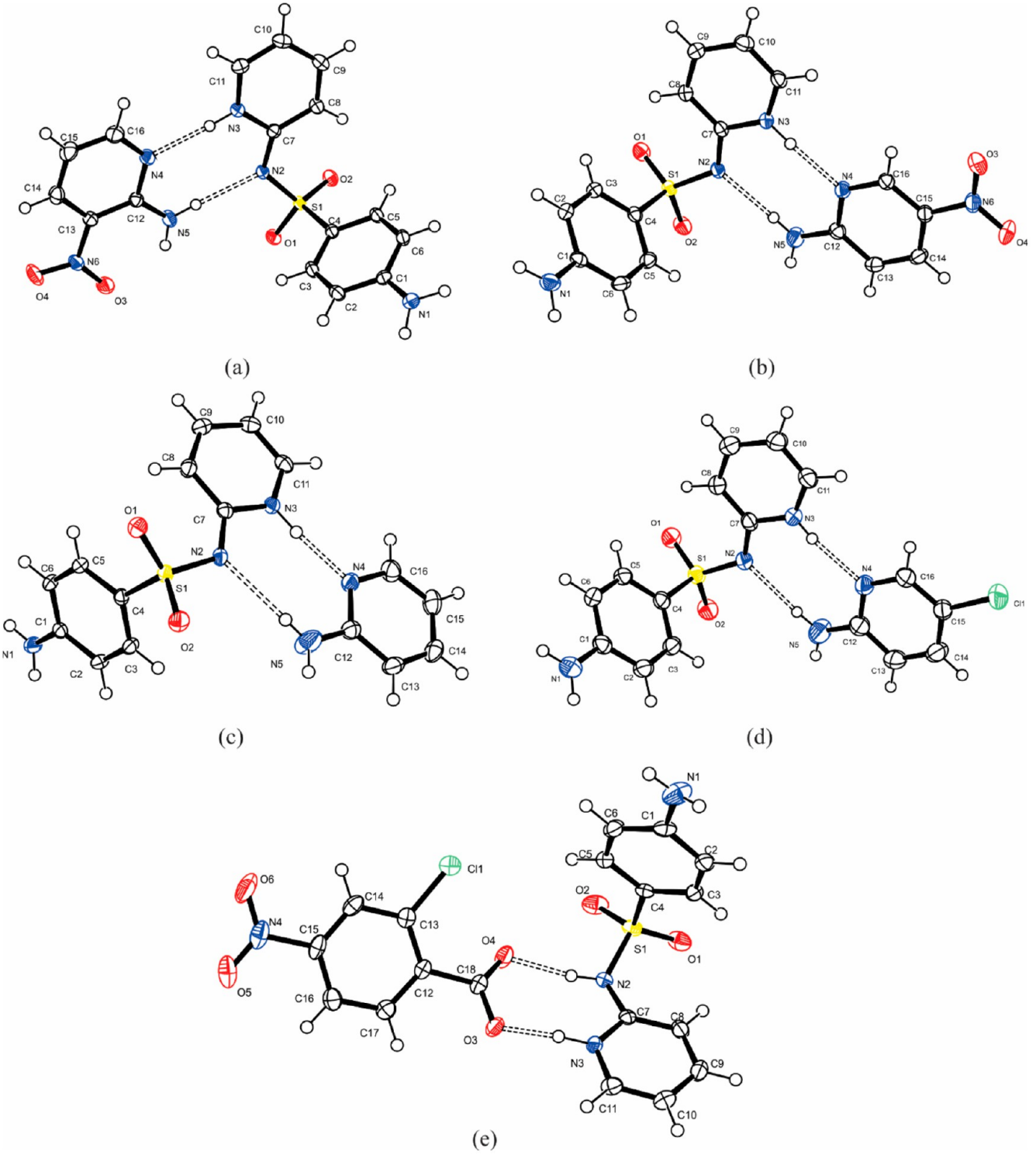


Figure 9. Ortep diagrams for (a) **sp** + **2a3np**, (b) **sp** + **2a5np**, (c) **sp** + **2ap**, (d) **sp** + **2a5clp**, and (e) **spH**$^+$ + **2c4n**$^-$.

hydrogen bond motifs, which include the one described above and the one formed by four **sp** molecules, connected by the aniline−sulfone hydrogen bonds (N1−H1A···O2 and N1−H1B···O2, respectively), as seen in Figure 10a (see Table 7 for bond distances and angles). **sp** + **2a5clp**, **sp** + **2a5np**, and **sp** + **2ap**, like their **st** counterparts, also feature a chain hydrogen bond motif, formed from the sulfone−aniline hydrogen bonds (N1−H1A···O2 and N1−H1B···O1 for **sp** + **2a5clp** and **sp** + **2a5np** and N1−H1A···O1 and N1−H1B···O2 for **sp** + **2ap**). The crystal structure packing mimics the cocrystal counterparts of **st** closely, albeit in a different orientation with respect to the unit cell axes. Like the packing of **st** + **2a3np**, the packing of **sp** +**2a3np** is made up of layers of **2a3np** and the pyridine portion of **sp** with the aniline portion separating said layers, as observed in Figure 10b.

Crystal Structure of the Molecular Salt spH$^+$ + 2c4n$^-$. **spH**$^+$ forms a molecular salt with **2c4n**$^-$, crystallizing as yellow

https://doi.org/10.1021/acs.cgd.1c00448
Cryst. Growth Des. 2022, 22, 98−122

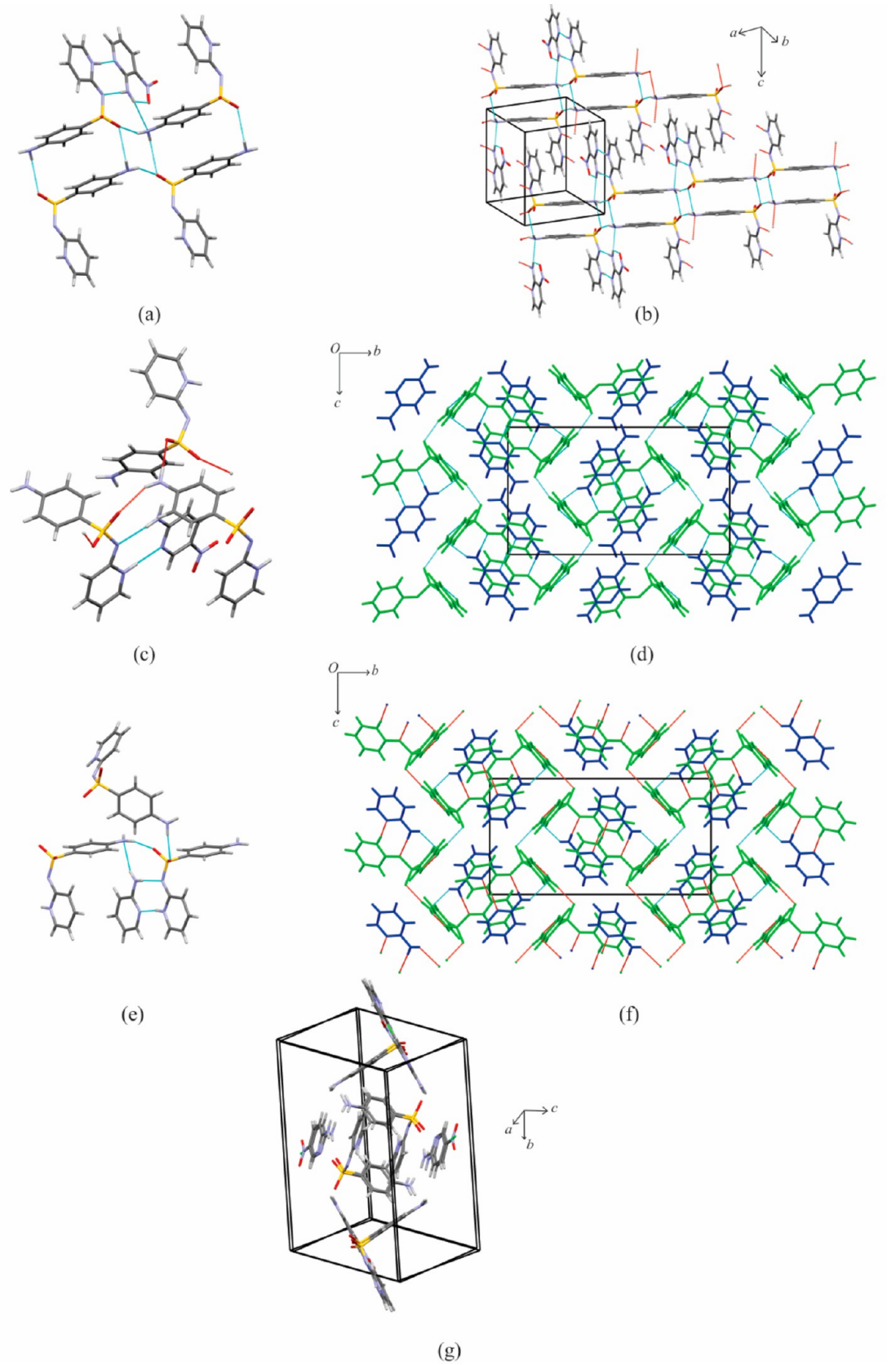


Figure 10. Crystal structures of (a) the hydrogen bonding present in **sp + 2a3np**, (b) the packing of **sp + 2a3np**, (c) the hydrogen bonding present in **sp + 2a5np**, (d) the packing of **sp + 2a5np**, (e) the hydrogen bonding present in **sp + 2ap**, (f) the packing of **sp + 2ap**, and (g) an overlay of **sp + 2a5np** and **sp + 2a5clp** showing that they are isostructural.

https://doi.org/10.1021/acs.cgd.1c00448
Cryst. Growth Des. 2022, 22, 98−122

Table 7. Hydrogen Bond Table for cocrystals and molecular salt containing sp

D−H···A[a]	d(D−H)	d(H···A)	d(D···A)	∠(DHA)
sp + 2a3np				
N1−H1A···N6	0.88	2.02	2.8921(16)	174
N3−H3A···O1 (i)	0.88	2.19	3.0143(15)	157
N5−H5A···N2	0.88	2.16	3.0337(16)	171
N5−H5B···N3 (iii)	0.88	2.30	3.0508(17)	144
N5−H5B···O3	0.88	2.07	2.6842(16)	126
sp + 2a5clp				
N1−H1A···N4	0.88	1.93	2.804(2)	170
N3−H3A···O2 (i)	0.88	2.23	3.067(2)	158
N3−H3B···S1 (iv)	0.88	2.99	3.8092(19)	156
N3−H3B···O1 (iv)	0.88	2.12	2.971(2)	161
N5−H5A···N2	0.88	2.20	3.060(3)	166
N5−H5B···N3 (iii)	0.88	2.39	3.097(3)	138
sp + 2a5np				
N1−H1A···N5	0.86	2.01	2.8676(14)	175
N3−H3A···O1 (v)	0.86	2.13	2.9911(14)	175
N3−H3B···O2 (i)	0.86	2.23	3.0495(15)	158
N4−H4A···N2	0.86	2.10	2.9510(16)	171
N4−H4B···N3(iii)	0.86	2.29	3.0559(16)	148
sp + 2ap				
N1−H1A···N5	0.86	1.95	2.806(2)	172
N3−H3A···O2 (iii)	0.86	2.13	2.964(2)	164
N3−H3B···O1 (vi)	0.86	2.10	2.954(2)	171
N4−H4A···N2	0.86	2.18	3.038(2)	175
N4−H4B···N3 (i)	0.86	2.47	3.145(2)	136
spH$^+$ + 2c4n$^-$				
N1−H1A···O3	0.88	1.71	2.584(3)	171.6
N3−H3A···O4 (vii)	0.88	2.48	3.046(4)	122.6
N3−H3B···O2 (viii)	0.88	2.65	3.320(4)	133.3
O4−H4A···N2	0.84	1.91	2.726(3)	165.3

[a]Symmetry transformations used to generate equivalent atoms: (i) $x + 1, y, z$; (ii) $-x + 1, -y, -z$; (iii) $x - 1, y, z$; (iv) $x + 1/2, -y + 3/2, z - 1/2$; (v) $x + 1/2, -y + 1/2, z - 1/2$; (vi) $x - 1/2, -y + 3/2, z + 1/2$; (vii) $x, y + 1, z$; (viii) $-x + 1, -y + 1, z - 1/2$.

plates. The asymmetric unit consists of one ion of each **2c4n**$^-$ and **spH**$^+$, crystallizing in the $Pca2_1$ space group. A proton transfer occurs between the carboxylic acid of **2c4n**$^-$ and the sulfonamide group of **sp**. **2c4n**$^-$ and **sp** form a hydrogen bond ring $R_2^2(8)$ from the carboxylate to the sulfonamide group, effectively forming a dimer (Figure 11a). The oxygen part of the carboxylate C18−O4 forms part of a bifurcated hydrogen bond system, which accepts one hydrogen bond from the previously described ring and the second to the aniline group (C14−O4···H1A). Packing of this structure is made up of alternating rows of **spH**$^+$ and **2c4n**$^-$, with alternating pairs of **sp** molecules giving a "W" formation when viewed down the *c*-axis Figure 11b.

FTIR Analysis. FTIR is a useful technique to distinguish between the different functional groups present in a solid, as well as to measure the strength of the intermolecular interactions between the different functional groups. For molecular salts and cocrystals, it is expected that the FTIR spectra will differ from the spectra of the individual components, not just due to the addition of potential new functional groups but also due to the different intermolecular interactions occurring (i.e., new hydrogen bonds, etc.). In particular, hydrogen bonds will cause a shift of significant IR peaks, which will be dependent on the strength or degree of the hydrogen bond in question. As such, an easy way to analyze the spectra of the cocrystals and molecular salts is to compare them to the spectrum of the sulfa drug present. Therefore, the spectrum of each cocrystal and molecular salt is presented together with the spectrum of the individual sulfa drug of interest. The comparative spectra of the cocrystals and molecular salts of **st**, **sm**, and **sp** are presented together in Figure 12, Figure 13, and Figure 14 respectively. (The separate spectra of each cocrystal and molecular salt have been included in the Supporting Information). The functional groups of most interest, which are present in each of the sulfa drugs regardless of heterocyclic ring present, are the amine ($-NH_2$), the sulfone ($-SO_2-$) and sulfonamide ($-SO_2-NH-$) functional groups. A summary of the position of these peaks are presented in Table 8. Some peaks could not be absolutely assigned, as they may be merged with other peaks or are simply not relevant to the crystal system in question.

The FTIR spectrum of each cocrystal or molecular salt also contains information on the molecular vibrations of the coformer as well. For example, for the nitrile containing compounds like **3cnp** and **4cnp**, the key peak for the C≡N stretch is a medium intense peak typically located around the 2200 cm^{-1} point, which for the cocrystals of **sm + 3cnp** and **sm + 4cnp** has been observed in their spectra at 2241 and 2247 cm^{-1}, respectively. Molecular vibrations for the C−Cl bonds could not be assigned absolutely, as the peaks coincide with deformation vibrations associated with the various other bonds present in the solid. However, Cl-containing compounds that yielded successful cocrystals or molecular salts also contain a nitro group, which could be identified more easily, and thus one could verify the formation of the respective cocrystal or molecular salt. The symmetrical nitro stretch can prove to be difficult to distinguish from the S═O stretch bands, as both stretches can overlap in the same frequency range. However, the asymmetrical nitro group stretch can be identified more easily and, where appropriate, is presented in Table 8. For the cocrystals containing **2ap** and **bipy**, which share the same set of functional groups with the sulfa drugs, their spectra is obviously different when compared to the respective spectrum of the sulfa drug. Thus, FTIR can prove to be an effective method for the quick identification of the formation of the respective cocrystal or molecular salt.

Thermal Analysis (DSC and TGA). Differential scanning calorimetry can provide useful information regarding the thermodynamics of materials and certain solid-state properties such as the melting point and enthalpy of fusion. TGA was used to determine the thermal stability of each sample. Each individual TGA is presented in the Supporting Information. Multicomponent crystals will often have significantly different melting points compared to their coformers. DSC and TGA curves were obtained for each of the multicomponent crystals. In each case, only a distinct endotherm was observed in the DSC curve. These peaks occurred over a temperature range different from the melting points of the pure sulfa drug or pure coformer. Usually these large peaks correspond to the melting point of the sample. The TGA curves show that after the temperature range in which this endotherm occurs, significant weight loss occurs of the components, indicating decomposition. This is confirmed by the absence of any recrystallization peaks on the cooling cycle of the DSC. The temperature ranges in which the sulfa drug undergoes decomposition are similar to those reported in the literature.[53] Table 9 contains a list of the onset temperatures and enthalpies of the decomposition points obtained from the DSC.

https://doi.org/10.1021/acs.cgd.1c00448
Cryst. Growth Des. 2022, 22, 98−122

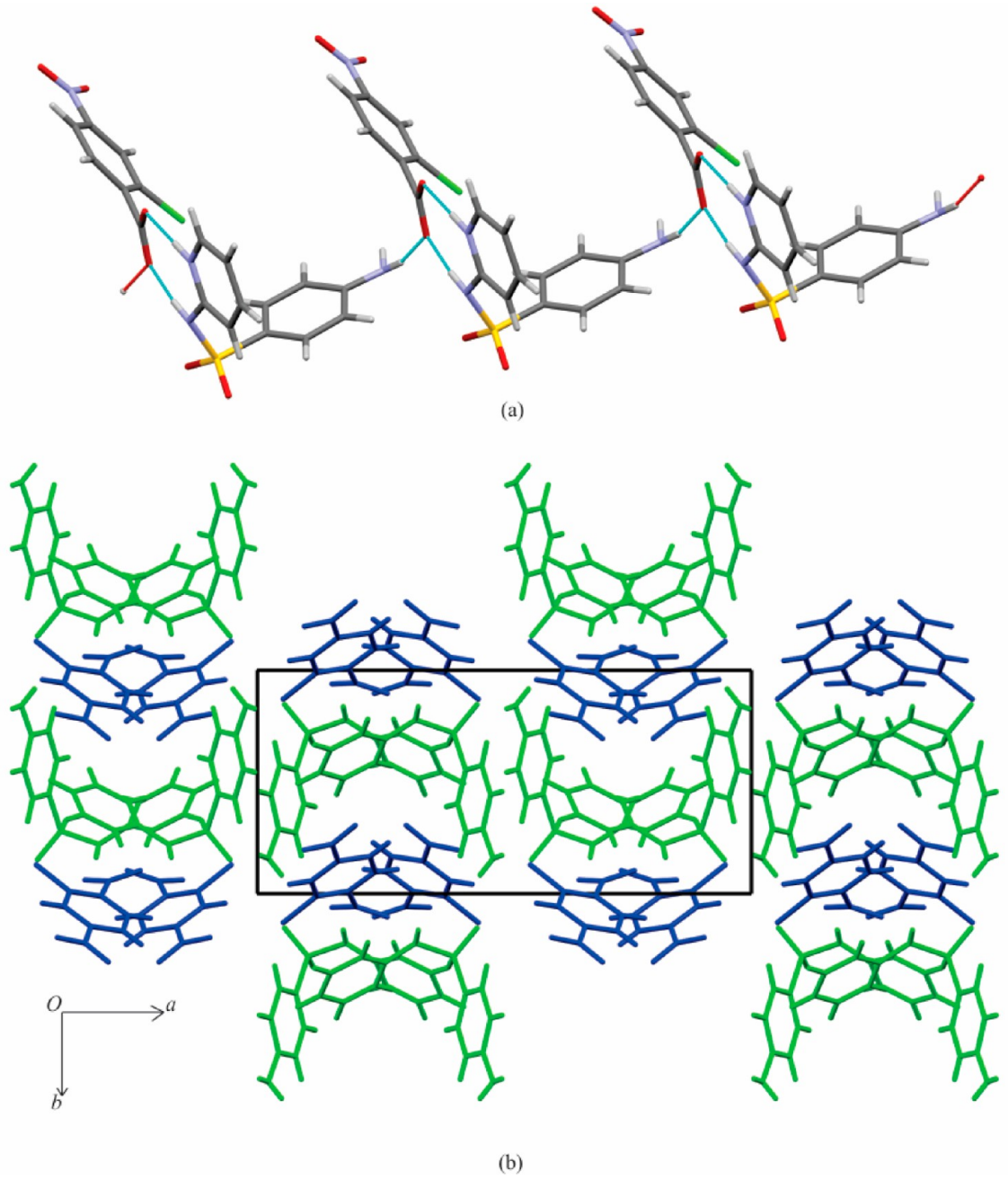


Figure 11. Crystal structure of **spH**$^+$ + **2c4n**$^-$ showing (a) the hydrogen bonding between molecules and the 1D tape structure and (b) the crystal structure packing viewed down the *c*-axis.

Comparison of the Cocrystals and Solvates of Sulfa Drugs. Typically, it would be useful to compare new molecular salts and cocrystals to those reported previously reported in the literature. However, the number of cocrystals or molecular salts reported in the CSD for **sp**, **st**, and **sm** is limited; 21 molecular salts and cocrystals containing **st** and 12 molecular salts and cocrystals containing **sm** have been reported in the CSD. No cocrystals or molecular salts containing **sp** have been listed in the CSD. Due to the varied nature of the coformers reported for these different multicomponent systems, only some general trends can be derived. In terms of the tautomeric forms where applicable, **st** and **sp** formed in the imidine form while **sm** formed in the amidine form, which should not be too surprising when compared to the various polymorphs of each sulfa drug.

The set of coformers that gave the greatest amount of success was **2ap** and its derivatives. Typically, if the coformer is a pyridine, the major interaction is between the pyridyl nitrogen and the sulfonamide hydrogen (observed in **st** + **bipy**). However, in the case of **2ap** and its derivatives, the amino group offers an additional set of interactions to the sulfa drug. The amino group, together with the pyridyl nitrogen, forms a ring hydrogen bond motif $R_2^2(8)$ with the sulfa drug at the 2′ position nitrogen and the sulfonamide group. The second hydrogen from the amino group of the coformer forms a hydrogen bond to the aniline group on a second sulfa drug molecule. This should not be surprising, since **sm** is often coupled together with trimethoprim as a molecular salt (Figure 15),[36] as well as the fact that the cocrystals presented by Wojnarska et al. were even

https://doi.org/10.1021/acs.cgd.1c00448
Cryst. Growth Des. 2022, 22, 98−122

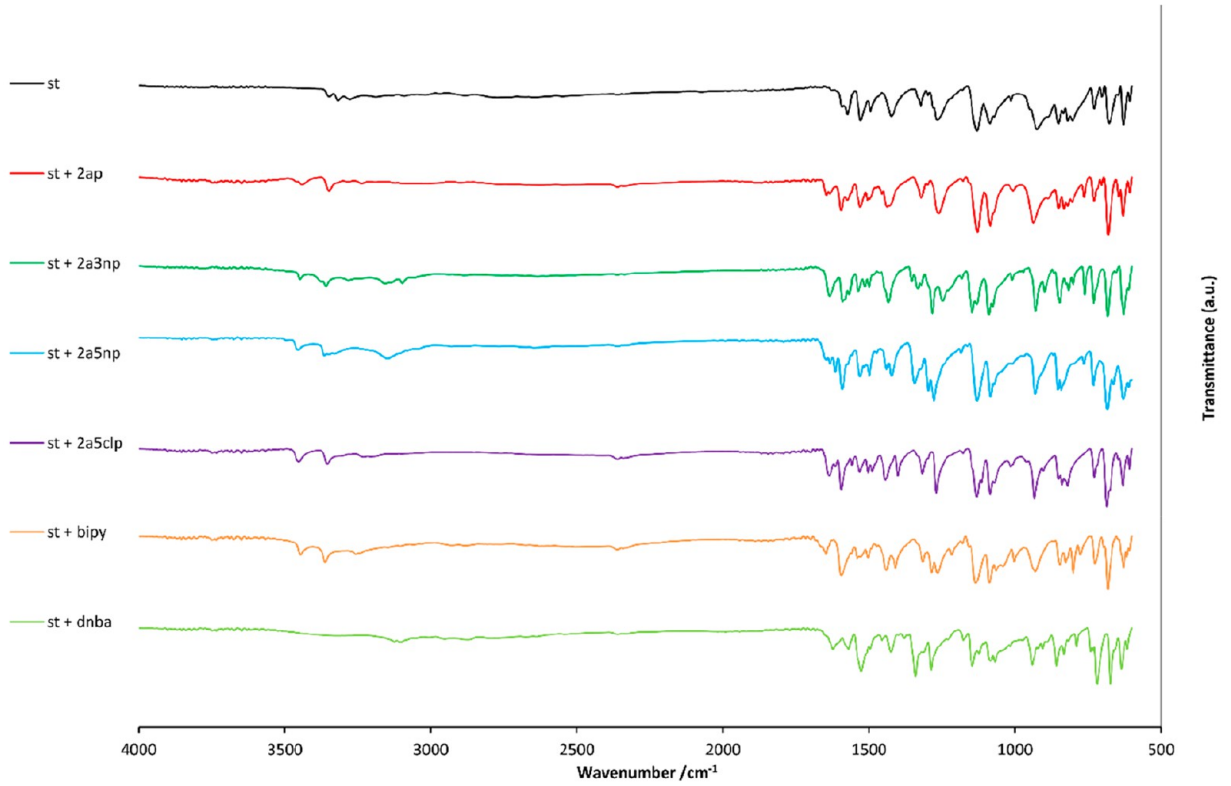


Figure 12. FTIR spectra of **st** and its cocrystals/molecular salt.

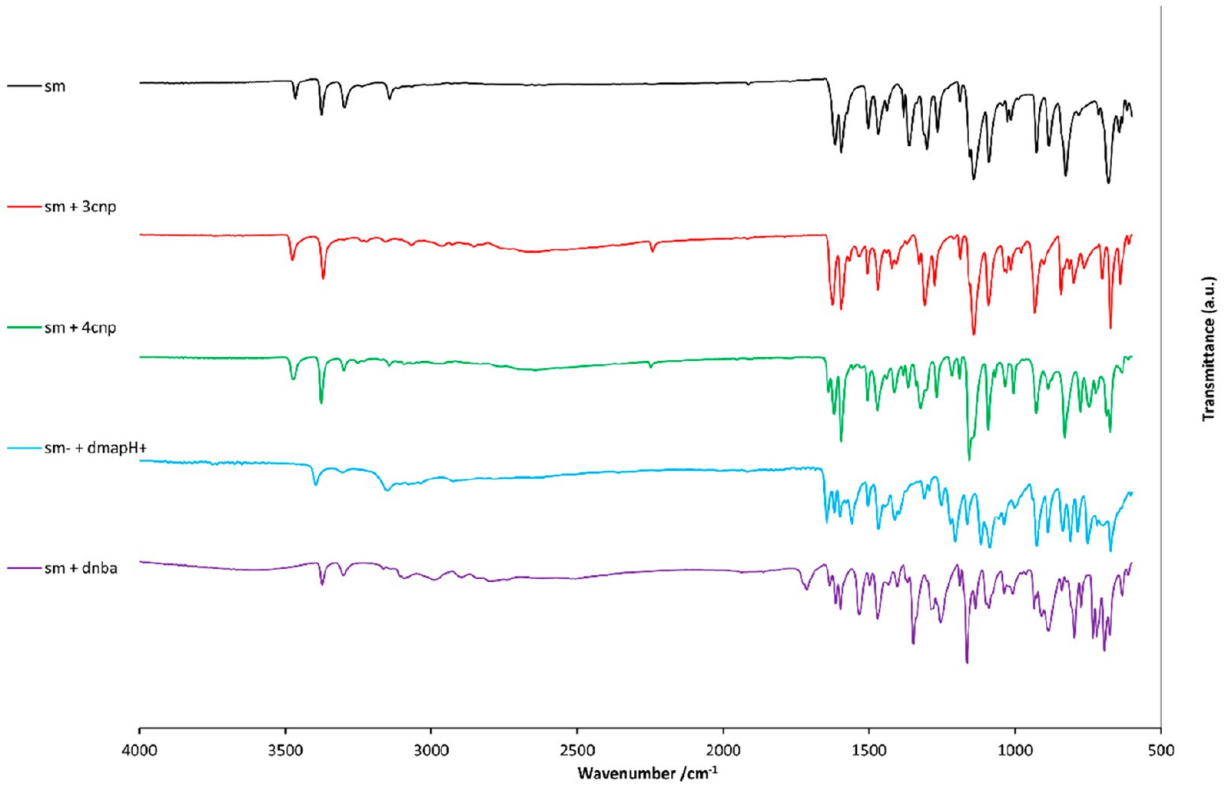


Figure 13. FTIR spectra of **sm** and its cocrystals/molecular salt.

isostructural with respect to each other.[51] Although the major driving force for the formation of the molecular salt of **sm** and trimethoprim is the ionic bond, some comparisons can be drawn from the hydrogen bonds that are present. Trimethoprim consists of a pyrimidine ring with two amino groups at the 2′ and 4′ positions, which in essence interacts with **sm** in a similar

https://doi.org/10.1021/acs.cgd.1c00448
Cryst. Growth Des. 2022, 22, 98−122

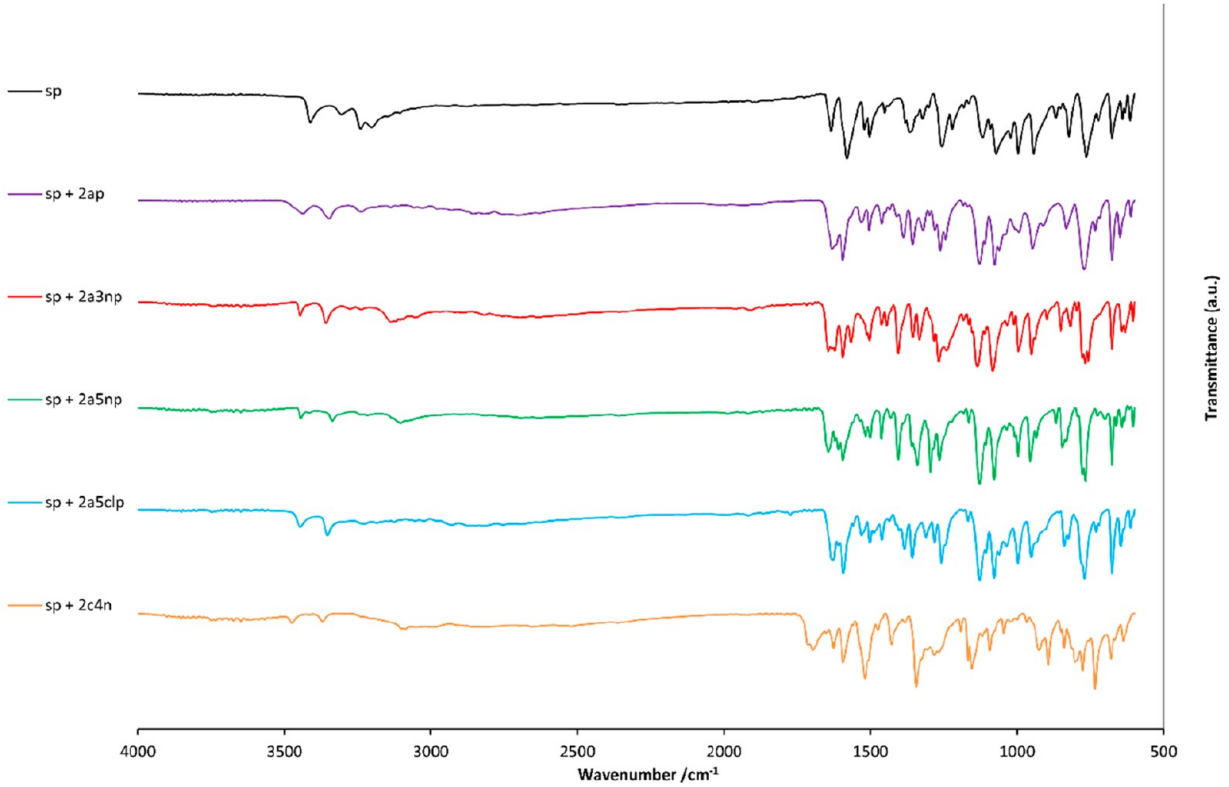


Figure 14. FTIR spectra of **sp** and its cocrystals/molecular salt.

Table 8. Some Assignments of the Peaks for the FTIR Spectra of st, sm and sp and Their Respective Derivatives[a]

solid form	ν_{asym} ($-NH_2$)	ν_{sym} ($-NH_2$)	ν ($-NH-$)	δ ($-NH-$)	ν_{asym} ($-SO_2-$)	ν_{sym} ($-SO_2-$)	ν ($-NH_3^+$)	ν_{asym} ($-NO_2-$)
Sulfathiazole and Its Complexes								
st	3348, m	3317, m	3277, m	1494, m	1322, s	1129, s		
st + 2ap	3441, m	3349, m	3349, m	1530, m	1321, s	1128, s		
st + 2a3np	3448, m	3359, m	3359, m	1514, m				1590, s
st + 2a5np	3453, m	3364, m	3148, m		1343, s	1184, s		1594, s
st + 2a5clp	3452, m	3355, m	3230, m, br	1535, m	1316, s	1130, s		
st + bipy	3446, m	3362, m	3257, m	1540, m	1315, s	1134, s		
stH$^+$ + dnba$^-$	-		3102, m	1526, s	1341, s	1146, s	3102, m, br	1590, s
Sulfamethoxazole and Its Complexes								
sm	3466, m	3376, m	3297, m	1501, m	1302, m	1141, s		
sm + 3cnp	3476, m	3371, m		1504, m	1309, s	1141, s		
sm + 4cnp	3473, m	3377, m	3299, m	1504, m	1323, m	1157, s		
sm$^-$ + 4dmapH$^+$	3395, m	3299, w			1293, m	1163, m		
sm + dnba	3374, m	3300, m		4898, m	1348, m	1165, vs		
Sulfapyridine and Its Complexes								
sp	3412, m	3305, m	3241, m	1503, m	1321, s	1221, m		
sp + 2ap	3436, m	3347, m	3235, m	1504, m	1280, s	1128, s		
sp + 2a3np	3446, m	3358, m	3158, m, br	1503, m	1355, s	1135, s		1590, s
sp +2a5np	3444, m	3337, m	3104, m, br	1500, m	1295, s	1127, s		1594, s
sp + 2a5clp	3445, m	3352, m		1501, m	1280, s	1127, s		
spH$^+$ + 2c4n$^-$	3474, m	3369, m		1593, m	1344, s	1093, m	3087, m, br	1519, s

[a] ν is the respective symmetrical and asymmetrical stretching bands, and δ is the scissoring band.

manner to **2ap** and its derivatives. This combination grants stability to this molecular complex and thus allows a cocrystal to form between the sulfa drug and **2ap** and its derivatives. Although theoretically, **2ap** and its derivatives should have formed a cocrystal or molecular salt with **sm**, they did not. It is plausible that the reason for this may be a combination of sterics as well as electronic effects.

Multicomponent crystals containing the sulfa drug and a coformer that is a derivative form of benzoic acid have no repeating hydrogen bond pattern between the different combinations. Based on the results of multicomponent crystals containing sulfamethazine[15−17] and work by Shunje,[50] it was expected that most of the multicomponent crystals containing benzoic acid and its derivatives would form either synthon iv or

https://doi.org/10.1021/acs.cgd.1c00448
Cryst. Growth Des. 2022, 22, 98−122

Table 9. List of the Onset Temperatures and Enthalpies for the Multicomponent Crystals Presented in This Work from the DSC Results

cocrystal or molecular salt	onset (°C)	peak (°C)	ΔH_{fus}[a] (kJ mol^{-1})
sm + 3cnp	142.1	143.8	55.6
sm + 4cnp	123.1	127.4	45.1
sm + dnba	187.9	190.4	74.4
smH$^+$ + 4dmap$^-$	195.6	198.5	56.2
st + 2ap	160.9	162.9	50.6
st + 2a3np	195.5	196.6	72.9
st + 2a5np	171.1	174.1	133.8
st + 2a5clp	183.8	185.9	64.1
st + bipy	179.6	181.8	82.7
stH$^+$ + dnba$^-$	189.4	190.9	69.0
sp + 2ap	143.2	145.7	40.4
sp + 2a3np	174.1	177.2	72.9
sp + 2a5np	188.4	191.9	90.7
sp + 2a5clp	167.4	170.9	65.9
spH$^+$ + 2c4n$^-$	143.0	145.1	43.4

[a]Heat of fusion.

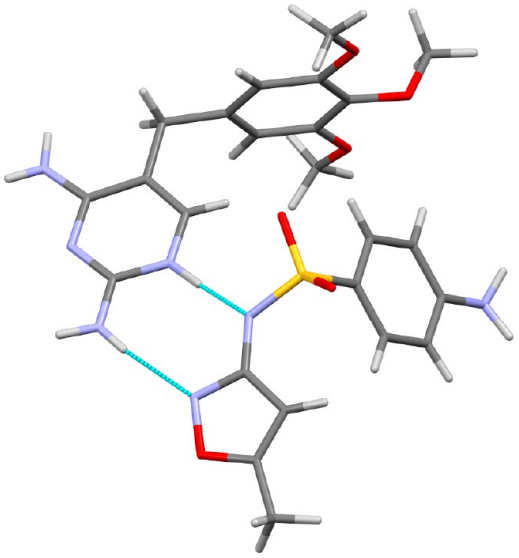


Figure 15. Molecular salt of **sm** + trimethoprim (refcode SMZTMP01).

synthon v shown in Scheme 5. However, not only did most of the cocrystallization attempts fail, only one formed with one of the expected synthons. Other examples in the literature of multicomponent crystals that involve a benzoic acid derivative with **st** and **sm** include **st + 4nba** (refcode FIZFUR), **st** + 2,4-dinitrobenzoic acid/2,4-dinitrobenzoate[38] (refcode KUFWIT), and **sm** with 2-hydroxy, 3,5-dinitrobenzoate[54] (refcode TUJPEV). However, in these cases the hydrogen bonding is different from those reported here: in **st + 4nba** both coformers form homodimers and only interact with each other via $\pi-\pi$ interactions and weak C−H···X hydrogen bonds, while the other two form a ring hydrogen bond motif consisting of the sulfonamide group, the protonated amino group from the aniline ring, and the carboxylate group (Figure 16). Out of the possible 30 multicomponent crystals that could have formed with benzoic acid derivatives attempted here, only three formed (two molecular salts and one cocrystal). This indicates that although it is possible to form a multicomponent crystal involving a sulfa drug compound and benzoic acid conformer, chances are probably low for success, and the choice of the hydrogen bonding site or interaction remains varied.

Both molecular salts and cocrystals were formed in this work. There are two sites where proton transfer can occur, indicated in Scheme 3. The ΔpK_a of the site where the major hydrogen bonding or proton transfer occurs in the multicomponent crystals reported in this work is given in Table 10. From this table, the pK_a rule worked well and predicted most cases correctly. However, pK_a rule does not necessarily take into account the presence of additional hydrogen bond donors or acceptors or predict which hydrogen bonding site is preferred. For example, **2ap** and its derivatives will most likely form the previously described ring hydrogen bond motif and most likely ignore the formation of say a pyridine−aniline group hydrogen bond pair. For the case of sulfa drugs + benzoic acids, predicting which hydrogen bonding site would be preferred based on the pK_a rule alone proves unreliable. The other problem lies in that most pK_a values are reported for water, whereas most of the crystallizations from this work were crystallized using organic solvents, which would yield different pK_a values. This is most notable with **stH$^+$ + dnba$^-$**, where the result based on water would have yielded a cocrystal instead of a salt. Although the use of using the pK_a rule is useful in determining if a molecular salt or cocrystal would form, it does not give any insight in predicting where or how the sulfa drugs would interact with the coformer.

One hydrogen bond interaction to take note of is that of the aniline forming a hydrogen bond with the sulfone group in a neighboring sulfa molecule (synthon vii). In all cases of polymorphs of the sulfa drugs, at least one of these hydrogen bonds exists. In most cases, this sulfone−aniline hydrogen bond can yield several different chain hydrogen bond motifs in multicomponent crystals, such as those observed in **sm + 3cnp** and **sm + 4cnp**. A few exceptions do arise, such as in the case of **sm + dnba** reported here and **st** + *N*-formylpiperidine.[56] In such cases, the coformer would consist of a hydrogen bond acceptor that may be too bulky to interact with the sulfonamide hydrogen or have several hydrogen bond acceptors that out-compete the sulfone group. Regardless, it is still worthwhile to take note of such interactions when choosing coformers for future cocrystallization attempts.

CONCLUSIONS

From the 25 coformers used for this work, only 13 new cocrystals and molecular salts were successful. Five cocrystals and one molecular salt with **st**, four cocrystals and one molecular salt with **sp**, and three cocrystals and one molecular salt with **sm** were synthesized and characterized. Both traditional solvent evaporation methods and mechanochemical methods were deployed, but overall solvent methods proved to be the most reliable method to obtain cocrystals or molecular salts, while mechanochemical methods (both dry milling and LAG) were able to obtain the same cocrystals or molecular salts of **sp** and **st** as the solvent based methods, while mechanochemical methods failed to produce a cocrystal or molecular salt of **sm**. Most of the coformers that formed a multicomponent crystal with the sulfa drugs were **2ap** and its various derivatives, which is a result of a ring hydrogen bond motif (synthon ii). The chance to form a successful cocrystal containing the sulfa drug and benzoic acid or one of its derivatives is low, and the best chance for success is to choose a derivative of benzoic acid that will undergo definite proton transfer to allow the formation of a molecular salt. The aniline group should also be considered as an important hydrogen bonding site in addition to the suflonamide/N-containing heterocycle pair when attempting to synthesize cocrystals or

https://doi.org/10.1021/acs.cgd.1c00448
Cryst. Growth Des. 2022, 22, 98−122

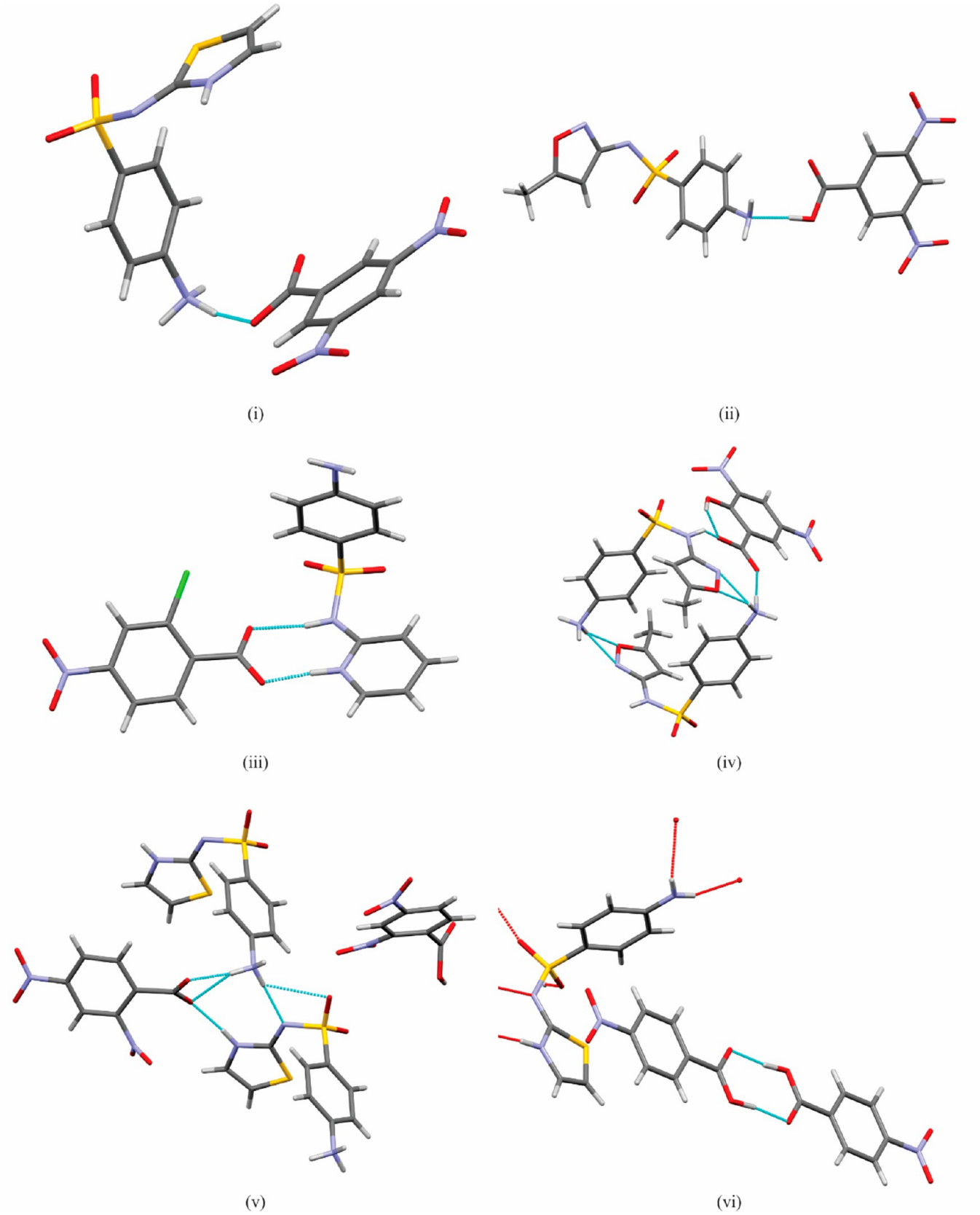


Figure 16. Crystal structures of multicomponent crystals featuring different sulfa drugs and benzoic acid derivatives showing different hydrogen bonding interactions: (i) **stH**$^+$ + **dnba**$^-$, (ii) **sm** + **dnba**, (iii) **spH**$^+$ + **2c4n**$^-$, (iv) 2,4-dinitrobenzoic acid (refcode KUFWIT), (v) 3,5-dinitrosalicylic acid (refcode TUJPEV), and (vi) **st** + **4nba** (refcode FIZFUR).

https://doi.org/10.1021/acs.cgd.1c00448
Cryst. Growth Des. 2022, 22, 98−122

Table 10. ΔpK_a Values for the Multicomponent Crystals Reported in This Work[a]

cocrystal or molecular salt	ΔpK_a	predicted result	actual result
st + 2ap	−0.57	cocrystal	cocrystal
st + 2a5clp	−2.57	cocrystal	cocrystal
st + 2a3np	−4.84	cocrystal	cocrystal
st + 2a5np	−4.42	cocrystal	cocrystal
st + bipy	−3.97	cocrystal	cocrystal
stH^+ + $dnba^-$	−0.58	cocrystal	molecular salt
sm + 3cnp	−3.82	cocrystal	cocrystal
sm + 4cnp	−3.68	cocrystal	cocrystal
sm^- + $4dmapH^+$	3.92	molecular salt	molecular salt
sm + dnba	−0.94	cocrystal	cocrystal
sp + 2ap	−1.76	cocrystal	cocrystal
sp + 2a5clp	−3.76	cocrystal	cocrystal
sp + 2a3np	−6.03	cocrystal	cocrystal
sp + 2a5np	−5.61	cocrystal	cocrystal
spH^+ + $2c4n^-$	6.39	molecular salt	molecular salt

[a]The pK_a used for the respective sulfa drug is based on where the major hydrogen bonding or proton transfer occurs between the sulfa drug and coformer.

molecular salts consisting of sulfa drugs and benzoic acid derivatives. For future work, coformers containing **2ap**, which also preserves the interaction of the aniline amino group to the sulfone group could yield more successful results. It may also be worthwhile in determining if the physicochemical properties of the successful multicomponent crystals improved over the single component forms as a result.

■ ASSOCIATED CONTENT

Supporting Information

The Supporting Information is available free of charge at https://pubs.acs.org/doi/10.1021/acs.cgd.1c00448.

Mass amounts used, powder X-ray diffraction data, differential scanning calorimetry data, thermal gravimetric analysis data, and Fourier-transform infrared spectroscopy (PDF)

Accession Codes

CCDC 2078040−2078054 contain the supplementary crystallographic data for this paper. These data can be obtained free of charge via www.ccdc.cam.ac.uk/data_request/cif, or by emailing data_request@ccdc.cam.ac.uk, or by contacting The Cambridge Crystallographic Data Centre, 12 Union Road, Cambridge CB2 1EZ, UK; fax: +44 1223 336033.

■ AUTHOR INFORMATION

Corresponding Author

Andreas Lemmerer − *Molecular Sciences Institute, School of Chemistry, University of the Witwatersrand, 2050 Johannesburg, South Africa;* orcid.org/0000-0003-1569-2831; Phone: +27-11-717-6711; Email: Andreas.Lemmerer@wits.ac.za; Fax: +27-11-717-6749

Author

Matthew C. Scheepers − *Molecular Sciences Institute, School of Chemistry, University of the Witwatersrand, 2050 Johannesburg, South Africa*

Complete contact information is available at: https://pubs.acs.org/10.1021/acs.cgd.1c00448

Notes

The authors declare no competing financial interest.

■ ACKNOWLEDGMENTS

This material is based upon work supported financially by the University of the Witwatersrand and the Molecular Sciences Institute. The National Research Foundation National Equipment Programme (UID 78572) is thanked for financing the purchase of the single-crystal diffractometer, and the DSI/NRF Centre of Excellence in Strong Materials is thanked for use of the D2-phaser.

■ REFERENCES

(1) Kawakami, K. Modification of Physicochemical Characteristics of Active Pharmaceutical Ingredients and Application of Supersaturatable Dosage Forms for Improving Bioavailability of Poorly Absorbed Drugs. *Adv. Drug Delivery Rev.* **2012**, *64* (6), 480−495.

(2) Blagden, N.; de Matas, M.; Gavan, P. T.; York, P. Crystal Engineering of Active Pharmaceutical Ingredients to Improve Solubility and Dissolution Rates. *Adv. Drug Delivery Rev.* **2007**, *59* (7), 617−630.

(3) Qiao, N.; Li, M.; Schlindwein, W.; Malek, N.; Davies, A.; Trappitt, G. Pharmaceutical Cocrystals: An Overview. *Int. J. Pharm.* **2011**, *419* (1−2), 1−11.

(4) Vishweshwar, P.; McMahon, J. A.; Peterson, M. L.; Hickey, M. B.; Shattock, T. R.; Zaworotko, M. J. Crystal Engineering of Pharmaceutical Co-Crystals from Polymorphic Active Pharmaceutical Ingredients. *Chem. Commun.* **2005**, *10* (36), 4601−4603.

(5) Desiraju, G. R. Crystal Engineering: From Molecule to Crystal. *J. Am. Chem. Soc.* **2013**, *135* (27), 9952−9967.

(6) Moulton, B.; Zaworotko, M. J. From Molecules to Crystal Engineering: Supramolecular Isomerism and Polymorphism in Network Solids. *Chem. Rev.* **2001**, *101* (6), 1629−1658.

(7) Schultheiss, N.; Newman, A. Pharmaceutical Cocrystals and Their Physicochemical Properties. *Cryst. Growth Des.* **2009**, *9* (6), 2950−2967.

(8) Vishweshwar, P.; McMahon, J. A.; Bis, J. A.; Zaworotko, M. J. Pharmaceutical Co-Crystals. *J. Pharm. Sci.* **2006**, *95* (3), 499−516.

(9) Nechipadappu, S. K.; Tekuri, V.; Trivedi, D. R. Pharmaceutical Co-Crystal of Flufenamic Acid: Synthesis and Characterization of Two Novel Drug-Drug Co-Crystal. *J. Pharm. Sci.* **2017**, *106* (5), 1384−1390.

(10) Bučar, D. K.; Day, G. M.; Halasz, I.; Zhang, G. G. Z.; Sander, J. R. G.; Reid, D. G.; MacGillivray, L. R.; Duer, M. J.; Jones, W. The Curious Case of (Caffeine)·(Benzoic Acid): How Heteronuclear Seeding Allowed the Formation of an Elusive Cocrystal. *Chem. Sci.* **2013**, *4* (12), 4417−4425.

(11) Kołaczek, A.; Fusiarz, I.; Lawecka, J.; Branowska, D. Biological Activity and Synthesis of Sulfonamide Derivatives: A Brief Review. *Chemik* **2014**, *68* (7), 620−628.

(12) Perlovich, G. L.; Ryzhakov, A. M.; Tkachev, V. V.; Hansen, L. K. Sulfonamide Molecular Crystals: Thermodynamic and Structural Aspects. *Cryst. Growth Des.* **2011**, *11* (4), 1067−1081.

(13) Bar, I.; Bernstein, J. Conformational Polymorphism VI: The Crystal and Molecular Structures of Form II, Form III, and Form V of 4-amino-N-2-pyridinylbenzenesulfonamide (Sulfapyridine). *J. Pharm. Sci.* **1985**, *74* (3), 255−263.

(14) Gelbrich, T.; Threlfall, T. L.; Bingham, A. L.; Hursthouse, M. B. Polymorph VI of Sulfapyridine: Inter-Penetrating Two- and Three-Dimensional Hydrogen-Bonded Nets Formed from Two Tautomeric Forms. *Acta Crystallogr. Sect. C Cryst. Struct. Commun.* **2007**, *63* (6), o323−o326.

(15) Basak, A. K.; Chaudhuri, S.; Mazumdar, S. K. Structure of 4-Amino-N-2-Pyridylbenzenesuphonamide (Sulphapyridine), C11H11N3O2S. *Acta Crystallogr., Sect. C: Cryst. Struct. Commun.* **1984**, *40* (11), 1848−1851.

(16) Gelbrich, T.; Hughes, D. S.; Hursthouse, M. B.; Threlfall, T. L. Packing Similarity in Polymorphs of Sulfathiazole. *CrystEngComm* **2008**, *10* (10), 1328−1334.

(17) Hughes, D. S.; Hursthouse, M. B.; Threlfall, T.; Tavener, S. A New Polymorph of Sulfathiazole. *Acta Crystallogr., Sect. C: Cryst. Struct. Commun.* **1999**, *55* (11), 1831−1833.
(18) Sovago, I.; Gutmann, M. J.; Hill, J. G.; Senn, H. M.; Thomas, L. H.; Wilson, C. C.; Farrugia, L. J. Experimental Electron Density and Neutron Diffraction Studies on the Polymorphs of Sulfathiazole. *Cryst. Growth Des.* **2014**, *14* (3), 1227−1239.
(19) Perlovich, G. L.; Ryzhakov, A. M.; Tkachev, V. V.; Hansen, L. K.; Raevsky, O. A. Sulfonamide Molecular Crystals: Structure, Sublimation Thermodynamic Characteristics, Molecular Packing, Hydrogen Bonds Networks. *Cryst. Growth Des.* **2013**, *13* (9), 4002−4016.
(20) Price, C. P.; Grzesiak, A. L.; Matzger, A. J. Crystalline Polymorph Selection and Discovery with Polymer Heteronuclei. *J. Am. Chem. Soc.* **2005**, *127* (15), 5512−5517.
(21) Aakeröy, C. B.; Beatty, A. M.; Helfrich, B. A.; Nieuwenhuyzen, M. Do Polymorphic Compounds Make Good Cocrystallizing Agents? A Structural Case Study That Demonstrates the Importance of Synthon Flexibility. *Cryst. Growth Des.* **2003**, *3* (2), 159−165.
(22) Cruz-Cabeza, A. J.; Groom, C. R. Identification, Classification and Relative Stability of Tautomers in the Cambridge Structural Database. *CrystEngComm* **2011**, *13* (1), 93−98.
(23) Wang, T.; Stevens, J. S.; Vetter, T.; Whitehead, G. F. S.; Vitorica-Yrezabal, I. J.; Hao, H.; Cruz-Cabeza, A. J. Salts, Cocrystals, and Ionic Cocrystals of a "Simple" Tautomeric Compound. *Cryst. Growth Des.* **2018**, *18* (11), 6973−6983.
(24) Velraj, G.; Soundharam, S. Structure, Vibrational, Electronic, NBO and NMR Analyses of 4-Amino-N-[2-Pyridinyl] Benzene Sulfonamide (Sulfapyridine) by Experimental and Theoretical Approach. *J. Mol. Struct.* **2014**, *1074*, 475−486.
(25) Salem, A. A.; Mossa, H. A.; Barsoum, B. N. Application of Nuclear Magnetic Resonance Spectroscopy for Quantitative Analysis of Miconazole, Metronidazole and Sulfamethoxazole in Pharmaceutical and Urine Samples. *J. Pharm. Biomed. Anal.* **2006**, *41* (2), 654−661.
(26) Scheepers, M. C.; Lemmerer, A. Synthesis and Characterization of a Series of Sulfamethazine Multicomponent Crystals with Various Benzoic Acids. *Cryst. Growth Des.* **2020**, *20* (2), 813−823.
(27) Lu, J.; Cruz-Cabeza, A. J.; Rohani, S.; Jennings, M. C. A 2:1 Sulfamethazine-Theophylline Cocrystal Exhibiting Two Tautomers of Sulfamethazine. *Acta Crystallogr. Sect. C Cryst. Struct. Commun.* **2011**, *67* (8), o306−o309.
(28) Fu, X.; Li, J.; Wang, L.; Wu, B.; Xu, X.; Deng, Z.; Zhang, H. Pharmaceutical Crystalline Complexes of Sulfamethazine with Saccharin: Same Interaction Site but Different Ionization States. *RSC Adv.* **2016**, *6* (31), 26474−26478.
(29) Ghosh, S.; Bag, P. P.; Reddy, C. M. Co-Crystals of Sulfamethazine with Some Carboxylic Acids and Amides: Co-Former Assisted Tautomerism in an Active Pharmaceutical Ingredient and Hydrogen Bond Competition Study. *Cryst. Growth Des.* **2011**, *11* (8), 3489−3503.
(30) Singh, M. P.; Baruah, J. B. Combinations of Tautomeric Forms and Neutral-Cationic Forms in the Cocrystals of Sulfamethazine with Carboxylic Acids. *ACS Omega* **2019**, *4* (7), 11609−11620.
(31) Elacqua, E.; Bučar, D. K.; Henry, R. F.; Zhang, G. G. Z.; MacGillivray, L. R. Supramolecular Complexes of Sulfadiazine and Pyridines: Reconfigurable Exteriors and Chameleon-like Behavior of Tautomers at the Co-Crystal-Salt Boundary. *Cryst. Growth Des.* **2013**, *13* (1), 393−403.
(32) Braschi, I.; Paul, G.; Gatti, G.; Cossi, M.; Marchese, L. Embedding Monomers and Dimers of Sulfonamide Antibiotics into High Silica Zeolite Y: An Experimental and Computational Study of the Tautomeric Forms Involved. *RSC Adv.* **2013**, *3* (20), 7427−7437.
(33) Cruz-Cabeza, A. J. Acid-Base Crystalline Complexes and the PKa Rule. *CrystEngComm* **2012**, *14* (20), 6362−6365.
(34) Lemmerer, A.; Govindraju, S.; Johnston, M.; Motloung, X.; Savig, K. L. Co-Crystals and Molecular Salts of Carboxylic Acid/Pyridine Complexes: Can Calculated PKa's Predict Proton Transfer? A Case Study of Nine Complexes. *CrystEngComm* **2015**, *17* (19), 3591−3595.
(35) Kumar, V.; Thaimattam, R.; Dutta, S.; Munshi, P.; Ramanan, A. Structural Landscape of Multicomponent Solids Based on Sulfa Drugs. *CrystEngComm* **2017**, *19* (21), 2914−2924.
(36) Nakai, H.; Takasuka, M.; Shiro, M. X-Ray and Infrared Spectral Studies of the Ionic Structure of Trimethoprim - Sulfamethoxazole 1 : 1 Molecular Complex. *J. Chem. Soc. Perkin Trans. 2* **1984**, No. 9, 1459−1464.
(37) Malathy, S.; Nirmalram, J. S.; Muthiah, P. T. Crystal Structure of 4-[(5-Methylisoxazol-3-Yl)Aminosulfonyl]Anilinium 3,5-Dinitrosalicylate. *Acta Crystallogr. Sect. E Crystallogr. Commun.* **2015**, *71* (10), 618−620.
(38) Samanta, R.; Kanaujia, S.; Reddy, C. M. New Co-Crystal and Salt Form of Sulfathiazole with Carboxylic Acid and Amide. *J. Chem. Sci.* **2014**, *126* (5), 1363−1367.
(39) Ruiz-Palomero, C.; Kennedy, S. R.; Soriano, M. L.; Jones, C. D.; Valcárcel, M.; Steed, J. W. Pharmaceutical Crystallization with Nanocellulose Organogels. *Chem. Commun.* **2016**, *52* (50), 7782−7785.
(40) Pratt, J.; Hutchinson, J.; Klein Stevens, C. L. Sulfapyridine (Polymorph III), Sulfapyridine Dioxane Solvate, Sulfapyridine Tetra-Hydro-Furan Solvate and Sulfapyri-Dine Piperi-Dine Solvate, All at 173 K. *Acta Crystallogr. Sect. C Cryst. Struct. Commun.* **2011**, *67* (12), o487−o491.
(41) Alsubaie, M.; Aljohani, M.; Erxleben, A.; McArdle, P. Cocrystal Forms of the BCS Class IV Drug Sulfamethoxazole. *Cryst. Growth Des.* **2018**, *18* (7), 3902−3912.
(42) Shefter, E.; Sackman, P. Structural Studies on Molecular Complexes V: Crystal Structures of Sulfathiazole—Sulfanilamide and Sulfathiazole—Theophylline Complexes. *J. Pharm. Sci.* **1971**, *60* (2), 282−286.
(43) Oruganti, M.; Trivedi, D. R. 4-Nitrobenzoic Acid-Sulfathiazole (1/1). *Acta Crystallogr. Sect. E Struct. Reports Online* **2014**, *70* (1), o85.
(44) Bruker. *SAINT+* (Including XPREP). Bruker AXS Inc.: Madison, Wisconsin, USA, 2012.
(45) Farrugia, L. J. WinGX Suite for Small-Molecule Single-Crystal Crystallography. *J. Appl. Crystallogr.* **1999**, *32* (4), 837−838.
(46) Sheldrick, G. M. SHELXT - Integrated Space-Group and Crystal-Structure Determination. *Acta Crystallogr., Sect. A: Found. Adv.* **2015**, *71* (1), 3−8.
(47) Farrugia, L. J. ORTEP-3 for Windows - A Version of ORTEP-III with a Graphical User Interface (GUI). *J. Appl. Crystallogr.* **1997**, *30* (5), 565.
(48) Macrae, C. F.; Edgington, P. R.; McCabe, P.; Pidcock, E.; Shields, G. P.; Taylor, R.; Towler, M.; Van De Streek, J. Mercury: Visualization and Analysis of Crystal Structures. *J. Appl. Crystallogr.* **2006**, *39* (3), 453−457.
(49) Groom, C. R.; Bruno, I. J.; Lightfoot, M. P.; Ward, S. C. The Cambridge Structural Database. *Acta Crystallogr., Sect. B: Struct. Sci., Cryst. Eng. Mater.* **2016**, *72* (2), 171−179.
(50) Shunje, K. N.Multicomponent Crystals of Sulfapyridine and Sulfadiazine. Masters Thesis, Cape Peninsula University of Technology, 2017; DOI: 10.1107/s2053273318089994.
(51) Wojnarska, J.; Gryl, M.; Seidler, T.; Stadnicka, K. M. Effect of Substituent Exchange on Optical Anisotropy in Multicomponent Isostructural Materials Containing Sulfathiazole and 2-Aminopyridine Derivatives. *Cryst. Growth Des.* **2020**, *20* (10), 6535−6544.
(52) Maury, L.; Rambaud, J.; Pauvert, B.; Lasserre, Y.; Berge, G.; Audran, M. Étude Physico-Chimique, Spectres De Vibration Et Structure Du Sulfaméthoxazole. *Can. J. Chem.* **1985**, *63* (11), 3012−3018.
(53) Dubey, R. P.; Patel, U. H.; Tailor, S. M. DFT Studies, Hirshfeld Surface Analysis and Crystal Structure of Novel Silver Complex of Sulfapyridine with Secondary Ligand Pyridine. *Mol. Cryst. Liq. Cryst.* **2017**, *656* (1), 139−152.
(54) Fábry, J. A Resonance-Assisted Intramolecular Hydrogen Bond in Compounds Containing 2-Hydroxy-3,5-Dinitrobenzoic Acid and Its Various Deprotonated Forms: Redetermination of Several Related Structures. *Acta Crystallogr. Sect. E Crystallogr. Commun.* **2018**, *74*, 1344−1357.
(55) *SciFinder*https://scifinder.cas.org/scifinder/view/scifinder/scifinderExplore.jsf (accessed Mar 22, 2021).
(56) Bingham, A. L.; Hughes, D. S.; Hursthouse, M. B.; Lancaster, R. W.; Tavener, S.; Threlfall, T. L. Over One Hundred Solvates of Sulfathiazole. *Chem. Commun.* **2001**, No. 7, 603−604.

Chapter 5 Exploring the Crystal Structure Landscape of 3,5-Dinitrobenzoic Acid through Various Multicomponent Molecular Complexes

5.1 Introduction

Seven multi-component crystals containing **dnba** were synthesized and characterized. A diverse range of coformers were used to synthesize these multi-component crystals. Hirshfeld analysis was used to analyse the weaker intermolecular interactions, while the CSD database was used to analyse trends involving crystal structures containing **dnba**.

Authors: Scheepers, M.C., Lemmerer A.

Journal: *Crystal Growth & Design*

Date Published: 24 December 2020

Volume Number: 21

Pages: 344-356

Number of citations as of 10 November 2022: 5

CRYSTAL GROWTH & DESIGN

pubs.acs.org/crystal

Article

Exploring the Crystal Structure Landscape of 3,5-Dinitrobenzoic Acid through Various Multicomponent Molecular Complexes

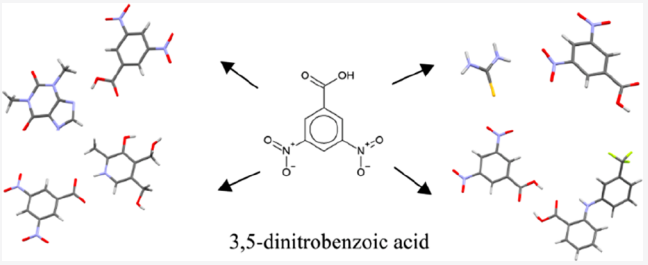
Matthew C. Scheepers and Andreas Lemmerer*

Cite This: *Cryst. Growth Des.* 2021, 21, 344–356

Read Online

ACCESS | Metrics & More | Article Recommendations | Supporting Information

ABSTRACT: Seven new multicomponent crystals, including one hydrate, one solvate, one molecular salt, and four cocrystals, consisting of 3,5-dinitrobenzoic acid with various coformers were synthesized and presented. These coformers include 2-acetylpyridine, 3-cyanopyridine, flufenamic acid, dimethylaminobenzophenone, pyridoxine, theophylline, and thiourea. Both hydrogen-bonding and weaker intermolecular forces such as C−H···π bonding, π-hole, and π···π contribute significantly to the overall packing scheme of each structure. Hirshfeld surfaces were used to identify these intermolecular forces. These structures were compared to those in the literature using the Cambridge Structural Database (CSD). These multicomponent crystals were characterized by single-crystal X-ray diffraction (SC-XRD) and differential scanning calorimetry (DSC).



Downloaded via UNIV OF THE WITWATERSRAND on June 13, 2022 at 09:14:21 (UTC).
See https://pubs.acs.org/sharingguidelines for options on how to legitimately share published articles.

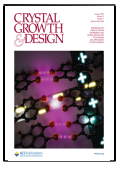
INTRODUCTION

The search for alternative methods for improving currently existing active pharmaceutical ingredients (APIs) with poor properties without modifying the drug itself has become critical. The formulation of APIs consisting of either a salt or a cocrystal has increased in the past few decades.[1−3] Cocrystals and molecular salts often have properties which differ significantly from those of the respective coformers. For pharmaceutical drugs improving properties such as solubility, tabletability, and intrinsic dissolution rates are critical, and the use of cocrystals has achieved this.[4,5] For this reason it makes the search for new multicomponent crystals so attractive.

3,5-Dinitrobenzoic acid (**dnba**), the molecule of interest in this work, consists of a carboxylic acid group and two nitro groups, all in a positions meta to each other. Several multicomponent crystal structures, both binary and ternary, involving **dnba** have been published in the Cambridge Structural Database (CSD),[6] including those which include various APIs.[7−9] A total of 278 results of cocrystals and molecular salts have been reported. Studies involving **dnba** include high energy density related materials,[10,11] short, strong hydrogen bonding[12] and the crystal engineering of APIs.[13−15] Although the primary interactions will be due to the formation of a hydrogen bond between the carboxylic acid and a suitable hydrogen bond acceptor of the coformer, other types of weaker interactions exist and could contribute significantly. For example, π holes from the nitro groups can form directional intermolecular interactions between neighboring molecules.[16] Due to the strongly electron withdrawing nitro groups the ring of **dnba** is relatively π-electron poor, which therefore makes **dnba** a potential charge-transfer acceptor molecule.

In this work we present seven new multicomponent crystals of **dnba**, which formed one solvate, one hydrate, one molecular salt, and four cocrystals. Most of the coformers chosen consist of N-containing heterocycles, with the rest consisting of various functional groups. These coformers include 2-acetylpyridine (**2acp**), 3-cyanopyridine (**3cnp**), flufenamic acid (**fa**), dimethylaminobenzophenone (**dmabp**), pyridoxine (**pyd**), theophylline (**thp**), and thiourea (**tu**) (see Scheme 1). Two of these coformers are APIs: **fa** is a nonsteroidal anti-inflammatory (NSAID) drug, while **thp** is used as a muscle relaxant or vasodilator in the treatment of respiratory issues such as asthma.[17,18] **pyd**, also referred to as vitamin B_6, is a nitrogen-containing heterocycle with several hydroxyl groups which can form potential hydrogen bonds with the nitro groups of **dnba**. **3cnp** and **2acp** were chosen to explore more crystal forms of these compounds as well, since not many crystal structures involving these compounds have been reported. **dmabp**, a derivative of benzophenone, is generally used as a photoinhibitor.[19] **dmabp** is structurally similar to Michler's ketone, which is used as an intermediate in the synthesis of various dyes. Although various benzophenone derivatives have been explored as potential coformers with **dnba**, only **dmabp** formed a multicomponent crystal. The aim

Received: September 1, 2020
Revised: December 3, 2020
Published: December 24, 2020



ACS Publications

© 2020 American Chemical Society

Scheme 1. Structures of dnba and the Coformers Used for This Work

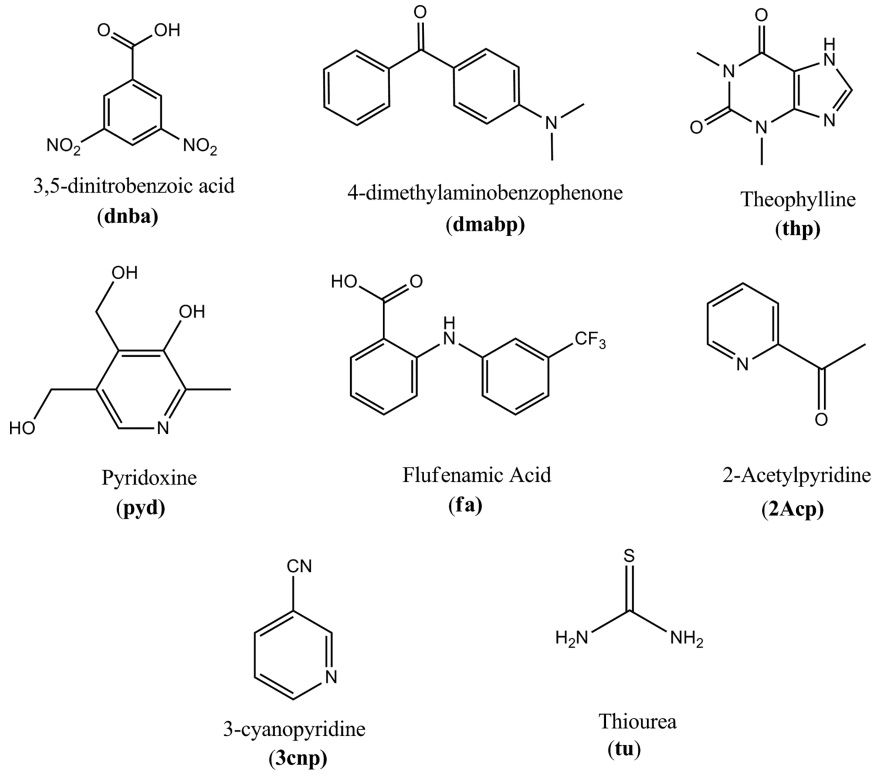


Table 1. Solvent System Used to Synthesize the Respective Multicomponent Molecular Complex

coformer	mass used (g)	solvent system
2-acetylpyridine	1.08 (1 mL, 8.915 mmol)	ethanol
3-cyanopyridine	0.049 (0.471 mmol)	ethanol
diethylaminobenzophenone	0.106 (0.471 mmol)	methanol[a]
flufenamic acid	0.133 (0.471 mmol)	ethanol/water (1/1 v/v)/ acetic acid
pyridoxine	0.080 (0.471 mmol)	ethanol
theophylline monohydrate	0.093 (0.471 mmol)	ethyl acetate
thiourea	0.036 (0.471 mmol)	ethyl acetate
3-aminopyridine	0.049 (0.471 mmol)	ethanol

[a]It should be noted that trace amounts of water were present in the starting material for methanol. This, along with the possibility of water from the atmosphere, resulted in the formation of the hydrate.

of this work is to observe new supramolecular assemblies with **dnba**, using a diverse range of coformers.

EXPERIMENTAL SECTION

All reagents used for synthesis and characterization were of analytical grade and were purchased from Sigma-Aldrich. Reagents were used as received, without further purification. Equimolar amounts of **dnba** (100 mg, 0.471 mmol) and the respective coformers were stirred in a heated solution of the respective solvent until no solid remained. This solution was left loosely covered, which evaporated to yield the respective cocrystal/salt. See Table 1 for the solvent systems used.

It should be noted that although several different solvents were used in an attempt to obtain a multicomponent crystal in a relatively high yield and pure form, those solvents did not yield the desired multicomponent crystal. In addition, several molar ratios were used (e.g. 2:1, 1:2, etc. **dnba**:coformer), but this yielded a mixture of the desired multicomponent crystal (in a 1:1 ratio) with the excess component. Heating was found to be essential in most of the cases (the multicomponent crystals consisting of the pyridine-based coformers did not essentially need heating, although heating helped in acquiring complete dissolution quickly), otherwise the desired multicomponent crystal could not be obtained.

Powder X-ray Diffraction (PXRD). Powder X-ray diffraction data for all compounds were measured at 293 K on a Bruker D2 Phaser diffractometer which employed a sealed-tube Co X-ray source (λ = 1.78896 Å), operating at 30 kV and 10 mA, and a LynxEye PSD detector in Bragg–Brentano geometry. Powder patterns for each sample are given in the Supporting Information, where the experimentally obtained data are compared to the calculated patterns obtained from the SC-XRD data.

Single Crystal X-ray Diffraction (SC-XRD). A Bruker D8 VENTURE PHOTON CMOS 100 area detector diffractometer, equipped with a graphite-monochromated Mo Kα_1 sealed tube (50 kV, 30 mA), was used to collect all of the intensity data. Crystal structures were determined at 173 K to achieve satisfactory thermal ellipsoids. The program SAINT+, version 6.02,[20] was used to integrate the data, and the program SADABS[21] was used to make empirical absorption corrections. Space group assignments were made using XPREP[21] on all compounds. In all cases, the structures were solved in the WinGX Suite of programs[21] by direct methods using SHELXS-97[21] and refined using full-matrix least-squares/difference Fourier techniques on F^2 using SHELXL-97.[21] All non-hydrogen atoms were refined anisotropically. All carbon-bound hydrogen atoms were placed at idealized positions and refined as riding atoms with its

https://dx.doi.org/10.1021/acs.cgd.0c01217
Cryst. Growth Des. 2021, 21, 344−356

U_{iso} parameter being 1.2 or 1.5 times those of their parent atoms. Unless otherwise stated, nitrogen-bound and oxygen-bound hydrogen atoms were located in the difference Fourier map and their coordinates and isotropic displacement parameters refined freely. Diagrams and publication material were generated using ORTEP-3[22] and Mercury.[23]

Cambridge Structural Database Analysis. The Cambridge Structural Database (CSD)[6] was analyzed to determine any common trends occurring among different multicomponent structures consisting of **dnba**. A combined query using both the carboxylic acid form of **dnba** and the carboxylate form was used to search for entries. Entries were filtered using 3D coordinates and organics. Entries containing salts with alkali or alkali-earth cations, heavily disordered molecules, and/or solvates were not examined. Mercury[23] was used to inspect the crystal structures.

Crystal structures were determined to be binary, ternary, or greater and consist of either or both the protonated (carboxylic acid form) and deprotonated (carboxylate) forms. In the case of a ternary or greater structure, only the interactions involving **dnba** were considered. In the case of multiple entries of the same crystal structure, only one entry was inspected and counted.

Hirshfeld Surface Analysis. Hirshfeld surface analysis is a computational method that can be used to explore intermolecular interactions in molecular crystals that are weaker than hydrogen bonds,[24−26] as well as to determine the "shape" of molecular fragments, which are key to understanding the overall packing. The figures and fingerprint plots presented in this work were generated using Crystal Explorer 17.5.[27] All images were generated using a high (standard) resolution.

Differential Scanning Calorimetry (DSC). Differential scanning calorimetry data were collected using a Mettler Toledo 822^e instrument with aluminum pans under nitrogen gas (flow rate 10 mL/min). Exothermic events were shown as peaks. Samples were heated and cooled to determine melting points as well as any additional phase transitions. The temperature and energy calibrations were performed using pure indium (purity 99.99%, mp 156.6 °C, heat of fusion 28.45 J g^{-1}) and pure zinc (purity 99.99%, mp 479.5 °C, heat of fusion 107.5 J g^{-1}).

RESULTS AND DISCUSSION

Seven multicomponent crystals containing **dnba** have been synthesized, of which four are cocrystals, one is a hydrate, one is a solvate, and one is a salt. It should be noted that for the pyridine derivatives and theophylline it is possible for either a salt or a cocrystal to form. A "rule of thumb" exists that if the pK_a values of both compounds are known, it is possible to predict whether a salt or cocrystal will form. This is done by calculating the ΔpK_a, which is given by the formula,

$$\Delta pK_a = pK_a(\text{conjugate acid of base}) - pK_a(\text{acid})$$

If the ΔpK_a value is less than zero a cocrystal would form (if it forms), whereas a value greater than 2−3 should lead to a salt. Values between 0 and 3 can predict neither case and are 0 for the crystal systems in question.[27] For this work, **dnba** could have formed either a salt or a cocrystal with **2acp**, **3cnp**, **pyd**, **thp** and **tu**. Table 2 gives the comparison of the results predicted by the pK_a rule vs the actual results of the crystal structures formed. It shows that the rule works for at least three of the five multicomponent crystal structures.

Table 2. Comparison of the Result Predicted by the pK_a Rule vs the Actual Result of the Crystal Structures Formed[a]

coformer	pK_a of coformer	ΔpK_a	result based on rule	actual result
2acp	3.00	0.33	undetermined	cocrystal
3cnp	1.78	0.23	undetermined	cocrystal
Pyd	9.63	6.86	salt	salt
thp	8.60	5.83	salt	cocrystal
tu	1.44	−1.33	cocrystal	cocrystal

[a] pK_a for **dnba** = 2.77. Values from SciFinder.[28]

These crystals were characterized, and a description of each crystal structure is given below (Figure 1). Crystallographic data and hydrogen bonds are given in Tables 3 and 4, respectively. Hirshfeld surfaces for d_i, d_e, d_{norm}, the shape index, and curvedness and the respective fingerprint plots were generated and are presented in the Supporting Information unless stated otherwise. The discussion of each of the Hirshfeld surfaces generated for each molecular complex are discussed together with the description of the crystal structures.

Crystal Structure Descriptions of Dnba Complexes. ***dnba* + *2acp*.** **dnba** formed a solvate with **2acp**, forming colorless plates (Figure 2). The solvate crystallizes in the $P2_1/n$ space group, with the asymmetric unit consisting of one molecule each of **dnba** and **2acp**. **dnba** forms a discrete hydrogen bond to the pyridinium of **2acp** with the carboxylic acid group. This dimer forms 2D sheets which stack together.

The Hirshfeld surfaces generated revealed additional intermolecular interactions present in the crystal. Red spots on the d_{norm} surface indicate the presence of weak C−H···O hydrogen bond interactions, with both the acetyl and nitro groups being involved. The shape index shows that N−O···π and C−O···π formed from the nitro and acetyl groups, respectively. The shape index does not indicate the presence of any π···π type interactions, which is normally indicated by the presence of a red and blue triangle touching each other. These surfaces correlate well with the observed overall packing pattern of the crystal: the weak C−H···O hydrogen bonds favor the formation of different "layers", while the N−O···π and C−O···π interactions allows the "layers" to stack together.

***dnba* + *3cnp*.** **dnba** formed a cocrystal with **3cnp**, forming colorless needles (Figure 3). The cocrystal crystallizes in the $P2_1/c$ space group, with the asymmetric unit consisting of one molecule each of **dnba** and **3cnp**. **dnba** forms a discrete hydrogen bond to the pyridine of **3cnp** with the carboxylic acid group. The **3cnp** and **dnba** molecules form alternating columns of each molecule which then stack together with inversion of molecules along its column.

The Hirshfeld surface revealed additional interactions. From the d_{norm} red spots occurring at the cyano nitrogen (N4) and one of the aromatic hydrogens (H10) indicates the formation of a 3-cyanopyridine dimer, with a the graph set $R_2^2(10)$. Large red spots near the nitro groups are indicative of π-hole type interactions. Two cases exist: one where the partially positive π system of the ring of **dnba** interacts with the oxygen of a nitro group that is on a neighboring **dnba** and the other case one of oxygen of the carboxylic acid interacting with the nitrogen of the nitro group of a neighboring **dnba** molecule. Smaller red spots on the d_{norm} indicate the presence of C−H···π type interactions. As a result of the presence of the π-hole-type interactions, the shape index consists of various large "bumps" and "hollows", as indicated by regions of large blue and red spots, respectively, giving rise to various small regions of "flatness", as indicated by the curvedness. As a result, the columns of **dnba** and **3cnp** are held together by π-hole and weak C−H···N interactions, respectively, while the strong hydrogen bond between **dnba** and **3cnp** as well as a few C−

https://dx.doi.org/10.1021/acs.cgd.0c01217
Cryst. Growth Des. 2021, 21, 344−356

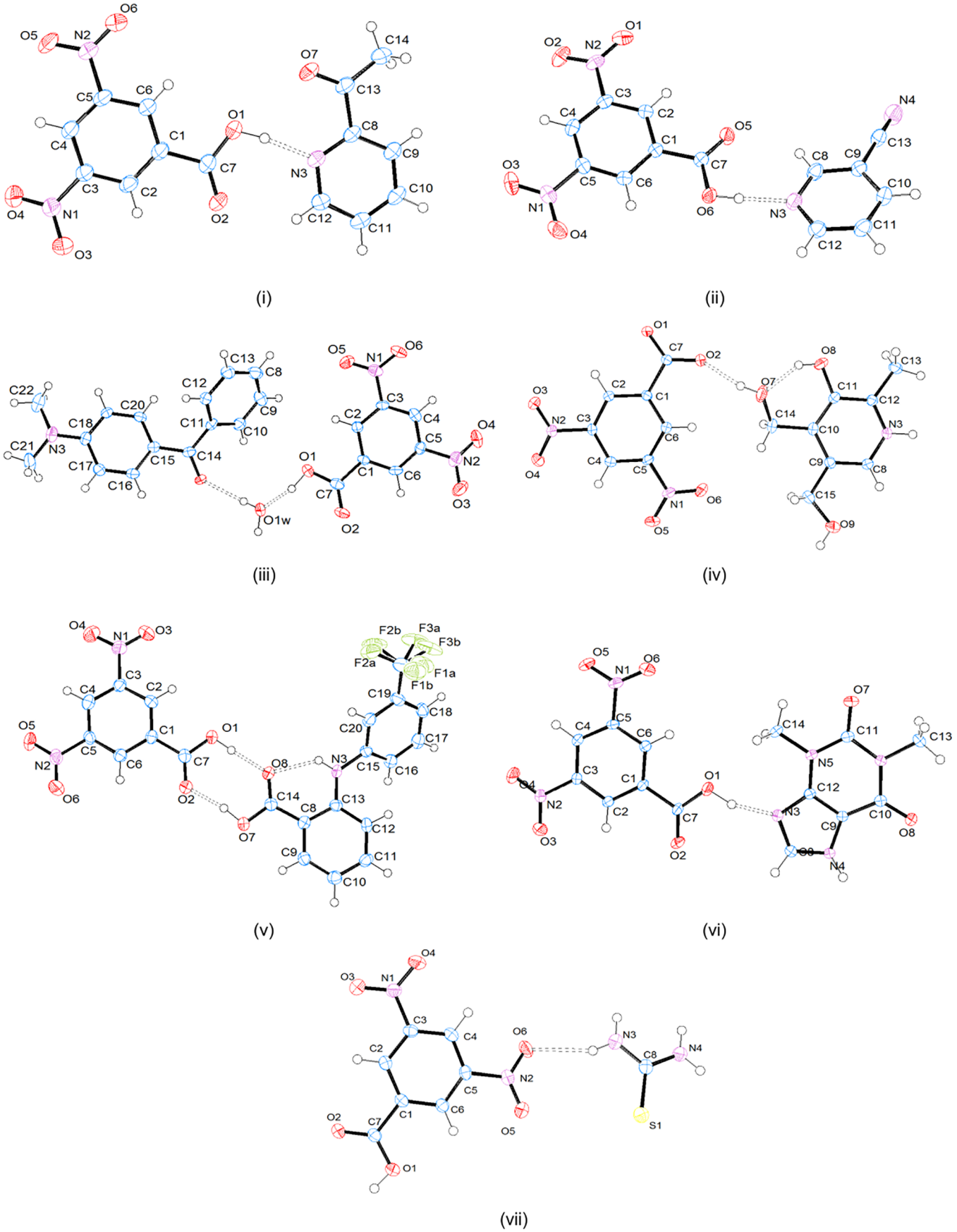


Figure 1. Ortep diagrams for the asymmetric units for the crystal structures of (i) **dnba** + **2acp**, (ii) **dnba** +**3cnp**, (iii) **dnba** + **dmabp**, (iv) **dnba** + **pyd**, (v) **dnba** + **fa**, (vi) **dnba** + **thp**, and (vii) **dnba** + **tu**, which shows the atom-numbering scheme. Displacement ellipsoids are drawn at the 50% probability level, and H atoms are shown as small spheres of arbitrary radii. The symmetry-independent hydrogen bonds are shown as dashed lines.

https://dx.doi.org/10.1021/acs.cgd.0c01217
Cryst. Growth Des. 2021, 21, 344−356

Table 3. Summary of Crystallographic Data

	cocrystal + salt			
	dnba + 2acp	**dnba + 3cnp**	**dnba + dmabp**	**dnba + fa**
empirical formula	$C_{14}H_{11}N_3O_7$	$C_{13}H_8N_4O_6$	$C_{22}H_{21}N_3O_8$	$C_{21}H_{14}N_3O_8F_3$
formula wt	333.26	316.23	455.42	493.35
temp (K)	173(2)	173(2)	173(2)	173(2)
cryst syst	monoclinic	monoclinic	monoclinic	triclinic
space group	$P2_1/n$	$P2_1/c$	$P2_1/n$	$P\bar{1}$
a (Å)	8.9295(9)	6.1678(3)	10.0968(2)	7.6667(4)
b (Å)	13.9281(14)	9.2276(5)	21.2232(5)	10.7718(5)
c (Å)	11.8082(11)	24.0942(13)	10.3367(3)	13.4392(5)
α (deg)	90	90	90	70.846(2)
β (deg)	100.347(3)	96.703(2)	101.2240(10)	84.228(2)
γ (deg)	90	90	90	88.073(2)
V (Å^3)	1444.7(2)	1361.92(12)	2172.65(9)	1043.11(8)
Z	4	4	4	2
density (g/cm^3)	1.532	1.542	1.392	1.571
μ (mm^{-1})	0.126	0.126	0.108	0.139
F(000)	688	648	952	504
crystal size (mm^3)	0.512 × 0.248 × 0.248	0.347 × 0.258 × 0.159	0.213 × 0.221 × 0.268	0.142 × 0.117 × 0.052
2θ range for data collection (deg)	4.566−56.922	6.652−55.984	1.919−28.335	3.222−50.998
no. of rflns collected	13893	27504	41576	15916
no. of indep rflns	3638 (R(int) = 0.0717, $R(\sigma)$ = 0.0614)	3286 (R(int) = 0.0451, $R(\sigma)$ = 0.0289)	2901 (R(int) = 0.0953, $R(\sigma)$ = 0.0361)	3871 (R(int) = 0.0746, $R(\sigma)$ = 0.0776)
goodness of fit on F^2	1.022	1.037	1.015	1.098
final R indexes ($I \geq 2\sigma(I)$)	R1 = 0.0553, wR2 = 0.1420	R1 = 0.0473, wR2 = 0.1032	R1 = 0.0458, wR2 = 0.0944	R1 = 0.0660, wR2 = 0.1413
final R indexes (all data)	R1 = 0.0936, wR2 = 0.1678	R1 = 0.0679, wR2 = 0.1124	R1 = = 0.0759, wR2 = 0.1037	R1 = 0.1308, wR2 = 0.1636
CCDC	2026651	2026652	2026653	2026654

	cocrystal/salt		
	dnba + pyd	**dnba + thp**	**dnba + tu**
empirical formula	$C_{15}H_{15}N_3O_9$	$C_{14}H_{12}N_6O_8$	$C_8H_8N_4O_6S$
formula wt	381.3	392.3	288.24
temp (K)	173(2)	173(2)	173(2)
cryst syst	monoclinic	monoclinic	monoclinic
space group	$P2_1/n$	$C2/c$	$P2_1/c$
a (Å)	9.2152(5)	18.7625(6)	13.0957(2)
b (Å)	14.1356(7)	15.4699(6)	9.0162(2)
c (Å)	12.5534(6)	12.6823(4)	9.8594(2)
α (deg)	90	90	90
β (deg)	104.378(2)	117.917(2)	92.6450(10)
γ (deg)	90	90	90
V (Å^3)	1584.02(14)	3252.7(2)	1162.89(4)
Z	4	8	4
density (g/cm^3)	1.599	1.602	1.646
μ (mm^{-1})	0.135	0.134	0.31
F(000)	792	1616	592
crystal size (mm^3)	0.215 × 0.436 × 0.080	0.415 × 0.401 × 0.206	0.243 × 0.193 × 0.163
2θ range for data collection (deg)	6.296−55.984	5.266−55.998	3.114−55.994
no. of rflns collected	36275	36969	17130
no. of indep rflns	3814 (R(int) = 0.0344, $R(\sigma)$ = 0.0172)	3044 (R(int) = 0.0357, $R(\sigma)$ = 0.0219)	2797 (R(int) = 0.0506, $R(\sigma)$ = 0.0393)
goodness of fit on F^2	1.061	1.061	1.014
final R indexes ($I \geq 2\sigma(I)$)	R1 = 0.0405, wR2 = 0.1108	R1 = 0.0427, wR2 = 0.1186	R1 = 0.0368, wR2 = 0.0819
final R indexes (all data)	R1 = 0.0521, wR2 = 0.1227	R1 = 0.0501, wR2 = 0.1247	R1 = 0.0616, wR2 = 0.0933
CCDC	2026655	2026656	2026657

H···π interactions allow the columns to alternate with each other, as observed in the overall packing.

dnba + pyd. **dnba** and **pyd** formed molecular salts, which crystallized as yellow prismatic crystals (Figure 4). The asymmetric unit consists of one molecule each of **dnba** and **pyd**, which crystallized in the $P2_1/n$ space group. A proton transfer occurred between the carboxylic acid of **dnba** and the pyridinium of **pyd**. One of the hydroxyl groups forms an intramolecular hydrogen bond with another neighboring hydroxyl group (O8−H8···O7). **dnba** and **pyd** form several different hydrogen bonds that form a continuous 2D lattice, with these lattices stacking on top of each other.

https://dx.doi.org/10.1021/acs.cgd.0c01217
Cryst. Growth Des. 2021, 21, 344−356

Table 4. Hydrogen Bonds

D−H···A	d(D−H) (Å)	d(H···A) (Å)	d(D···A) (Å)	∠(DHA) (deg)
dnba + 2acp				
O1−H1···N3	0.98(3)	1.73(3)	2.707(2)	171(3)
dnba + 3cnp				
O6−H6···N3	0.93(2)	1.74(3)	2.6684(19)	175(2)
dnba + dmabp				
O1W−H1WA···O7[a]	0.92(6)	1.93(6)	2.842(5)	170(5)
O1W−H1WB···O7	0.77(6)	2.02(6)	2.789(5)	180(6)
O1−H2A···O1W	1.01(7)	1.57(6)	2.558(4)	164(6)
dnba + fa				
O1−H1···O8	0.92(5)	1.72(5)	2.625(4)	167(5)
N3−H3···O1[b]	0.98(2)	1.65(2)	2.6269(15)	174(2)
N3−H3···O2[b]	0.98(2)	2.57(2)	3.2529(15)	126(2)
O9−H9···O4[c]	0.88(3)	2.15(3)	3.0239(17)	175(2)
O7−H7···O2	0.87(3)	1.76(3)	2.6019(15)	162(2)
O8−H8···O7	0.86(3)	1.80(3)	2.5685(17)	147(3)
dnba + thp				
N4−H4···O8[d]	0.98(3)	1.76(3)	2.7264(16)	172(2)
O1−H1···N3	1.01(3)	1.66(3)	2.6264(15)	160(3)
dnba + pyd				
N3−H3···O1[h]	0.98(2)	1.65(2)	2.6269(15)	174(2)
N3−H3···O2[h]	0.98(2)	2.57(2)	3.2529(15)	126(2)
O9−H9···O4[c]	0.88(3)	2.15(3)	3.0239(17)	175(2)
O7−H7···O2	0.87(3)	1.76(3)	2.6019(15)	162(2)
O8−H8···O7	0.86(3)	1.80(3)	2.5685(17)	147(3)
dnba + tu				
N4−H4B···S1[e]	0.89(2)	2.49(2)	3.3773(18)	173(2)
N3−H3A···O6	0.82(2)	2.39(2)	3.108(2)	146(2)
N4−H4A···S1[f]	0.85(2)	2.66(2)	3.4502(19)	157(2)
N3−H3B···S1[f]	0.89(2)	2.66(3)	3.470(2)	152(2)
O1−H1···O2[g]	0.88(3)	1.77(3)	2.6524(18)	176(3)
N4−H4B···S1[e]	0.89(2)	2.49(2)	3.3773(18)	173(2)

[a] $-x+1, -y+1, -z+2$. [b] $x-1/2, -y+1/2, z+1/2$. [c] $x-1/2, -y+3/2, z+1/2$. [d] $-x+3/2, -y+3/2, -z+1$. [e] $-x+1, -y+1, -z$. [f] $-x+1, y+1/2, -z+1/2$. [g] $-x+2, -y, -z+2$. [h] $x-1/2, -y+1/2, z+1/2$.

The Hirshfeld surfaces for the molecular salt of **dnba + pyd** show that the hydrogen bond is the most significant intermolecular interaction present. The large, bright red spots present in the d_{norm} are involved with hydrogen bonding, with a few smaller and dimmer set of red spots which are involved with weaker C−H···O hydrogen bonding. Although the shape index has the presence of red and blue triangles that are typical indicators for the presence of a $\pi\cdots\pi$ interaction, the blue edges on the curvedness surface indicate otherwise. Most likely the 2D lattices formed are stacked together by a combination of both ionic forces and weak C−H···O interactions.

dnba + dmbp Hydrate. **dnba** and **dmabp** formed a hydrated molecular complex and crystallized as fragile orange plates (Figure 5). This molecular complex crystallized in the $P2_1/n$ space group with the asymmetric unit consisting of one molecule of each **dnba**, **dmabp**, and water. **dnba**, **dmabp**, and water form part of a dimer, where water acts as the primary hydrogen bond donor and acceptor. In this structure, water forms a bridge between **dnba** and **dmabp** by acting as a hydrogen bond acceptor from **dnba** and as a hydrogen bond donor to **dmabp** and another water molecule. These dimers formed 2D sheets which stack to form a layered structure.

The Hirshfeld surface reveals the presence of both π-hole and $\pi-\pi$ stacking in addition to the hydrogen bonding present. The bright red spots observed on the d_{norm} surface are related to the previously described strong hydrogen bonding. A few red spots appear over the nitro group O5−N1−O6 which indicates the presence of a π-hole-type interaction to the carboxylic acid group of an adjacent **dnba** molecule. The shape index indicates the presence of several $\pi-\pi$ stacking type interactions due to the presence of adjacent red and blue triangles on the surface. The first of these is between adjacent benzene rings (C8−C13) of **dmabp**, while the second of these is between the rings of **dnba** and the ring containing the dimethylamino group of **dmabp** (C15−C20). The curvedness shows regions which would allow for the possibility of $\pi-\pi$ stacking. This indicates that while hydrogen bonding yields the formation of the 2D sheets, these sheets are held together via π-hole and $\pi-\pi$ stacking interactions.

dnba + fa. **dnba** formed a cocrystal with **fa**, which crystallized as fragile, orange platelike crystals. The cocrystal crystallizes in the $P\bar{1}$ space group with the asymmetric unit consisting of one molecule of each **dnba** and **fa**. Rotational disorder is present within the trifluoro group on the **fa** molecules. Hydrogen bonding exists between the carboxylic acids of both **dnba** and **fa**, which give the $R_2^2(8)$ ring dimer. The Hirshfeld surface of the **dnba + fa** cocrystal reveals more types of interactions. Red spots of various sizes appear on the

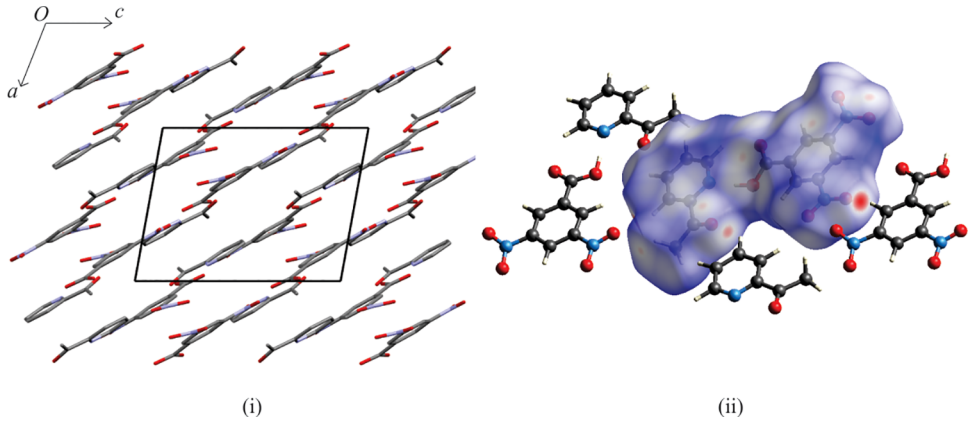


Figure 2. Crystal structure of the solvate **dnba + 2acp** showing (i) the packing (with hydrogen atoms omitted) and (ii) the d_{norm} showing some of the C−H···O interactions (surface mapped between −0.2267 and +1.0880 Å).

https://dx.doi.org/10.1021/acs.cgd.0c01217
Cryst. Growth Des. 2021, 21, 344−356

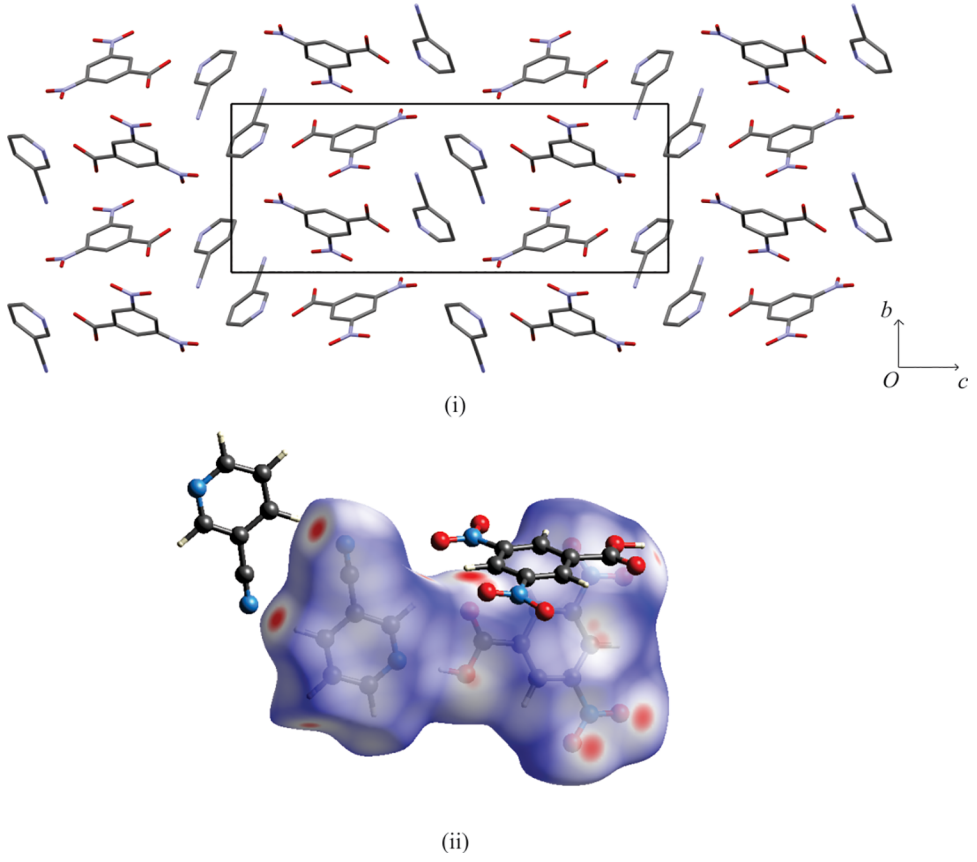


Figure 3. Crystal structure of **dnba** + **3cnp** showing (i) the packing of (with hydrogen atoms omitted) and (ii) the d_{norm} of **dnba** + **3cnp** showing the **3cnp** dimer as well as the π-hole interaction between the carboxylic acid group and one of the nitro groups (surface mapped from −0.1939 to +1.1896 Å).

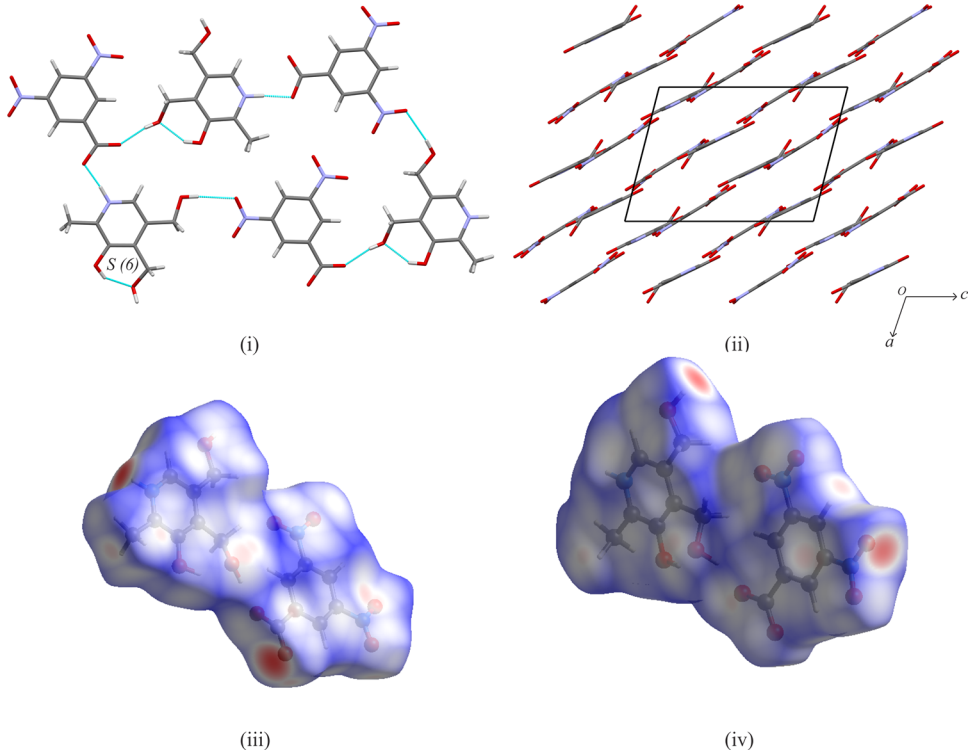


Figure 4. Crystal structure of **dnba** + **pyd** showing (i) the hydrogen bonding and (ii) the packing (with hydrogen atoms omitted) and (iii, iv) the d_{norm} from two different perspectives, where the brightest red spots are due to hydrogen bonding.

https://dx.doi.org/10.1021/acs.cgd.0c01217
Cryst. Growth Des. 2021, 21, 344−356

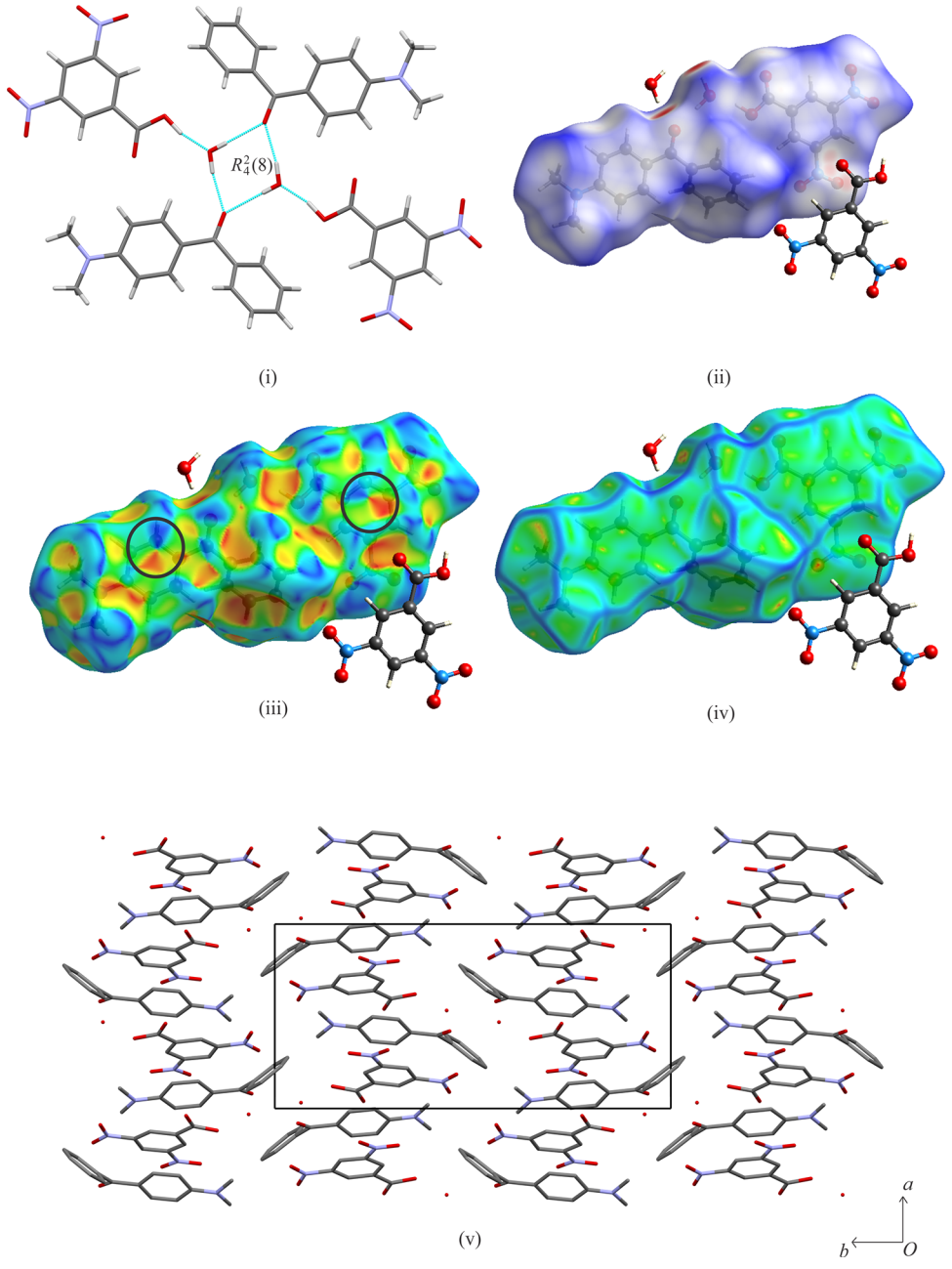


Figure 5. Crystal structure of **dnba** + **dmabp** showing (i) the hydrogen-bonded "water ring", (ii) the d_{norm} showing the π-hole interactions (mapped from −0.5738 to +1.4262 Å), (iii) the shape index with circles showing possible $\pi-\pi$ interactions, (iv) curvedness showing flat regions that could possibly allow for $\pi-\pi$ interactions, and (v) the packing diagram (with hydrogens omitted).

d_{norm}, which indicates the presence of various weak C−H···O, C−H···π, C−O···π and N−O···π interactions. Figure 6(ii) shows where some of these weak interactions may be occurring. The shape index indicates the possibility of $\pi-\pi$ stacking interactions, as indicated by the red and blue triangles in Figure 6(iii) and the presence of a flat region in the curvedness which could allow for such an interaction to exist. This $\pi-\pi$ stacking occurs between inverted dimers: i.e., between **dnba** and the benzoic acid portion of **fa**. This would lead to a layered-type packing in the structure, with the trifluorotoluene portion of **fa** separating different layers.

dnba + ***thp***. **dnba** formed a cocrystal with **thp**, which crystallized as colorless blocks (Figure 7). The asymmetric unit consists of one molecule of each **dnba** and **thp**, crystallizing in the *C*2/*c* space group. The hydrogen H1 was placed geometrically with respect to O1, since this hydrogen could not be found accurately in the Fourier map. **dnba** forms a discrete hydrogen bond between the carboxylic acid O1−H1 to nitrogen N3 of **thp**. **thp** forms part of a dimer held together by two molecules of **thp** forming a ring between N4−H8···O8, with a ring graph set of $R_2^2(10)$. The overall packing is made up of several rows and columns of alternating **dnba** and **thp** molecules.

The Hirshfeld surface shows an additional set of important interactions. The brighter red spots that appear on the d_{norm} surface correspond to the stronger hydrogen bonds described previously, while the less bright spots represent weaker C−H hydrogen bonds. In addition to the strong hydrogen bond

https://dx.doi.org/10.1021/acs.cgd.0c01217
Cryst. Growth Des. 2021, 21, 344−356

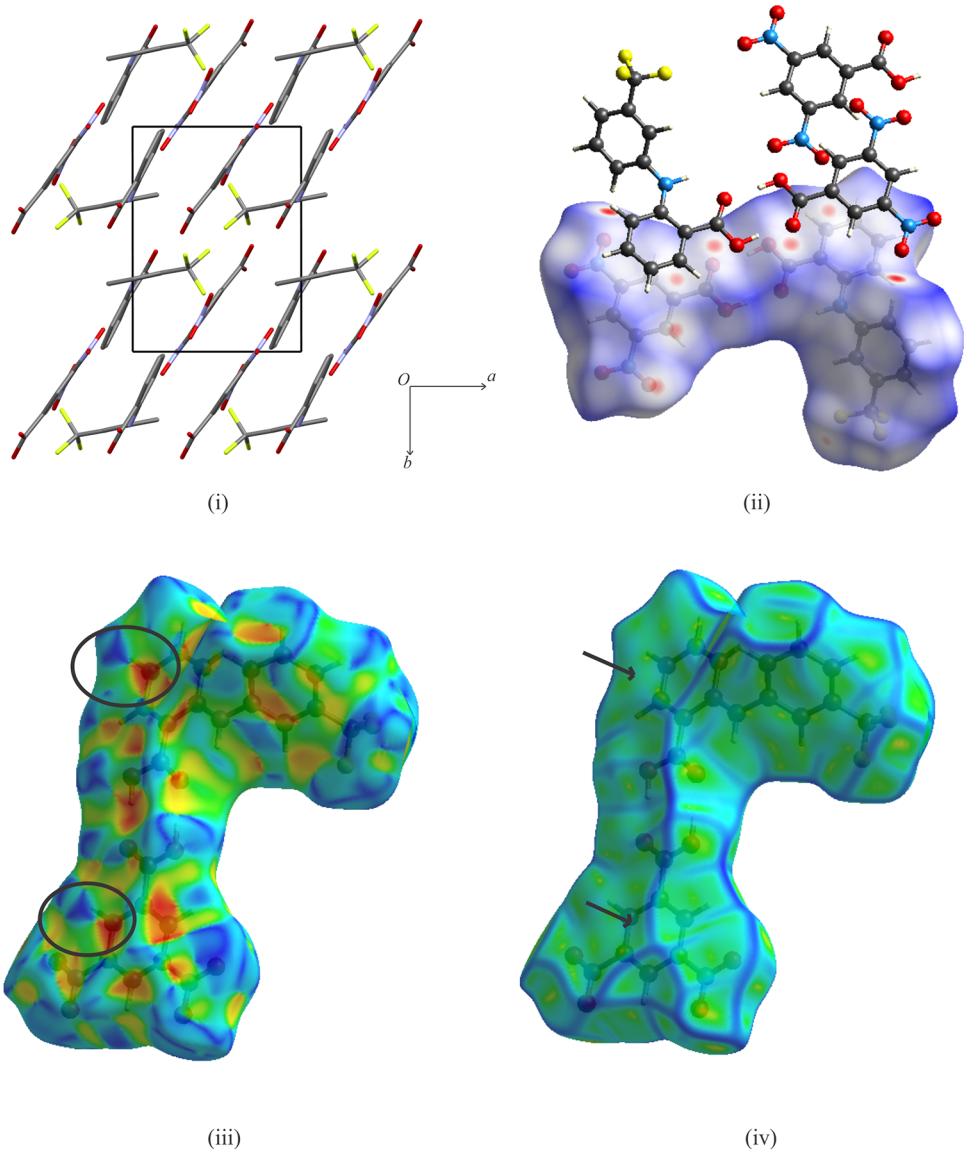


Figure 6. Crystal structure of **dnba** + **fa** showing (i) the packing (with hydrogen atoms omitted), (ii) the d_{norm} showing some of the weaker interactions present (mapped from 0.1410 to 1.4528 Å), (iii) the shape index with circles indicating the presence of some $\pi-\pi$ stacking, and (iv) the curvedness with arrows showing some flat regions where $\pi-\pi$ stacking may be possible.

between **dnba** and **thp** described previously, the weak hydrogen bond C8−H8···O2 forms. In addition, weaker hydrogen bonds form between different neighboring **dnba** molecules via C2−H2···O6 and C4−H4···O2. The presence of red and blue triangles on the shape index on both the ring of **dnba** and imidazole portion of **thp**, as well as the curvedness being flat over the aforementioned regions, indicates the presence of $\pi\cdots\pi$ stacking, which would dominate the overall packing observed in this cocrystal.

***dnba* + *tu*.** **dnba** formed a cocrystal with **tu** and crystallized as pale yellow blocks (Figure 8). This cocrystal crystallizes in the $P2_1/c$ group with the asymmetric unit consisting of one molecule each of **dnba** and **tu**. Both **dnba** and **tu** form a $R_2^2(8)$ homosynthon, which forms a set of two dimers. These dimers interact with each other via the amino group (the group not involved in the homodimer) and one of the nitro groups. In addition, a bifurcated hydrogen-bonded system arises between two **tu** molecules related to each other via the 2-fold screw axis through N4−H4A···S1 and N3−H3B···S1. The Hirshfeld surfaces indicate a π-hole-type interaction in the d_{norm} with the nitro group O3−N1−O4 interacting with the carboxylic acid group of a nearby **dnba** molecule. The packing of this cocrystal is made up of rows of **dnba** molecules alternating with channels of **tu** molecules.

Cambridge Structural Database Analysis. The analysis of the CSD indicates several trends in previously reported multicomponent crystal structures involving **dnba**. The search result of the combined query yielded 362 results. After salts containing alkali or alkakine-earth cations, heavily disordered molecules, and solvates were removed, 259 multicomponent crystal structures were examined further. Some notable examples are given in Table 5. A total of 186 of these results were binary and 73 were ternary or greater. A total of 131 entries consisted of the protonated (carboxylic acid) form, and 186 entries consisted of the deprotonated (carboxylate) form. At least 25 hydrates were reported. Only 5 entries show the formation of the carboxylic acid heterodimer $R_2^2(8)$ ring motif

https://dx.doi.org/10.1021/acs.cgd.0c01217
Cryst. Growth Des. 2021, 21, 344−356

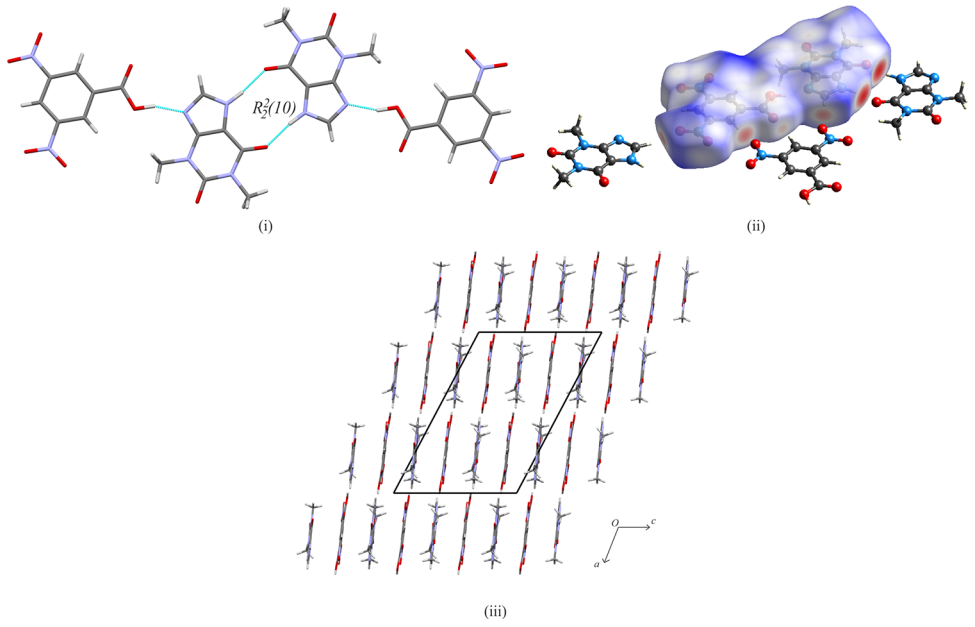


Figure 7. Crystal structure of **dnba** + **thp** showing (i) the hydrogen bonding, (ii), the d_{norm} showing some of the additional weaker hydrogen bonds (mapped from −0.5738−1.4262 Å), and (iii) the packing.

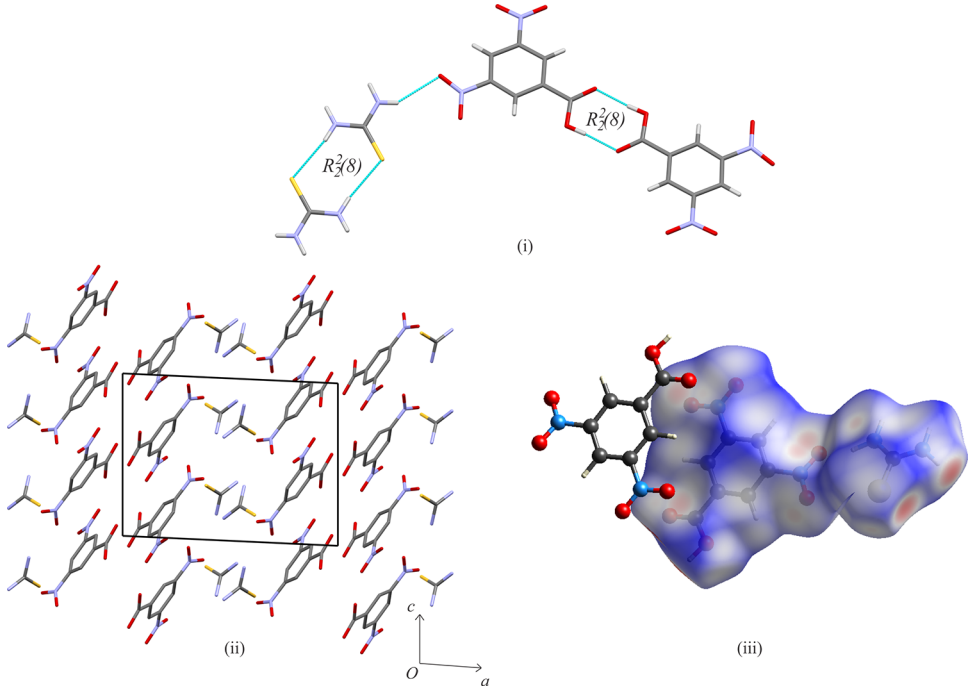


Figure 8. Crystal structure of **dnba** + **tu** showing (i) the hydrogen bonding, (ii) the packing (with hydrogen atoms omitted), and (iii) the d_{norm} showing the π-hole interaction between the nitro group and carboxylic acid (mapped from −0.7297 to +1.5105 Å).

such as that observed for the **dnba** + **fa** crystal structure, which makes the formation of this heterodimer rather rare.

One of the most common features of previously reported structures are that many coformers contain a nitrogen atom that can either act as a hydrogen bond acceptor or accepts a proton as a base and becomes ionized. Out of the total number of N-containing coformers, 66 entries include a N-containing compound that acts as a hydrogen bond acceptor (no proton transfer) and 140 consist of a proton transfer occurring from **dnba** to the N-containing compound. This result is reasonable, since **dnba** is relatively more acidic than benzoic acid (pK_a = 4.20), which will more likely result in the formation of a salt than of a cocrystal. Although most of the multicomponent crystals consisting of N-containing coformers presented in this work resulted in a cocrystal, it should be noted the multicomponent crystals present here are more an exception, rather than a part of the norm.

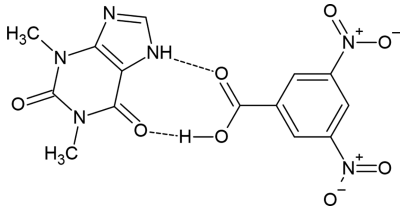
From Figures 2, 4, 7, and to some extent Figure 6 it seems that **dnba** tends to favor forming a layered-type structure. From the CSD, multicomponent structures which contain coformers that are relatively planar tend to favor forming a layered-type structure. This is not an absolute trend: for

https://dx.doi.org/10.1021/acs.cgd.0c01217
Cryst. Growth Des. 2021, 21, 344−356

Table 5. Some Notable Examples of Multicomponent Crystals of dnba Presented in Other Work

refcode	comment
COLKUL	another benzoic acid derivative forming a carboxylic acid ring motif $R_2^2(8)$; also a hydrate
RAVLIM	cocrystal formed between **dnba** and 4-pyridinecarboxaldehyde; has π-hole interactions; crystals are elastic[29]
XILTAO	hydrate consisting of the carboxylate of **dnba** and 3-aminopyridinium
GAUTAM	cocrystal consisting of 4-dimethylaminobenzoic acid and **dnba**; consists of two homodimers
GOBJUQ	cocrystal consisting of **dnba** and indole-2-carboxylic acid; forms a heterodimer; layered structure
HORWIX	cocrystal consisting of carbamazepine and **dnba**; forms a heterodimer while a nitro group forms a hydrogen bond to amide not involved with the ring synthon
IDUNUQ	molecular salt formed from the proton transfer of **dnba** to 3-hydroxypyridine; carboxylate forms a hydrogen bond between the hydroxyl group and pyridyl nitrogen on two independent 3-hydroxypyridine groups
KIZQIT, KIZQOZ, KIZQUF, KIZREQ	series of charge transfer complexes formed between **dnba** and various N-substituted carbazoles; **dnba** formed a homodimer
NEMSUT	cocrystal formed between the interaction of **dnba** and phenylurea; **dnba** forms a ring synthon $R_2^2(8)$ between the carboxylic acid and amide group; remaining N−H groups form hydrogen bonds to nitro group
XAMHAX	molecular salt of **dnba** and benzimidazole; salt forms hydrogen bonds with nitro group over carboxylate

Scheme 2. Theoretical Ring Hydrogen Bond Motif between dnba and thp



example, in the hydrate consisting of **dnba** and 4-aminosalicylic acid (refcode COLKUL) the coformers may be described as being relatively planar but the resulting structure was not simply layered.

Out of the 259 structures examined for this work, only 57 entries exhibit a hydrogen bond formed with the nitro group. In most cases, the carboxylic acid group of **dnba** dominates as the major interaction with the coformer, as observed in multicomponent crystal structures containing N-containing heterocycles. Even in cases where multiple hydrogen bond donors are available, it is not guaranteed that a hydrogen bond to the nitro group will form. It is probable that the formation of the π-hole interaction, together with other weaker interactions, is more favorable than forming a hydrogen bond with the nitro group.

For the cocrystal of **dnba** + **thp**, it should be noted that **dnba** could have formed a heterodimer, with ring synthon $R_2^2(9)$ as shown in Scheme 2. This type of heterodimer is common with cocrystals consisting of **thp** and a benzoic acid derivative, such as that occurring between **thp** and 4-aminobenzoic acid (refcode HUMNEK). However, the **thp** homodimer that was observed in **dnba** + **thp** is also common in other cocrystals involving **dnba** and a benzoic acid derivative, such as the **thp** + salicylic acid cocrystal (refcode KIGLES). The layered type structure appears to also be a common means of packing for such cocrystal systems, although exceptions do arise.

Hirshfeld Surface Analysis of dnba Complexes. It would be of interest to compare the contact contribution of **dnba** between the different multicomponent crystals presented. The percentages of the contributions from different interacting pairs is calculated by first calculating the Hirshfeld surface of **dnba** by itself and then using the values obtained from the fingerprint plots to plot a bar graph as presented in Figure 9. From Figure 9 the largest contribution comes from the O−H/H−O set of contacts, which naturally comes from the main contributing hydrogen bonds formed between **dnba**

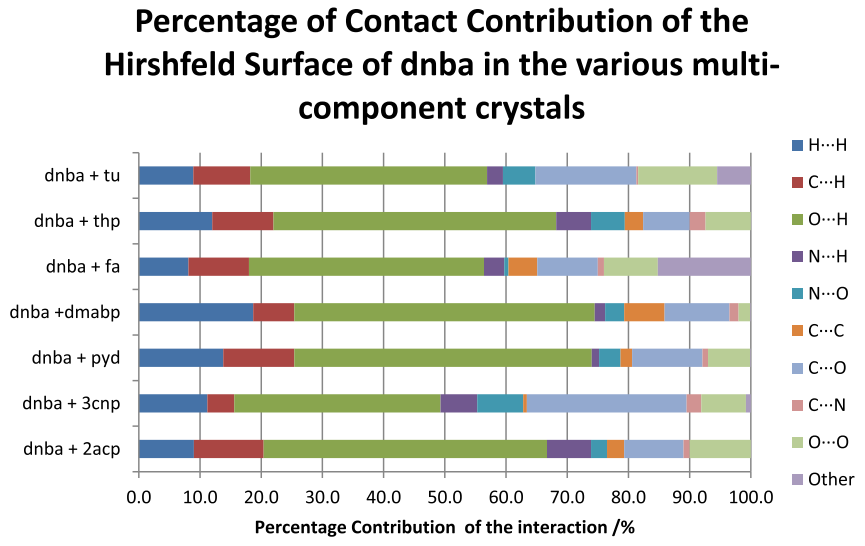


Figure 9. Percentage contribution of contacts due to **dnba**. For the cocrystal of **dnba** + **fa** the percentage contributions of F···H and O···F in other are 8.5% and 5.8%, respectively.

https://dx.doi.org/10.1021/acs.cgd.0c01217
Cryst. Growth Des. 2021, 21, 344−356

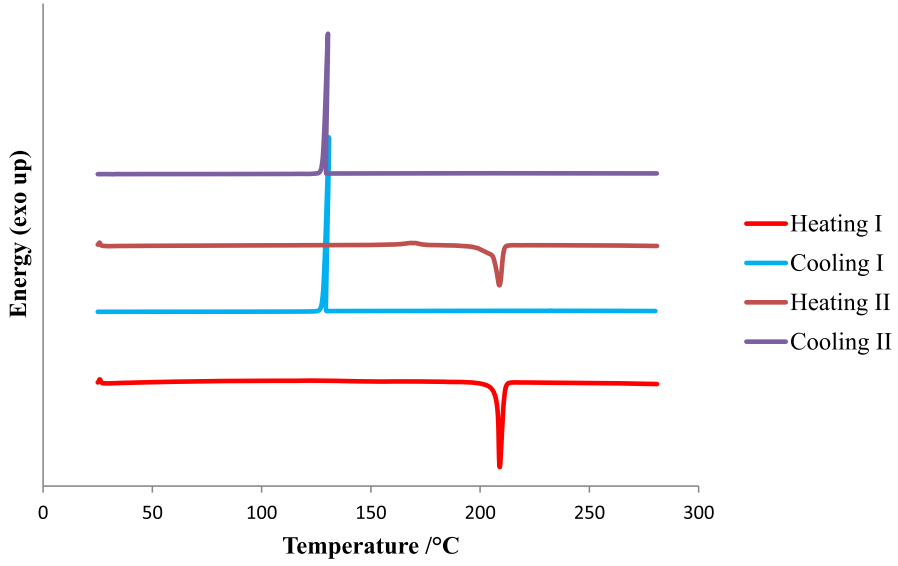


Figure 10. DSC curves for **dnba** + **2-acp**.

Table 6. Thermodynamic Data for the Melting of the Multicomponent Crystals of dnba

cocrystal/molecular salt	onset (°C)	peak (°C)	heat of fusion ΔH_{fus} (kJ mol^{-1})
dnba + **thp**	194.2	203.9	128.5
dnba + **pyd**	161.6	168.5	70.4
dnba + **2acp** (solvate)	76.8	80.9	96.4
dnba + **3cnp**	134.4	135.6	204.3
dnba + **dmabp** hydrate	86.8	93.0	91.8
dnba + **fa**	136.8	141.0	111.2
dnba + **tu**	153.2	156.3	179.5

and its respective coformer(s). Other notable sets of contacts include C···H and C···O. The C···O set of contacts contributes to a large percentage toward the total, especially for the **dnba** + **3cnp**. These arise due to the π-hole-type interactions present across the various multicomponent crystals. The C···H contacts arise due to the C−H···π, and its significance has been noted before. The percentage of C−C contacts in the cocrystal of **dnba** + **fa** and the hydrate of **dnba** + **dmabp** is much higher than the rest due to the presence of π−π stacking interactions. Overall the contact contributions of the different contacts across the different multicomponents are similar to each other to an extent.

Differential Scanning Calorimetry. Differential scanning calorimetry was carried out on all samples. In each case, the sample was heated to 250 °C and then cooled to 40 °C twice at a heating/cooling rate of 10 °C/min under ambient conditions. In each case only one thermal event was observed—the melting peak with no recrystallization. The exceptions to this are the cocrystals of **dnba** + **thp** and **dnba** + **3cnp** and the solvate **dnba** + **2acp**. In these crystal systems, upon cooling back to 25 °C, a peak corresponding to recrystallization is observed. Upon heating and cooling a second time, the same peaks are observed, indicating a degree of reversibility. The DSC curves for the heating and cooling of **dnba** + **2acp** are represented in Figure 10, as an example of the thermal behavior observed for **dnba** + **thp** and **dnba** + **2acp**. The rest of the DSC curves are available in the Supporting Information. Table 6 contains the thermodynamic behavior related to the melting of each of the multicomponent crystals.

CONCLUSIONS

Seven multicomponent crystals, of which five are cocrystals, one is a solvate, and one is a molecular salt, consisting of **dnba** were synthesized and characterized. These crystals showed various hydrogen-bonding interactions between **dnba** and the coformer. Hirshfeld surfaces show that a number of weaker interactions exist within each crystal, which contributes to the overall structure and packing of the molecules in the crystals. For future work, it would be of use to determine if the cocrystals of **dnba** + **thp** and **dnba** + **fa** have any improved properties such as solubility over the parent API molecule. Overall, this work shows that **dnba** can be a versatile molecule to consider in the development of new multicomponent crystals involving APIs.

ASSOCIATED CONTENT

Supporting Information

The Supporting Information is available free of charge at https://pubs.acs.org/doi/10.1021/acs.cgd.0c01217.

Powder X-ray diffraction data, differential scanning calorimetry data, and the Hirshfeld surface diagrams and fingerprint plots (PDF)

Accession Codes

CCDC 2026651−2026657 contain the supplementary crystallographic data for this paper. These data can be obtained free of charge via www.ccdc.cam.ac.uk/data_request/cif, or by emailing data_request@ccdc.cam.ac.uk, or by contacting The Cambridge Crystallographic Data Centre, 12 Union Road, Cambridge CB2 1EZ, UK; fax: +44 1223 336033.

AUTHOR INFORMATION

Corresponding Author

Andreas Lemmerer − *Molecular Sciences Institute, School of Chemistry, University of the Witwatersrand, 2050 Johannesburg, South Africa;* orcid.org/0000-0003-1569-2831; Phone: +27-11-717-6711;

https://dx.doi.org/10.1021/acs.cgd.0c01217
Cryst. Growth Des. 2021, 21, 344−356

Email: andreas.lemmerer@wits.ac.za; Fax: +27-11-717-6749

Author

Matthew C. Scheepers − *Molecular Sciences Institute, School of Chemistry, University of the Witwatersrand, 2050 Johannesburg, South Africa*

Complete contact information is available at: https://pubs.acs.org/10.1021/acs.cgd.0c01217

Notes

The authors declare no competing financial interest.

■ ACKNOWLEDGMENTS

We acknowledge and thank the DSI/NRF Centre of Excellence in Strong Materials as well as the NRF for funding the Bruker D2 Phaser diffractometer.

■ REFERENCES

(1) Vishweshwar, P.; McMahon, J. A.; Bis, J. A.; Zaworotko, M. J. Pharmaceutical Co-Crystals. *J. Pharm. Sci.* **2006**, *95*, 499−516.
(2) Schultheiss, N.; Newman, A. Pharmaceutical Cocrystals and Their Physicochemical Properties. *Cryst. Growth Des.* **2009**, *9*, 2950−2967.
(3) Karimi-Jafari, M.; Padrela, L.; Walker, G. M.; Croker, D. M. Creating Cocrystals: A review of Pharmaceutical Cocrystal Preparation Routes and Applications. *Cryst. Growth Des.* **2018**, *18*, 6370−6387.
(4) Zhou, Z.; Li, W.; Sun, W. J.; Lu, T.; Tong, H. H. Y.; Sun, C. C.; Zheng, Y. Resveratrol cocrystals with enhanced solubility and tabletability. *Int. J. Pharm.* **2016**, *509*, 391−399.
(5) Stanton, M. K.; Kelly, R. C.; Colletti, A.; Kiang, Y. H.; Langley, M.; Munson, E. J.; Peterson, M. L.; Roberts, J.; Wells, M. Improved Pharmacokinetics of AMG 517 Through Co-Crystallization Part 1: Comparison of Two Acids With Corresponding Amide Co-crystals. *J. Pharm. Sci.* **2010**, *99*, 3769−3778.
(6) Groom, C. R.; Bruno, I. J.; Lightfoot, M. P.; Ward, S. C. The Cambridge Structural Database. *Acta Crystallogr., Sect. B: Struct. Sci., Cryst. Eng. Mater.* **2016**, *72*, 171−179.
(7) Shaibah, M. A. E; Yathirajan, H. S.; Rathore, R. S.; Furuya, T.; Haraguchi, T.; Akitsu, T.; Glidewell, C. Co-crystallization of 3,5-dinitrobenzoic acid with two antipsychotic agents: a simple 1:1 salt with trihexyphenidyl and a 1:2 acid salt containing a very short O—H···O hydrogen bond with chlorprothixene. *Acta Cryst. Sect. E* **2019**, *75*, 292−298.
(8) Aitipamula, S.; Chow, P. S.; Tan, R. B. H. Polymorphs and Solvates of a Cocrystal Involving an Analgesic Drug, Ethenzamide, and 3,5-Dinitrobenzoic Acid. *Cryst. Growth Des.* **2010**, *10*, 2229−2238.
(9) Pawlędzio, S.; Trzybiński, D.; Woźniak, K. Crystal structure and energetic features of the cocrystal of carbamazepine with 3,5-dinitrobenzoic acid. *Acta Crystallogr., Sect. C: Struct. Chem.* **2019**, *75*, 1150−1156.
(10) Liu, X.; Su, Z.; Ji, W.; Chen, S.; Wei, Q.; Xie, G.; Yang, X.; Gao, S. Structure, Physicochemical Properties, and Density Functional Theory Calculation of High-Energy-Density Materials Constructed with Intermolecular Interaction: Nitro Group Charge Determines Sensitivity. *J. Phys. Chem. C* **2014**, *118*, 23487−23498.
(11) Hill, T. N.; Levendis, D. C.; Lemmerer, A. Binary and ternary co-crystals and molecular salts of 3,5-dinitrobenzoic acid: A many-faceted supramolecular reagent. *J. Mol. Struct.* **2018**, *1168*, 28−38.
(12) Ford, S. J.; McIntyre, G. J.; Johnson, M. R.; Evans, I. R. Structure and dynamics studies of the short strong hydrogen bond in the 3,5-dinitrobenzoic acid−nicotinic acid molecular complex. *CrystEngComm* **2013**, *15*, 7576−7582.
(13) Tothadi, S.; Desiraju, G. R. Unusual co-crystal of isonicotinamide: the structural landscape in crystal engineering. *Philos. Trans. R. Soc., A* **2012**, *370*, 2900−2915.
(14) Santiago de Oliveira, Y.; Saraiva Costa, W.; Ferreira Borges, P.; Silmara Alves de Santana, M.; Ayala, A. P. The design of novel metronidazole benzoate structures: exploring stoichiometric diversity. *Acta Crystallogr., Sect. C: Struct. Chem.* **2019**, *75*, 483−495.
(15) Girisha, M.; Yathirajan, H. S.; Jasinski, J. P.; Glidewell, C. Different acid−base behaviour of a pyrazole and an isoxazole with organic acids: crystal and molecular structures of the salt 3-(4-fluorophenyl)-1H-pyrazolium 2,4,6-trinitrophenolate and of the cocrystal 4-amino-N-(3,4-dimethyl-1,2-oxazol-5-yl)-benzenesulfonamide−3,5-dinitrobenzoic acid (1/1). *Acta Crystallogr., Sect. C: Struct. Chem.* **2016**, *72*, 612−618.
(16) Bauzá, A.; Mooibroek, T. J.; Frontera, A. Directionality of π-holes in nitro compounds. *Chem. Commun.* **2015**, *51*, 1491−1493.
(17) Ebisuzaki, Y.; Boyle, P. D.; Smith, J. A. Methylxanthines. I. Anhydrous Theophylline. *Acta Crystallogr., Sect. C: Cryst. Struct. Commun.* **1997**, *53*, 777−779.
(18) Rossi, F.; Cerreia Vioglio, P.; Bordignon, S.; Giorgio, V.; Nervi, C.; Priola, E.; Gobetto, R.; Yazawa, K.; Chierotti, M. R. Unraveling the Hydrogen Bond Network in a Theophylline−Pyridoxine Salt Cocrystal by a Combined X-ray Diffraction, Solid-State NMR, and Computational Approach. *Cryst. Growth Des.* **2018**, *18*, 2225−2233.
(19) Van Hoeck, E.; De Schaetzen, T.; Pacquet, C.; Bolle, F.; Boxus, L.; Van Loco, J. Analysis of benzophenone and 4-methylbenzophenone in breakfast cereals using ultrasonic extraction in combination with gas chromatography−tandem mass spectrometry (GC−MS n). *Anal. Chim. Acta* **2010**, *663*, 55−59.
(20) *Bruker, SAINT+, ver. 6.02 (including XPREP)*, Bruker AXS Inc.: Madison, WI, USA, 1999. Cruz-Cabeza, A. J. Acid−base crystalline complexes and the pK_a rule. *CrystEngComm.* **2012**, *14*, 6362−6365.
(21) Sheldrick, G. M.; *SHELX, release 97-2 (includes SHELXS and SHELXL)*; University of Göttingen: 1997.
(22) Farrugia, L. J. ORTEP-3 for Windows - a version of ORTEP-III with a Graphical User Interface (GUI). *J. Appl. Crystallogr.* **1997**, *30*, 565−565.
(23) Macrae, C. F.; Edgington, P. R.; McCabe, P.; Pidcock, E.; Shields, G. P.; Taylor, R.; Towler, M.; van de Streek, J. Mercury: visualization and analysis of crystal structures. *J. Appl. Crystallogr.* **2006**, *39*, 453−457.
(24) Spackman, M. A.; McKinnon, J. J. Hirshfeld surface analysis. *CrystEngComm* **2002**, *4*, 378−392.
(25) McKinnon, J. J.; Spackman, M. A.; Mitchell, A. S. Novel tools for visualizing and exploring intermolecular interactions in molecular crystals. *Acta Crystallogr., Sect. B: Struct. Sci.* **2004**, *60*, 627−668.
(26) Turner, M. J.; McKinnon, J. J.; Wolff, S. K.; Grimwood, D. J.; Spackman, P. R.; Jayatilaka, D.; Spackman, M. A.; *CrystalExplorer 17.5*; The University of Western Australia: 2017.
(27) Cruz-Cabeza, A. J. Acid−base crystalline complexes and the pKa rule. *CrystEngComm* **2012**, *14*, 6362−6365.
(28) SciFinder: https://scifinder.cas.org/scifinder/view/scifinder/scifinderExplore.jsf. Date of Access: September 19−22, 2018.
(29) Saha, S.; Desiraju, G. R. σ-Hole and π-Hole Synthon Mimicry in Third-Generation Crystal Engineering: Design of Elastic Crystals. *Chem. - Eur. J.* **2017**, *23*, 4936−4943.

Chapter 6 Chains or rings? Polymorphism of an isoniazid derivative derivatized with diacetone alcohol

6.1 Introduction

For this work, **iz4h4m2p** was synthesized using the method described in the experimental section. This compound was found to be polymorphic, existing in two forms, form **I** and form **II**. Both forms exhibited unique hydrogen bonding from each other, with form **I** forming a chain hydrogen bond motif while form **II** forms a ring hydrogen bond motif.

Authors: Scheepers, M.C., Lemmerer A.

Journal: *RSC Advances*

Date Published: 3 April 2022

Volume Number: 12

Pages: 11658-11664

Number of citations as of 10 November 2022: 1

RSC Advances

PAPER

View Article Online
View Journal | View Issue

Check for updates

Cite this: *RSC Adv.*, 2022, **12**, 11658

Chains or rings? Polymorphism of an isoniazid derivative derivatized with diacetone alcohol†

Matthew C. Scheepers, Manuel A. Fernandes and Andreas Lemmerer *

Received 31st March 2022
Accepted 3rd April 2022

DOI: 10.1039/d2ra02057b

rsc.li/rsc-advances

Isoniazid was derivated with diacetone alcohol in a Schiff-base reaction in order to yield *N*′-[(2*E*)-4-hydroxy-4-methylpentan-2-ylidene]pyridine-4-carbohydrazide. The resulting product was determined to be polymorphic, exhibiting two crystal forms: form I and form II. From the crystal structure determination using SC-XRD it was determined that form I crystalizes in the *C*2/*c* space group while form II crystalizes in the $P2_1/c$ space group. The hydrogen bonding patterns of both forms are distinctively different from each other: form I forms a chain hydrogen bond motif by forming a hydrogen bond between the hydroxyl group and the oxygen of the amide group while form II forms dimers with a ring hydrogen bond motif forming between the hydroxyl group and the pyridine group. From DSC analysis form I and form II are enantiotropically related, with form I converting to form II at 132.3 °C before melting at 142.3 °C. Based on both experimental and computational evidence, we conclude that form I is a metastable form, with form II being the most stable form. This is another case of a "disappearing polymorph."

Open Access Article. Published on 14 April 2022. Downloaded on 6/13/2022 10:14:39 AM.
This article is licensed under a Creative Commons Attribution-NonCommercial 3.0 Unported Licence.

1 Introduction

Polymorphism is the phenomenon where a compound can exist in more than one crystal structure.[1,2] Many APIs have been determined to be polymorphic, with the number of known polymorphic forms being dependent on the time and effort used to search for more forms. For APIs, properties such as solubility, dissolution rate, appearance, *etc.*[3,4] can differ between different polymorphs. For pharmaceuticals this becomes significant. On one hand it is possible to obtain a new polymorph with better properties than the older known form.[5,6] On the other hand, the appearance of a new polymorph can be detrimental, such as the case of Ritonavir, where the new form was thermodynamically more stable than the original form with poorer physicochemical properties that led to Abbott withdrawing the drug from the market and losing millions of dollars in the process. Therefore, for new and existing APIs the need to adequately screen for polymorphs and characterize them becomes crucial for the success of an API entering the market.

Isoniazid, an anti-bacterial often combined with *p*-aminosalicylic acid and streptomycin, is used as an effective treatment for tuberculosis (TB).[7] Isoniazid itself is a fairly simple drug molecule consisting of primarily an amide, a pyridine and a hydrazine group. Only until recently was isoniazid considered to be monomorphic, with at least three forms reported in total so far.[8] The first and most stable crystal structure of isoniazid consists of a series of interconnected N–H···N hydrogen bonds that form a spiral-type structure.[9,10] These interactions can be reduced by changing the primary amine to either a secondary amine or to an imine.[11–17] This effectively could leave the amide group as the only strong hydrogen bond donor, and thus could possibly allow one to design co-crystals with more robust intermolecular interactions involving the pyridine ring.[18] These hydrazine derivatives of isoniazid also tend to be polymorphic.[11,19–21] From a crystal engineering perspective, this offers two significant advantages: the first being better control over the hydrogen bond pairs (and thus also gives greater degree of predictability and ease of control),[22,23] and two, properties which are further tuneable by selecting the polymorph with better physicochemical properties or stability. Together with the possibility of improving the inherent bioavailability of isoniazid, the advantages of derivatizing isoniazid should prove advantageous.

The title compound *N*′-[(2*E*)-4-hydroxy-4-methylpentan-2-ylidene]pyridine-4-carbohydrazide (iz4h4m2p, see Scheme 1) was synthesized by reacting isoniazid with diacetone alcohol (4-hydroxy-4-methyl-2-pentanone, 4h4m2p) in a Schiff-base reaction. iz4h4m2p was first reported in a previous work in a co-crystal with 4-*tert*-butylbenzoic acid[24] but the crystal structure of iz4h4m2p by itself had not been reported. 4h4m2p was used due to the presence of the hydroxyl group, which could possibly allow the formation of an intramolecular hydrogen bond between the hydroxyl group and amide, while the remainder of

Molecular Sciences Institute, School of Chemistry, University of the Witwatersrand, Private Bag 3, 2050, Johannesburg, South Africa. E-mail: andreas.lemmerer@wits.ac.za; Fax: +27-11-717-6749; Tel: +27-11-717-6711

† Electronic supplementary information (ESI) available: Crystallographic information, PXRD patterns and Hirshfeld surface finger plots. CCDC 2133557–2133558. For ESI and crystallographic data in CIF or other electronic format see **https://doi.org/10.1039/d2ra02057b**

© 2022 The Author(s). Published by the Royal Society of Chemistry

Open Access Article. Published on 14 April 2022. Downloaded on 6/13/2022 10:14:39 AM.
This article is licensed under a Creative Commons Attribution-NonCommercial 3.0 Unported Licence.

the aliphatic backbone could be used to increase the lipophilic character of isoniazid, which has been an approach used to improve isoniazid.[25] We wanted to explore the potential of a Schiff-base derivatised form of isoniazid with varying functional groups to expand the range of potential coformers that could be used for different crystal engineering purposes. This required an understanding of the intermolecular interactions present in the pure form of iz4h4m2p in a crystal structure. In an effort to characterize said structure, it was discovered that this compound was polymorphic. Hence, the objective of this work was to explore the polymorphism of this compound using traditional screening methods. Two polymorphic forms of iz4h4m2p were discovered, which were then characterized by SC-XRD, PXRD, DSC and FTIR.

2 Experiment

2.1 Materials

All materials were purchased from Sigma-Aldrich, and were used as is without further purification.

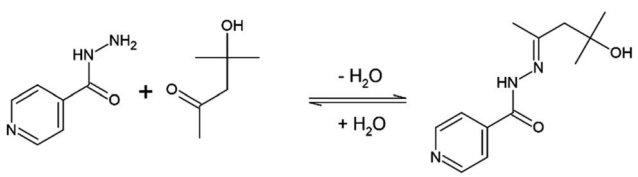
2.2 General procedure for synthesis of iz4h4m2p

A general method of obtaining iz4h4m2p is given as follows: 0.250 g of isoniazid (1.82 mmol) was dissolved in 10 mL of ethanol (absolute). A few drops (0.5 mL) of 4h4m2p was added to this mixture. This solution was refluxed for 18 h, after which it was transferred to vial, which was kept loosely open. Crystals of were grown from this mixture after several days. The different methods used to obtain the different crystal forms is given in the results and discussion.

2.3 General procedures for characterization methods

Powder X-ray diffraction (PXRD). Powder X-ray diffraction is used to determine the bulk phase purity of each sample. PXRD data for all forms were measured at 293 K on a Bruker D2 Phaser diffractometer which employs a sealed tube Co X-ray source (λ = 1.78896 Å), operating at 30 kV and 10 mA, and LynxEye PSD detector in Bragg–Brentano geometry. Powder patterns for both forms is present in the ESI,† where the experimentally measured pattern is compared to the calculated patterns obtained from the SC-XRD data (Fig. 1).

Single crystal X-ray diffraction (SC-XRD). The Bruker D8 VENTURE PHOTON CMOS 100 area detector diffractometer, equipped with a graphite monochromated MoKα_1 (λ = 0.71073 Å) sealed tube (50 kV, 30 mA), was used to collect all the intensity data. Crystal structures were determined at 173 K and



Scheme 1 Schiff-base reaction of isoniazid with 4h4m2p to form iz4h4m2p.

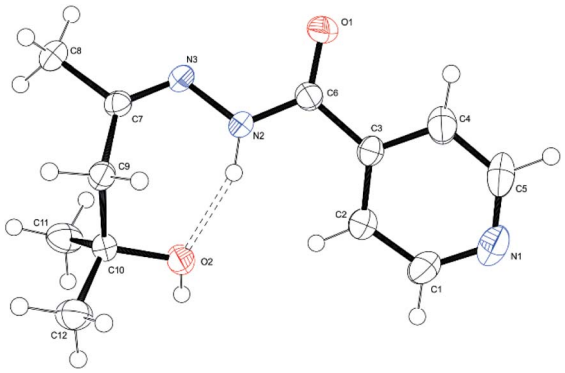


Fig. 1 Ortep diagram of form I. Atomic numbering used is the same for both forms.

to achieve satisfactory thermal ellipsoids. The program SAINT+, vers. 6.02 was used to integrate the data and the program SADABS[27] was used to make empirical absorption corrections. Space group assignments were made using XPREP[26] on all compounds. In all cases, the structures were solved in the WinGX[28] Suite of programs by intrinsic phasing using SHELXT[29] and refined using full-matrix least-squares/difference Fourier techniques on F^2 using SHELXL.[29] All non-hydrogen atoms were refined anisotropically. All carbon-bound hydrogen atoms were placed at idealized positions and refined as riding atoms with U_{iso} parameter 1.2 or 1.5 times those of their parent atoms.

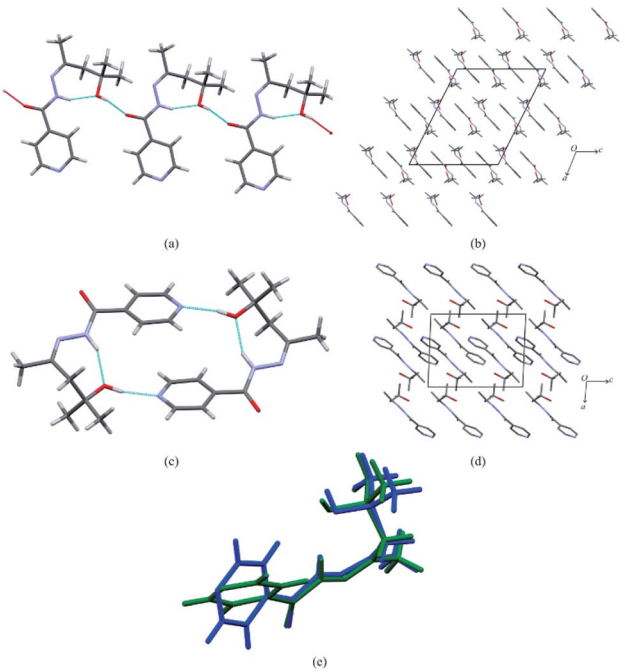


Fig. 2 The crystals structures of form I and form II showing: (a) the chain hydrogen bond motif found in form I, (b) the crystal structure packing of form I (with hydrogen omitted for clarity), (c) the dimer with the ring hydrogen bond motif, (d) the crystal structure packing of form II (with hydrogen omitted for clarity) and (e) the molecular overlay of iz4h4m2p molecules from the asymmetric units of form I (blue) and form II (green).

© 2022 The Author(s). Published by the Royal Society of Chemistry

Open Access Article. Published on 14 April 2022. Downloaded on 6/13/2022 10:14:39 AM.
This article is licensed under a Creative Commons Attribution-NonCommercial 3.0 Unported Licence.

Table 1 Hydrogen bond table for the crystal structures of form I and form II of iz4h4m2p

D–H···A	d(D–H)	d(H···A)	d(D···A)	∠(DHA)
Form I				
N2–H2A···O2	0.888(19)	1.888(19)	2.7220(18)	156(2)
O2–H2B···O1 (i)	0.84(2)	1.89(2)	2.7088(15)	164(2)
Form II				
N2–H2A···O2	0.898(15)	1.913(15)	2.7370(13)	152(12)
O2–H2B···N1 (ii)	0.892(19)	1.903(19)	2.7778(13)	166(16)

Symmetry transformations used to generate equivalent atoms: (i) $x, y-1, z$ (ii) $-x+1, -y+1, -z+1$.

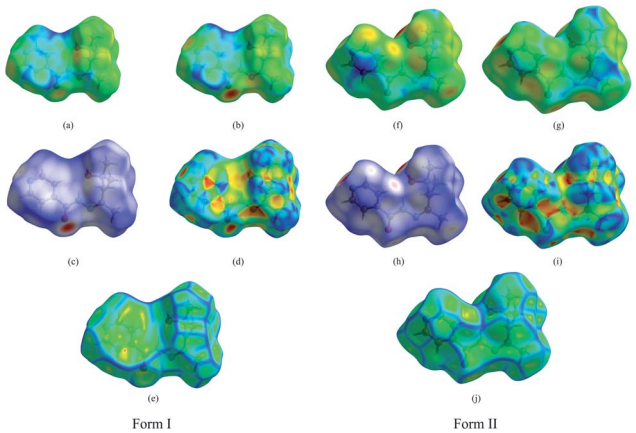


Fig. 3 The Hirshfeld surfaces for form I and form II with (a)–(e) representing the d_i, d_e, d_{norm}, shape index and curvedness respectively for form I and (f)–(j) representing the d_i, d_e, d_{norm}, shape index and curvedness respectively for form II.

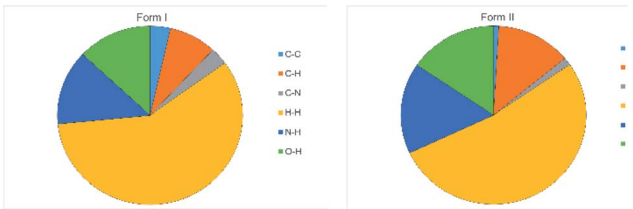


Fig. 4 The comparison of the contributions for each contact towards the Hirshfeld surface area between form I and form II.

Nitrogen-bound and oxygen-bound hydrogen atoms were located in the difference Fourier map and their coordinates and isotropic displacement parameters refined freely. Diagrams and publication material were generated using ORTEP-3 [30] and MERCURY.[31] The crystallographic information can be found in the ESI in Table S1.†

Hirshfeld surface analysis. Hirshfeld surface analysis is a computational method that can be used to explore intermolecular interactions in molecular crystals that are weaker than hydrogen bonds, as well as to determine the 'shape' of molecular fragments, which are key to understanding the overall packing. The figures and fingerprint plots presented in this work were generated using Crystal Explorer 17.5.[32] All images were generated using a high (standard) resolution.

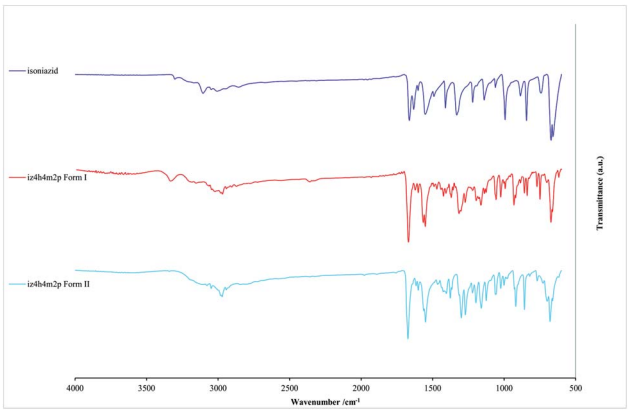


Fig. 5 The FTIR spectra for isoniazid, form I and form II of iz4h4m2p.

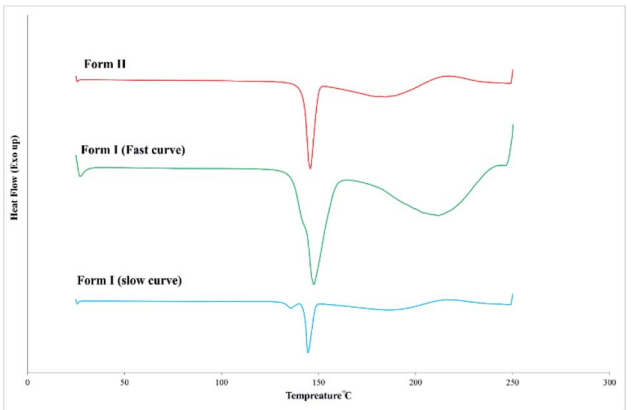


Fig. 6 DSC curves for the polymorphs of iz4h4m2p.

Table 2 Thermodynamic information regarding the DSC curves

Property	Form I	Form II
T_{fus} [a] [°C]	139.7 ± 0.1	142.6 ± 0.1 [b] 142.1 ± 0.1 [c]
$\Delta_{fus}H$ [kJ mol^{-1}]	32.3 ± 0.8	33.93 ± 0.8 [b] 33.17 ± 0.9 [c]
$\Delta_{fus}S$ [d] [J K^{-1} mol^{-1}]	78.2 ± 1.9	81.6 ± 1.9 [b] 79.9 ± 1.9 [c]
Transition to mod	I → II	—
T_{trans}	132.29 ± 0.1 [b]	—
$\Delta_{trans}H$ [kJ mol^{-1}]	3.51 ± 0.8 [b]	—
$\Delta_{trans}S$ [J K^{-1} mol^{-1}]	8.65 ± 1.9 [b]	—

[a] This is the onset temperature. These melting peaks may not necessarily represents pure melting, as the sample may have started decomposing beyond this point. [b] From the slow curve of form I. [c] From the curve of form II. [d] From the expression $\Delta S = \Delta H/T$.

FTIR analysis. FTIR spectra was collected using the Bruker Alpha II model equipped with the Eco-ATR sampling module. Background noise was subtracted and small amount of the

© 2022 The Author(s). Published by the Royal Society of Chemistry

Open Access Article. Published on 14 April 2022. Downloaded on 6/13/2022 10:14:39 AM.
This article is licensed under a Creative Commons Attribution-NonCommercial 3.0 Unported Licence.

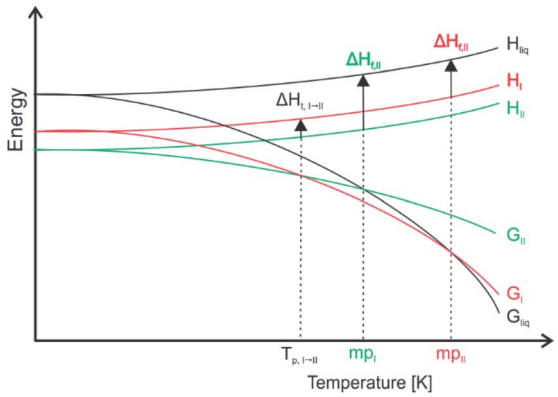


Fig. 7 The energy *vs.* temperature diagram showing the enantiotropic relation between form I and form II.

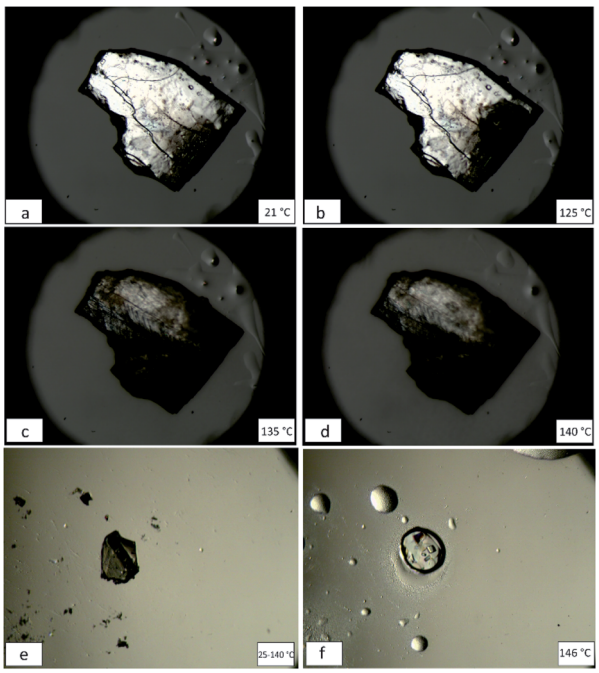


Fig. 8 Hot stage microscopy images showing a block of form I at room temperature (a). The crystal starts undergoing a phase transition at 125 °C (b) before finishing at around 135 °C (c). Melting occurs after 140 °C (d). Form II for most of its time from 25–140 °C until melting (f).

sample of interest was placed onto the ATR crystal. Spectra were measured from 600 to 4000 cm^{-1} range, resolution 4 cm^{-1} with 24 scans per sample. Spectra were collected using the ATR-FTIR in a room with air conditioning set at 22 °C. After spectral acquisition the ATR crystal was cleaned using isopropanol.

Differential scanning calorimetry (DSC). Differential scanning calorimetry data were collected using a Mettler Toledo DSC 3 with aluminium pans under nitrogen gas (flow rate = 10 mL min^{-1}). Exothermic events were shown as peaks. Samples were heated and cooled to determine melting points as well as any additional phase transitions. The temperature and energy calibrations were performed using pure indium (purity 99.99%, m.p. 156.6 °C, heat of fusion: 28.45 J g^{-1}) and pure zinc (purity 99.99%, m.p. 479.5 °C, heat of fusion: 107.5 J g^{-1}). Samples were heated to 250 °C from 25 °C before being cooled back down at 25 °C at a heating or cooling rate of 10 °C min^{-1} or 40 °C min^{-1}.

Hot stage microscopy. Hot stage microscopy was done on an Olympus SZ61 equipped with a Kofler hot bench. Images were captured using an Olympus EP50 camera. Various heating and cooling techniques were applied to capture the phase transitions.

Calculations. Intermolecular energies at 0 K of form I and II were calculated using PIXEL[33,34] as incorporated in the August 2014 version of the CLP[35] package. The calculations were carried out as described within the CLP manual. The calculation was initialized by geometrically normalizing bonds involving H to neutron distances within CLP, followed by the calculation of an *ab initio* MP2/6-31G(d,p) molecular electron density using Gaussian-09 (ref. 36) revision E.01. This molecular electron density description was then used as input by PIXEL to carry out the calculations.

Intramolecular energy DFT calculations for the molecules in form I and II were computed at the M06-2X-6-311G(d,p)[37] level at 0 K in the gas phase using Gaussian-09. Grimme dispersion corrections (D3) were applied to all calculations.[38] In the calculations, the molecular geometry (angles and torsion angles) derived from the crystal coordinates for all atoms (except hydrogens) were kept frozen but bond lengths allowed to optimise, while H atom positions were allowed to fully optimize.

3 Results and discussion

3.1. Obtaining form I and form II

During our investigation, our initial goal was to find an optimal method for the synthesis iz4h4m2p. From our initial batches we obtained form I. This was obtained using the method described above, with crystals obtained from slow evaporation of the reaction mixture. This procedure was repeated using the exact same method when form II was discovered. However, we failed to obtain form I again using this procedure. To try overcome this, several different methods were deployed. One of the first was to recrystallize form I using different solvents in a slow evaporation method. The solvents used included acetonitrile, methanol, dichloromethane, isopropanol and *n*-propanol. However, these attempts failed as we obtained form II each time. Another attempt included altering the reaction conditions. This included changing the solvent, altering the amount of 4h4m2p (for example, using 1.03 mmol of 4h4m2p with 1.82 mmol of isoniazid using the same synthesis procedure), reaction times (from 2 hours to 48 hours), temperatures (doing room temperature reactions to reflux) *etc.* Despite all this, we still exclusively obtained form II. From these experiments we conclude that form I is the metastable form, whose formation was kinetically favoured and is a chance discovery, while form II is the most stable form. Despite this, we were still able to isolate enough to characterize form I by the methods described above. To further confirm the stability, we used slurry methods where we mixed equal masses (0.050 g) of each form I and form II with

© 2022 The Author(s). Published by the Royal Society of Chemistry

Open Access Article. Published on 14 April 2022. Downloaded on 6/13/2022 10:14:39 AM.
This article is licensed under a Creative Commons Attribution-NonCommercial 3.0 Unported Licence.

0.5 mL of hexane. The resulting powder consisted of purely form II, with no trace of form I. Even in our attempts at seeding form I, where powders of form I added to a supersaturated solution of iz4h4m2p (from form II), showed the conversion of form I to form II.

We also attempted to obtain more polymorphic forms using sublimation experiments. Both crystals of form I and form II were used in sublimation experiments. These experiments involved heating crystals at around 130–140 °C on a Kofler hot bench. Unfortunately the crystals obtained from these experiments were that of isoniazid, which indicates that at high temperatures iz4h4m2p is unstable and may be prone to reversing the Schiff base reaction (see Scheme 1, we assume water vapor in the atmosphere allowed this reaction to occur).

3.2. Crystal structures of form I and form II

Form I formed colourless blocks while form II formed as colourless plates. Form I crystalizes in the $C2/c$ space group while form II crystalizes in the $P2_1/c$ space group. For both crystal structures, the amide group forms an intramolecular hydrogen bond to the hydroxyl group (N2–H2A···O2). Apart from this, the hydrogen bonding for both crystal structures differs significantly. In form I a hydrogen bond forms between the hydroxyl group to the oxygen atom of the amide group (O2–H2B···O1), forming a chain hydrogen bond motif $C_2^2(6)$ (see Fig. 2a). It should be noted that in form I, the pyridyl nitrogen (N1) is not involved in any strong hydrogen bonding. Form II on the other hand forms a ring based hydrogen bond motif $R_3^3(18)$, with the hydroxyl group forming a hydrogen bond to the pyridal nitrogen (N1). This effectively forms dimers (see Fig. 2c). In the case of form II, the amide N–H group or the hydroxyl group does not form a strong hydrogen bond to the oxygen of the amide group (O1). iz4h4m2p also exhibits conformational polymorphism, which is most notable due to the different torsional angle of the pyridyl ring (Fig. 2e). The torsional angle between the ring and the amide group (C4–C3–C6–O1) for form I and form II respectively is 14.48° and 31.77°. This contrast may be due to the effect of the hydrogen bonding present: form I is not restricted by hydrogen bonding and will accept a conformation with a low energy. Intramolecular DFT calculations show that the molecule in form I is more stable compared to the molecule in form II by 3.1 kJ mol^{-1}. On the other hand form II will be locked to a conformation that allows the formation of the hydrogen bond between the pyridine ring and hydroxyl group. Consequently, because of the different hydrogen bonding interactions, each form will packing differently. Form I overall forms layered type packing, with each chain forming rows with the pyridine ring forming π···π stacking between adjacent chains (Fig. 2b). This π···π stacking does not exist for form II, which is a consequence of the hydrogen bonded dimers (Fig. 2d). The packing coefficients (calculated using PLATON[39]) for both form I and form II are 67.7% and 69.7% respectively, which indicates that form II is more efficient at packing than form I by 2%.

Intermolecular energy calculations using PIXEL indicates the intermolecular energy of form II (−164.7 kJ mol^{-1}) is lower than form I (−145.3 kJ mol^{-1}) by 19.4 kJ mol^{-1}. Adding the intermolecular and intramolecular energies leads to the lattice energy ($E_{\text{latt}} = U_{\text{inter}} + \Delta E_{\text{intra}}$), which is −145.3 and −161.6 kJ mol^{-1} for form I and form II respectively. The calculated lattice energies show that form II is more stable than form I by 16.2 kJ mol^{-1}. Thus the intramolecular energies for the individual molecules are not that different, but the intermolecular interactions in form II make this form considerably more favoured, and it is not surprising that we did not manage to crystallise form I again (Table 1).

3.3. Hirshfeld analysis

Hirshfeld surface diagrams were generated for both form I and form II and both are presented in Fig. 3. One of the most noticeable differences between the two Hirshfeld surfaces is in the large red spot at the pyridyl nitrogen of form II (Fig. 3g and h), which is much smaller in form I. This arises due to the strong hydrogen bonding described previously. The small red spot on the pyridyl nitrogen on form I arises from a weak C–H hydrogen bond (C9–H9···N1). Conversely, for form II a weaker hydrogen bond between the oxygen (O1) from the amide group also exist (C4–H4···O1). One other noticeable weak C–H hydrogen bond in form II is that of C1–H1···N3, indicating that the imine might also be involved in some weak hydrogen bonding, although this has not been observed for form I. A pair of red and blue triangles spotted on the shape index of form I (Fig. 3d) along with the relatively flat region on the curvedness of form I (Fig. 3e) confirms that form I consists of a series of chains of iz4h4m2p stacked together by π···π stacking interactions. Conversely, the shape index and curvedness of form II (Fig. 3i and j) does not share this feature, indicates that packing of form II does not involve π···π stacking, but rather is organized by other weak interactions instead such as C–H hydrogen bonding. This is supported by an increased amount of surface contact arising from C–H interactions found in form II when comparing form I and form II, as seen in Fig. 4.

3.4. FTIR spectra

FTIR spectroscopy can be used for the quick identification of the polymorphs of iz4h4m2p. The FTIR spectra for form I and form II as well as that of isoniazid were measured. These spectra are compared with each other and are presented in Fig. 5. It first should be noted that although the hydroxyl groups typically forms a broad medium to strong band in the 3550–3230 cm^{-1} range, the hydrazide functional group (O=C–NH–NH$_2$) also forms a medium to strong band in the same region as the hydroxyl group, giving the spectra a similar shape in this region. However, it is still possible to distinguish between isoniazid and iz4h4m2p, as well as between the two forms of iz4h4m2p by using other vibrational peaks. One of the first noticeable differences between isoniazid and that of both forms of iz4h4m2p should be the lack of a –NH$_2$ group. This can easily be observed by the absence of a medium-strong peak in the 1635–1600 cm^{-1} region that is associated with the –NH$_2$ deformation vibration (which is not to be confused the strong peak

© 2022 The Author(s). Published by the Royal Society of Chemistry

Open Access Article. Published on 14 April 2022. Downloaded on 6/13/2022 10:14:39 AM.
This article is licensed under a Creative Commons Attribution-NonCommercial 3.0 Unported Licence.

appearing in the 1680–1635 cm^{-1} region that is associated with the carbonyl stretch).

One notable difference between the spectra of form I and form II is the absence of a medium peak around the 3300–3350 cm^{-1} region in form II, which appears as a weak band instead. This peak is most likely associated with the N–H stretch of an amide group. This increase in the intensity of form I is most likely the result of the chain hydrogen bond motif described previously, as the carbonyl group forming a hydrogen bond may have affected the dipole moment of the N–H group in form I. This peak can be used as a signature peak when a quick comparison is needed.

3.5. DSC curves

The DSC curves obtained for both forms of iz4h4m2p is presented in Fig. 6. The curve of form I heated at 10 °C min^{-1} will be referred to as the slow curve, while the one heated at 40 °C min^{-1} will be referred to as the fast curve. Measurements were done in triplicate to determine errors. From the slow curve for form I it can be observed that two significant peaks are observed occurring almost one after the other. The first small peak represents the solid-state phase transition of form I to form II. This is supported by the temperature range of the second, larger peak coinciding closely to the same temperature for the melting/decomposition of form II obtained from the curve of form II. The curve for form II does not show any other significant peaks before the melting/decomposition one. In order to determine the melting point and heat of fusion of form I alone without transforming to form II, the sample was heated quickly at 40 °C min^{-1} (fast curve) to prevent the sample having enough time to transform from form I to form II. From the fast curve of form I the melting/decomposition peak was found to be 139.7 °C, which is roughly 2 °C below the melting/decomposition peak of form II. Both forms showed no significant peaks on the cooling cycle. The onset temperatures along with the associated enthalpies is tabulated in Table 2. To determine whether the two forms are monotropically or enantiotropically related, several rules can be applied. The heat-of-fusion rule states that for an enantiotropic system, the form with the higher melting point will have a lower heat-of-fusion.[40] For this system, this rule is difficult to apply since the enthalpies are similar in size and have a margin of error between them. However, the heat-of-transition rule provides a clearer interpretation. It states that "if an endothermal transition is observed at some temperature it may be assumed that there is a transition point below it".[40] From the slow curve of form I an endothermic peak was observed, with a subsequent endothermic peak matching closely to the melting peak of form II. This is best represented by the qualitative energy *vs.* temperature curves observed in Fig. 7, in particular $\Delta H_{I\rightarrow II}$. Based on this observation it can be observed unambiguously that form I and form II are enantiotropically related.

3.6. Hot stage microscopy

A block-like crystal of form I was placed on a glass microscope slide and covered by a glass cover slip. This was heated until melting, and significant changes were captured. For form I no significant changes were observed until heated to 125 °C (Fig. 8b). This block started to move and become darker, with a clear phase transformation occurring. This process occurs and finishes around 135 °C (Fig. 8c). Melting starts occurring after 140 °C and finishes at 145 °C (see video part of ESI†). After cooling, a wax-like solid remained, which indicated that no recrystallization occurred, as expected from comparing the DSC curve. Form II was also examined part of the hot stage microscopy. The crystal of form II remained unchanged until melting (Fig. 8e and f). Upon cooling, like form I, a wax-like solid remained, indicating no recrystallization occurred. Videos depicting the melting of form I and its phase transition are available as ESI.†

4 Conclusions

Two polymorphic forms of iz4h4m2p were discovered and characterized. Form I is a metastable phase that proved to be elusive to obtain again, while form II is the most stable form, and obtained repeatedly from most solvents. From the crystal structure analysis of both forms it is revealed that the two forms can be differentiated by two different hydrogen bond motifs: form I using a chain hydrogen bond motif and form II using a ring hydrogen bond motif. Form I utilises $\pi\cdots\pi$ stacking, while form II uses different weaker hydrogen bonding (C–H) to stabilise its packing. From the DSC analysis, form I has an enantiotropic thermal relation to form II. Computational studies confirm our observations that form II is much more stable than form I, despite the molecular conformation of iz4h4m2p in form I to be more stable than the conformation of iz4h4m2p in form II. This is due to the overall intermolecular energy of form II being much lower than form I. Here we have presented a case of a "disappearing" polymorphic system,[41] where the formation of one form (form I) is overtaken by the formation of another (form II). Thus, for future work it may prove to be worthwhile to find and characterize more polymorphs, while also finding a more reliable and consistent method of obtaining form I.

Conflicts of interest

There are no conflicts to declare.

Acknowledgements

This material is based upon work supported financially by the University of the Witwatersrand and the Molecular Sciences Institute. The National Research Foundation National Equipment Programme (UID 78572) is thanked for financing the purchase of the single-crystal diffractometer, and the DSI/NRF Centre of Excellence in Strong Materials is thanked for use of the D2-phaser.

Notes and references

1 P. H. Karpinski, *Chem. Eng. Technol.*, 2006, **29**, 233–237.

© 2022 The Author(s). Published by the Royal Society of Chemistry

Open Access Article. Published on 14 April 2022. Downloaded on 6/13/2022 10:14:39 AM.
This article is licensed under a Creative Commons Attribution-NonCommercial 3.0 Unported Licence.

2 J. Lu and S. Rohani, *Curr. Med. Chem.*, 2009, **16**, 884–905.
3 V. R. Vázquez Marrero, C. Piñero Berriós, L. De Dios Rodríguez, T. Stelzer and V. López-Mejías, *Cryst. Growth Des.*, 2019, **19**, 4101–4108.
4 A. Lévesque, T. Maris and J. D. Wuest, *J. Am. Chem. Soc.*, 2020, **142**, 11873–11883.
5 H. M. Wolff, L. Quere and J. Riedner, US8232414B2, 2012.
6 K. Higashi, K. Ueda and K. Moribe, *Adv. Drug Delivery Rev.*, 2017, **117**, 71–85.
7 M. D. Iseman, *Eur. Respir. J.*, 2002, **20**, 87–94.
8 K. Zhang, N. Fellah, A. G. Shtukenberg, X. Fu, C. Hu and M. D. Ward, *CrystEngComm*, 2020, **22**, 2705–2708.
9 L. H. Jensen, *J. Am. Chem. Soc.*, 1954, **265**, 4663–4667.
10 G. Rajalakshmi, V. R. Hathwar and P. Kumaradhas, *Acta Crystallogr., Sect. B: Struct. Sci., Cryst. Eng. Mater.*, 2014, **70**, 331–341.
11 D. Hean, T. Gelbrich, U. J. Griesser, J. P. Michael and A. Lemmerer, *CrystEngComm*, 2015, **17**, 5143–5153.
12 D. Hean, J. P. Michael and A. Lemmerer, *J. Mol. Struct.*, 2018, **1157**, 693–707.
13 A. Lemmerer, J. Bernstein and V. Kahlenberg, *CrystEngComm*, 2010, **12**, 2856–2864.
14 S. Y. Wang, X. M. Song and L. X. Duan, *Acta Crystallogr., Sect. E: Struct. Rep. Online*, 2008, **64**, o1880.
15 Z. L. Lu, B. Z. Shan, C. Y. Duan, Y. P. Tian, X. Z. You, H. K. Fun and K. Sivakumar, *Acta Crystallogr., Sect. C: Cryst. Struct. Commun.*, 1996, **52**, 1720–1722.
16 V. Meenatchi, K. Muthu, M. Rajasekar and S. Meenakshisundaram, *Spectrochim. Acta, Part A*, 2014, **124**, 423–428.
17 V. Jayaprakash, A. K. Timiri, V. Vijayan, B. N. Sinha and V. Devadasan, *J. Pharm. Chem.*, 2019, **6**, 1–4.
18 T. R. Shattock, K. K. Arora, P. Vishweshwar and M. J. Zaworotko, *Cryst. Growth Des.*, 2008, **8**, 4533–4545.
19 V. Vrdoljak, B. Prugovečki, I. Primožič, T. Hrenar, D. Cvijanović, J. Parlov Vuković, R. Odžak, M. Skočibušić, S. Prugovečki, J. Lovrić, D. Matković-Čalogović and M. Cindrić, *New J. Chem.*, 2018, **42**, 11697–11707.
20 L. Tom, V. Smolenski, J. Jasinski and M. R. P. Kurup, *ChemRxiv*, 2018, DOI: **10.26434/chemrxiv.6489425**.
21 C. R. Taylor, M. T. Mulvee, D. S. Perenyi, M. R. Probert, G. M. Day and J. W. Steed, *J. Am. Chem. Soc.*, 2020, **142**, 16668–16680.
22 A. Lemmerer, J. Bernstein and V. Kahlenberg, *CrystEngComm*, 2011, **13**, 5692–5708.
23 A. Lemmerer, *CrystEngComm*, 2012, **14**, 2465–2478.
24 L. G. Madeley, D. C. Levendis and A. Lemmerer, *Acta Crystallogr., Sect. C: Struct. Chem.*, 2019, **75**, 200–207.
25 C. F. de Faria, T. Moreira, P. Lopes, H. Costa, J. R. Krewall, C. M. Barton, S. Santos, D. Goodwin, D. Machado, M. Viveiros, M. Machuqueiro and F. Martins, *Biomed. Pharmacother.*, 2021, **144**, 112362.
26 Bruker, *SAINT+ and XPREP*, Bruker AXS Inc., Madison, Wisconsin, USA, 2012.
27 Bruker, *SADABS*, Bruker AXS Inc., Madison, Wisconsin, USA, 2001.
28 L. J. Farrugia, *J. Appl. Crystallogr.*, 1999, **32**, 837–838.
29 G. M. Sheldrick, *Acta Crystallogr., Sect. A: Found. Crystallogr.*, 2015, **71**, 3–8.
30 L. J. Farrugia, *J. Appl. Crystallogr.*, 2012, **45**, 849–854.
31 C. F. Macrae, I. Sovago, S. J. Cottrell, P. T. A. Galek, P. McCabe, E. Pidcock, M. Platings, G. P. Shields, J. S. Stevens, M. Towler and P. A. Wood, *J. Appl. Crystallogr.*, 2020, **53**, 226–235.
32 P. R. Spackman, M. J. Turner, J. J. McKinnon, S. K. Wolff, D. J. Grimwood, D. Jayatilaka and M. A. Spackman, *J. Appl. Crystallogr.*, 2021, **54**, 1006–1011.
33 A. Gavezzotti, *J. Phys. Chem. B*, 2003, **107**, 2344–2353.
34 A. Gavezzotti, *Z. Krystallog.*, 2005, **220**, 499–510.
35 A. Gavezzotti, *New J. Chem.*, 2011, **35**, 1360–1368.
36 M. J. Frisch, G. W. Trucks, H. B. Schlegel, G. E. Scuseria, M. A. Robb, J. R. Cheeseman, G. Scalmani, V. Barone, B. Mennucci, G. A. Petersson, H. Nakatsuji, M. Caricato, X. Li, H. P. Hratchian, A. F. Izmaylov, J. Bloino, G. Zheng, J. L. Sonnenberg, M. Hada, M. Ehara, K. Toyota, R. Fukuda, J. Hasegawa, M. Ishida, T. Nakajima, Y. Honda, O. Kitao, H. Nakai, T. Vreven, J. J. A. Montgomery, J. E. Peralta, F. Ogliaro, M. Bearpark, J. J. Heyd, E. Brothers, K. N. Kudin, V. N. Staroverov, R. Kobayashi, J. Normand, K. Raghavachari, A. Rendell, J. C. Burant, S. S. Iyengar, J. Tomasi, M. Cossi, N. Rega, N. J. Millam, M. Klene, J. E. Knox, J. B. Cross, V. Bakken, C. Adamo, J. Jaramillo, R. Gomperts, R. E. Stratmann, O. Yazyev, A. J. Austin, R. Cammi, C. Pomelli, J. W. Ochterski, R. L. Martin, K. Morokuma, V. G. Zakrzewski, G. A. Voth, P. Salvador, J. J. Dannenberg, S. Dapprich, A. D. Daniels, O. Farkas, J. B. Foresman, J. V. Ortiz, J. Cioslowski and D. J. Fox, *Gaussian-09, Revision E.01*, Gaussian Inc., Wallingford, CT, U.S.A., 2009.
37 Y. Zhao and D. G. Truhlar, *Theor. Chem. Acc.*, 2008, **120**, 215–241.
38 S. Grimme, *Wiley Interdiscip. Rev.: Comput. Mol. Sci.*, 2011, **1**, 211–228.
39 A. L. Spek, *J. Appl. Crystallogr.*, 2003, **36**, 7–13.
40 A. Burger and R. Ramberfer, *Mikrochim. Acta*, 1979, **2**, 259–271.
41 J. D. Dunitz and J. Bernstein, *Acc. Chem. Res.*, 1995, **28**, 193–200.

© 2022 The Author(s). Published by the Royal Society of Chemistry

Chapter 7 Design of a series of cocrystals featuring isoniazid modified with diacetone alcohol

7.1 Introduction

In this paper eight cocrystals containing **iz4h4m2p** and a carboxylic acid were synthesized and characterized. Each of the cocrystals features a hydrogen bond formed between the pyridine ring of **iz4h4m2p** and the carboxylic acid. Most of the cocrystals featured a similar hydrogen bond scheme overall, with exceptions arising where an additional hydroxyl group was present on the carboxylic acid molecule.

Authors: Scheepers, M.C., Lemmerer A.
Journal: Acta Crystallographica Section B
Date Published: 27 Spetember 2022
Volume Number: B78
Pages: 1-11

STRUCTURAL SCIENCE
CRYSTAL ENGINEERING
MATERIALS

ISSN 2052-5206

Design of a series of cocrystals featuring isoniazid modified with diacetone alcohol

Matthew Clarke Scheepers and Andreas Lemmerer*

Molecular Sciences Institute, School of Chemistry, University of the Witwatersrand, Private Bag 3, Johannesburg, Gauteng 2050, South Africa. *Correspondence e-mail: andreas.lemmerer@wits.ac.za

Received 25 July 2022
Accepted 27 September 2022

Edited by A. Nangia, CSIR–National Chemical Laboratory, India

Keywords: isoniazid; cocrystal; covalent-assisted supramolecular synthesis; crystal structure; pharmaceutical.

CCDC references: 2177244; 2177245; 2177246; 2177247; 2177248; 2177249; 2177250; 2177251

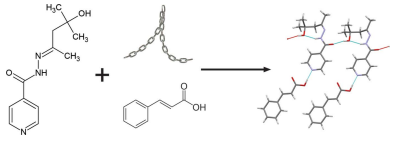
Supporting information: this article has supporting information at journals.iucr.org/b

Eight cocrystals containing an isoniazid derivative derivatized with diacetone alcohol [*N*′-[(2*E*)-4-hydroxy-4-methylpentan-2-ylidene]pyridine-4-carbohydrazide, **iz4h4m2p**] were synthesized and characterized. All coformers used in this work feature at least one carboxylic acid functional group. These coformers include: succinic acid, 3,5-dinitrobenzoic acid, 4-nitrobenzoic acid, 2-chloro-4-nitrobenzoic acid, 2,5-dihydroxybenzoic acid, 3-hydroxybenzoic acid, 4-hydroxybenzoic acid and cinammic acid. Crystal structures were obtained using single crystal X-ray diffraction, which shows that cocrystals containing **iz4h4m2p** feature a similar chain hydrogen bond between molecules of **iz4h4m2p** in addition to the expected carboxylic acid···pyridine hydrogen-bond interaction. Differences between the structures arise when additional hydroxyl group(s) are present, such as the case featuring the hydroxybenzoic acids. These structures are compared to their isoniazid counterparts presented previously in the literature. All cocrystals were also characterized with differential scanning calorimetry and Fourier transform infrared spectroscopy.

1. Introduction

Isoniazid or isonicotinic acid hydrazide (**inh**) is an antibacterial prodrug, often used together with a combination of other drugs as part of an effective treatment for tuberculosis (TB). Originally it was combined with *p*-aminosalicylic acid and streptomycin (Iseman, 2002). **inh** itself is a fairly simple prodrug molecule consisting of primarily a pyridine ring and a hydrazine group. It is converted into the active isonicotinic acyl radical form by the catalase–peroxidase enzyme KatG present in *Mycobacterium tuberculosis* (de Faria *et al.*, 2021). When treating TB, a single oral dose which contains all the necessary active pharmaceutical ingredients (APIs) in a fixed-dose combination (FDC) is preferred. However, it is known that **inh** can degrade in the presence of other APIs (Bhutani *et al.*, 2004; Diniz *et al.*, 2018). As such, this proves to be problematic. Several different strategies can be used to solve this problem.

One of these potential solutions is to use cocrystals. Although no universal agreement of the exact definition of a cocrystal exists, several proposed definitions are available. The definition of a cocrystal proposed by the FDA is: '*Solids that are crystalline materials composed of two or more molecules in the same crystal lattice.*' (Aitipamula *et al.*, 2012). Aitipamula *et al.* (2012) proposed several different definitions that included the presence of ions to avoid separating cocrystals and salts from falling under different regulations. Grothe *et al.* (2016) proposed that a cocrystal is a '*crystal with a coformer molecule plus either another coformer or at least two ions*' with further classifications into different classes. Cocrystals offer the advantage in that the intermolecular interactions between API and coformer can be planned, in addition to the oppor-



OPEN ACCESS
Published under a CC BY 4.0 licence

tunity to patent new intellectual properties (Oruganti *et al.*, 2016). Cocrystals can potentially offer the advantage of improved properties such as solubility, bioavailability and dissolution rates over the pure material (Blagden *et al.*, 2007; Ganie *et al.*, 2022). For pharmaceutical cocrystals the ideal strategy is to use a Generally Regarded As Safe (GRAS) or a pharmaceutically-accepted compound which can form complementary hydrogen bonds with the targeted API (Trask, 2007). However, in practise, this strategy may prove difficult, as the number of suitable GRAS or pharmaceutically acceptable compounds that could be used is limited. Even if a potentially suitable conformer is found, cocrystallization may not occur due to unknown factors such as kinetic and/or thermodynamic barriers (Bučar *et al.*, 2013). Therefore, it becomes imperative to explore the structural landscape of new and already existing APIs.

One approach to finding a product with improved properties is to modify an already existing API. Although modifying an API would involve starting clinical trials from scratch, it may prove worthwhile in the long term if the modified API is better than the original form. From a crystal engineering perspective, the modification is a crystal engineering opportunity that can either simplify complex intermolecular interactions or introduce functional groups that can become involved in new intermolecular interactions. For **inh** the hydrazine group is targeted because it can be easily modified (Hearn & Cynamon, 2004). One of these modifications involves a Schiff-base condensation reaction between **inh** and a ketone or aldehyde of choice. In particular, derivatives using 2-propanone (Wang *et al.*, 2008; Lemmerer, 2012; Oruganti *et al.*, 2016; Boles *et al.*, 2021) or 2-butanone (Lemmerer *et al.*, 2011; Madeley *et al.*, 2019; Setshedi & Smith, 2021) as the ketones and aldehydes (Ganie *et al.*, 2022) including salinazid (Surov *et al.*, 2016) have been reported in the literature in crystal engineering studies. This changes the hydrazide group to an amide and an imine group. From a crystal engineering perspective, these modified **inh** can have a reduced number of hydrogen bond donors. Although this may reduce the chances of forming a cocrystal since the only hydrogen pair donor remaining will be the amide and hydrogen bond acceptors will be the oxygen from the amide and the pyridine ring; however, this should not be a big problem, as carboxylic acids have been shown to form a robust interaction with pyridines (either a hydrogen bond or a proton transfer) very easily (Shattock *et al.*, 2008).

In a previous work (Scheepers *et al.*, 2022), we presented *N*′-[(2*E*)-4-hydroxy-4-methylpentan-2-ylidene]pyridine-4-carbohydrazide (**iz4h4m2p**), which is **inh** derivatized using diacetone alcohol (4-hydroxy-4-methyl-2-pentanone) *via* a Schiff-base condensation reaction. This ketone consists of a five carbon length alkyl chain with an extra methyl group and a hydroxyl group. This compound was determined to be polymorphic in our previous study (Scheepers *et al.*, 2022), consisting of a metastable form, form **I** and a stable form, form **II** (Scheepers *et al.*, 2022). The major difference between the two forms is the different hydrogen bonding present in each form: form **I** forms a chain hydrogen-bond motif between the hydroxyl group to the oxygen atom from the amide group from a neighbouring **iz4h4m2p** molecule, while form **II** forms a ring hydrogen-bond motif where the hydroxyl group forms a hydrogen bond to the pyridine ring, which subsequently combines to form dimers (Fig. 1). Like the other hydrazone derivatives of **inh** mentioned, **iz4h4m2p** still features a bulky alkyl chain backbone. However, the newly introduced hydroxyl group should allow for some variation from the previously observed cocrystals of the hydrazone derivatives of **inh**. Since **iz4h4m2p** contains a pyridine, it should readily interact with molecules containing a carboxylic acid group. This interaction can potentially reduce the supramolecular assembly from 2D sheets to a 1D ribbon (Lemmerer *et al.*, 2011). This increases the chances of forming cocrystals with more predictable supramolecular assemblies.

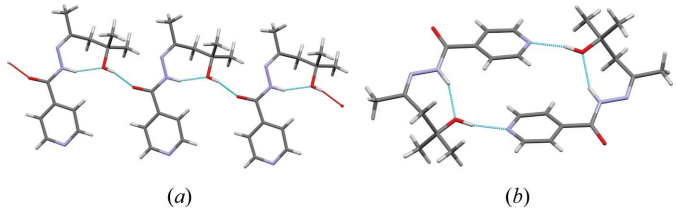


Figure 1
The structures of **iz4h4m2p** and the different hydrogen-bonding schemes between (*a*) form **I** and (*b*) form **II**.

So far, only one cocrystal containing **iz4h4m2p** has been reported (Madeley *et al.*, 2019) and it contained 4-*tert*-butylbenzoic acid. This cocrystal consists of a hydrogen bond formed between the pyridine ring of **iz4h4m2p** and the carboxylic acid group, while a chain hydrogen-bond motif exists between the hydroxyl group of the **iz4h4m2p** molecule to the oxygen of the amide group from a neighbouring **iz4h4m2p** molecule. Based on this, would other **iz4h4m2p** cocrystals with carboxylic acid coformers form similar structures with similar hydrogen-bond motifs? Will additional hydrogen-bond donors/acceptors from the coformers have a considerable effect on the structure of these cocrystals? Hence, the objective for this work is to explore the multicomponent crystal landscape of **iz4h4m2p**. This involves designing and synthesizing cocrystals of **iz4h4m2p** with coformers containing the carboxylic acid group.

2. Experimental

2.1. Materials

All materials were purchased from Sigma-Aldrich and were used as is without further purification.

2.2. General procedure for synthesis of iz4h4m2p and its cocrystals

iz4h4m2p was synthesized using a previously described method. **inh** and diacetone alcohol were dissolved in absolute ethanol (5 ml) in a small glass vial containing a magnetic stirrer bar. This vial was closed and stirred for 24 h at room temperature (∼295–300 K). After which, the lid of the vial was

replaced with another lid with a small hole in it to allow solvent to evaporate out. After several days crystals of **iz4h4m2p** were obtained. These crystals were of form **II**.

The general procedure for the synthesizing cocrystals was as follows: stoichiometric amounts of **iz4h4m2p** and the respective coformer were dissolved in an appropriate solvent/solvent combination in a small glass vial at room temperature. The vial is closed using a lid with a small hole in it to allow solvent to evaporate out. Crystals are obtained after several days.

2.3. Powder X-ray diffraction

Powder X-ray diffraction (PXRD) is used to determine the bulk phase purity of each sample. PXRD data for all forms were measured at 293 K on a Bruker D2 Phaser diffractometer which employs a sealed tube Co X-ray source (λ = 1.78896 Å), operating at 30 kV and 10 mA, and LynxEye PSD detector in Bragg–Brentano geometry. Powder patterns for the cocrystals are presented in the supporting information, where the experimentally measured pattern is compared to the calculated patterns obtained from the SC-XRD data.

2.4. Single crystal X-ray diffraction

A Bruker D8 Venture Photon CMOS 100 area detector diffractometer, equipped with a graphite-monochromated Mo $K\alpha_1$ (λ = 0.71073 Å) sealed tube (50 kV, 30 mA), was used to collect all the intensity data. Crystal structures were determined at 173 K. The program *SAINT+* (version 6.02) (Bruker, 2012) was used to integrate the data and the program *SADABS* (Krause *et al.*, 2015) was used to make empirical absorption corrections. Space group assignments were made using *XPREP* (Bruker, 2012) for all compounds. In all cases except for the case of **iz4h4m2p** + **4hba**, the structures were solved in the *WinGX* suite of programs (Farrugia, 1999) by intrinsic phasing using *SHELXT* (Sheldrick, 2015) and refined using full-matrix least-squares/difference Fourier techniques on F^2 using *SHELXL* (Sheldrick, 2018). All non-hydrogen atoms were refined anisotropically. All carbon-bound hydrogen atoms were placed at idealized positions and refined as riding atoms with the U_{iso} parameter 1.2 or 1.5 times that of their parent atoms. Nitrogen-bound and oxygen-bound hydrogen atoms were located in a difference Fourier map and their coordinates and isotropic displacement parameters refined freely. *Olex2* (version 1.3) (Dolomanov *et al.*, 2009) was used to solve the disordered system of **iz4h4m2p** + **4hba**. Diagrams and publication material were generated using *ORTEP-3* (Farrugia, 2012) and *MERCURY* (Macrae *et al.*, 2020). The crystallographic information can be found in Table 1.

2.5. The Cambridge Structural Database

The Cambridge Structural Database (CSD version 2022.1.0) (Groom *et al.*, 2016) was used to compare the cocrystals presented in this work with the cocrystals of **inh**, as well as the cocrystals of any notable **inh** derivative. The only restriction was that entries must be classified as being organic. *MERCURY* (Macrae *et al.*, 2020) was used to inspect the crystal structures. The aromatic analyser tool of *MERCURY* was used to inspect the aromatic interactions of the aryl rings. The crystal structure similarity tool was used to compare the structural similarity of selected structures.

Table 1
Coformers, molar ratios and solvent systems used to synthesize cocrystals presented in this work.

3hba: 3-hydroxybenzoic acid, **4hba**: 4-hydroxybenzoic acid, **2,5hba**: 2,5-dihydroxybenzoic acid, **2c4n**: 2-chloro-4-nitrobenzoic acid, **4nba**: 4-nitrobenzoic acid, **dnba**: 3,5-dinitrobenzoic acid, **ca**: cinammic acid, **sa**: succinic acid.

Coformer	Molar ratio (**iz4h4m2p**:coformer)	Solvent system
3hba	1:1	Ethanol
4hba	1:1	Ethanol
2,5-dhba	1:1	Methanol or 1:1 *v*/*v* methanol : acetonitrile
2c4n	1:1	Ethanol
4nba	1:1	Ethanol
dnba	1:1	Ethanol
ca	1:1	Methanol
sa	2:1	Ethanol

2.6. Differential scanning calorimetry

Differential scanning calorimetry (DSC) data were collected using a Mettler Toledo DSC 3 with aluminium pans under nitrogen gas (flow rate = 10 ml min^{-1}). Exothermic events were shown as peaks. Samples were heated and cooled to determine melting points as well as any additional phase transitions. The temperature and energy calibrations were performed using pure indium (purity 99.99%, m.p. 156.6°C, heat of fusion: 28.45 J g^{-1}) and pure zinc (purity 99.99%, m.p. 479.5°C, heat of fusion: 107.5 J g^{-1}). Samples were heated to 250°C from 25°C before being cooled back down at 25°C at a heating or cooling rate of 10°C min^{-1}.

2.7. Fourier transform infrared analysis

FTIR spectra were collected using the Bruker Alpha II spectrometer equipped with an Eco-ATR sampling module. Background noise was subtracted and a small amount of the sample of interest was placed onto the ATR crystal. Spectra were measured in the 600 to 4000 cm^{-1} range, resolution was 4 cm^{-1} with 24 scans per sample. Spectra were collected in a room with air conditioning set at 295 K. After spectral acquisition the ATR crystal was cleaned using isopropanol.

3. Results and discussion

3.1. Obtaining cocrystals

In order to obtain cocrystals containing **iz4h4m2p** with molecules containing at least one carboxylic acid, several coformers were used. Most of these consist of Generally Regarded As Safe (GRAS) compounds, such as succinic acid (**sa**) and gentisic acid (2,5-dihydroxybenzoic acid, **2,5-dhba**). These coformers include ones which have either one or two carboxylic acid groups. A full list of all the coformers used is

Table 2
Crystallographic information for cocrystals presented in this work.

For all structures: Mo $K\alpha$ radiation, Bruker APEX-II CCD diffractometer, multi-scan absorption correction using *SADABS* (Krause *et al.*, 2015). H atoms treated by a mixture of independent and constrained refinement.

	iz4h4m2p + 2c4n	**iz4h4m2p + 3hba**	**iz4h4m2p + ca**	**iz4h4m2p + dnba**
Crystal data				
Chemical formula	$C_{12}H_{17}N_3O_2{\cdot}C_7H_4NO_4Cl$	$C_7H_6O_3{\cdot}C_{12}H_{17}N_3O_2$	$C_{12}H_{17}N_3O_2{\cdot}C_9H_8O_2$	$C_{12}H_{17}N_3O_2{\cdot}C_7H_4N_2O_6$
M_r	436.85	373.4	383.44	447.41
Crystal system, space group	Triclinic, $P\overline{1}$	Monoclinic, $P2_1/n$	Triclinic, $P\overline{1}$	Monoclinic, $P2_1/n$
Temperature (K)	173	173	173	173
a, b, c (Å)	7.0381 (1), 12.2643 (2), 12.4636 (2)	8.7472 (3), 16.9734 (5), 13.2480 (4)	6.9734 (3), 11.2540 (5), 13.4029 (6)	6.9538 (3), 18.9491 (8), 15.9042 (7)
α, β, γ (°)	103.215 (1), 97.797 (1), 93.497 (1)	90, 94.886 (1), 90	89.949 (2), 82.689 (2), 74.261 (2)	90, 99.261 (2), 90
V (Å^3)	1032.92 (3)	1959.78 (11)	1003.55 (8)	2068.35 (15)
Z	2	4	2	4
μ (mm^{-1})	0.23	0.09	0.09	0.11
Crystal size (mm)	0.52 × 0.25 × 0.21	0.59 × 0.48 × 0.22	0.37 × 0.18 × 0.10	0.39 × 0.29 × 0.13
Data collection				
T_{min}, T_{max}	0.674, 0.746	0.686, 0.747	0.631, 0.746	0.699, 0.747
No. of measured, independent and observed $I > 2\sigma(I)$] reflections	49833, 7362, 4908	78332, 8649, 7062	47711, 4995, 4111	196011, 11136, 9039
R_{int}	0.039	0.033	0.078	0.082
(sin $\theta/\lambda)_{max}$ (Å^{-1})	0.753	0.809	0.668	0.864
Refinement				
$R[F^2 > 2\sigma(F^2)]$, $wR(F^2)$, S	0.044, 0.117, 1.06	0.051, 0.145, 1.06	0.039, 0.107, 1.03	0.054, 0.140, 1.07
No. of reflections	7362	8649	4995	11136
No. of parameters	286	263	268	304
$\Delta\rho_{max}$, $\Delta\rho_{min}$ (e Å^{-3})	0.42, −0.35	0.50, −0.20	0.25, −0.20	0.54, −0.30

	iz4h4m2p + sa	**iz4h4m2p + 4nba**	**iz4h4m2p + 25dhba**	**iz4h4m2p + 4hba**
Crystal data				
Chemical formula	$C_{12}H_{17}N_3O_2{\cdot}C_2H_3O_2$	$C_{12}H_{17}N_3O_2{\cdot}C_7H_5NO_4$	$C_{12}H_{17}N_3O_2{\cdot}C_7H_6O_4$	$C_{12}H_{16}N_3O_2{\cdot}2(C_7H_6O_3)$
M_r	294.33	402.4	389.4	884.92
Crystal system, space group	Monoclinic, $P2_1/c$	Triclinic, $P\overline{1}$	Monoclinic, $P2_1/n$	Monoclinic, $C2/c$
Temperature (K)	173	173	133	173
a, b, c (Å)	6.9773 (4), 20.6482 (11), 10.5035 (5)	6.8701 (3), 12.1647 (6), 12.1779 (6)	8.5777 (5), 17.5407 (9), 13.2200 (8)	41.700 (2), 8.2992 (4), 12.9536 (8)
α, β, γ (°)	90, 98.764 (2), 90	101.130 (2), 92.818 (2), 105.005 (2)	90, 96.605 (2), 90	90, 97.033 (2), 90
V (Å^3)	1495.56 (14)	959.26 (8)	1975.86 (19)	4449.2 (4)
Z	4	2	4	4
μ (mm^{-1})	0.10	0.11	0.10	0.09
Crystal size (mm)	0.52 × 0.23 × 0.07	0.57 × 0.42 × 0.11	0.58 × 0.49 × 0.27	0.55 × 0.26 × 0.14
Data collection				
T_{min}, T_{max}	0.676, 0.746	0.642, 0.746	0.689, 0.746	0.600, 0.746
No. of measured, independent and observed [$I > 2\sigma(I)$] reflections	45682, 3733, 3131	42678, 5857, 4742	41489, 4917, 4391	54732, 5529, 5529
R_{int}	0.089	0.047	0.028	0.088
(sin $\theta/\lambda)_{max}$ (Å^{-1})	0.668	0.715	0.668	0.667
Refinement				
$R[F^2 > 2\sigma(F^2)]$, $wR(F^2)$, S	0.044, 0.113, 1.03	0.045, 0.136, 1.07	0.038, 0.105, 0.99	0.056, 0.150, 1.04
No. of reflections	3733	5857	4917	5529
No. of parameters	205	277	273	352
$\Delta\rho_{max}$, $\Delta\rho_{min}$ (e Å^{-3})	0.33, −0.21	0.34, −0.27	0.30, −0.21	0.29, −0.27

Computer programs: *SAINT* (v. 8.40B) (Bruker, 2016), *SHELXT-2018/2* (Sheldrick, 2015), *SHELXL2018/3* (Sheldrick, 2018), *ORTEP for Windows* (Farrugia, 2012), *Olex2* (v. 1.3) (Dolomanov *et al.*, 2009), *WinGX* publication routines (Farrugia, 2012).

included in the supporting information. For this work, we used various stoichiometric ratios such as 1:1, 2:1 and 1:2 of **iz4h4m2p**: coformer with different solvents (methanol, ethanol, acetonitrile, water) and solvent mixtures (1:1 ratios of solvent 1:solvent 2). It should be noted that we avoided heating the solution, as **iz4h4m2p** can decompose in a hot solution, resulting in an oil. Thus we relied on stirring the solution for 10–20 min at room temperature to ensure complete dissolution. Out of a list of 28 coformers used, only eight formed cocrystals. The reasons why we did not obtain more were due to the possibility that some of the acids still produced oils as opposed to crystals, while in other cases the

coformers precipitated out separately without forming a cocrystal. The eight cocrystals that were synthesized used the following coformers: 3,5-dinitrobenzoic acid (**dnba**), succinic acid, **2,5-dhba**, 3-hydroxybenzoic acid (**3hba**), 4-hydroxybenzoic acid (**4hba**), 4-nitrobenzoic acid (**4nba**), 2-chloro-4-nitrobenzoic acid (**2c4n**) and cinammic acid. The molar ratios and solvents used to synthesize these are presented in Table 1. The results are presented below in four separate sections because of some similarities and major differences between certain crystal structures and/or coformers. These sections are: (i) **iz4h4m2p** + **sa** and **iz4h4m2p** + **ca**, (ii) **iz4h4m2p** + **dnba**, **iz4h4m2p** + **2c4n** and **iz4h4m2p** + **4nba**, (iii) **iz4h4m2p** + **4hba**, (iv) **iz4h4m2p** + **2,5-dhba** and **iz4h4m2p** + **3hba**. The reasoning for splitting these cocrystals into these sections is as follows: (i) it was suspected that **iz4h4m2p** + **ca** and **iz4h4m2p** + **sa** to have a similar hydrogen-bonding patterns due to the absence of additional hydrogen bond donors/acceptors, (ii)) in **iz4h4m2p** + **dnba**, **iz4h4m2p** + **2c4n**, and **iz4h4m2p** + **4nba** the coformers all feature a nitro group, which may or may not have had a significant impact on the crystal structure formation while (iii) and (iv) the additional hydrogen bond donors had a significant impact in the overall hydrogen bond interactions observed that made the structures unique in comparison to the structures described in (i) and (ii). The crystal structure information is presented in Table 2, while *ORTEP* diagrams are presented in Fig. 2. Graph sets have been used to describe some of the hydrogen bonding observed in the crystal structures (Etter *et al.*, 1990).

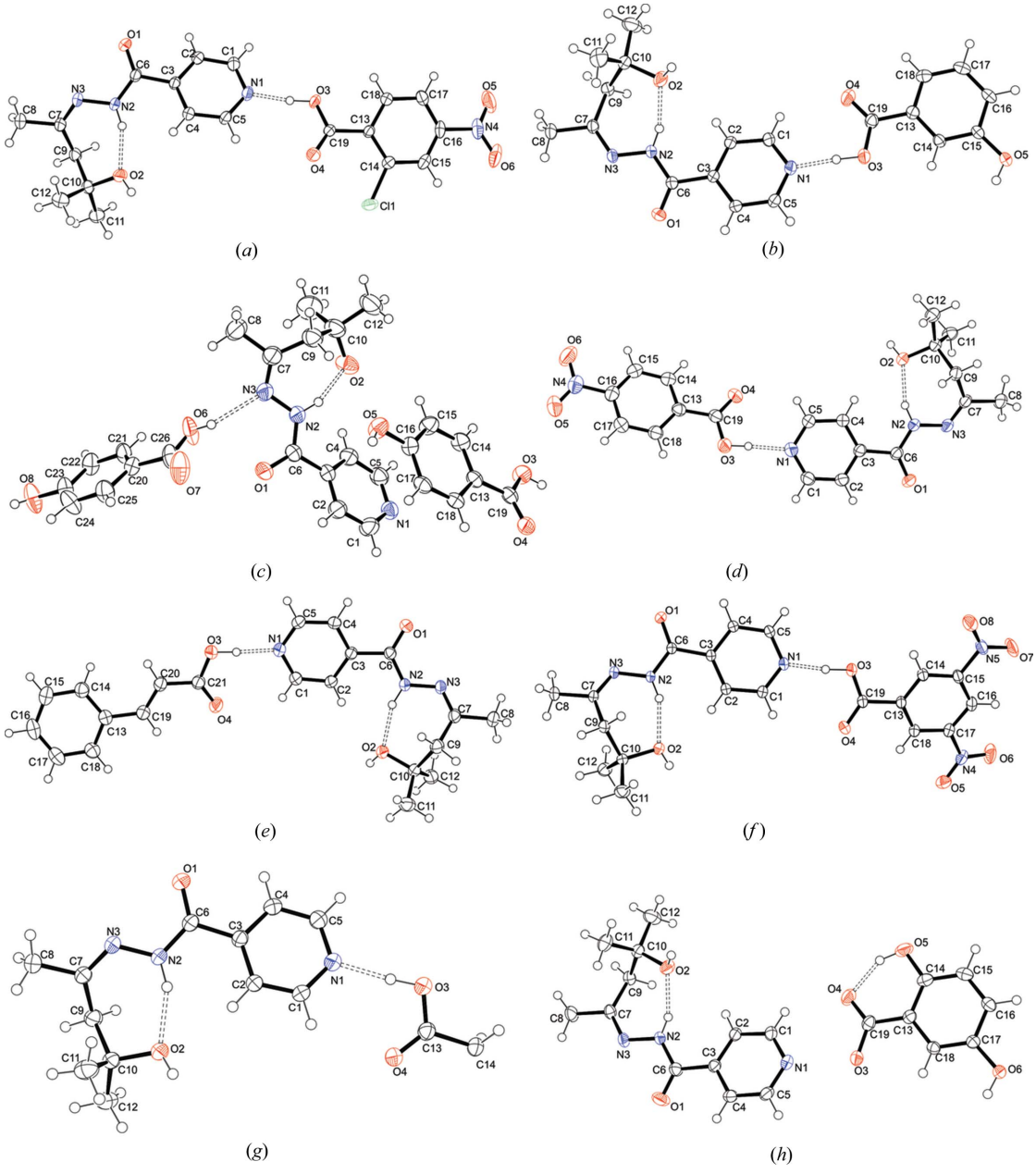


Figure 2
ORTEP diagrams of (*a*) **iz4h4m2p** + **2c4n**, (*b*) **iz4h4m2p** + **3hba**, (*c*) **iz4h4m2p** + **4hba**, (*d*) **iz4h4m2p** + **4nba**, (*e*) **iz4h4m2p** + **ca**, (*f*) **iz4h4m2p** + **dnba**, (*g*) **iz4h4m2p** + **sa** and (*h*) **iz4h4m2p** + **2,5-dhba**.

3.2. Crystal structures of iz4h4m2p + sa and iz4h4m2p + ca

iz4h4m2p formed cocrystals with succinic acid and cinammic acid, forming colourless needles and colourless plates, respectively. The asymmetric unit of **iz4h4m2p** + **ca** consists of one molecule each of **iz4h4m2p** and **ca** and crystallizes in space group $P\overline{1}$, while the asymmetric unit of **iz4h4m2p** + **sa** consists of one molecule of **iz4h4m2p** and half a molecule of succinic acid (which sits on a special crystallographic site), and crystallizes in space group $P2_1/c$. In each case the respective carboxylic acid forms a hydrogen bond with the pyridyl nitrogen of **iz4h4m2p**. Furthermore, this results in the hydroxyl group of **iz4h4m2p** forming a hydrogen bond with the oxygen of the amide from a neighbouring **iz4h4m2p** molecule, which forms a $C_2^2(6)$ chain hydrogen-bond motif similar to the one observed in form **I** of **iz4h4m2p**. Additionally, for **iz4h4m2p** + **ca**, $\pi\cdots\pi$ stacking exists between the rings of adjacent **ca** molecules and pyridine rings of **iz4h4m2p** ($Cg\cdots Cg$ = 4.01 Å). Although both crystal structures form 1D ribbons (Fig. 3), the packing between the two are different. The ribbons in **iz4h4m2p** + **ca** feature a more stacked or layered structure, with cinammic acid and **iz4h4m2p** separated by alternating layers [Figs. 4(*a*) and 4(*b*)], while the ribbons from the cocrystal of **iz4h4m2p** + **sa** form a zigzag pattern [Fig. 4(*c*)].

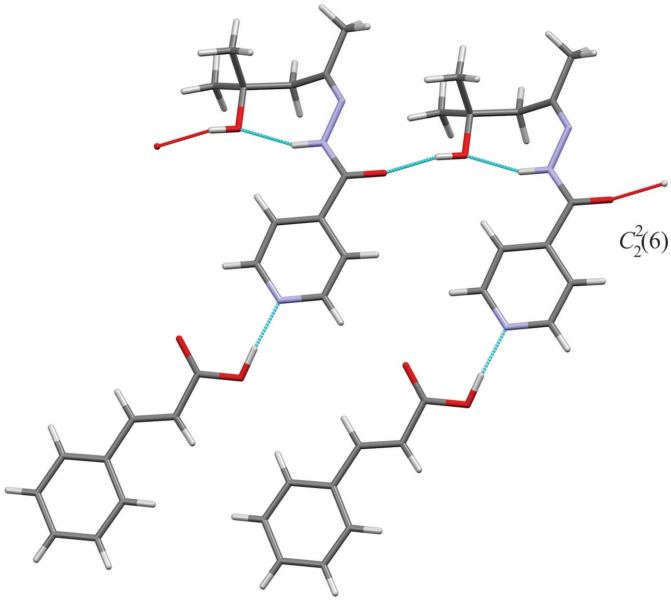


Figure 3
Hydrogen bonding in **iz4h4m2p** + **ca** which is the standard hydrogen-bonding scheme in most of the structures presented.

3.3. Crystal structures of iz4h4m2p + dnba, iz4h4m2p + 2c4n and iz4h4m2p + 4nba

iz4h4m2p formed cocrystals with **dnba**, **2c4n** and **4nba**, yielding colourless plates, colourless blocks and colourless plates, respectively. Each cocrystal contains one molecule of **iz4h4m2p** and one molecule of the respective coformer in the asymmetric unit. Both **iz4h4m2p** + **2c4n** and **iz4h4m2p** + **4nba** crystallize in space group $P\overline{1}$, while **iz4h4m2p** + **dnba** crystallizes in the space group $P2_1/n$. It should be noted that the cocrystals of **iz4h4m2p** + **2c4n** and **iz4h4m2p** + **4nba** share similar unit-cell parameters and the same space group, which would imply the structures may be isostructural. Using the crystal structure similarity tool and restricting the size of the cluster to 30 molecules, there is a strong correlation that shows that the two structures may be isostructural to a degree, as seen in Fig. 5(*d*), despite some deviations observed (such as, for example, some of the pyridine ring having different torsion angles). This slight difference is due to the presence of the chlorine atom in **2c4n**. The major hydrogen bonding for all three structures is the same as the one described in the previously discussed structures: the carboxylic acid···pyridine ring hydrogen bond and the amide···hydroxyl···amide chain hydrogen bond. Nitro groups in all structures do not participate in any hydrogen bonding. $\pi\cdots\pi$ stacking exists between **2c4n** molecules to **2c4n** molecules and **iz4h4m2p** molecules to **iz4h4m2p** molecules in the structure of **iz4h4m2p** + **2c4n** (**2c4n**···**2c4n**: $Cg\cdots Cg$ = 3.58 Å and **iz4h4m2p**···**iz4h4m2p**: $Cg\cdots Cg$ = 3.74 Å). A similar pattern of $\pi\cdots\pi$ stacking was observed for the structure of **iz4h4m2p** + **4nba** (**4nba**···**4nba**: $Cg\cdots Cg$ = 3.66 Å and **iz4h4m2p**···**iz4h4m2p**: $Cg\cdots Cg$ = 3.81 Å). For **iz4h4m2p** + **dnba,** the only $\pi\cdots\pi$ stacking observed was between adjacent **dnba** molecules ($Cg\cdots Cg$ = 3.90 Å). The packing of **iz4h4m2p** + **dnba**, **iz4h4m2p** + **2c4n** and **iz4h4m2p** + **4nba** is similar: alternating rows of 1D ribbons formed from the chain hydrogen-bond motif [Figs. 5(*a*)–5(*c*)].

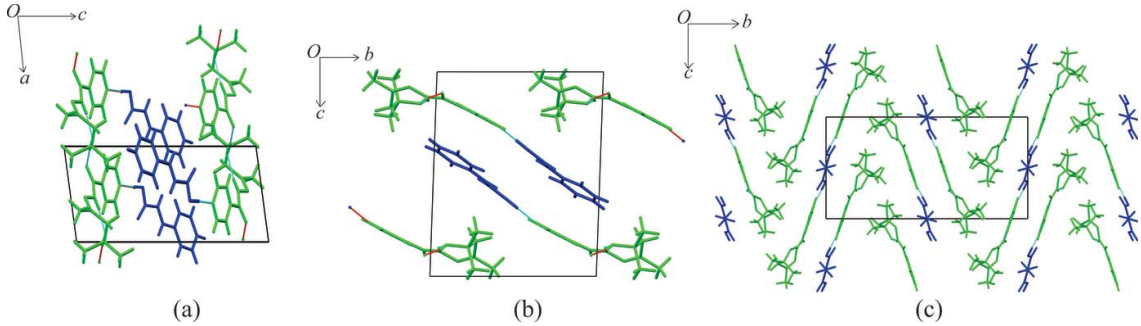


Figure 4
Crystal structure packing of (*a*) **iz4h4m2p** + **ca** (down the *b*-axis), (*b*) **iz4h4m2p** + **ca** (down the *a*-axis) and (*c*) **iz4h4m2p** + **sa** (down the *a*-axis). **Iz4h4m2p** molecules are presented in green while the respective coformers are in blue.

3.4. Crystal structure of iz4h4m2p + 4hba

iz4h4m2p and **4hba** formed a cocrystal, forming colourless plates. This cocrystal contains one molecule of **iz4h4m2p** and two molecules **4hba** in the asymmetric unit and crystallizes in space group *C*2/*c*. One of the two molecules of **4hba**, the one located at a special crystallographic site, is disordered. This causes the disordered **4hba** molecule to exist in one of two possible orientations at these sites. To distinguish between the two **4hba** molecules, they will be referred to as either the disordered or non-disordered **4hba** molecule. Not all the hydrogens attached to an oxygen atom could be found precisely and were placed geometrically with respect to the oxygen atom. These hydrogen atoms are H3, H6 and H8. Like the previous structures, the hydroxyl group of **iz4h4m2p** forms a hydrogen bond to the oxygen of the amide group from a neighbouring **iz4h4m2p** molecule (O2—H2···O1), while the carboxylic acid group of the non-disordered **4hba** molecule forms a hydrogen bond with the pyridine ring of **iz4h2m2p**. The hydroxyl group of the non-disordered **4hba** molecule forms a hydrogen bond with one of the oxygen atoms of the carboxylic acid group from a neighbouring **4hba** molecule (O5—H5*A*···O4) [Fig. 6(*a*)]. A $\pi\cdots\pi$ stacking interaction between the pyridine ring of **iz4h4m2p** and the aromatic ring of the non-disordered **4hba** molecule is present ($Cg\cdots Cg$ = 3.695 Å). Due to the nature of the varied orientation of the disordered **4hba** molecule and it sitting on an inversion site, two sets of almost identical hydrogen bonding are present. The hydrogen atoms from the carboxylic acid group (O6—H6) and the hydroxyl group (O8—H8) to the one nitrogen atom of the hydrazine group (N3) and the oxygen atom of the amide (O1).

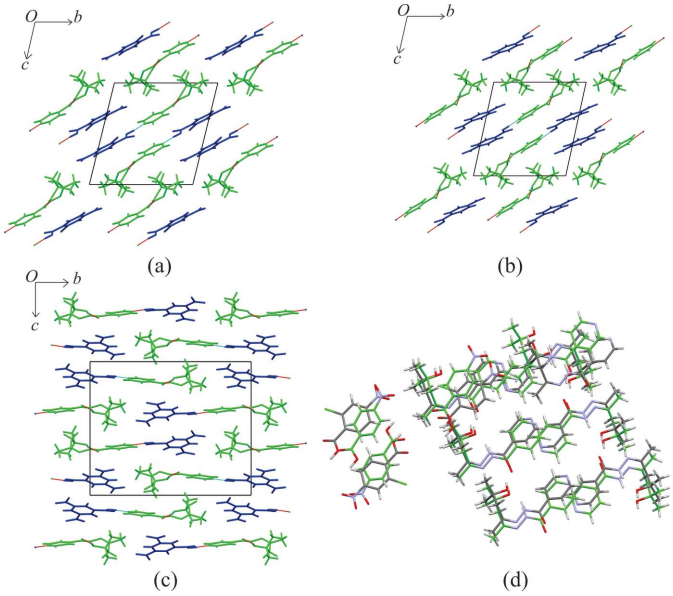


Figure 5
Crystal structure packing of (*a*) **iz4h4m2p** + **2c4n** (viewed down the *a*-axis), (*b*) **iz4h4m2p** + **4nba** (viewed down the *a*-axis), (*c*) **iz4h4m2p** + **dnba** (viewed down the *a*-axis). In (*a*)–(*c*) **iz4h4m2p** molecules are presented in green while the respective coformer is shown in blue. (*d*) The overlay of molecules from **iz4h4m2p** + **4nba** (represented as green molecules) and **iz4h4m2p** + **2c4n** (using standard colours).

The packing is made up of a series of alternating layers of the disordered **4hba** molecules, **iz4h4m2p** molecules and non-disordered **4hba** molecules.

3.5. Crystal structures of iz4h4m2p + 2,5-dhba and iz4h4m2p + 3hba

iz4h4m2p formed cocrystals with **2,5-dhba** and **3hba,** forming colourless blocks and colourless plates, respectively. The asymmetric unit for both structures consists of one molecule of each **iz4h4m2p** and the respective coformer, forming in space group $P2_1/n$. In our initial refinement of the crystal structure for **iz4h4m2p** + **2,5-dhba** we observed some electron density that located around one of the inversion sites. It is plausible that this electron density could correlate to some methanol molecules partially occupying these sites. However, this electron density was determined to be too weak to be refined as proper atoms, therefore we used the *SQUEEZE* program of *PLATON* to remove it (Spek, 2020). In addition, the hydrogen atom H3 in **iz4h4m2p** + **2,5-dhba** could not be found precisely, and was placed geometrically with respect to

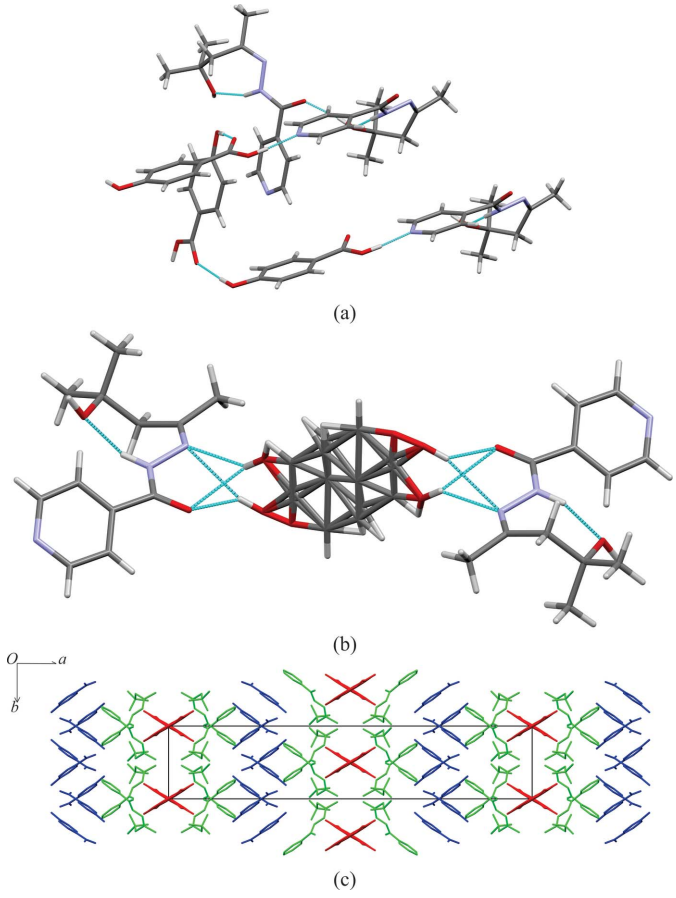


Figure 6
The crystal structure of **iz4h4m2p** + **4hba** showing (*a*) the hydrogen bonding between the non-disordered **4hba** molecules and **iz4h4m2p** (excluding the disordered **4hba** molecule), (*b*) the hydrogen bonding between the disordered **4hba** molecules and **iz4h4m2p** and (*c*) the packing of the structure down the *c*-axis [with hydrogens omitted for clarity; the molecules are colour-coded as follows: green: **iz4h4m2p**, blue: **4hba** (non-disordered) and red: **4hba** (disordered)].

the O3 atom. Due to both structures having similar unit-cell parameters, the crystal structure similarity tool in *MERCURY* was used to confirm whether both structures are isostructural. The search was restricted to a cluster of 15 molecules and molecular differences were allowed. From Fig. 7(*a*) it can be seen that all 15 molecules matched, which is indicative of both structures being isostructural. This should not be too surprising, since the difference between **3hba** and **2,5-dhba** is simply the additional hydroxyl group on **2,5-dhba**, which ultimately forms an intramolecular hydrogen bond with the carboxylic acid group. Both structures are also unusual with respect to most of the other cocrystals presented here, as the amide···hydroxyl···amide (**iz4h4m2p**) chain hydrogen-bond motif does not exist. Instead, the hydroxyl group of the carboxylic acid forms a bifurcated hydrogen bond with the amide and imine group's nitrogen (O5—H5*A*···O1 and O5—H5*A*···N3 for **iz4h4m2p** + **3hba** and O6—H6···N3 and O6—H6···O1 for **iz4h4m2p** + **2,5-dhba**). The hydroxyl group of **iz4h4m2p** then forms a hydrogen bond to the phenol of the benzoic acid (in place of the amide group from a neighbouring **iz4h4m2p** molecule). This, in turn, forms a new chain hydrogen-bond motif $C_3^3(7)$, which alternates between **iz4h4m2p** and the respective benzoic acid molecules [Fig. 7(*b*)]. Due to this chain hydrogen-bond motif, the packing of **iz4h4m2p** + **2,5-dhba** forms a series of zigzag ribbons [Fig. 7(*c*)].

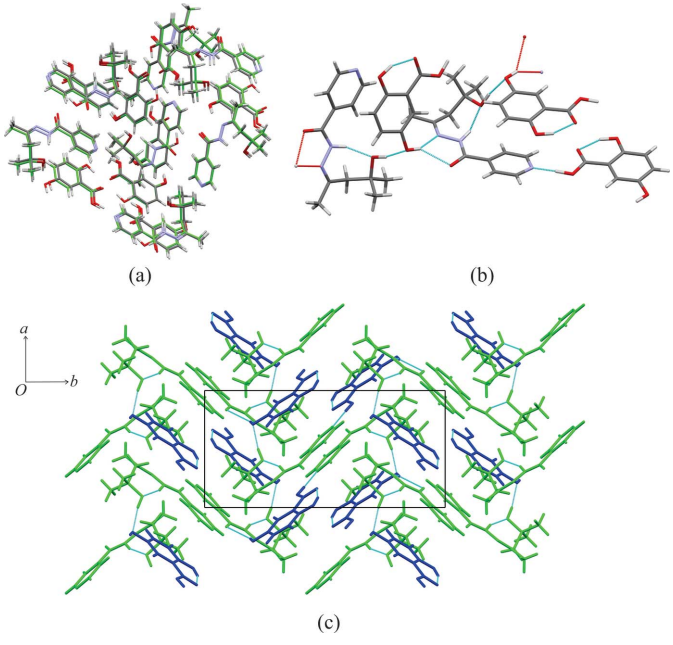


Figure 7
The crystal structure of **iz4h4m2p** + **2,5-dhba** showing (*a*) the overlap of **iz4h4m2p** + **3hba** and **iz4h4m2p** + **2,5-dhba** using the crystal structure similarity tool in *MERCURY* (**iz4h4m2p** + **3hba** in standard colours while the carbon atoms in **iz4h4m2p** + **2,5-dhba** are in green), (*b*) the hydrogen bonding present and (*c*) the packing diagram (**iz4h4m2p** is presented in green while **2,5-dhba** is presented in blue).

3.6. Comparison of cocrystals with literature examples

The CSD was used to evaluate and compare the cocrystals presented in this work with other cocrystals containing **inh** (or a Schiff-based derivative of **inh**). A complete list of CSD entries with their refcodes used to make these comparisons is included in the supporting information. First, for cocrystals and molecular salts containing **inh**, 78 results were obtained after removing duplicate entries, alkali or alkali metal salts, inorganic acids and other derivatives of **inh**. Almost all cocrystals of **inh** were formed using a coformer with a carboxylic acid functional group, forming either a carboxylic acid···pyridine ring hydrogen bond or a proton transfer if the result was a molecular salt. Nine cocrystals containing a coformer without a carboxylic were found which include the following: hydrochlorothiazide (CSD refcode: DADLUS), cyanuric acid (CSD refcode: MOXNAR), 2,4,6-trinitrophenolate (CSD refcode: PEZVAU), 5-fluorocytosine, (CSD refcode: PINJII), 5,7-dihydroxy-2-(4-hydroxyphenyl)-2,3-dihydro-4*H*-1-benzopyran-4-one (CSD refcode: UDUJIP), 1,5-naphthalenedisulfonic acid (CSD refcode: VEGHUN), resveratrol (CSD refcode: VOPQEZ), naphthalene-2,7-diol (CSD refcode: KEBLUC) and nitrofurantoin monohydrate (CSD refcode: KEFXOM). The CSD contains 433 hits of Schiff-based **inh** derivatives with the imine functional group, of which 227 contain more than one chemical entity (molecules, ions *etc.*), of which 131 were hydrates. After removing inorganic salts and solvates, only 53 cocrystals and molecular salts containing a Schiff-based **inh**-derivative remained. Like **inh**, most of the coformers used to synthesize these cocrystals and molecular salts contains a carboxylic acid functional group. Exceptions include 2,4,6-trinitrophenolate (CSD refcodes: CETWEF, EPISAY, LIGXEG and ZECXEN), saccharin (CSD refcodes: ZUVWUK and ZUVXAR) and acesulfame (CSD refcode: OKAVUT).

Similar to the cocrystals of **iz4h4m2p** presented here, cocrystals featuring a carboxylic acid will form a carboxylic acid···pyridine ring hydrogen-bond motif. A large degree of variability in hydrogen bonding exists in cocrystals containing **inh**. Cocrystals featuring an isoniazid derivative have a limited degree of variability in the hydrogen bonding, most of which stems from the nature of the coformer chosen. The variability of hydrogen bonding in **inh** cocrystals can include forming the following hydrogen-bond motifs: homodimers between the hydrazide groups, tetramers and chains. The packing can vary drastically in crystals containing **inh** molecules, which can range from 1D ribbons to 3D networks, which is due to the different combinations of hydrogen-bond pairing. For the cocrystals containing an isoniazid derivative with a reduced number of hydrogen pair donors, most packing is reduced to 1D ribbons, which can stack either parallel (such as **iz4h4m2p** + **dnba**, **iz4h4m2p** + **2c4n** and **iz4h4m2p** + **4nba**) or zigzag (such as **iz4h4m2p** + **2,5-dhba** and **iz4h4m2p** + **sa**).

Some exceptional cases arise. For example, in the cocrystal of the isoniazid derivative derivatized using acetone [*N*′-(propan-2-ylidene)isonicotinohydrazide] and **2c4n** (CSD refcode: LATLID) (Lemmerer, 2012) contains both neutral

and ionized species in the same asymmetric unit. Not only is this crystal structure chiral, the pyridine rings alternate in alignment along the chain hydrogen-bond motif at different points, which has not been observed in any of the cocrystals of **iz4h4m2p**. Polymorphism exists for the case of **inh** and cinammic acid, where three different forms exist (CSD refcodes: SETSAN01, SETSAN02, SETSAN03) (Sarcevica *et al.*, 2013, 2014). All three polymorphs featured forming an $R_4^4(16)$ ring-based tetramer, connected using the carboxylic acid···pyridine hydrogen pair as well as one of the hydrazide hydrogens forming a hydrogen pair to the oxygen of the carboxylic acid, similar to the one reported for **inh** + **dnba**. Form **I** and form **II** exhibit the same hydrogen bonding pattern, which forms tetramers. The difference between form **I** and form **II** is the orientation in which the tetramers exist in relation to each other: the tetramers in form **I** are parallel while in form **II** some of the tetramers lie at an angle. Form **III** has different hydrogen bonding compared to the form **I** and form **II**, which features a bifurcated hydrogen bond between the one oxygen of the carboxylic acid to two hydrogens from the hydrazide group from different **inh** molecules. The packing of form **III** is similar to form **I**, a layered packing. In comparison, **iz4h4m2p** + **ca** forms a zigzag packing. This is a clear example that derivatizing **inh** using a Schiff-base reaction and reducing the number of hydrogen bond donors can reduce the complexity of a structure to a simpler one.

3.7. FTIR spectra

FTIR spectroscopy is a useful technique to identify the different functional groups present in a solid, as well as to measure the strength of the intermolecular interactions between the different functional groups. For cocrystals, it is expected that FTIR spectra will differ to the spectra of the individual components, not just due to the addition of potential new functional groups but also due to the different intermolecular interactions occurring (*i.e.* new hydrogen bonds *etc.*). In particular, hydrogen bonds will cause a shift of significant FTIR peaks, which will be dependent on the strength or degree of the hydrogen bond in question. The FTIR spectra are represented together in Fig. 8, while each spectra is presented separately in the supporting information. The spectral assignments for the carboxylic acid functional group (or for **iz4h4m2p** the hydroxyl and carbonyl groups) for the cocrystals and both forms of **iz4h4m2p** have been included in Table 3. Another important use of FTIR here is to determine whether proton transfer occurred or not in the cocrystal of **iz4h4m2p** + **2,5-dhba**. As noted before, the acidic protons from **2,5-dhba** could not be located precisely in the difference Fourier maps, which were assigned geometrically with respect to the carboxylic acid. FTIR can be used to determine whether proton transfer has occurred or not. To determine whether a proton transfer has occurred, one could check to see if stretching band of either the carbonyl group (C═O) or the hydroxyl group (O—H) is present or absent. If these characteristic peaks are absent, a salt would be present. Unfortunately **iz4h4m2p** has both a carbonyl (associated with the amide) and hydroxyl groups present, making identification of a salt using this method difficult. However, a carboxylate group can also be identified by strong peaks associated with the symmetric and asymmetric stretching of the CO_2^- group in the 1450–1360 cm^{-1} and 1650–1540 cm^{-1} ranges, respectively. With the exception of **iz4h4m2p** + **dnba** these peaks are absent in each spectrum, indicating that no proton transfer occurs.

Table 3
IR spectral assignments of the wavenumbers for **iz4h4m2p** and its cocrystals to the carboxylic acid functional and/or the hydroxyl and carbonyl functional groups.

Sample	C═O stretch (cm^{-1})	O—H stretch (cm^{-1})	C—O stretch (cm^{-1})	O—H bend in-plane (cm^{-1})	O—H bend out-plane (cm^{-1})
i4h4m2p (form **I**)	1660	2969	1273	1407	932
i4h4m2p (form **II**)	1673	2971	1271	1404	919
iz4h4m2p + **2c4n**	1662	2980	1309	1408	924
iz4h4m2p + **3hba**	1674	2964	1292	1412	924
iz4h4m2p + **4nba**	1662	2982	1285	1410	925
iz4h4m2p + **ca**	1667	2975	1281	1409	927
iz4h4m2p + **sa**	1662	2968	1309	1407	925
iz4h4m2p + **dnba**	1655	2976	1286	1412	912
iz4h4m2p + **4hba**	1651	2962	1271	1415	926
iz4h4m2p + **2,5-dhba**	1673	2972	1305	1413	928

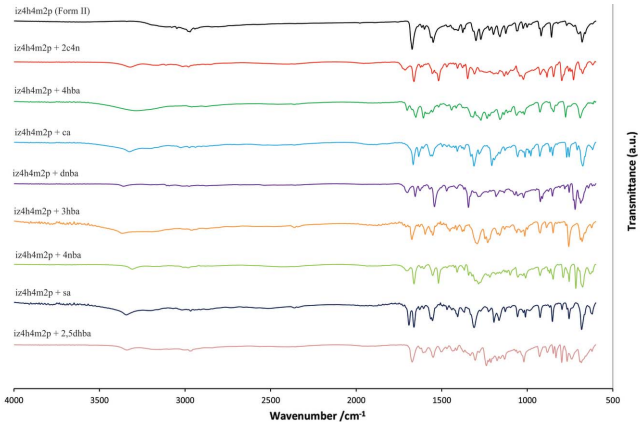


Figure 8
FTIR spectra of **iz4h4m2p** (form **II**) and its cocrystals.

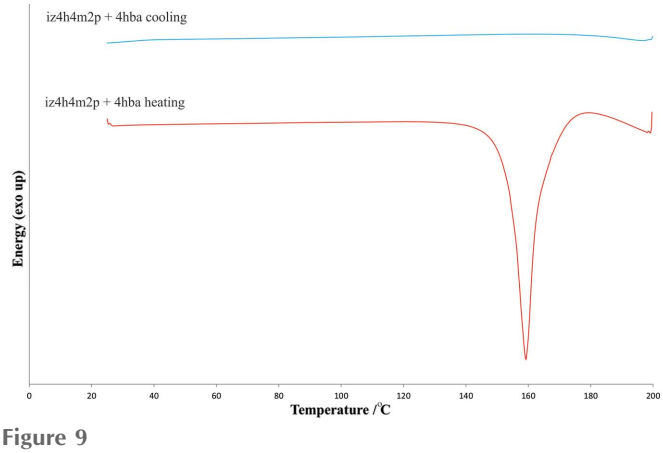


Figure 9
DSC diagrams of **iz4h4m2p** + **4hba** representing the typical behaviour of DSC curves of all cocrystals of **iz4h4m2p**.

Table 4
Onset temperatures and associated enthalpies for thermal events observed in DSC curves for the cocrystals presented in this work.

The melting/decomposition points of both polymorphic forms of **iz4h4m2p** are also given for comparison purposes (Scheepers *et al.*, 2022).

Thermal event	Onset (°C)	Enthalpy (J g^{-1})
iz4h4m2p (form **I**) melting/decomposition	139.7 ± 0.1	137.2 ± 2.3
iz4h4m2p (form **II**) melting/decomposition	142.1 ± 0.1	144.2 ± 2.4
iz4h4m2p + **2c4n** melting/decomposition	117.1 ± 0.2	237.7 ± 2.3
iz4h4m2p + **3hba** melting/decomposition	145.6 ± 0.2	276.8 ± 4.3
iz4h4m2p + **4nba** melting/decomposition	155.8 ± 0.2	279.9 ± 5.2
iz4h4m2p + **ca** melting/decomposition	103.4 ± 0.1	102.3 ± 6.6
iz4h4m2p + **dnba** melting/decomposition	130.5 ± 0.2	263.2 ± 2.8
iz4h4m2p + **sa** melting/decomposition	119.8 ± 0.1	102.2 ± 1.3
iz4h4m2p + **4hba** melting/decomposition	153.2 ± 0.2	233.9 ± 3.2
iz4h4m2p + **2,5-dhba** melting/decomposition	149.4 ± 0.2	300.6 ± 2.4

For the case of **iz4h4m2p** + **dnba**, the asymmetric stretching of the nitro groups occurs in the same range of the asymmetric stretching of the CO_2^- group, making this identification elusive. However, based on the absent strong CO_2^- group symmetric stretching band, it is more likely **iz4h4m2p** + **dnba** is a cocrystal as opposed to a salt.

3.8. Thermal analysis

DSC curves were collected for all eight cocrystals. Two of the DSC curves are presented in Fig. 9, with the curve of **iz4h4m2p** + **4hba** being a representative DSC curve for all the cocrystals. The DSCs of the other cocrystals are presented in the supporting information. The associated onset temperatures and enthalpies are represented in Table 4. For most of the samples, a single large endothermic peak was observed (corresponding to the melting/decomposition point of the sample) on the heating cycle, while no thermal events were observed on the cooling cycle which corresponds closely to the behaviour of form **II** of **iz4h4m2p**. It should be noted that only one large endothermic peak was observed for **iz4h4m2p** + **4hba**, which indicates that desolvation does not occur before melting.

4. Conclusions

Eight cocrystals containing **iz4h4m2p** were synthesized and characterized. Most of the cocrystals were uniform with regard to their hydrogen bonding, with two major hydrogen-bonding motifs observed: the carboxylic acid···pyridine hydrogen bond and the chain hydrogen-bond motif formed between the amide and hydroxyl groups, which is the same hydrogen-bond motif observed in form **I**. Exceptions to this arose when the carboxylic acid coformer had additional hydrogen bond donors (the hydroxybenzoic acids), which caused the overall hydrogen-bonding patterns to deviate from the expected hydrogen-bonding motifs. Packing of the structures featured either a zigzag or a layered formation, which indicates a greater degree of predicting the supramolecular assimilation. Most cocrystals did not feature any additional thermal events in their DSC curves. The derivatization of **inh** with diacetone alcohol made the cocrystals of **iz4h4m2p** more predictable than the cocrystals formed with **inh**. This could potentially prove useful in the design and synthesis of new FDC drugs. As such it would prove useful to evaluate the biological activity of **iz4h4m2p** and its cocrystals with GRAS compounds, as well as stability studies in the presence of these other drugs.

Acknowledgements

We would like to acknowledge and thank the DSI/NRF Centre of Excellence in Strong Materials as well as the NRF for funding the Bruker D2 Phaser diffractometer. We would also like to thank Professor Manuel Fernandes for his assistance with the solution of the **iz4h4m2p** + **4hba** crystal structure.

References

Aitipamula, S., Banerjee, R., Bansal, A. K., Biradha, K., Cheney, M. L., Choudhury, A. R., Desiraju, G. R., Dikundwar, A. G., Dubey, R., Duggirala, N., Ghogale, P. P., Ghosh, S., Goswami, P. K., Goud, N. R., Jetti, R. R. K. R., Karpinski, P., Kaushik, P., Kumar, D., Kumar, V., Moulton, B., Mukherjee, A., Mukherjee, G., Myerson, A. S., Puri, V., Ramanan, A., Rajamannar, T., Reddy, C. M., Rodriguez-hornedo, N., Rogers, R. D., Row, T. N. G., Sanphui, P., Shan, N., Shete, G., Singh, A., Sun, C. C., Swift, J. A., Thaimattam, R., Thakur, T. S., Thaper, R. K., Thomas, S. P., Tothadi, S., Vangala, V. R., Variankaval, N., Vishweshwar, P., Weyna, D. R. & Zaworotko, M. J. (2012). *Cryst. Growth Des.* **12**, 2147–2152.
Bhutani, H., Mariappan, T. T. & Singh, S. (2004). *Drug Dev. Ind. Pharm.* **30**, 667–672.
Blagden, N., de Matas, M., Gavan, P. T. & York, P. (2007). *Adv. Drug Deliv. Rev.* **59**, 617–630.
Boles, J. E., Ellaby, R. J., Shepherd, H. J. & Hiscock, J. R. (2021). *RSC Adv.* **11**, 9550–9556.
Bruker (2012). *SAINT*+ (version 6.02), *SAINT* (version 8.40B) and *XREP*. Bruker AXS Inc., Madison, Wisconsin, USA.
Bučar, D. K., Day, G. M., Halasz, I., Zhang, G. G. Z., Sander, J. R. G., Reid, D. G., MacGillivray, L. R., Duer, M. J. & Jones, W. (2013). *Chem. Sci.* **4**, 4417–4425.
Diniz, L. F., Souza, M. S., Carvalho, P. S., da Silva, C. C. P., D'Vries, R. F. & Ellena, J. (2018). *J. Mol. Struct.* **1153**, 58–68.
Dolomanov, O. V., Bourhis, L. J., Gildea, R. J., Howard, J. A. K. & Puschmann, H. (2009). *J. Appl. Cryst.* **42**, 339–341.
Etter, M. C., MacDonald, J. C. & Bernstein, J. (1990). *Acta Cryst.* B**46**, 256–262.
Faria, C. F. de, Moreira, T., Lopes, P., Costa, H., Krewall, J. R., Barton, C. M., Santos, S., Goodwin, D., Machado, D., Viveiros, M., Machuqueiro, M. & Martins, F. (2021). *Biomed. Pharmacother.* **144**, 112362.
Farrugia, L. J. (1999). *J. Appl. Cryst.* **32**, 837–838.
Farrugia, L. J. (2012). *J. Appl. Cryst.* **45**, 849–854.
Ganie, A. A., Marimuthu, R., Islam, S. T., Narang, S. & Dar, A. A. (2022). *J. Solid State Chem.* **307**, 122762.
Groom, C. R., Bruno, I. J., Lightfoot, M. P. & Ward, S. C. (2016). *Acta Cryst.* B**72**, 171–179.
Grothe, E., Meekes, H., Vlieg, E., ter Horst, J. H. & de Gelder, R. (2016). *Cryst. Growth Des.* **16**, 3237–3243.
Hearn, M. J. & Cynamon, M. H. (2004). *J. Antimicrob. Chemother.* **53**, 185–191.
Iseman, M. D. (2002). *Eur. Respir. J. Suppl.* **20**, 87S–94S.
Krause, L., Herbst-Irmer, R., Sheldrick, G. M. & Stalke, D. (2015). *J. Appl. Cryst.* **48**, 3–10.
Lemmerer, A. (2012). *CrystEngComm*, **14**, 2465–2478.

Lemmerer, A., Bernstein, J. & Kahlenberg, V. (2011). *CrystEngComm*, **13**, 5692–5708.

Macrae, C. F., Sovago, I., Cottrell, S. J., Galek, P. T. A., McCabe, P., Pidcock, E., Platings, M., Shields, G. P., Stevens, J. S., Towler, M. & Wood, P. A. (2020). *J. Appl. Cryst.* **53**, 226–235.

Madeley, L. G., Levendis, D. C. & Lemmerer, A. (2019). *Acta Cryst.* C**75**, 200–207.

Oruganti, M., Khade, P., Das, U. K. & Trivedi, D. R. (2016). *RSC Adv.* **6**, 15868–15876.

Sarcevica, I., Orola, L., Veidis, M. V. & Belyakov, S. (2014). *Acta Cryst.* C**70**, 392–395.

Sarcevica, I., Orola, L., Veidis, M. V., Podjava, A. & Belyakov, S. (2013). *Cryst. Growth Des.* **13**, 1082–1090.

Scheepers, M. C., Fernandes, M. A. & Lemmerer, A. (2022). *RSC Adv.* **12**, 11658–11664.

Setshedi, I. B. & Smith, M. G. (2021). *Z. Kristallogr. New Cryst. Struct.* **236**, 1093–1095.

Shattock, T. R., Arora, K. K., Vishweshwar, P. & Zaworotko, M. J. (2008). *Cryst. Growth Des.* **8**, 4533–4545.

Sheldrick, G. M. (2015). *Acta Cryst.* A**71**, 3–8.

Sheldrick, G. M. (2015). *Acta Cryst.* C**71**, 3–9.

Spek, A. L. (2020). *Acta Cryst.* E**76**, 1–11.

Surov, A. O., Voronin, A. P., Simagina, A. A., Churakov, A. V. & Perlovich, G. L. (2016). *Cryst. Growth Des.* **16**, 2605–2617.

Trask, A. V. (2007). *Mol. Pharm.* **4**, 301–309.

Wang, S. Y., Song, X. M. & Duan, L. X. (2008). *Acta Cryst.* E**64**, o1880.

Chapter 8 Conclusions

In this work the crystal engineering of a series of sulfa drugs, **dnba** and an isoniazid derivative was explored. Here a number of new cocrystal and molecular salts were synthesized and characterized. Each of these new solid forms showcase different intermolecular interactions compared with the original starting material.

For the sulfa drugs, **sp**, **st**, **sm** and **sz** a number of new molecular salts and cocrystals were synthesized and characterized. The co-formers used were mostly benzoic acid derivatives or pyridine derivatives. For **sz** benzoic acids proved to be the most successful co-former to use. In each case the carboxylic acid interacted with **sz** to form a $R_2^2(8)$ ring based hydrogen bond motif. The only molecular salts formed from this study that contained **sz** was **sz** + **2c4n** and **sz** + **3hba**, in which a proton was transferred from the carboxylate to the sulfonamide and pyrimidine ring. For the case of **sz** and a hydroxybenzoic acid (**2hba**, **3hba** and **4hba**), **sz** + **2hba** and **sz** + **3hba** were isostructural, with **sz** forming the sulfonamide tautomer, while **sz** + **4hba** differed significantly by forming the sulfonimide tautomer (the only case from this work) and having a different packing altogether. In comparison, **sp**, **st** and **sm** formed cocrystals and molecular salts more easily with pyridines than with carboxylic acids. **2ap** and its derivatives formed cocrystals easily with **st** and **sp**, forming a $R_2^2(8)$ ring hydrogen bond motif. In addition **dnba** formed a molecular salt and a cocrystal with **st** and **sm** respectively. In these cases, **dnba** did not interact with the sulfonamide and N-containing hetrerocycle, but interacted with the amine group of the aniline ring instead. **sm** did not form any cocrystals or molecular salts with **2ap** or its derivatives. Instead it formed cocrystals with **3cnp** and **4cnp** and a molecular salt with **4dmap**, which interacted with the sulfonamide group. Overall there are both similarities and differences between each of the sulfa drugs investigated. Both carboxylic acids and pyridines produced new solid forms of the sulfa drugs but the sulfa drugs tended to have a clear preference of one over the other. The chance of forming cocrystals and/or molecular salts

containing sulfa drugs proved to be elusive, and it may be necessary to use more exotic crystalizing techniques to obtain cocrystals and/or molecular salts with specific coformers.

A diverse range of new multi-component crystals containing **dnba** was obtained. This included API's such as **fa** and **thp**, in addition to the title compounds. From this work it has been shown that **dnba** is an excellent coformer, not only being a strong hydrogen bond donor, but also good at forming meaningful weaker interactions, such as C−H···π bonding, π-hole, and π···π stacking. Hirshfeld surfaces showed that these weaker interactions contributed significantly to the overall packing of these multi-component crystals. An examination of the CSD highlighted some interesting trends concerning **dnba**, such as forming a layered type packing or the tendency of the nitro group to not form strong hydrogen bonds. Overall **dnba** remains a good cocrystalizing agent.

Finally **iz4h4m2p** was determined to be polymorphic, with two polymorphic forms: form I (the metastable form) and form **II** (the most stable form). The major difference between the two is in the hydrogen bonding motifs observed: form **I** favoured a chain hydrogen bond motif formed between the oxygen of the amide and hydroxyl group of neighbouring **iz4h4m2p** molecules while form **II** favoured a ring based where the hydroxyl group formed a hydrogen bond to the pyridine ring which resulted in the formation of dimers. The torsional angle between the pyridine ring and amide was significantly different between the two, which resulted in a conformational difference between the two. From the Intramolecular DFT calculations it was found the conformation of **iz4h4m2p** in form **I** was more energetically favoured over form **II** by 3.1 kJ mol^{-1}. However, *PIXEL* calculations showed that the intermolecular energy of form **II** was much lower than form **I** by 19.4 kJ mol^{-1}, which explains why we could not obtain form **I** again. Form **I** shows conversion to form **II** upon heating at around 132.29 °C before melting at 142.6 °C. Form **II** showed no other phase transition other than melting. **iz4h4m2p** formed

cocrystals with carboxylic acids. Two major hydrogen bond motifs were observed: the carboxylic acid···pyridine hydrogen bond and the chain hydrogen bond motif formed between the hydroxyl group to the oxygen of the amide (reminiscent of the hydrogen bonding of form **I**). The only exception to this were the cases where an additional hydrogen bond donor was present of the conformer. The majority of the structures packed using either a zig-zag type structure or a layered structure. These cocrystals did not show any other phase transitions other than melting. These cocrystals show that derivatising the hydrazine group of **inh** with a diacetone alcohol can produce a molecule with a predictable and controllable structural landscape.

In future it would be useful to see if more exotic crystallization techniques can be used to obtain either a cocrystal or molecular salt for combinations that "failed." It may also prove useful to investigate the properties of the successful cocrystals and molecular salts obtained. Overall the crystal engineering of the above compounds yielded useful insight into their respective structural landscapes. These cases prove that the formation of certain cocrystals and molecular salts or the formation of polymorphic forms are non-trivial, and that a great deal of crystal engineering still needs to be investigated.

References

(1) Unit Cell https://en.wikipedia.org/wiki/Unit_cell (accessed Jun 28, 2022).

(2) Mighell, A. D.; Himes, V. L.; Rodgers, J. R. Revised Space-group Frequencies for Organic Compounds. *Acta Crystallogr. Sect. A* **1983**, *A39*, 737–740. https://doi.org/10.1107/S010876738500040X.

(3) De Yoreo, J. J. Principles of Crystal Nucleation and Growth. *Rev. Mineral. Geochemistry* **2003**, *54* (1), 57–93. https://doi.org/10.2113/0540057.

(4) Gebauer, D.; Kellermeier, M.; Gale, J. D.; Bergström, L.; Cölfen, H. Pre-Nucleation Clusters as Solute Precursors in Crystallisation. *Chem. Soc. Rev.* **2014**, *43* (7), 2348–2371. https://doi.org/10.1039/c3cs60451a.

(5) Desiraju, G. R. Crystal Engineering: A Holistic View. *Angew. Chemie - Int. Ed.* **2007**, *46* (44), 8342–8356. https://doi.org/10.1002/anie.200700534.

(6) Watson, J. D.; Crick, F. H. The Structure of DNA. *Cold Spring Harb Symp Quant Biol* **1953**, *18*, 123–131. https://doi.org/10.1101/SQB.1953.018.01.020.

(7) Arunan, E.; Desiraju, G. R.; Klein, R. A.; Sadlej, J.; Scheiner, S.; Alkorta, I.; Clary, D. C.; Crabtree, R. H.; Dannenberg, J. J.; Hobza, P.; Kjaergaard, H. G.; Legon, A. C.; Mennucci, B.; Nesbitt, D. J. Defining the Hydrogen Bond: An Account (IUPAC Technical Report). *Pure Appl. Chem.* **2011**, *83* (8), 1619–1636. https://doi.org/10.1351/PAC-REP-10-01-01.

(8) Steiner, T. The Hydrogen Bond in the Solid State. *Angew. Chemie Int. Ed.* **2002**, *41*, 48–76.

(9) Aakeröy, C. B.; Seddon, K. R. The Hydrogen Bond and Crystal Engineering. *Chem. Soc. Rev.* **1993**, *22* (6), 397–407. https://doi.org/10.1039/CS9932200397.

(10) Fuller, W. Hydrogen Bond Lengths and Angles Observed in Crystals. *J. Phys. Chem.* **1959**, *63* (10), 1705–1717.

(11) Etter, M. C.; MacDonald, J. C.; Bernstein, J. Graph-set Analysis of Hydrogen-bond Patterns in Organic Crystals. *Acta Crystallogr. Sect. B* **1990**, *46* (2), 256–262. https://doi.org/10.1107/S0108768189012929.

(12) Martinez, C. R.; Iverson, B. L. Rethinking the Term "Pi-Stacking." *Chem. Sci.* **2012**, *3* (7), 2191–2201. https://doi.org/10.1039/c2sc20045g.

(13) Hunter, C. A.; Sanders, J. K. M. The Nature of Pi-Pi Interactions. *J. Am. Chem. Soc.* **1990**, *112* (14), 5525–5534. https://doi.org/10.1021/ja00170a016.

(14) Williams, J. H.; Cockcroft, J. K.; Fitch, A. N. Structure of the Lowest Temperature Phase of the Solid Benzene-Hexafluorobenzene Adduct. *Angew. Chemie - Int. Ed.* **1992**, *31* (12), 1655–1657.

(15) Host-Guest Chemistry and π-π stacking interactions https://chem.libretexts.org/Bookshelves/Inorganic_Chemistry/Map%3A_Inorganic_Chemistry_(Miessler_Fischer_Tarr)/06%3A_Acid-Base_and_Donor-Acceptor_Chemistry/6.05%3A_Intermolecular_Forces/6.5.01%3A_Host-Guest_Chemistry_and_-_stacking_interactions (accessed Jun 28, 2022).

(16) Lu, J.; Rohani, S. Polymorphism and Crystallization of Active Pharmaceutical Ingredients (APIs). *Curr. Med. Chem.* **2009**, *16* (7), 884–905. https://doi.org/10.2174/092986709787549299.

(17) Groom, C. R.; Bruno, I. J.; Lightfoot, M. P.; Ward, S. C. The Cambridge Structural Database.

Acta Crystallogr. Sect. B **2016**, *72* (2), 171–179. https://doi.org/10.1107/S2052520616003954.

(18) Vishweshwar, P.; McMahon, J. A.; Peterson, M. L.; Hickey, M. B.; Shattock, T. R.; Zaworotko, M. J. Crystal Engineering of Pharmaceutical Co-Crystals from Polymorphic Active Pharmaceutical Ingredients. *Chem. Commun.* **2005**, *10* (36), 4601–4603. https://doi.org/10.1039/b501304f.

(19) Bernstein, J. Crystal Growth, Polymorphism and Structure-Property Relationships in Organic Crystals. *J. Phys. D. Appl. Phys.* **1993**, *26* (8), B66–B76. https://doi.org/10.1088/0022-3727/26/8B/010.

(20) Harris, R. K. NMR Studies of Organic Polymorphs & Solvates. *Analyst* **2006**, *131* (3), 351–373. https://doi.org/10.1039/b516057j.

(21) Bernstein, J. Polymorphism - A Perspective. *Cryst. Growth Des.* **2011**, *11* (3), 632–650. https://doi.org/10.1021/cg1013335.

(22) Lévesque, A.; Maris, T.; Wuest, J. D. ROY Reclaims Its Crown: New Ways to Increase Polymorphic Diversity. *J. Am. Chem. Soc.* **2020**, *142* (27), 11873–11883. https://doi.org/10.1021/jacs.0c04434.

(23) Zhang, K.; Fellah, N.; Shtukenberg, A. G.; Fu, X.; Hu, C.; Ward, M. D. Discovery of New Polymorphs of the Tuberculosis Drug Isoniazid. *CrystEngComm* **2020**, *22* (16), 2705–2708. https://doi.org/10.1039/d0ce00440e.

(24) Varughese, S.; Kiran, M. S. R. N.; Solanko, K. A.; Bond, A. D.; Ramamurty, U.; Desiraju, G. R. Interaction Anisotropy and Shear Instability of Aspirin Polymorphs Established by Nanoindentation. *Chem. Sci.* **2011**, *2* (11), 2236–2242. https://doi.org/10.1039/c1sc00430a.

(25) Shtukenberg, A. G.; Hu, C. T.; Zhu, Q.; Schmidt, M. U.; Xu, W.; Tan, M.; Kahr, B. The Third Ambient Aspirin Polymorph. *Cryst. Growth Des.* **2017**, *17* (6), 3562–3566. https://doi.org/10.1021/acs.cgd.7b00673.

(26) Corpinot, M. K.; Bučar, D. K. A Practical Guide to the Design of Molecular Crystals. *Cryst. Growth Des.* **2019**, *19* (2), 1426–1453. https://doi.org/10.1021/acs.cgd.8b00972.

(27) Brittain, H. G. Polymorphism and Solvatomorphism 2010. *J. Pharm. Sci.* **2011**, *101* (2), 464–484. https://doi.org/10.1002/jps.

(28) Bauer, J.; Spanton, S.; Henry, R.; Quick, J.; Dziki, W.; Porter, W.; Morris, J. Ritonavir: An Extraordinary Example of Conformational Polymorphism. *Pharm. Res.* **2001**, *18* (6), 859–866. https://doi.org/10.1023/A:1011052932607.

(29) Haleblian, J.; McCrone, W. Pharmaceutical Applications of Polymorphism. *J. Pharm. Sci.* **1969**, *58* (8), 911–929. https://doi.org/10.1002/jps.2600580802.

(30) Burger, A.; Ramberfer, R. On the Polymorphism of Pharmaceuticals and Other Molecular Crystals. I Theory of Thermodynamic Rules. *Mikrochim. Acta* **1979**, *2*, 259–271.

(31) Bernstein, J. *Polymorphism in Molecular Crystals*, 2nd Editio.; International Union of Crystal; Oxford University Press: Oxford, 2020.

(32) Bs, S. Pharmaceutical Co-Crystals - a Review. *Ars Pharm.* **2009**, *50* (Figure 1), 99–117.

(33) Rossini, E.; Netz, R. R.; Knapp, E. W. Computing PKa Values in Different Solvents by Electrostatic Transformation. *J. Chem. Theory Comput.* **2016**, *12* (7), 3360–3369. https://doi.org/10.1021/acs.jctc.6b00446.

(34) Cruz-Cabeza, A. J. Acid-Base Crystalline Complexes and the PKa Rule. *CrystEngComm* **2012**, *14* (20), 6362–6365. https://doi.org/10.1039/c2ce26055g.

(35) Lemmerer, A.; Govindraju, S.; Johnston, M.; Motloung, X.; Savig, K. L. Co-Crystals and Molecular Salts of Carboxylic Acid/Pyridine Complexes: Can Calculated PKa's Predict Proton Transfer? A Case Study of Nine Complexes. *CrystEngComm* **2015**, *17* (19), 3591–3595. https://doi.org/10.1039/c5ce00102a.

(36) Aitpamula, S.; Zaigun, Y.; Chow, P. S.; Tan, R. B. H. Pharmaceutical Co-Crystals - Molecular Design and Process Development. In *Co-crystals Preparation, Characterization and Applications*; Aakeröy, C. B., Sinha, A. S., Eds.; Cambridge, 2018; pp 194–230.

(37) Schultheiss, N.; Newman, A. Pharmaceutical Cocrystals and Their Physicochemical Properties. *Cryst. Growth &Design* **2009**, *9* (6), 2950–2967.

(38) Nechipadappu, S. K.; Tekuri, V.; Trivedi, D. R. Pharmaceutical Co-Crystal of Flufenamic Acid: Synthesis and Characterization of Two Novel Drug-Drug Co-Crystal. *J. Pharm. Sci.* **2017**, *106* (5), 1384–1390. https://doi.org/10.1016/j.xphs.2017.01.033.

(39) Co-trimoxazole Monograph for Professionals - Drugs.com https://www.drugs.com/monograph/co-trimoxazole.html (accessed Mar 24, 2021).

(40) Blagden, N.; Berry, D. J.; Parkin, A.; Javed, H.; Ibrahim, A.; Gavan, P. T.; De Matos, L. L.; Seaton, C. C. Current Directions in Co-Crystal Growth. *New J. Chem.* **2008**, *32* (10), 1659–1672. https://doi.org/10.1039/b803866j.

(41) Desiraju, G. R. Supramolecular Synthons in Crystal Engineering—A New Organic Synthesis. *Angew. Chemie Int. Ed. English* **1995**, *34* (21), 2311–2327. https://doi.org/10.1002/anie.199523111.

(42) Shattock, T. R.; Arora, K. K.; Vishweshwar, P.; Zaworotko, M. J. Hierarchy of Supramolecular Synthons: Persistent Carboxylic Acid···pyridine Hydrogen Bonds in Cocrystals That Also Contain a Hydroxyl Moiety. *Cryst. Growth Des.* **2008**, *8* (12), 4533–4545. https://doi.org/10.1021/cg800565a.

(43) Gelbrich, T.; Threlfall, T. L.; Bingham, A. L.; Hursthouse, M. B. Polymorph VI of Sulfapyridine: Inter-Penetrating Two- and Three-Dimensional Hydrogen-Bonded Nets Formed from Two Tautomeric Forms. *Acta Crystallogr. Sect. C Cryst. Struct. Commun.* **2007**, *63* (6), 323–326. https://doi.org/10.1107/S0108270107017817.

(44) Lu, J.; Cruz-Cabeza, A. J.; Rohani, S.; Jennings, M. C. A 2:1 Sulfamethazine-Theophylline Cocrystal Exhibiting Two Tautomers of Sulfamethazine. *Acta Crystallogr. Sect. C Cryst. Struct. Commun.* **2011**, *67* (8), 306–309. https://doi.org/10.1107/S0108270111024280.

(45) Velraj, G.; Soundharam, S. Structure, Vibrational, Electronic, NBO and NMR Analyses of 4-Amino-N-[2-Pyridinyl] Benzene Sulfonamide (Sulfapyridine) by Experimental and Theoretical Approach. *J. Mol. Struct.* **2014**, *1074*, 475–486. https://doi.org/10.1016/j.molstruc.2014.06.003.

(46) Bernstein, J. Polymorph IV of 4-Amino-N-2-Pyridinylbenzenesulfonamide (Sulfapyridine). *Acta Crystallogr. C.* **1988**, *44 (Pt 5)* (1972), 900–902. https://doi.org/10.1107/s0108270188001180.

(47) Pratt, J.; Hutchinson, J.; Klein Stevens, C. L. Sulfapyridine (Polymorph III), Sulfapyridine Dioxane Solvate, Sulfapyridine Tetra-Hydro-Furan Solvate and Sulfapyri-Dine Piperi-Dine Solvate, All at 173 K. *Acta Crystallogr. Sect. C Cryst. Struct. Commun.* **2011**, *67* (12), 487–491. https://doi.org/10.1107/S0108270111041825.

(48) Bar, I.; Bernstein, J. Conformational Polymorphism VI: The Crystal and Molecular Structures of Form II, Form III, and Form V of 4-amino-N-2-pyridinylbenzenesulfonamide (Sulfapyridine). *J. Pharm. Sci.* **1985**, *74* (3), 255–263. https://doi.org/10.1002/jps.2600740307.

(49) Sugawara, T.; Takasu, I. Tautomerism in the Solid State. *Adv. Phys. Org. Chem.* **1999**, *32* (C),

219–265. https://doi.org/10.1016/S0065-3160(08)60008-8.

(50) McKinnon, J. J.; Spackman, M. A.; Mitchell, A. S. *Novel Tools for Visualizing and Exploring Intermolecular Interactions in Molecular Crystals*; International Union of Crystallography, 2004; Vol. 60. https://doi.org/10.1107/S0108768104020300.

(51) Shambaugh, G. E. History of Sulfonamides. *Arch Otolaryngol.* **1966**, *83* (1), 27–28.

(52) Scholar, E. Sulfanilamide. In *xPharm: The Comprehensive Pharmacology Reference*; Enna, S. J., Bylund, D. B., Eds.; Elsevier: New York, 2007; pp 1–5. https://doi.org/https://doi.org/10.1016/B978-008055232-3.62694-7.

(53) Whitby, L. E. H. Chemotherapy of Pneumococcal and Other Infections with 2-(p-Aminobenzenesulphonamidopyridine). *Lancet* **1938**, *231* (5987), 1210–1212. https://doi.org/10.1016/S0140-6736(46)91304-9.

(54) Christensen, S. B. *Drugs That Changed Society: History and Current Status of the Early Antibiotics: Salvarsan, Sulfonamides, and β-Lactams*; 2021; Vol. 26. https://doi.org/10.3390/molecules26196057.

(55) Basak, A. K.; Chaudhuri, S.; Mazumdar, S. K. Structure of 4-Amino-N-2-Pyridylbenzenesuphonamide (Sulphapyridine), C11H11N3O2S. *Acta Crystallogr. Sect. C Cryst. Struct. Commun.* **1984**, *40* (11), 1848–1851. https://doi.org/10.1107/s0108270184009811.

(56) Castle, R. N.; Witt, N. F. The Polymorphism of Sulfapyridine. *J. Am. Chem. Soc.* **1946**, *68* (1), 64–66. https://doi.org/10.1021/ja01205a020.

(57) Adsmond, D. A.; Grant, D. J. W. Hydrogen Bonding in Sulfonamides. *J. Pharm. Sci.* **2001**, *90* (12), 2058–2077. https://doi.org/10.1002/jps.1157.

(58) Coles, S. J.; Hursthouse, M. B.; Mayer, T. A.; Threlfall, T. L. 4-Amino-N-Pyridin-2-Yl-Benzenesulfonamide with Formic Acid Butyl Ester. February 2000. https://doi.org/doi:10.5258/ecrystals/196.

(59) Ruiz-Palomero, C.; Kennedy, S. R.; Soriano, M. L.; Jones, C. D.; Valcárcel, M.; Steed, J. W. Pharmaceutical Crystallization with Nanocellulose Organogels. *Chem. Commun.* **2016**, *52* (50), 7782–7785. https://doi.org/10.1039/c6cc03088b.

(60) Shunje, K. N. Multicomponent Crystals of Sulfapyridine and Sulfadiazine, Cape Peninsula University of Technology, 2017. https://doi.org/10.1107/s2053273318089994.

(61) Swann, J. P. The 1941 Sulfathiazole Disaster and the Birth of Good Manufacturing Practices. *PDA J. Pharm. Sci. Technol.* **1999**, *53* (3), 148–153.

(62) Parmar, M. M.; Khan, O.; Seton, L.; Ford, J. L. Polymorph Selection with Morphology Control Using Solvents. *Cryst. Growth Des.* **2007**, *7* (9), 1635–1642. https://doi.org/10.1021/cg070074n.

(63) Bingham, A. L.; Hughes, D. S.; Hursthouse, M. B.; Lancaster, R. W.; Tavener, S.; Threlfall, T. L. Over One Hundred Solvates of Sulfathiazole. *Chem. Commun.* **2001**, No. 7, 603–604. https://doi.org/10.1039/b009540k.

(64) Gelbrich, T.; Hughes, D. S.; Hursthouse, M. B.; Threlfall, T. L. Packing Similarity in Polymorphs of Sulfathiazole. *CrystEngComm* **2008**, *10* (10), 1328–1334. https://doi.org/10.1039/b807898j.

(65) McArdle, P.; Hu, Y.; Lyons, A.; Dark, R. Predicting and Understanding Crystal Morphology: The Morphology of Benzoic Acid and the Polymorphs of Sulfathiazole. *CrystEngComm* **2010**, *12* (10), 3119–3125. https://doi.org/10.1039/c001071e.

(66) Shefter, E.; Sackman, P. Structural Studies on Molecular Complexes V: Crystal Structures of Sulfathiazole—Sulfanilamide and Sulfathiazole—Theophylline Complexes. *J. Pharm. Sci.* **1971**, *60* (2), 282–286. https://doi.org/10.1002/jps.2600600228.

(67) Oruganti, M.; Trivedi, D. R. 4-Nitrobenzoic Acid-Sulfathiazole (1/1). *Acta Crystallogr. Sect. E Struct. Reports Online* **2014**, *70* (1). https://doi.org/10.1107/S1600536813034004.

(68) Samanta, R.; Kanaujia, S.; Reddy, C. M. New Co-Crystal and Salt Form of Sulfathiazole with Carboxylic Acid and Amide. *J. Chem. Sci.* **2014**, *126* (5), 1363–1367. https://doi.org/10.1007/s12039-014-0698-5.

(69) Hu, Y.; Gniado, K.; Erxleben, A.; McArdle, P. Mechanochemical Reaction of Sulfathiazole with Carboxylic Acids: Formation of a Cocrystal, a Salt, and Coamorphous Solids. *Cryst. Growth Des.* **2014**, *14* (2), 803–813. https://doi.org/10.1021/cg401673z.

(70) Deo, N.; Tiwari, R. K.; Singh, T. P. Crystallization and X-Ray Crystal Data of Sulfonamides. *J. Sci. Res* **1980**, *2* (2), 137.

(71) Maury, L.; Rambaud, J.; Pauvert, B.; Lasserre, Y.; Berge, G.; Audran, M. Étude Physico-Chimique, Spectres De Vibration Et Structure Du Sulfaméthoxazole. *Can. J. Chem.* **1985**, *63* (11), 3012–3018. https://doi.org/10.1139/v85-500.

(72) Price, C. P.; Grzesiak, A. L.; Matzger, A. J. Crystalline Polymorph Selection and Discovery with Polymer Heteronuclei. *J. Am. Chem. Soc.* **2005**, *127* (15), 5512–5517. https://doi.org/10.1021/ja042561m.

(73) Rambaud, J.; Roques, R.; Alberola, S.; Sabon, F. Structure Cristalline et Moleculaire Du Sulfabenzamide. *Bull. Soc. Chim. Fr.* **1980**, *1*, 51–55.

(74) Giuseppetti, G.; Tadini, C. Structure of 2,4-Diamino-5-(3,4,5-Trimethoxybenzyl)Pyrimidinium Benzoate (Trimethoprim Monobenzoate), C 14H19N40 3"C7H50 2. *Acta Crystallogr. Sect. C Cryst. Struct. Commun.* **1984**, *C40*, 650–653.

(75) Nakai, H.; Takasuka, M.; Shiro, M. X-Ray and Infrared Spectral Studies of the Ionic Structure of Trimethoprim - Sulfamethoxazole 1 : 1 Molecular Complex. *J. Chem. Soc. Perkin Trans. 2* **1984**, No. 9, 1459–1464. https://doi.org/10.1039/p29840001459.

(76) Alsubaie, M.; Aljohani, M.; Erxleben, A.; McArdle, P. Cocrystal Forms of the BCS Class IV Drug Sulfamethoxazole. *Cryst. Growth Des.* **2018**, *18* (7), 3902–3912. https://doi.org/10.1021/acs.cgd.8b00216.

(77) Lynch, D. E.; Sandhu, P.; Parsons, S. 1 : 1 Molecular Complexes of 4-Amino-N-(4,6-Dimethylpyrimidin-2-Yl)Benzene-Sulfonamide (Sulfamethazine) with Indole-2-Carboxylic Acid and 2,4-Dinitrobenzoic Acid. *Aust. J. Chem.* **2000**, *53* (5), 383–387. https://doi.org/10.1071/ch00021.

(78) Wang, R.; Yuan, P.; Yang, D.; Zhang, B.; Zhang, L.; Lu, Y.; Du, G. Structural Features and Interactions of New Sulfamethazine Salt and Cocrystal. *J. Mol. Struct.* **2021**, *1229*, 129596. https://doi.org/10.1016/j.molstruc.2020.129596.

(79) Maury, L.; Rambaud, J.; Pauvert, B.; Lasserre, Y.; Bergé, G.; Audran, M. Physicochemical and Structural Study of Sulfamethazine. *J. Pharm. Sci.* **1985**, *74* (4), 422–426. https://doi.org/10.1002/jps.2600740411.

(80) Perumalla, S. R.; Wang, C.; Guo, Y.; Shi, L.; Sun, C. C. Robust Bulk Preparation and Characterization of Sulfamethazine and Saccharine Salt and Cocrystal Polymorphs. *CrystEngComm* **2019**, *21* (13), 2089–2096. https://doi.org/10.1039/c8ce01076e.

(81) Smith, G.; Wermuth, U. D. 4-Amino-N-(4,6-Dimethylpyrimidin-2-Yl)Benzenesulfonamide-4-Nitrobenzoic Acid (1/1). *Acta Crystallogr. Sect. E Struct. Reports Online* **2012**, *68* (6).

https://doi.org/10.1107/S1600536812019563.

(82) Ghosh, S.; Bag, P. P.; Reddy, C. M. Co-Crystals of Sulfamethazine with Some Carboxylic Acids and Amides: Co-Former Assisted Tautomerism in an Active Pharmaceutical Ingredient and Hydrogen Bond Competition Study. *Cryst. Growth Des.* **2011**, *11* (8), 3489–3503. https://doi.org/10.1021/cg200334m.

(83) Kumar, V.; Thaimattam, R.; Dutta, S.; Munshi, P.; Ramanan, A. Structural Landscape of Multicomponent Solids Based on Sulfa Drugs. *CrystEngComm* **2017**, *19* (21), 2914–2924. https://doi.org/10.1039/c7ce00217c.

(84) Singh, M. P.; Baruah, J. B. Combinations of Tautomeric Forms and Neutral-Cationic Forms in the Cocrystals of Sulfamethazine with Carboxylic Acids. *ACS Omega* **2019**, *4* (7), 11609–11620. https://doi.org/10.1021/acsomega.9b01437.

(85) Iseman, M. D. Tuberculosis Therapy: Past, Present and Future. *Eur. Respir. Journal, Suppl.* **2002**, *20* (36), 87–94. https://doi.org/10.1183/09031936.02.00309102.

(86) Diniz, L. F.; Souza, M. S.; Carvalho, P. S.; da Silva, C. C. P.; D'Vries, R. F.; Ellena, J. Novel Isoniazid Cocrystals with Aromatic Carboxylic Acids: Crystal Engineering, Spectroscopy and Thermochemical Investigations. *J. Mol. Struct.* **2018**, *1153*, 58–68. https://doi.org/10.1016/j.molstruc.2017.09.115.

(87) de Faria, C. F.; Moreira, T.; Lopes, P.; Costa, H.; Krewall, J. R.; Barton, C. M.; Santos, S.; Goodwin, D.; Machado, D.; Viveiros, M.; Machuqueiro, M.; Martins, F. Designing New Antitubercular Isoniazid Derivatives with Improved Reactivity and Membrane Trafficking Abilities. *Biomed. Pharmacother.* **2021**, *144*, 112362. https://doi.org/10.1016/j.biopha.2021.112362.

(88) Jensen, L. H. The Crystal Structure of Isonicotinic Acid Hydrazide. *J. Am. Chem. Soc.* **1954**, *265* (3), 4663–4667. https://doi.org/https://doi.org/10.1021/ja01647a053.

(89) Bhat, T. N.; Singh, T. P.; Vijayan, M. Isonicotinic Acid Hydrazide {--} a Reinvestigation. *Acta Cryst. Sect. B* **1974**, *3* (12), 2921–2922.

(90) Lemmerer, A. Covalent Assistance to Supramolecular Synthesis: Modifying the Drug Functionality of the Antituberculosis API Isoniazid in Situ during Co-Crystallization with GRAS and API Compounds. *CrystEngComm* **2012**, *14* (7), 2465–2478. https://doi.org/10.1039/c1ce06310c.

(91) Rajalakshmi, G.; Hathwar, V. R.; Kumaradhas, P. Topological Analysis of Electron Density and the Electrostatic Properties of Isoniazid: An Experimental and Theoretical Study. *Acta Crystallogr. Sect. B Struct. Sci. Cryst. Eng. Mater.* **2014**, *70* (2), 331–341. https://doi.org/10.1107/S2052520613033209.

(92) Lemmerer, A.; Adsmond, D. A.; Esterhuysen, C.; Bernstein, J. Polymorphic Co-Crystals from Polymorphic Co-Crystal Formers: Competition between Carboxylic Acid···pyridine and Phenol···pyridine Hydrogen Bonds. *Cryst. Growth Des.* **2013**, *13* (9), 3935–3952. https://doi.org/10.1021/cg4006357.

(93) Lemmerer, A.; Bernstein, J.; Kahlenberg, V. Covalent Assistance in Supramolecular Synthesis: In Situ Modification and Masking of the Hydrogen Bonding Functionality of the Supramolecular Reagent Isoniazid in Co-Crystals. *CrystEngComm* **2011**, *13* (19), 5692–5708. https://doi.org/10.1039/c1ce05152k.

(94) Lemmerer, A.; Bernstein, J.; Kahlenberg, V. One-Pot Covalent and Supramolecular Synthesis of Pharmaceutical Co-Crystals Using the API Isoniazid: A Potential Supramolecular Reagent. *CrystEngComm* **2010**, *12* (10), 2856–2864. https://doi.org/10.1039/c000473a.

(95) Hean, D.; Gelbrich, T.; Griesser, U. J.; Michael, J. P.; Lemmerer, A. Structural Insights into

the Hexamorphic System of an Isoniazid Derivative. *CrystEngComm* **2015**, *17* (28), 5143–5153. https://doi.org/10.1039/c5ce00275c.

(96) Sarcevica, I.; Orola, L.; Veidis, M. V.; Podjava, A.; Belyakov, S. Crystal and Molecular Structure and Stability of Isoniazid Cocrystals with Selected Carboxylic Acids. *Cryst. Growth Des.* **2013**, *13* (3), 1082–1090. https://doi.org/10.1021/cg301356h.

(97) Sarcevica, I.; Orola, L.; Veidis, M. V.; Belyakov, S. Cinnamic Acid Hydrogen Bonds to Isoniazid and N'-(Propan-2-Ylidene) Isonicotinohydrazide, an in Situ Reaction Product of Isoniazid and Acetone. *Acta Crystallogr. Sect. C Struct. Chem.* **2014**, *70* (4), 392–395. https://doi.org/10.1107/S2053229614003684.

(98) Mashhadi, S. M. A.; Yufit, D.; Liu, H.; Hodgkinson, P.; Yunus, U. Synthesis and Structural Characterization of Cocrystals of Isoniazid and Cinnamic Acid Derivatives. *J. Mol. Struct.* **2020**, *1219*, 1–8. https://doi.org/10.1016/j.molstruc.2020.128621.

(99) Aitipamula, S.; Wong, A. B. H.; Chow, P. S.; Tan, R. B. H. Novel Solid Forms of the Anti-Tuberculosis Drug, Isoniazid: Ternary and Polymorphic Cocrystals. *CrystEngComm* **2013**, *15* (29), 5877–5887. https://doi.org/10.1039/c3ce40729b.

(100) Sarceviča, I.; Kons, A.; Orola, L. Isoniazid Cocrystallisation with Dicarboxylic Acids: Vapochemical, Mechanochemical and Thermal Methods. *CrystEngComm* **2016**, *18* (9), 1625–1635. https://doi.org/10.1039/c5ce01774b.

(101) Aakeröy, C. B.; Beatty, A. M.; Helfrich, B. A.; Nieuwenhuyzen, M. Do Polymorphic Compounds Make Good Cocrystallizing Agents? A Structural Case Study That Demonstrates the Importance of Synthon Flexibility. *Cryst. Growth Des.* **2003**, *3* (2), 159–165. https://doi.org/10.1021/cg025593z.

(102) Bruker. SAINT+ (Including XPREP). Bruker AXS Inc.: Madison, Wisconsin, USA 2012.

(103) Farrugia, L. J. WinGX Suite for Small-Molecule Single-Crystal Crystallography. *J. Appl. Crystallogr.* **1999**, *32* (4), 837–838. https://doi.org/10.1107/S0021889899006020.

(104) Sheldrick, G. M. SHELXS-97 and SHELXL-97, Program for Crystal Structure Solution and Refinement. University of Gottingen: Gottingen 1997.

(105) Sheldrick, G. M. SHELXT - Integrated Space-Group and Crystal-Structure Determination. *Acta Crystallogr. Sect. A Found. Crystallogr.* **2015**, *71* (1), 3–8. https://doi.org/10.1107/S2053273314026370.

(106) Farrugia, L. J. ORTEP-3 for Windows - A Version of ORTEP-III with a Graphical User Interface (GUI). *J. Appl. Crystallogr.* **1997**, *30* (5), 565. https://doi.org/10.1107/S0021889897003117.

(107) Macrae, C. F.; Edgington, P. R.; McCabe, P.; Pidcock, E.; Shields, G. P.; Taylor, R.; Towler, M.; Van De Streek, J. Mercury: Visualization and Analysis of Crystal Structures. *J. Appl. Crystallogr.* **2006**, *39* (3), 453–457. https://doi.org/10.1107/S002188980600731X.

(108) Spackman, P. R.; Turner, M. J.; McKinnon, J. J.; Wolff, S. K.; Grimwood, D. J.; Jayatilaka, D.; Spackman, M. A. CrystalExplorer: A Program for Hirshfeld Surface Analysis, Visualization and Quantitative Analysis of Molecular Crystals. *J. Appl. Crystallogr.* **2021**, *54*, 1006–1011. https://doi.org/10.1107/S1600576721002910.

Appendix

The appendix is presented as they appear for each of the research articles.

Chapter 3

Synthesis and Characterization of a series of sulfamethazine multi-component crystals with various benzoic acids

Matthew Scheepers and Andreas Lemmerer

Supplementary Information

Powder X-ray Patterns (PXRD)

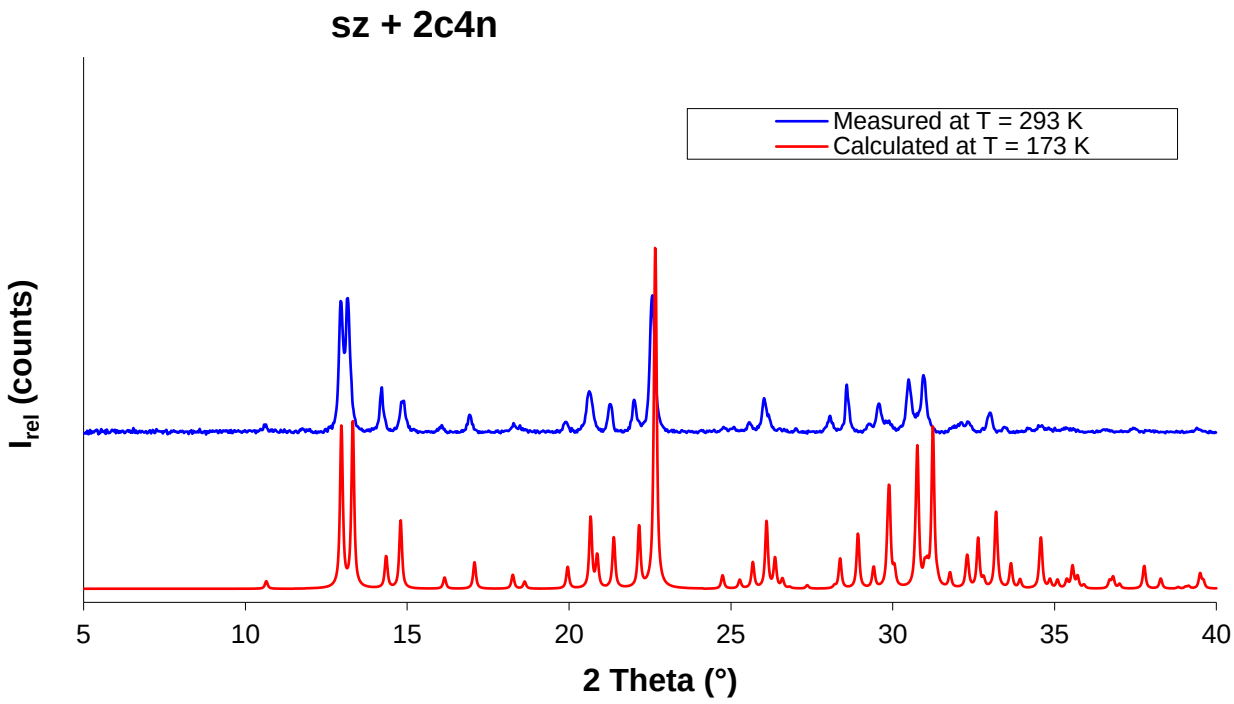


Fig S1 The PXRD pattern for the molecular salt of sz + 2c4n showing the calculated and experimentally obtained patterns.

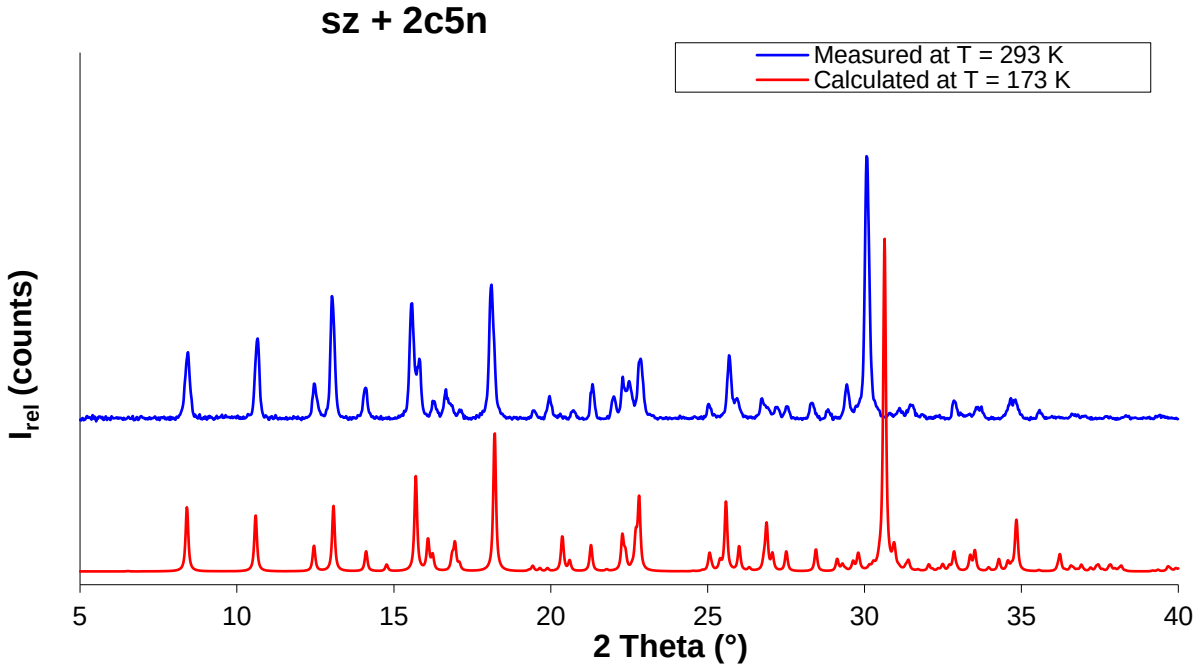


Fig S2 The PXRD pattern for the molecular salt of sz + 2c5n showing the calculated and experimentally obtained patterns.

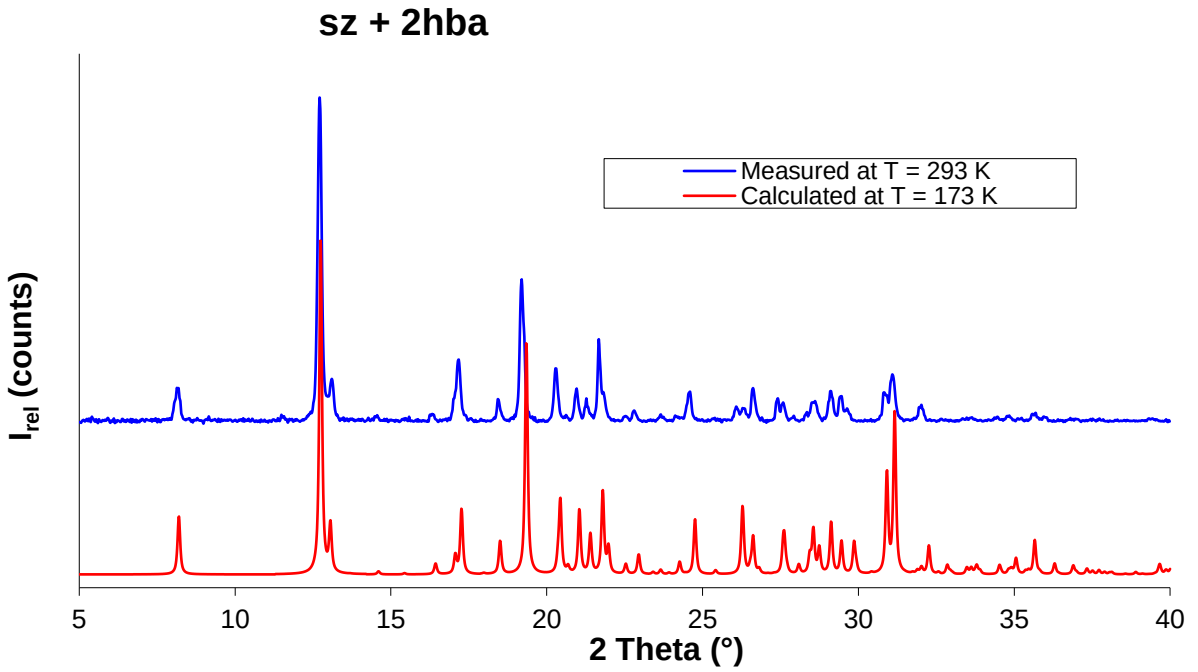


Fig S3 The PXRD pattern for the molecular salt of sz + 2hba showing the calculated and experimentally obtained patterns.

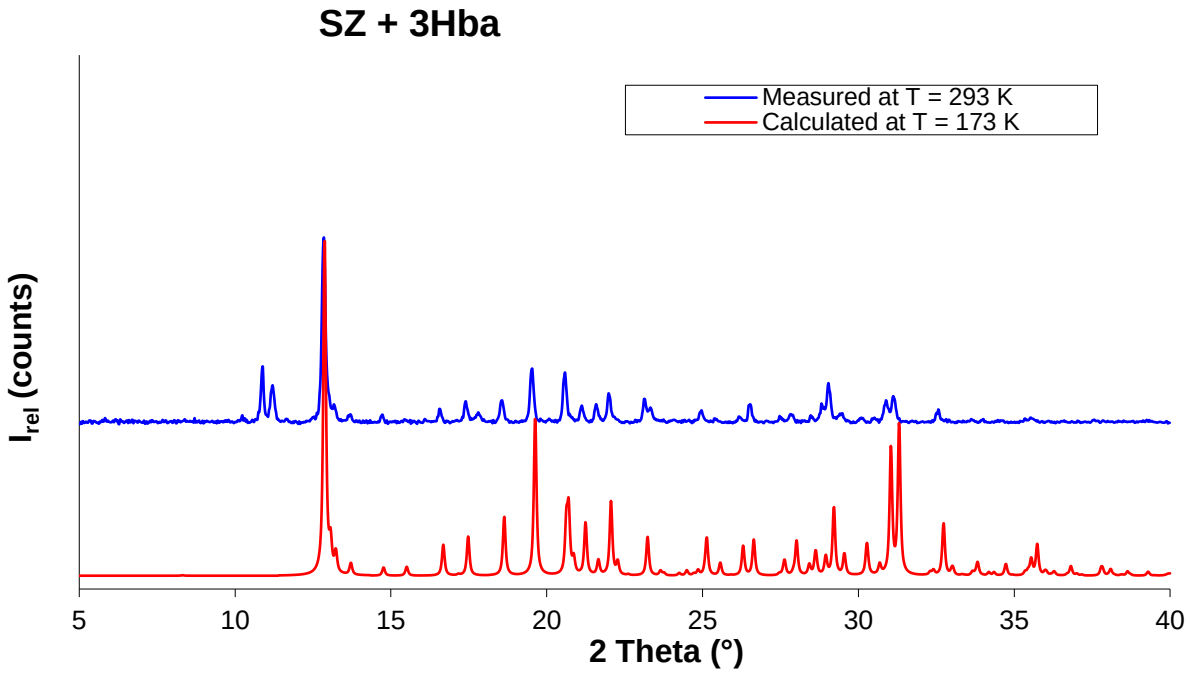


Fig S4 The PXRD pattern for the molecular salt of sz + 3hba showing the calculated and experimentally obtained patterns.

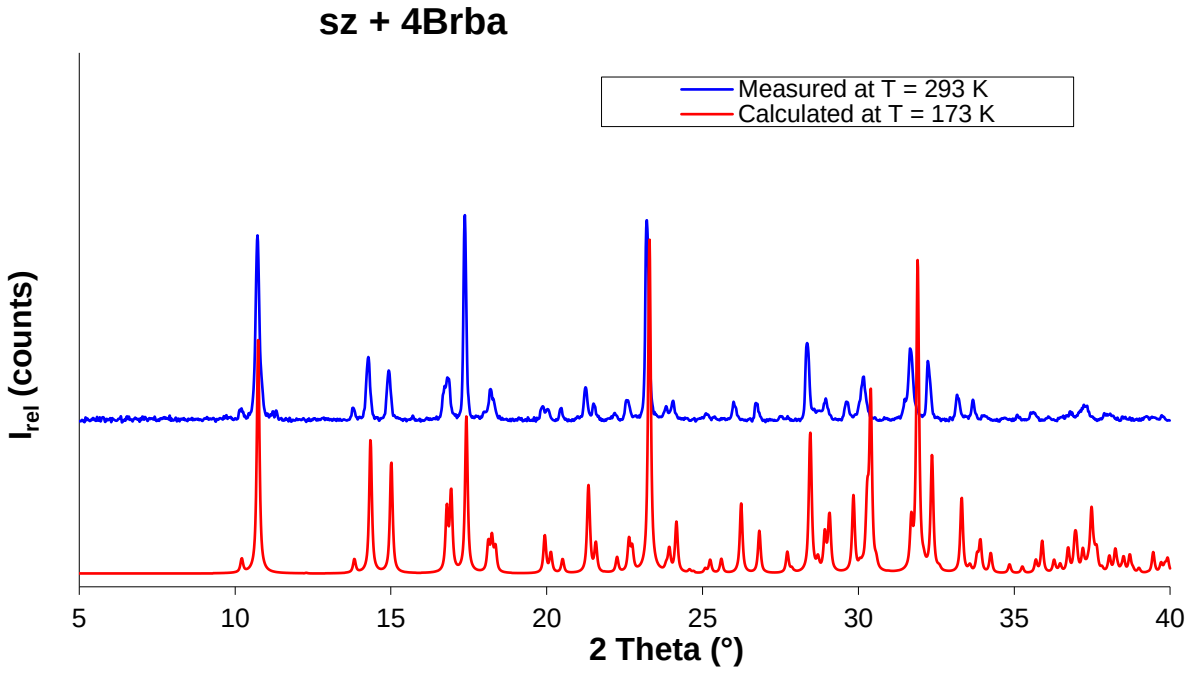


Fig S5 The PXRD pattern for the molecular salt of sz + 4Brba showing the calculated and experimentally obtained patterns.

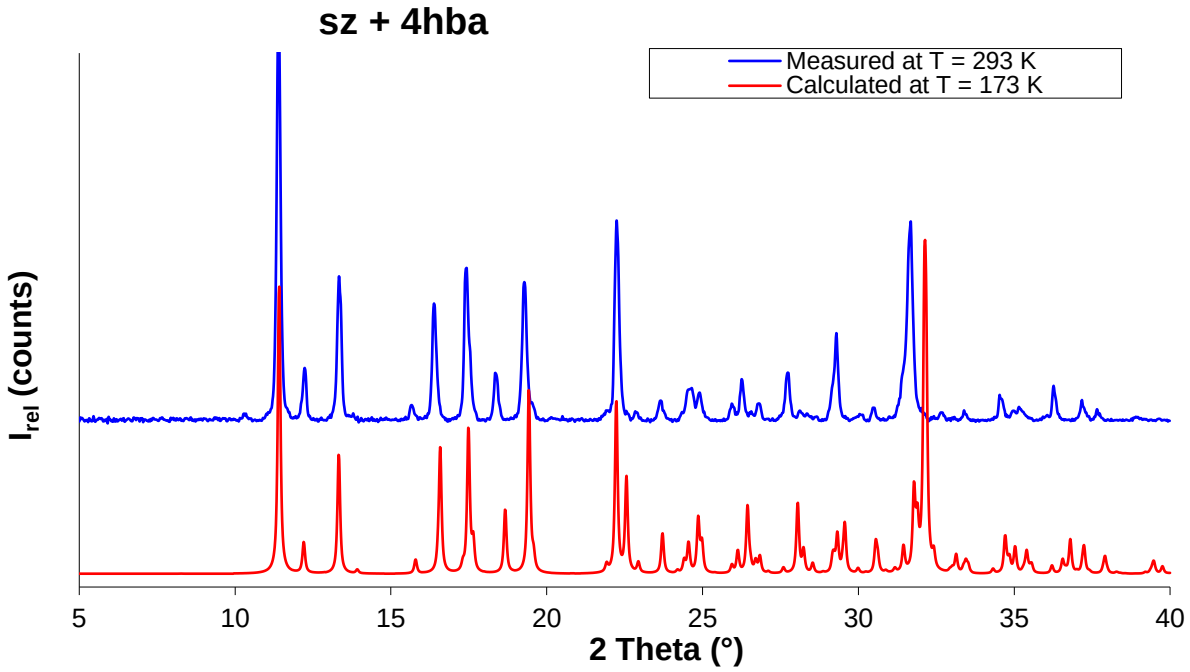


Fig S6 The PXRD pattern for the molecular salt of sz + 4hba showing the calculated and experimentally obtained patterns.

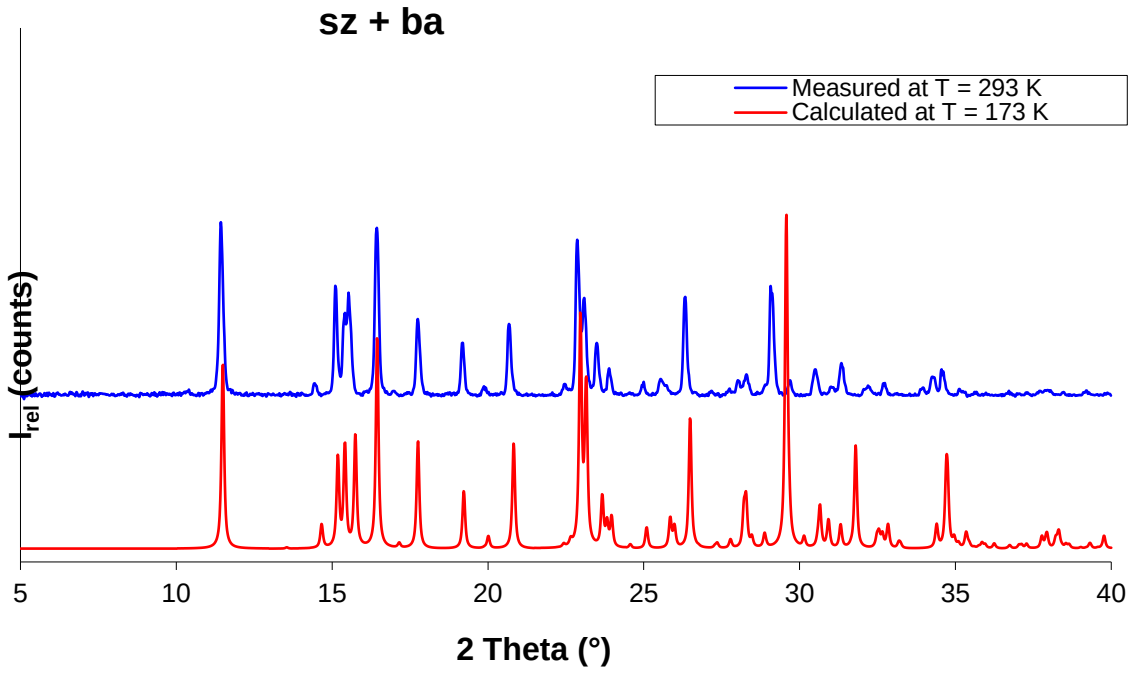


Fig S7 The PXRD pattern for the molecular salt of sz + ba showing the calculated and experimentally obtained patterns.

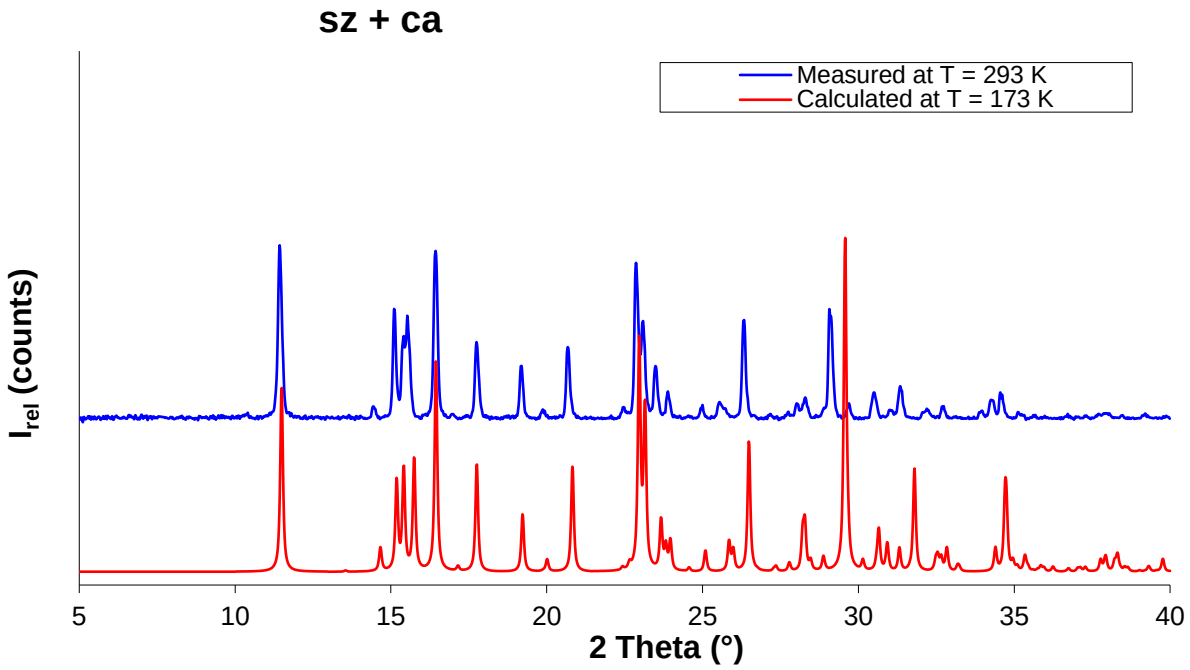


Fig S8 The PXRD pattern for the molecular salt of sz + ca showing the calculated and experimentally obtained patterns.

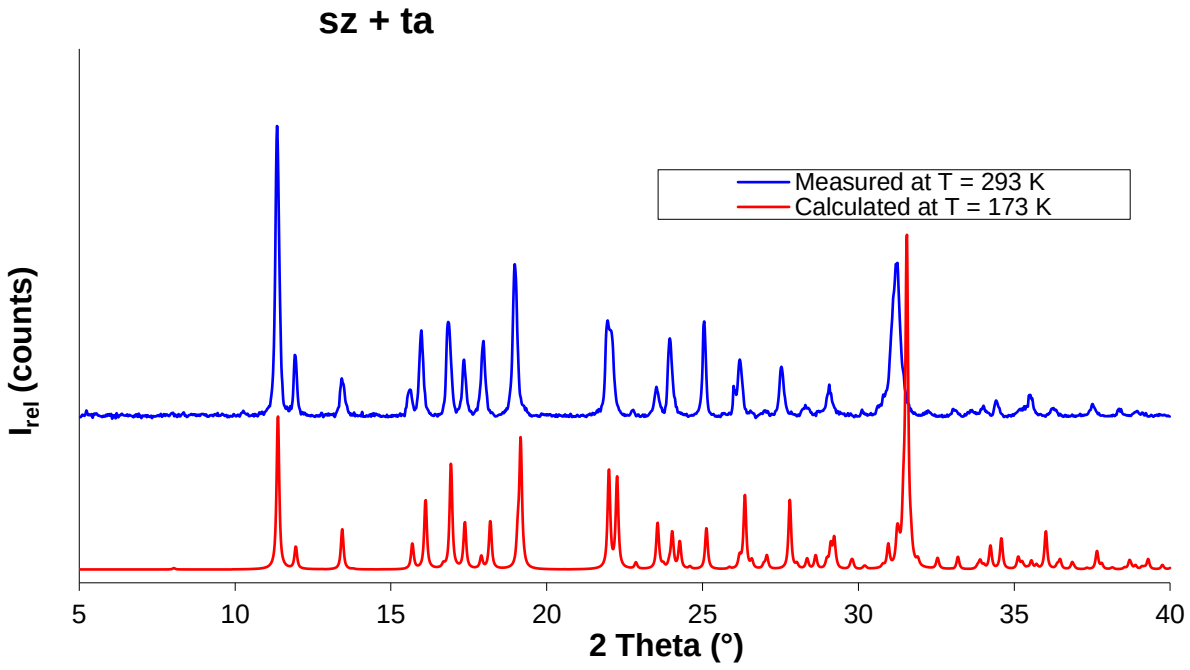


Fig S9 The PXRD pattern for the molecular salt of sz + ta showing the calculated and experimentally obtained patterns.

Chapter 4

In pursuit of multi-component crystals of the sulfa-drugs sulfapyridine, sulfathiazole and sulfamethoxazole

Matthew C. Scheepers and Andreas Lemmerer*‡

Supplementary Information

Table of contents

1. Mass amounts
2. PXRD patterns
3. DSC curves
4. TGA curves
5. FTIR spectra

1. Mass Amounts

Table 1 Masses used for each co-former in equimolar amounts to 0.050 g of the sulfa-drug.

Co-former	Masses used for **sp**/g	Masses used for **st**/g	Masses used for **sm**/g
3-cyanopyridine	0.021	0.020	0.020
4-cyanopyridine	0.021	0.020	0.020
4-dimethylaminopyridine	0.025	0.024	0.024
2-aminopyridine	0.019	0.018	0.018
3-aminopyridine	0.019	0.018	0.018
4-aminopyridine	0.019	0.018	0.018
2-hydroxypyridine	0.019	0.019	0.019
3-hydroxypyridine	0.019	0.019	0.019
4-hydroxypyridine	0.019	0.019	0.019
2-amino-3-nitropyridine	0.028	0.027	0.027
2-amino-5-nitropyridine	0.028	0.027	0.027
4,4’-bipyridine	0.031	0.031	0.031
2-amino-5-chloropyridine	0.026	0.025	0.025
3,5-dinitrobenzoic acid	0.043	0.042	0.042
4-nitrobenzoic acid	0.034	0.033	0.033
2-chloro-4-nitrobenzoic acid	0.040	0.039	0.039
2-chloro-5-nitrobenzoic acid	0.040	0.039	0.039
2-hydroxybenzoic acid (Salicylic acid)	0.028	0.027	0.027
3-hydroxybenoic acid	0.028	0.027	0.027
4-hydroxybenzoic acid	0.028	0.027	0.027
3,4-dichlorobenzoic acid	0.038	0.037	0.037
Toluic Acid	0.027	0.027	0.027

Saccharine	0.037	0.036	0.036
Succinic acid	0.024	0.023	0.023
Cinnamic Acid (*trans*)	0.030	0.029	0.029

Table 2 Successful crystallization experiments and solvent systems used.

Multi-component crystal	Mass of sulfa drug /g	Mass of co-former used/ g	Solvent system used
sm + **3cnp**	0.050	0.020	THF
sm + **4cnp**	0.050	0.020	Acetonitrile
sm + **4dmap**	0.050	0.024	THF
sm + **dnba**	0.050	0.042	Methanol
st + **2a3np**	0.050	0.027	1:1 v/v Ethanol/Acetonitrile
st + **2a5np**	0.100	0.027	1:1 v/v Ethanol/Acetonitrile
st + **2ap**	0.050	0.018	1:1 v/v Ethanol/Acetonitrile
st + **2a5clp**	0.050	0.025	1:1 v/v Ethanol/Acetonitrile
st + **bipy**	0.100	0.031	1:1 v/v Ethanol/Acetonitrile
st + **dnba**	0.050	0.042	1:1 v/v Ethanol/Acetonitrile
sp + **2a3np**	0.050	0.028	1:1 v/v Ethanol/Acetonitrile

sp + **2a5np**	0.050	0.028	Acetonitrile
sp + **2ap**	0.050	0.019	1:1 v/v Ethanol/Acetonitrile
sp + **2a5clp**	0.050	0.026	THF
sp + **2c4n**	0.050	0.040	1:1 v/v Water/isopropanol

2. Powder X-ray diffraction patterns

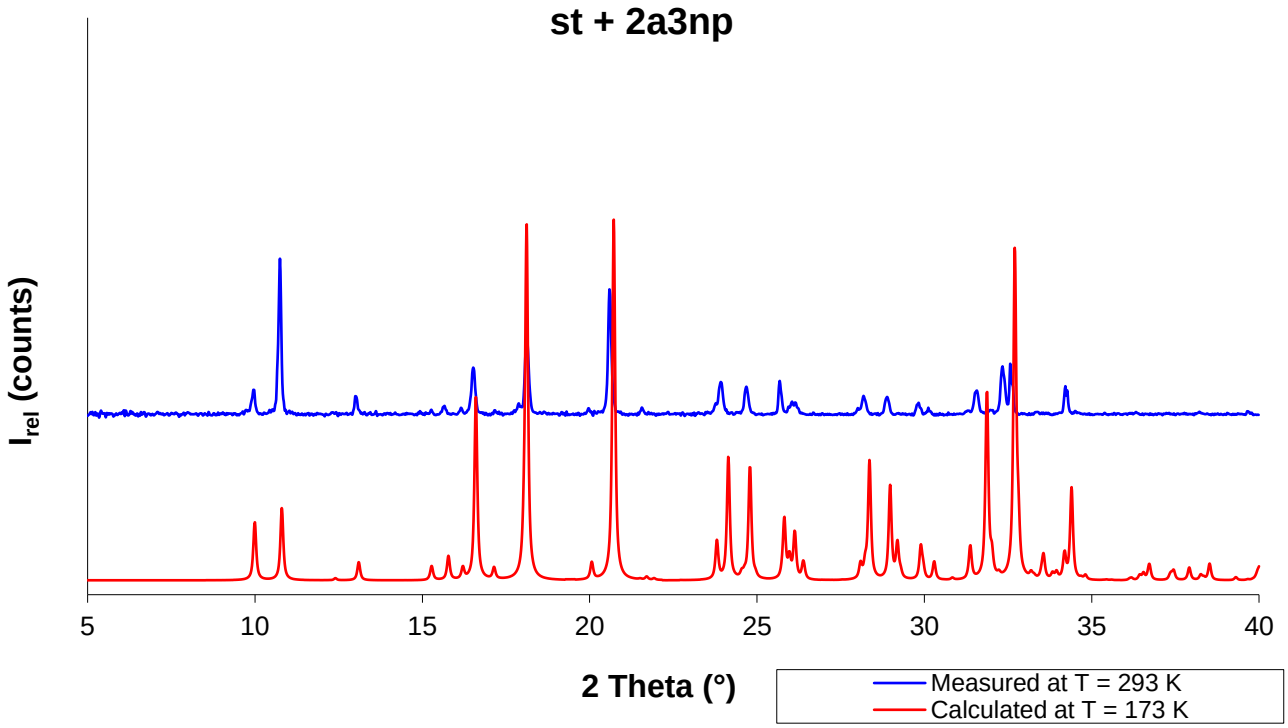


Figure S2.1 PXRD pattern for the co-crystal of **st + 2a3np**

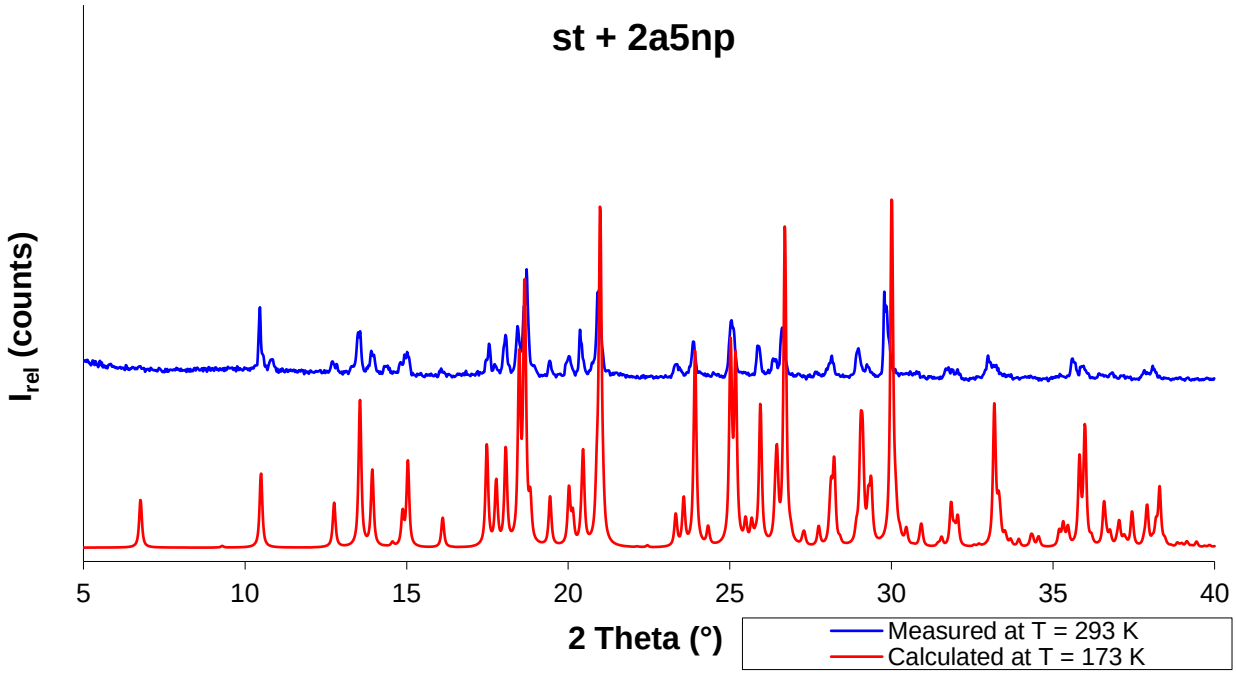


Figure S2.2 PXRD pattern for the co-crystal of **st + 2a5np**

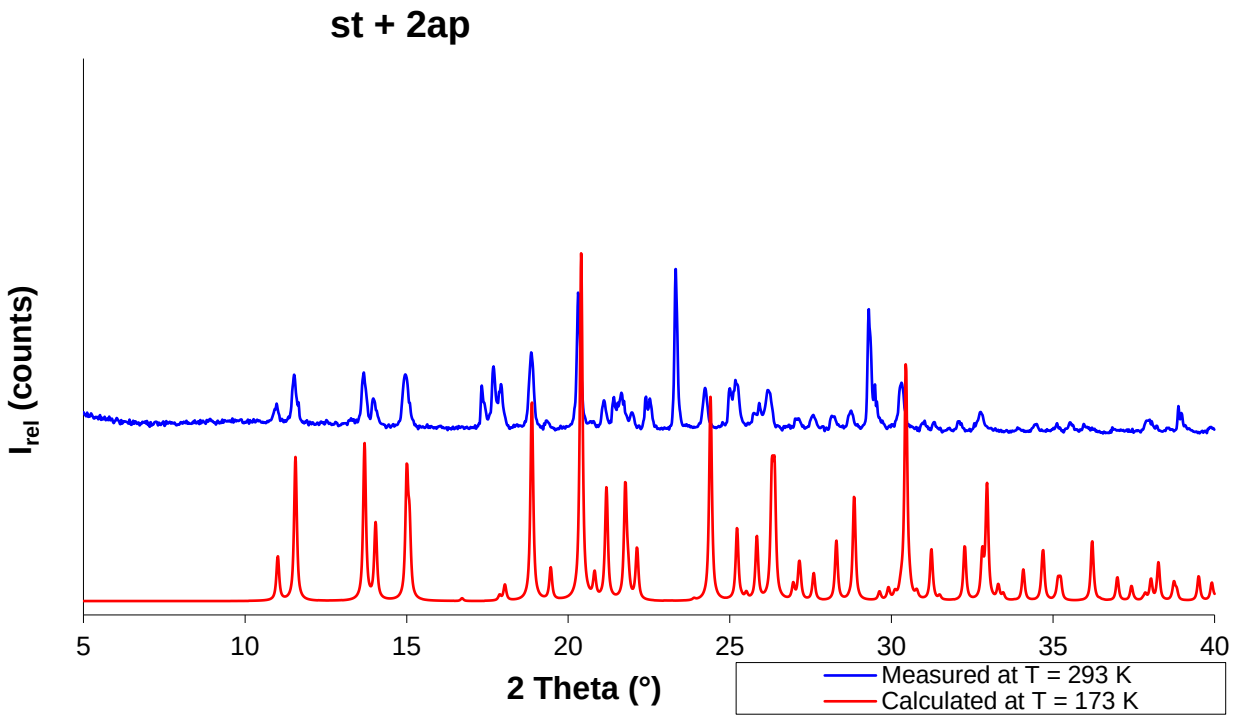


Figure S2.3 PXRD pattern for the co-crystal of **st + 2ap**

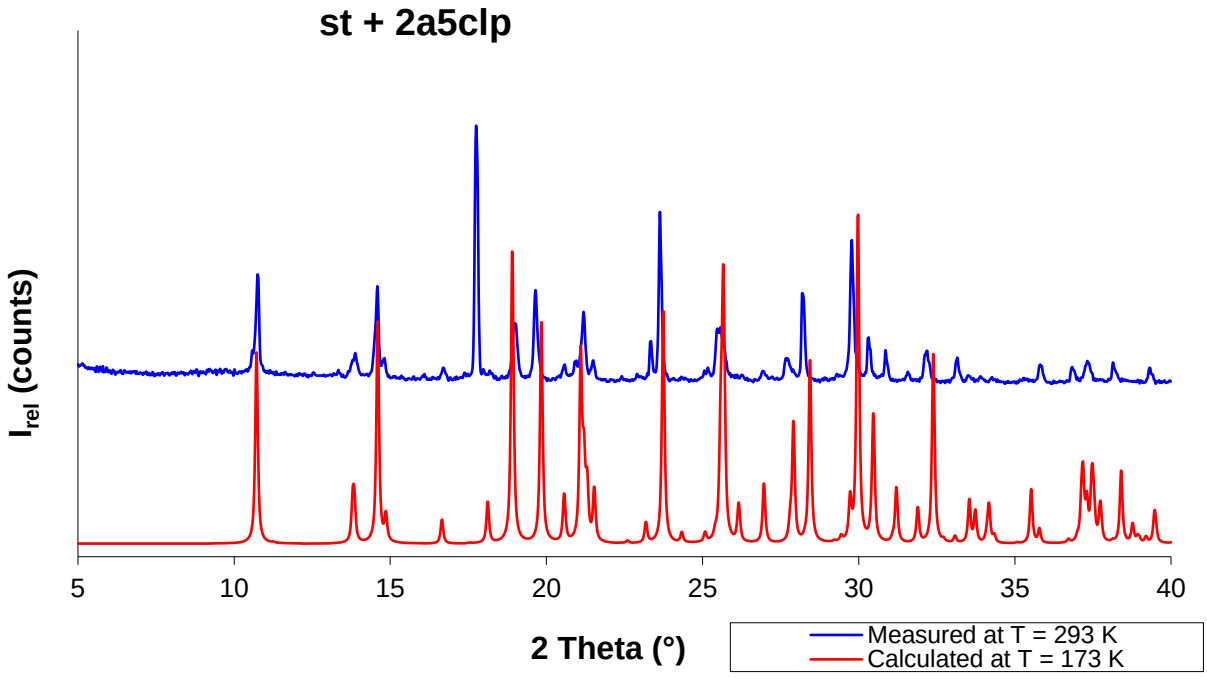


Figure S2.4 PXRD pattern for the co-crystal of **st + 2a5clp**

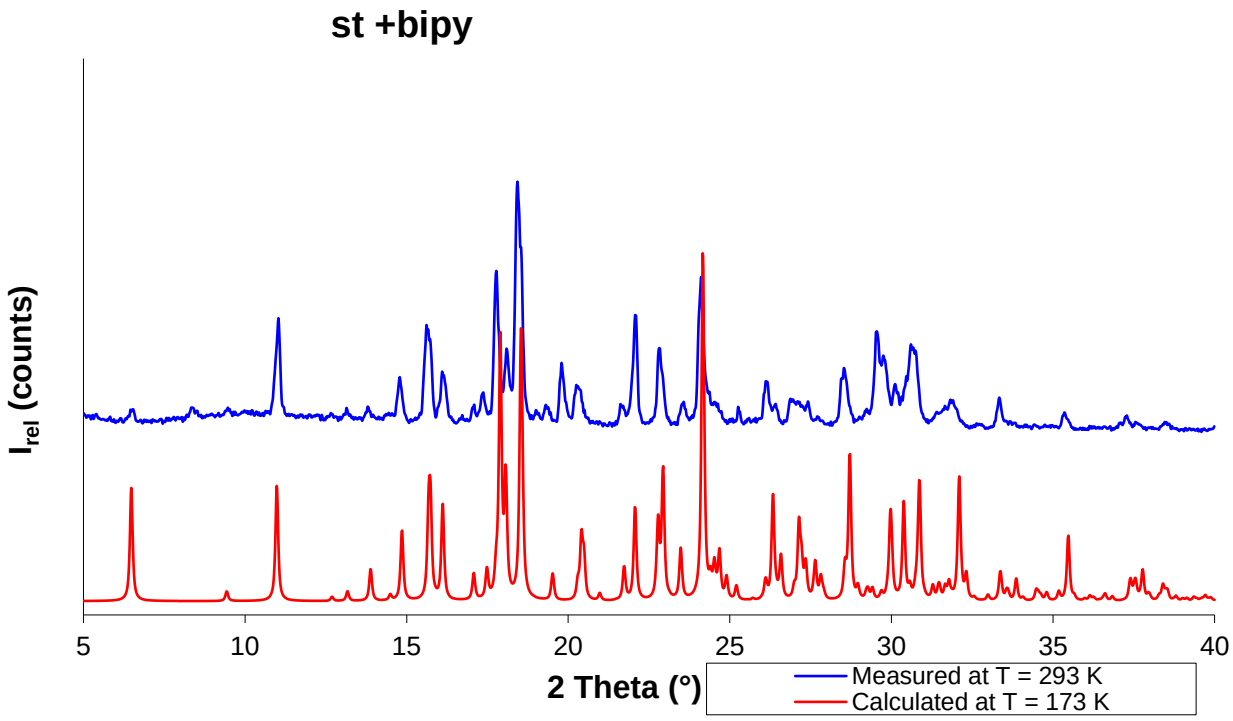


Figure S2.5 PXRD pattern for the co-crystal of **st** + **bipy**

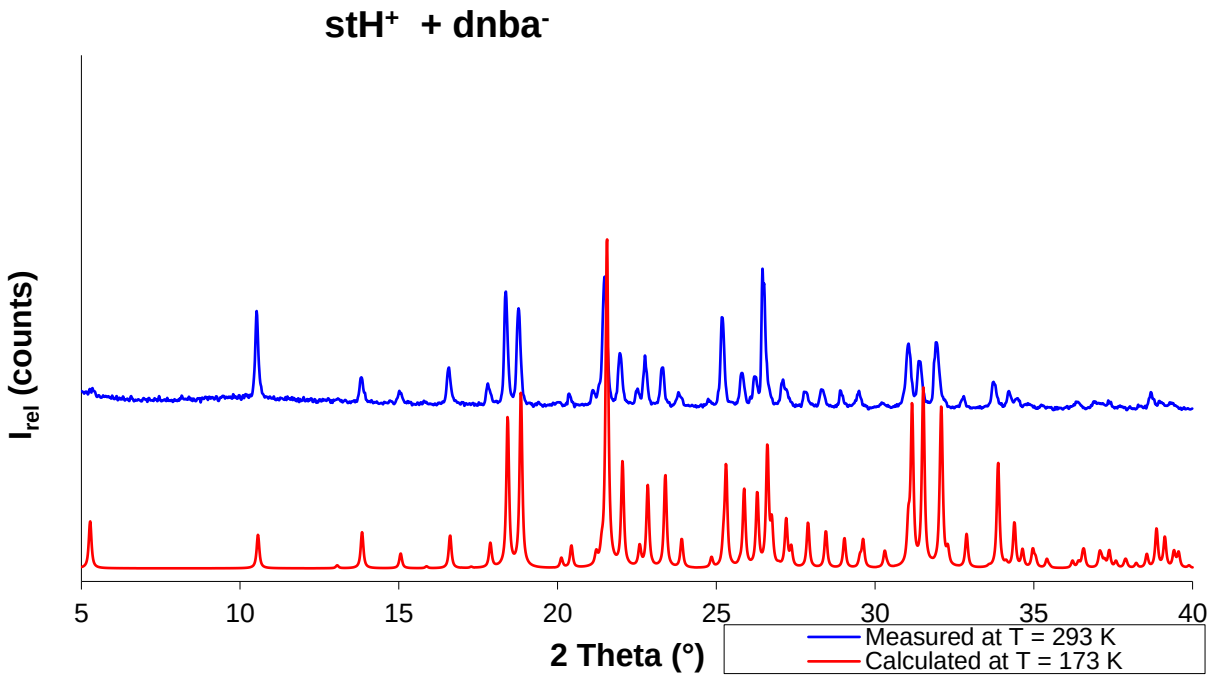


Figure S2.6 PXRD pattern for the co-crystal of **stH$^+$ + dnba$^-$**

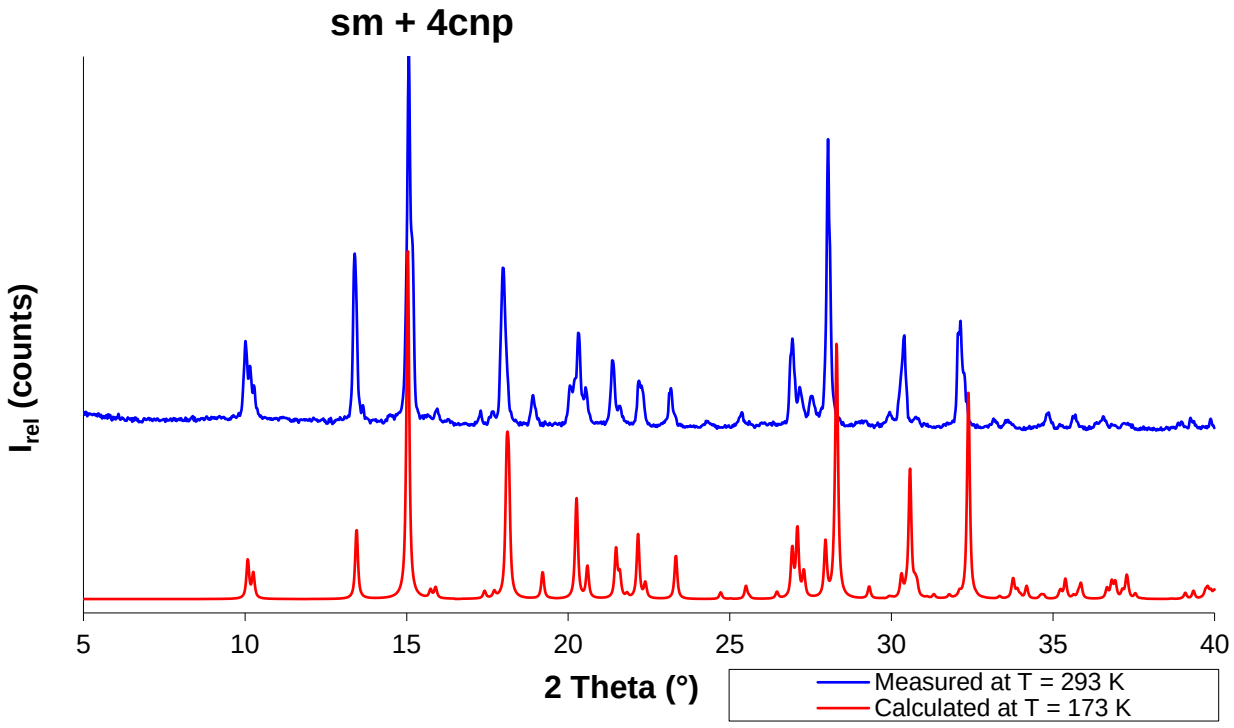


Figure S2.7 PXRD pattern for the co-crystal of **sm + 4cnp**

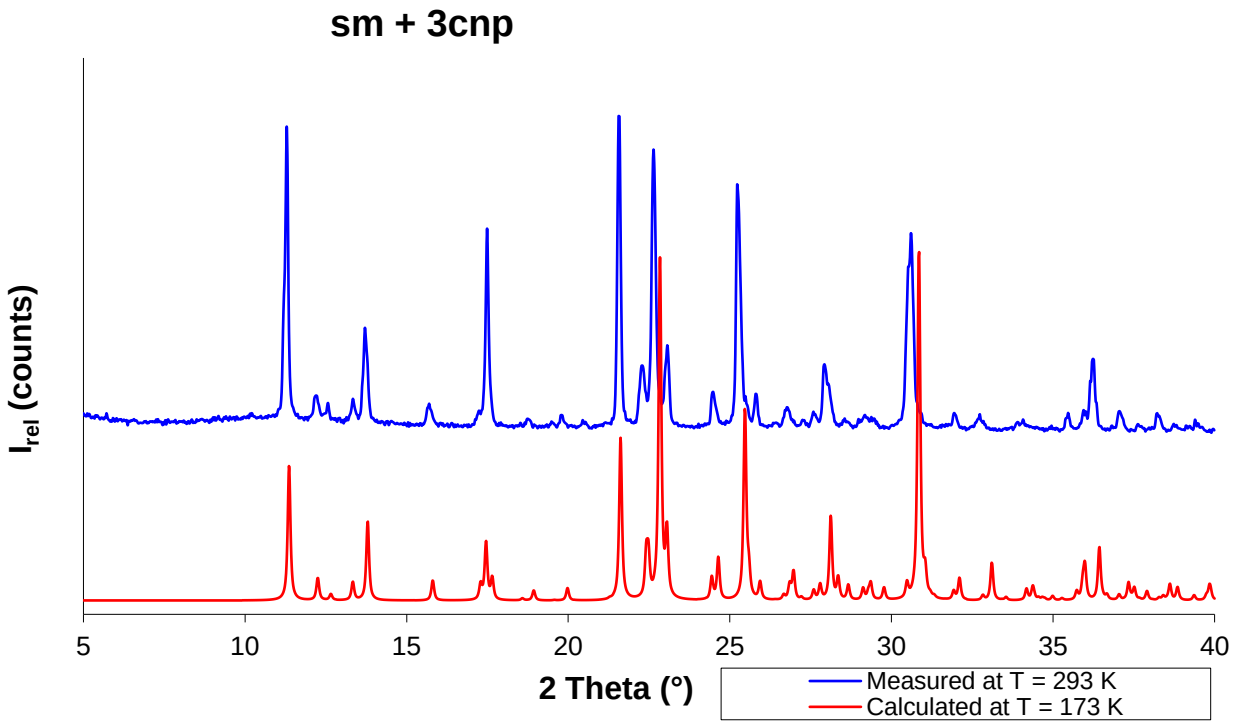


Figure S2.8 PXRD pattern for the co-crystal of **sm + 3cnp**

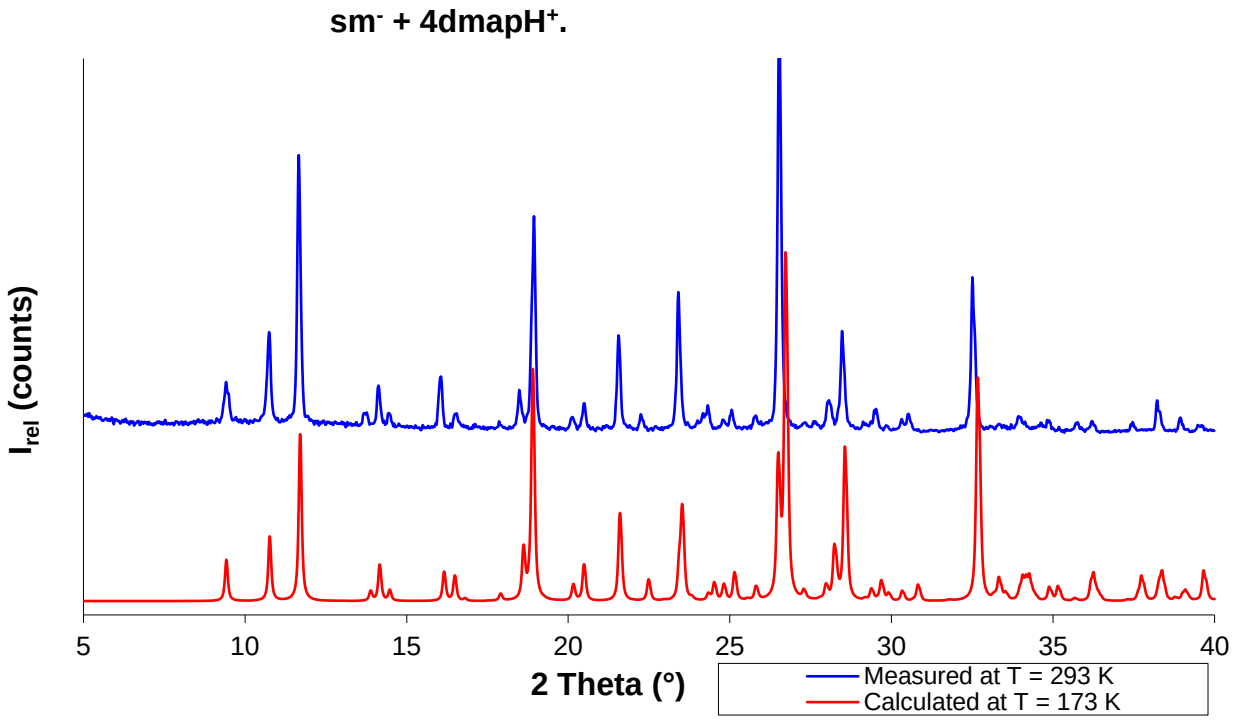


Figure S2.9 PXRD pattern for the co-crystal of **sm**$^{-}$ + **4dmapH**$^{+}$.

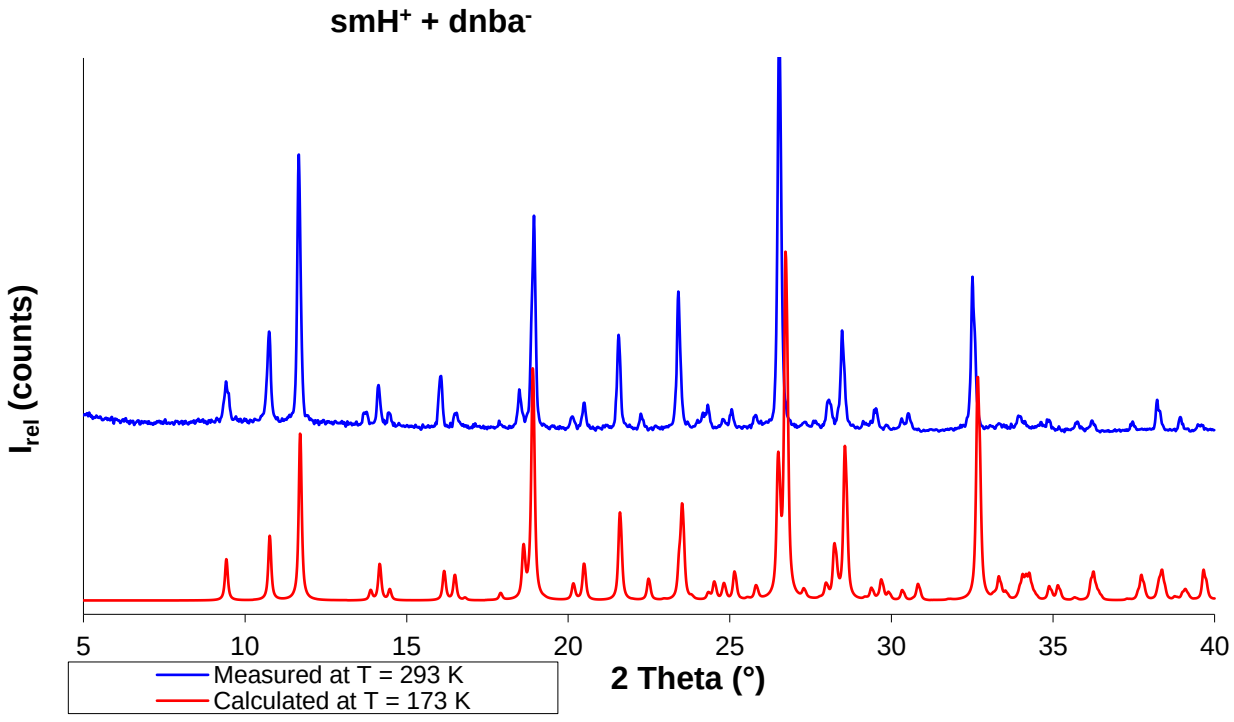


Figure S2.10 PXRD pattern for the co-crystal of **smH**$^{+}$ + **dnba**$^{-}$

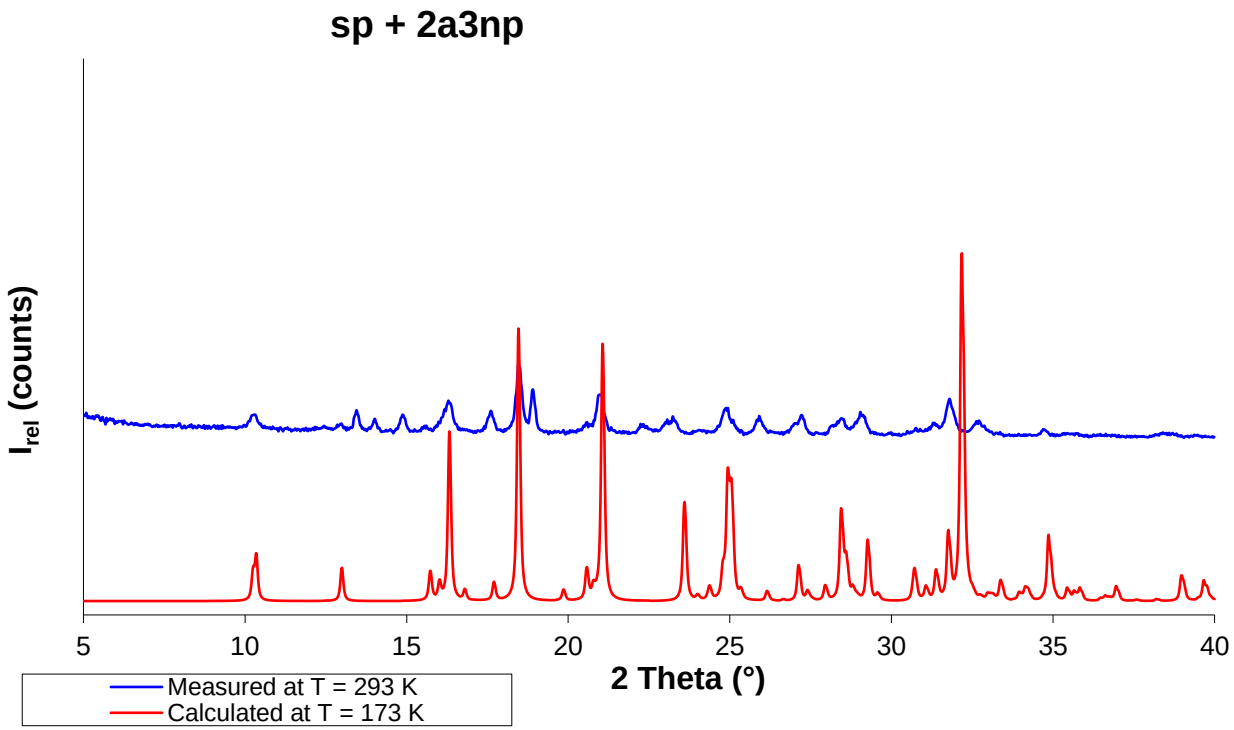


Figure S2.11 PXRD pattern for the co-crystal of **sp + 2a3np**

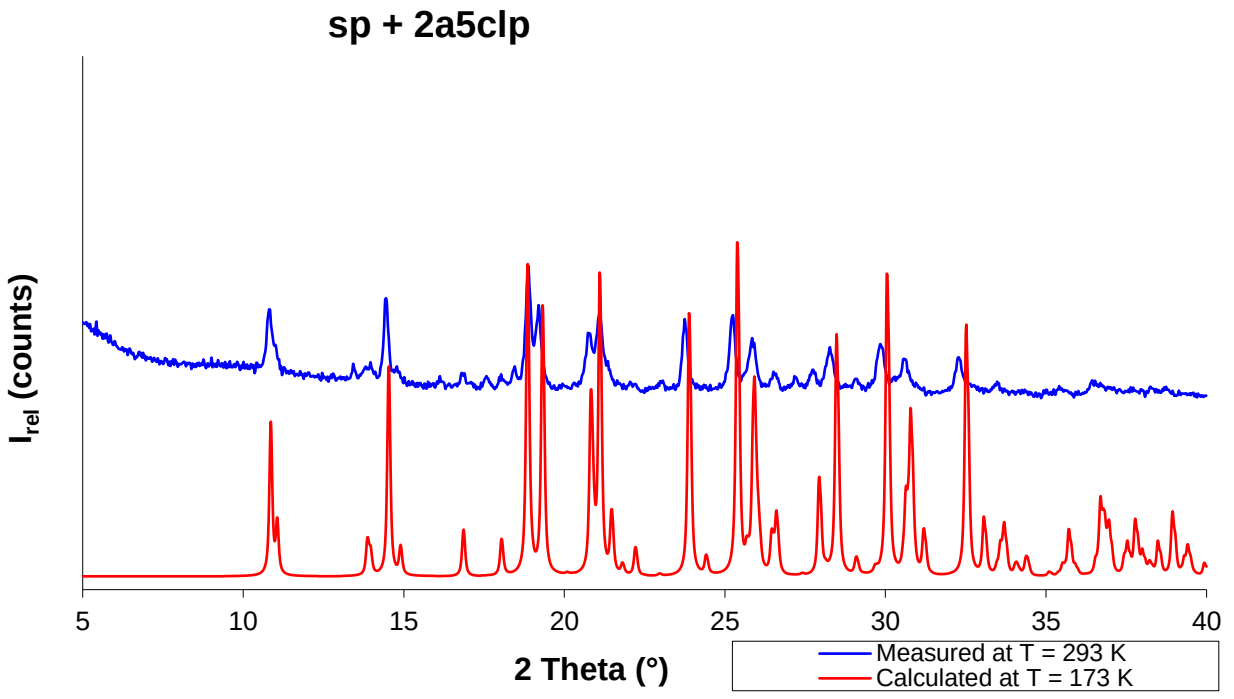


Figure S2.12 PXRD pattern for the co-crystal of **sp + 2a5clp**

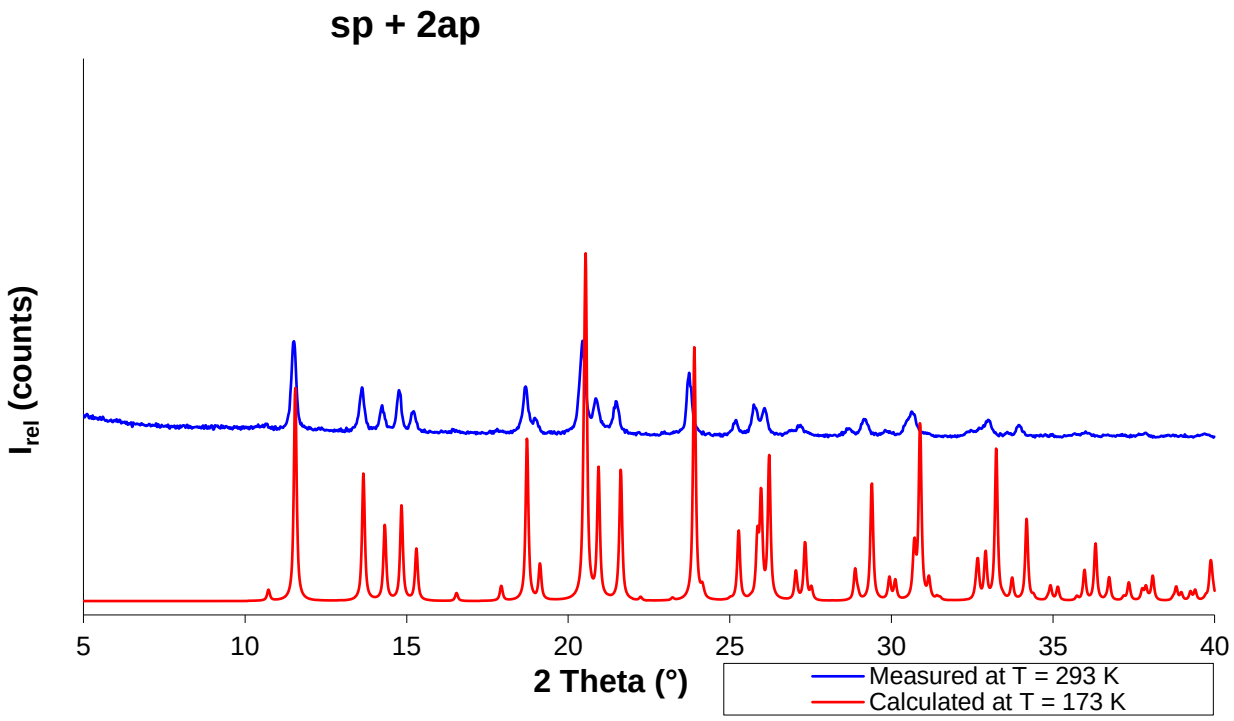


Figure S2.13 PXRD pattern for the co-crystal of **sp + 2ap**

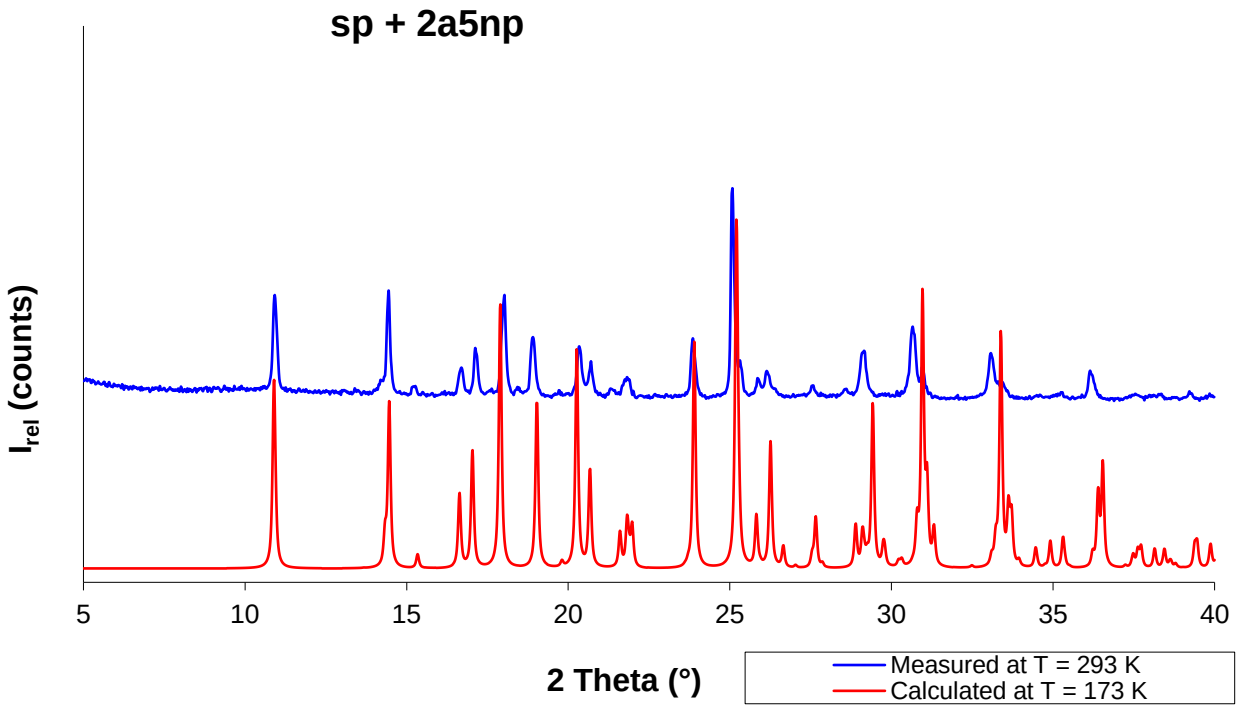


Figure S2.14 PXRD pattern for the co-crystal of **sp + 2a5np**

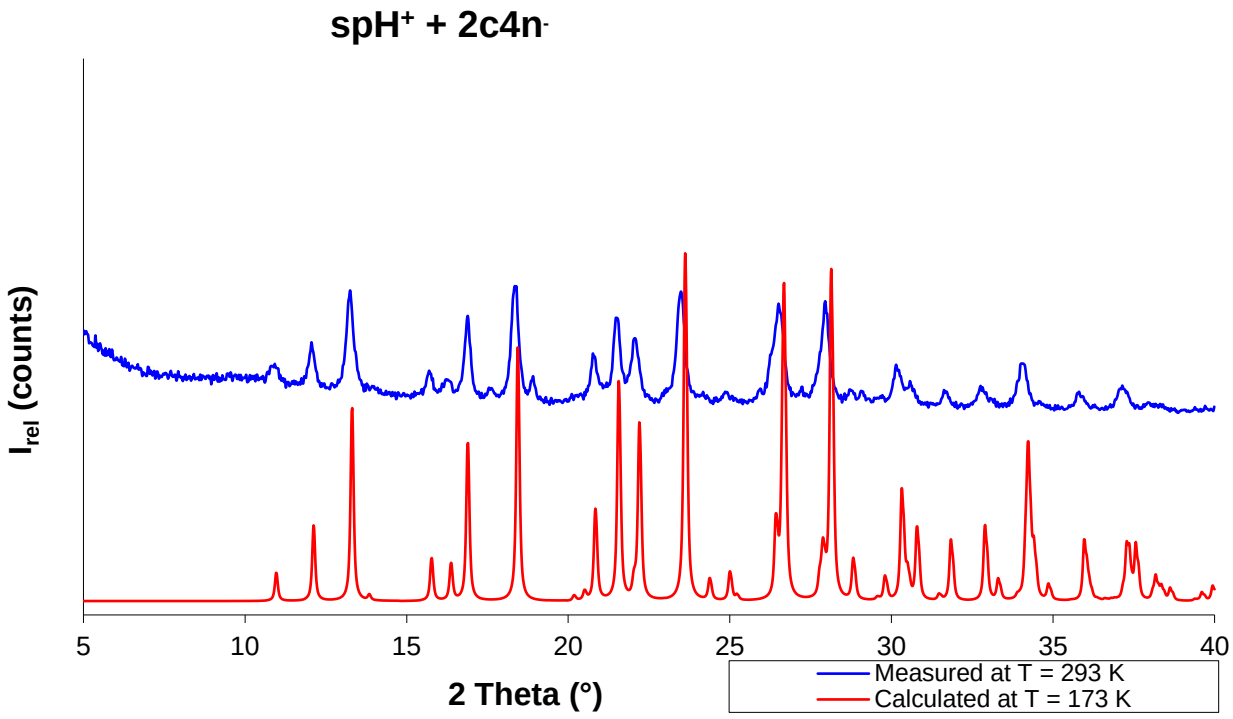


Figure S2.15 PXRD pattern for the co-crystal of **spH$^+$ + 2c4n$^-$**

3. Differential Scanning Calorimetry Curves

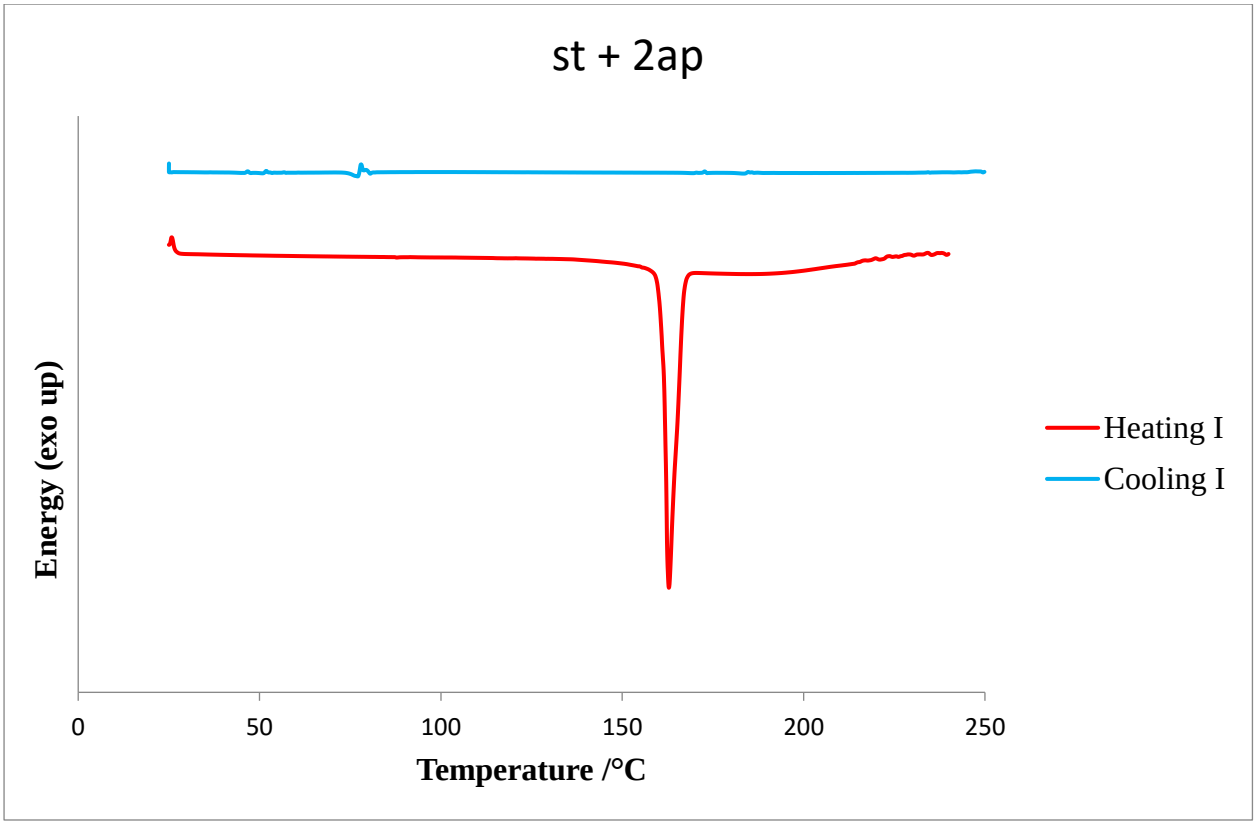


Figure S3.1 DSC curve for **st + 2ap**

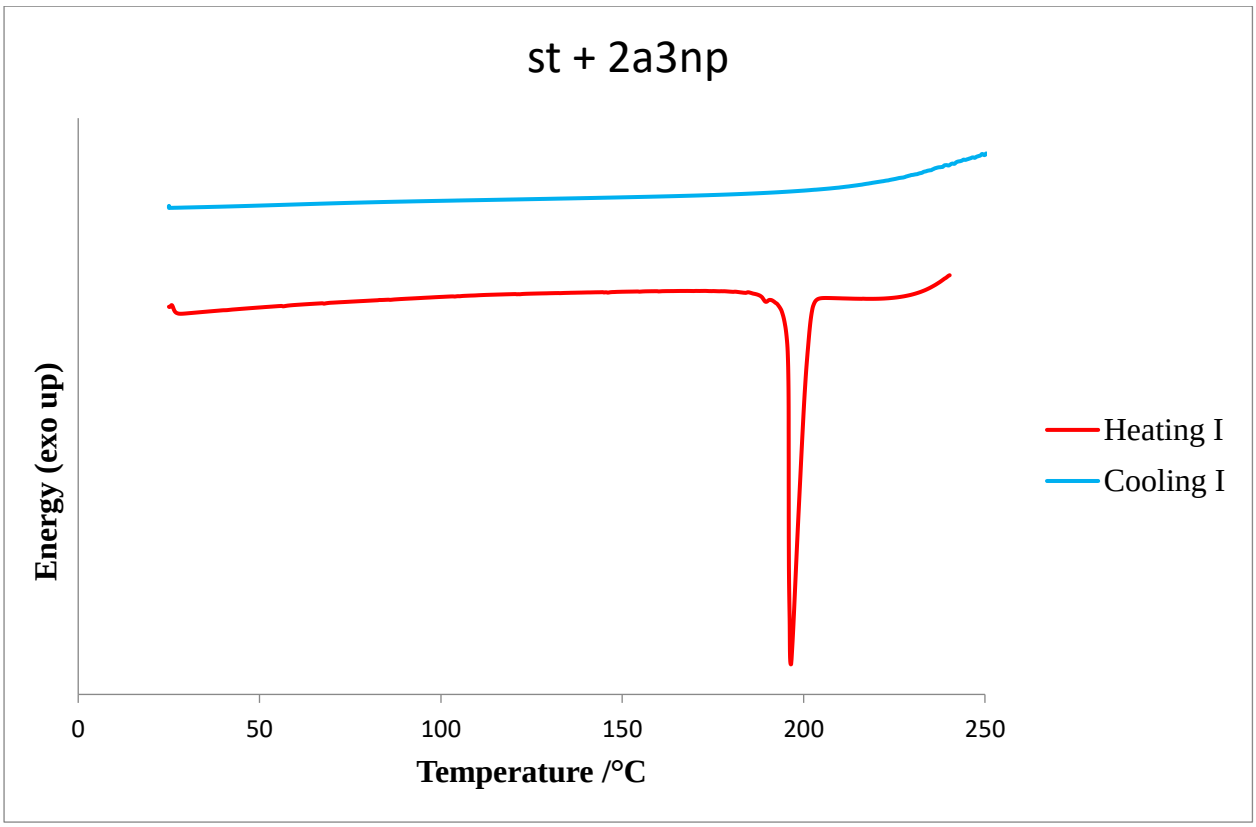


Figure S3.2 DSC curve for **st + 2a3np**

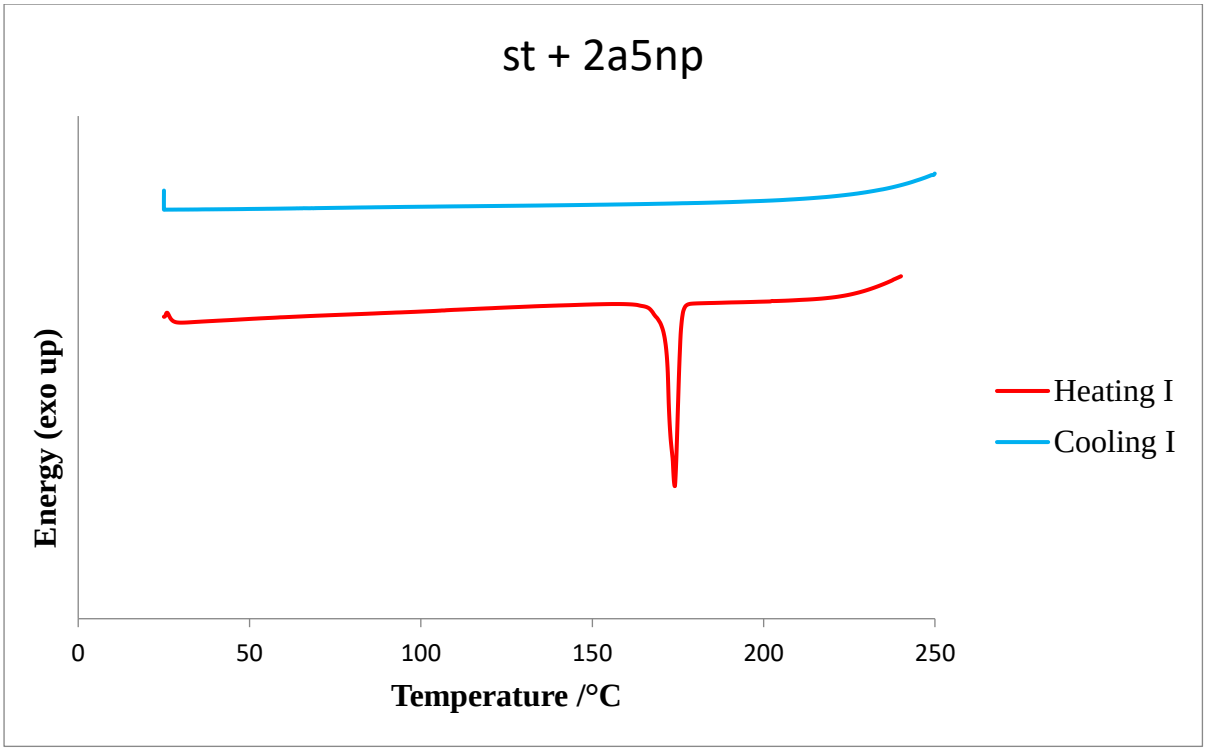


Figure S3.3 DSC curve for **st + 2a5np**

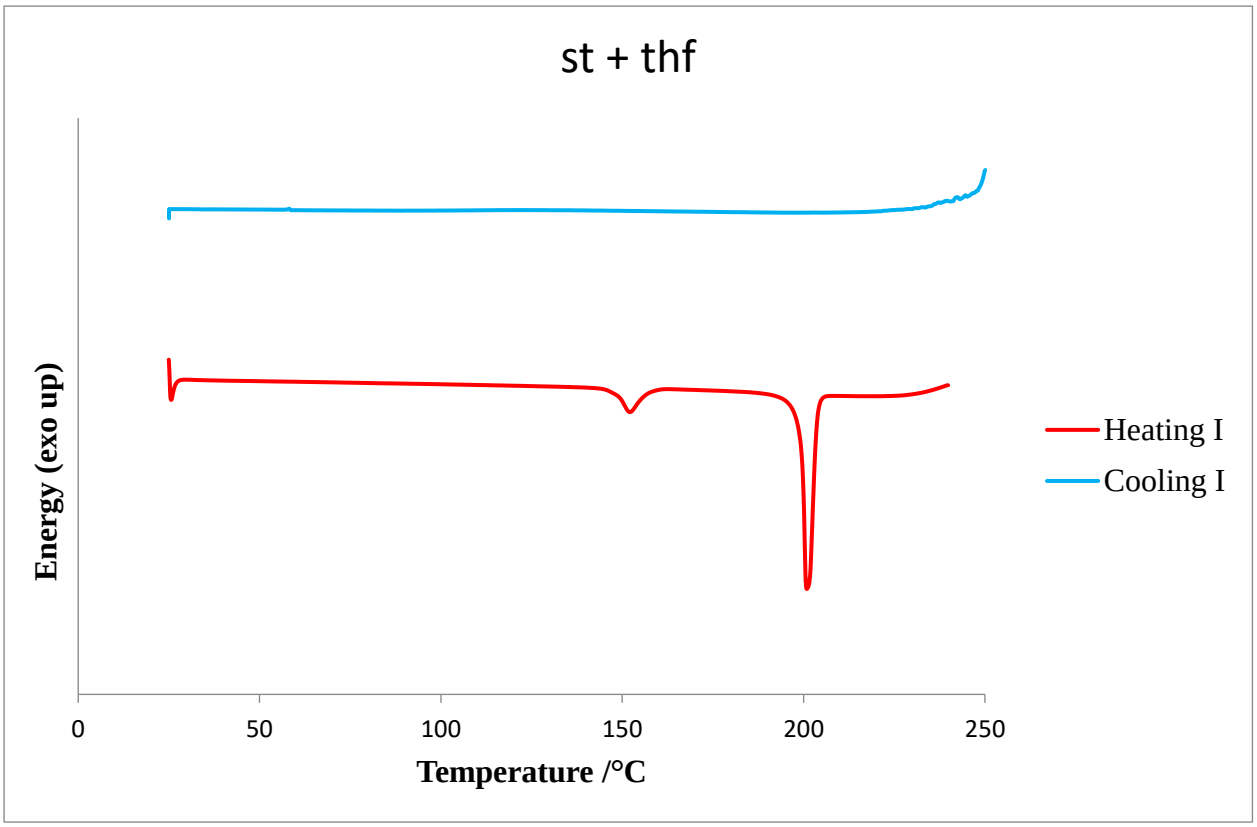


Figure S3.3 DSC curve for **st + thf**

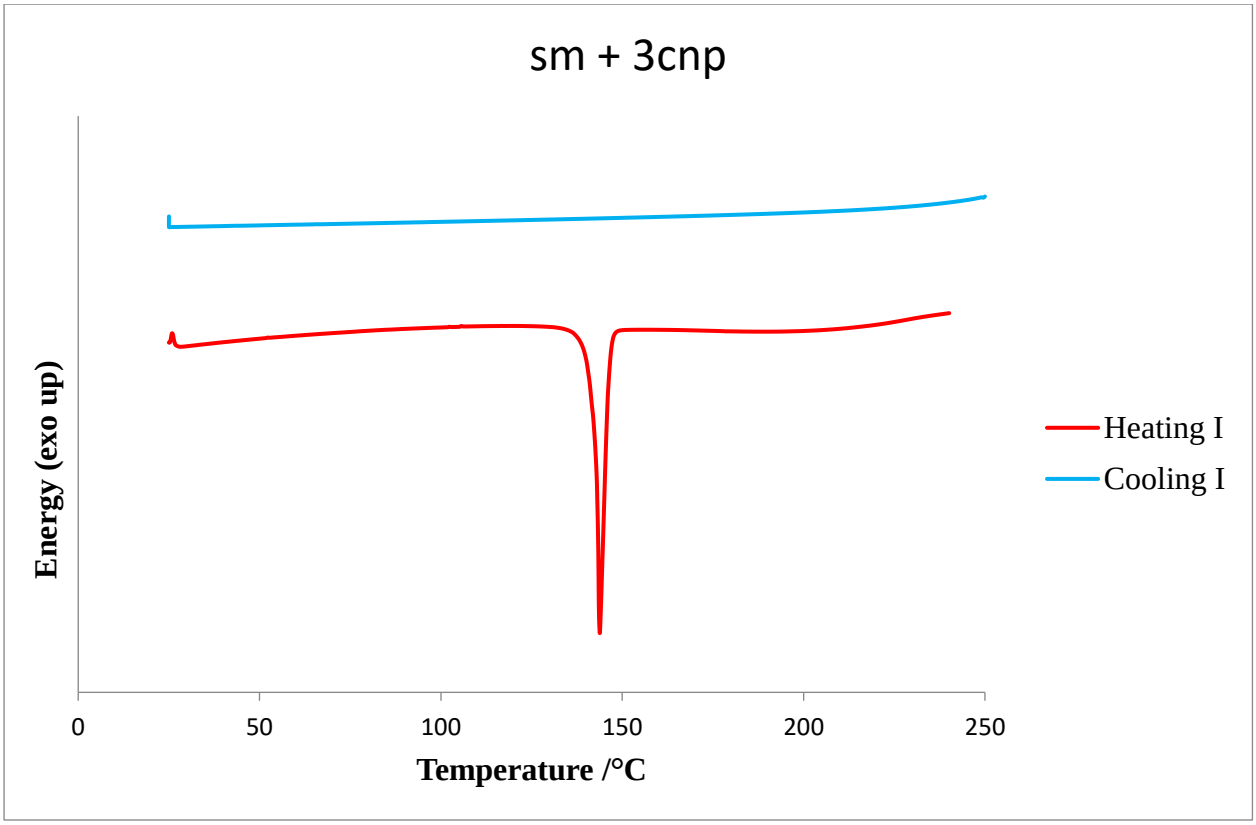


Figure S3.4 DSC curve for **sm + 3cnp**

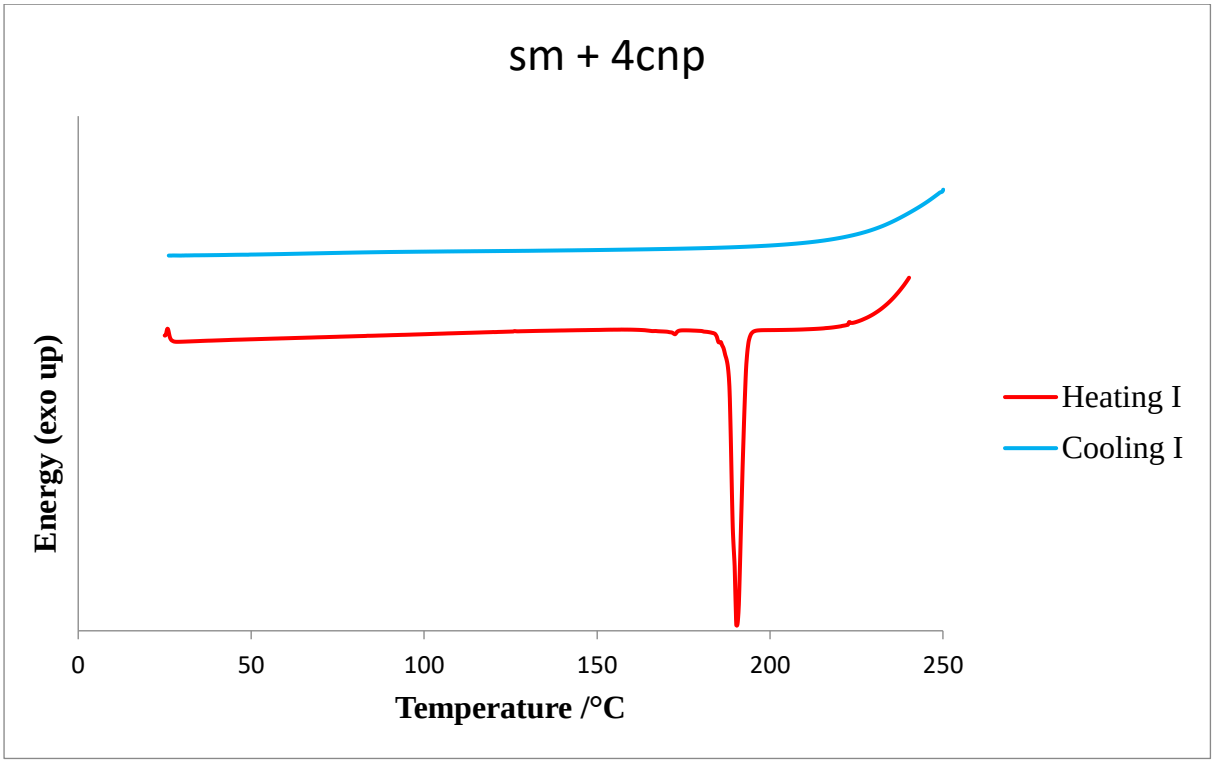


Figure S3.5 DSC curve for **sm + 4cnp**

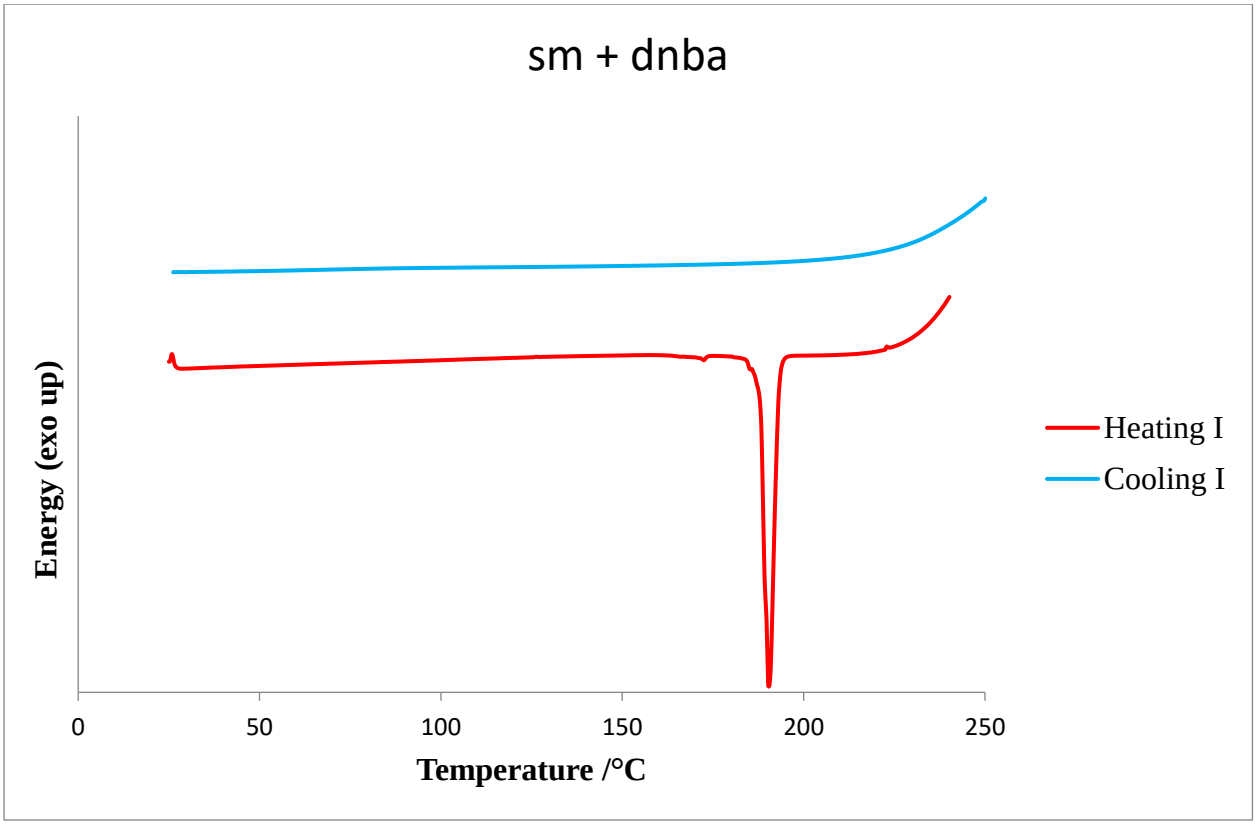


Figure S3.6 DSC curve for **sm + dnba**

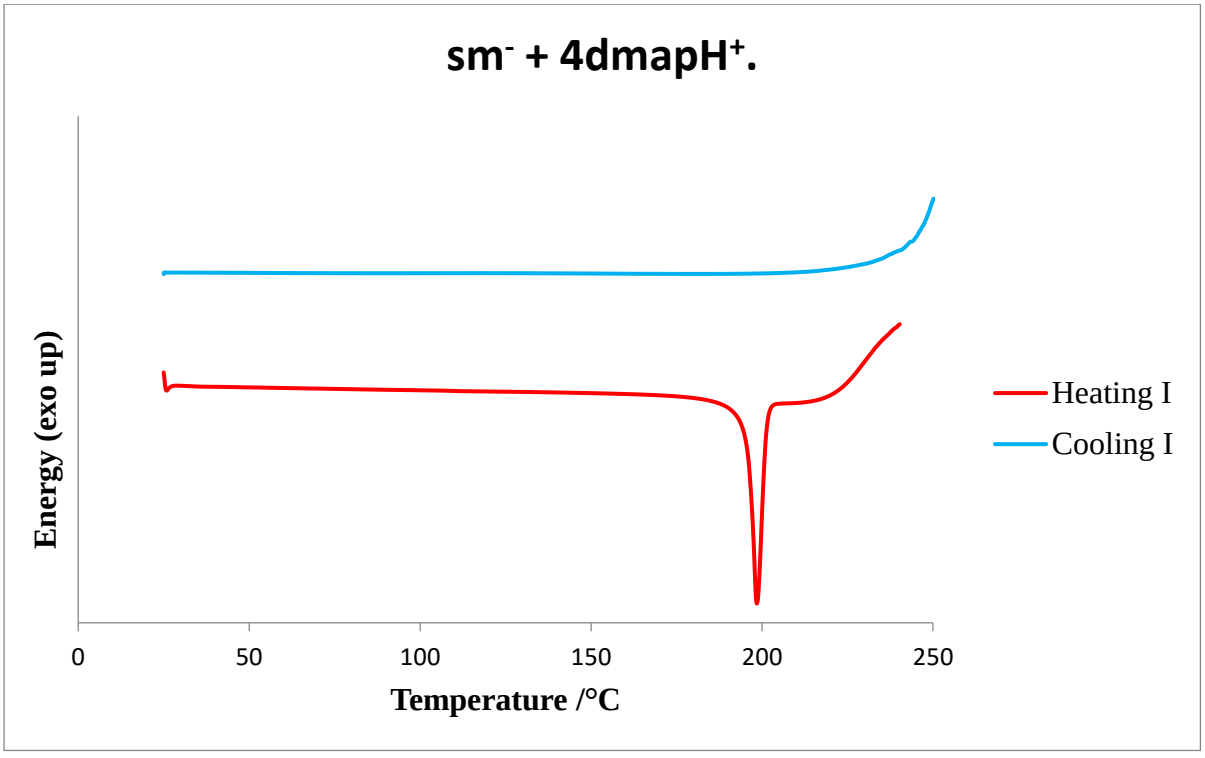


Figure S3.6 DSC curve for **sm$^-$ + 4dmapH$^+$**.

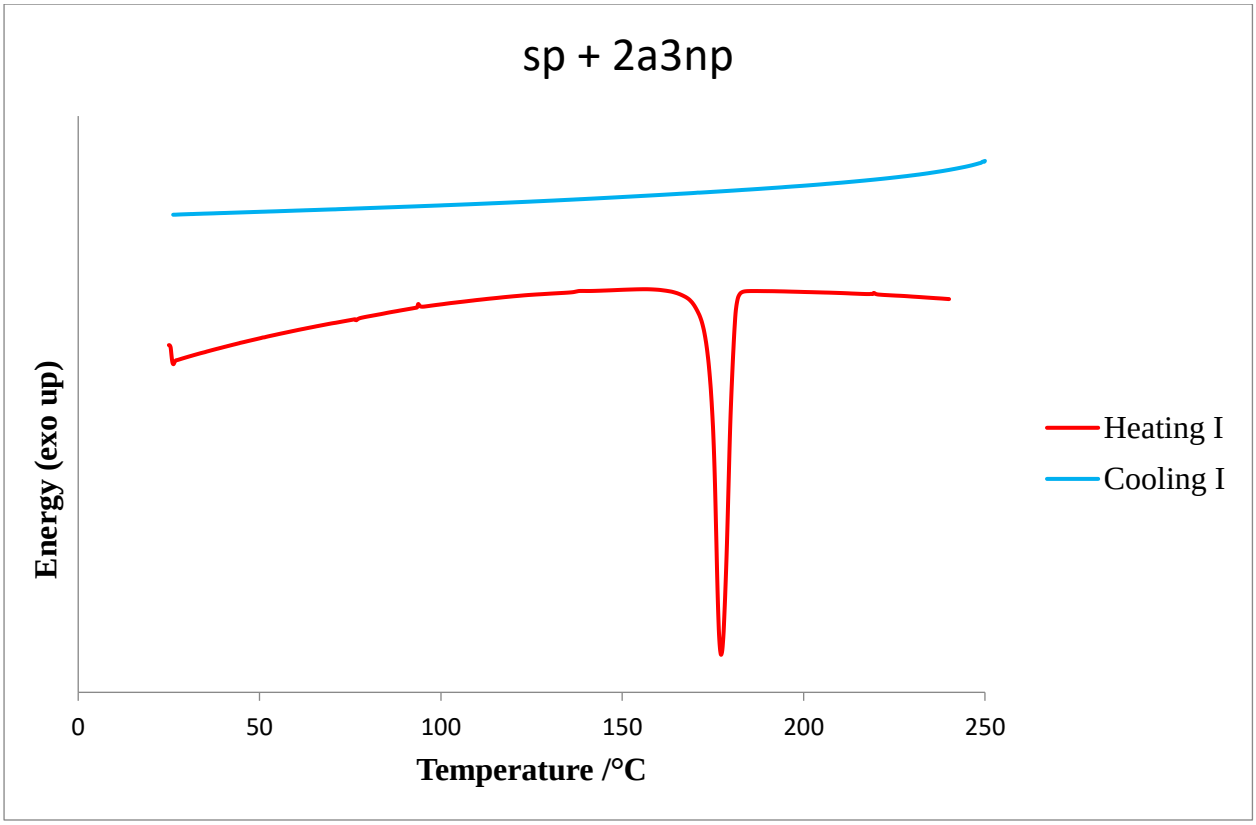


Figure S3.7 DSC curve for **sp + 2a3np**

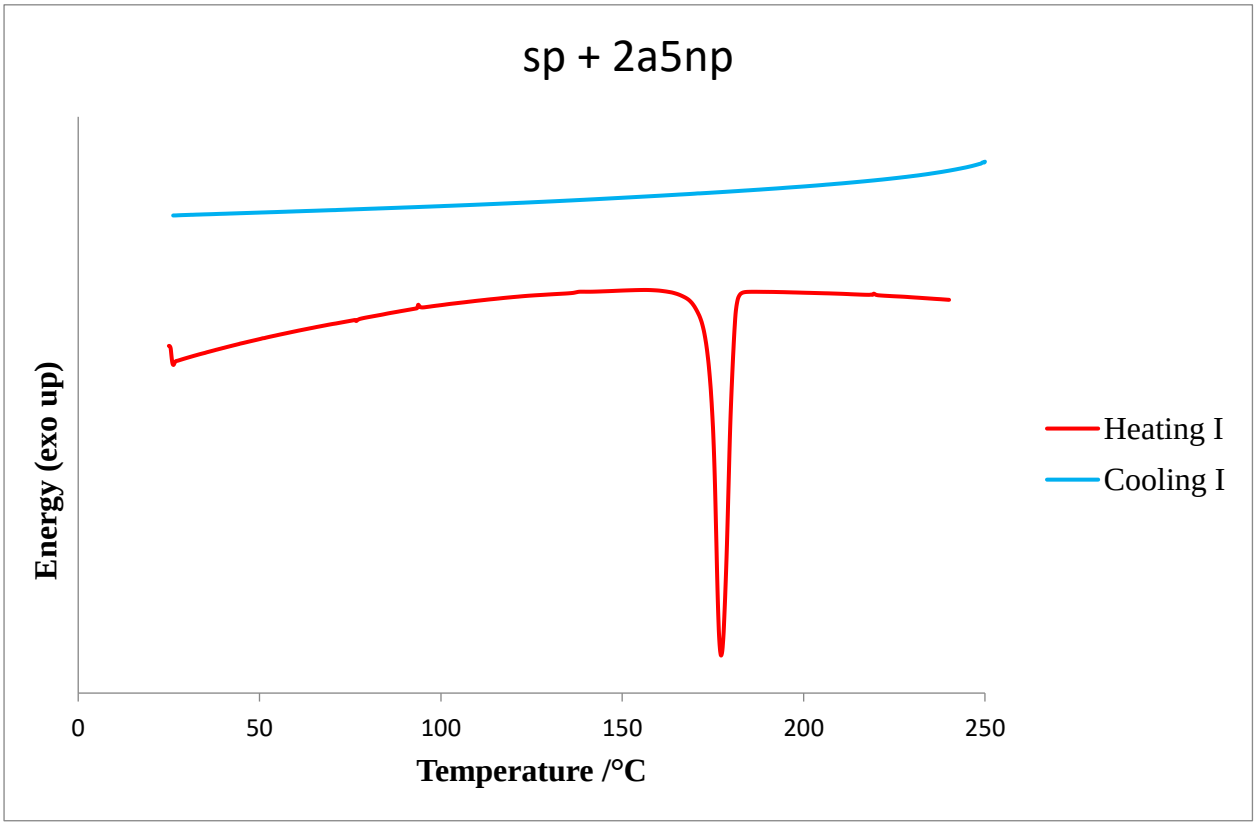


Figure S3.8 DSC curve for **sp + 2a5np**

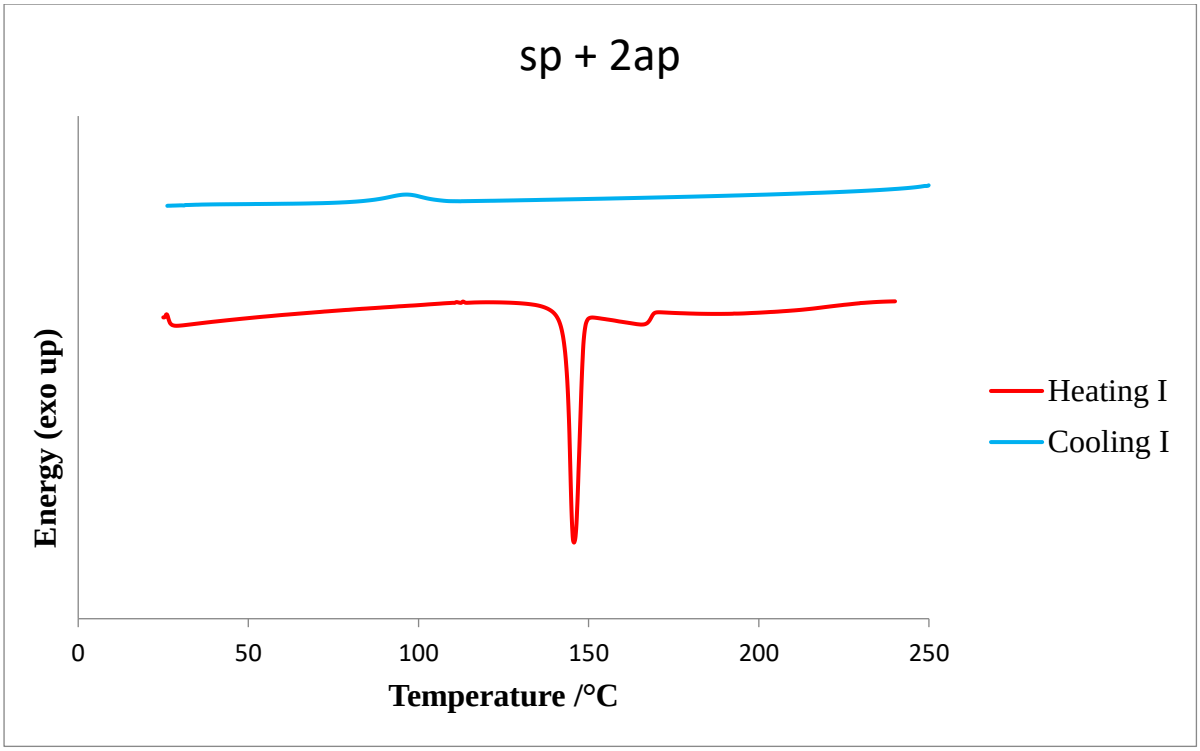


Figure S3.9 DSC curve for **sp + 2ap**

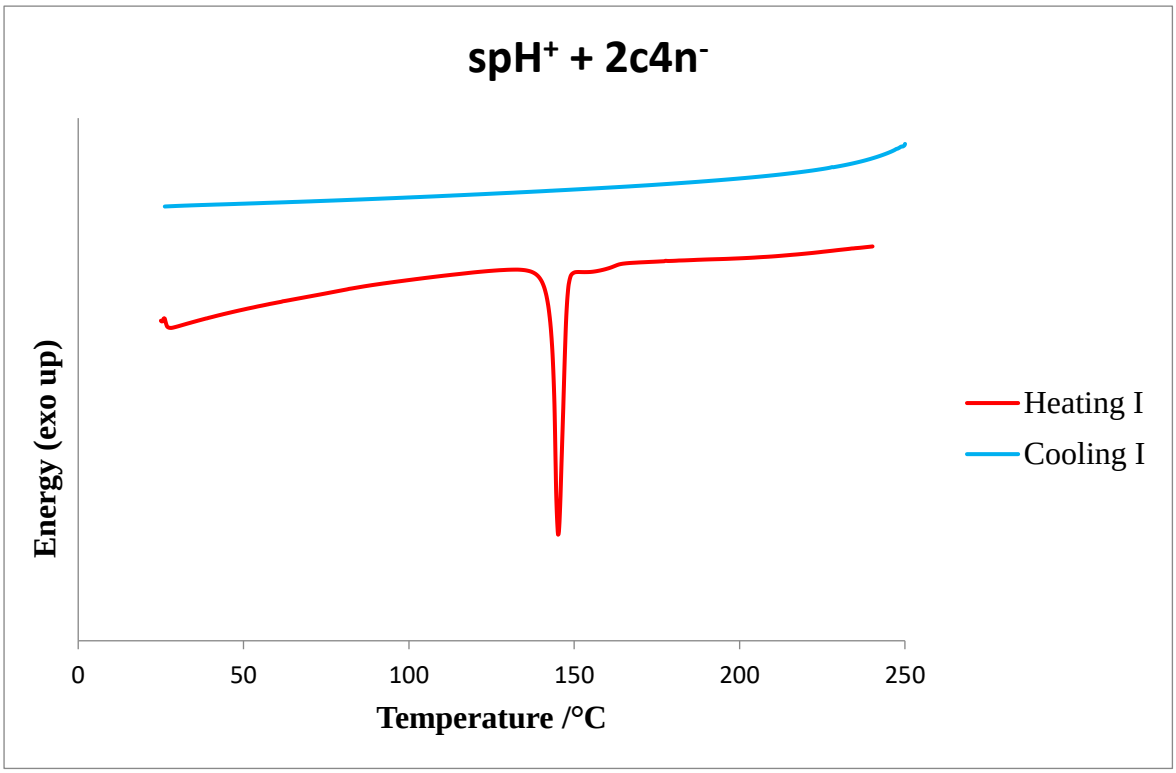


Figure S3.10 DSC curve for **spH$^+$ + 2c4n$^-$**

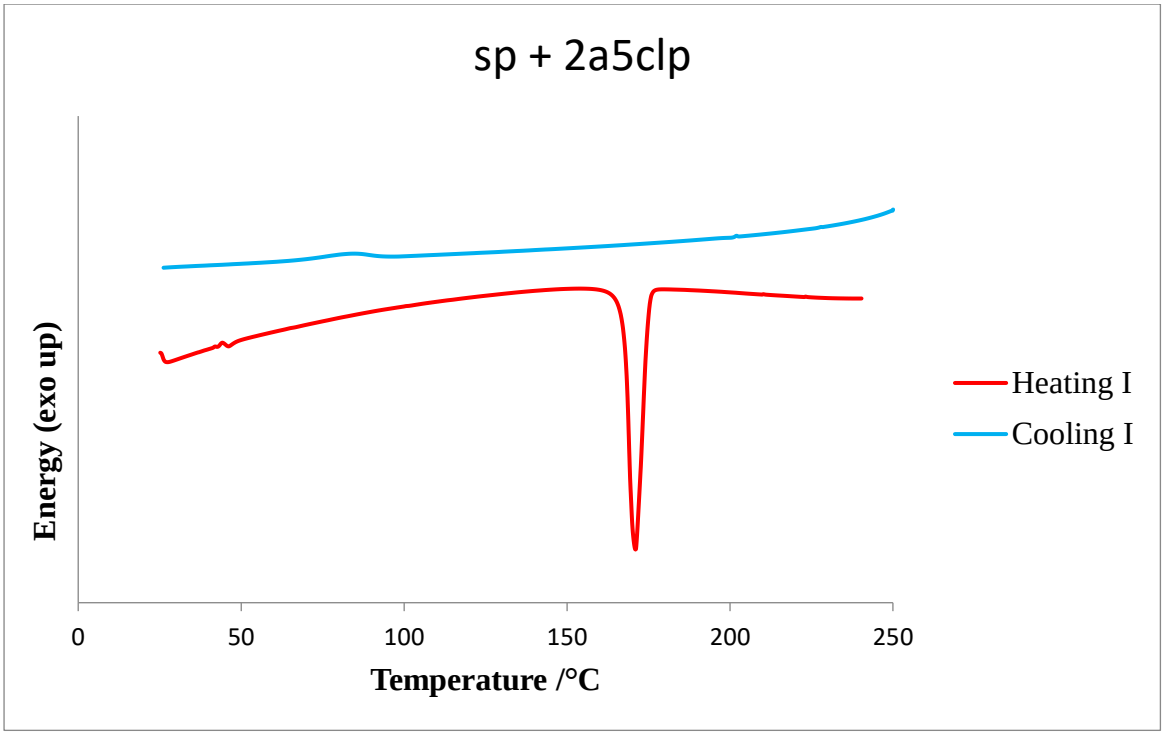


Figure S3.11 DSC curve for **sp + 2a5clp**

4. TGA Curves

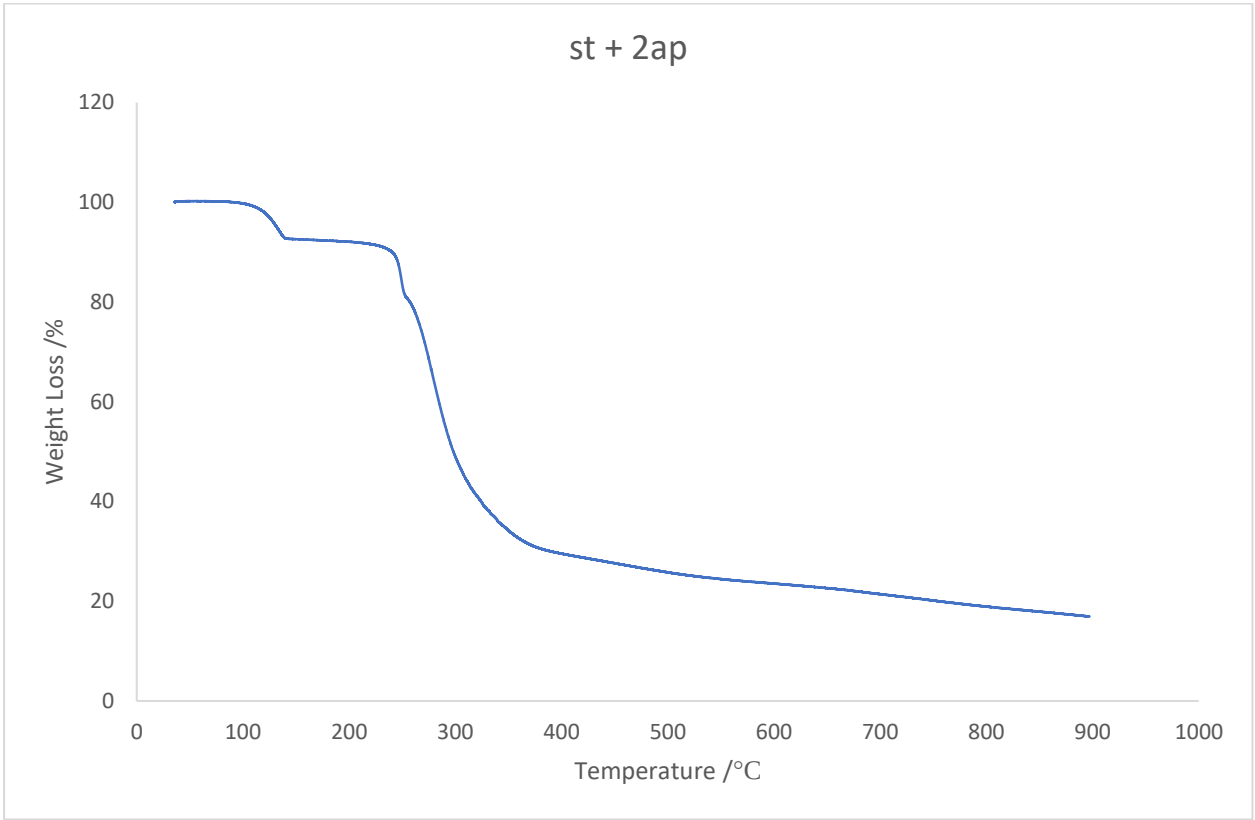


Figure S4.1 TGA curve of **st + 2ap**.

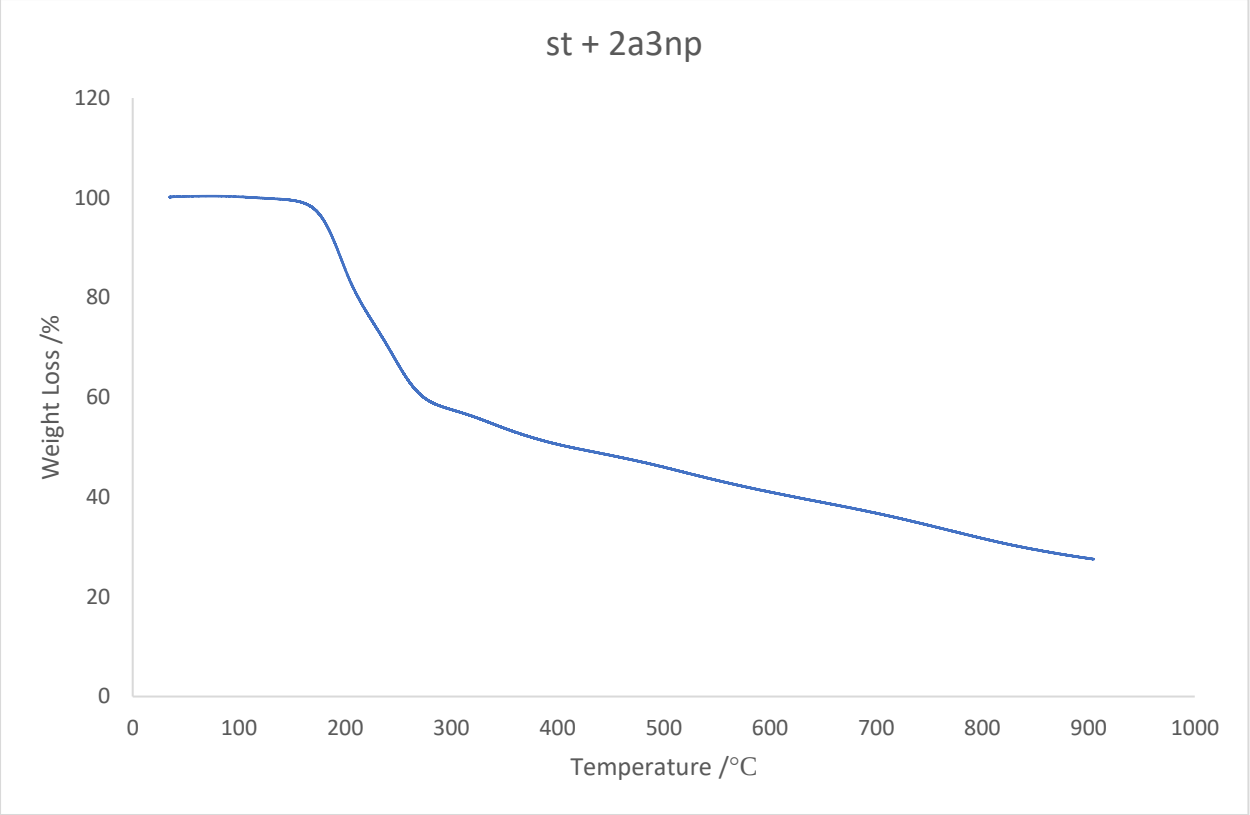


Figure S4.2 TGA curve of **st + 2a3np**.

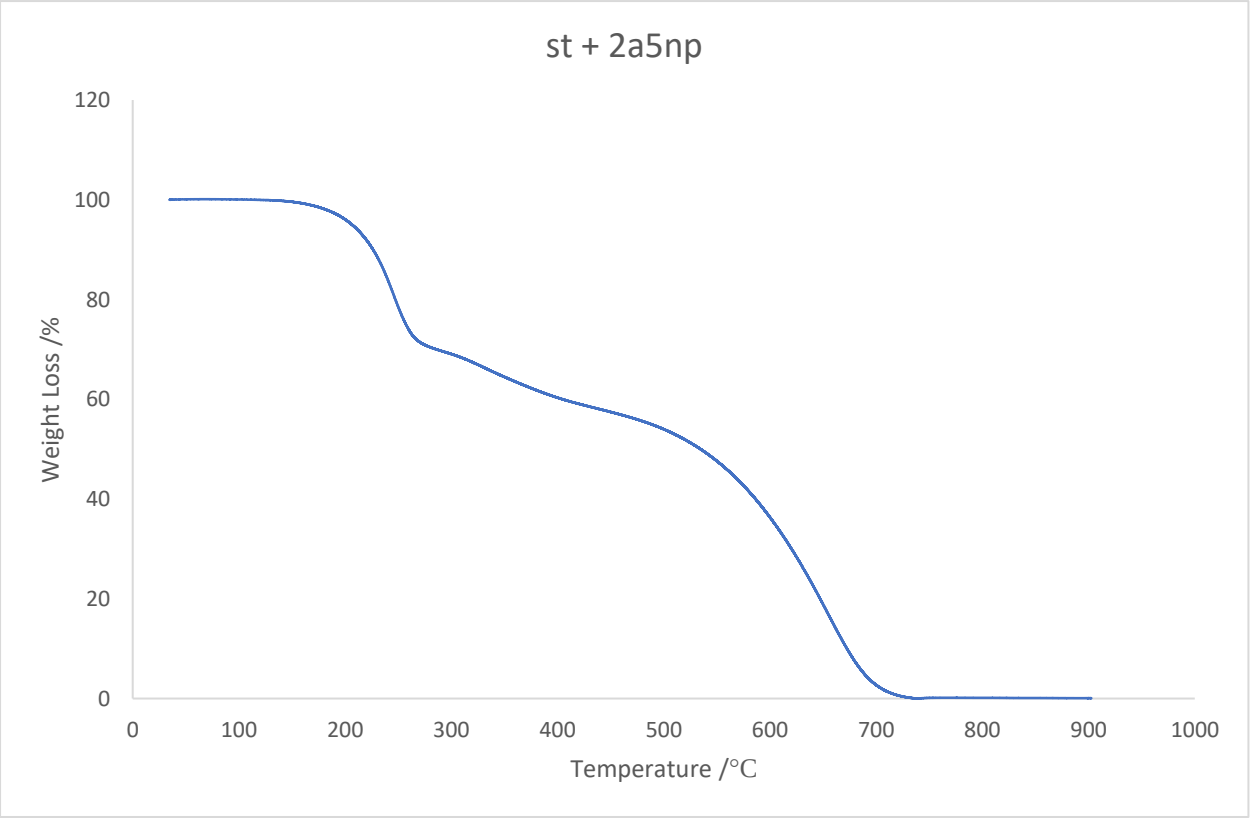


Figure S4.3 TGA curve of **st + 2a5np**.

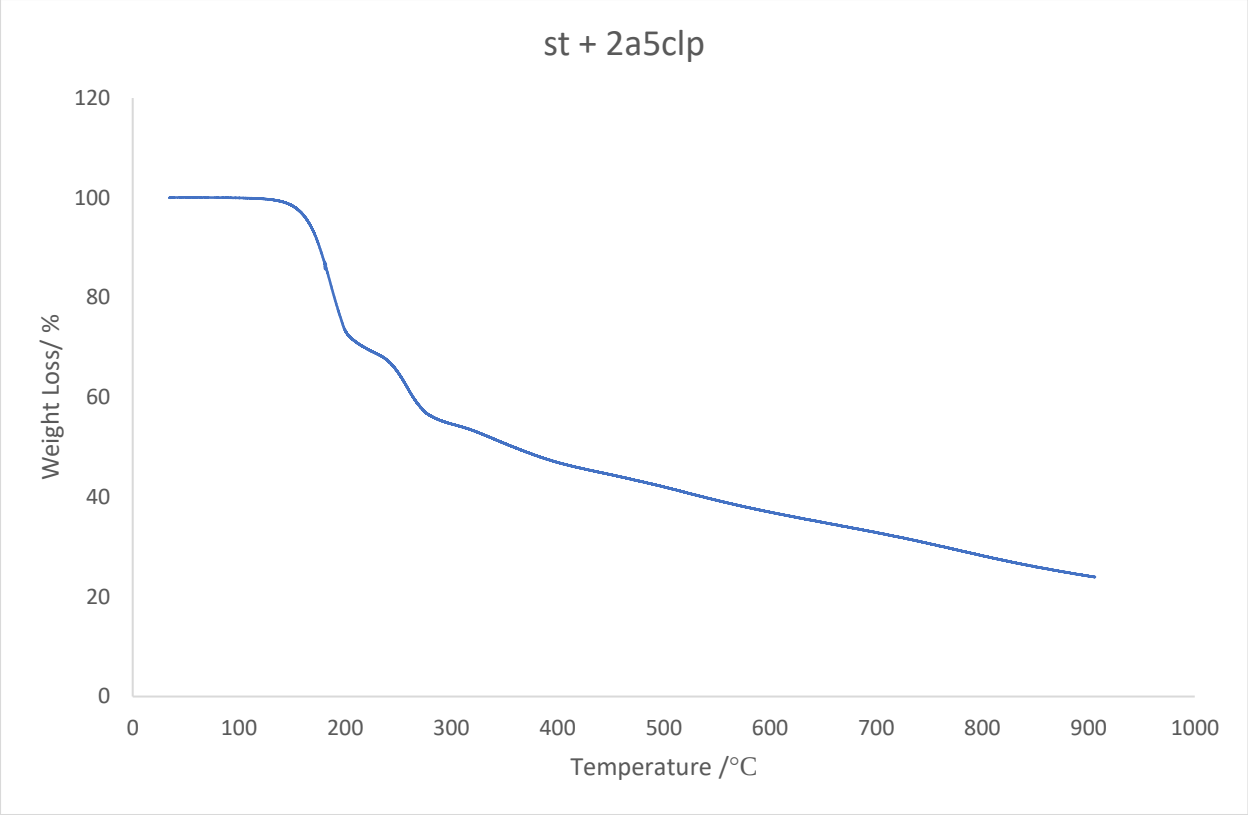


Figure S4.4 TGA curve of **st + 2a5clp**.

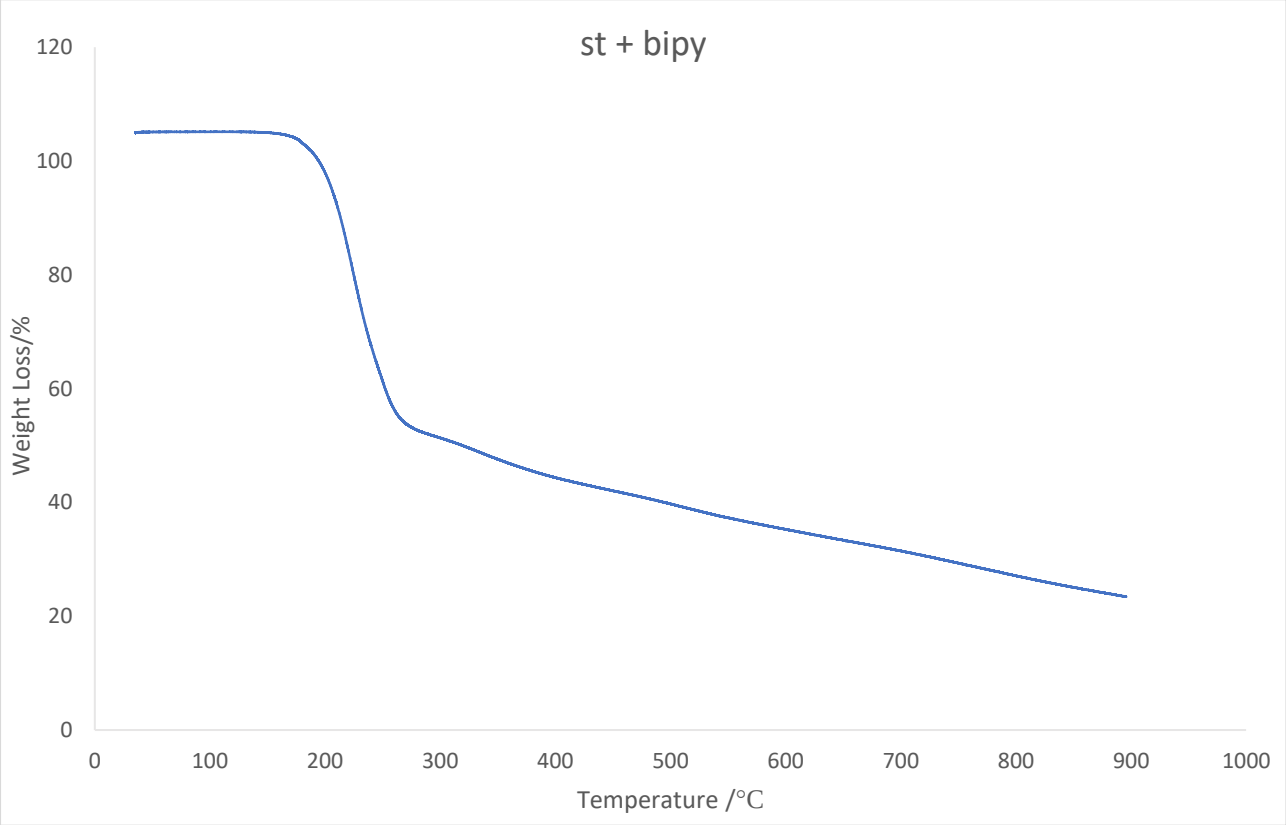


Figure S4.5 TGA curve of **st + bipy**.

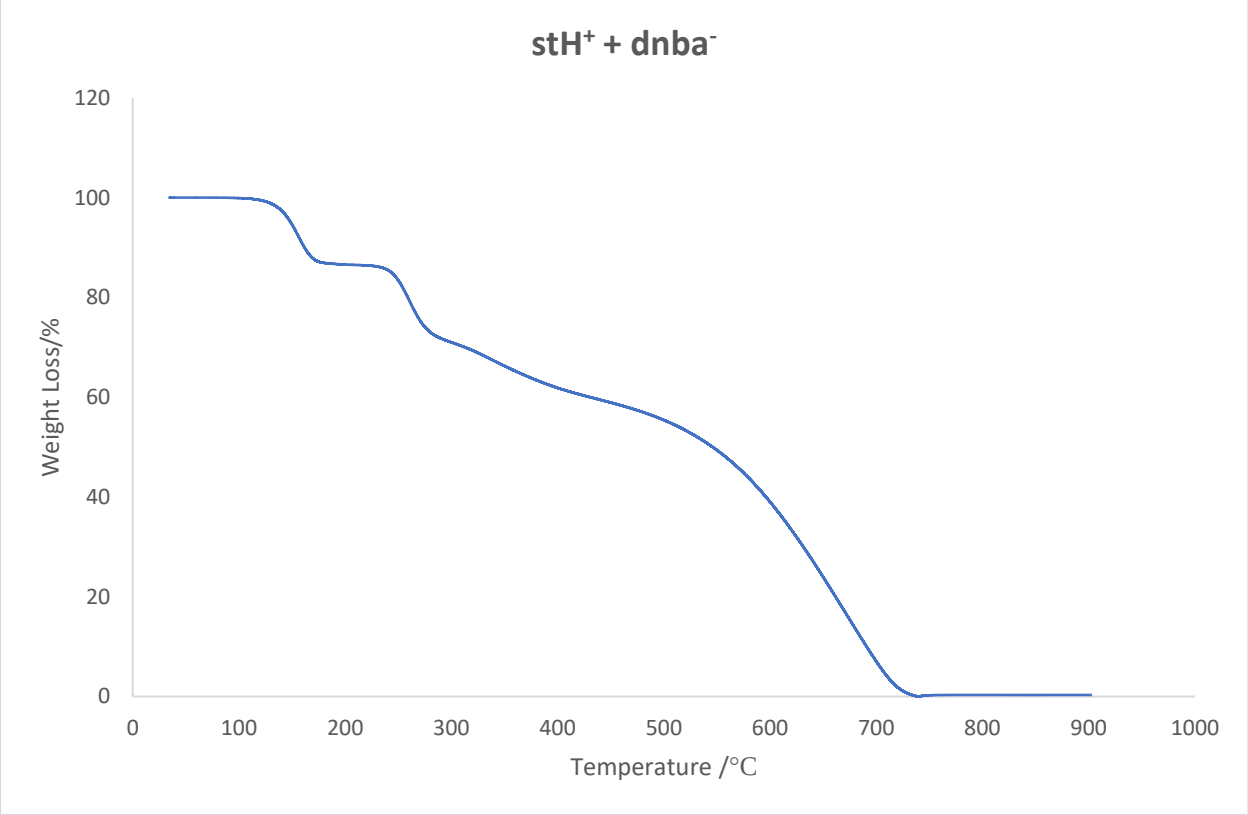


Figure S4.6 TGA curve of **stH$^+$ + dnba$^-$**.

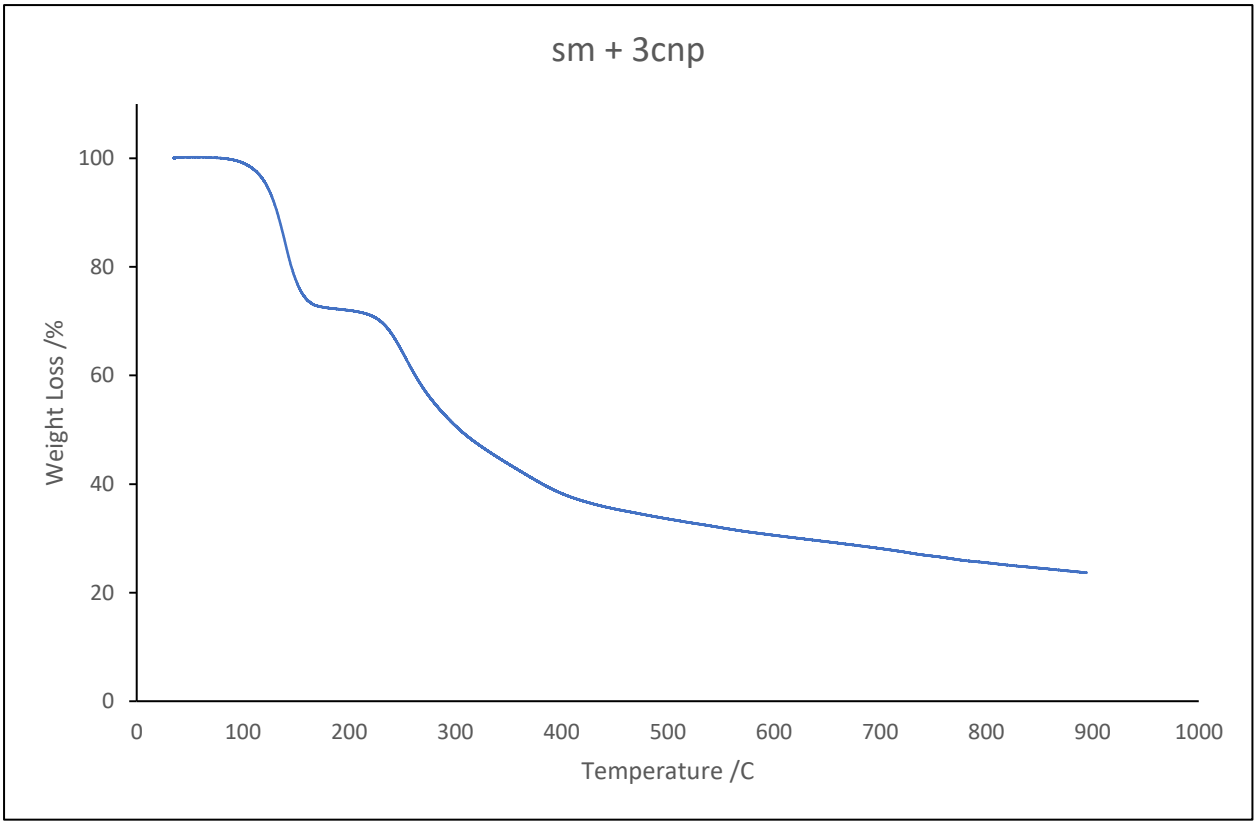


Figure S4.7 TGA curve of **sm + 3cnp**.

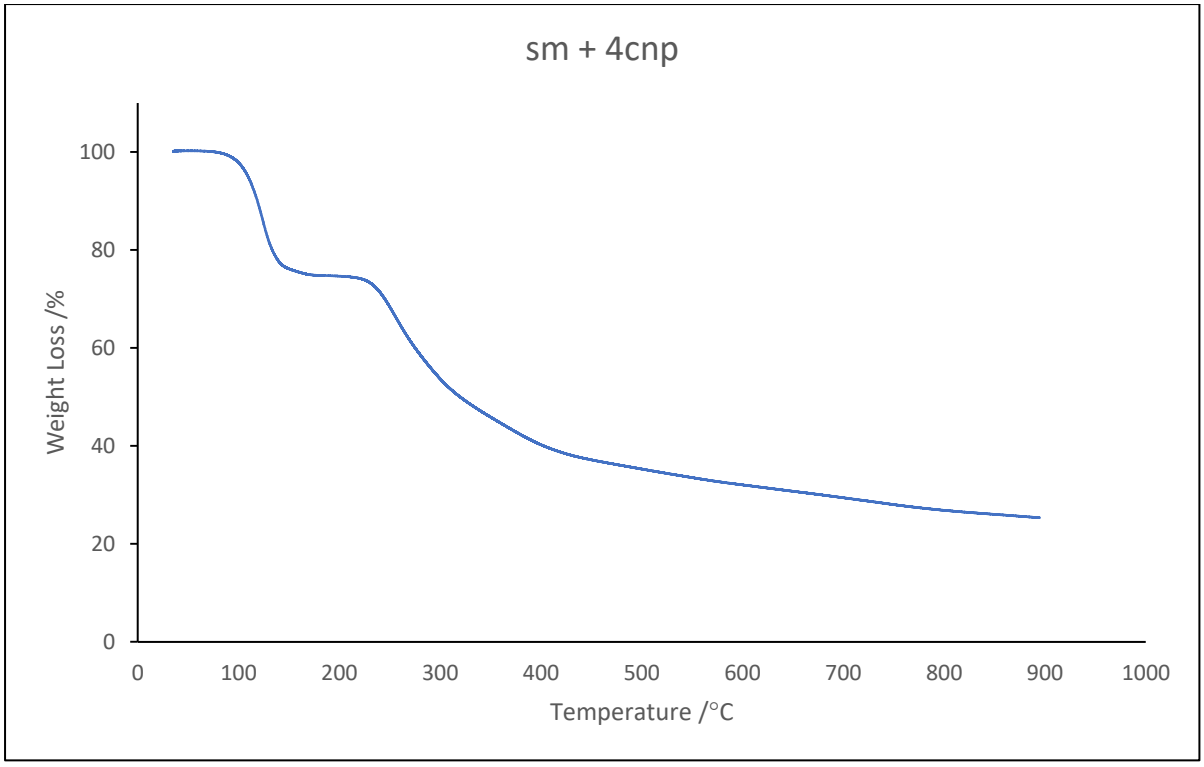


Figure S4.8 TGA curve of **sm + 4cnp**.

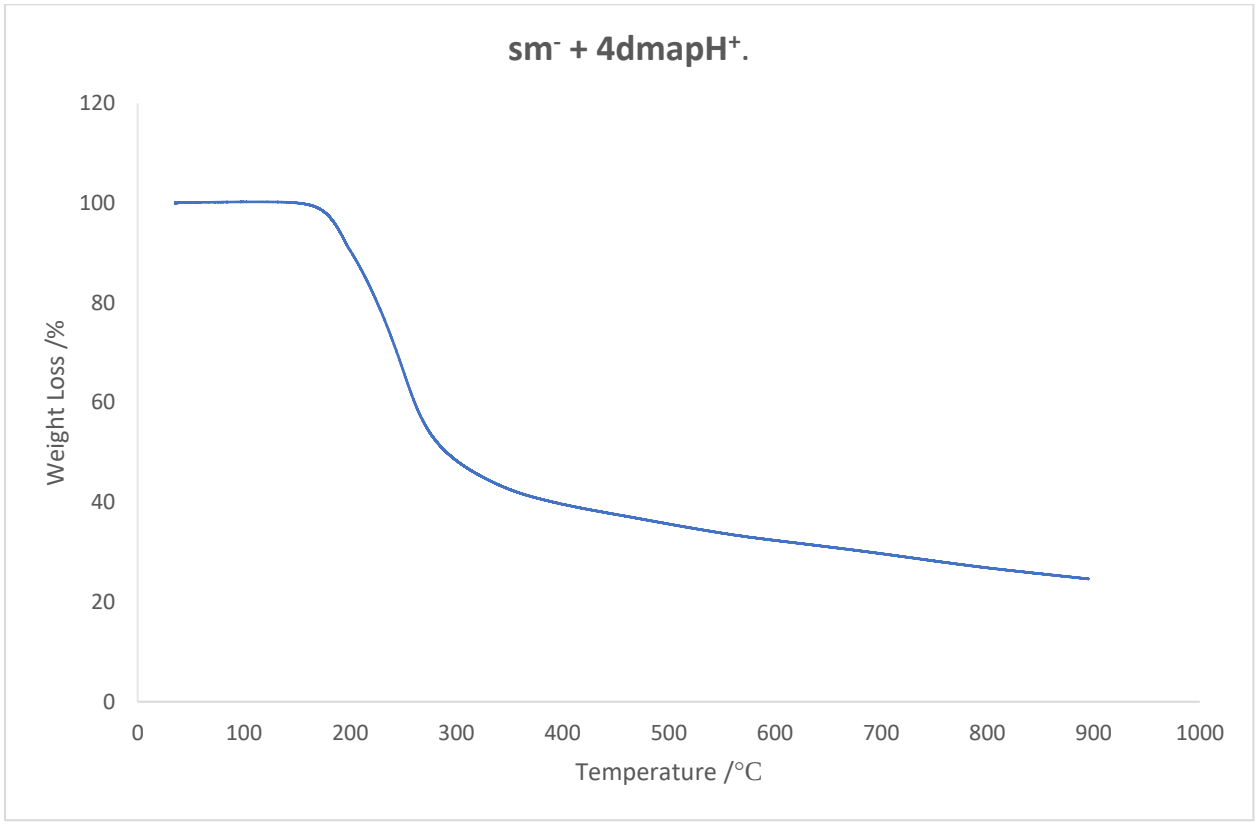


Figure S4.9 TGA curve of **sm⁻ + 4dmapH⁺**.

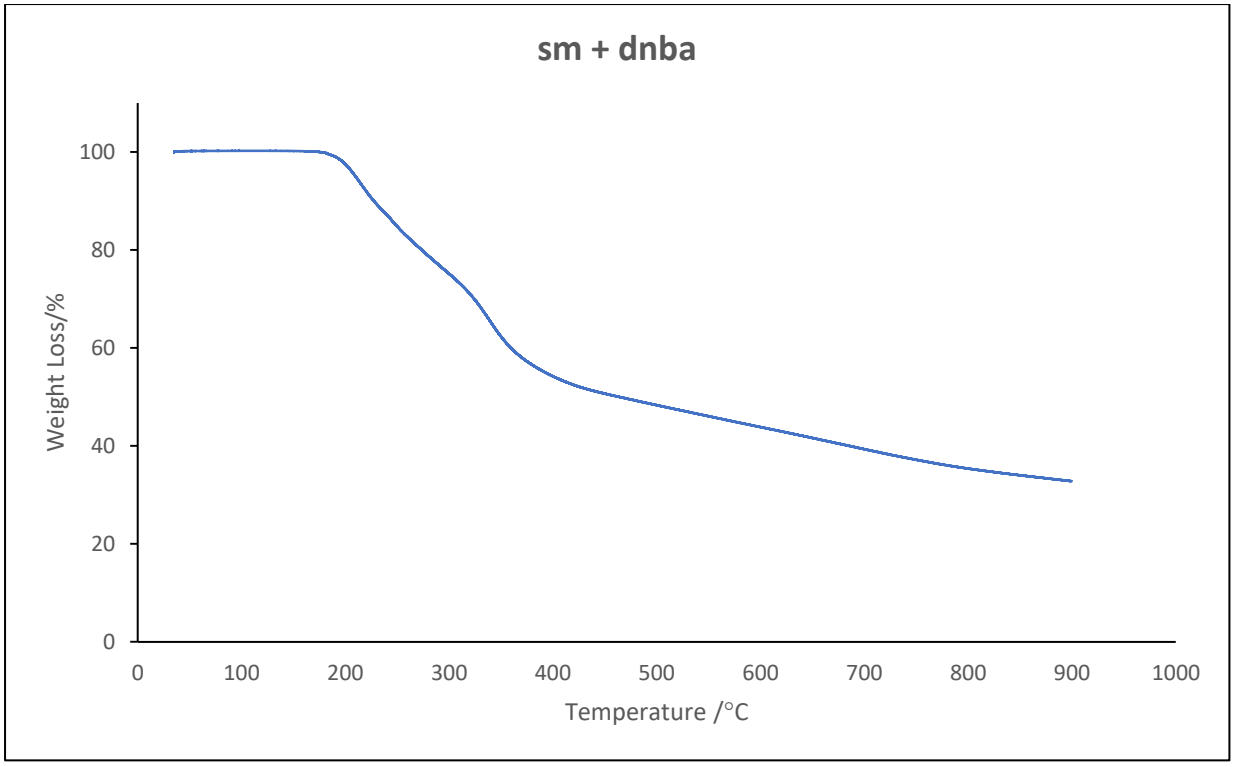


Figure S4.10 TGA curve of **sm + dnba**.

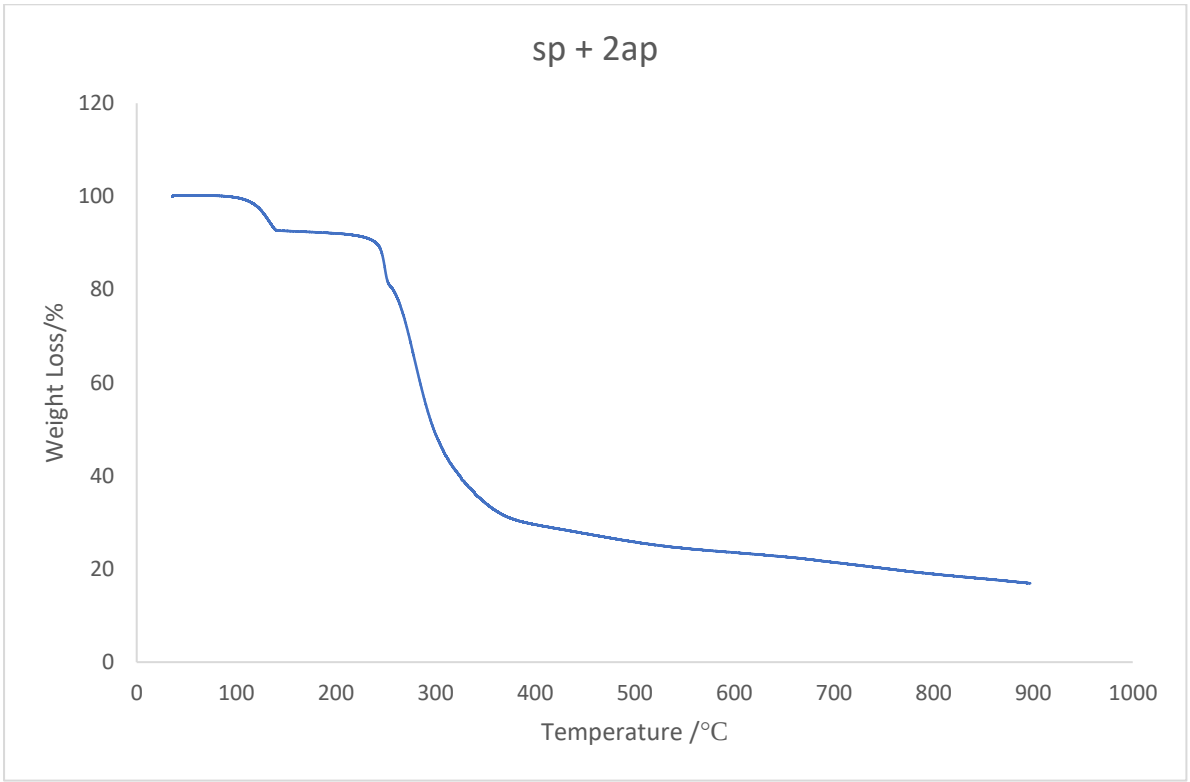


Figure S4.11 TGA curve of **sp + 2ap.**

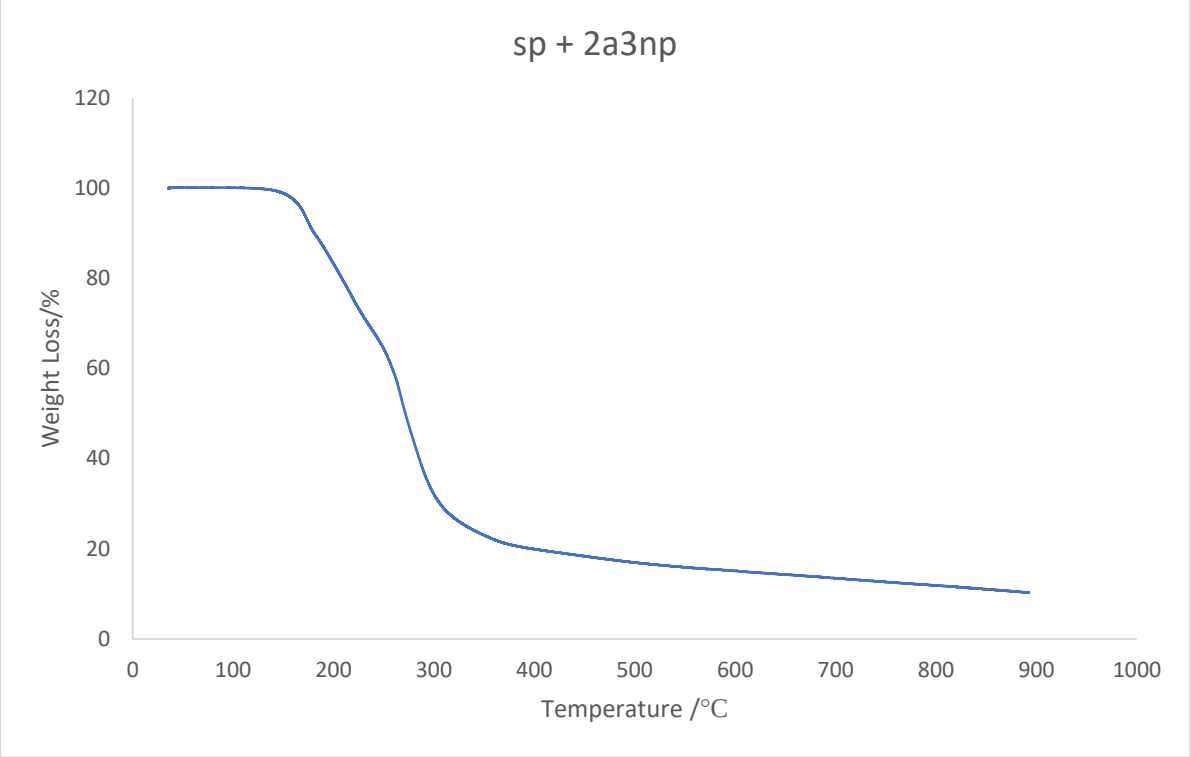


Figure S4.12 TGA curve of **sp + 2a3np.**

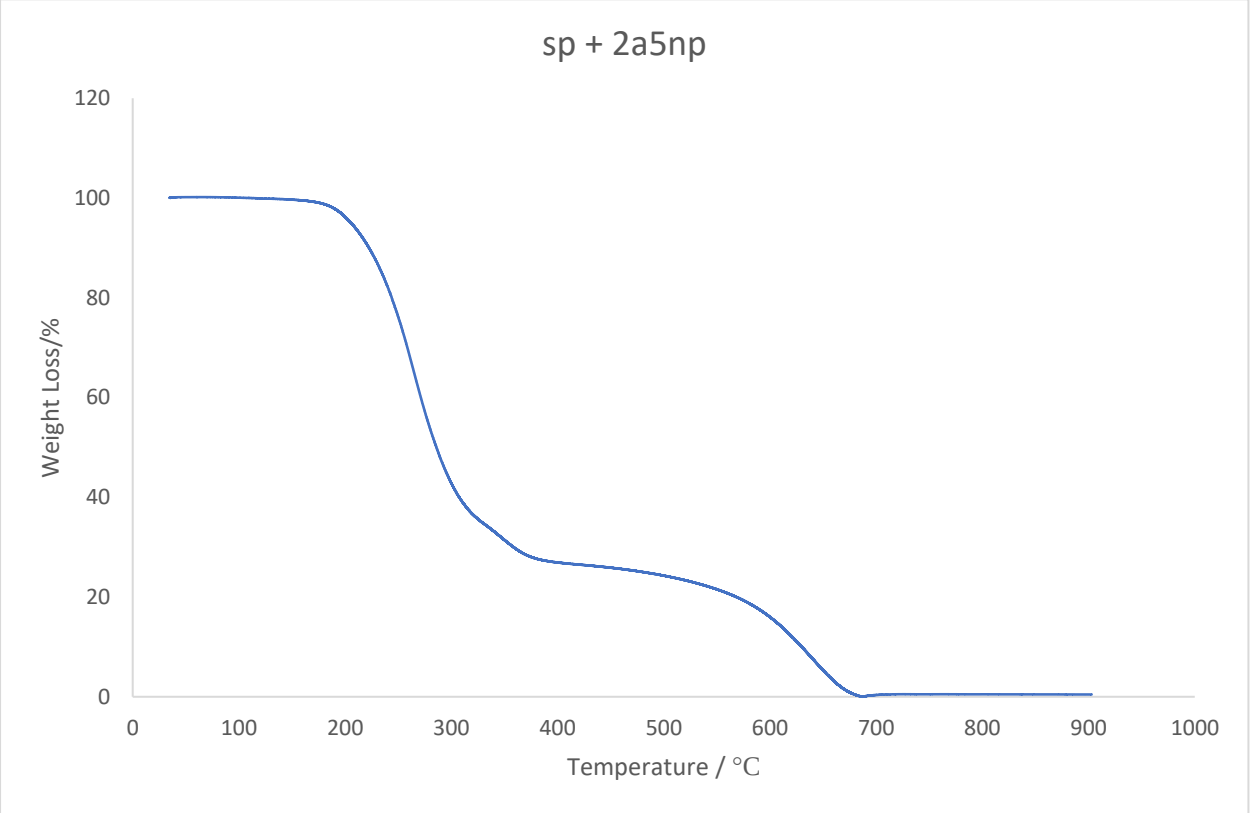


Figure S4.13 TGA curve of **sp + 2a5np.**

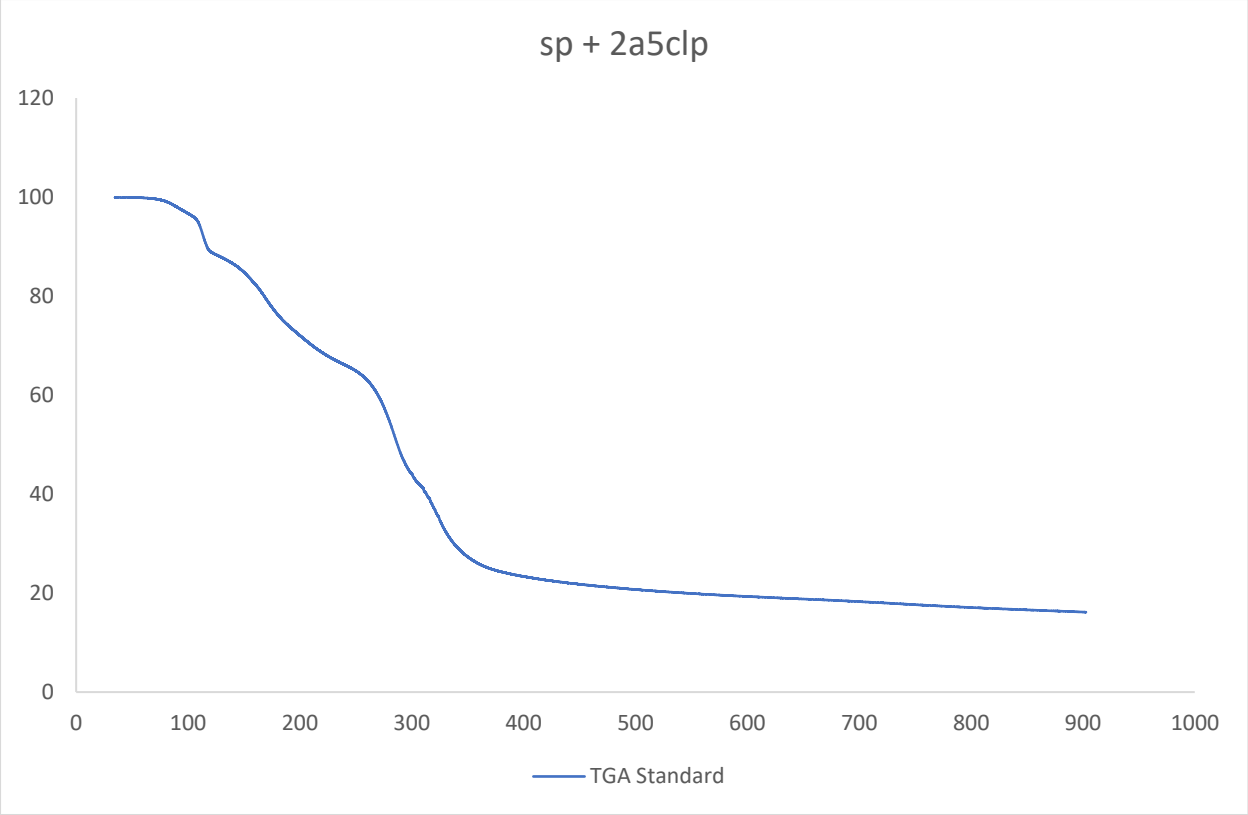


Figure S4.14 TGA curve of **sp + 2a5clp.**

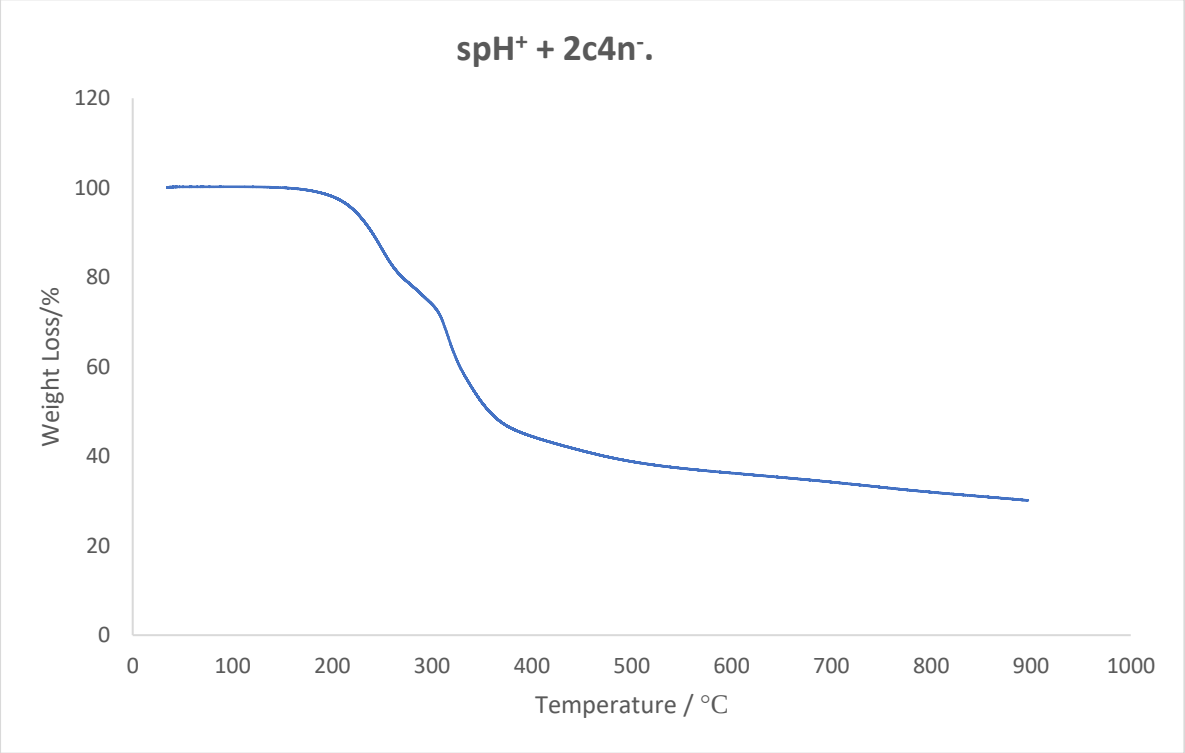


Figure S4.15 TGA curve of **spH$^+$ + 2c4n$^-$.**

5. FTIR Spectra

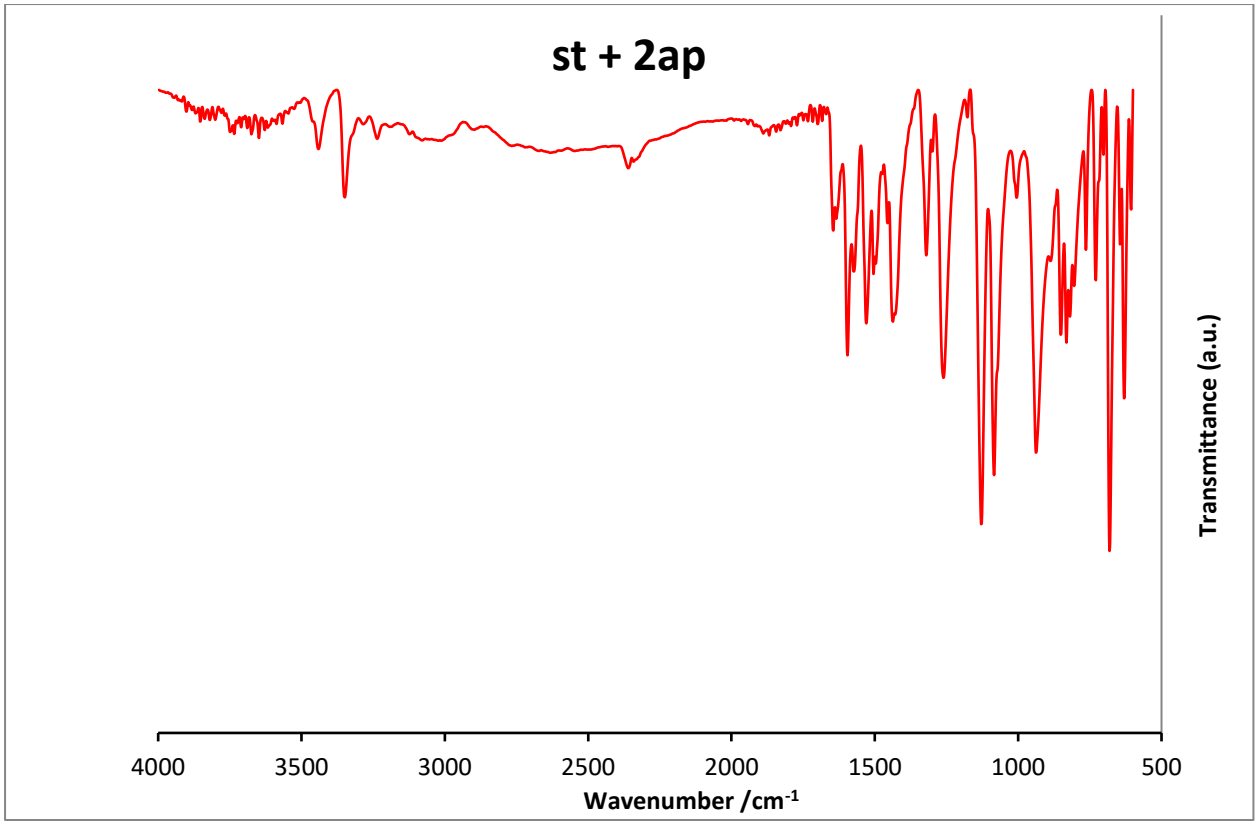


Figure S5.1 FTIR spectra of the cocrystal **st + 2ap**

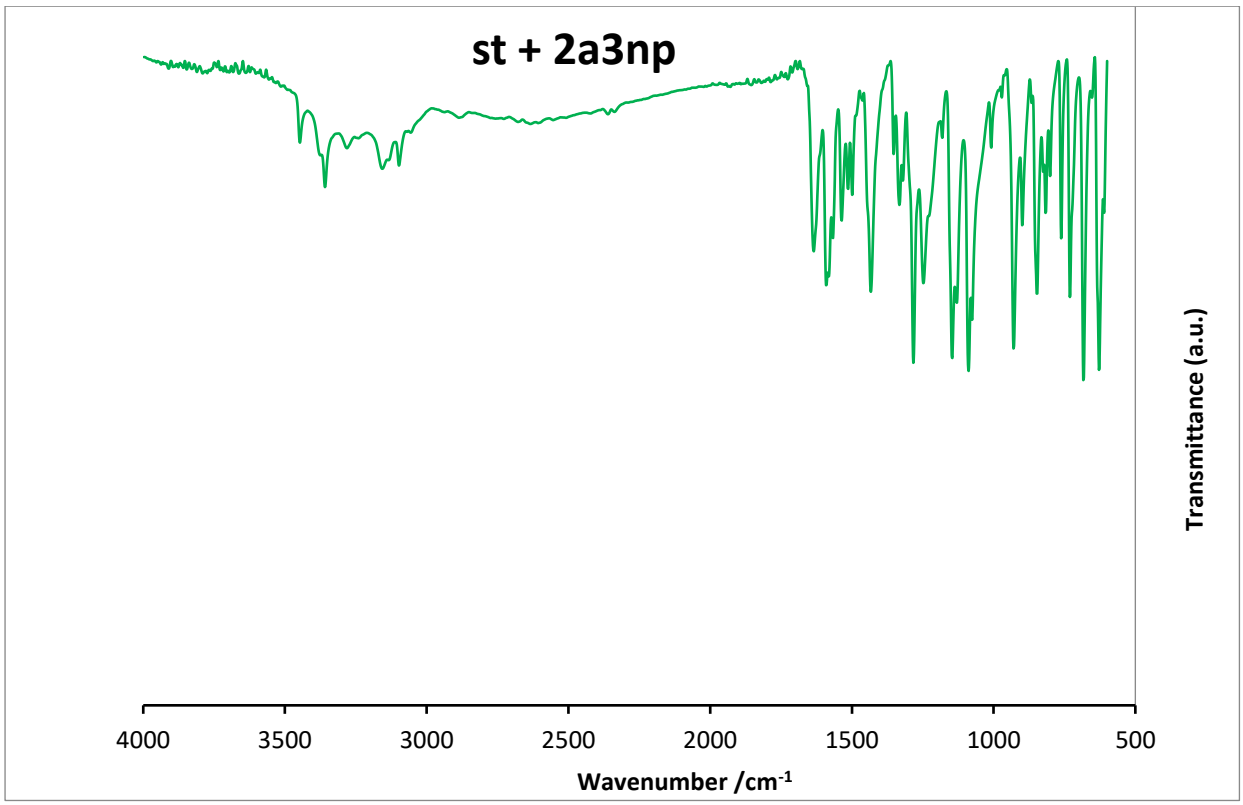


Figure S5.2 FTIR spectra of the cocrystal **st + 2a3np**

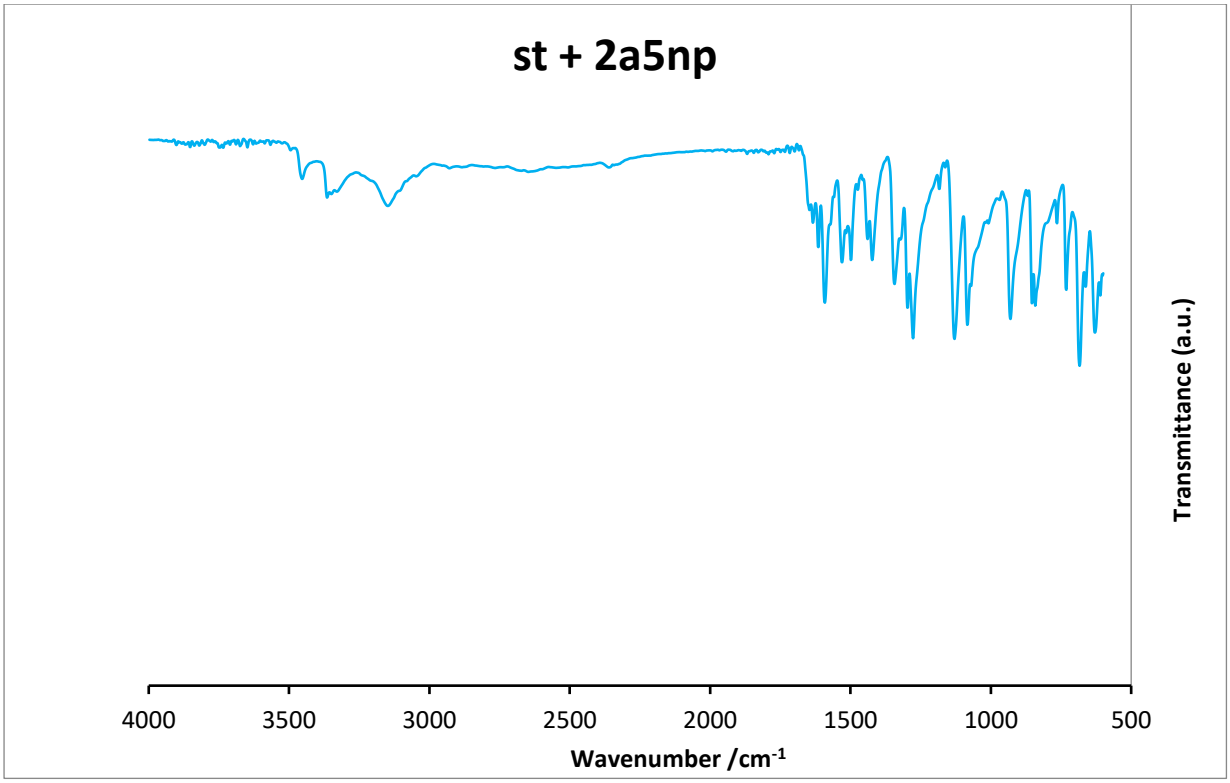


Figure S5.3 FTIR spectra of the cocrystal **st + 2a5np**

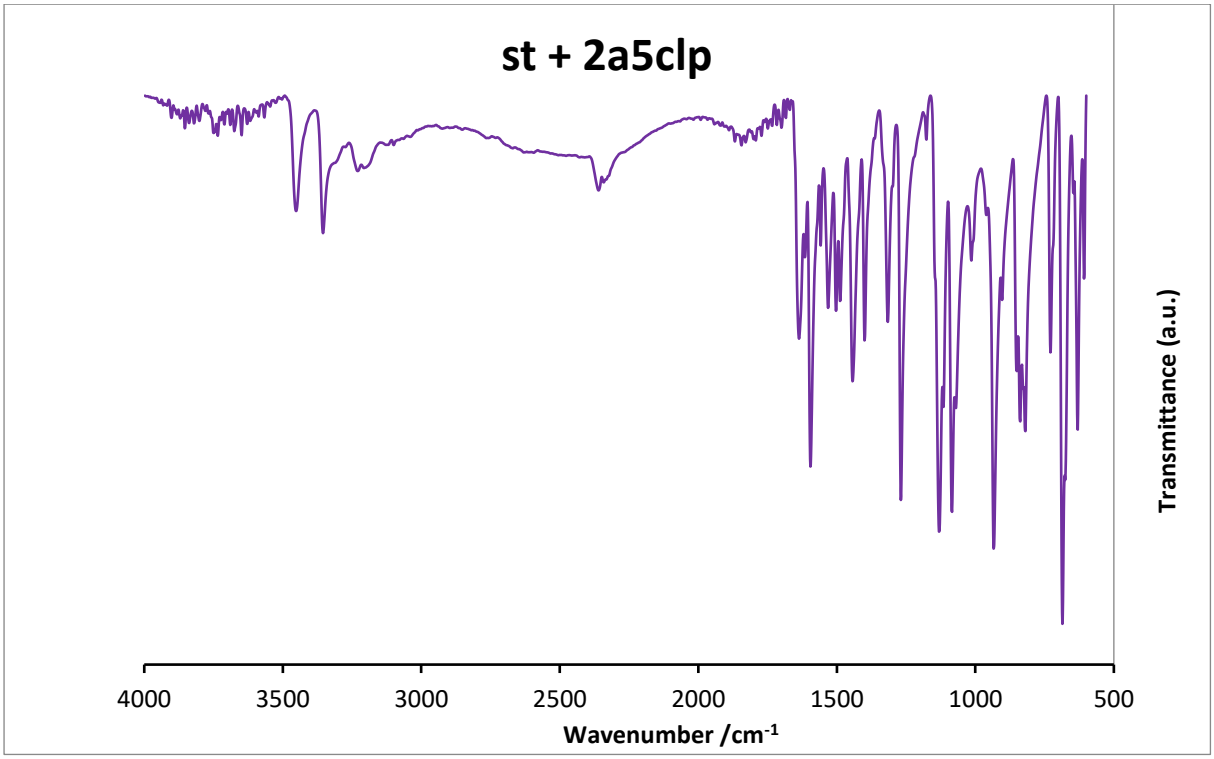


Figure S5.4 FTIR spectra of the cocrystal **st + 2a5clp**

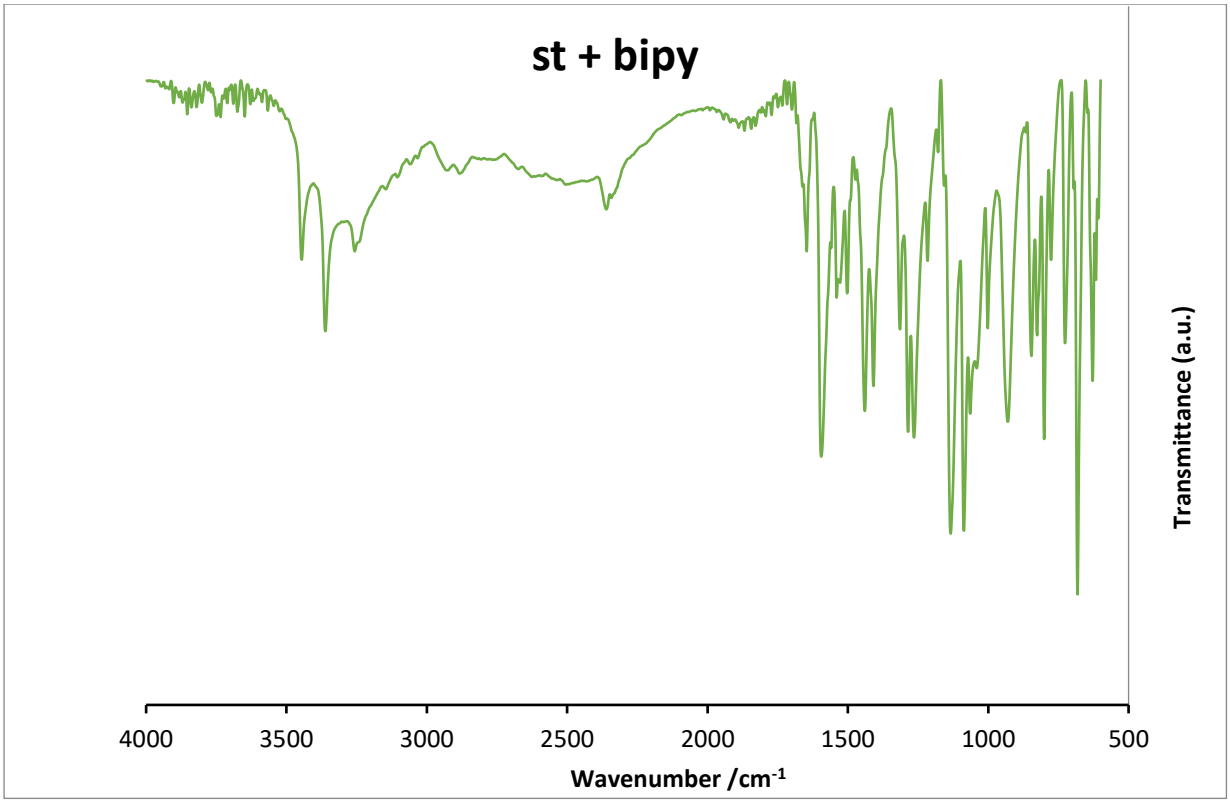


Figure S5.5 FTIR spectra of the cocrystal **st** + **bipy**

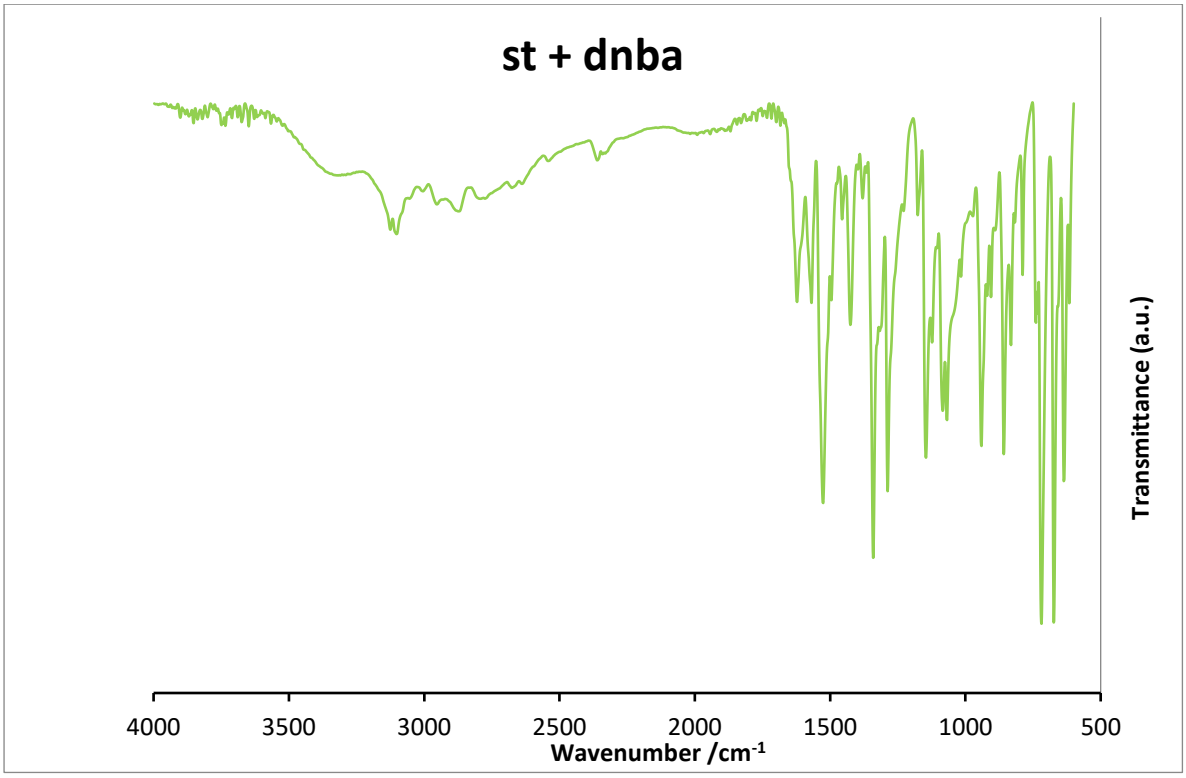


Figure S5.6 FTIR spectra of the cocrystal **stH**$^{+}$ + **dnba**$^{-}$

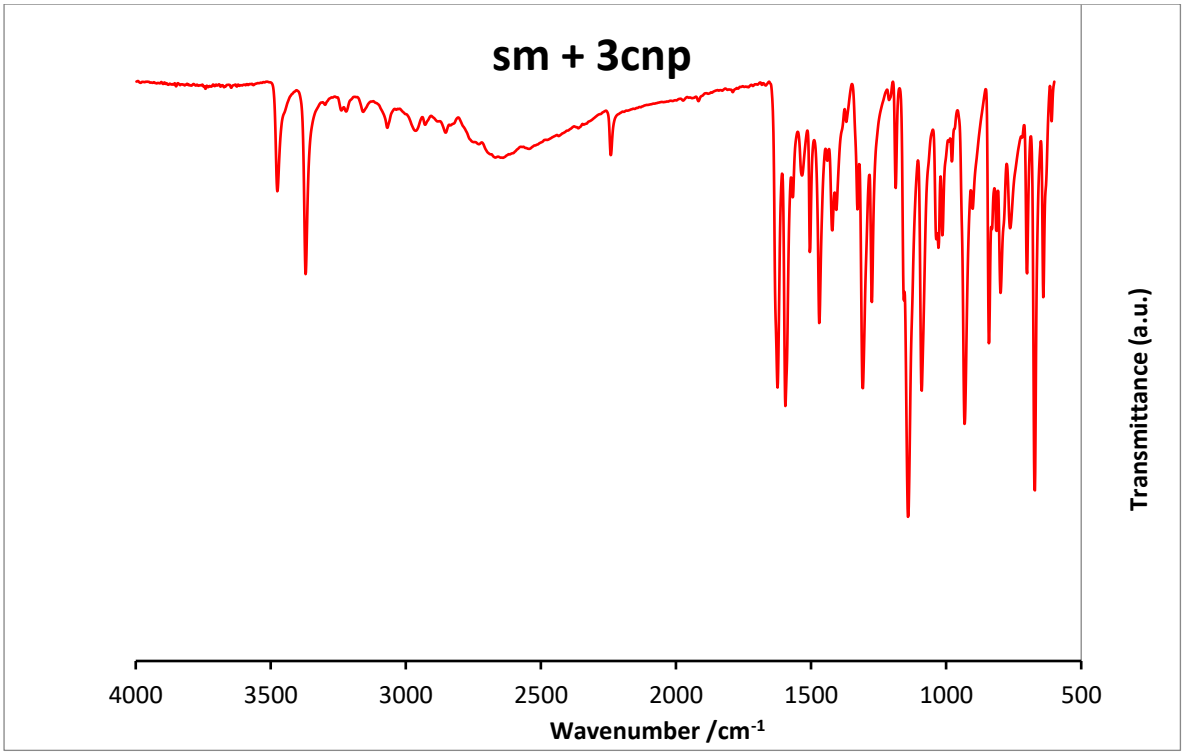


Figure S5.7 FTIR spectra of the cocrystal **sm** + **3cnp**

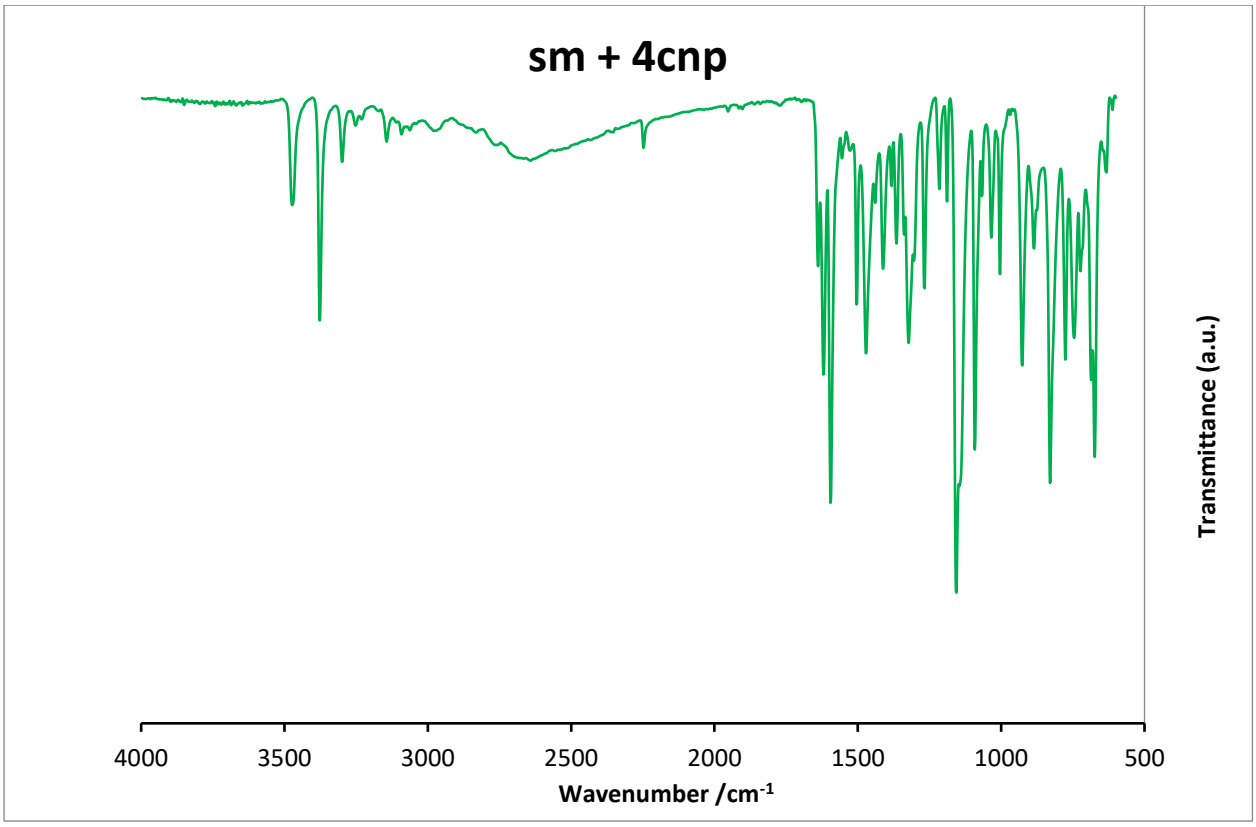


Figure S5.8 FTIR spectra of the cocrystal of **sm** + **4cnp**

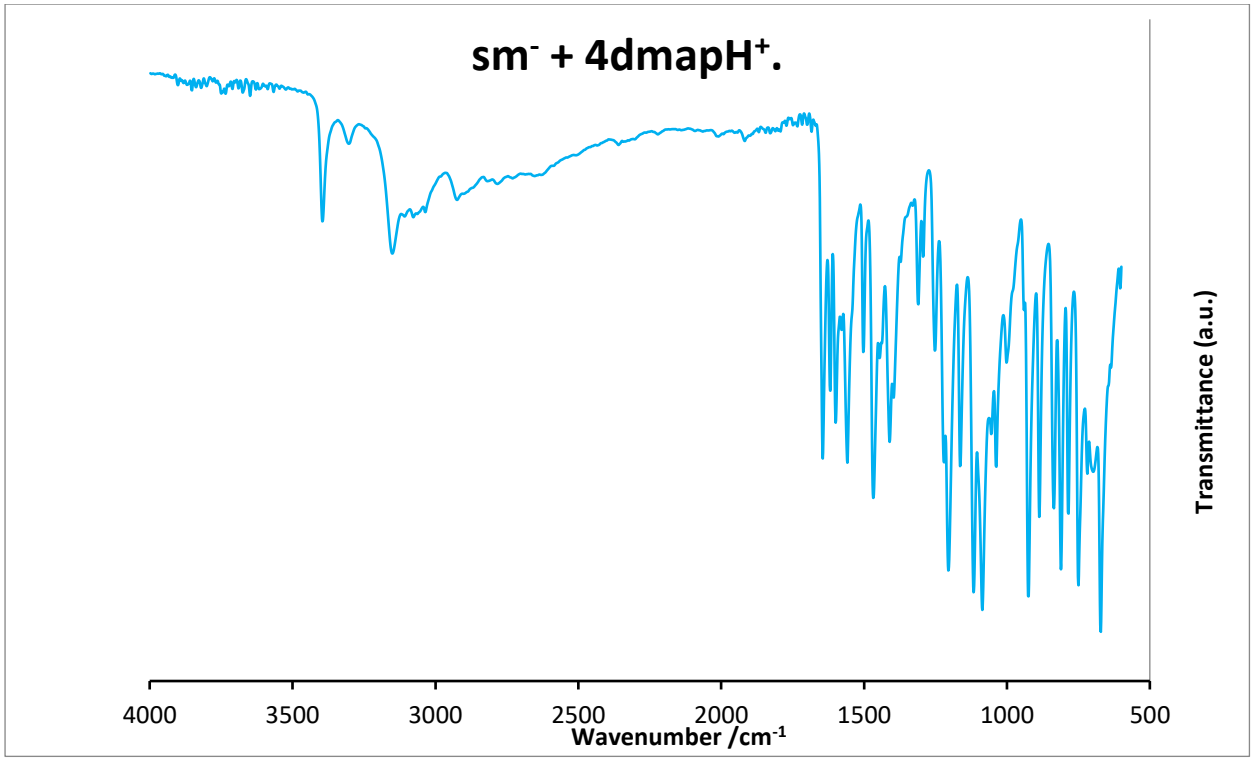


Figure S5.9 FTIR spectra of the molecular salt of **sm** + **dmap**

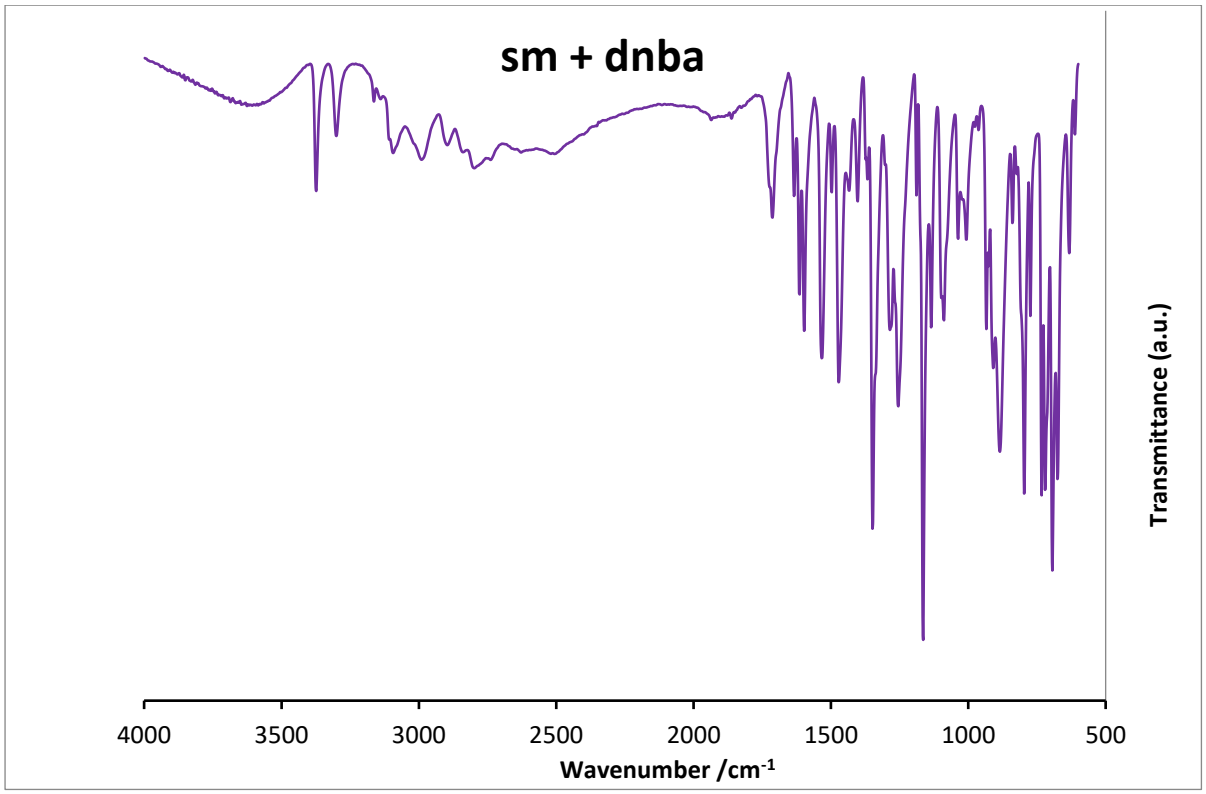


Figure S5.10 FTIR spectra of the cocrystal of **sm** + **dnba**

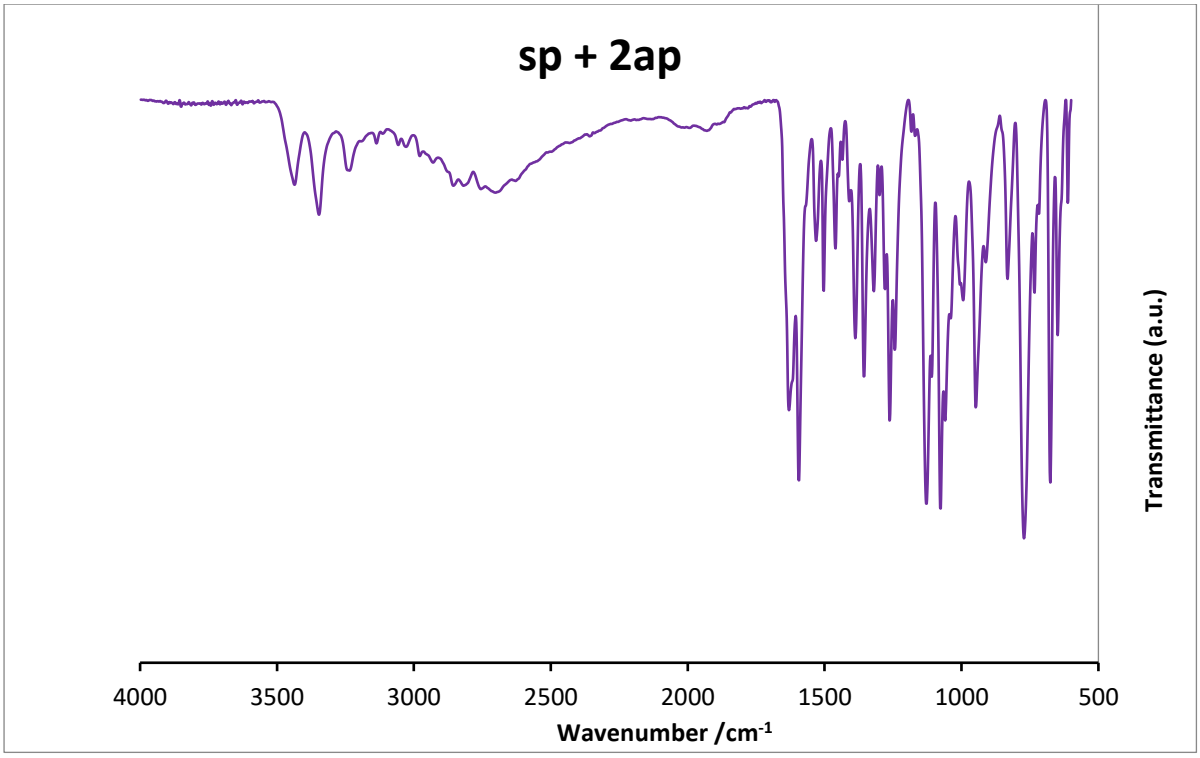


Figure S5.11 FTIR spectra of the cocrystal **sp + 2ap**

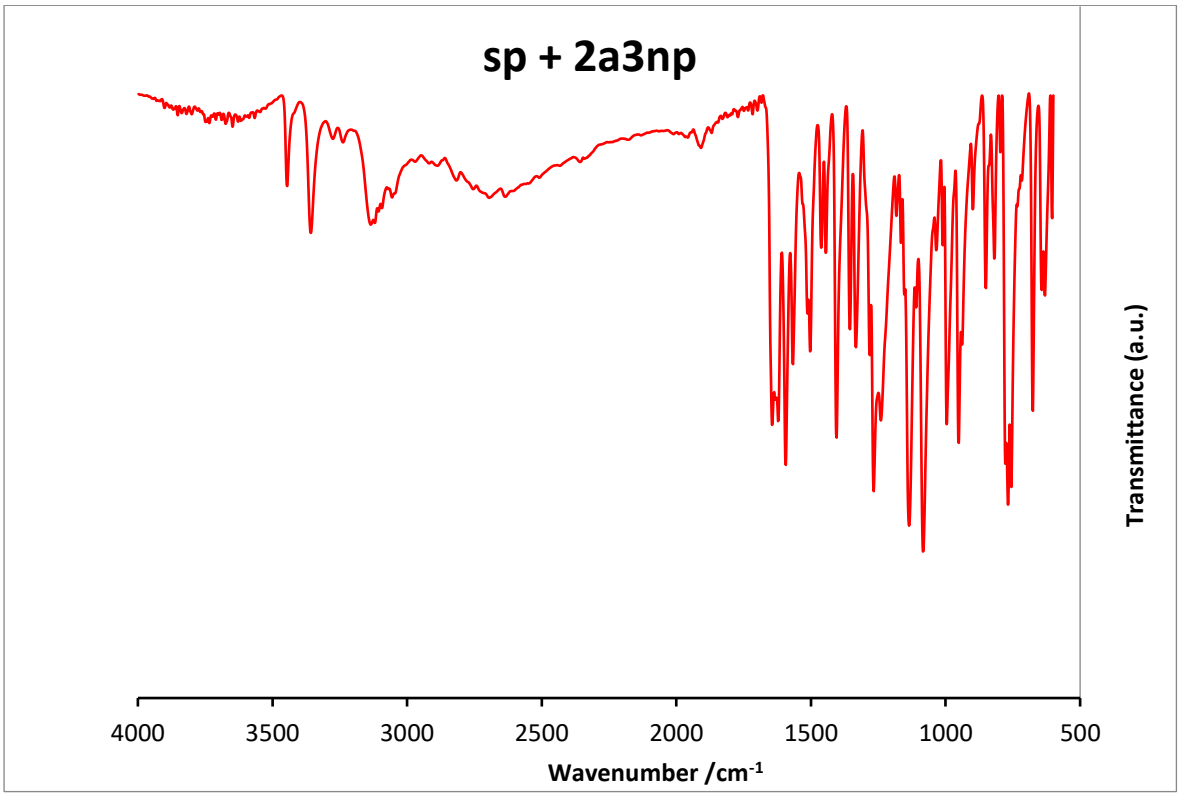


Figure S5.12 FTIR spectra of the cocrystal of **sp + 2a3np**

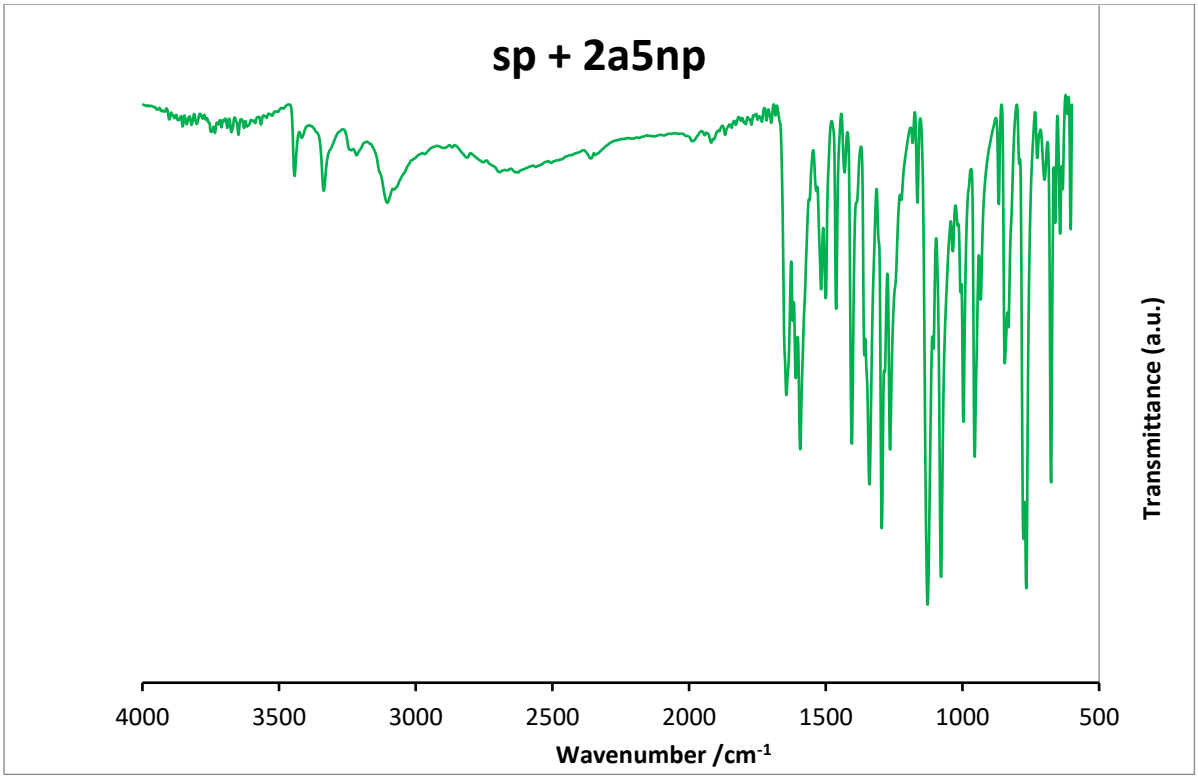


Figure S5.13 FTIR spectra of the cocrystal of **sp + 2a5np**

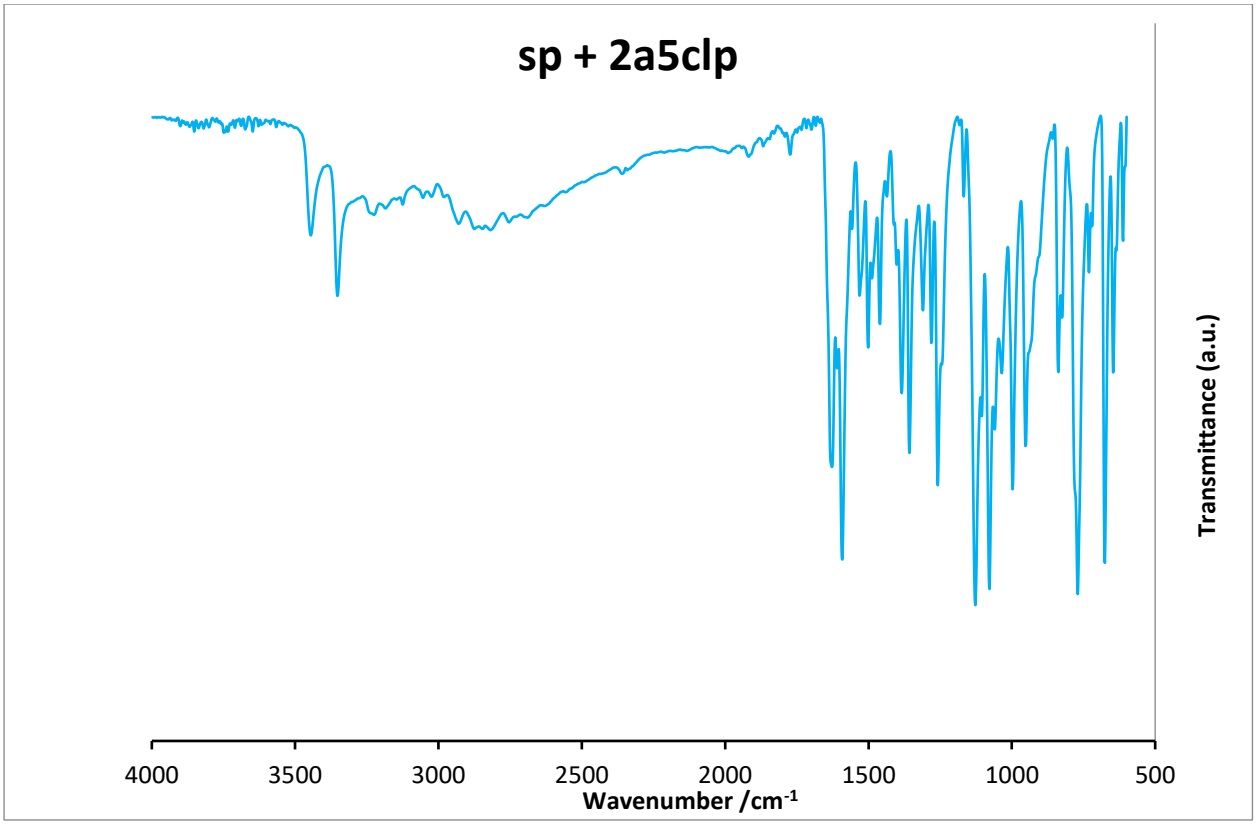


Figure S5.14 FTIR spectra of the cocrystal of **sp + 2a5clp**

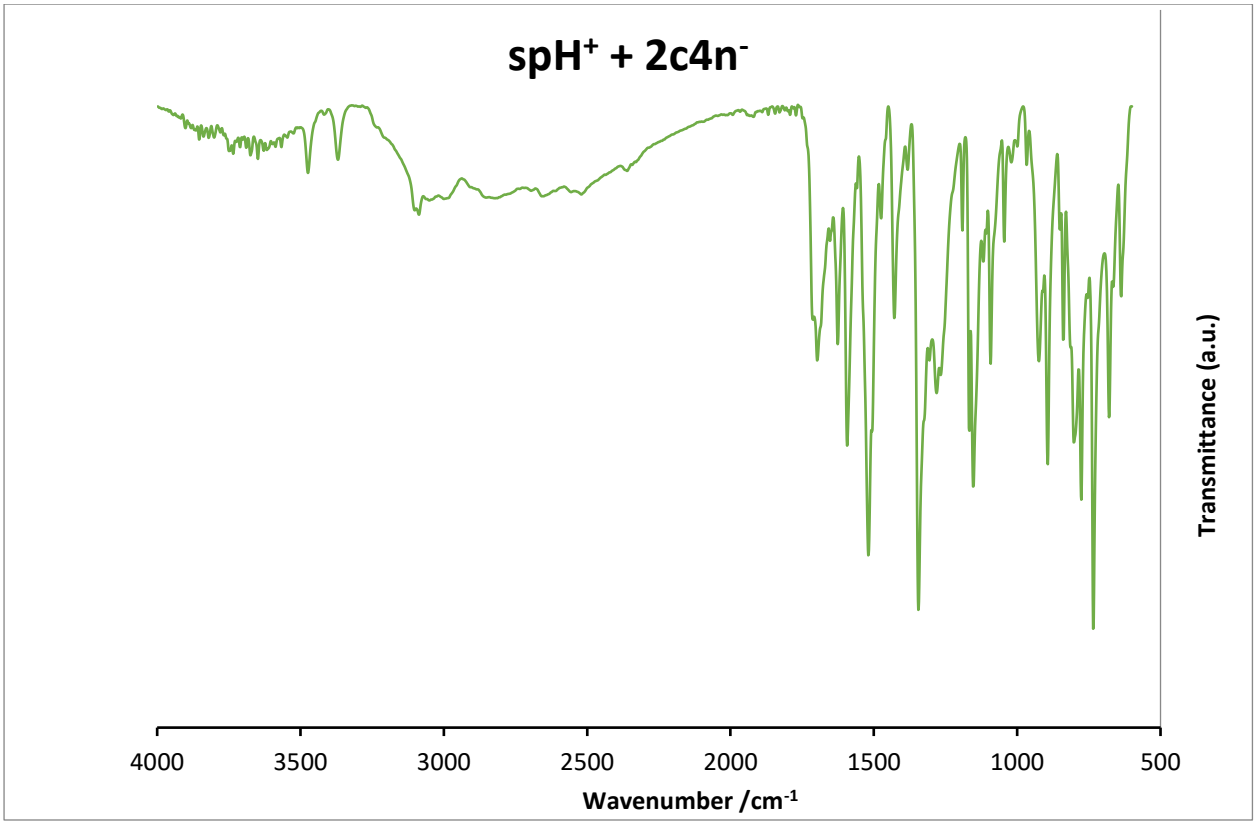


Figure S5.15 FTIR spectra of the molecular salt of **spH$^+$ + 2c4n$^-$**

Chapter 5

Supporting Information

Exploring the crystal structural landscape of 3,5-dinitrobenzoic acid through various multi-component molecular complexes

Matthew C. Scheepers and Andreas Lemmerer*[‡]

[‡]*Molecular Sciences Institute, School of Chemistry, University of the Witwatersrand, 2050, Johannesburg, South Africa*

To whom correspondence should be addressed:

Prof. Andreas Lemmerer, Molecular Sciences Institute, School of Chemistry, University of the Witwatersrand, Private Bag 3, 2050, Johannesburg, South Africa.

E-mail: andreas.lemmerer@wits.ac.za. Fax: +27-11-717-6749. Tel: +27-11-717-6711.

Contents

1. Powder X-ray diffraction data
2. Differential Scanning Calorimetry Data
3. Hirshfeld surface diagrams and fingerplots

1. PXRD results

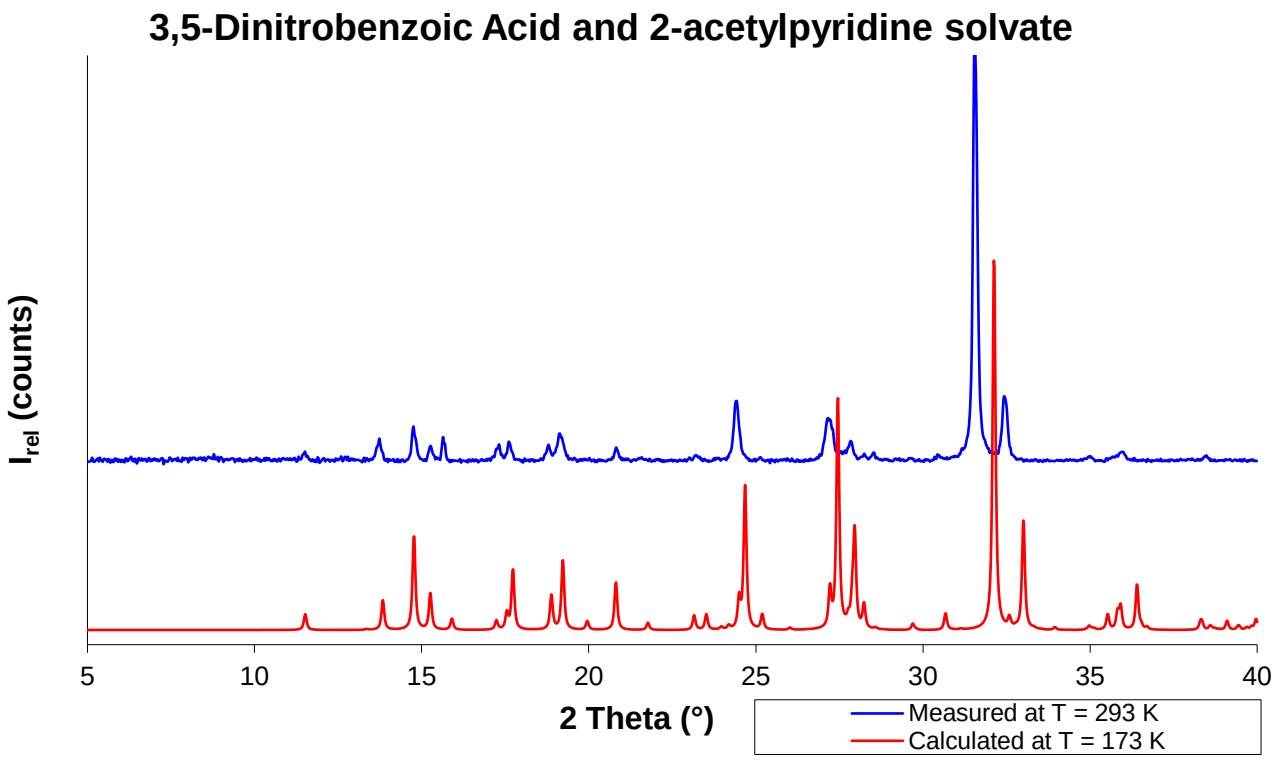


Figure A1 Calculated and measured PXRD Pattern for **dnba** + **2OAcp** solvate

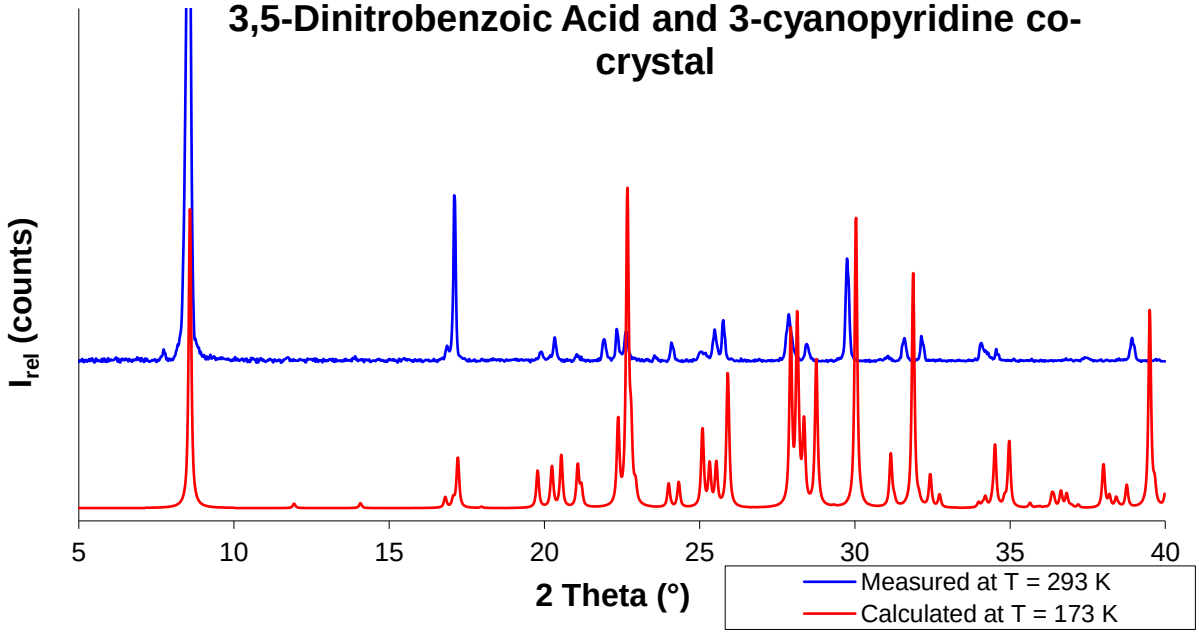


Figure A2 Calculated and measured PXRD Pattern for **dnba** + **3cnp** co-crystal

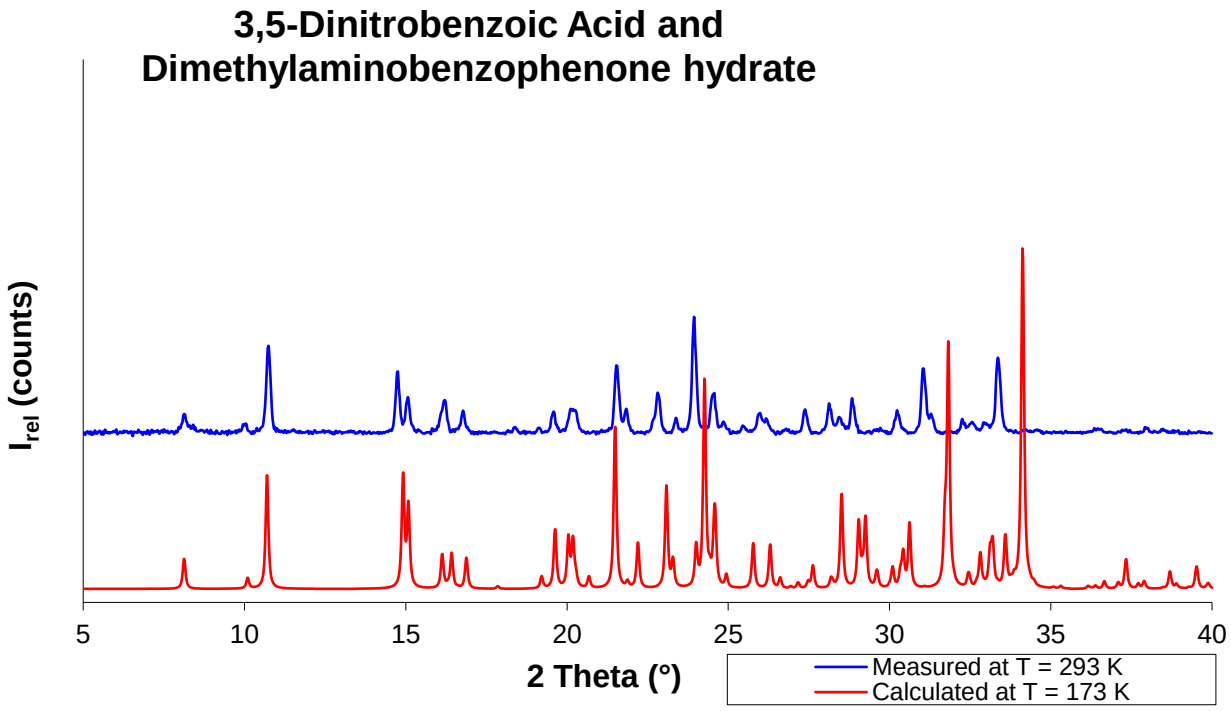


Figure A3 Calculated and measured PXRD Pattern for **dnba** + **dmabp** hydrate

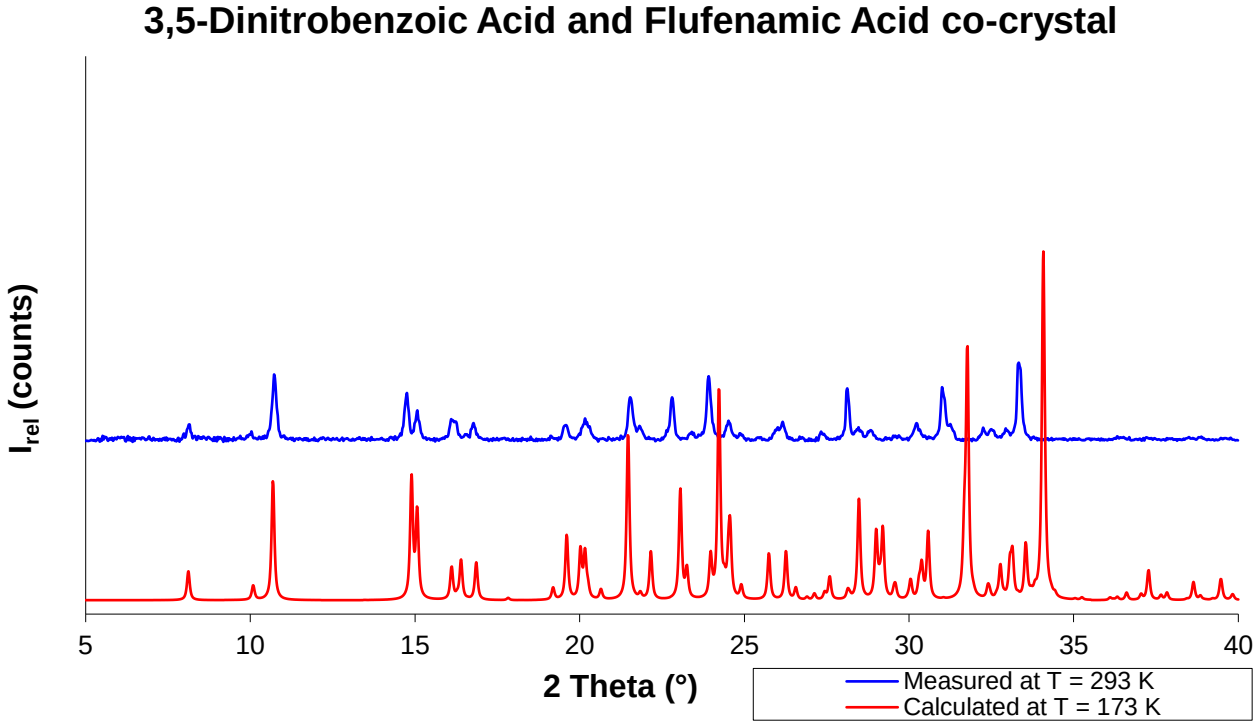


Figure A4 Calculated and measured PXRD Pattern for **dnba** + **fa** co-crystal

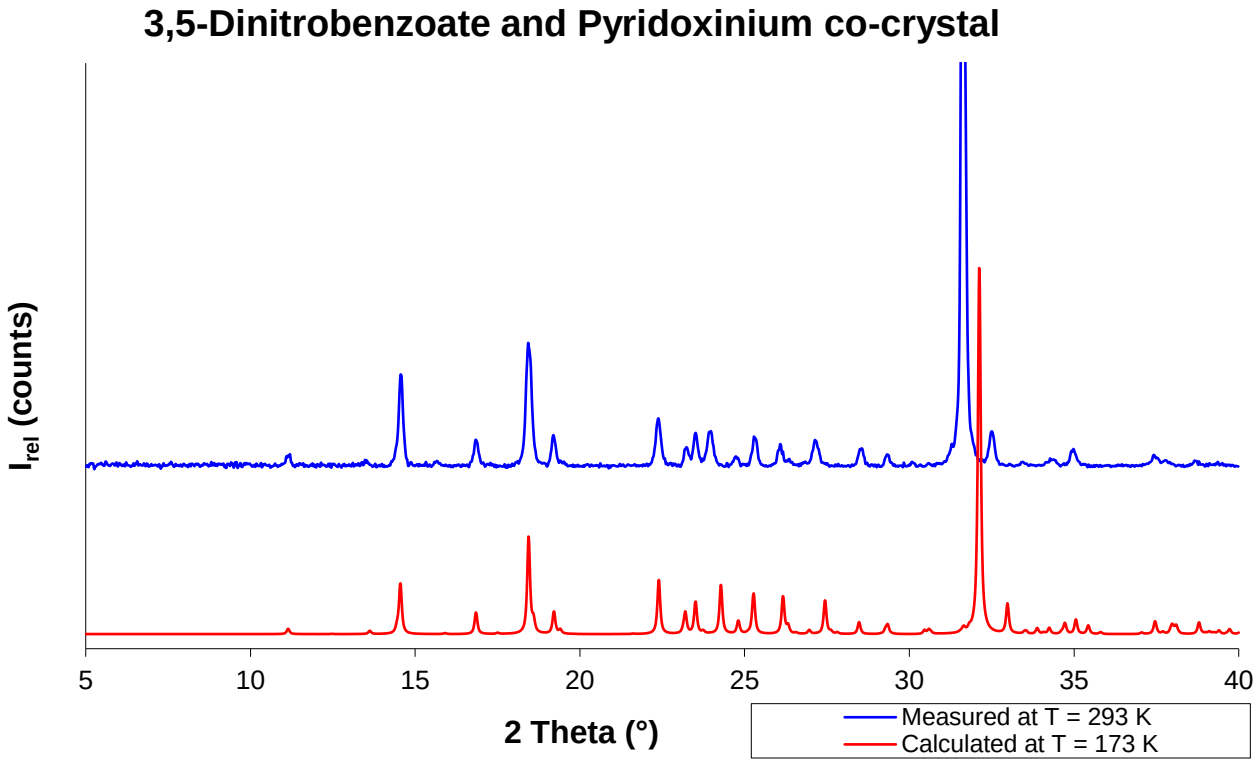


Figure A5 Calculated and measured PXRD Pattern for **dnba** + **pyd** molecular salt

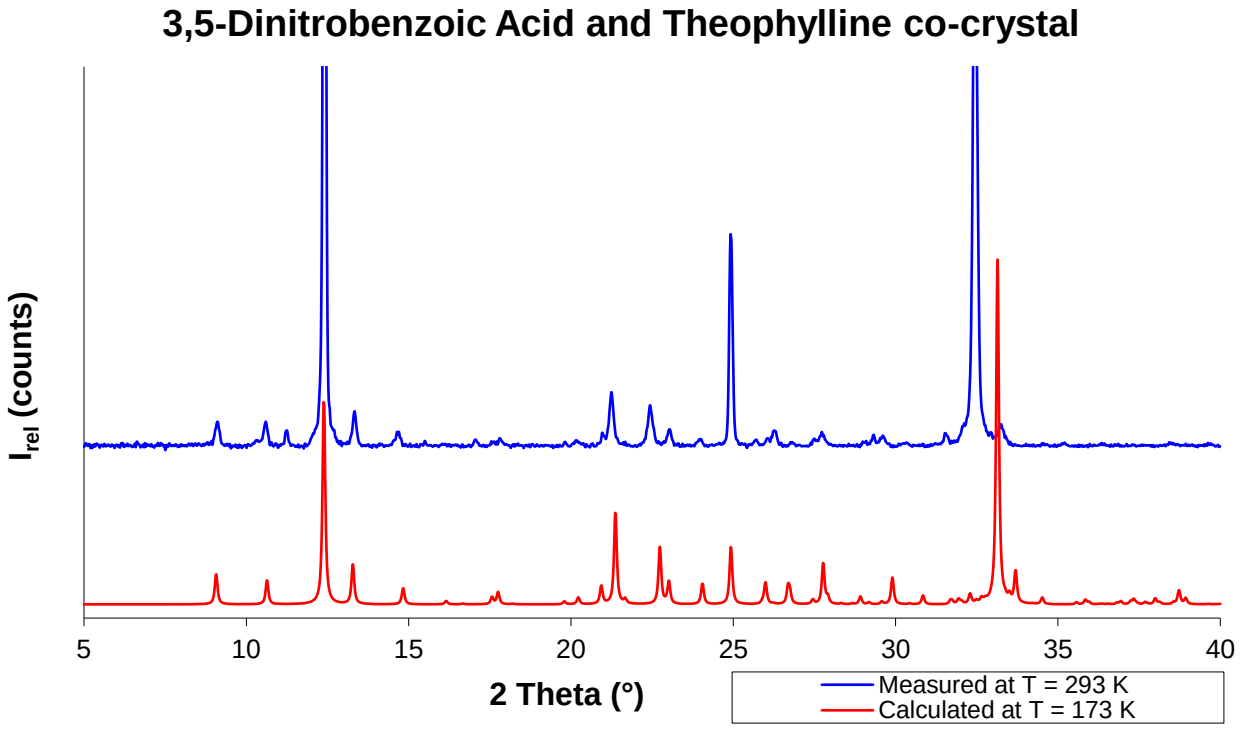


Figure A6 Calculated and measured PXRD Pattern for **dnba** + **thp** co-crystal

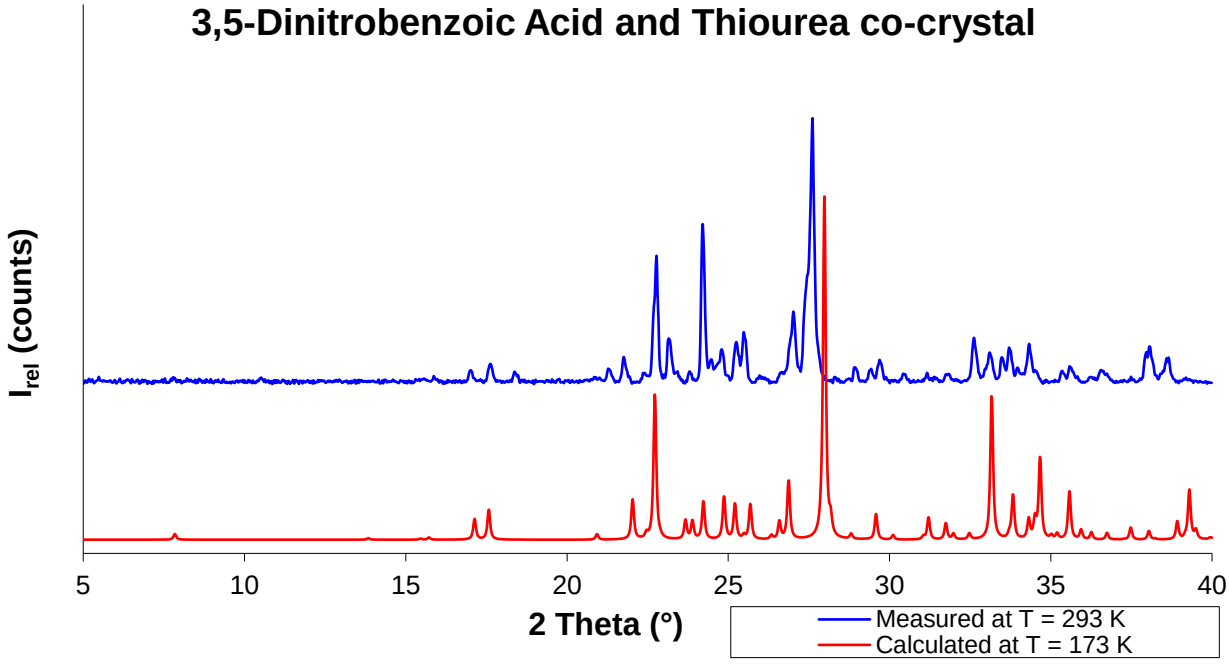


Figure A7 Calculated and measured PXRD Pattern for **dnba** + **tu** co-crystal

2. Differential Scanning Calorimetry Data

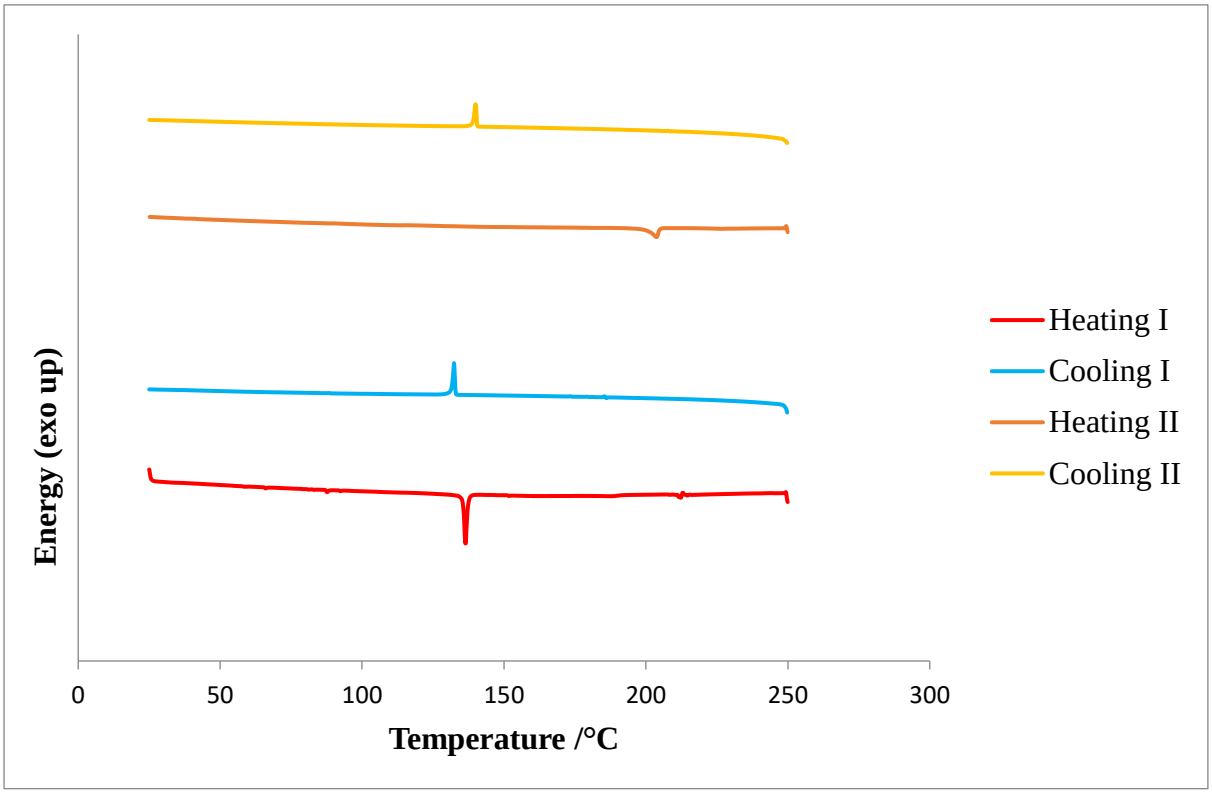


Figure B2 DSC curves for **dnba** + **3cnp** co-crystal

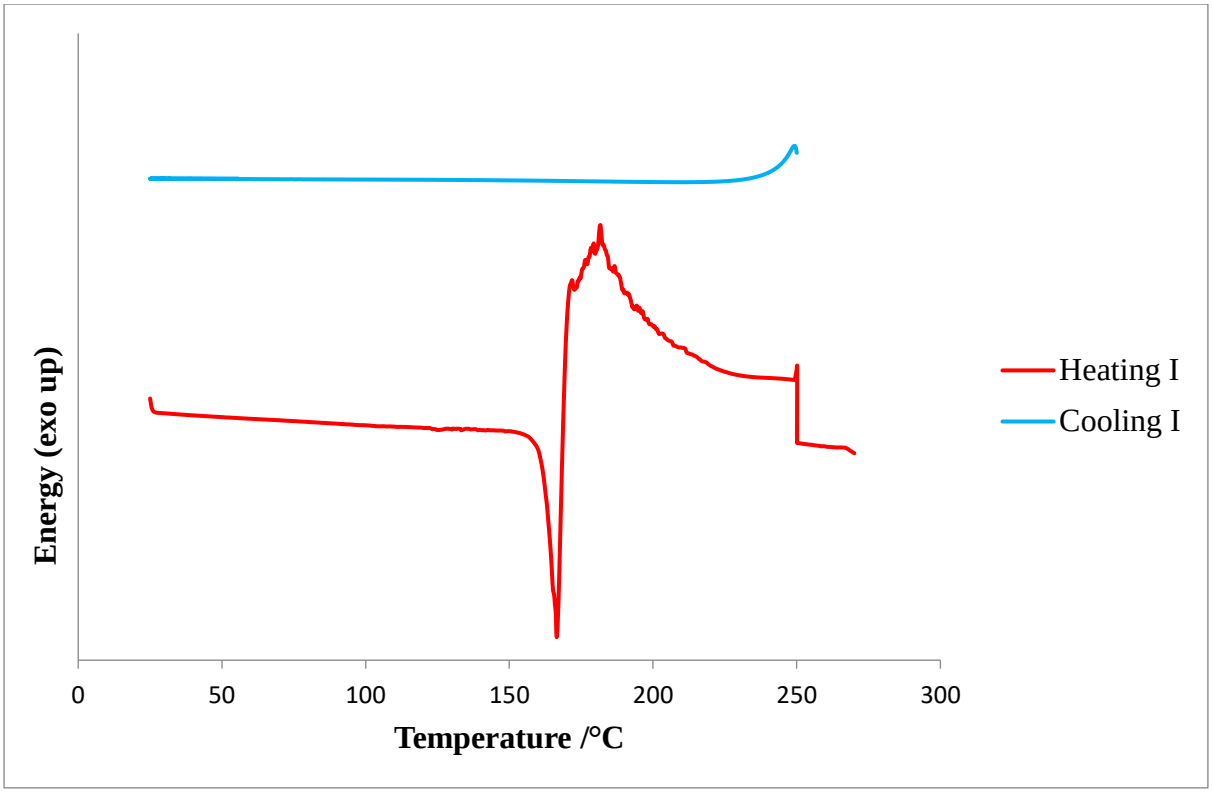


Figure B3 DSC curves for **dnba** + **pyd** molecular salt

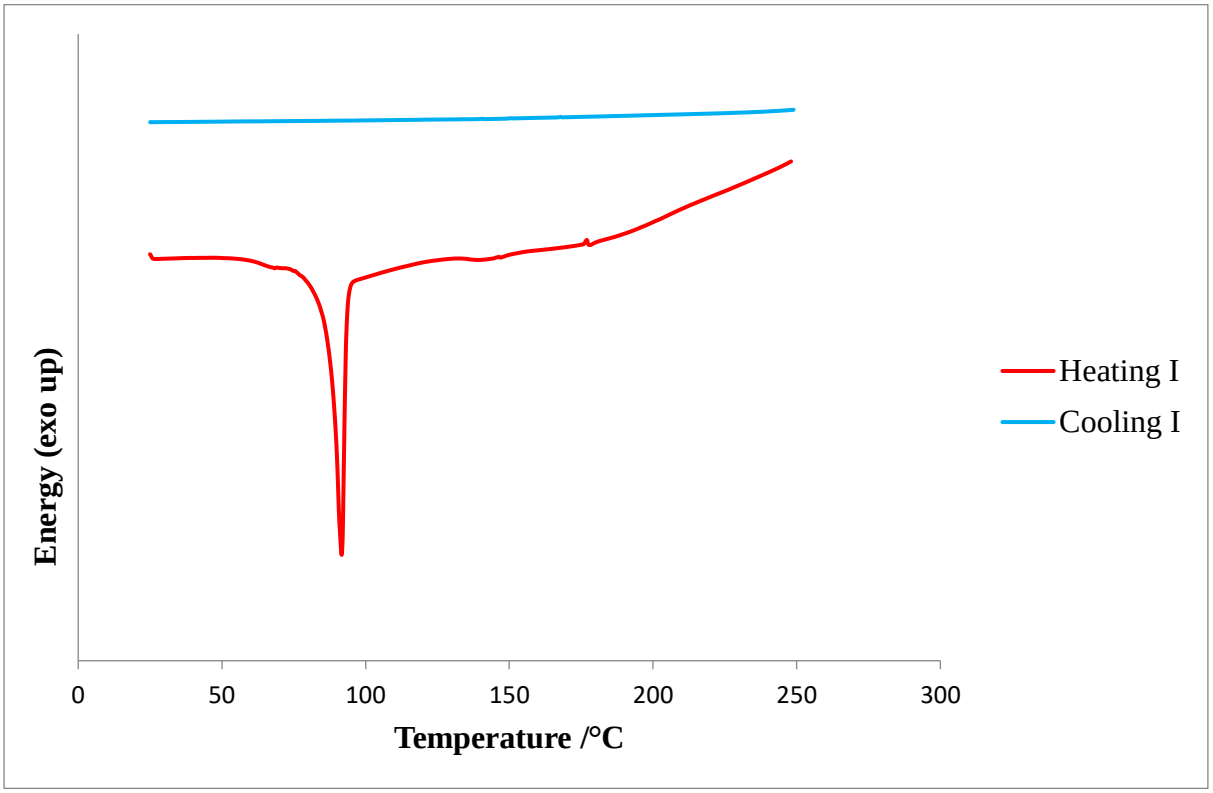


Figure B5 DSC curves for **dnba** + **dmabp** molecular complex

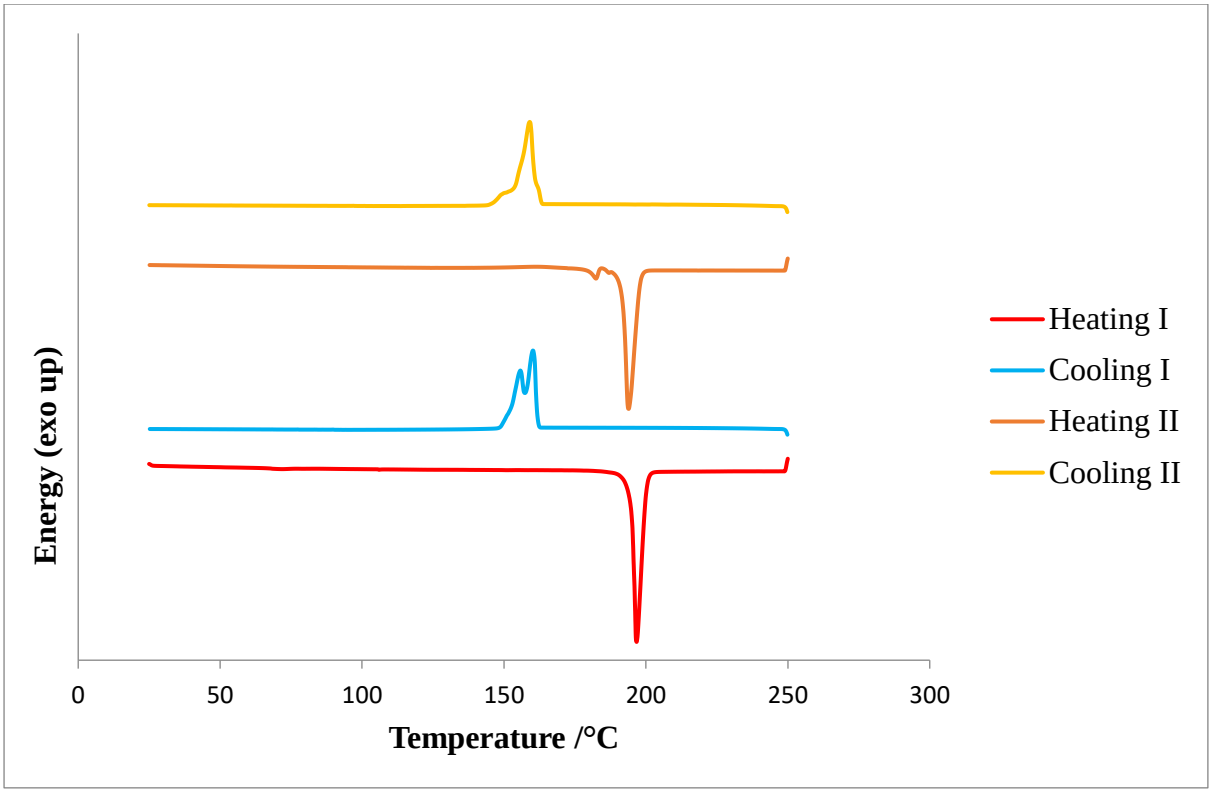


Figure B5 DSC curves for **dnba** + **thp** co-crystal

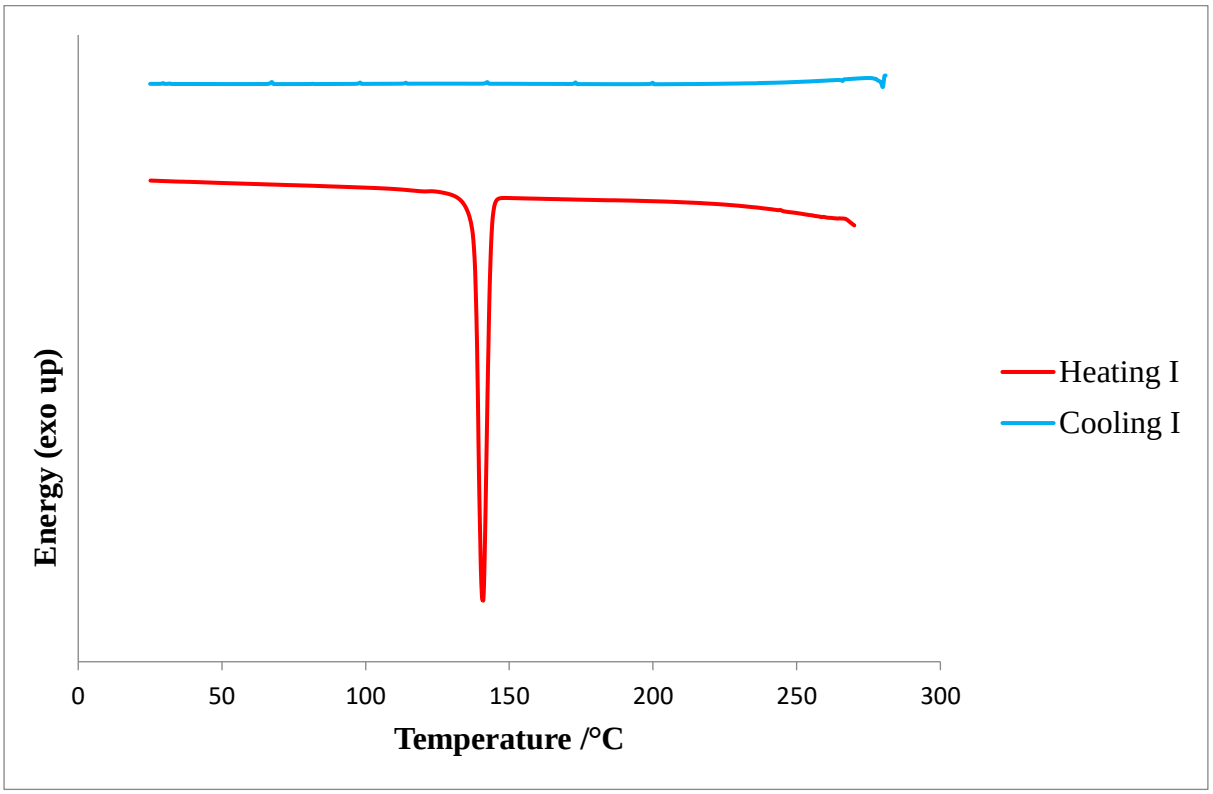


Figure B6 DSC curves for **dnba** + **fa** co-crystal

4. Hirshfeld Surfaces

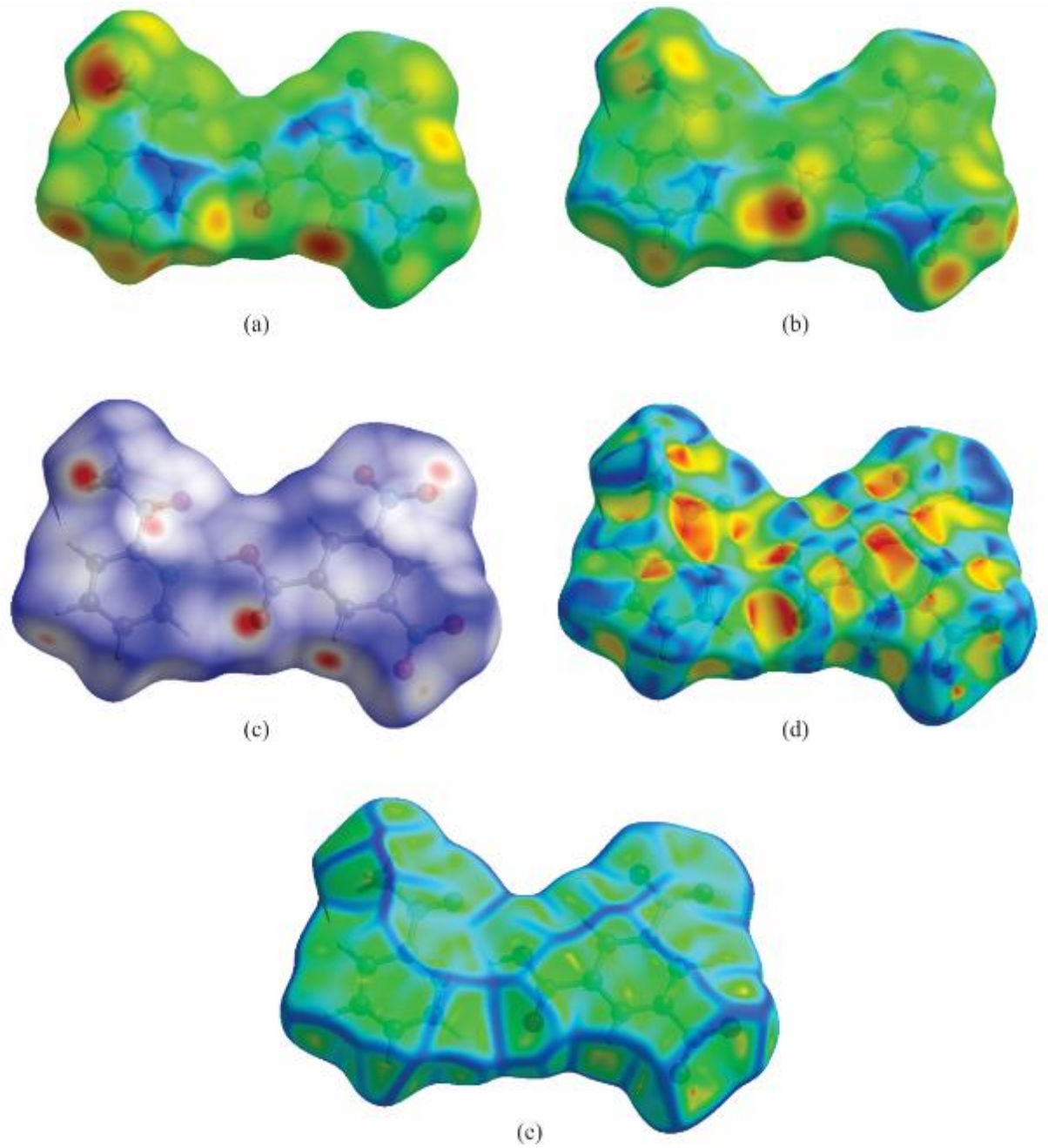


Figure C1 The Hirshfeld Surfaces of the solvate **dnba + 2acp** showing (a) d_i, (b) d_e (c) d_{norm}, (d) the shape index and (e) the curvedness

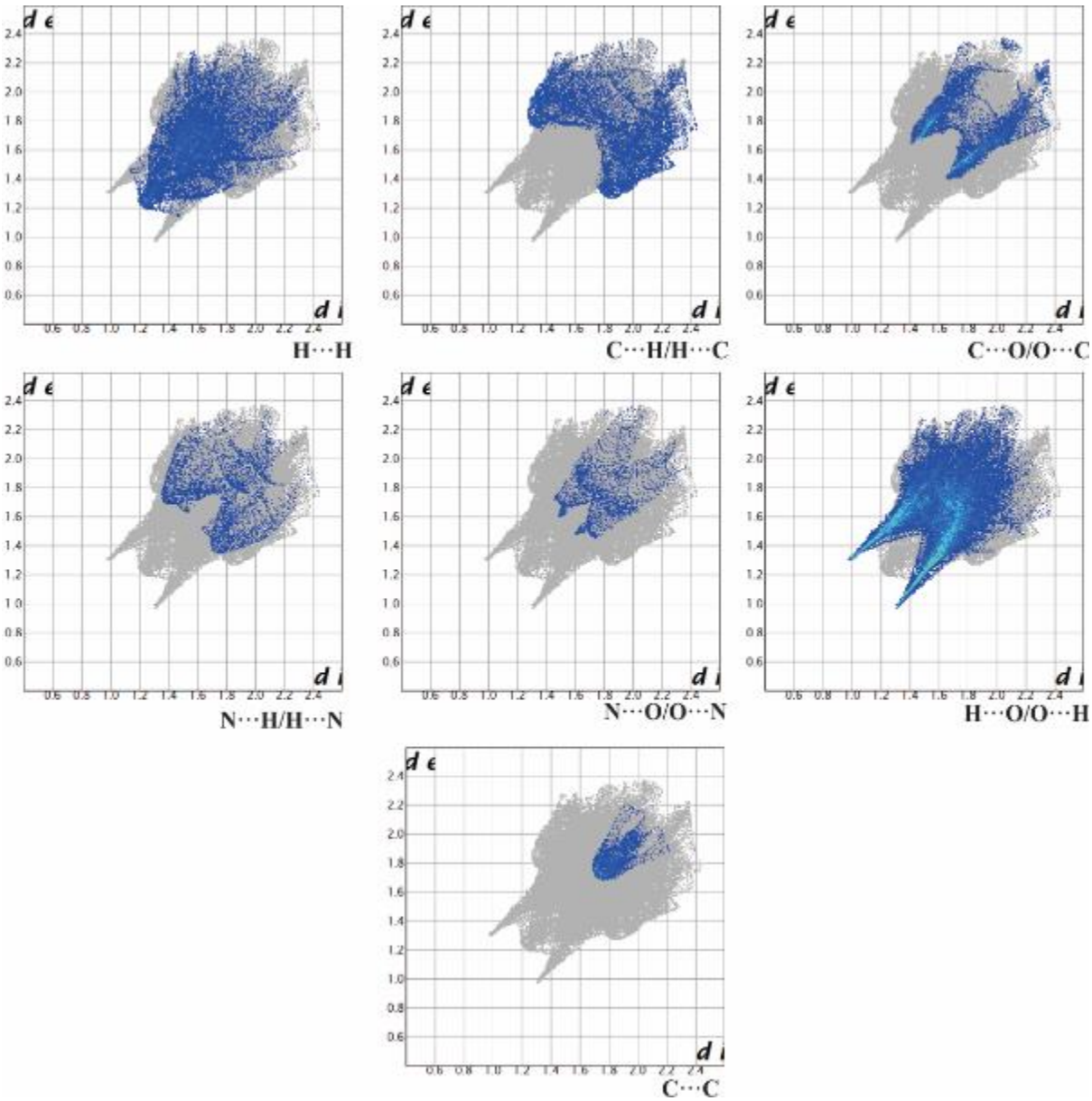


Figure C2 The Fingerprint plots for **dnba + 2acp**

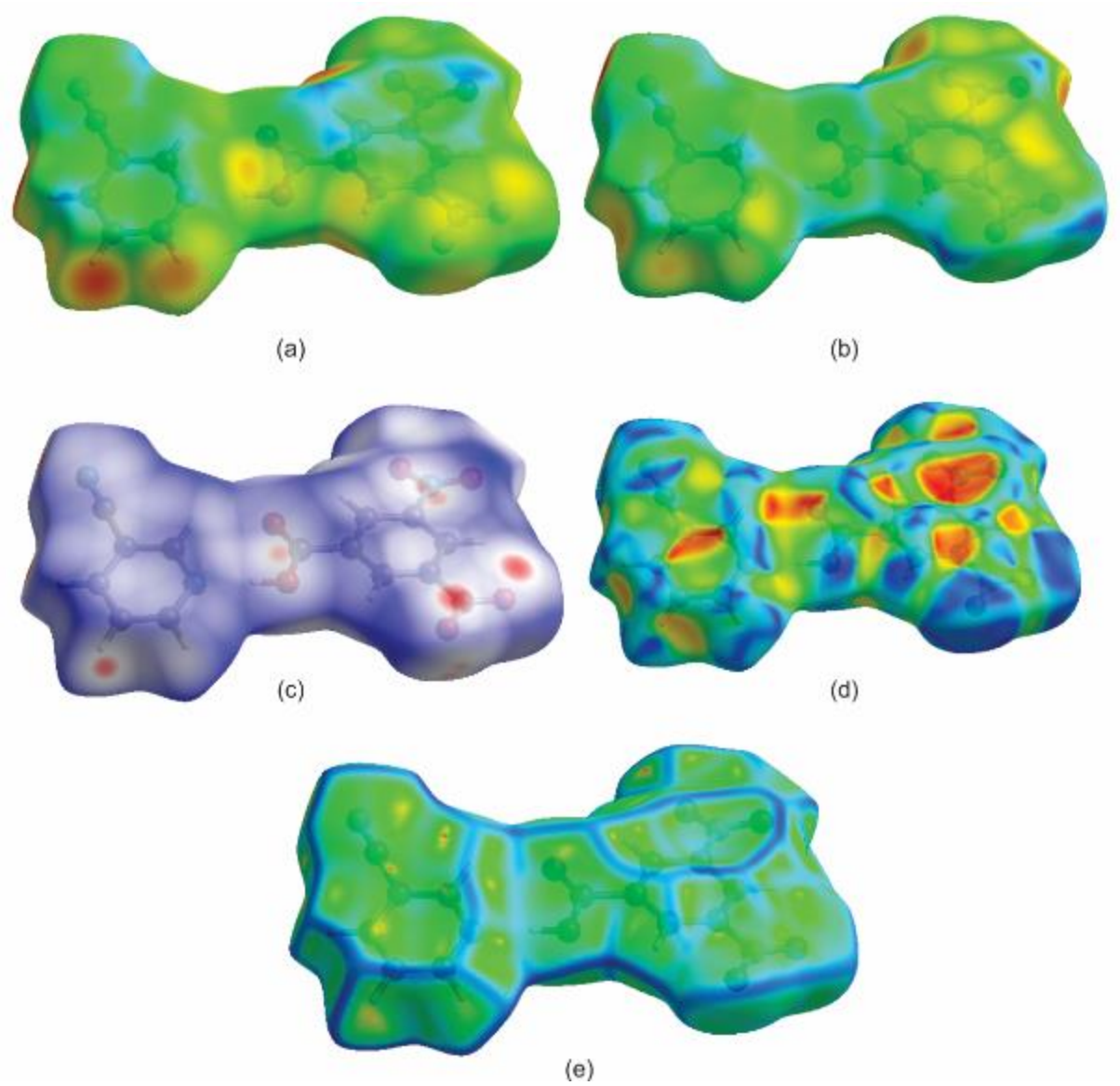


Figure C3 The Hirshfeld Surfaces of the co-crystal **dnba + 3cnp** showing (a) d_i, (b) d_e (c) d_{norm}, (d) the shape index and (e) the curvedness.

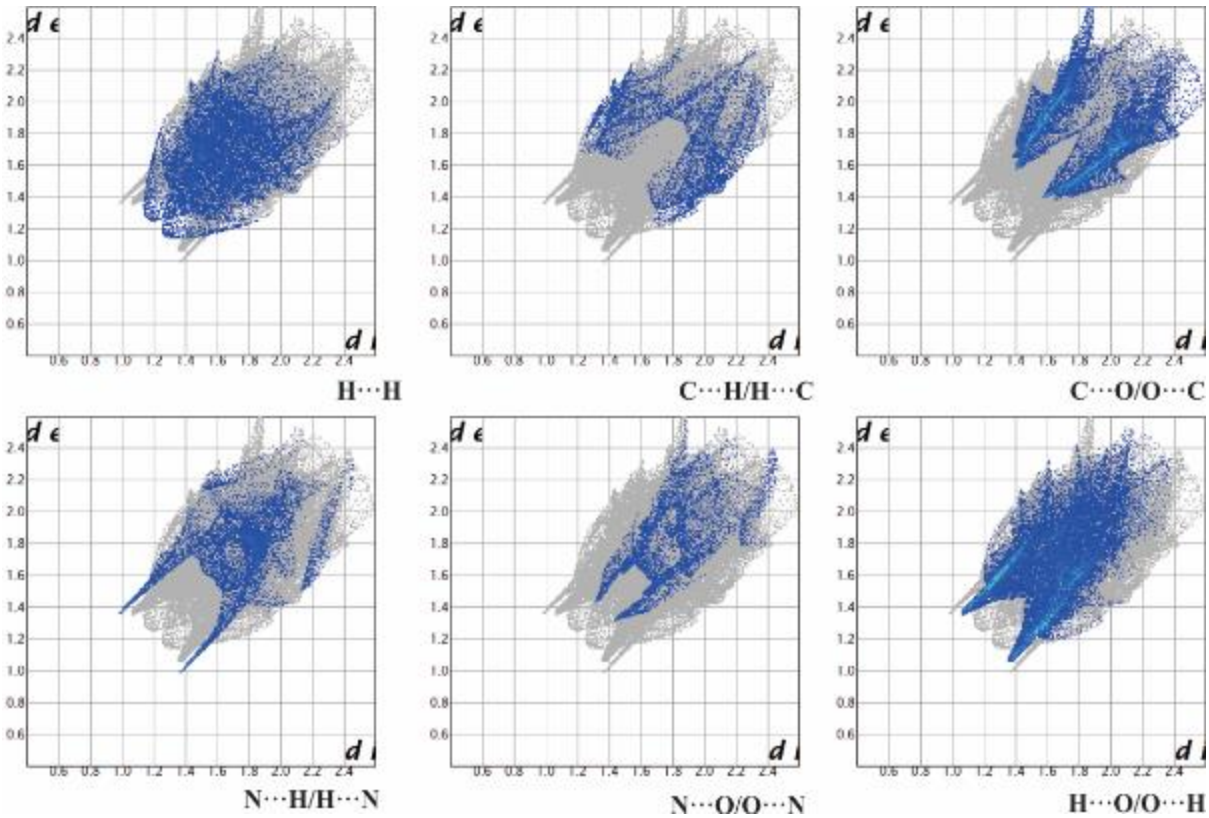


Figure C4 The Fingerprint plots for **dnba + 3cnp.**

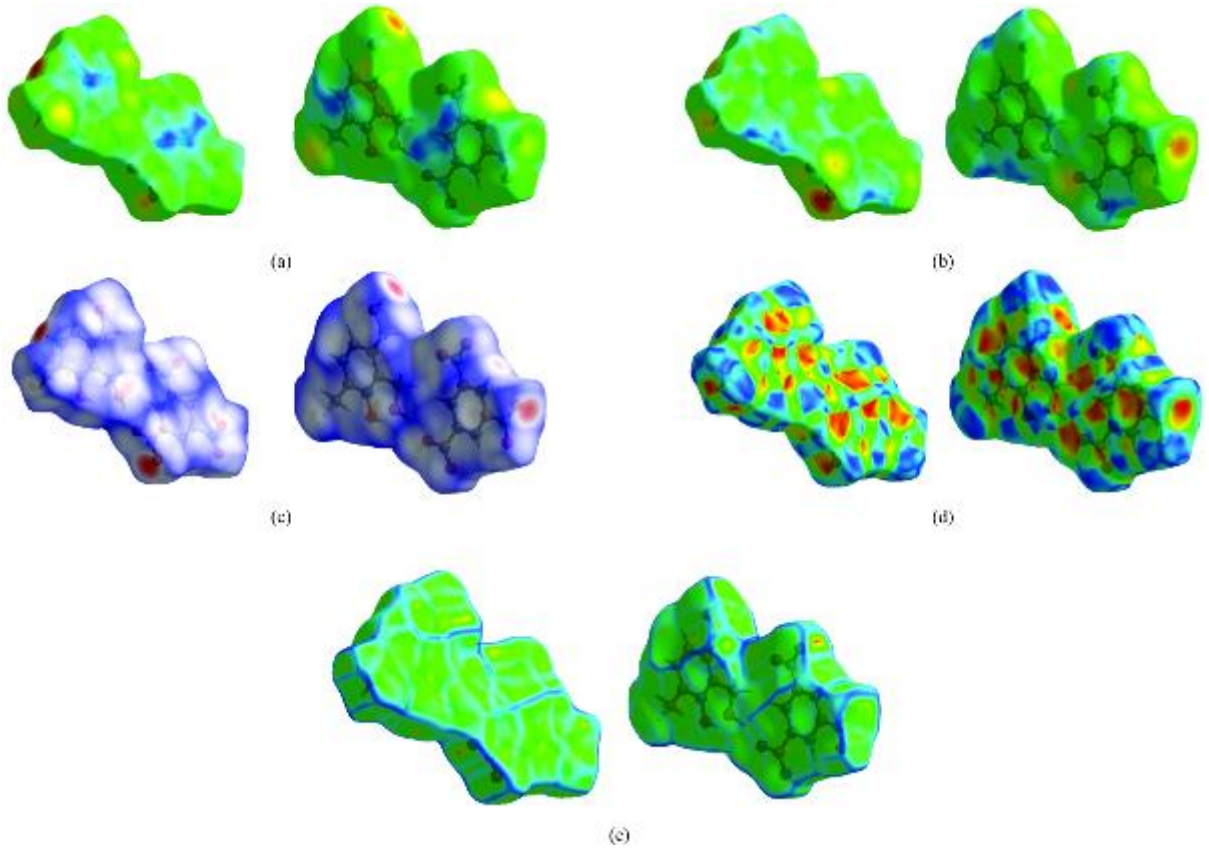


Figure C5 The Hirshfeld Surfaces of the molecular salt **dnba + pyd** showing (a) d_i, (b) d_e (c) d_{norm}, (d) the shape index and (e) the curvedness.

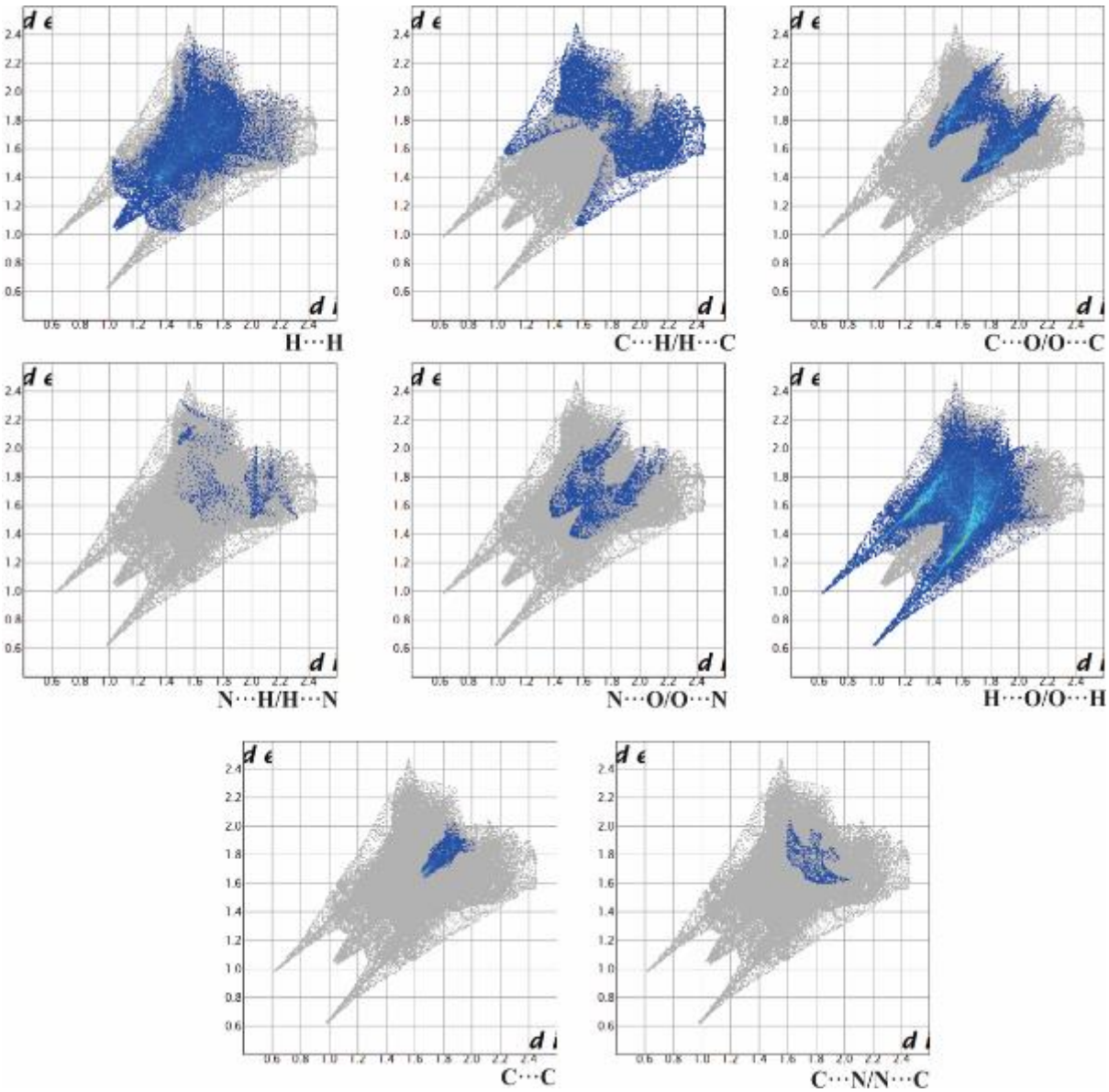


Figure C6 The Fingerprint plots for **dnba + pyd.**

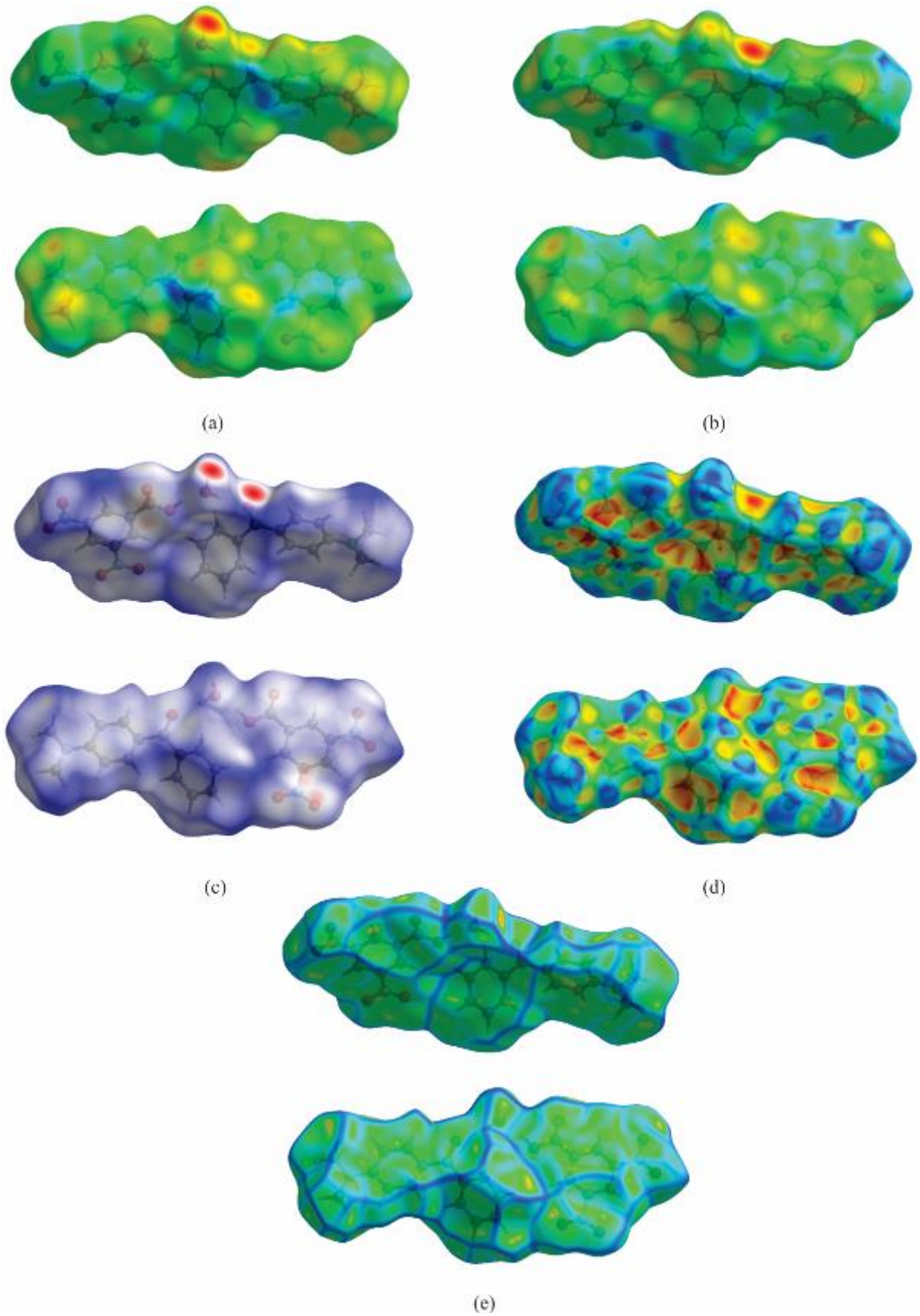


Figure C7 The Hirshfeld Surfaces of the hydrate **dnba + pyd** showing (a) d_i, (b) d_e (c) d_{norm}, (d) the shape index and (e) the curvedness.

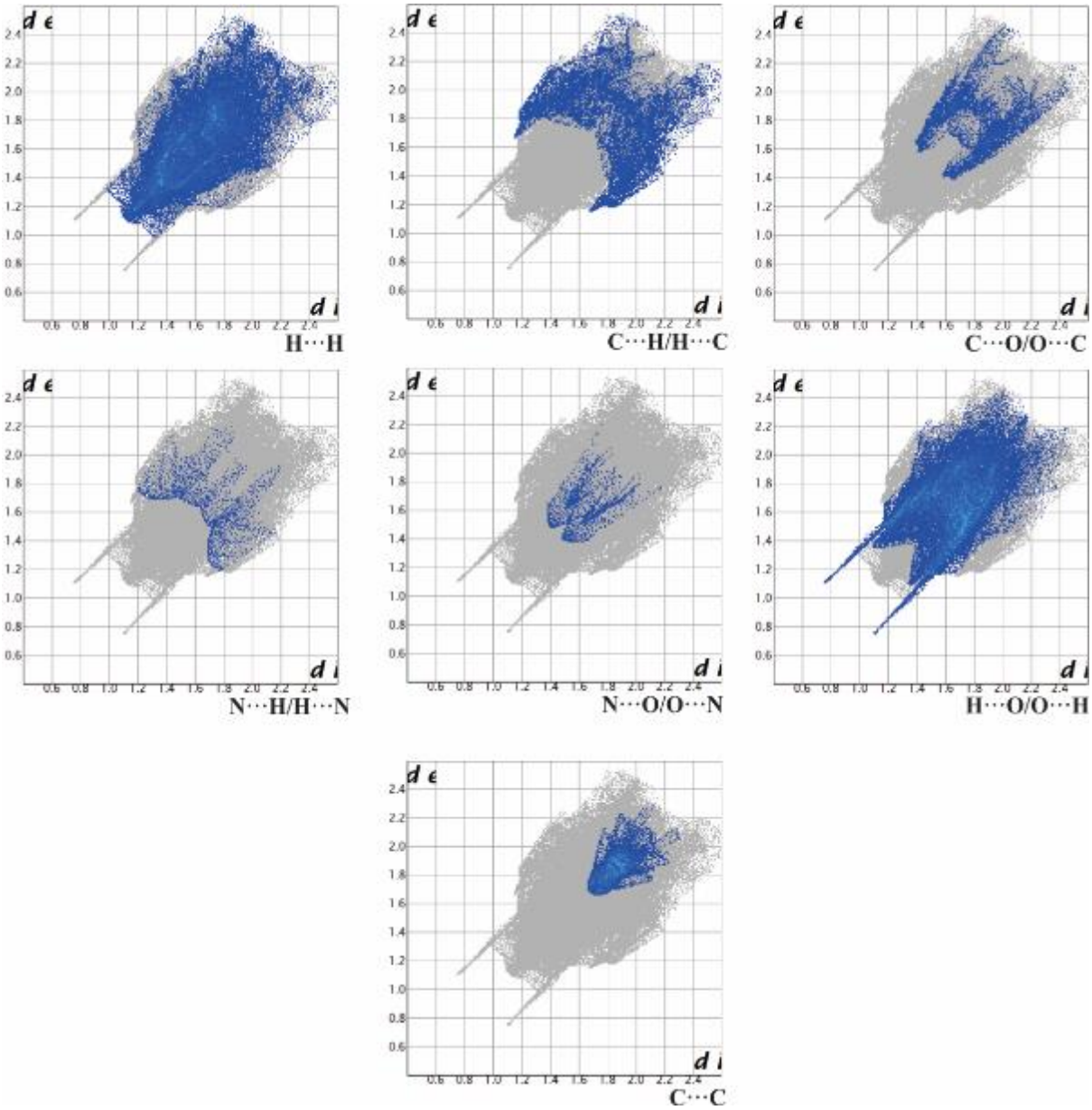


Figure C8 The Fingerprint plots for **dnba + dmabp.**

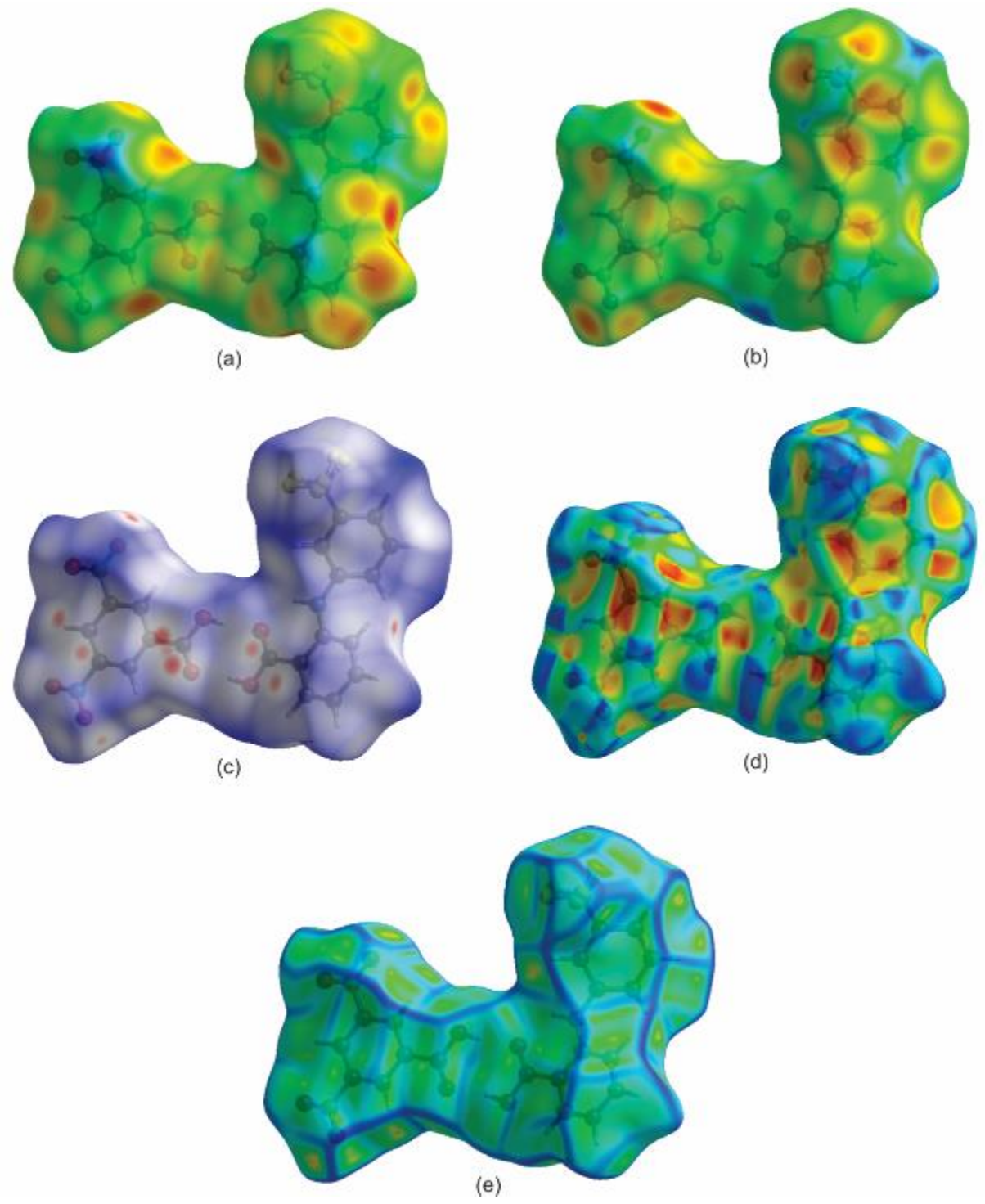


Figure C9 The Hirshfeld Surfaces of the co-crystal **dnba + fa** showing (a) d_i, (b) d_e (c) d_{norm}, (d) the shape index and (e) the curvedness.

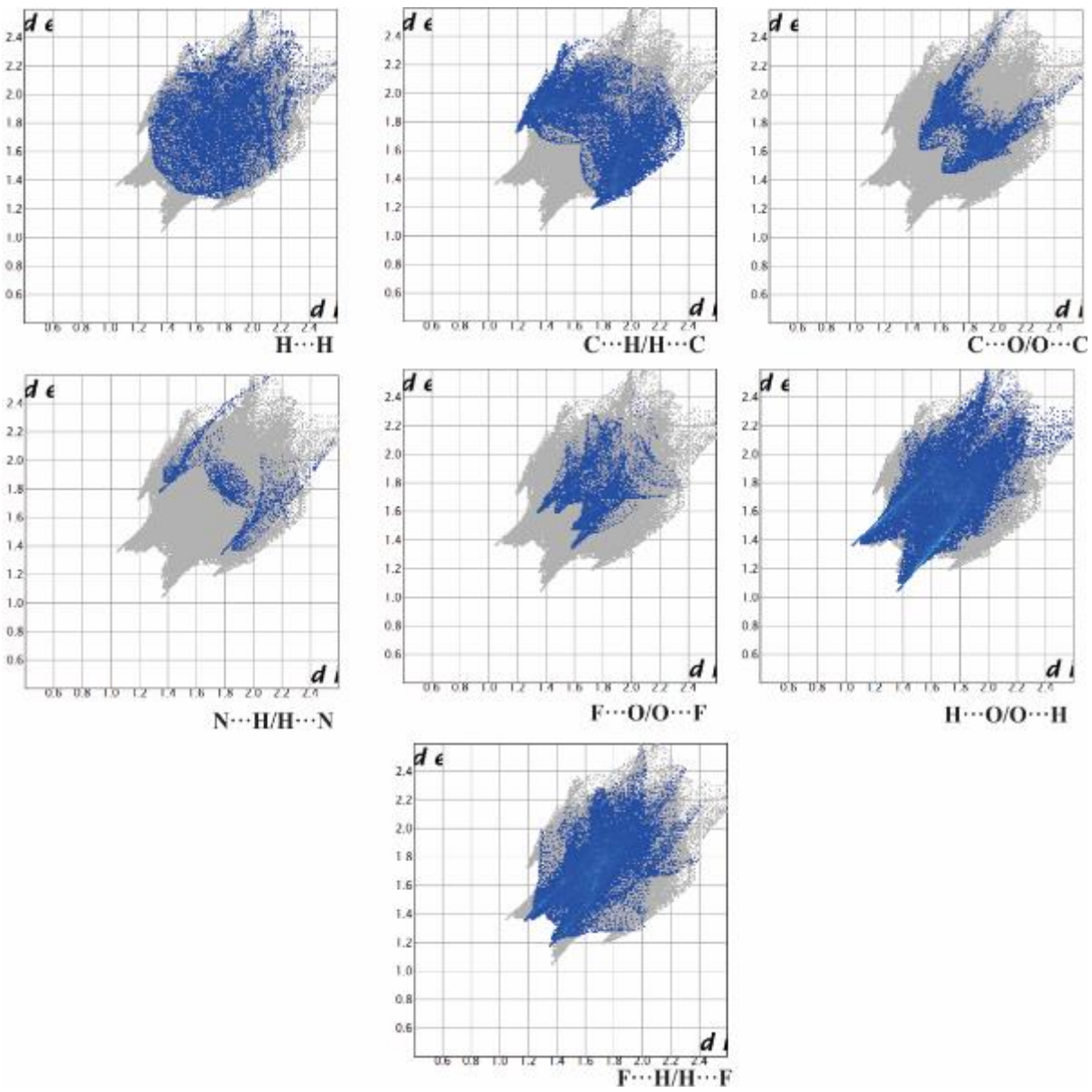


Figure C10 The Fingerprint plots for **dnba + fa.**

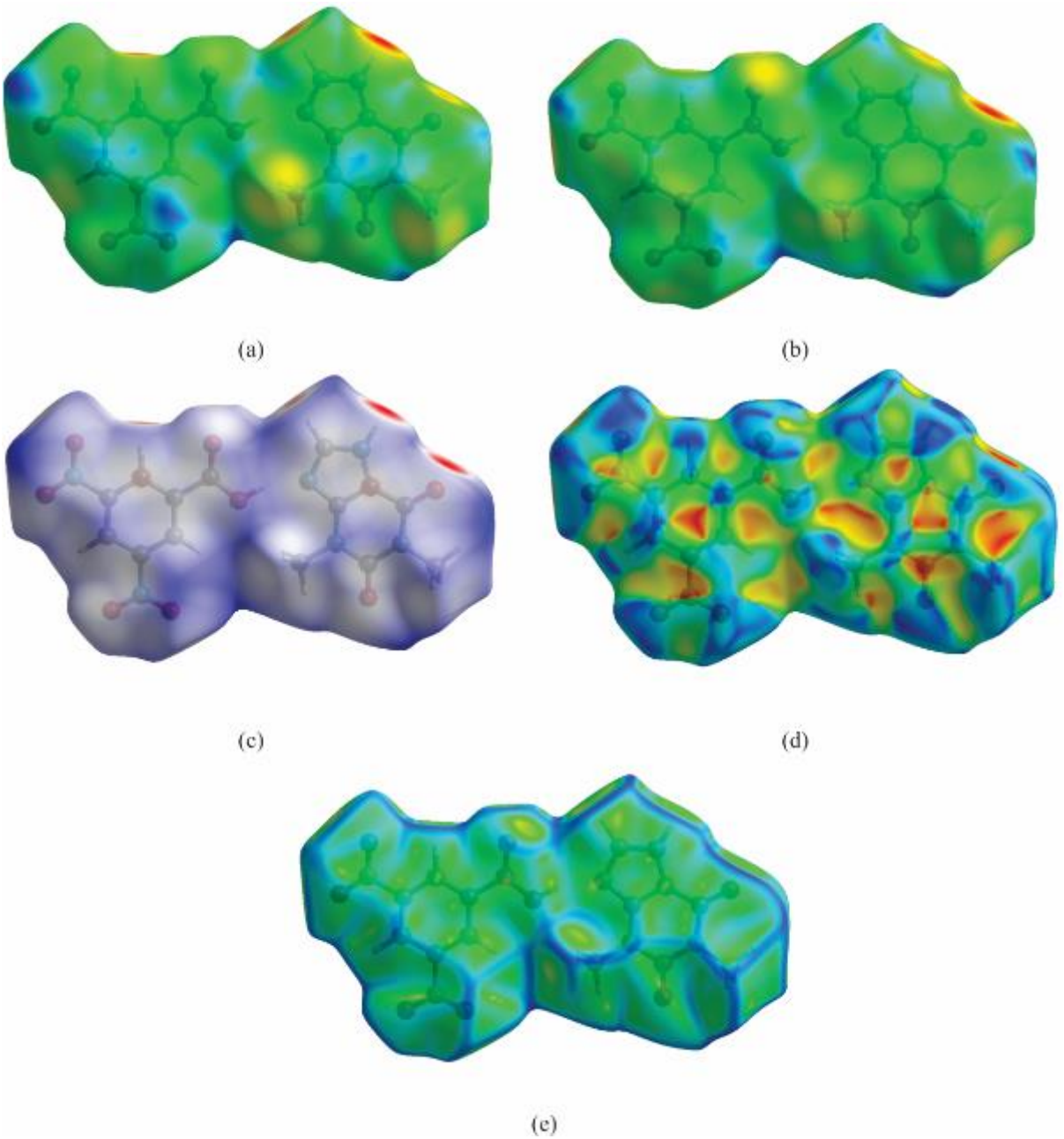


Figure C11 The Hirshfeld Surfaces of the co-crystal **dnba + thp** showing (a) d_i, (b) d_e (c) d_{norm}, (d) the shape index and (e) the curvedness.

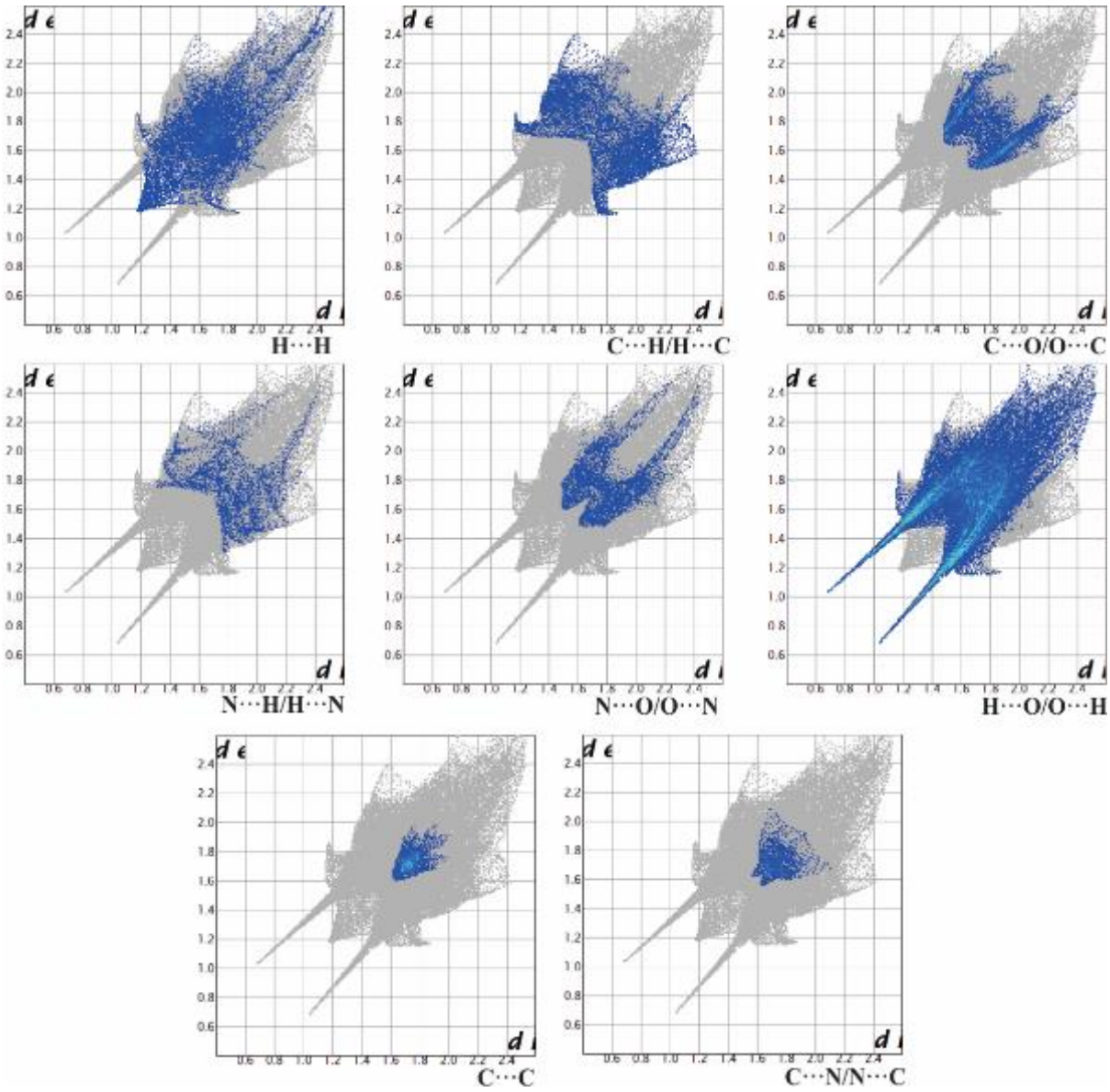


Figure C12 The Fingerprint plots for **dnba + thp.**

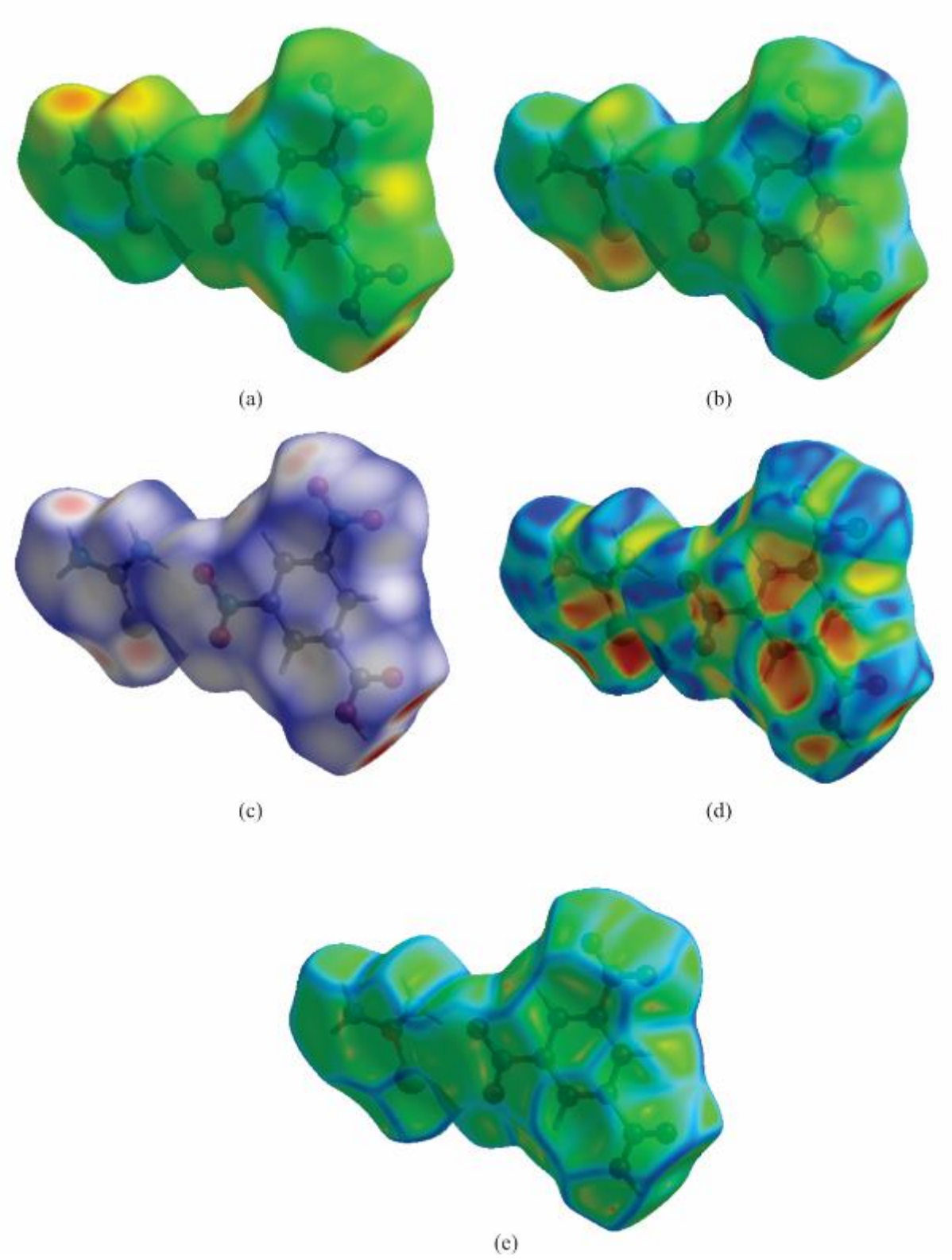


Figure C13 The Hirshfeld Surfaces of the co-crystal **dnba + tu** showing (a) d_i, (b) d_e (c) d_{norm}, (d) the shape index and (e) the curvedness.

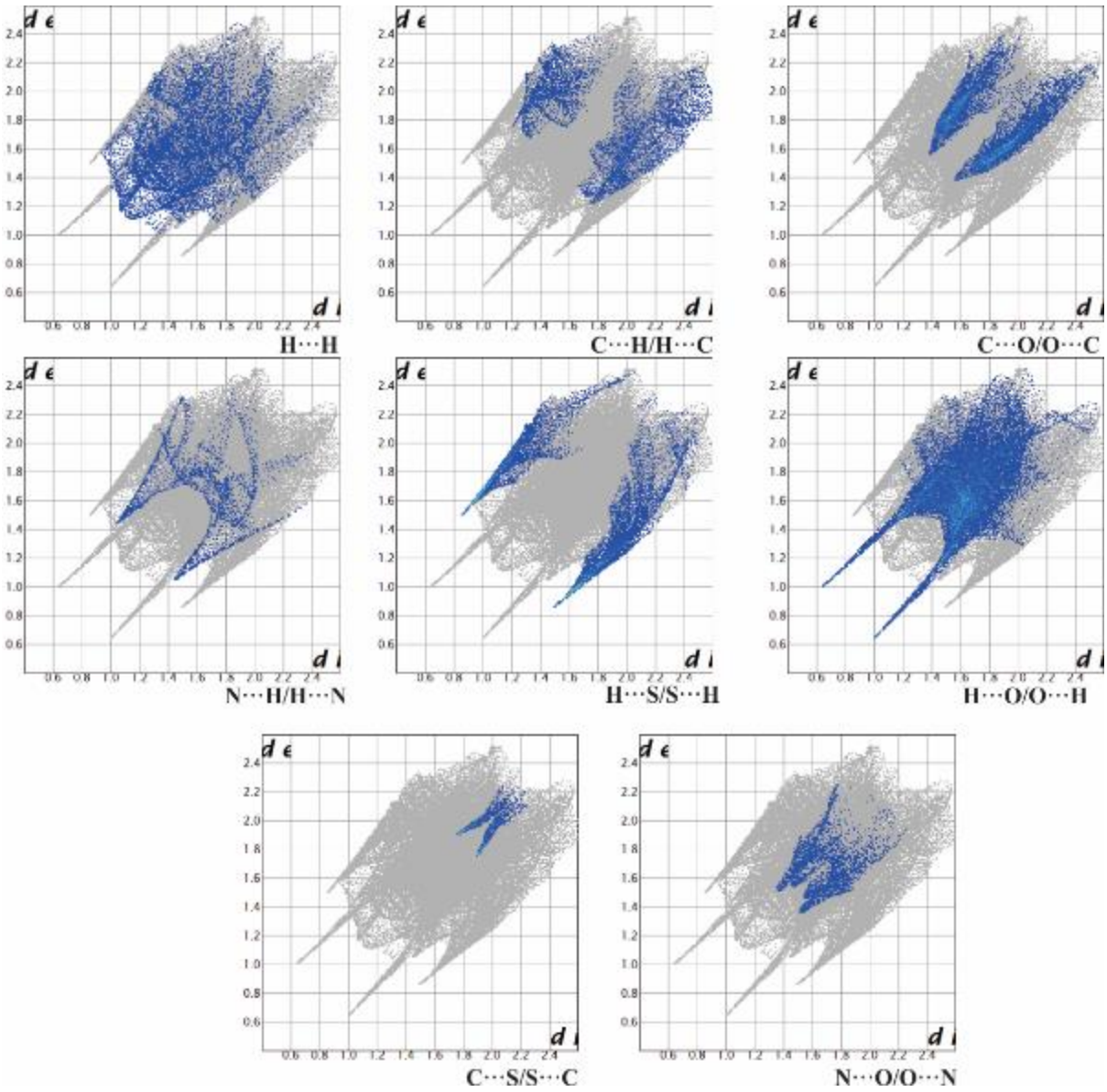


Figure C14 The Fingerprint plots for **dnba + tu.**

Chapter 6

Chains or Rings? Polymorphism of an isoniazid derivative derivatized with diacetone alcohol

Matthew C. Scheepers and Andreas Lemmerer*‡

Supplementary Information

1. **Table S1** Crystallographic information for the crystal structures of **Form I** and **Form II**

Crystal Form	**Form I**	**Form II**
Empirical formula	$C_{12}H_{17}N_3O_2$	$C_{12}H_{17}N_3O_2$
Formula weight	235.28	235.28
Temperature/K	173(2)	173(2)
Crystal system	Monoclinic	Monoclinic
Space group	*C*2/c	$P2_1/c$
a/Å	21.8108(4)	9.2041(2)
b/Å	7.0776(2)	11.1274(3)
c/Å	18.1625(5)	11.9383(3)
α/°	90	90
β/°	116.465(3)	92.3570(10)
γ/°	90	90
Volume/Å^3	2509.90(12)	1221.66(5)
Z	8	4
Density/ g/cm^3	1.245	1.279
μ/mm-1	0.087	0.089
F(000)	1008	504
Crystal size/mm^3	0.255 x 0.184 x 0.152	0.728 x 0.495 x 0.228
2Θ range for data collection/°	2.086 to 28.420	2.215 to 28.330
Reflections collected	37052	50485
Independent reflections	3065 [*R*(int) = 0.1191]	3029 [R(int) = 0.0395]
Goodness-of-fit on F^2	0.863	1.066
Final *R* indexes [I>=2σ (I)]	R_1 = 0.0452, wR_2 = 0.0978	R_1 = 0.0382, wR_2 = 0.0896
Final *R* indexes [all data]	R_1 = 0.0933, wR_2 = 0.1115	R_1 = 0.0578, wR_2 = 0.0987
CCDC	2133557	2133558

2. PXRD patterns

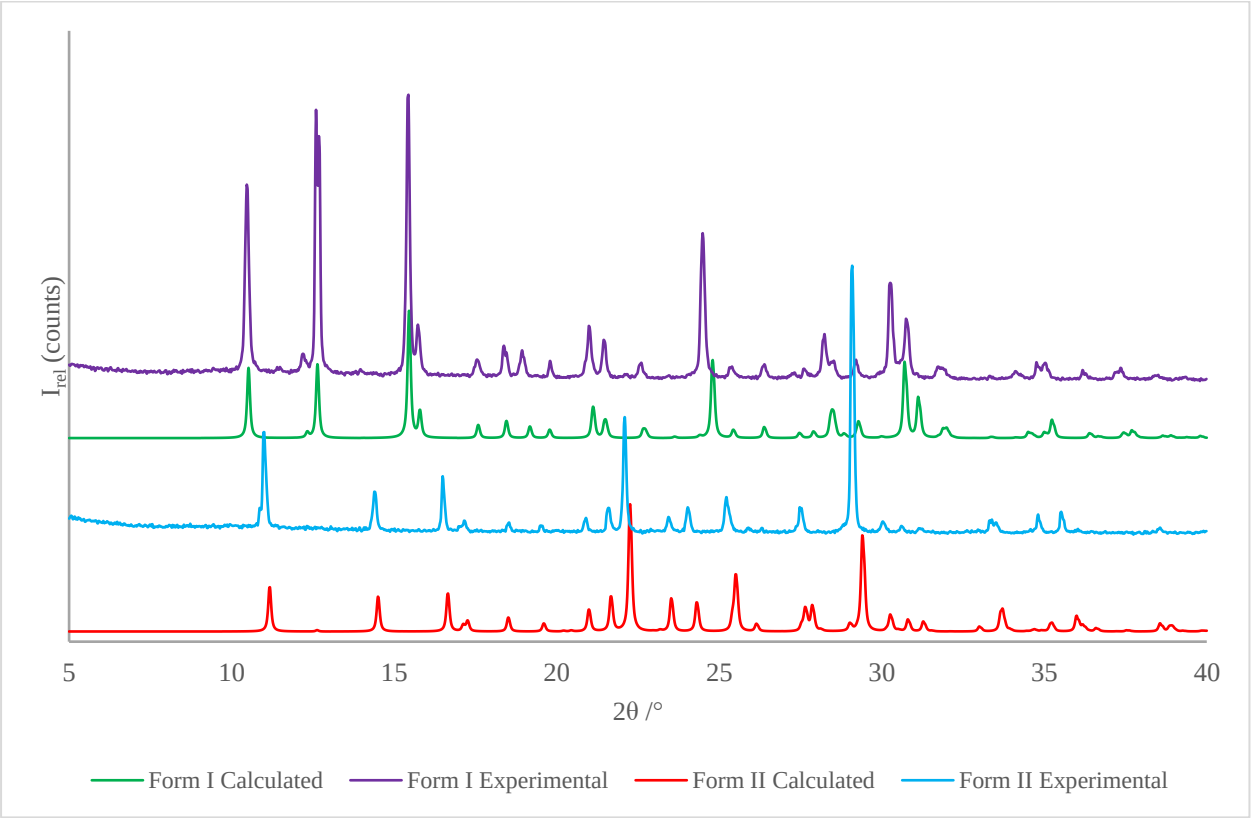


Figure S1 PXRD Patterns for both **Form I** and **Form II,** calculated and experimental.

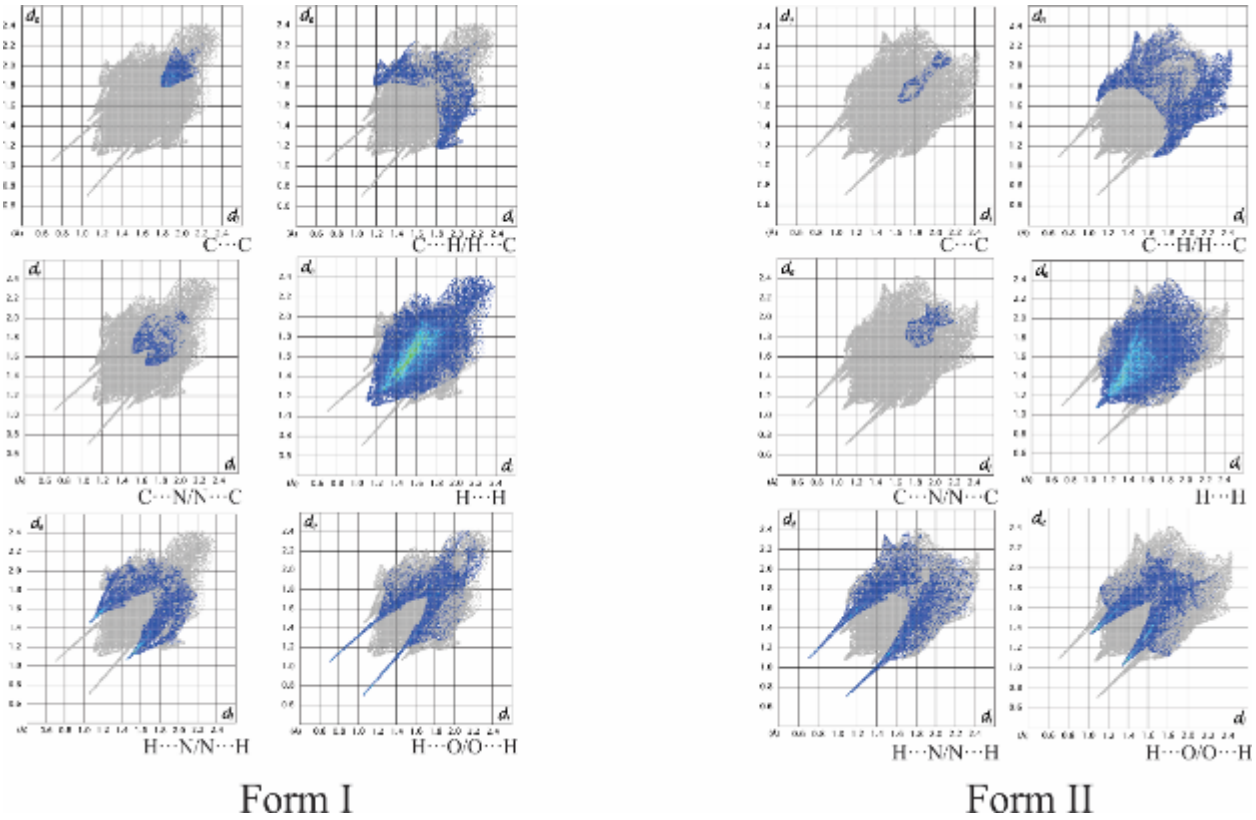


Figure S2 Hirshfeld Surface Fingerprint spots for both **Form I** and **Form II**

Chapter 7

Acta Cryst. (2022). B**78**, https://doi.org/10.1107/S2052520622009532 Supporting information



STRUCTURAL SCIENCE
CRYSTAL ENGINEERING
MATERIALS

Volume 78 (2022)

Supporting information for article:

Design of a series of cocrystals featuring isoniazid modified with diacetone alcohol

Matthew Clarke Scheepers and Andreas Lemmerer

S1. Coformers used for this work

Table S1 Complete list of coformers used for this study.

Coformer	Mass used for a 1:1 stoichiometric amount relative to 50 mg of iz4h4m2p/ g
2-hydroxybenzoic acid (salicylic acid)	0.029
3-hydroxybenzoic acid	0.029
4-hydroxybenzoic acid	0.029
1-naphthionic acid	0.037
2-chloro-4-nitrobenzoic acid	0.043
2-chloro-5-nitrobenzoic acid	0.043
4-nitrobenzoic acid	0.036
3,5-dinitrobenzoic acid	0.045
Benzoic acid	0.026
2-aminobenzoic acid	0.029
3-aminobenzoic acid	0.029
4-aminobenzoic acid	0.029
Succinic acid	0.012
4-methoxybenzoic acid (methyl paraben)	0.032
trans-Cinnamic acid	0.031
Tartaric acid	0.032
2,4-dihydroxybenzoic acid	0.033
2,5-dihydroxybenzoic acid	0.033
3,4-dihydroxybenzoic acid	0.033
3,5-dihydroxybenzoic acid	0.033
Acetylsalicylic acid	0.038
Mendelic acid	0.032
Glycolic acid	0.008
2-chlorobenzoic acid	0.033
3-chlorobenzoic acid	0.033
4-chlorobenzoic acid	0.033
Toluic acid	0.029
1,4-dicarboxylicecyclohexane	0.037
4-iodobenzoic acid	0.053
4-bromobenzoic acid	0.043

S2. PXRD patterns

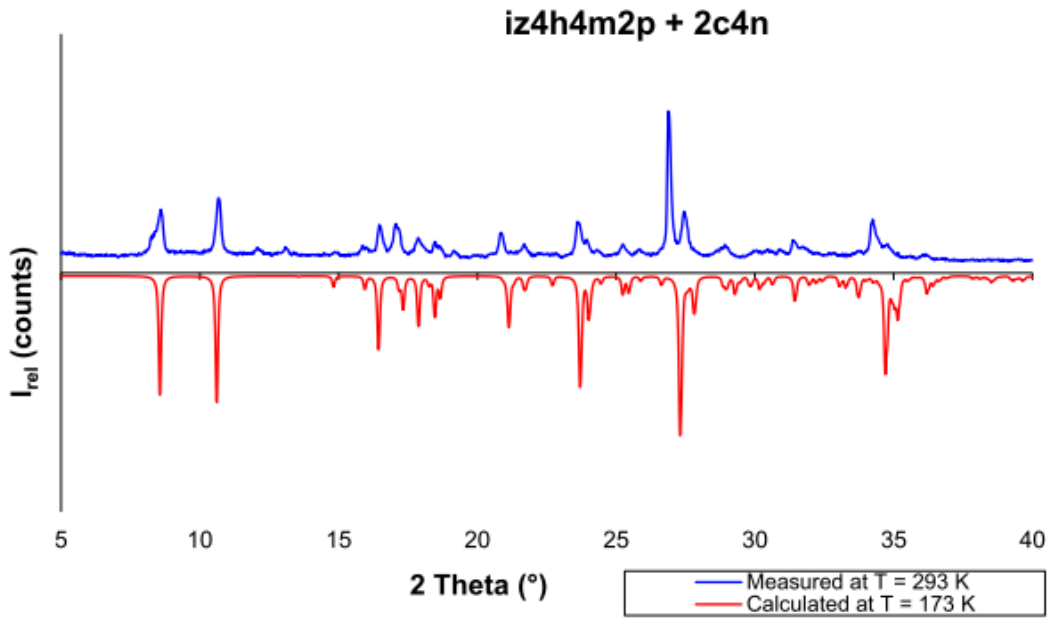


Figure S1 PXRD pattern for **iz4h4m2p** + **2c4n**

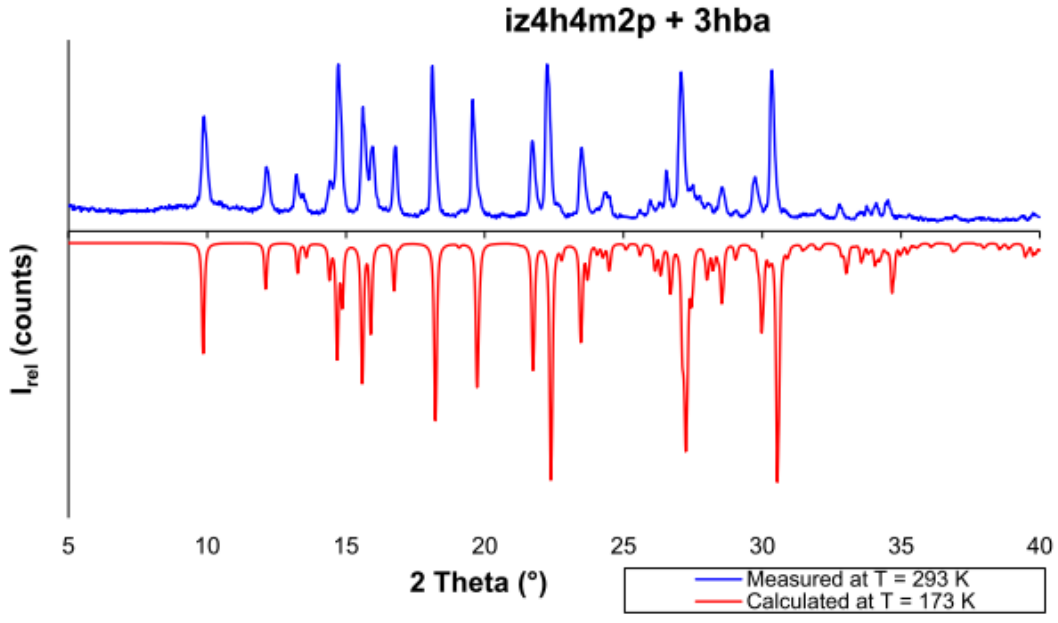


Figure S2 PXRD pattern for **iz4h4m2p** + **3hba**

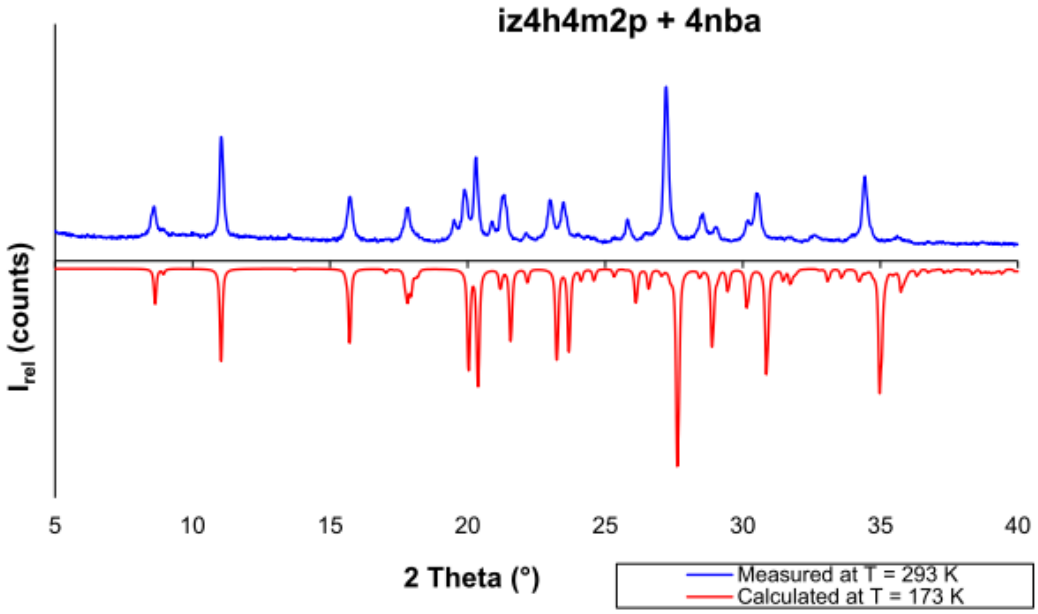


Figure S3 PXRD pattern for **iz4h4m2p** + **4nba**

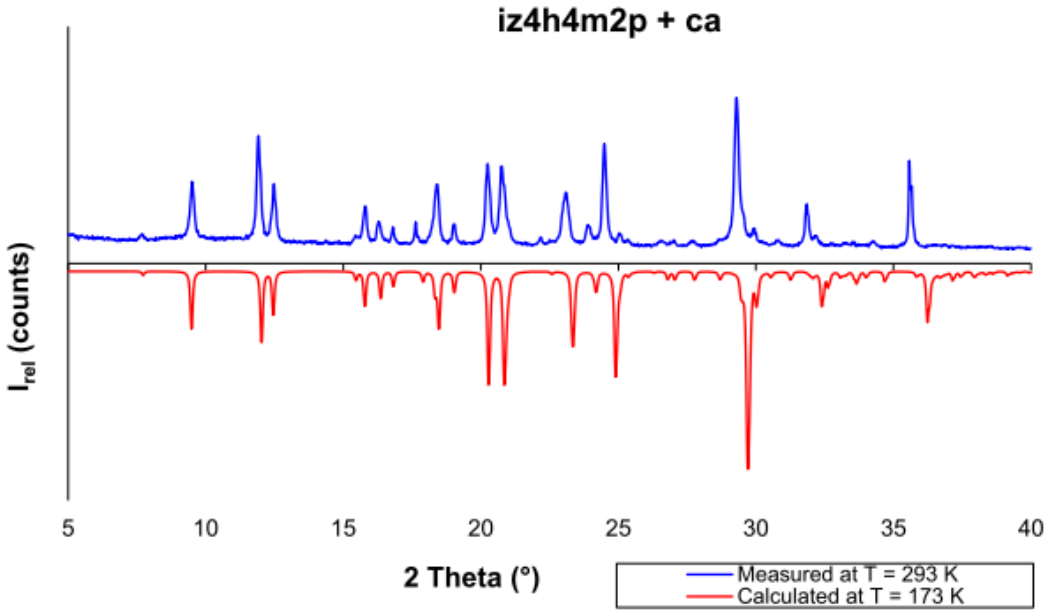


Figure S4 PXRD pattern for **iz4h4m2p** + ca

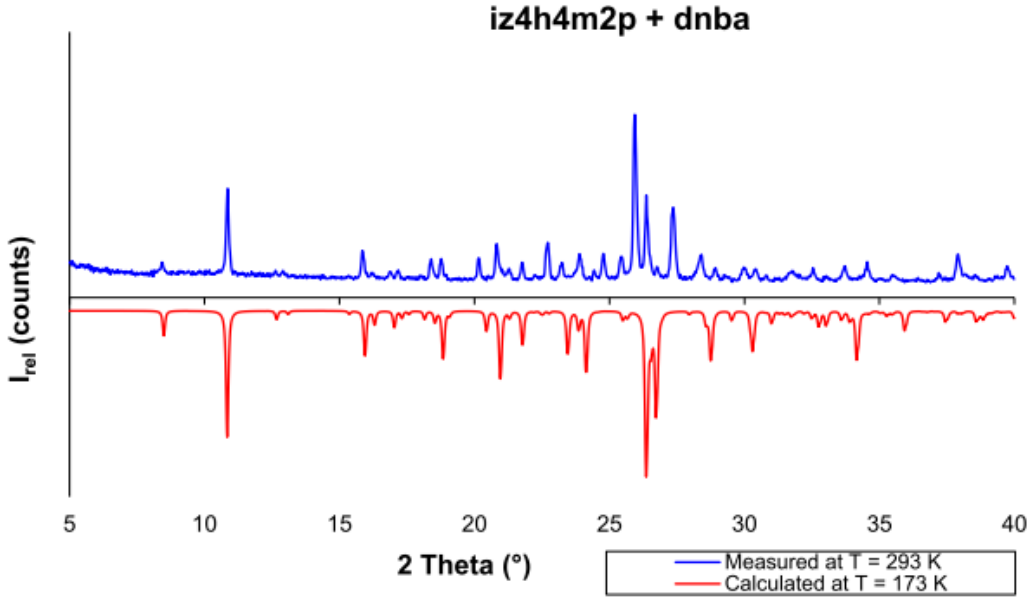


Figure S5 PXRD pattern for **iz4h4m2p** + **dnba**

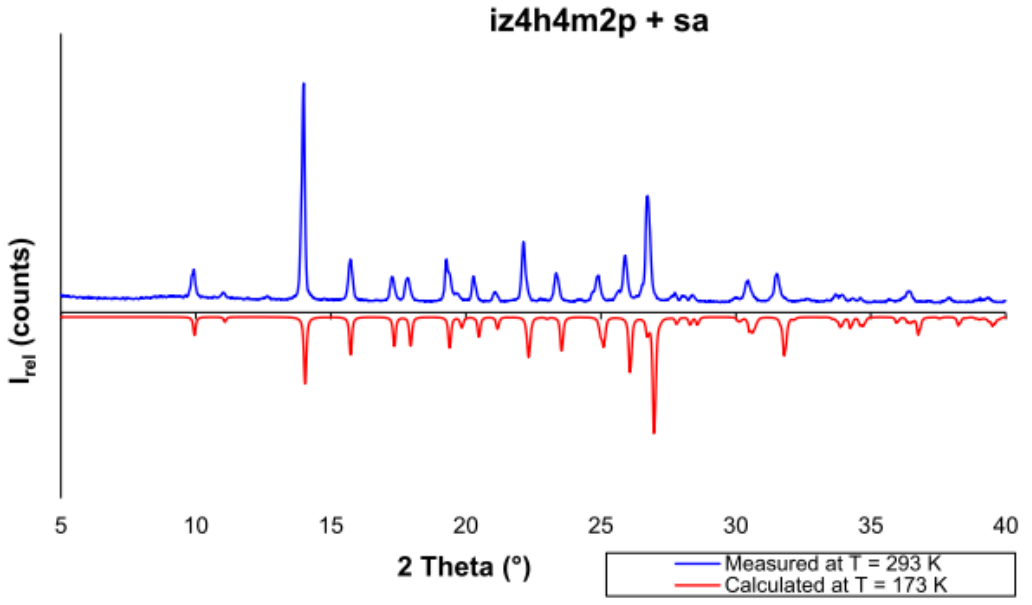


Figure S6 PXRD pattern for **iz4h4m2p** + sa

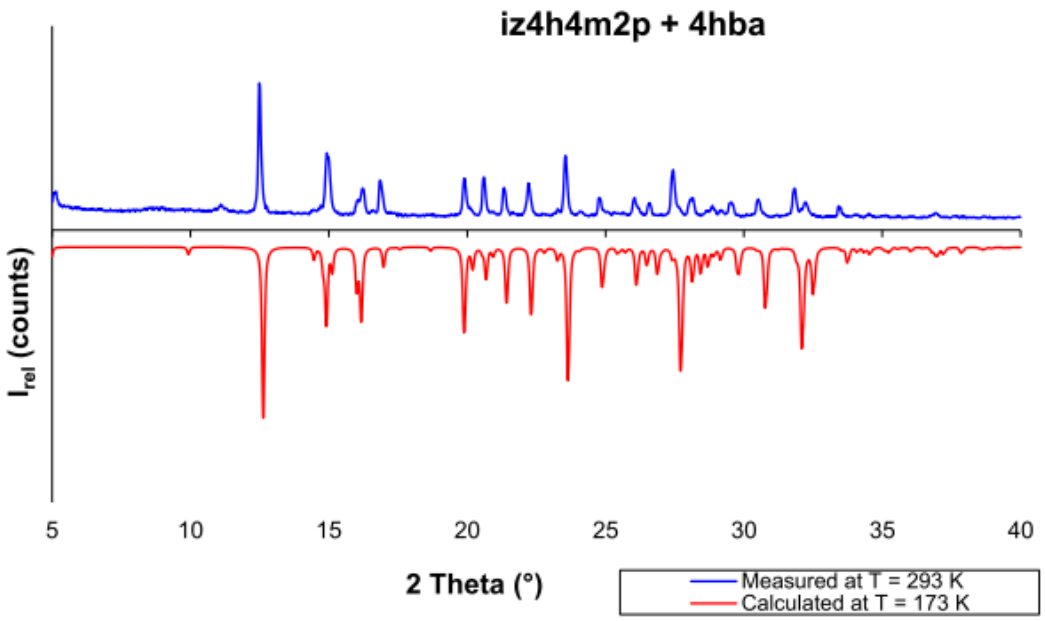


Figure S7 PXRD pattern for iz4h4m2p + 4hba

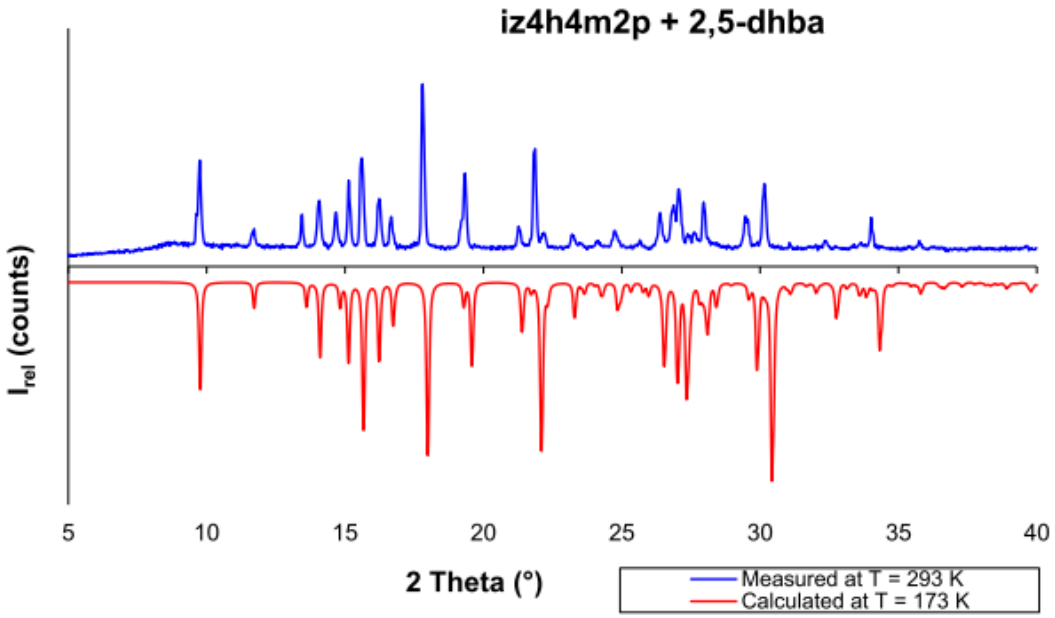


Figure S8 PXRD pattern for **iz4h4m2p + 2,5-dhba**

S3. Individual FTIR spectra

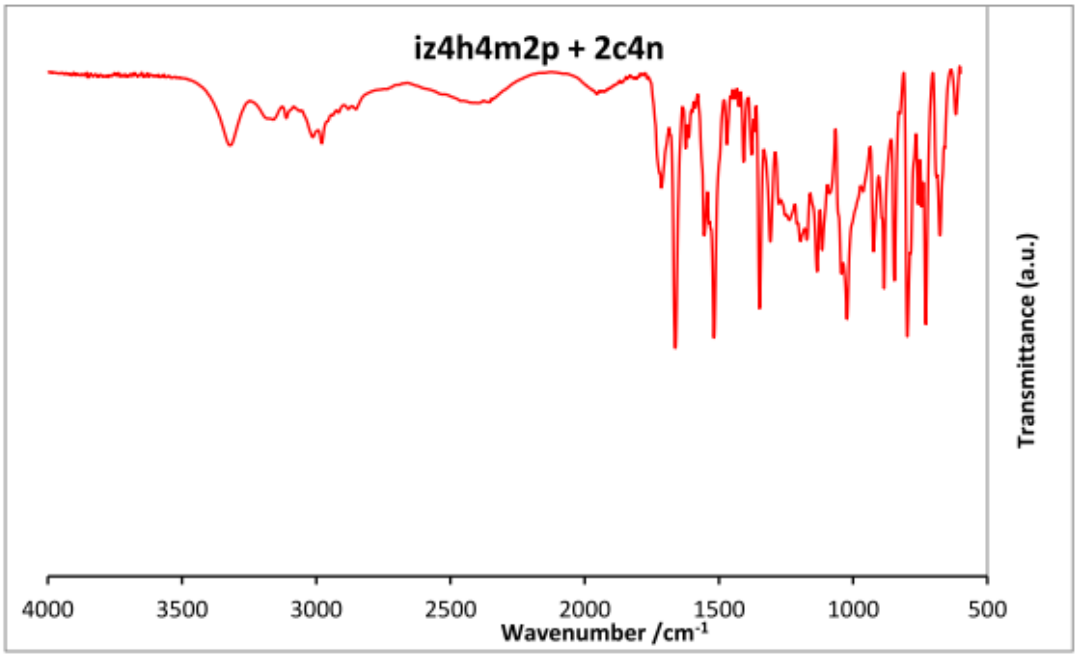


Figure S9 FTIR for the cocrystal of **iz4h4m2p** + **2c4n**

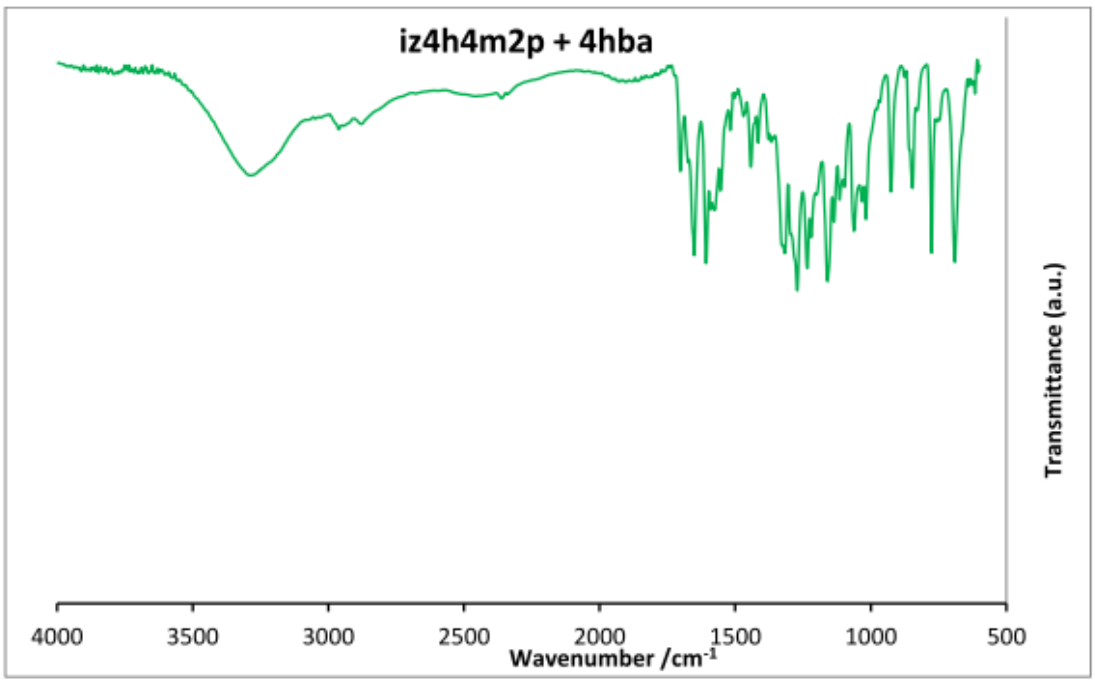


Figure S10 FTIR for the cocrystal of **iz4h4m2p** + **4hba**

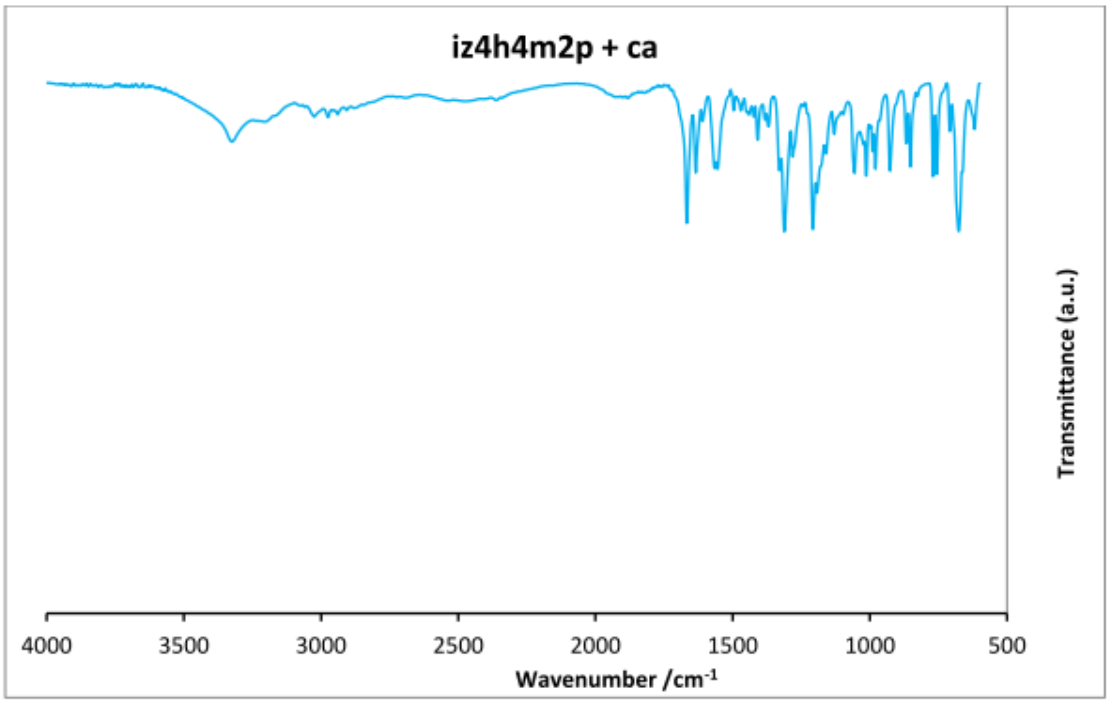


Figure S11 FTIR for the cocrystal of **iz4h4m2p** + **4hba**

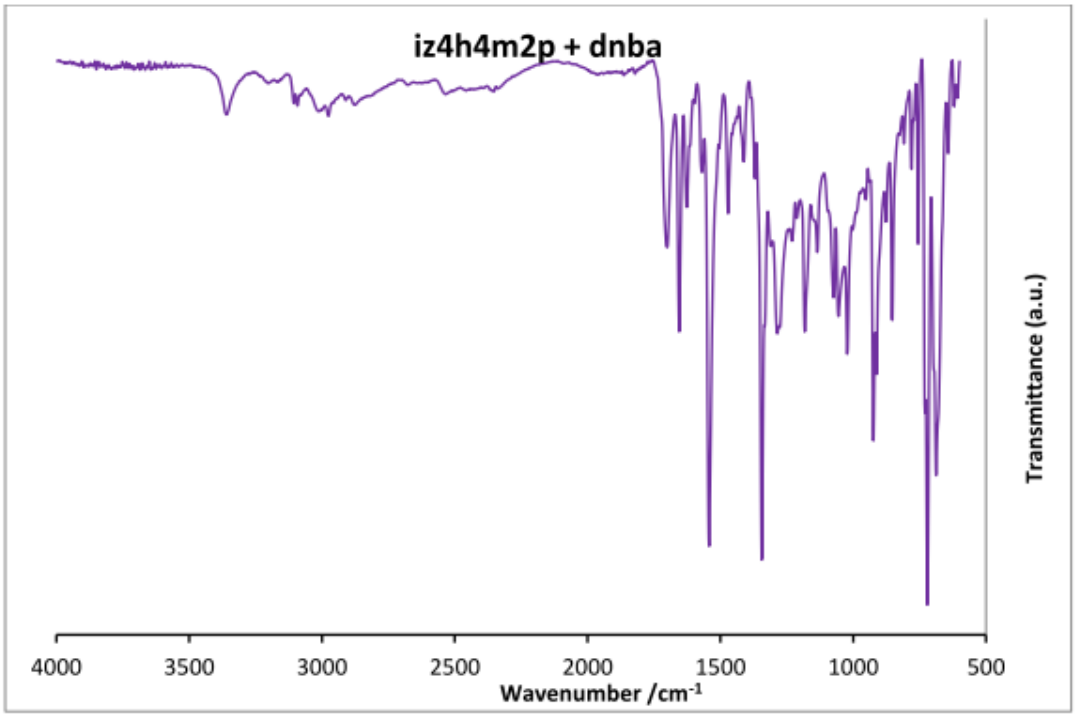


Figure S12 FTIR for the cocrystal of **iz4h4m2p** + **dnba**

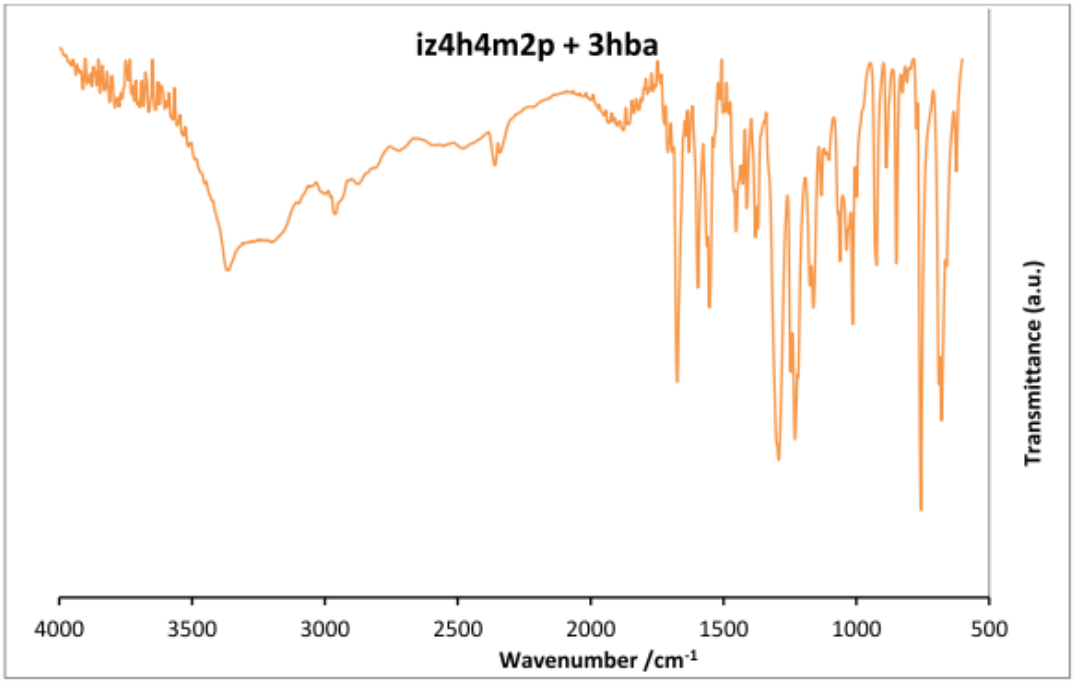


Figure S13 FTIR for the cocrystal of **iz4h4m2p** + **3hba**

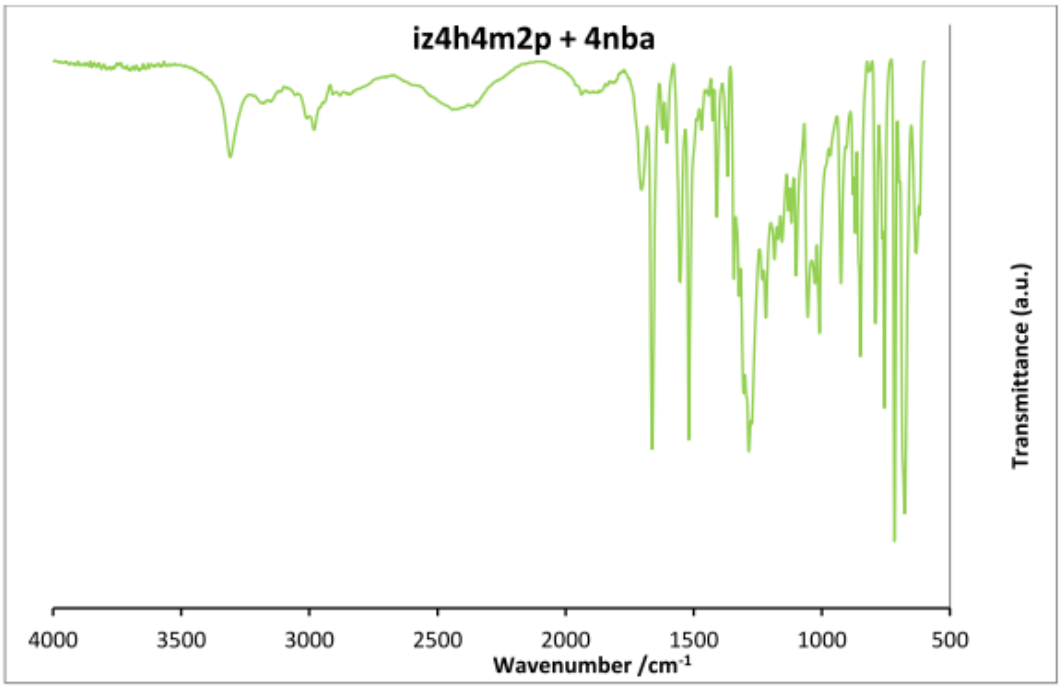


Figure S14 FTIR for the cocrystal of **iz4h4m2p** + **4nba**

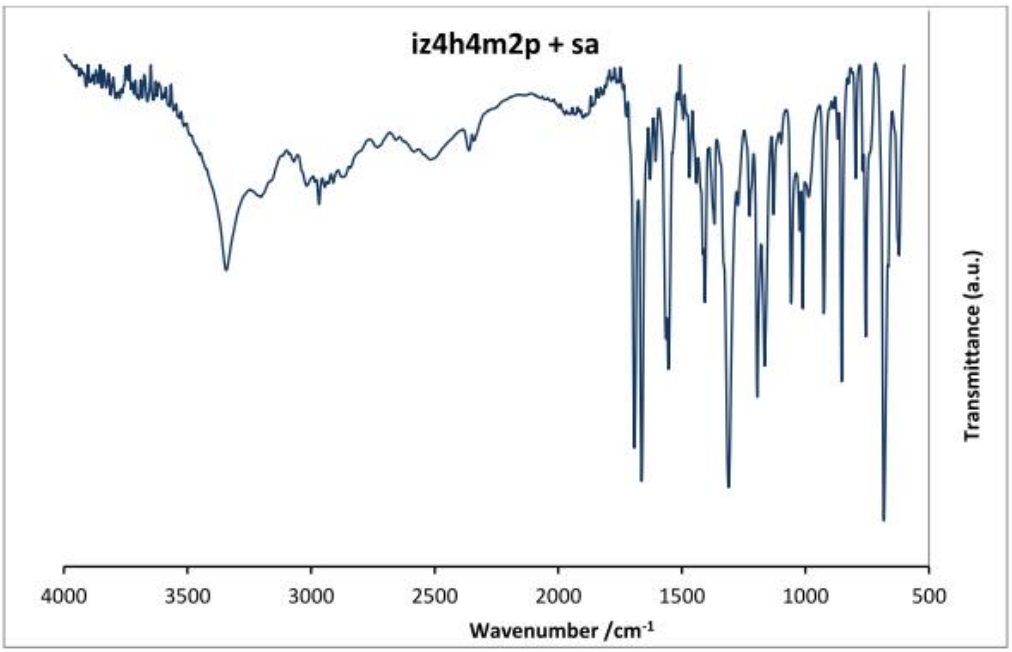


Figure S15 FTIR for the cocrystal of **iz4h4m2p** + **sa**

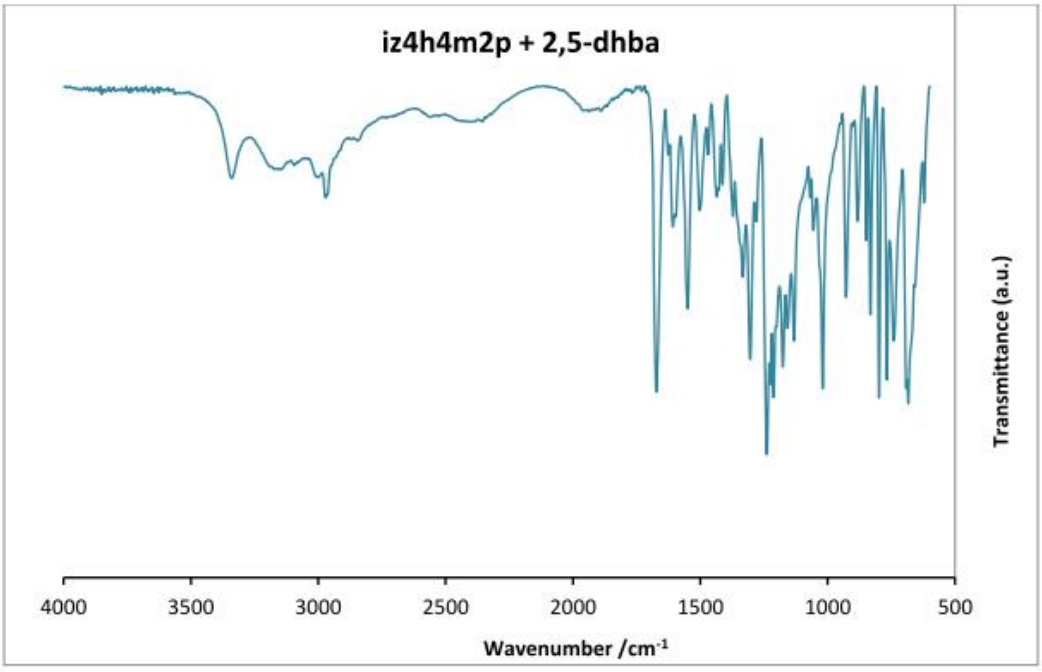


Figure S16 FTIR for the cocrystal of **iz4h4m2p** + **2,5-dhba**

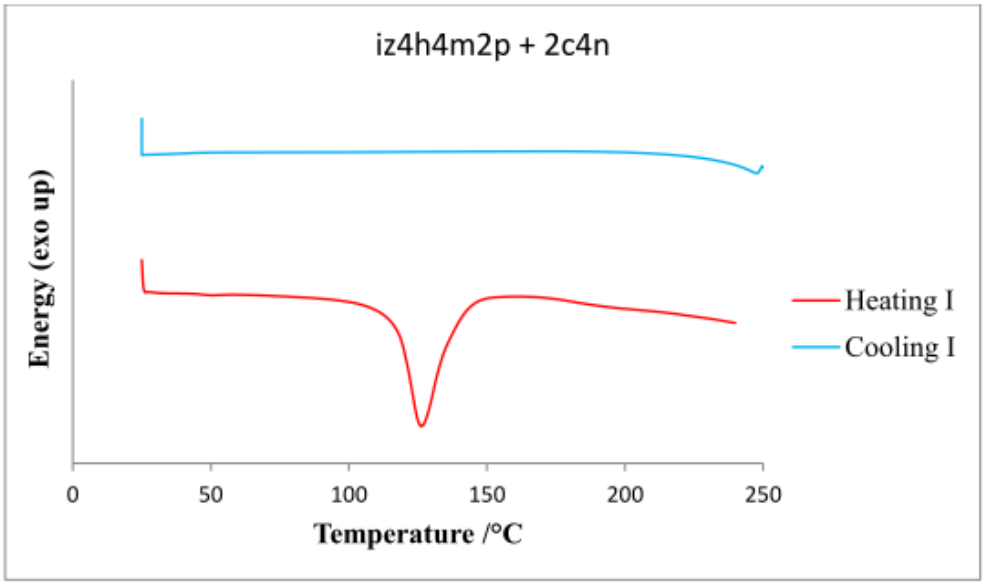


Figure S17 DSC curve for the cocrystal of **iz4h4m2p** + **2c4n**

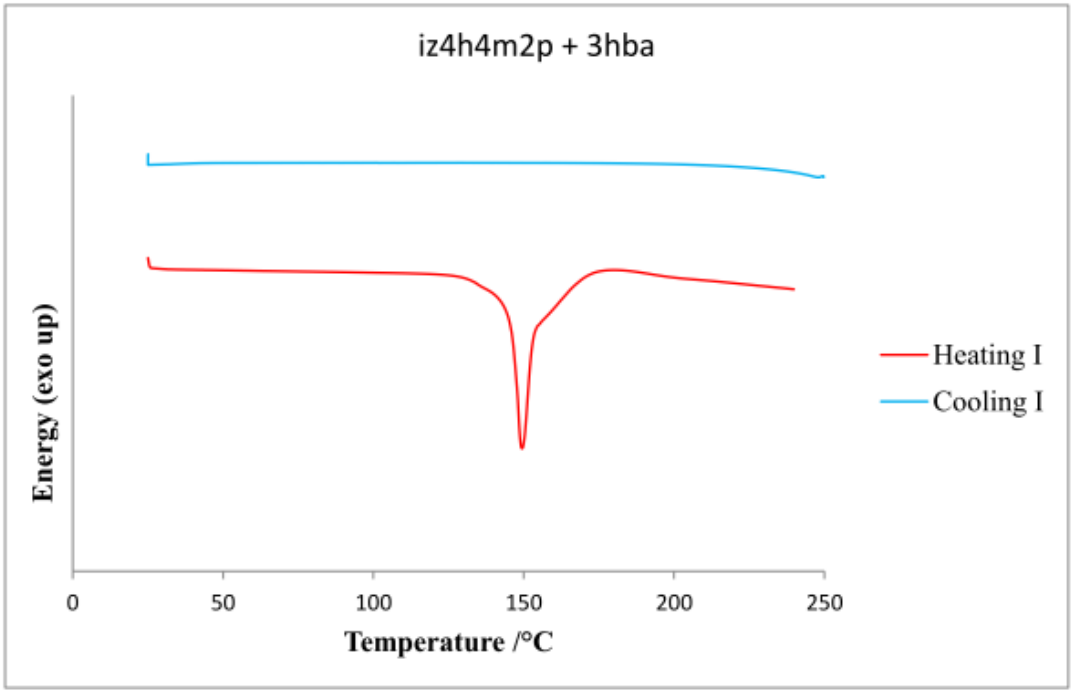


Figure S18 DSC curve for the cocrystal of **iz4h4m2p** + **3hba**

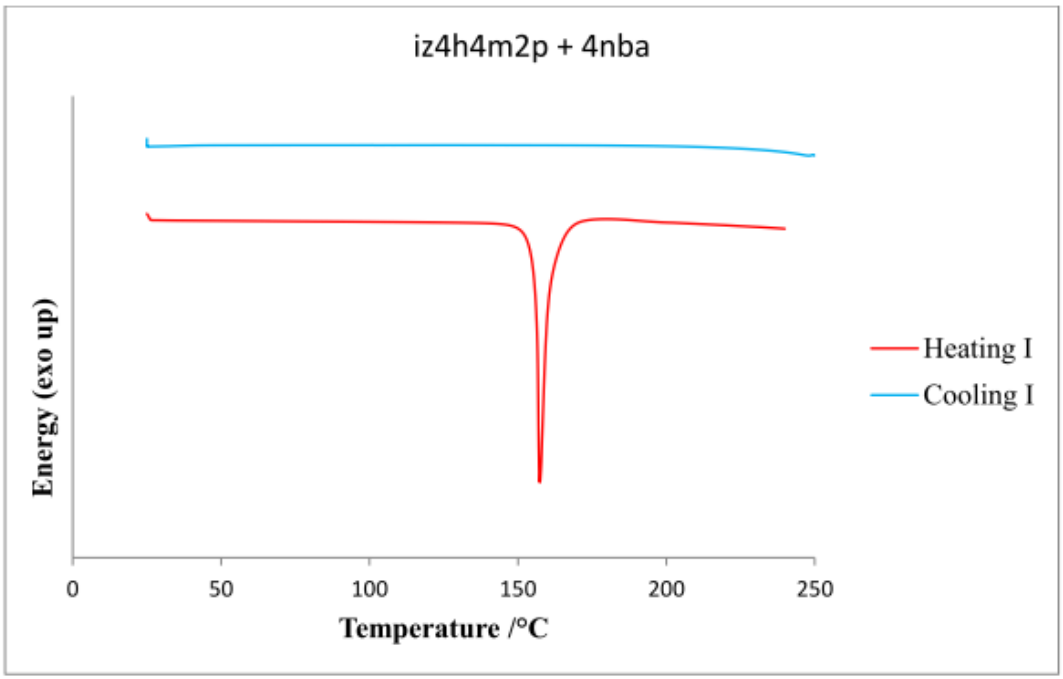


Figure S19 DSC curve for the cocrystal of **iz4h4m2p** + **4nba**.

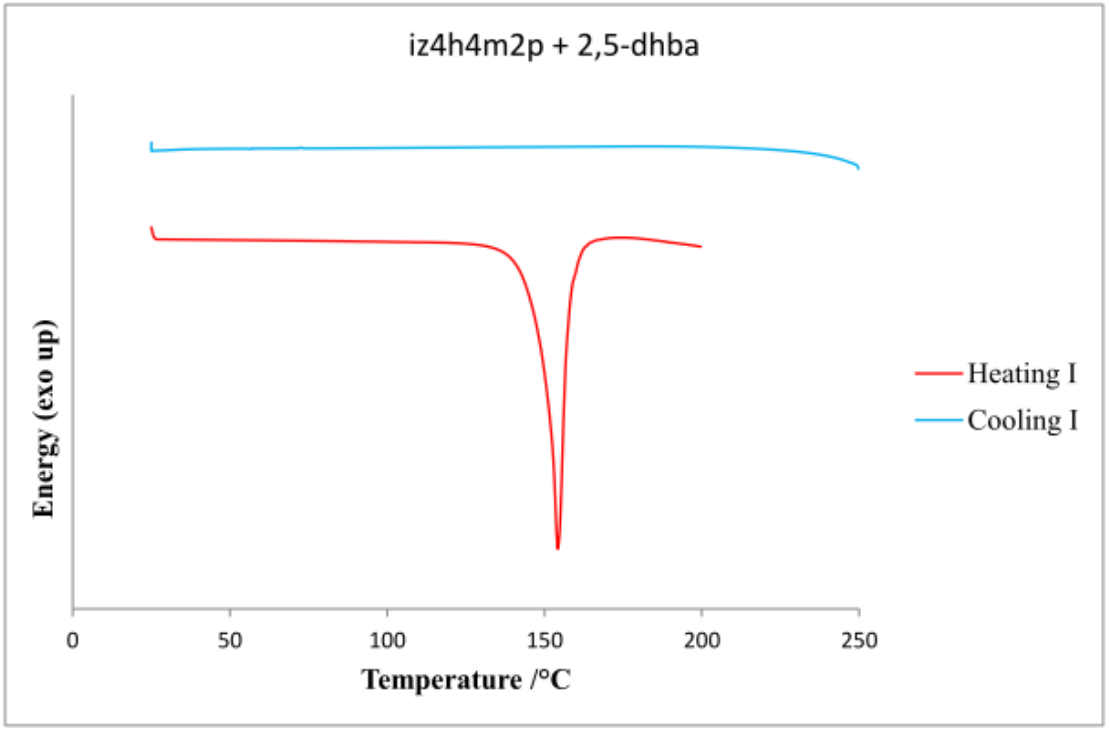


Figure S20 DSC curve for the cocrystal of **iz4h4m2p** + **2,5-dhba**.

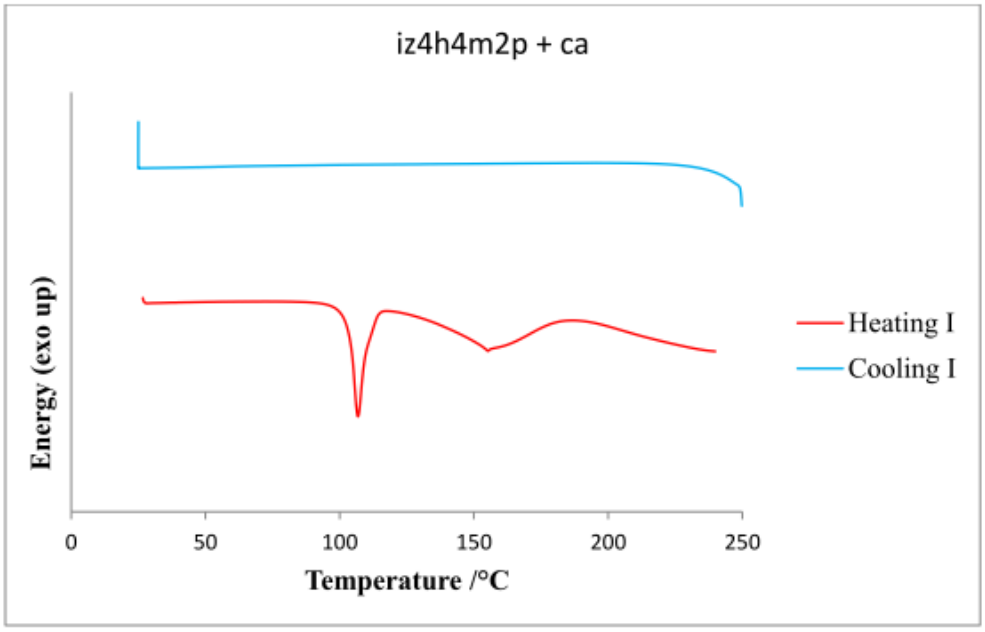


Figure S21 DSC curve for the cocrystal **iz4h4m2p** + ca

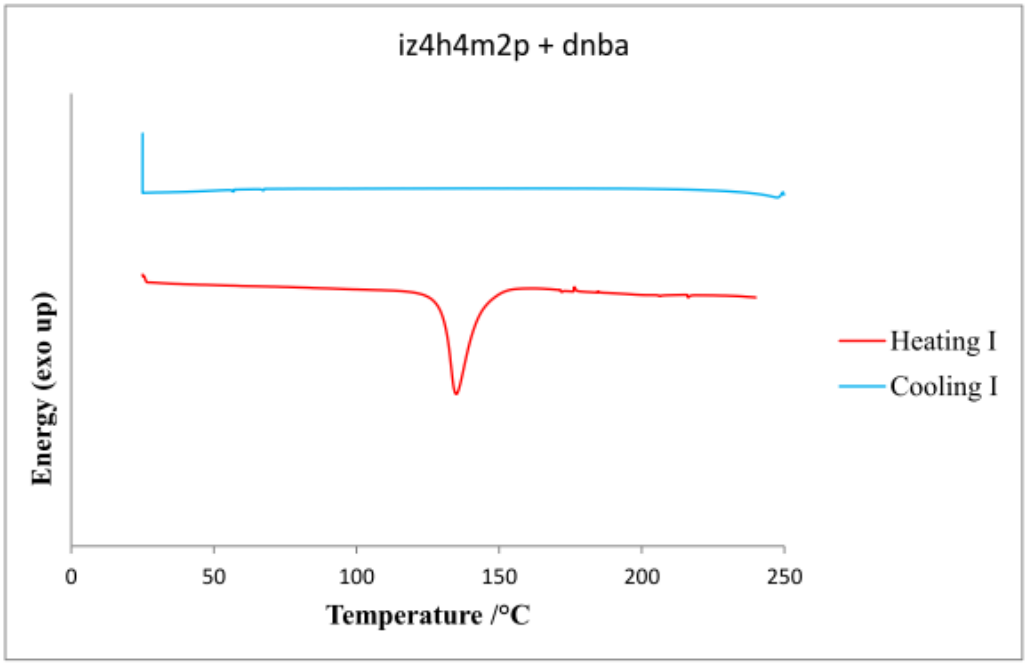


Figure S22 DSC curve for the cocrystal of **iz4h4m2p** + **dnba**.

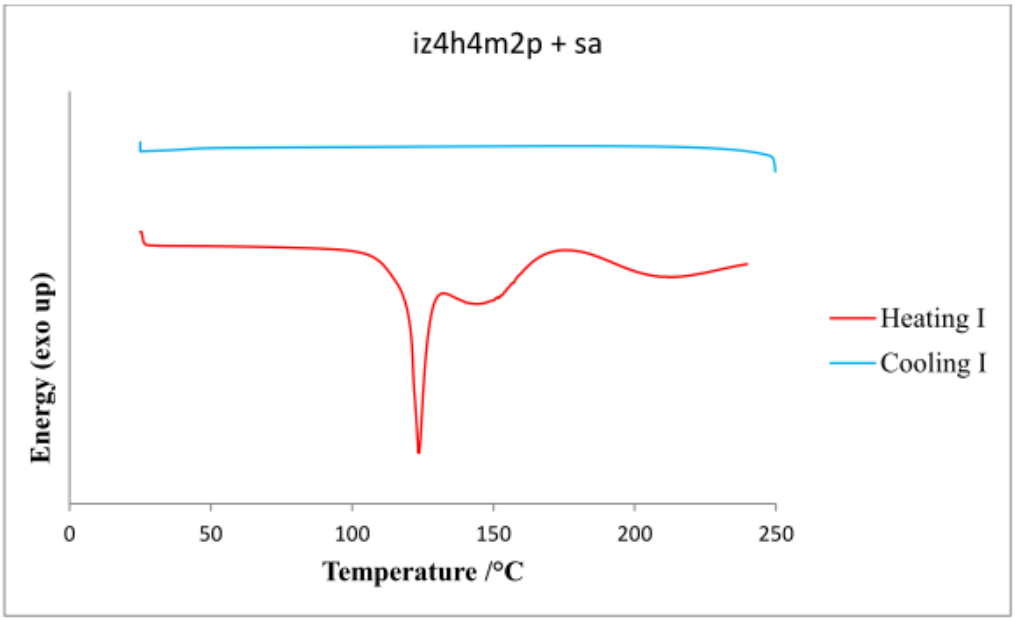


Figure S23 DSC curve for the cocrystal of **iz4h4m2p** + sa.

Table S2 List of cocrystals and moleculars salts of **inh** and Schiff-based derivatives of **inh** respectively

Refcodes of cocrystals and molecular salts of inh	Refcodes of cocrystals and molecular salts of Schiff-based inh derivatives
BAJXAP	CEFZEU
BAJXET	CETWEF
CAQPIX	EPISAY
ACUDAG	FADHOJ
ACUDEK	FADHUP
ACUDEK01	GIYMAF
ACUDIO	GIYMEJ
BICQAH	GIYMIN
BICQEL	GIYMOT
BICQUB	JILXIO
BICQUB01	JILXIO01
BIZMAZ	JILXOU
BOMBOW	JILYAH

BOMBUC	JILYEL
BOMCAJ	JILYIP
BUQTEP	JILYOV
BUVQER	LATKEY
COSKUT	LATKIC
DADLUS	LATKOI
EJOYEJ	LATLAV
FADGEY	LATLID
FADGIC	LEFQUK
FADGIC01	LIGXEG
FADGOI	NAKYOQ
FADGUO	NAKZIL
FADGUO01	OKAVED
FADGUO02	OKAVIH
FADHAV	OKAVON
FADHEZ	OKAVUT
FADHID	SAYNOX
FOSFIE	SAYNUD
FOSFOK	SAYPAL
FOSFUQ	SAYPEP
FOSFUQ01	SIKTEO
FOSMIL	UBILAW
FOSMIL01	UMUZAG
FOSMIL02	WOCFAX
FOSMIL03	XOPYEJ
GIYLUY	XOPYUZ
LATKUO	XOPZOU
LATLEZ	YUJJOE
LATSUW	YUJJOE01
LATTAD	YUJKAR
LATTAD01	YUJKEV
LODHIX	YUJNAU
LODHOD	YUJNEY
MOXNAR	YUJQUR

NAKZOR	YUJRAY
ORAWIO	ZECXEN
PEHFUF	ZUVWUK
PEHFUF01	ZUVXAR
PEZVAU	FEDRIT
PINJII	FEDTIV
PUMFOV	
PUMGAI	
PUMGOW	
QICJOE	
SETRIU	
SETROA	
SETRUG	
SETSAN01	
SETSAN02	
SETSAN03	
UDUJIP	
ULOSOG	
UQEKAF	
URUDER	
VAXROD	
VEGHOH	
VEGHUN	
VOPQEZ	
WETZAZ	
WIWNAU	
YEVBAF	
YIFXOB	
KEBLUC	
KEFXOM	
PEZVAU01	